NANYANG TECHNOLOGICAL UNIVERSITY

FIELD MEASUREMENTS AND NUMERICAL ANALYSIS OF INTERACTION BETWEEN CLOSELY SPACED BORED TUNNELS

CHUA HENG CHOON

SCHOOL OF CIVIL AND ENVIRONMENTAL ENGINEERING

2016

FIELD MEASUREMENTS AND NUMERICAL ANALYSIS OF INTERACTION BETWEEN CLOSELY SPACED BORED TUNNELS

CHUA HENG CHOON

School of Civil and Environmental Engineering

A thesis submitted to the Nanyang Technological University

in partial fulfilment of the requirement for the degree of

Doctor of Philosophy

2016

ACKNOWLEDGEMENTS

I would like to take this opportunity to express my appreciation and gratitude to my former supervisor Dr Wong Kai Sin and present supervisor Associate Professor Anthony Goh Teck Chee for their guidance, suggestions and invaluable advice throughout the research study.

I would also like to express my gratitude to the following personnel from Land Transport Authority (LTA) of Singapore, Main Contractors and Subcontractors involved in the Circle Line (CCL) Project for their kind assistance:

LTA Teams for the Circle Line Project

1. Mr Venktaramana A/L V Vijayaragavan (Director, Circle Line Stage 5)
2. Mr Tan Kian Thong (Director, Circle Line Stage 3)
3. Mr Ow Chun Nam (Director, Circle Line Stage 4)
4. Mr Lim Kim Kwang (Senior Project Manager, Circle Line C852)
5. Mr Ramesh s/o Sreedharan Nair (Deputy Project Manager, Circle Line C854)
6. Mr Ho Kee Sang (Deputy Project Manager, Circle Line C855)
7. Mr Tan Ming Wooi (Senior Design Engineer, Circle Line C852)
8. Mr Alan Khoo Rongwen (Project Engineer, Circle Line C855)
9. Mr Mahesh P Shelke (Technical Officer, Circle Line C854)

Main Contractors for the Circle Line Project

1. Sembawang Engineers & Constructors Pte. Ltd.
2. Taisei Corporation
3. Woh Hup Pte. Ltd. - Shanghai Tunnel Engineering Co., Ltd. - Alpine Mayreder Bau GmbH Joint Venture

Subcontractors (Geotechnical Instrumentations) for the Circle Line Project

1. Tritech Engineering & Testing (Singapore) Pte. Ltd.

2. Soil & Foundation Pte. Ltd.

Without their consent, support and guidance during data acquisition, my research study at NTU would not be made possible.

As a full time research staff of NTU for the Jurong Rock Caverns (JRC) Project (2009 – 2012), my heartfelt appreciation goes to my project supervisor Associate Professor Anthony Goh Teck Chee and all the personnel from JTC Corporation involved in the JRC Project. Their support and kind consideration facilitated my part-time research study at NTU.

This thesis could also not be made possible without the knowledge imparted by my former project supervisor of NTU for the research project on the Deep Tunnel Sewerage System (DTSS), Dr Ashraf Mohamed Hefny, who had patiently shared his precious engineering experience and expertise in the area of underground construction. Therefore, I would like to say a special thank you for his previous guidance and invaluable advice.

I would also like to thank Associate Professor Leong Eng Choon and Associate Professor Zhao Zhiye for giving me the opportunity to learn from them during the complementary site investigation at Banyan Basin, Jurong Island, for the JRC Project (2006 – 2007) and JRC Project (2007 – 2009).

Many thanks to Mr Eugene Tan Hiap Guan and Mr Vincent Heng Hiang Kim of Geotechnics Laboratory, who have in one way or another assisted me during the course of this research study.

Towards finalisation of my thesis, I began making overtures of friendship. A big thank you to Zhang Wei, Chen Yi, Zou Chunjiang, Zhang Wengang, Huang Wengui, Si Jinhua, Weng Jian and many others for mutual recognition of friendship. As an

interested party, I would like to thank Chong Chee Siew, who appeared to be implacably opposed to my plan of being featured as a “professor”, despite myself (see photo and passage in MEMORABILIA).

It may be worth to mention that another particularly enjoyable part of the finalisation of this thesis was in “fouling up” badly with Kelly Zong Fuli, the only daughter and heiress of beverage tycoon Zong Qinghou and Shi Youzhen, who openly search for Prince Charming since January 2013. Thus in what follows, I sent umpteen of emails to her which I never dreamt that I would actually pursue such action! In retrospect, those emails indeed served as a “wonderFuli” pastime (see photos in MEMORABILIA).

Finally, my deep appreciation and thank you to my mother Teh Kin Moi (a ten-generation descendant of 郑成功), my deceased father Chua OPeng Pui, my brothers and my sisters for their encouragement and understanding, as well as my potential Ms Right, whom I have yet to find, for her forbearance.

TABLE OF CONTENTS

ABSTRACT

The recent construction of the Circle Line (CCL) Mass Rapid Transit (MRT) Tunnels in Singapore has provided an opportunity to investigate the effects of interaction between closely spaced bored tunnels. The primary objectives of the research are two-fold. The first is to investigate the effects of interaction between closely spaced bored tunnels on ground surface settlements as well as the stresses and deformation induced in the tunnel lining of the pre-existing bored tunnel. This is achieved by analysing the field measurements from Contract 856 of Circle Line Stage 5, followed by conducting detailed two-dimensional (2D) numerical studies to investigate the ground surface responses and complex interaction mechanisms of closely spaced bored tunnels. The second objective is to propose a simplified methodology, empirical equations and design charts which will be practically useful to tunnel engineers in their preliminary design.

Review of literatures relevant to the present research study was performed. Although a great deal of insights has been gained from the published literatures, the problems and shortcomings of some works were surveyed and summarised.

The background of the Circle Line Contract 856 was introduced. The geological conditions as well as the engineering properties of soils and rocks encountered along the bored tunnel alignments were described in detail. Field measurements of ground surface settlements were classified according to groups of ground compositions. The interrelationship between ground surface settlements and Earth Pressure Balance Machine (EPBM) parameters was explored.

Back analyses of the ground surface settlements for Circle Line Contract 856 using the 2D finite element program PLAXIS were carried out. Both the Mohr-Coulomb (MC) and Hardening Soil (HS) models were considered for bored tunnelling through stiff ground of Jurong Formation and mixed ground of Jurong Formation and Kallang

Formation. The results demonstrated reasonably good agreement between the field measurements and the 2D finite element analyses. The HS model with its capability to model the non-linear stress-strain behaviour and also to take into account of both loading and unloading was found to be suitable for analysing tunnelling through stiff ground of Jurong Formation.

A procedure that utilises the Excel spreadsheet built-in optimisation routine Solver to estimate the trough width parameter i and location of maximum surface settlement Loc S_{max} for single and closely spaced bored tunnels was developed. It is shown that the highly scattered field measurements were not completely in the range of the trough width parameter i proposed by Peck (1969).

A comprehensive finite element study was carried out from which empirical equations were developed for estimating the trough width parameter i and location of maximum surface settlement Loc S_{max} for closely spaced bored tunnels with the same volume loss condition. The proposed empirical equations were found to be in good agreement with results of additional finite element analyses as well as with the results of finite element back analyses for selected field case studies.

Further numerical parametric studies were then performed to investigate the interaction between closely spaced bored tunnels. The effects of tunnel geometric parameters as well as soil and lining deformation properties on the stresses and deformation induced in the pre-existing bored tunnel were studied. The results of the parametric studies indicated the complex interaction mechanisms governing the stresses and deformation induced in the pre-existing bored tunnel after construction of the second adjacent bored tunnel. The possibility of idealising the overall interaction mechanisms has been discussed. Based on the results obtained, design charts were proposed for estimating the induced incremental maximum bending moment as well as the vertical and horizontal diameter changes of the pre-existing bored tunnel after construction of the

second closely spaced bored tunnel. The validity of the design charts was affirmed based on seven published case histories.

For the more complex situation where joints are incorporated into the tunnel lining, a parametric study was carried out to assess the feasibility of simplifying the exact simulation. For all the cases analysed by the finite element approach, the stresses and total displacements generated by the 4-joint+key is close to the 5-joint for cases involving single bored tunnel. The same phenomena can be considered valid for interaction between closely spaced parallel bored tunnels. Further simplification of the 4-joint+key to non-jointed tunnel lining can be achieved by considering the effect of K_o.

The present research has improved the understanding on the effects of interaction between closely spaced bored tunnels on the ground surface settlements and tunnel lining response of the pre-existing bored tunnel. The proposed methodology, empirical equations and design charts are useful as rapid and inexpensive tools for preliminary design considerations as well as for the interpretations of the field measurements.

LIST OF TABLES

LIST OF FIGURES

LIST OF SYMBOLS

Symbol	Description
N	Blow count of standard penetration test (SPT)
D_{10}, d_{10}	Grain size at which 10 per cent of the sample is finer than
c_u, c, s_u	Undrained shear strength; undrained cohesion
OF, N_t, N_c	Overload factor; stability number; stability factor
H, z_o	Depth to tunnel axis; depth of cover; tunnel depth; depth of tunnel below ground (at tunnel springline); depth of burial; depth of the tunnel centre below ground surface
γ, γ_s, γ_{sat}	Unit weight of soil; saturated unit weight of soil
σ_o	Total Overburden pressure or applied axial stress
P_o	Air pressure or confining pressure
σ_s	Surcharge acting on the ground surface
OFS	Overload ratio
D	Tunnel diameter
H/D, z_o/D	Dimensionless depth of burial; tunnel cover to diameter ratio
$\gamma D/c_u$	Ratio controls the localized failures to occur at the tunnel face
LF	Load factor
N_{TC}	Stability ratio at collapse
P	Unsupported length of tunnel excavation
C	Cover to tunnel crown; depth of cover
f	Seepage force
s'	Effective support pressure
γ_s'	Submerged unit weight

Symbol	Description
c'	Effective cohesion
Δh	Head difference
F_o, F_1, F_2, F_3	Coefficients as functions of the friction angle ϕ'
ϕ', ϕ	Friction angle; effective friction angle; internal friction angle of cohesive-frictional soil
h_o-h_f	Hydraulic head difference
Δp	Difference in pressure
S_{max}, δ_{max}	Maximum settlement
i, σ	Distance to the point of inflection; trough width parameter; standard deviation of the normal probability curve
S	Settlement at distance x from the centreline of the tunnel
x	Distance x from the centreline of the tunnel; coordinate
V_s	Volume of a unit length of the settlement trough
K, k'	Constant which depends on ground properties; empirical constant; constant of proportionality which is known as the trough width parameter
n	Empirical factor
R	Tunnel radius
α	Empirical constant
k	Ground permeability
K_x	Lateral stress perpendicular to the tunnel axis
L_T	Lagging distance between the twin tunnels excavated faces
K_o	Coefficient of earth pressure at rest; coefficient of lateral earth pressure at rest
n_o	Soil stiffness ratio

Symbol	Description
E'_h	Horizontal effective Young's modulus
E'_v	Vertical effective Young's modulus
OCR	Overconsolidation ratio
α_{dec}	Ratio of stress release
L_{dec}	Length of unlined zone
L_{lin}	Length of the excavated section at each step
p	Uniform face pressure
σ_{ho}	Initial axial stress at the tunnel axis
G_{layer}/G_{soil}	Stiffness of the upper layer relative to that of the saturated clay
s_p	Distance between the centres of the tunnels
m	Rate of increase of cohesion with depth for purely cohesive clay
S	Clear spacing between the tunnels
RQD	Rock quality designation
E_u, E_s	Modulus of elasticity; undrained elastic modulus; undrained Young's modulus; undrained modulus; deformation modulus
ψ	Angle of dilatancy
E_{50}^{ref}	Reference secant stiffness in standard drained triaxial test
ϕ_u	Undrained friction angle
E_{50}	Secant stiffness in standard drained triaxial test; secant Young's modulus
E_{ur}	Unloading / reloading stiffness
σ'_3	Confining stress
p^{ref}	Reference confining pressure

Symbol	Description
m	Power for stress-level dependency of stiffness
E_{oed}^{ref}	Reference tangent stiffness for primary oedometer loading
E_{ur}^{ref}	Reference unloading / reloading stiffness
ν_{ur}	Poisson's ratio for unloading-reloading
K_o^{nc}	K_o-value for normal consolidation
R_f , $\frac{q_f}{q_a}$	Failure ratio
z	Depth
E_p	Pressuremeter modulus; reload modulus
G	Shear modulus
E'	Drained Young's modulus
ν, ν_d, ν_u	Poisson's ratio of soil ("d" denotes drained and "u" denotes undrained)
D_r	Relative density
t	Thickness of tunnel lining
γ_l	Unit weight of tunnel lining
E_l	Deformation modulus of tunnel lining
ν_l	Poisson's ratio of tunnel lining
VL	Volume loss in percentage
H'	Distance of horizontal bottom boundary below the tunnel axis
Loc S_{max}, μ	Location of maximum surface settlement; mean of the normal probability curve
D_i	Error function
$S(x)_G$	Magnitude of the Gaussian probability curve

Symbol	Description
$S(x)_M$	Magnitude of the measured ground surface settlement
W/D	Dimensionless pillar width
H_{JF}	Strata thickness for Jurong Formation (interval)
H_{MC}	Strata thickness for Marine Clay (interval)
W	Pillar width
R^2	Coefficient of determination
$i_{R0.5}$	Trough width parameter (residual soil with volume loss of 0.5 per cent)
$i_{R5.0}$	Trough width parameter (residual soil with volume loss of 5 per cent)
$i_{M0.5}$	Trough width parameter (mixed soils with volume loss of 0.5 per cent)
$i_{M5.0}$	Trough width parameter (mixed soils with volume loss of 5 per cent)
i_{FEM}	Trough width parameter (finite element analyses)
$i_{FEM\ (Field)}$	Trough width parameter (finite element analyses of field measurements)
Loc $S_{max\ R0.5}$	Location of maximum surface settlement (residual soil with volume loss of 0.5 per cent)
Loc $S_{max\ R5.0}$	Location of maximum surface settlement (residual soil with volume loss of 5 per cent)
Loc $S_{max\ M0.5}$	Location of maximum surface settlement (mixed soils with volume loss of 0.5 per cent)
Loc $S_{max\ M5.0}$	Location of maximum surface settlement (mixed soils with volume loss of 5 per cent)
Loc $S_{max\ FEM}$	Location of maximum surface settlement (finite element analyses)
Loc $S_{max\ FEM\ (Field)}$	Location of maximum surface settlement (finite element analyses of field measurements)
VL(1)	Volume loss induced in the first bored tunnel
VL(2)	Volume loss induced in the second bored tunnel

Symbol	Description
VL(1,2)	Volume loss induced in the first and second bored tunnels
θ	Tunnel angular relative position
E_s/E_l	Relative stiffness
F	Flexibility ratio; lining flexibility
R_{inter}	Interface strength
ΔM_{max}	Incremental maximum bending moment
M_c	Constrained modulus
ΔM_p	Incremental maximum moment coefficient for primary effect
ΔD_p	Deformation coefficient for primary effect
ΔM_{VL}	Incremental maximum moment coefficient per unit volume loss for volume loss effects
ΔD_{VL}	Deformation coefficient per unit volume loss for volume loss effects
ΔM_{max}	Incremental maximum bending moment
$\Delta D_{H/V}$	Vertical (V) or horizontal (H) diameter change
I_l	Moment of inertia of the cross section per unit length along the axis of the tunnel
n_e	Number of equal segments
I_e	Effective moment of inertia
I_j	Second moment of area at the joint
C_r	Compressibility ratio
T	Thrust
M	Bending moment
ΔD	Diameter change

Symbol	Description
η	Reduction factor
E_lI_l	Bending rigidity of the actual tunnel lining
$(E_lI_l)_e$	Effective bending rigidity of the equivalent continuous tunnel
$(E_lI_l)_e/(E_lI_l)$	Effective rigidity ratio
$K_\theta l/E_lI_l$	Joint stiffness ratio
K_s	Coefficient of soil resistance
θ_j	Orientation of reference joint

CHAPTER 1 INTRODUCTION

1.1 Background

The utilization of underground space for various development purposes, e.g. underground transportation system, communication and utility network such as electric cable systems and sewerage systems, has gained considerable interests in countries where rapid urbanization and land scarcity are major issues, e.g. Singapore. In Singapore, the construction of the Circle Line (CCL) Mass Rapid Transit (MRT) Tunnels commenced in 2002. The multi-billion dollar Circle Line MRT Tunnels were constructed on the central-south of Singapore. The construction of this underground MRT system is crucial as it shortens the travelling time of the commuters by allowing the commuters to bypass some of the busy interchanges in Singapore, as well as freeing up surface land for other higher value activities, which is considered as a critical advantage for a land-scarce country like Singapore.

The construction of the Circle Line MRT Tunnels has provided an opportunity to investigate the effects of interaction between closely spaced bored tunnels. The Circle Line Project implemented in 5 stages, i.e. Stage 1 to Stage 5, involves the construction of the twin running bored tunnels of 37 kilometres long with 32 stations using various types of Tunnel Boring Machines (TBMs). The Contract in which this research are based upon included the construction of the bored tunnels from West Coast (Haw Par Villa Station) to Harbour Front Station with a connecting tunnel to a ventilation shaft of Circle Line Contract 856 (Stage 5).

The subsurface ground conditions encountered along the tunnel alignments consist of various weathering grades of sedimentary rocks of Jurong Formation overlain by softer soils of Kallang Formation. In addition, mixed-face ground conditions were also encountered at some sections of the tunnel alignments.

Along the tunnel alignments, comprehensive geotechnical instrumentations were deployed to monitor both the ground and structure responses to bored tunnelling.

This database of geotechnical instrumentations has provided opportunities for real scale studying of the interaction between closely spaced bored tunnelling. It should be noted, however, that the mechanisms of interactions between closely spaced bored tunnels are highly complex due to large number of variables involved. Hence, a comprehensive study on the behaviour of tunnel interaction is conducted using finite element analysis. The measured field data thus provides an invaluable benchmark for calibration of the numerical model for the parametric studies.

For closely spaced bored tunnelling, the state of stress and strain around the bored tunnels may be highly modified. Subsequently, this may lead to excessive ground movements (see Figures 1.1 to 1.3) which can adversely affect the stability of the adjacent structures, both underground and above ground. To date, the Gaussian distribution curve proposed by Peck (1969) remains the most popular method used for estimating the surface settlement profile for single tunnels. This empirical method that was developed mostly based on field measurements observed from hand mining as well as open face shield mining enables the distance to the point of inflection to be determined by plotting the settlement ratio against the square of the distance from the line of symmetry to the monitoring point. A plot tends to appear as a straight line when the ground surface settlement trough follows the Gaussian form. On the other hand, a curvy line may render the settlement parameter indeterminable. The use of a simple spreadsheet algorithm enables the settlement parameters from Peck's method to be determined for both straight and curvy lines. Accordingly, the settlement parameter for the measured ground surface settlements induced by closely spaced bored tunnelling may also be determined. Apart from developing a technique to facilitate the back analysis of field measurements, development of a potentially useful predictive method is important to aid the engineering design process and serve as a form of knowledge gained.

For structural design of tunnel lining, closed-form analytical solutions and various analytical methods have been proposed by Morgan (1961), Peck et al. (1972), Muir Wood (1975) and Duddeck and Erdmann (1982). However, fewer studies were conducted for assessing the additional impact of interaction between closely spaced

bored tunnels (see Figures 1.4 and 1.5), in particular for cases involving a wide range of flexibility of tunnel lining. The precast segmental linings (see Figure 1.6) are commonly used as the primary lining in bored tunnelling projects. However, the presence of key segment and joints in between the precast segmental linings which may significantly influence the stresses and displacements induced in the tunnel lining have seldom been investigated.

Based on the problems identified, the present research investigates the field performance of closely spaced bored tunnelling based on field measurements consisting of ground surface settlements and Earth Pressure Balance Machine (EPBM) parameters for Circle Line Contract 856. This is followed by assessing the use of the two-dimensional (2D) finite element method program PLAXIS for estimating ground surface settlements induced by closely spaced bored tunnelling, where comparisons will be made with the field measurements and the soil models adopted for the computation will be validated. Subsequently, the effects of interaction between closely spaced bored tunnels on the ground surface settlement as well as stresses and displacements induced in the first bored tunnel will be studied. Factors affecting the magnitude and extent of ground surface settlement trough as well as the magnitude of interaction effects between closely spaced bored tunnels will be identified. Some differences do exist between the monolithic tunnel lining and jointed precast segmental linings. These differences will be investigated for single bored tunnel and closely spaced bored tunnels. Finally, it is the main thrust of this research to generalise the results obtained from the numerical studies to produce practical predictive methods for rapid and inexpensive evaluations of the magnitude of tunnel interaction to facilitate preliminary design considerations as well as interpretations of field monitoring results for closely spaced bored tunnels.

Figure 1.1 Temporary restriction on access to left lane due to ground surface settlement

Figure 1.2 Temporary restriction on access to median due to ground surface settlement

Figure 1.3 Ground surface settlement trough

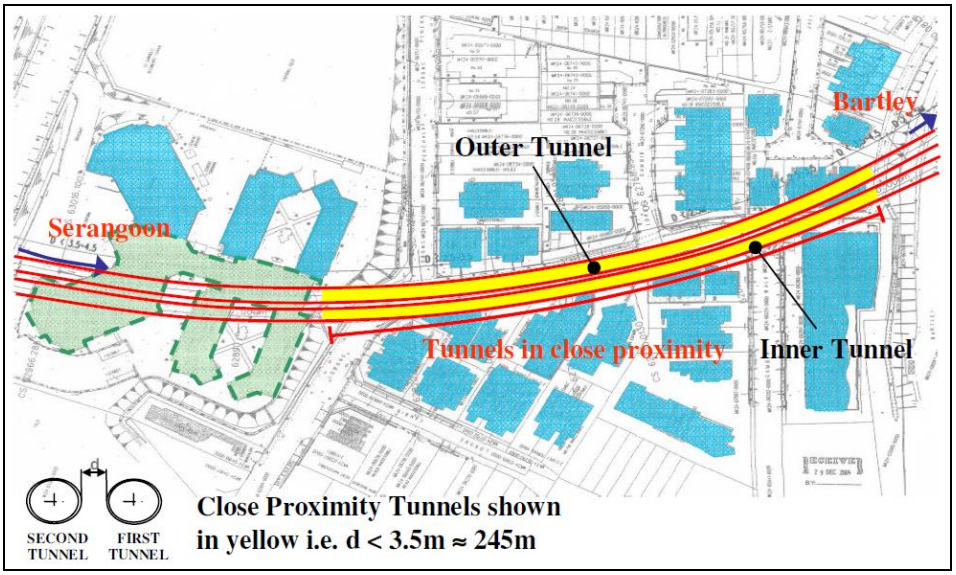

Figure 1.4 Tunnels between Serangoon and Bartley Stations in close proximity (Circle Line Contract 852) (after Lim et al., 2008)

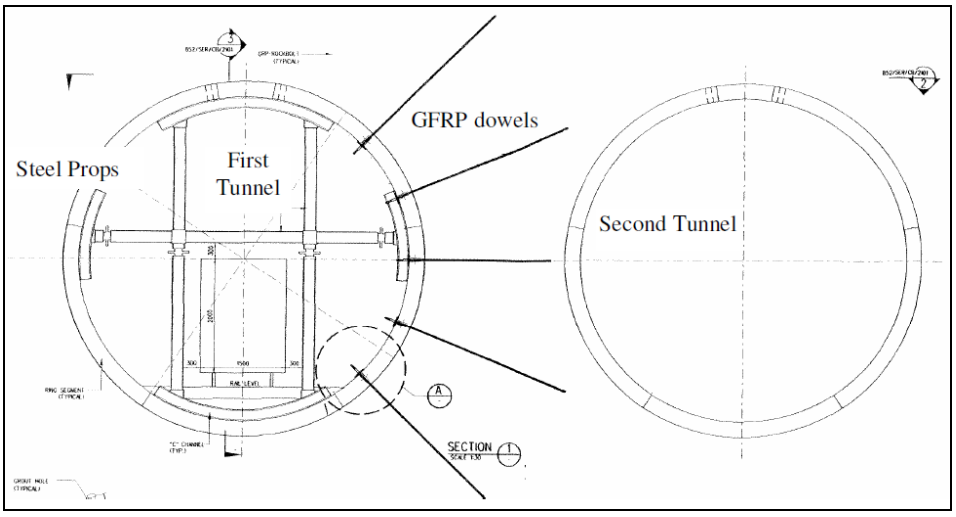

Figure 1.5 Temporary bracing and GFRP dowels for first tunnel (Circle Line Contract 852) (after Lim et al., 2008)

Figure 1.6 Jointed precast segmental linings

1.2 Research Objectives

This research involves an extensive assessment of field measurements as well as performing a series of comprehensive 2D finite element analyses. Following are the objectives of this research:

1. To examine the ground surface settlements induced by closely spaced bored tunnelling through: (a) Weathering grades of sedimentary rocks of Jurong Formation; (b) Weathering grades of sedimentary rocks of Jurong Formation overlain by softer soils of Kallang Formation and; (c) Mixed-face ground of weathering grades of sedimentary rocks of Jurong Formation and softer soils of Kallang Formation based on the EPBM parameters in order to identify various sources of volume loss influencing the ground surface settlements.
2. To evaluate the performance of Mohr-Coulomb (MC) elastic perfectly plastic model and Hardening Soil (HS) non-linear hyperbolic model in estimating the ground surface settlements above: (a) Weathering grades of sedimentary rocks of Jurong Formation; (b) Weathering grades of sedimentary rocks of Jurong Formation overlain by softer soils of Kallang Formation and; (c) Mixed-face ground of weathering grades of sedimentary rocks of Jurong Formation and softer soils of Kallang Formation.
3. To investigate numerically the important factors affecting the ground surface settlement trough induced by the closely spaced bored tunnelling through (a) Weathering grades of sedimentary rocks of Jurong Formation and; (b) Mixed-face ground of weathering grades of sedimentary rocks of Jurong Formation and softer soils of Kallang Formation.
4. To establish a predictive method for assessing the ground surface settlement parameters for ground surface settlement trough induced by closely spaced bored tunnelling through: (a) Weathering grades of sedimentary rocks of Jurong Formation and; (b) Mixed-face ground of weathering grades of sedimentary rocks of Jurong Formation and softer soils of Kallang Formation.
5. To investigate numerically the important factors affecting the magnitude of interaction effects between closely spaced bored tunnels and to identify the

contribution of each fundamental interaction effect towards the complex interaction effects.

6. To establish a predictive method for assessing the magnitude of interaction effects between closely spaced bored tunnels.

1.3 Research Scope

The scope of work includes:

1. Conduct literature review on the following aspects of tunnelling:

a. Classifications of soft ground for tunnelling and operating techniques adopted in the state-of-the-art Tunnel Boring Machines (TBMs), i.e. EPBM and Slurry Machine, in controlling ground movements during bored tunnelling as well as methods for estimating face pressure and factor of safety for EPBM and Slurry Machine, respectively.

b. Approaches for estimating ground surface settlement.

c. Some recent published works related to measurements made during tunnelling, physical modelling and numerical studies of interaction between closely spaced tunnels.

d. Summarize the relevance of previous works to the present research.

2. Collate field data of Circle Line Contract 856

a. Characterise geological conditions and their corresponding engineering properties along the sites studied.

b. Classify the field data into groups of similar subsurface conditions at the tunnel level.

3. Evaluate field performance of bored tunnelling of Circle Line Contract 856

a. Identify the relationship between longitudinal ground surface response and EPBM parameters.

4. **Conduct back analysis of Circle Line Contract 856**

a. Assess the adequacy of the 2D numerical analysis in estimating ground surface settlement profiles.

b. Calibrate the numerical model.

5. **Develop a method for determination of trough width parameter**

a. Assess the general acceptability of the proposed method.

6. **Develop empirical equations for predicting trough width parameters**

a. Validate the proposed empirical equations.

7. **Investigate the factors affecting interaction between bored tunnels**

a. Conduct numerical parametric studies on closely spaced bored tunnels.

8. **Develop design charts for estimating magnitude of interaction between bored tunnels**

a. Validate the proposed design charts.

9. **Investigate the behaviour of jointed tunnel lining**

a. Summarise the existing methods for estimating stresses induced in the monolithic and jointed tunnel lining.

b. Identify the influence of the presence of key segment and joints between segmental linings.

1.4 Layout of Thesis

Chapter 2 presents an overview of the soil behaviouristic classification system commonly adopted for soft ground tunnelling. The chapter also reviews the suitability of adopting each of the state-of-the-art EPBM and Slurry Machine methods for tunnelling through different ground conditions. The common operating parameters of EPBM and Slurry Machine methods are discussed and the differences

in functioning principle of each machine in stabilising the tunnel face during operation as well as method for estimating face pressure are highlighted.

Chapter 3 summarises the previous research related to single tunnel and interaction between closely spaced tunnels. The chapter contains the common approaches proposed by researchers for estimating the ground surface response to tunnelling as well as field observations, laboratory experimental studies and numerical analyses of interaction between closely spaced tunnels.

Chapter 4 contains detailed descriptions of the instrumented sites of the Circle Line Contract 856. Both geological and geotechnical aspects of the Jurong Formation and Kallang Formation are presented.

Chapter 5 investigates the relationship between longitudinal ground surface settlements associated with construction of two closely spaced bored tunnels through Jurong Formation and mixed-face ground condition with EPBM parameters.

Chapter 6 investigates the adequacy of 2D finite element analysis and selected soil models adopted for estimating the transverse settlement profile induced by construction of closely spaced bored tunnels. The results of the back-analyses using 2D plane strain model are compared with the field measurements.

Chapter 7 presents a method for determining the trough width parameter. The adequacy of the proposed method is compared with the trough width parameter proposed by other researchers.

Chapter 8 presents the development of empirical equations for predicting the trough width parameter. The proposed empirical equations are validated using results of finite element analyses and four case studies.

Chapter 9 investigates the effects of newly bored tunnel on the incremental stresses and displacements induced in the pre-existing bored tunnel. The mechanisms of

interaction between closely spaced parallel bored tunnels are studied in detail based on 2D finite element analysis.

Chapter 10 presents the development of a series of design charts for estimating the vertical and horizontal displacements induced in closely spaced parallel bored tunnels. The development procedures of the design charts are illustrated and some practical applications of the proposed design charts are highlighted. The validity of the proposed design charts for estimating the displacements induced in the pre-existing bored tunnel is affirmed based on published field data in the literature.

Chapter 11 presents a literature review on methods used for design of tunnel lining incorporating the effects of joints. The results of parametric studies for single bored tunnel and closely spaced bored tunnels incorporating the key segment and joints in the segmental linings are discussed.

Chapter 12 presents conclusions of the present research and proposals for future works.

CHAPTER 2 SOIL BEHAVIOURISTIC CLASSIFICATION SYSTEM AND TUNNEL BORING MACHINES

2.1 Introduction

This chapter provides an overview of the classification of the ground conditions for soft ground tunnelling and summarises the methods for evaluating the stability of granular soils and gravels as well as cohesive soils at the tunnel face. The capabilities of the Earth Pressure Balance Machine (EPBM) and Slurry Machine in controlling the ground surface settlement and heave are described. References were also made to the available methods for estimating the degree of support provided to the ground during bored tunnelling.

2.2 Classifications of Soft Ground for Tunnelling

Several methods have been proposed to evaluate ground behaviour for determining the tunnel stability. These methods include correlations based on ground behaviour classifications and modified overload factors. The behaviour of ground can be classified as follows:

Firm Ground

Ground has sufficient stand-up time for heading advanced by the tunnel boring machine. There is adequate time for the erection of the final lining before the ground movement begins. This ground includes stiff clays and cemented or cohesive granular material.

Ravelling Ground

Materials at the working face of the tunnel progressively drop out into the heading. This may lead to cavities above the tunnels or sinkholes at the ground surface. The ravelling is slower above the ground water table as compared to below the ground water table. This ground includes slightly cemented sands, silts and fine sands gaining their strength from apparent cohesion.

Running Ground

Materials run from the unsupported tunnel face and slope into the heading until a stable pile is built up at the angle of repose. This ground includes perfectly cohesionless granular soils above the ground water table such as dry sands and gravels.

Flowing Ground

Materials flow into the tunnel due to the built-up seepage pressures at the working face. This ground includes ravelling or running ground below the water table.

Squeezing Ground

Materials are squeezed into the tunnel plastically, where no visible fracturing or loss of continuity is observed. The squeezing behaviour is due to the overstressing of the soil. This ground includes soft to medium clays.

Swelling Ground

Materials absorb water and slowly swell into the tunnel. This ground includes swelling clays and desiccated soils.

2.3 Methods for Evaluation of Ground Behaviour

Terzaghi (1950) published the Tunnelman's Ground Classification System which relates the reaction of soil to tunnelling construction methods in use in the 1950s. This empirical evaluation was later modified by Heuer (1974) to present the classification system in engineering terms that reflect current terminology and usage, as illustrated in Table 2.1.

Table 2.1 Tunnelman's ground classification system (after Heuer, 1974)

Classification		Behaviour	Typical Soil Types
Firm		Heading can be advanced without initial support and final lining can be constructed before ground starts to move.	Loess above water table; hard clay, marl, cement sand and gravel when not highly overstressed.
Ravelling	Slow Ravelling	Chunks or flakes of material begin to drop out of the arch or walls sometimes after the ground has been exposed due to loosening or to overstress and "brittle" fracture (ground separates or breaks along distinct surfaces, opposed to squeezing ground). In fast ravelling ground, the process starts within a few minutes, otherwise the ground is slow ravelling.	Residual soils or sand with small amounts of binder may be fast ravelling below the water table, slow ravelling above. Stiff fissured clays may be slow or fast ravelling depending upon degree of overstress.
	Fast Ravelling		
Squeezing		Ground squeezes or extrudes plastically into tunnel without visible fracturing or loss of continuity and without perceptible increase in water content. Ductile, plastic yield and flow due to overstress.	Ground with low frictional strength. Rate of squeeze depends on degree of overstress. Occurs at shallow to medium depth in clay of very soft to medium consistency. Stiff to hard clay under high cover may move in combination of ravelling at execution surface and squeezing at depth behind surface.
Running	Cohesive Running	Granular materials without cohesion are unstable at a slope greater than their angle of repose (±30-35^{o}). When exposed at steeper slopes, they run like granulated sugar or dune sand until the slope flattens to the angle of repose.	Clean, dry granular materials. Apparent cohesion in moist sand or weak cementation in any granular soil may allow the material to stand for a brief period of ravelling before it breaks down and runs. Such behaviour is cohesive-running.
	Running		
Flowing		A mixture of soil and water flows into the tunnel like a viscous fluid. The material can enter the tunnel from the invert as well as from the face, crown and walls, and can flow for great distances, completely filling the tunnel in some cases.	Below the water table in silt, sand or gravel without enough clay content to give significant cohesion and plasticity. May also occur in highly sensitive clay when such material is disturbed.
Swelling		Ground absorbs water, increases in volume, and expands slowly into the tunnel.	Highly preconsolidated clay with plasticity index in excess of about 30, generally containing significant percentages of montmorillonite.

2.3.1 Ground Behaviour at Tunnel Face

A series of classification systems of the ground behaviour trends of each soil type to tunnelling operation has also been proposed by Schmidt (1974) and Heuer and Virgens (1987).

Granular Soils and Gravels above Ground Water Table

The behaviour of sands and silty sands is dependent on their relative density, grain size, fines percentage and angularity of grains. Heuer and Virgens (1987) developed approximate ground behaviour trends of dense silty sands (SPT N > 30) above water table for tunnelling operations, as shown in Figure 2.1. It was also pointed out by Heuer and Virgens (1987) that silts and fine sands behave much differently from clayey soils and may lead to potentially difficult tunnelling conditions.

Other than estimation of ground behaviour of non-cohesive silty sands based on D_{10} size, the ratio of overburden to unconfined compressive strength can also be used to classify the ground behaviour if the materials have sufficient cohesion or cementation to permit sampling and testing to define the unconfined compressive strength:

1. Firm ground: If the overburden pressure at tunnel depth is in the range of about 1/10 to 1/6 of the unconfined compressive strength or less;
2. Slow ravelling: If the overburden pressure is in the range of about 1/5 to 1/4 of the unconfined compressive strength; and
3. Fast ravelling: If the overburden pressure is in the range of about 1/3 to 1/2 of the unconfined compressive strength.

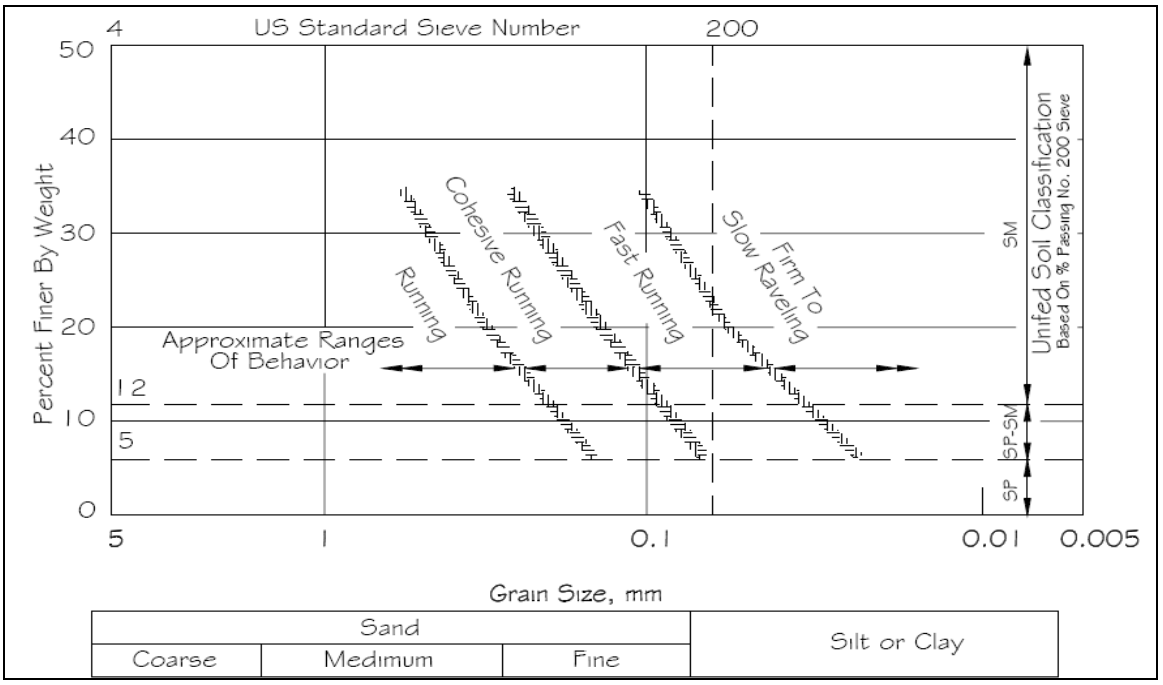

Figure 2.1 Anticipated ground behaviour based on D_{10} size dense soil N > 30 above ground water table (after Heuer and Virgens, 1987)

Granular Soils and Gravels below Ground Water Table

For silty sands, clean sands and gravels below the ground water table, the soils can also be classified as flowing ground according to the Tunnelman's Ground Classification System, where some forms of ground water control such as dewatering or the use of compressed air must be considered. The internal air pressure must approximately balance the external water head. Table 2.2 summarises the behaviour of sands and gravels in tunnelling by Terzaghi (1977).

The immediate ground movements of the classified soft ground conditions for tunnelling induce different volume loss, and in turn, different ground settlement profiles. Hence, selection of soft ground tunnelling techniques must be suitable for the expected ground conditions and considerations must be given to the ground behaviour at the tunnel face to ensure the stability of the tunnel face during the tunnelling.

Table 2.2 Tunnel behaviour: sands and gravels (after Terzaghi, 1977)

Designation	Degree of Compactness	Tunnel Behaviour	
		Above Water Table	Below Water Table
Very fine clean sand	Loose, N≤10 Dense, N>30	Cohesive running Fast ravelling	Flowing Flowing
Fine sand with clay binder	Loose, N≤10 Dense N>30	Rapid ravelling Firm or slowly ravelling	Flowing Slowly ravelling
Sand or sandy gravel with clay binder	Loose, N≤10 Dense N>30	Rapid ravelling Firm	Rapid ravelling or flowing Firm or slow ravelling
Sandy gravel and medium to coarse sand		Running ground. Uniform (c_u<3) and loose (N≤10) materials with round grains run much more freely than well-graded (c_u>6) and dense (N>30) ones with angular grains.	Flowing conditions combined with extremely heavy discharge of water.

Cohesive Soil

The overload factor OF also termed the stability number N_t provides measurement for the ground movements into the tunnel face. Broms and Bennermark (1967) defined the stability number N_t for tunnel in cohesive soil as:

$$N_t = \frac{\sigma_o - P_o}{c_u} \tag{2.1}$$

where σ_o is the total overburden pressure or applied axial stress, P_o is the air pressure or confining pressure and c_u is the undrained shear strength determined by unconfined compression tests, Swedish fall-cone tests or laboratory vane tests. This correlation has been identified as the fundamental ratio for characterising the instability of the face.

For cases involving surcharge acting on the ground surface σ_s, N_t can be expressed as follows:

$$N_t = \frac{\sigma_o + \sigma_s - P_o}{c_u} \tag{2.2}$$

From field observations, Peck (1969) indicated that N_t values of less than 5 permits tunnelling to be carried out without difficulties in cohesive soil. For N_t value ranging from 5 to 6, the rapid invasion of the clay into the tailpiece clearance may be expected. Table 2.3 summarises the tunnel behaviour in relation to the stability factor.

Table 2.3 Tunnel stability: cohesive soils (after Peck, 1969 and after Phienwaja, 1987)

Stability Factor, N_t	**Tunnel Behaviour**
1	Stable
2 – 3	Small creep
4 – 5	Creeping, usually slow enough to permit tunnelling
6	May produce general shear failure. Clay likely to invade tail space too quickly to handle

Clough and Schmidt (1981) reported that the theoretical potential ground loss is less than about 1 per cent when the overload factor OF is smaller than about 2. For OF between about 2 and 4, the potential ground loss might reach magnitudes of 10 per cent. In this case, the ground movements through the face are generally small and a shield can effectively restrain ground losses to a value smaller than 2 per cent or 3 per cent. An approximately 1/3 of the total ground losses in clay with OF values up to about 5 occurs through the tunnel face when a shield is used. Face support becomes important for OF greater than about 5. For OF = 6, the ground loss is between 30 per cent and 90 per cent. It was pointed out that the proposed relationship between ground loss and OF is not truly valid for very large strains.

For practical applications, Schmidt (1974) presented graphically the approximate relationship between overload ratio OFS and tunnel behaviour, where OFS is the ratio of the net overburden pressure at springline (after accounting for any air pressure) divided by the undrained shear strength c_u of clay. Schmidt (1974) indicated that the ground conditions are favourable for tunnelling so long as OFS < 3, whereas the shield becomes unmanageable when OFS = 6. This evaluation

method can be considered as a more detailed classification as it linked the stress level around the tunnel with the undrained shear strength of soil.

The guideline presented in ITA/AITES Report 2006 (2007) also indicated that in addition to overload factor, parameters H/D and $\gamma D/c_u$ which accounted for the effect of depth on the stability conditions as well as the possibility of localised failures to occur at the face also need to be considered, where H is the depth of the cover and D is the tunnel diameter. For $H/D < 2$, a detailed analysis of the face stability is required, whereas localised failure can occur at the face for $4 < \gamma D/c_u$.

Mair (1978) proposed a load factor for tunnelling in clayey ground as:

$$LF = \frac{N_t}{N_{TC}} \tag{2.3}$$

where N_{TC} is the stability ratio at collapse (see Figure 2.2), P is the unsupported length of tunnel excavation, D is the outer tunnel diameter and C is the cover to tunnel crown.

Therefore, LF = 0 when the tunnel support pressure corresponds to the overburden stress at tunnel axis level and increases to LF = 1 at failure with tunnel support pressure equal to tunnel support pressure at collapse.

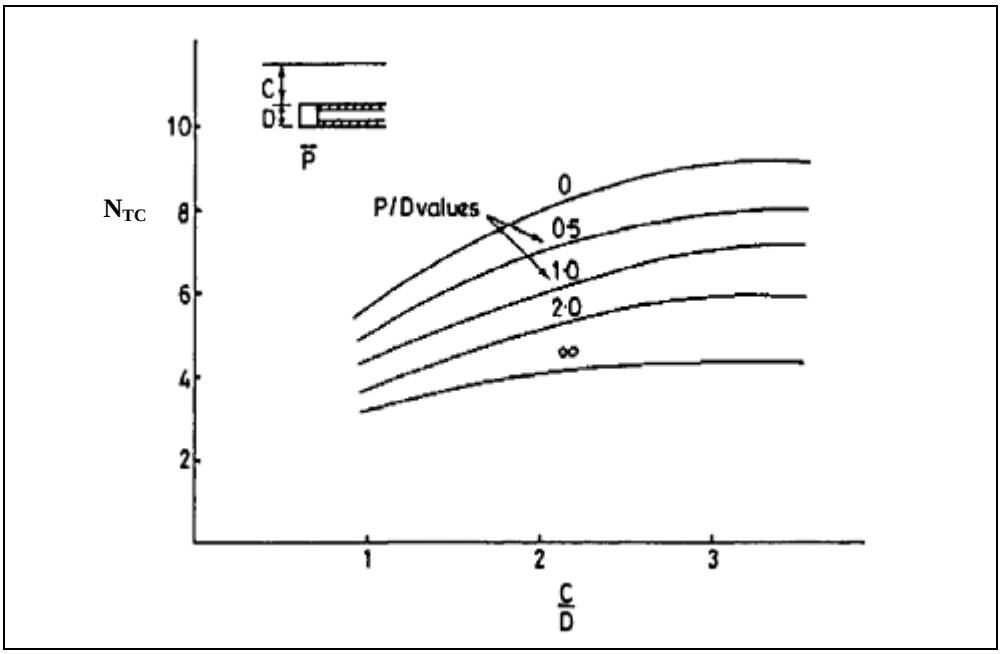

Figure 2.2 Influence of heading geometry and depth on the tunnel stability ratio at collapse (after Mair, 1978)

2.4 Tunnel Boring Machine

A Tunnel Boring Machine (TBM) is a complex set of equipment assembled to excavate a tunnel. The basic components of TBM include the cutterhead with cutting tools, shield, equipment for grouting and ground support installation, as well as steering systems and systems for power supply. In addition, there are also back-up equipment systems that provide muck transport, personnel and material conveyance, ventilation and utilities.

2.4.1 Components Affecting Excavation Performance of Tunnel Boring Machine

Cutting Wheel

The design of the cutting wheel is adapted to the geological conditions along the tunnel alignment. It can be designed for both soft ground and hard rock conditions with openings to ease the ground material transfer to the working chamber. The cutting tools may consist of a combination of the following components:

1. Scrapers as soft ground teeth
2. Disc cutters for harder ground excavation
3. Bucket lips or copy cutter as overcutting edge

In addition, the rotary unit with lead through for the injection of soil conditioning agents in front of the cutting wheel is also part of the components of the cutting wheel.

Shield

The steel structure of the shield is normally designed according to the specified earth pressure, hydrostatic pressure, live loads, the occurring operational loads and an operating load above atmospheric pressure of 4 bars. The shield generally consists of the following three main components:

1. Front shield with cutting wheel and main drive
2. Middle shield body which includes the thrust jacks
3. Tailskin in which the ring building systems is located

All connections and lead through required for operation of the TBM are integrated.

Front Shield and Middle Shield

The cutter section with welded pressure wall serves as an abutment for the cutting wheel drive. It separates the excavation chamber with working face chamber and is required for generating pressure for support of the working face and absorbs the force generated by the contact pressure of the cutting wheel. The earth pressure sensors are positioned in the pressure wall. The shield tail is connected to the cutter section by means of articulation jacks.

Tailskin

The tailskin connection to the shield body is a passive type articulated design. A short tailskin attached to the rear of the trailing shield provides the sealing surface for the articulated tailskin. Connection of the tailskin to the shield main body is by passive articulation cylinders.

The tailskin includes:

1. The row wire brush seals capable of withstanding the high water pressure
2. The double articulation seal consisting of packing of stuffing box (mechanically adjustable) and emergency seal (emergency inflatable)
3. The grease lines to each of the front and rear (welded on the tail plate)
4. The grout lines are integrated in the tailskin. The four lines are two components grouting type
5. Spring plates (protection from grout) are bolted on the outside of the tailskin
6. The grout lines are equipped with special access points to allow for cleaning in case of blockage
7. The accelerator hose including mixing chamber can be removed from within the tunnel using specific seal

Grouting Equipments

The mortar cal will pump directly from the grout pump outside the tunnel and transfer to the storage tank on the back-up systems. The injection of the mortar and accelerator will be done through the tailskin. The mixing of the accelerator and mortar is located behind the tailskin in order to reduce any risk of grouting the injection lines. Subsequently, the mixture flows a small distance out of the tailskin into the cavity to be filled where the mixture hardens within a short period of time. This back-filling process is both pressure and volume controlled.

2.5 Functioning Principle of Earth Pressure Balance Machine

The basic idea of the EPBM, as illustrated in Figure 2.3, is to maintain the excavated soil in contact with the tunnel face to prevent soil movements into the face. In the conventional EPBM, the ground is excavated with the rotating cutter wheel and the excavated soil are collected and compacted in the excavation chamber behind the cutter wheel. When the earth paste in the excavation chamber can no longer be compacted by the earth pressure and the water pressure, the balanced which provides support and stability to the face is achieved. At this stage, the earth pressure at the tunnel face approximately corresponds to the earth pressure

at rest. A further increase of the support pressure of the earth paste exceeding the balance results in a further compaction of the earth paste in the excavation chamber as well as on the tunnel face. This may lead to a heave of the area in front of the shield. However, reducing the earth pressure may lead to the intrusion of the ground material into the excavation chamber which subsequently causing settlements. The excavated material is discharged by a screw conveyor and is transported from the pressurised excavation chamber to the tunnel under atmospheric pressure.

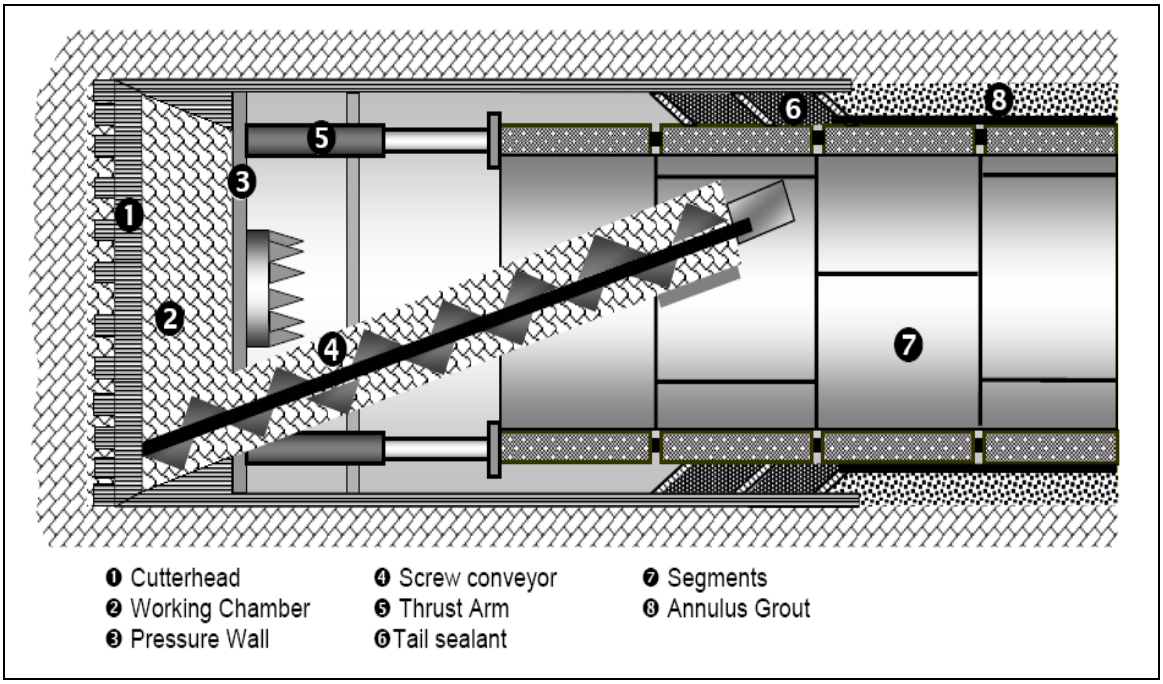

Figure 2.3 Schematic representation of EPBM (after EFNARC, 2005)

2.5.1 Operations of Earth Pressure Balance Machine

Screw Conveyor and Conveyor Belt

The screw conveyor is mounted to the connecting flange in the pressure wall of the cutter section and runs from the base of the shield to the discharge point of the conveyor belt. The front part of the spiral screw with shaft is protected against wear. The screw and core diameters determine the maximum allowable grain size along one edge. The material removed during the tunnelling operation is transported from the mixing chamber in the cutter section through the screw conveyor to the conveyor belt, which subsequently transports the material from the material

discharge point of the screw conveyor to the waiting muck car. A belt scanner device may be installed on the conveyor belt, which can monitor the volume of the excavated material automatically in real time. The monitored data will be recorded and transferred to the data acquisition system and the excavated mass can be monitored by applying a density of the excavated material.

Soil Conditioning

The use of foam as a conditioning medium for EPBM is suitable for high consistency heterogeneous soil conditions, as illustrated in Figure 2.4. The process requirements to a foam-conditioned soil are:

1. Support pressure transfer to the tunnel face
2. Sufficient ductility
3. Low water permeability
4. Elasticity
5. Reduction of adhesion at the TBM
6. Reduction of wear
7. Reduction of the drive power

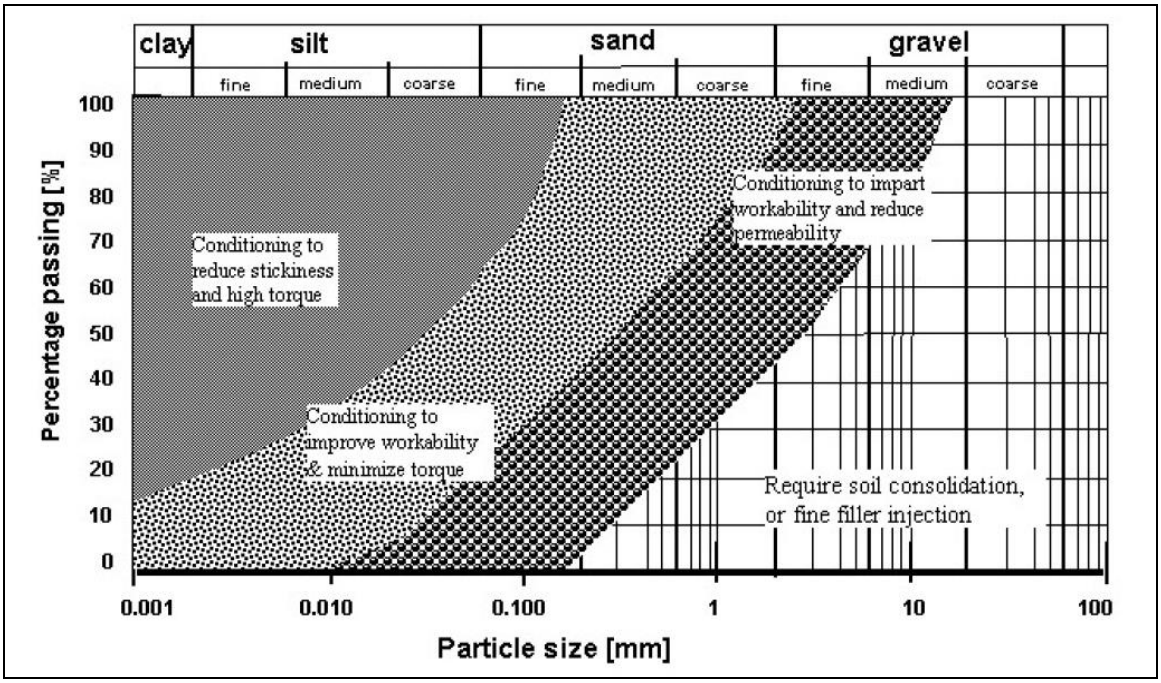

Figure 2.4 Soil conditioning needs of EPBM in different ground types (boundaries are only indicative) (after EFNARC, 2005)

Control of Earth Pressure

The EPBM keeps the earth pressure constant during tunnelling, where the pressure created in the excavation chamber has to compensate the pressure in front of the cutting wheel to avoid ground settlement and heave. The earth pressure is mainly influenced by the following factors:

1. Speed of screw conveyor
2. Advance rate
3. Volume of excavated materials
4. Additives for ground conditioning
5. Mode of operation (full EPB and open mode)

During tunnelling at a given speed, the earth pressure is usually controlled by changing the speed of the screw conveyor. When the ground is discharged more rapidly due to the higher speed of the screw, the earth pressure is falling. However, the opposite condition applies when decreasing the ground discharge rate. It is also possible to control the earth pressure by varying the advance rate of EPBM where reducing the advance rate of EPBM decreases the earth pressure, whereas increasing the advance rate increases the earth pressure. In addition, the rate of rotation of the cutting wheel can also be varied during tunnelling for mixing and ground conditioning, as well as to minimise the shield rolling.

Depending upon the severity of the ground conditions, the EPBM is capable of functioning at different modes, i.e. full EPB and open mode. For full EPB mode, the excavation chamber is closed with spoil being removed by the screw conveyor. The spoil is conditioned in the excavation chamber using the systems provided and creates a material consistency in the screw capable of retaining the confinement pressure. Control systems are supplied to interlock the screw speed and foam injection rate with the advance rate of EPBM to maintain the face pressure. The operation of EPBM in open mode can be achieved if the stability of the ground permits, where the spoil can be removed from the cutting wheel chamber by screw conveyor in the absence of the confinement pressure. Under such operation mode, no ground conditioning is required. The variations of earth pressure during the

operation period of the EPBM are visualised in the control cabin with the help of the earth pressure sensors installed at different levels on the pressure bulkhead.

2.5.2 Ground Conditions for Earth Pressure Balance Machine

The EPBM is particularly useful for binding grounds with a high content of clay and silt with the following characteristics:

1. High plasticity
2. Liquid to soft consistency
3. Low internal friction
4. Low water permeability

However, plastic clays can lead to blockage of muck conveying and can stick and cover the cutting tools and hence, reduce the excavation efficiency. In these cases, soil conditioning maybe injected ahead of the cutter head.

2.6 Slurry Machine

The Slurry Machine, illustrated in Figure 2.5, is capable of providing and maintaining positive pressure to control the tunnel face at all times during excavation. The positive pressure will be provided using slurry confined to a separate chamber (plenum chamber) where the excavation takes place. Excavation of the ground will be achieved by rotating cutterhead fitted with different configurations of cutting tools. The excavation chamber will remain filled with pressurized slurry at all times, thereby balancing the earth and hydrostatic pressure of the ground in front of the Slurry Machine.

The slurry feed and discharge flow metres as well as the slurry transducers mounted on the slurry shield bulkhead are linked to the central monitoring system where the information is processed. The slurry supply and discharge rate is controlled by adjusting the rotation speed of the slurry feed and discharge pump. This ensures that the required discharge flow rate necessary to allow smooth transportation of the spoil without sedimentation or segregation within the pipeline is kept at constant

level. The slurry feed density and slurry discharge density detectors are installed in the slurry feed line and discharge line respectively to control the excavated volume at all times during excavation.

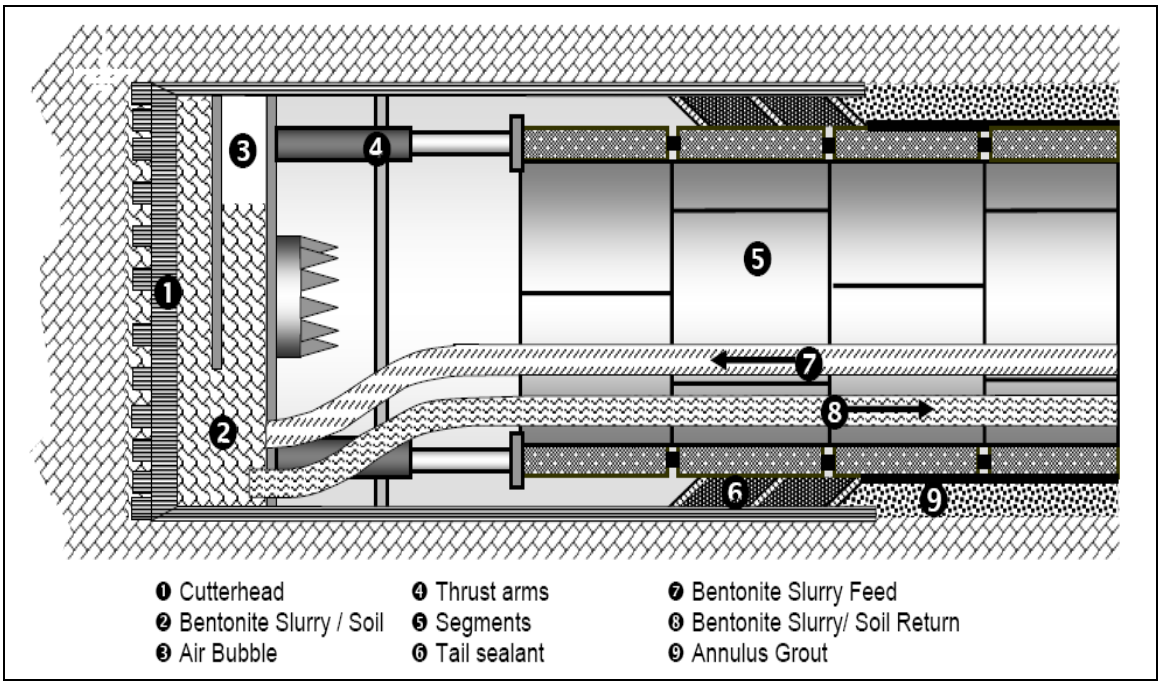

Figure 2.5 Schematic representation of Slurry Machine (after EFNARC, 2005)

2.6.1 Operations of Slurry Machine

Slurry and Characteristics Control

The slurry used to support the tunnel face during Slurry Machine tunnelling consists of a mixture of clay with a specified maximum particle size, water and polymers. The polymers are normally added to the slurry as binder, viscosifier and fluid loss reducer. The ratio of clay and polymers to be mixed with water to form slurry mixture is depending on the prevailing ground conditions. It will be ensured that all additives for the slurry will be biodegradable.

The slurry characteristics will be monitored continuously to maintain its ability to convey the spoil away from the excavation chamber at high velocity through the pipeline as well as to form a mud cake, i.e. impermeable membrane, at the tunnel

face for supporting the tunnel face as well as to facilitate separation from spoil at the treatment plant.

Slurry Supply and Return Lines

The slurry will be supplied to the Slurry Machine from the slurry treatment plant installed on the ground surface via a feeding line consisting of steel pipe of certain diameter and wall thickness. Similarly, the discharge slurry from the Slurry Machine will be conveyed out of the tunnel through a discharge line back to the treatment plant. The wall of the discharge pipe is thicker than the feeding pipe. In order to generate the required pressure in the return line, booster stations are normally installed inside the tunnel at a prescribed spacing. However, installation of addition booster pump for the feeding line to generate the required pressure at the tunnel face will be necessary only for long distance between the surface treatment plant and Slurry Machine.

Slurry Discharge Flow Rate

The slurry discharge flow rate needs to be maintained at constant level to allow smooth transportation of the excavated soil with aid of the slurry to the processing plant on the ground surface without causing sedimentation or segregation within the discharge line. An optimum flow rate is achieved by keeping the actual flow rate at the minimum level necessary to prevent settling of the soil particles within the line while maintaining the energy consumption of the pumps as low as possible and the capacity of the slurry plant installed on an economical level.

The optimum discharge flow rate will be determined by calculations for each soil type encountered at the tunnel horizon. It is a function of the pipe diameter, the specific gravity of the excavated soil and slurry, as well as the amount of excavated soil per minute.

Control of Slurry Pressure

The Slurry Machine is not feasible to operate in an open mode due to the fact that the support medium is used as transport medium to convey the excavated ground

out of the tunnel. The minimum pressure inside the excavation chamber is governed by the hydrostatic head between Slurry Machine and slurry tank on the ground surface subtracting the friction of the slurry within the pipe. This minimum pressure is generally in the range of 0.5 to 1.5 bars.

The tunnel heading will be supported by applying a positive pressure to the face using pressurized slurry contained in the plenum chamber of the Slurry Machine at all times. The slurry will continuously be circulated at specific rate to allow the excavated ground to be conveyed away from the face along with the slurry via pipelines to the separation plant installed on the ground surface.

The pressure of the slurry inside the plenum chamber will be controlled by adjusting the rotation speed of the slurry feed pump and the slurry discharge pump. A pressure transducer installed in the bulkhead of the plenum chamber near tunnel axis will be used to monitor the pressure inside the cutterhead. The face pressure to be applied using slurry in the plenum chamber of the Slurry Machine have been determined for every prescribed interval of the tunnel length and have been analyzed for drained and undrained stability conditions.

For Slurry Machine, the recommended face pressure is normally set higher than the design pressure. This is necessary to form the mud cake at the soil-slurry interface and to account for pressure loss due to slurry infiltration into the ground.

Recommended Face Pressure = Design Face Pressure + Excess Pressure

Some criteria have been established as general guidelines for selecting the minimum face pressure for Slurry Machine:

1. When tunnelling through soils with a low permeability and when a high penetration rate of Slurry Machine is encountered, face pressures are based on undrained condition
2. When tunnelling beneath or adjacent to sensitive structures, buildings and utilities, face pressure shall be equal to at least the pore pressure

3. During standstill or low penetration rate of Slurry Machine, the lower limit for the face pressure shall be equal to the pressures determined based on drained condition
4. For both Slurry Machine advance and standstill, the upper bound face pressure is equal to the octahedral stress where exceeding this limit may induce ground heave

The slurry pressure at the face will be measured with pressure transducer mounted on bulkhead and will be controlled within the allowable fluctuation range.

2.6.2 Ground Conditions for Slurry Machine

The Slurry Machine is mainly suitable for sands and gravelly soils and is best for operating in soils with small percentage of fine grain. Increase in the percentage of clay in the soil leads to difficulty during the separation process. The presence of coarse gravel may cause slurry leakage and hence, preventing the membrane formation. Under such circumstances, slurry consistency needs to be reconsidered to adapt to the situation. In addition, coarse gravel may also cause problem to the slurry pumping system by clogging up the discharge pipes. In this case, gravel may have to be crushed using special crusher usually installed at the excavation chamber of the machine.

2.7 Recommendations for Improvement in Shield Tunnelling (ITA/AITES Report 2006)

The modern TBMs are designed to act upon the settlement sources and prevent ground decompression ahead of the tunnel face, above the shield and at the tail skin.

Reduction of decompression ahead of the tunnel face can be achieved as follows:

1. Selection of appropriate face support method such as Earth Pressure Balance and Slurry

2. Equip machine with equipment allowing geophysical investigations to be performed through boring ahead of the face for appropriate application of face pressure
3. Equip machine with reliable sensor gauges to allow measurement of variations of all key parameters within the working chamber and spoil conveyor

Limiting ground losses along the shield can be achieved as follows:

1. Limiting amount of overcutting or using variable overcutting tool (elliptical overcutting)
2. Reducing the total length of the shield
3. Allowing bentonite grouting to be achieved through shield skin

In addition, tail void can be minimised by conducting backfilling using relevant grouting products maintained at the desired level during shield advancement.

2.8 Method for Estimating Face Pressure for Earth Pressure Balance Machine

Anagnostou and Kovári (1996) assessed the face stability by considering the limit equilibrium of a wedge and a prismatic body defined by slip surfaces beginning at the face and reaching the soil surface. The model proposed by Horn (1961) based upon the silo theory (Janssen, 1895), as illustrated in Figure 2.6, has been applied to the investigation of face stability with EPBM and Slurry Machine. Figure 2.7 illustrates the seepage force f and effective support pressure s'. From the results of the parametric studies on the effects of the advance rate (Anagnostou 1993, 1995), it was observed that drained conditions are to be expected when the permeability is higher than 10^{-7} m/s to 10^{-6} m/s and the net excavation advance rate is 0.1 m/hr to 1 m/hr or less. Although undrained strength will be applicable for assessing face stability during excavation in a clayey, low permeability soil, it was pointed out that drained analysis is more appropriate in the case of a standstill. The dimensional analysis performed by Anagnostou and Kovári (1996) has led to the following general form of the limit equilibrium condition:

$$s' = F_o \gamma_s' D - F_1 c' + F_2 \gamma_s' \Delta h - F_3 c' \frac{\Delta h}{D} \qquad (2.4)$$

where γ_s' is the submerged unit weight (for soil beneath the water table), D is the tunnel diameter, c' is the effective cohesion, Δh is the head difference and F_o to F_3 are coefficients as functions of the friction angle ϕ' and can be obtained from Figure 2.8, which have been computed numerically. It was also highlighted that reducing the head difference in the ground decreases the required effective face support, as illustrated in Figure 2.9. It is therefore concluded that lowering of the piezometric head into the ground by pump operation represents an extremely effective measure for face stabilisation in cases with exceptionally high piezometric heads.

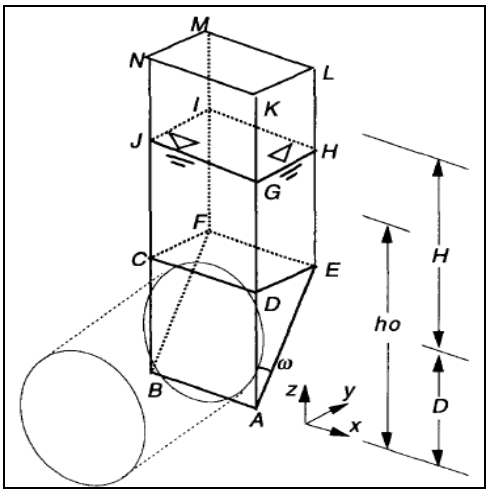

Figure 2.6 Sliding mechanism (after Horn, 1961)

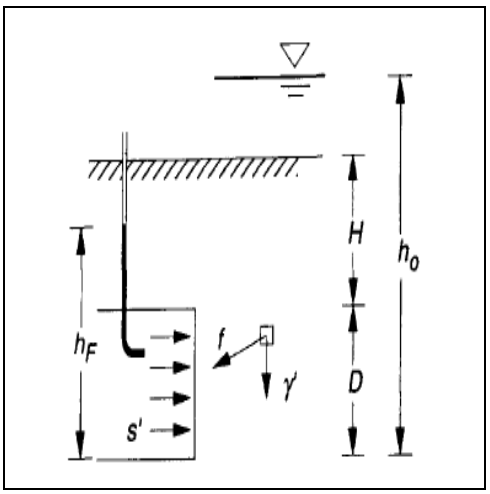

Figure 2.7 Seepage force f and effective support pressure s' (after Anagnostou and Kovári, 1996)

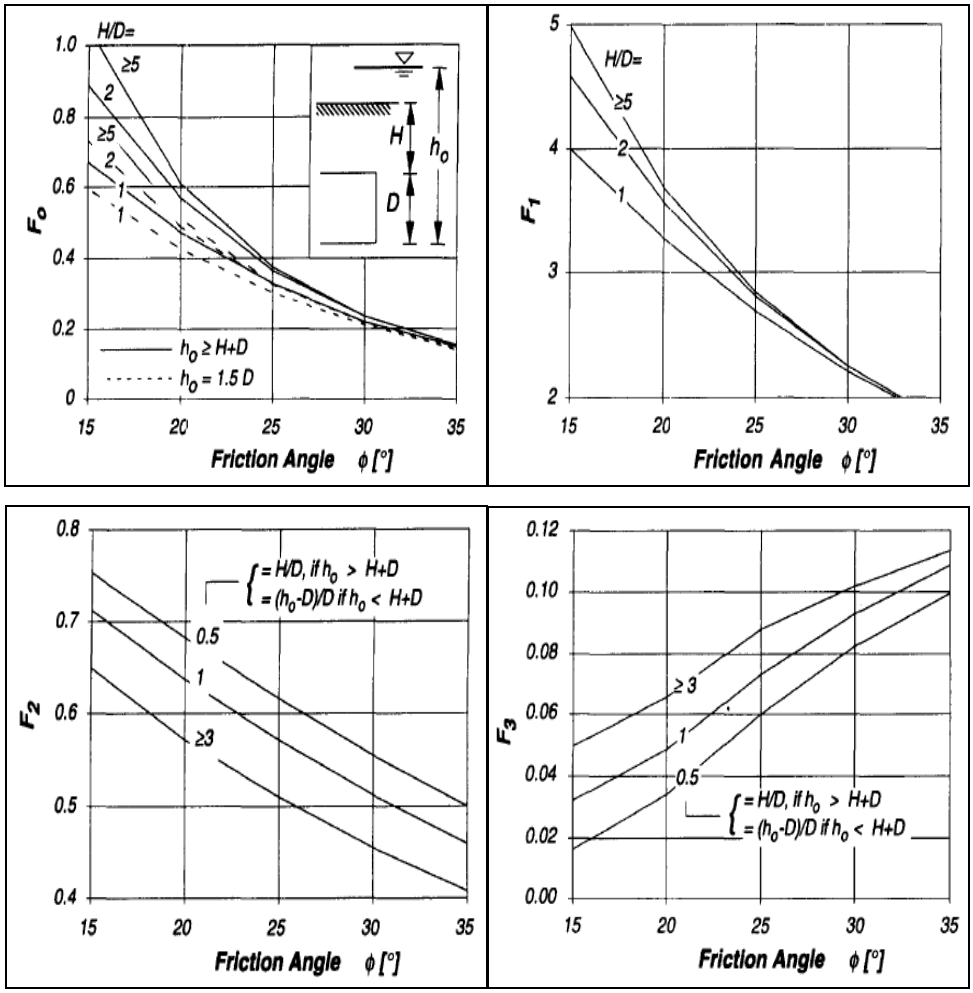

Figure 2.8 Nomograms for the dimensionless coefficients F_o, F_1, F_2 and F_3 (after Anagnostou and Kovári, 1996)

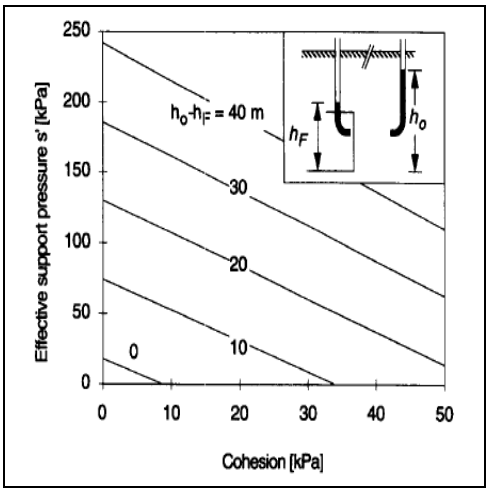

Figure 2.9 Effective support pressure as a function of cohesion c and of hydraulic head difference (h_o-h_f) for a given chainage of the Storebaelt Tunnel (after Anagnostou and Kovári, 1996)

2.9 Method for Estimating Factor of Safety for Slurry Machine

The slurry pressure must be higher than the ground water pressure in the soil in order to prevent a seepage flow towards the excavation face. As illustrated in Figure 2.10, the difference in pressure Δp will cause the slurry to infiltrate into the soil where the less the slurry penetrates, the greater the support force on the tunnel face. It was reported that lower excess pressure is sufficient to ensure the face stability of tunnel constructed in soil of high friction angle, as illustrated in Figure 2.11. Anagnostou and Kovári (1994) presented the safety factor as a function of the characteristic grain size d_{10}, for cases involving two different excess pressures and slurry yield strength, as illustrated in Figure 2.12. In addition, they also related the safety factor with time, critical advance rate and permeability, after considering the fact that the support force decreases with increasing infiltration distance which increases gradually over time during an excavation standstill. The time-dependent effects are illustrated in Figure 2.13.

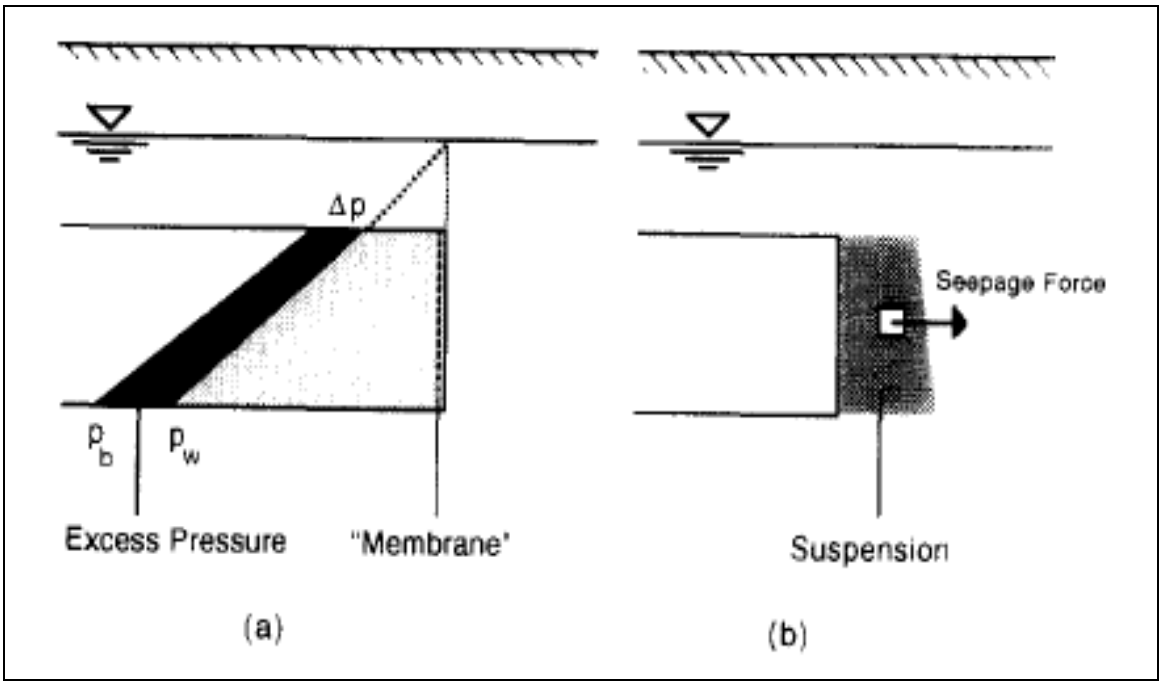

Figure 2.10 Stabilizing effect of the suspension: (a) without penetration into the ground and; (b) with penetration into the ground (after Anagnostou and Kovári, 1994)

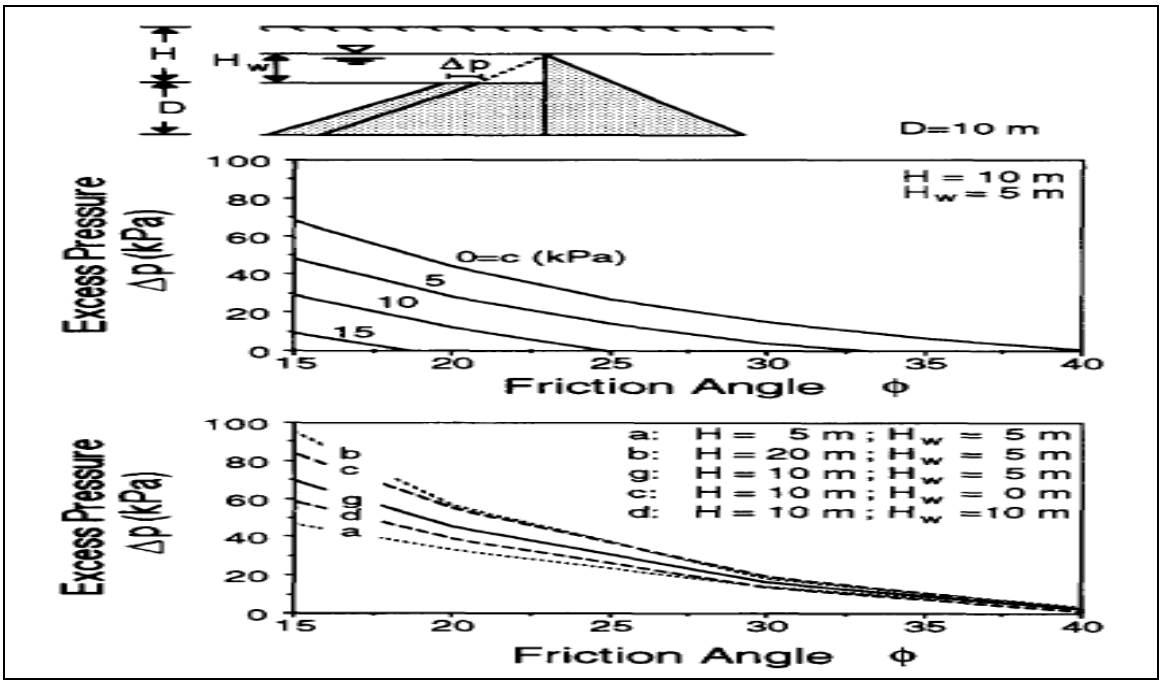

Figure 2.11 Limit equilibrium conditions for membrane model for a given set of parameters (after Anagnostou and Kovári, 1994)

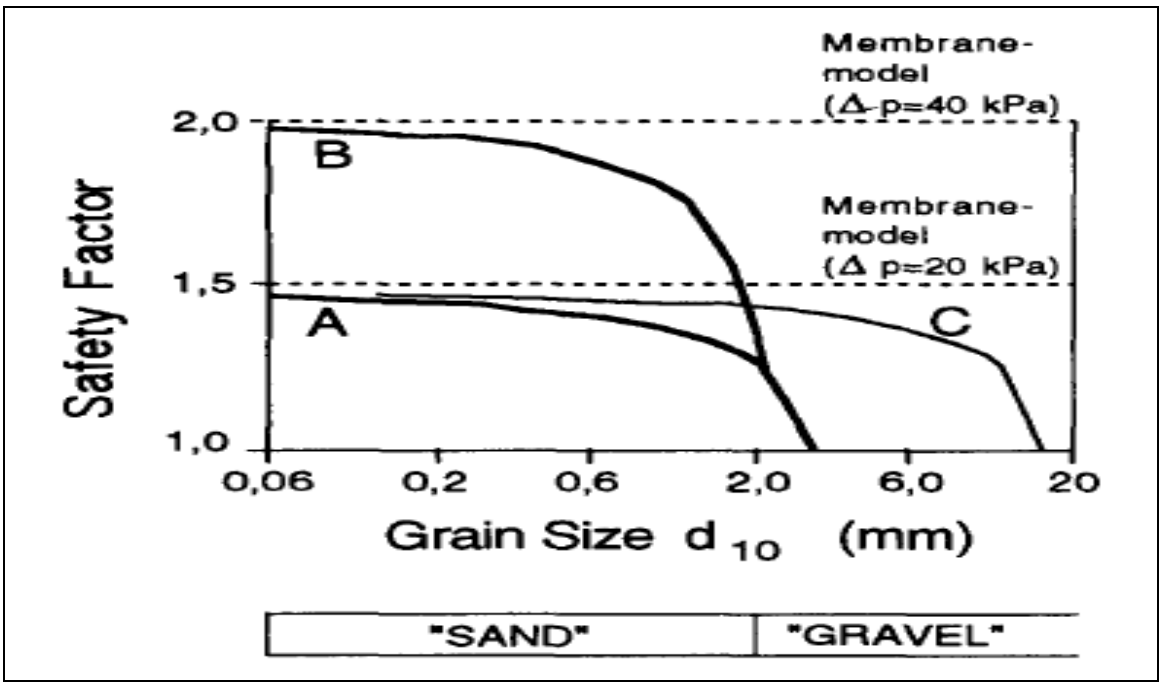

Figure 2.12 Safety factor as a function of characteristic grained size d_{10} (after Anagnostou and Kovári, 1994)

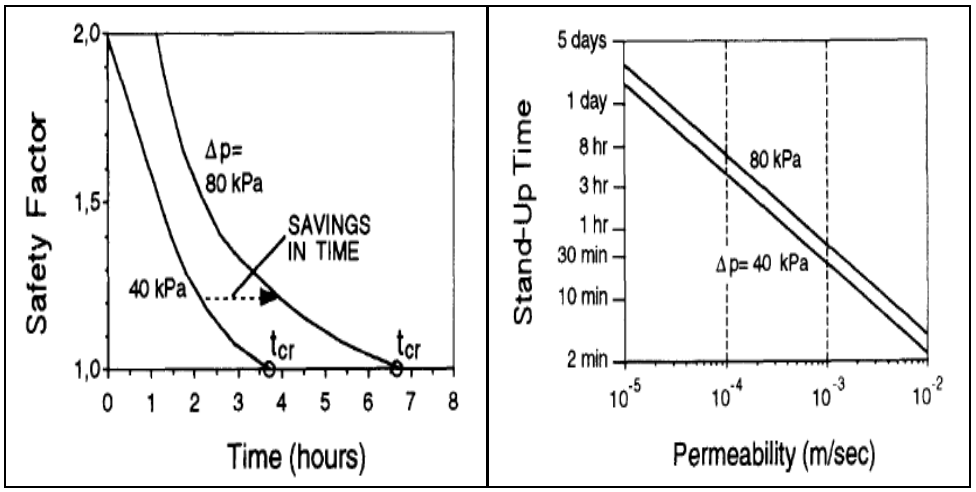

(a) (b)

Figure 2.13 (a) Safety factor as a function of time and; (b) stand-up time as a function of permeability (after Anagnostou and Kovári, 1994)

2.10 Summary

Different soil types behave differently during tunnelling. Face stability is one of the design considerations for open type manual shield tunnelling and semi-mechanised shield tunnelling where the stability of the tunnel face must be maintained at all times during tunnelling. Classification of ground behaviour and dimensionless parameters that provide measurement for the ground movements into the tunnel face were proposed by various researchers including Terzaghi (1950 and 1977), Broms and Bennermark (1967), Peck (1969), Heuer (1974), Schmidt (1974), Mair (1978), Clough and Schmidt (1981), Heuer and Virgens (1987), Phienwaja (1987). For full face TBM, the tunnelling methods involving EPBM and Slurry Machine must be suitable for the expected ground condition. The EPBM is suitable mainly for clays, silts and sands above the water table whereas the Slurry Machine is suitable mainly for sands and gravelly soil and is effective for driving through grounds with high groundwater pressure. The approaches to determine the effective support pressure and factor of safety for EPBM and Slurry Machine have been proposed by Anagnostou and Kovári (1994 and 1996).

CHAPTER 3 REVIEW ON ANALYSIS OF SINGLE TUNNEL AND CLOSELY SPACED TUNNELS

3.1 Introduction

Tunnelling in soft ground in urban areas has become necessary in many countries with rapid population growth and industrialisation. Any underground excavation will disturb the soil and the original stress distribution state which in turn will cause ground settlement around the excavation. Excessive ground movements can lead to damage to the surrounding structures and facilities. The problem is most significant in soft ground tunnels at shallow depth in urban areas.

3.2 Ground Surface Settlement over Bored Tunnel in Soft Ground

The important concept of ground settlements induced by tunnelling in soft ground was documented in the ITA/AITES Report 2006 (2007). The settlement induced by shield tunnelling can be classified into four categories:

1. **Settlement ahead and above the face**

   Displacement magnitude depends on the level of confining support at the excavation chamber, ground conditions and hydraulic conditions.

2. **Settlement along the shield**

   Displacements caused by overcutting induced by peripheral cutters, pitching angle of the shield, tapering of the shield, rolling of the shield which may induce shearing to the ground surrounding the shield.

3. **Settlement at the shield tail**

   Displacements caused by the gap between the shield and the excavated ground, thickness of the tail skin and the clearance between the inner face of the tail skin and the outer face of the liner. The displacement magnitude depends on the grouting parameters.

4. **Settlement due to lining deformation**

   Displacement magnitude depends on the relative flexibility of the lining due to presence of joints as well as ground conditions.

5. **Settlement due to ground consolidation**

   Displacement magnitude depends on the change of pore water pressure in the ground, as a result of seepage towards the tunnel or dissipation of excess pore water pressure generated after tunnelling.

It was pointed out that the influence of lining deformation on ground movements must be taken into account for the case involving large tunnel spans with limited cover.

The ITA/AITES Report 2006 (2007) illustrated that the volume loss caused by the face intake is around 10 per cent to 20 per cent of the total volume loss, as compared to 40 per cent to 50 per cent and 30 per cent to 40 per cent of the total volume loss produced along the shield and observed at the tail skin, respectively. However, the advances in construction techniques and methods, i.e. EPB, Slurry and Mixshield TBMs as well as grouting technologies have led to much smaller settlements ahead of the tunnel face as well as over the tail skin.

The following are some assumptions on displacement propagation towards the ground surface (ITA/AITES Report 2006 (2007)):

1. Ground is incompressible (no volume change in the ground) where the volume of settlement trough equals the volume of ground loss at the opening. The assumption is reported valid for shallow tunnel in cohesive grounds.
2. Lower volumes of settlement observed at the surface than at the tunnel level could be attributed to the following factors:
   a. Large depth of cover resulting in up to 80 per cent deformation dampening
   b. The presence of stiff layer over the tunnel (bridging effect)
   c. The presence of a layer of dilating material in the tunnel cover, e.g. dense sand.

These are useful information which can be used to explain some of the observed phenomena of ground surface settlement which deviate from what is expected from previous cases.

Shirlaw (2002) reported the relationship between face pressure and ground surface settlement for EPB tunnelling for the North East Line (NEL) of Singapore. To facilitate the study, the ground conditions encountered along the tunnel alignment were characterised into three broad groups: Group 1 consisting of weak, recent soils (e.g. Kallang Formation) where high face pressure is required at all times to control settlement; Group 2 consisting of stronger but soil-like materials where tunnelling can be carried out without a support pressure and; Group 3 consisting of highly variable weathered rocks where face pressure is required. Shirlaw (2002) pointed out that overcutting is one of the significant factors for settlement where for a typical 6 m diameter machine, the minimum overcutting expressed as a percentage of the face area is about 0.5 per cent, whereas additional overcutting due to 50 mm look-up (overhang) as well as additional overcutting due to 100 mm extension of copy cutter are 1.1 per cent and 4.8 per cent, respectively. It was also pointed out by Shirlaw (2002) that the volume loss of greater than 2 per cent are very likely to occur where Kallang Formation, interface of Jurong Formation and Kallang Formation as well as partial Jurong Formation with Kallang formation above are encountered at the tunnel face. While tunnelling through interface of Old Alluvium and Kallang Formation as well as Granite GII to GV residual soils each indicates a single case of volume loss of greater than 2 per cent, no such magnitude of volume loss was reported for tunnelling through Old Alluvium, Jurong Formation (sedimentary residual soils) as well as Boulder Clay. Shirlaw (2002) concluded that the following factors may lead to excessive ground surface settlement:

1. Launching of the shield
2. The ‘learning’ curve (immediately after the launch proper)
3. Any change in ground that requires a change in face pressure
4. Mixed face condition
5. Long stoppages without support pressure
6. Docking of the shield at the end of the drive

A series of useful diagrams showing the relationship between face pressure and volume loss for EPB shield tunnelling through various geological conditions in Singapore were also presented by Shirlaw (2002), as shown in Figures 3.1 to 3.4, where those observations have led to the proposal of the following guidelines for face pressure control:

1. For tunnelling through the soils of Kallang Formation, and any locations where there is less than 3 m cover to the Kallang Formation, face pressure of 0.9 to 1.2 times the total overburden pressure is ideal to minimise the settlement. The settlement increases rapidly with reduction in face pressure.
2. For tunnelling through Old Alluvium, the settlement was observed to be consistently low and independent of the face pressure.
3. For tunnelling through weathered rocks of the Jurong Formation with no Kallang Formation soils above tunnel, the settlement was observed to be uniformly low and independent of the face pressure.
4. For tunnelling through fault zones, completely weathered Sandstone and in the highly weathered Mudstones and Shales, high face pressure is needed to effectively support such materials and prevent overexcavation.
5. For tunnelling through residual soils of the Bukit Timah Granite, face pressure of greater than 0.5 times the total overburden pressure is needed to minimise the volume loss to less than 1 per cent. Similar observation was made for mixed rock and soil grades of the Bukit Timah Granite.

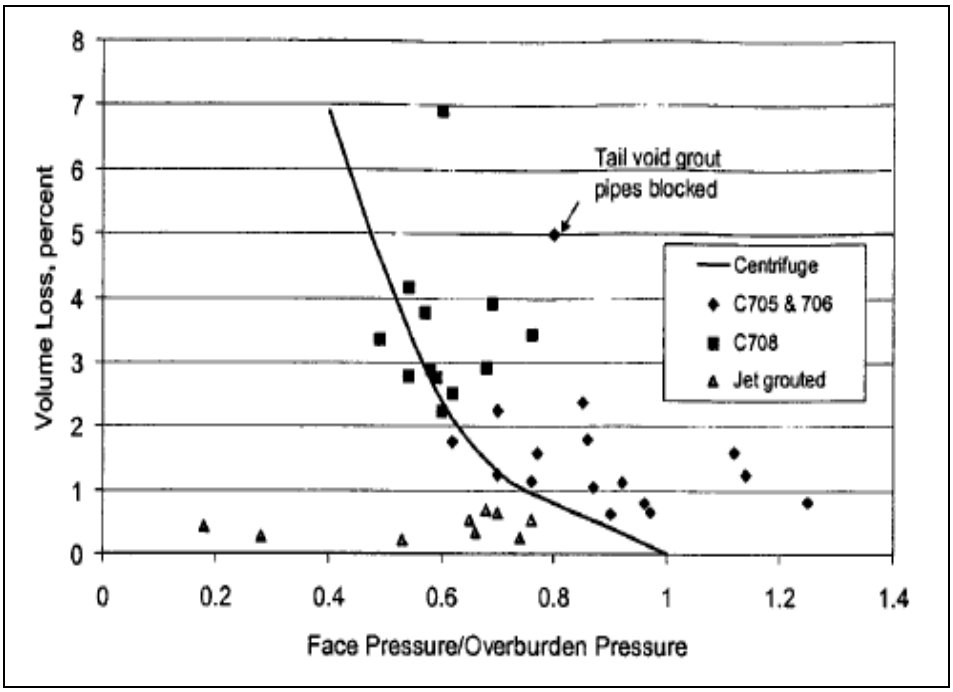

Figure 3.1 Relationship between face pressure and settlement, EPB tunnelling through soils of the Kallang Formation (after Shirlaw, 2002)

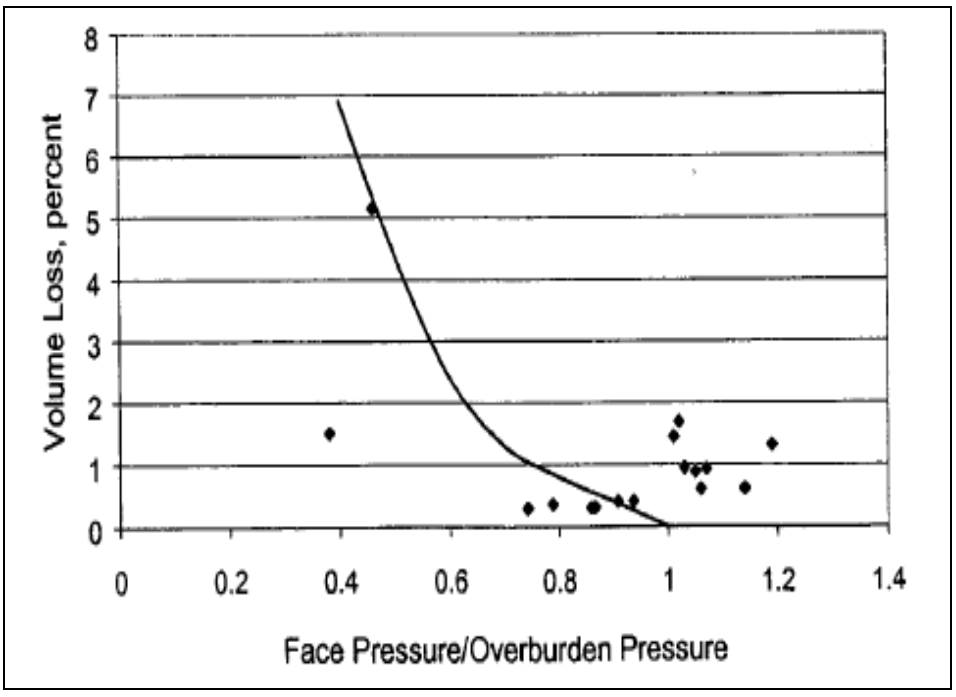

(a)

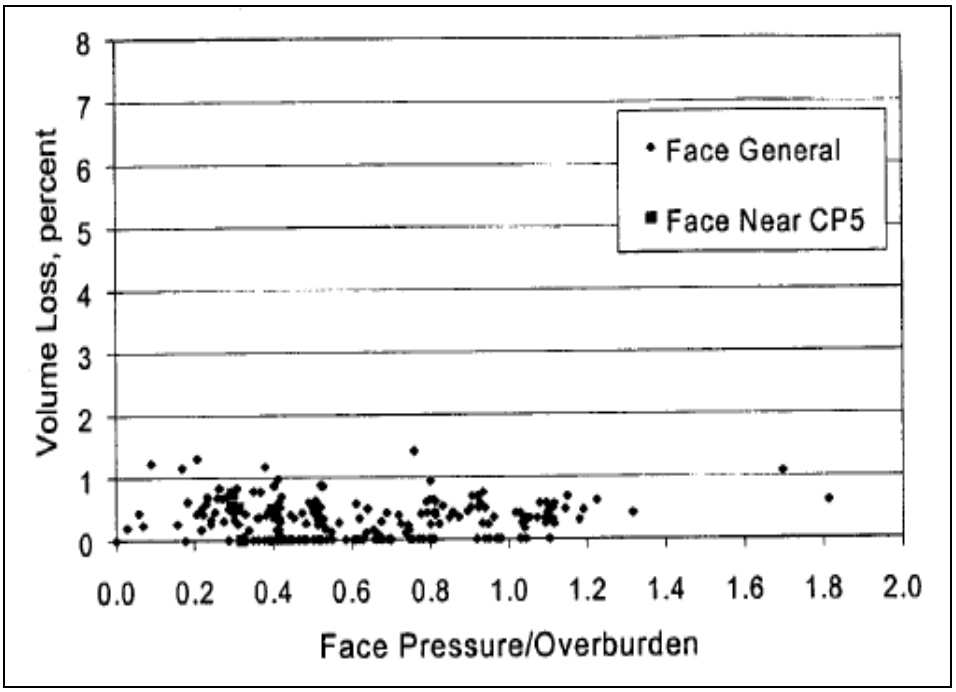

(b)

Figure 3.2 Relationship between face pressure and settlement for EPB tunnelling through (a) mixed face of Kallang Formation soils and Old Alluvium and; (b) Old Alluvium (after Shirlaw, 2002)

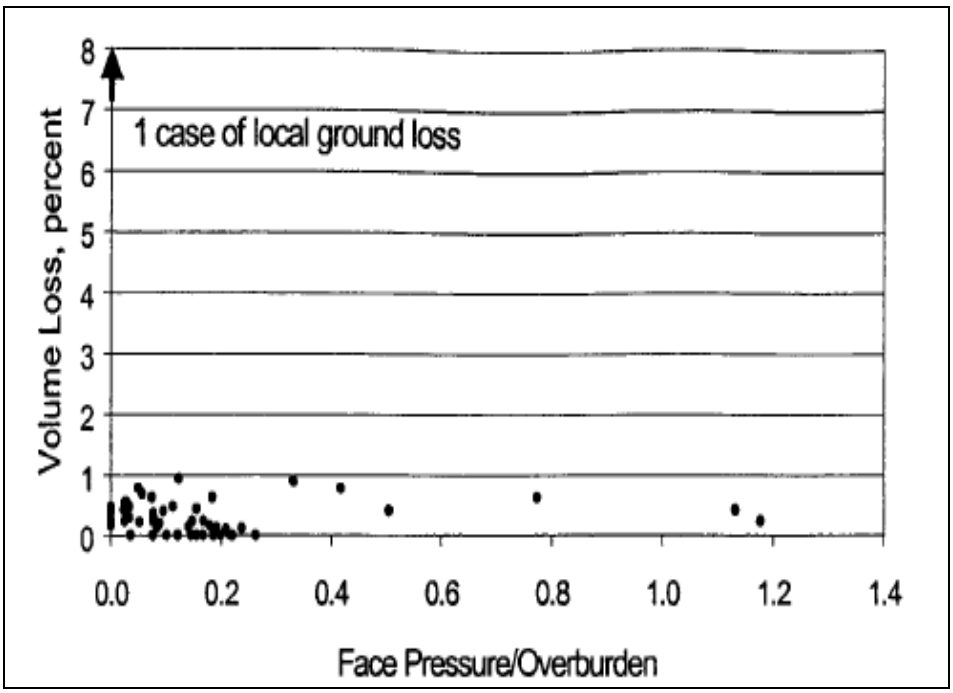

(a)

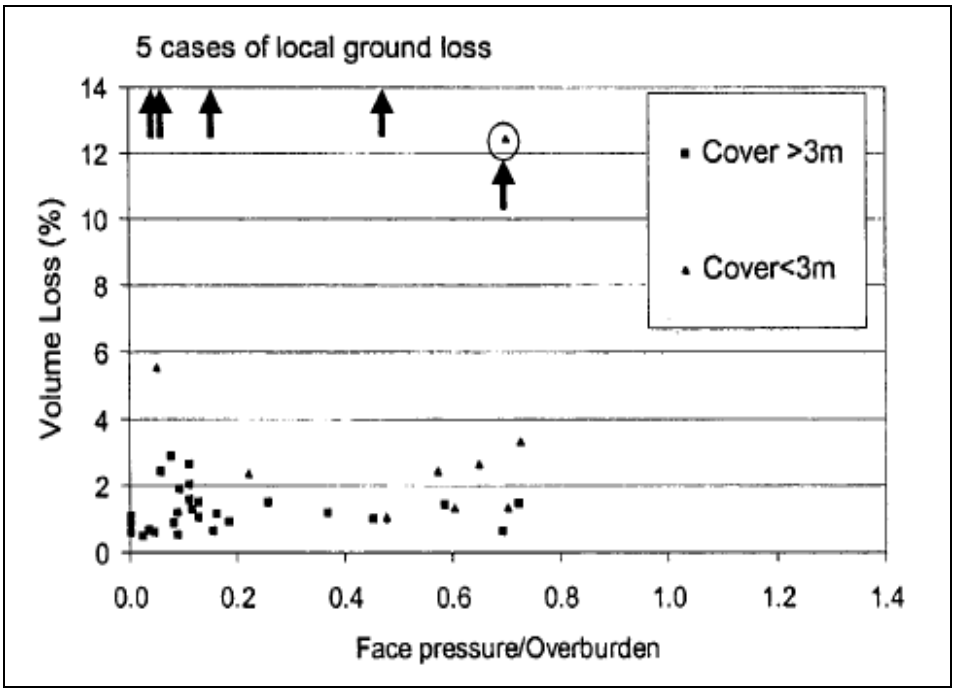

(b)

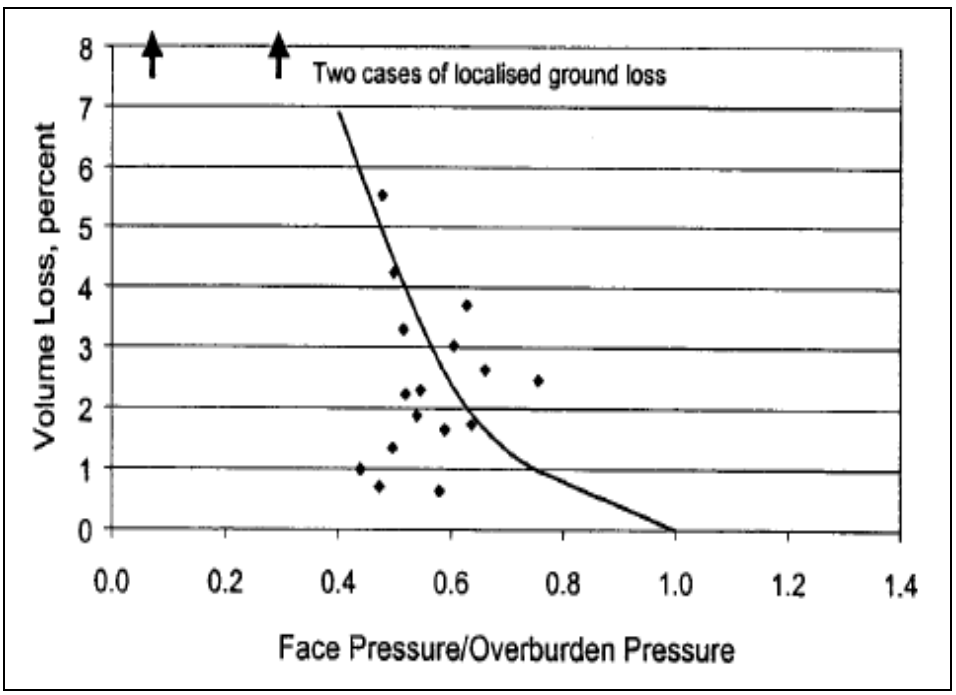

(c)

Figure 3.3 Relationship between face pressure and settlement for EPB tunnelling through weathered rocks of the Jurong Formation (a) no Kallang Formation soils above tunnel; (b) Kallang Formation soils present above tunnel and; (c) mixed face of Kallang Formation soils (after Shirlaw, 2002)

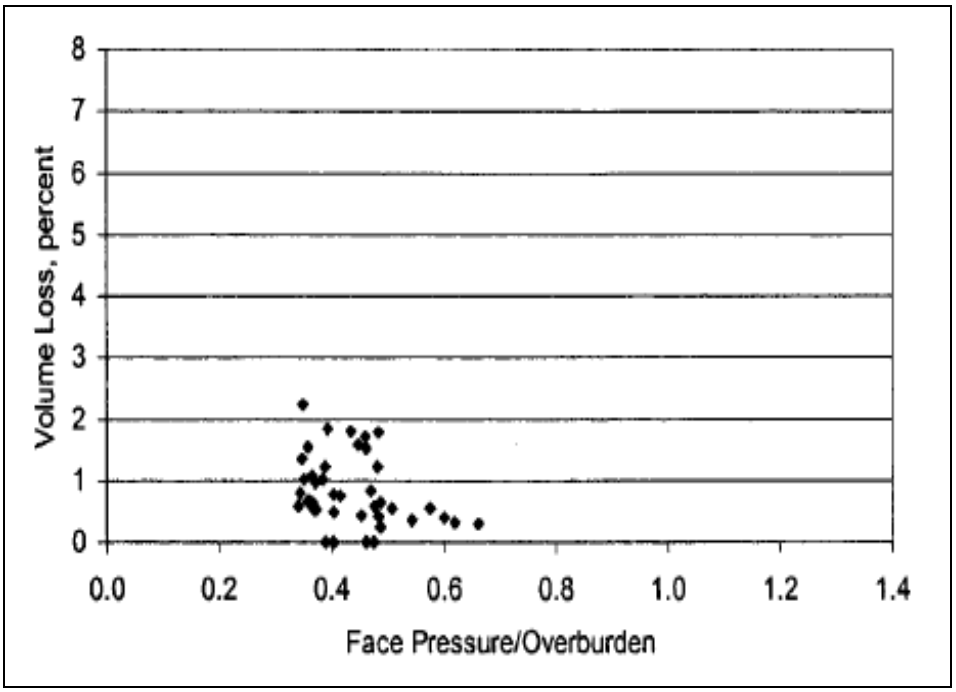

(a)

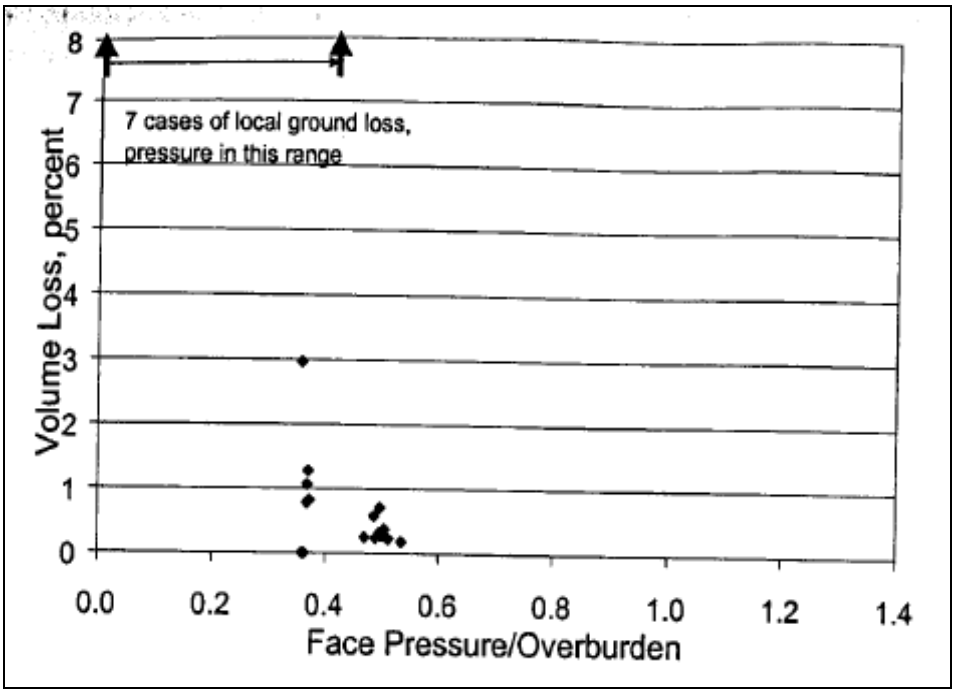

(b)

Figure 3.4 Relationship between face pressure and settlement due to EPB tunnelling through (a) residual soils and; (b) mixed rock and soil grades of the Bukit Timah Granite (after Shirlaw, 2002)

3.3 Methods for Estimating Ground Surface Settlement

Design in underground engineering is always one of the most difficult problems for tunnelling practitioners. The main reason is that problems such as determination of the ground response, stress distribution and displacement behaviour of the tunnel have not been thoroughly understood. However, engineers have been striving to obtain some empirical formulae or approximate results by way of the observational method. The approaches to estimate the ground response to tunnelling in soft ground can be classified into four types: empirical or semi-empirical approach, theoretical approach, numerical study as well as experimental and field study.

3.3.1 Empirical and Semi-Empirical Approach

Peck (1969) updated available empirical techniques to estimate the ground surface settlement due to tunnelling. He identified that the loss of ground into the tunnel is the major source of surface settlements and that loss of ground is related to the method of construction, type of soil, groundwater conditions, and geometry and depth of tunnel. He summarised field measurements to allow the engineer to estimate the loss of ground associated with various tunnelling sequences in different types of ground and discussed the effectiveness of various methods for reducing the loss of ground and thus the surface settlement. He showed that the pattern of surface settlements caused by loss of ground into single or two closely spaced tunnels can be approximated by a Gaussian probability curve, as illustrated in Figure 3.5. The curve is completely defined by the maximum settlement S_{max} (Figure 3.5 uses the symbol $\delta_{max.}$) and the point of inflection, i, as follows:

$$S = S_{max} \exp^{\frac{-x^2}{2i^2}} \tag{3.1}$$

where S is the settlement at distance x from the centreline of the tunnel.

The ground loss was defined as the ratio of volume of surface settlement to that of the theoretical volume of excavated tunnel, assuming no volume change in the

ground where the actual measured values are less than the theoretical values. The volume of a unit length of the settlement trough, V_s, can be obtained by integration, which results in the following expression:

$$V_s = \sqrt{2\pi i S_{\max}} \tag{3.2}$$

and can be approximated by:

$$V_s = 2.5 i S_{\max} \tag{3.3}$$

Peck (1969) suggested that the volume of ground loss can be assumed as 1 per cent of the volume of the tunnel. While the settlement may be as little as 0.5 per cent for exceptionally good ground conditions and workmanship, the value may be very large for the opposite conditions.

Deere et al. (1969), Peck (1969) and Schmidt (1969) recognized a strong dependence of the trough width parameter i on the geometry of the problem tunnel depth z_o and diameter D and hence, suggested an empirical relationship as shown in Equation 3.4.

$$\frac{i}{R} = K\left(\frac{z_o}{D}\right)^n \tag{3.4}$$

where K is a constant which depends on ground properties and n is an empirical factor. For majority of soft ground tunnels, values of K = 1.0 and n = 0.8 were suggested.

Peck (1969) also presented the relationship between tunnel depth and trough width as functions of the type of ground and groundwater conditions (Figure 3.6). Cording and Hansmire (1975) introduced the concept of the angle of draw which is used in the mining profession into tunnelling. They defined it as an angle from the vertical to the line connecting the springline and the edge of settlement trough at a distance

of 2.5i from the tunnel centreline. They showed that the boundary curves suggested by Peck (1969) could be approximated by straight lines corresponding to the angles of draw of 11, 33 and 50 degrees for the ratio z_o/D less than 4. These lines are also shown in Figure 3.6.

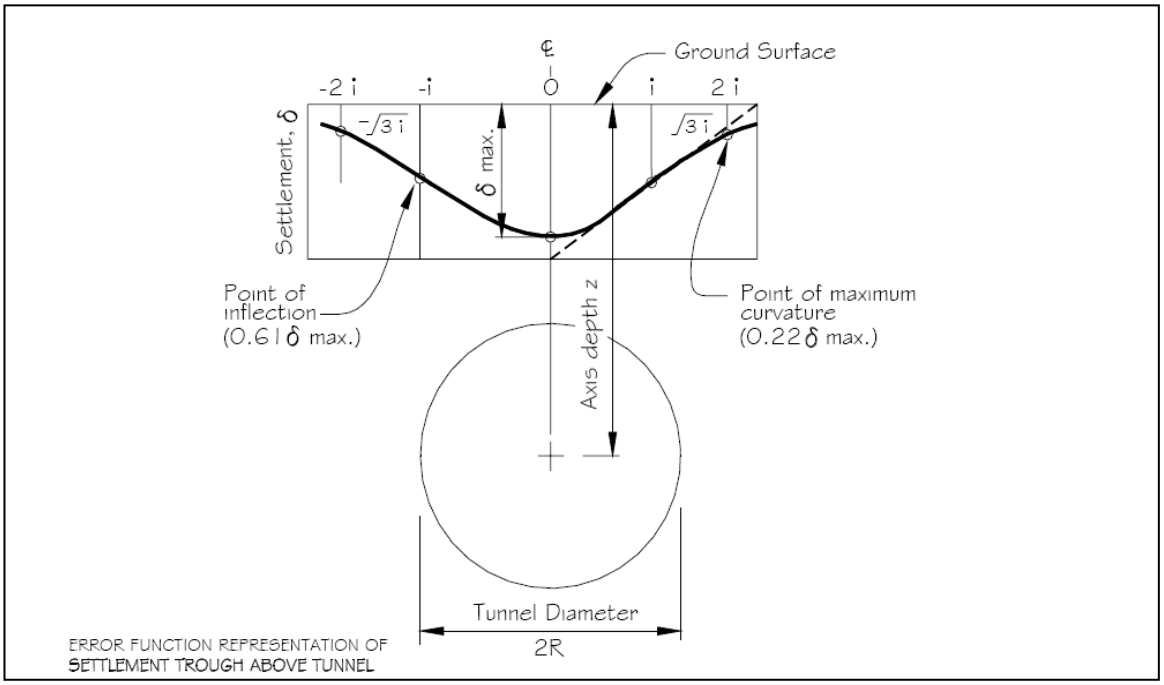

Figure 3.5 Gaussian distribution curve representation of settlement trough above tunnel (after Peck, 1969)

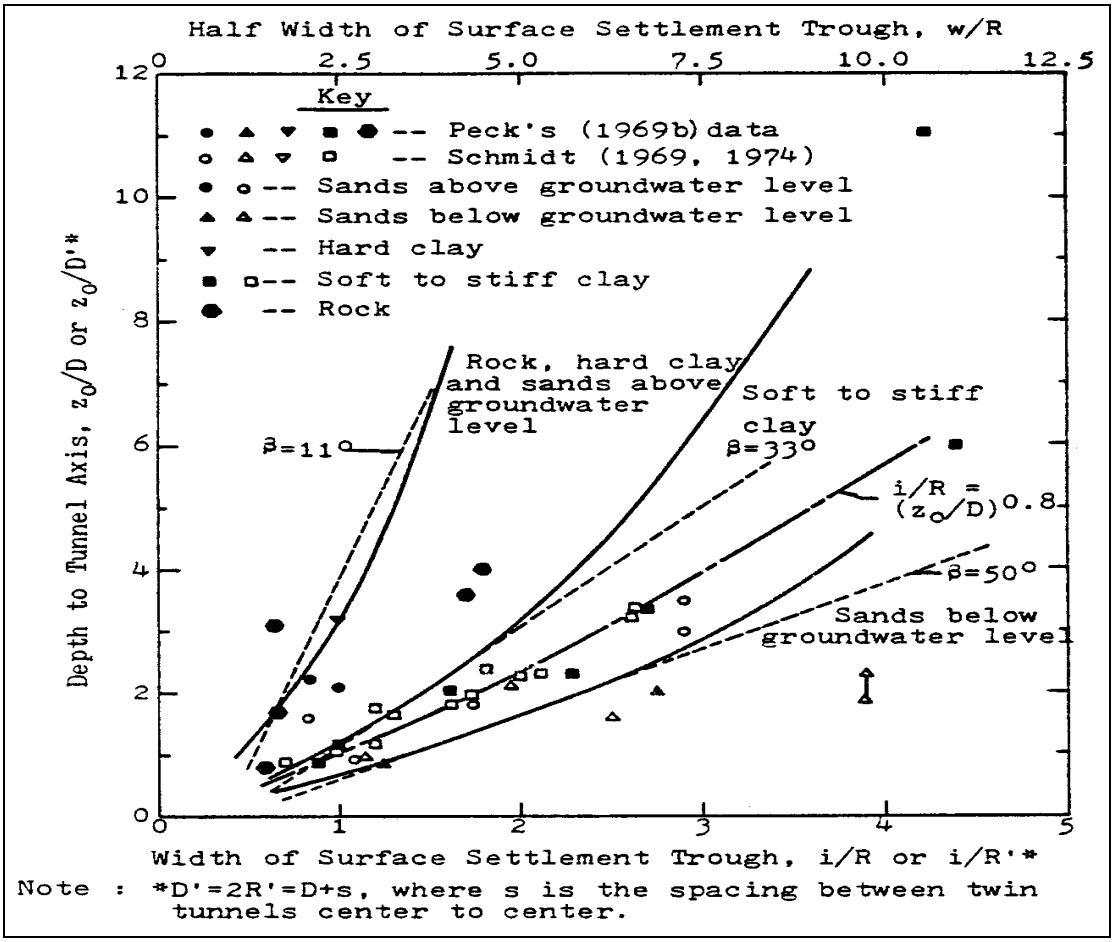

Figure 3.6 Relation between trough width and tunnel depth for various tunnels in different material (after Peck, 1969)

O'Reilly and New (1982) developed the Gaussian model by making the assumption that the ground loss could be represented by a radial flow of material towards the tunnel and that the trough could be related to the ground conditions through an empirical constant K.

$$S = S_{\max} \exp^{-\frac{x^2}{2(Kz_o)^2}} \tag{3.5}$$

$$K = \frac{i}{z_o} \tag{3.6}$$

where the trough width parameter i is an approximately linear function of the depth z_o and broadly independent of tunnel construction method, whereas K is an empirical constant which may be taken approximately as 0.5 and 0.25 for clays and sands or gravels, respectively. For practical design, the full width of the transverse settlement trough is usually taken as 6i. The estimation of trough width parameter i proposed by various researchers is summarised in Table 3.1.

Table 3.1 Comparisons of trough width parameter i recommended by various researchers

Researchers	**Trough Width Parameter i (m)**	**Remarks**
Peck (1969)	$i/R=(z_o/2R)^n$: n=0.8 to 1	Field observations
Attewell (1977)	$i/R=\alpha\,(z_o/2R)^n$: α =1 and n=1	Field observations of tunnels in U.K.
Atkinson & Potts (1979)	$i=0.25(z_o+R)$: loose sand, $i=0.25(1.5z_o+0.5R)$:dense sand and over consolidated clay	Field observations and model tests
Clough & Schmidt (1981)	$i/R=\alpha\,(z_o/2R)^n$: α =1 and n=0.8	Field observations of tunnels in U.S.
O'Reilly & New (1982)	$i=0.43z_o+1.1$:cohesive soil, $i=0.28z_o-0.1$:granular soil	Field observations of tunnels in U.K.
Leach (1985)	$i=(0.57+0.45z_o)\pm 1.01$	Sites where consolidation effects are insignificant
Mair and Taylor (1997)	$i=0.5z_o$	Field observations worldwide and centrifuge test

Note: z_o is the depth of tunnel below ground (at tunnel springline) and R is the tunnel radius.

3.3.2 Theoretical Approach

In this approach, the ground which deforms is idealised as a homogeneous and isotropic or transverse isotropic continuum which can be characterised by a relatively simple mathematical expression. Elastic (e.g. Deere et al., 1969; Schmidt, 1969), visco-elastic (e.g. Carter and Booker, 1984), plastic and elasto-plastic (e.g. González and Sagaseta, 2001) characterisation have been attempted. In some cases, a uniform stress field is assumed throughout the medium before the cavity is created which is equivalent to assuming that the medium is weightless. In other cases, it is assumed that the tunnel has materialised instantaneously and that the lining develops its full strength at the moment of excavation.

There have been few studies which were mainly concerned with stresses and strains in the ground near a tunnel (e.g. Sagaseta, 1987; Verruijt and Booker, 1996; Loganathan and Poulos, 1998) as well as deformations and forces acting on and induced in the lining (e.g. Morgan, 1961; Muir Wood, 1975). Kirsch 1898 (Timoshenko and Goodier, 1951) considered the stress state around a hole in a flat elastic plate subjected to a uniformly distributed uniaxial stress. His solution is approximate yet simple and adopted widely for either case of plane stress or plane strain condition under uniformly distributed biaxial stress state.

3.3.3 Numerical Studies

Another approach is to use a numerical method such as finite element method. Until recently, numerical analysis was usually carried out under the assumption of plane strain condition because of high costs associated with three-dimensional (3D) analysis. Nowadays, such sophisticated softwares like PLAXIS 3D (PLAXIS, 2015) and FLAC 3D (ITASCA^{TM} Consulting Group, Inc., 2015) are easily available. It is well known that the stress change and corresponding deformation near the tunnel heading are 3D. A 2D analysis may not be adequate to handle such a situation satisfactorily. Apart from that, 2D numerical approach has been shown to be a viable tool for carrying out parametric studies and for analysis and design of a site

specific problem where tunnelling approaches plane strain condition. In addition, 2D back analysis can be performed for calibration of the numerical model. As recommended by Clough and Mana (1976) that the numerical method be incorporated into an observational approach where the initial analysis based on reasonable estimate is adjusted and modified as more data from the observed behaviour are collected alongside construction progress.

Ghaboussi and Ranken (1977) studied interaction between two circular and parallel tunnels by linear elastic and elasto-plastic finite element analysis. The influence of depth of burial, tunnel spacing and construction sequence was investigated. They showed that the shear stress in the pillar increased as the pillar width was reduced. In addition, the minimum pillar width at which the two tunnels act independently increases with depth of tunnels. Ghaboussi and Ranken (1977) also reported that the interaction between two parallel tunnels resulted in settlements of ground surface larger than those obtained by superposition of the surface settlements from two single tunnels. The excess surface settlement volume was found to increase with the depth of the tunnel. They also studied the effects of excavating the two tunnels simultaneously i.e. symmetrical case and one after another, i.e. unsymmetrical case. In shallow tunnels of $z_o/D = 1.5$ the excess surface settlement volume for the symmetrical case was larger than that for the unsymmetrical case while in deep tunnels of $z_o/D = 5.5$, the excess surface settlement volume for both cases were found to be similar.

3.4 Recent Numerical and Analytical Studies on Tunnelling

Addenbrooke and Potts (2001) conducted finite element analyses of twin tunnel construction in stiff overconsolidated London Clay using the Imperial College Finite Element Programme (ICFEP). Their study focused on the influence of tunnel position, tunnel spacing, rest period, and sequence of excavation on the interaction between two parallel side-by-side tunnels as well as the second tunnel running above the first tunnel (piggyback). The results of the analyses indicated that for side-by-side tunnels, reducing pillar width led to the point of maximum settlement

being drawn towards the first tunnel, whereas the settlement profile is practically centred on the second tunnel at pillar width greater than 7 diameters. The analyses of piggyback tunnels indicated that the settlement profile above the second tunnel is distinctly different in shape to an equivalent greenfield profile. While it was pointed out that the volume loss into the second tunnel is greater than that into the first tunnel due to the reduction in soil stiffness around the second tunnel after excavation of the first tunnel, the length of rest period has negligible influence on these interaction effects.

Chi et al. (2001) applied an optimization technique for the back-analysis of tunnelling induced ground movement. The results of the back-analysis using the monitoring data of the Taipei Rapid Transit System suggests the angle of the influence zone of ground settlement for tunnelling in clayey soil to be approximately 45^o and that for sandy layers it ranges from 30^o to 50^o. In addition, backfill grouting is also expected to reduce the physical gap of the shield machine in the order of 60 per cent to 80 per cent and 70 per cent to 85 per cent for tunnelling in clayey soils and sandy layers, respectively.

Chou and Bobet (2002) proposed an analytical solution to predict the ground deformations in shallow tunnels in clay. The comparison with the field measurements affirmed the general validity of the analytical solution in predicting the ground movements due to the shield driven tunnels in medium to stiff clay, where small plastic deformation around the tunnel are expected and hence, shows an advantage over the empirical method since all variables can be taken into consideration. However, their analytical solution cannot be used for analyses of complex tunnel interaction cases unlike numerical analyses. Their study highlighted that for numerical analysis, the location of the bottom boundary of zero vertical deformation is critical to predict the vertical deformation of the ground. They recommended that the boundary should be located at a distance of two tunnel diameters below the tunnel centreline, or at the location of a stiff soil layer whichever is smaller.

Lin et al. (2002) carried out 3D numerical analyses of EPB shield tunnelling in stiff to hard clay using finite difference program FLAC 3D. A Mohr-Coulomb (MC) model with effective stress method was adopted to simulate the soil behaviour whereas linear elastic model was used for grouting material. Both the lining segment and shield machine were simulated using shell structural element which behaves as linear elastic material with no failure limit. The research has provided both the measured data of ground surface settlements and results of 2D and 3D analyses as presented in Figures 3.7 and 3.8 with the aim to show that a 2D analysis can be performed in substitution of the 3D analysis for estimation of transverse surface settlement if the section considered is far behind the tunnel face as the shield advancing.

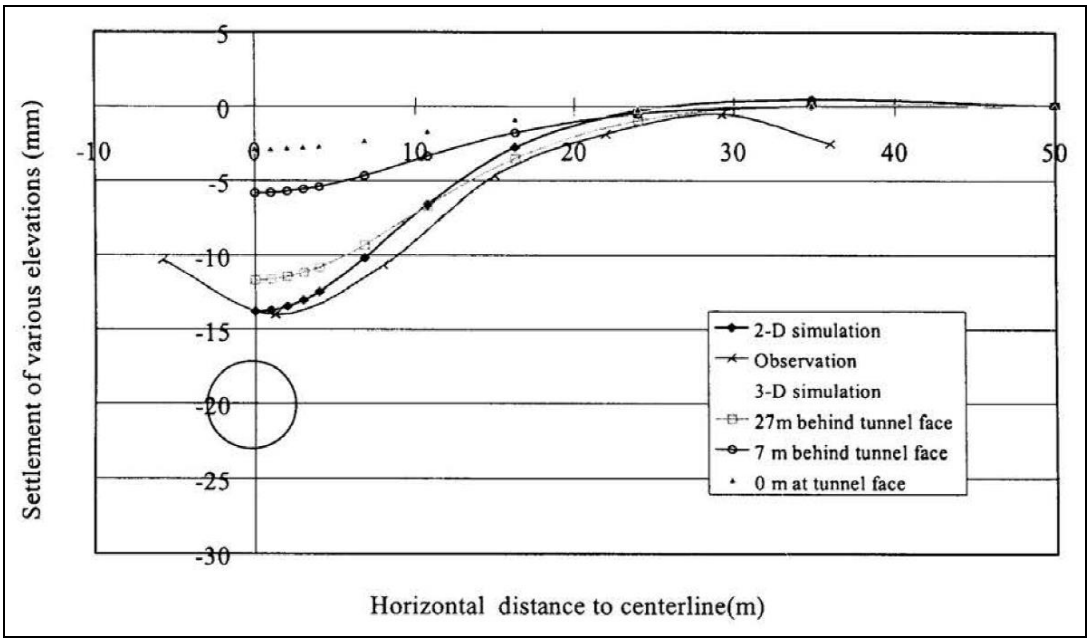

Figure 3.7 Comparison of ground settlement trough at various transverse sections with plane strain condition (MRTA) (after Lin et al., 2002)

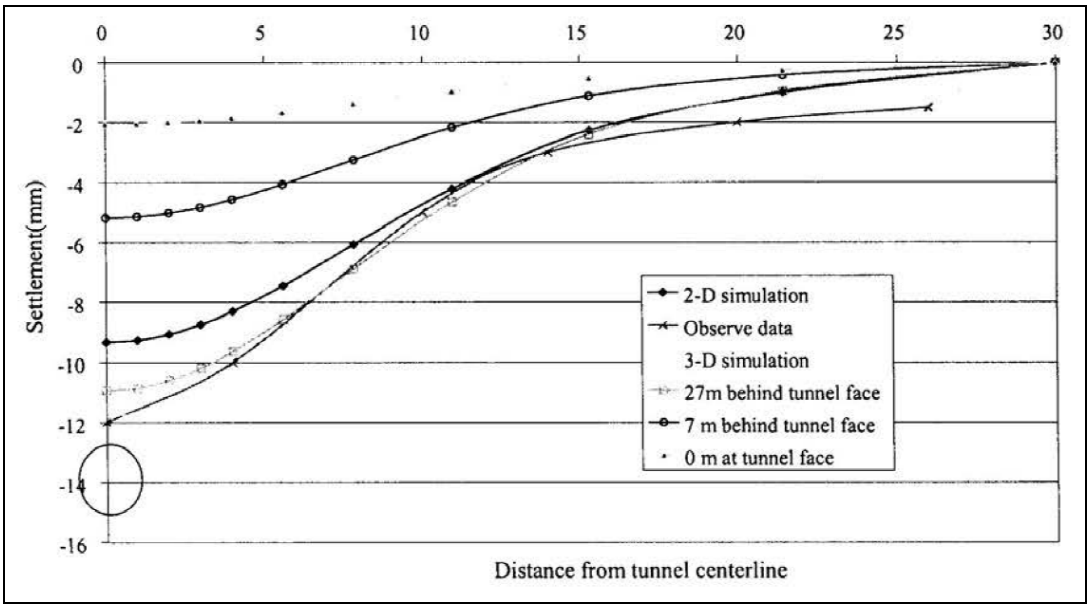

Figure 3.8 Comparison of ground settlement trough at various transverse sections with plane strain condition (MWA) (after Lin et al., 2002)

Melis et al. (2002) proposed a new numerical model generated using finite difference method, FLAC 3D, to simulate the EPB Shield excavation procedures for estimating ground subsidence. Full excavation sequences, including the chamber pressure on the tunnel face, void space between soil and shield (over excavation), tail piece void between soil and lining (gap parameter), injection grout pressure and the lining behaviour have been accounted in their proposed method of simulation. The linear elastic model was selected as one of the soil constitutive models for numerical analysis due to the very stiff nature of the Madrid soils where the plasticity effects are not very important for predicting ground subsidence. The Mohr-Coulomb model and Modified Cam-Clay model were also adopted to cater to the plastic deformation around the tunnel during excavation.

Liakos et al. (2003) conducted 2D and 3D finite element analyses to investigate the effect of consolidation on the ground-liner interaction. An axisymmetric model was adopted for the 2D modelling and the ground was assumed to be homogeneous and linear elastic. They showed that the ground consolidation led to an increase of the stresses in the liner. For ground permeability of $k = 10^{-7}$m/s, the tangential stress in the liner around the springline of the tunnel is found to increase by 10 percent,

whereas a decrease in the permeability to k = 10^{-9}m/s results in an increase of tangential stress by almost 100 percent. In addition, the limitation of the axisymmetric model to incorporate the lateral stress perpendicular to the tunnel axis, K_x was highlighted, where such limitation produced greater radial displacement as compared to 3D results for the case of K_x equal to unity and smaller radial displacement for the case of K_x equal to 0.5.

Koungelis and Augarde (2004) conducted numerical analyses of multiple tunnels using finite element program, PLAXIS, with the aim to improve prediction of minimum interaction distance between multiple tunnels constructed at shallow depths in soft ground. For comparison, soil stratigraphy and tunnel geometric parameters identical to Addenbrooke and Potts (2001) were adopted. Both the Thames Gravel and London Clay were modelled using elastic-perfectly plastic Mohr-Coulomb soil model, with increasing elastic stiffness with depth. They reported that the interaction effects are significant for pillar width of less than four tunnel diameters. Although comparison of results generated based on two different elastic soil stiffness indicated similar vertical displacement vectors of the tunnels, the first tunnel was observed to displace towards the second tunnel at low soil stiffness, whereas the opposite phenomenon was observed for the case involving higher soil stiffness. It should be pointed out, however, that no field observation was presented in the paper to substantiate such phenomenon. Koungelis and Augarde (2004) concluded that the numerical analysis using simple elastic-plastic Mohr-Coulomb soil model seems to generally agree well with the results generated by Addenbrooke and Potts (2001) using advance soil modelling technique and hence, indicating the general validity of using the Mohr-Coulomb soil model for parametric studies.

Ng et al. (2004) conducted 3D coupled finite element analyses to investigate the interactions between large parallel hypothetical twin tunnels constructed in stiff clay using the new Austrian tunnelling method (NATM). The analyses focused on the influence of the lagging distance between the twin tunnels excavated faces, L_T and the load transfer mechanism between the twin tunnels. It was observed that L_T

significantly affected the shortening of the horizontal diameter of the tunnels as compared to the vertical diameter. They concluded that the magnitude of the maximum settlement is, however, independent of L_T and increasing L_T increases the load transfer from the lagging tunnel to the leading tunnel which resulted in an increase in the stresses in the left tunnel.

Ding et al. (2004) proposed a 2D finite element model for the analysis of shield tunnels. The Drucker-Prager yield criterion and the Reyes elasto-plastic matrix were employed for the soils surrounding the tunnel. In addition, curve beam elements and joint elements were used to model the segments and the flexible contact between any two adjacent segments, respectively. The grout properties that can reflect the state of the grout at each construction stage were adopted for modelling the grout material. Comparisons of the results of numerical analysis with the field measurements indicated conservative prediction of bending moments induced around the circular segmental liner using the uniform grout pressure model (GP-A) for stage 3 (grout hardening) and stage 4 (hardened grout). It was observed that the grout models have small influence on the relative displacements at the joints. This may be partly attributed to the fact that the joint stiffness values are much greater than the grout stiffness values, and partly due to arching effects along the circular lining.

Chern and Hsiao (2005) proposed tunnel interaction assessment criteria based on the results of numerical analyses for estimating the severity of the interaction between closely spaced tunnels constructed in rock mass. They pointed out that both the tunnel spacing and the strength to stress ratio of the surrounding rock mass affected the interaction between tunnels. The interaction of the HsuehShan Tunnels was assessed using the proposed criterion and it was found that only a short section of the pilot tunnel was affected by the subsequent construction of the main tunnels. The proposed assessment criteria also indicated severe tunnel interaction occurred near the portal where poor rock condition was encountered and was subsequently stabilised by additional support system.

Franzius et al. (2005) conducted 2D and 3D finite element analyses of tunnel construction in London Clay to investigate the influence of 3D effects, soil anisotropic and K_o on the tunnelling induced ground settlement trough. They concluded that both 2D and 3D modelling have negligible effect on the shape of transverse settlement trough, where wider trough width was observed as compared to the field data. Although appropriate soil anisotropy for London Clay was included in the 2D study, the transverse settlement trough remains shallow even for a high degree of soil anisotropy. In addition, comparison of the longitudinal settlement profiles generated using 3D results with the field data demonstrated that the longitudinal trough extends too far in the longitudinal direction which prevent the steady-state settlement conditions behind the tunnel face from being achieved. The study indicated that steady state conditions can only be achieved when applying an unrealistically high degree of anisotropy combined with a low K_o, where both appear to be unreasonable assumptions for London Clay. However, this approach leads to high settlement as a result of the unrealistically high volume loss. These observations demonstrate the marginal effects of 3D modelling and elastic soil anisotropy in the prediction of tunnelling induced ground settlement profiles in London Clay. With hindsight, it is clear that the application of advanced soil parameters for numerical investigation may not necessary produce high quality results due to the complexity of the ground conditions.

Lee et al. (2005) investigate the interaction behaviour of the three parallel horse-shoe shape tunnels of Hsuehshan Tunnel Project using finite element program PLAXIS. The study shows that the excavation behaviour is closely affected by the geological conditions, depth of overburden, pillar width of tunnels and the lateral stress.

Ng and Lee (2005) used a finite element method to study the effects of the soil stiffness ratio, $n_o = E'_h/E'_v$ where E'_h is the horizontal effective Young's modulus and E'_v is the vertical effective Young's modulus, and the initial coefficient of earth pressure at rest, K_o on ground deformations and stress transfer mechanisms due to idealized open-face tunnelling using NATM. The results showed that increasing

stiffness ratio induced smaller plastic extension strain zones at the crown and at the invert, subsequently, led to a deeper and narrower transverse surface settlement trough, whereas the opposite phenomenon was observed with increasing initial K_o. They observed the total stress reduction zone fall within 2.0D ahead of the tunnel face. In addition, the results also indicated that the effective stress coefficient varied around the tunnel peripheral, for the initial ground condition of K_o equals to unity. Increasing K_o leads to the larger stress reduction zone and the smaller the percentage increase in the stress coefficient.

Park (2005) presented elastic solutions to predict the tunnelling induced ground movements for shallow and deep circular tunnel in soft ground. For practical purpose, it is often assumed that the uniform radial ground deformation pattern occurred around the tunnel opening. Although the results suggest the oval shape deformation pattern around the tunnel opening give larger surface and maximum subsurface settlement, it is not generally feasible to carry out detailed finite element analysis during routine design. Furthermore, shield advancements such as pitching and negotiating a curve, backfill grouting process, as well as the nature of interactions between closely spaced tunnels also influences the volume loss pattern around the tunnel opening.

Kasper and Meschke (2006) reported a 3D finite element study of a shield tunnelling problem. All relevant shield tunnelling components and the step-by-step construction process of the tunnel advance were considered in the numerical sensitivity studies for the analysis of ground settlement, shield movement and loading of the tunnel lining. The comparisons suggest that the face pressure, grouting pressure, length and the taper of the TBM have significant influence on the ground settlement. While the trailer loads is identified to have only a local influence on the stresses in the lining, the face pressure and the TBM length have the most important influence on the axial normal force in the tunnel lining. The grouting pressure is identified to have negligible influence on the stresses in the cross section of the tunnel lining. It was pointed out that the presented results are case specific and hence, can hardly be applied generally without further considerations.

Möller (2006) compared the results of both 2D and 3D finite element analyses using PLAXIS to measured data of ground surface settlements for Second Heinenoord slurry shield tunnel, as shown in Figures 3.9. A Hardening Soil (HS) model was adopted and grout pressure method was introduced in 2D analysis to compute the ground surface settlement trough. It is of interest to note that similar magnitude and pattern of ground surface settlement troughs were generated using both 2D and 3D approaches and good comparisons with field measurements were achieved. While Figure 3.10 shows a lower grout pressure applied at the tunnel crown for Hardening Soil model with small-strain stiffness (HS-Small) had resulted in better agreement with the field measurements as compared to HS and Mohr-Coulomb (MC) models, Figure 3.11 shows identical magnitude and pattern of transverse settlement troughs for HS-Small and MC models with field measurements based on the same grout pressure applied at the tunnel crown where recommendation was made on the superiority of the use of the MC model over the HS model for tunnel analysis using grout pressure method. In addition, comparisons were made between ground surface settlement troughs computed using HS-Small grout pressure method, HS-Small contraction method and HS-Small stress reduction method as shown in Figure 3.12, where the ground surface settlement troughs generated using HS-Small contraction and HS-Small stress reduction methods were described as flatter than the HS-Small grout pressure method. From these observations, it is apparent that the drawback of grout pressure method is the need to match the field measurements with different grout pressures in view of there is no exact method that can be used to predetermine the grout pressure for prediction of ground surface settlement trough. As pointed out by Burland (2001), precise prediction of ground movements caused by tunnelling is not realistic where reasonable estimates of the likely range of movements can be possibly made provided tunnelling is carried out under the control of suitably qualified and experienced engineers. Clearly, the strong temptation to precisely predict the ground surface settlement trough must be resisted, as can be observed from the result of grout pressure method using HS-Small model in Figures 3.12. Furthermore, evaluation of the result of 2D analysis using stress reduction method for Steinhaldenfeld conventionally driven tunnel in Figure 3.13 and the result of 2D analysis using HS-Small contraction method in Figure 3.12 has led to the identification of the link between the accuracy for computing the ground surface settlement trough where the former was determined by Möller (2006) as the best fit curve for the 2D analysis of ground surface settlement trough using HS model for comparison with 3D analysis. It is believed that the reliability of grout pressure method in generating the

representative magnitude and pattern of ground surface settlement trough can only be verified as more field measurements become available for comparisons.

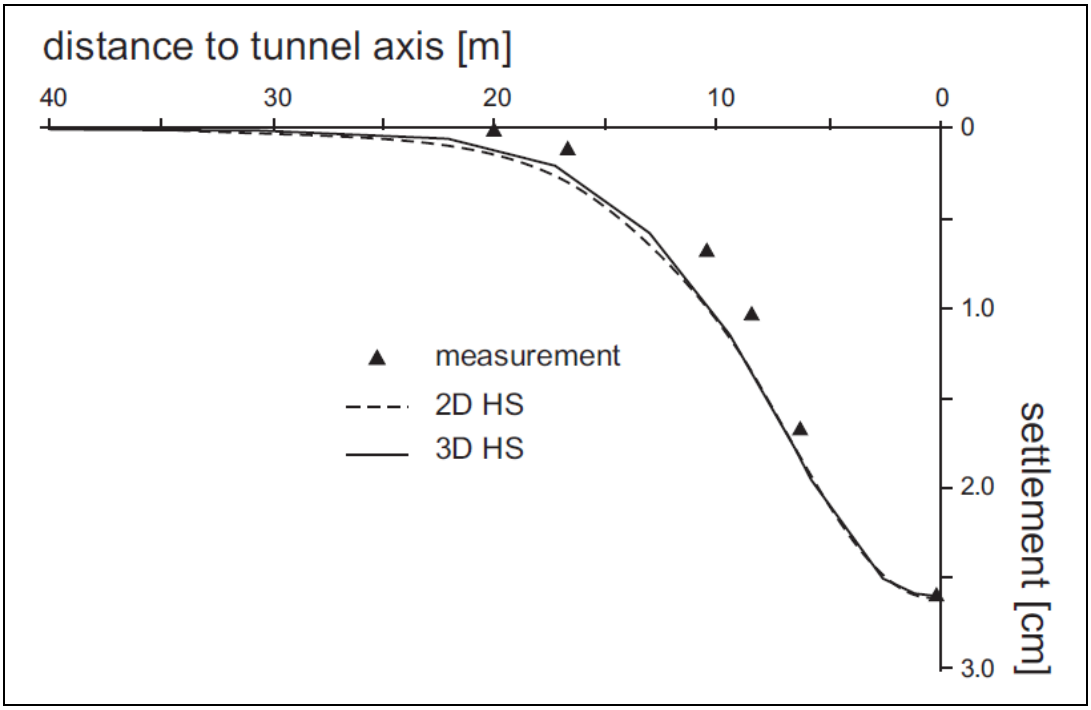

Figure 3.9 Comparison of 2D and 3D transverse surface settlement trough (after Möller, 2006)

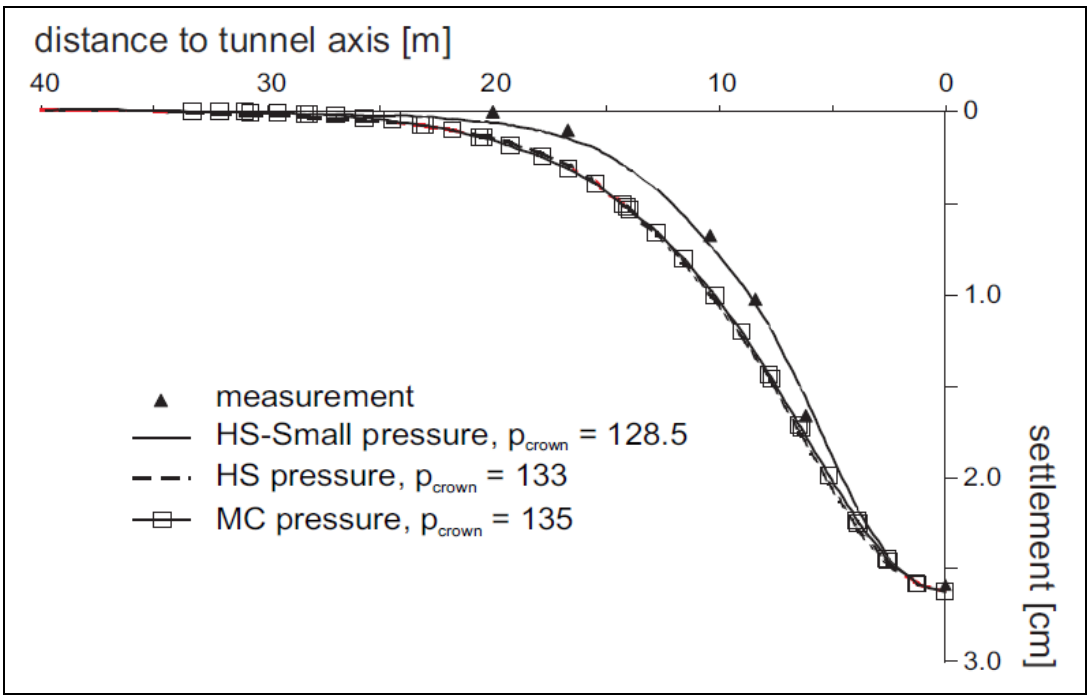

Figure 3.10 Transverse settlement trough using the grout pressure method and different constitutive models (after Möller, 2006)

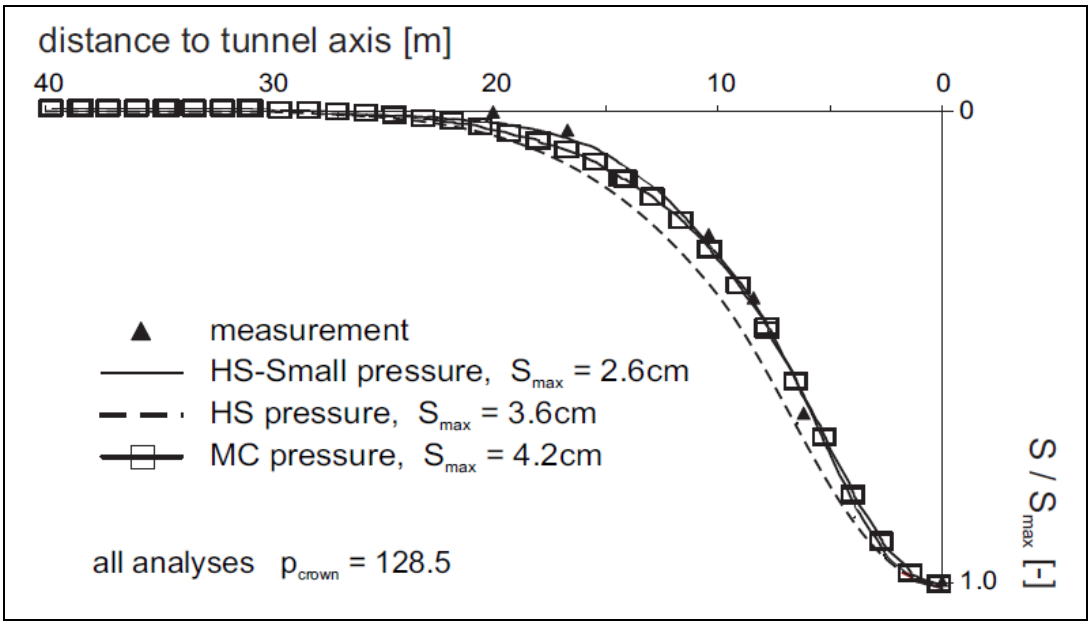

Figure 3.11 Normalized transverse settlement troughs of different constitutive models using the same crown pressure (after Möller, 2006)

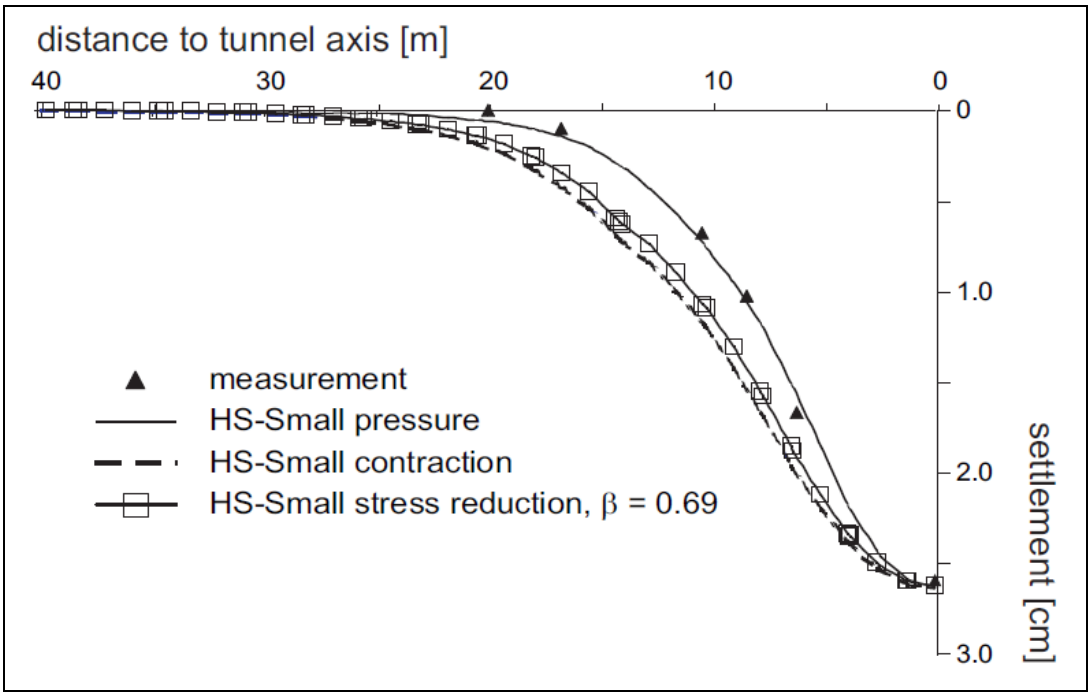

Figure 3.12 Transverse settlement troughs of different installation procedures (after Möller, 2006)

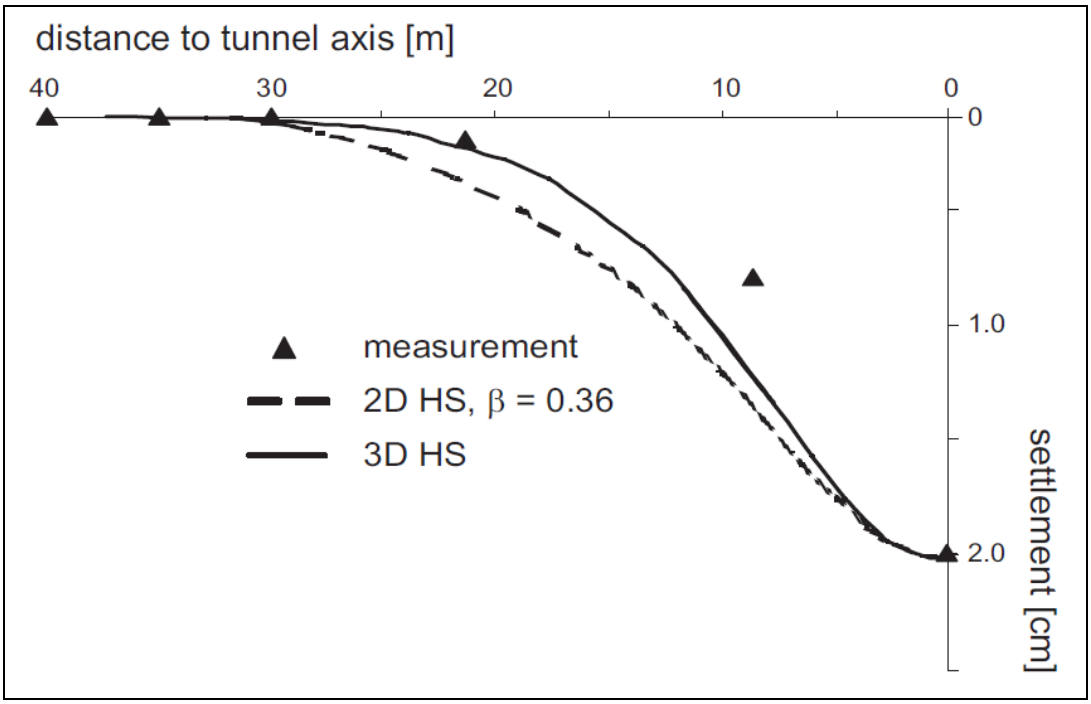

Figure 3.13 Comparison of surface settlements of 2D and 3D analyses (after Möller, 2006)

Dang and Meguid (2008) implemented a constitutive model based on a multilaminate framework into a finite element program to investigate the effects of soil structure on the ground response to tunnelling. The different soil parameters including bonding and anisotropy influence the shape of the settlement trough, maximum surface settlement and lining stresses. For a given anisotropy parameter, increasing overconsolidation ratio, OCR increases maximum vertical displacement, width of the settlement trough and lining stresses. The results also suggest that the width of the settlement trough and lining stresses increase with volume loss. However, it was observed that further volume loss after a critical value induced no additional stresses on the tunnel lining.

Möller and Vermeer (2008) presented the results of 2D finite element analyses using PLAXIS for open face conventional tunnelling and closed face shield tunnelling. Both Hardening Soil (HS) model and the Hardening Soil model with small-strain stiffness (HS-Small) were adopted and three different installation procedures, i.e. stress reduction method, grout pressure method and contraction method were

simulated. As highlighted, the HS-Small model is an extension of the HS model that includes the very high soil stiffness for very small strains and hence improves the steepness of the settlement trough. It was pointed out that the structural forces are less influenced by the choice of the constitutive model. Comparison of the results presented for transverse settlement trough in Figures 3.14, however, indicates the less conservative estimation of the ground surface settlement trough using HS-Small model as compared to HS model. As is evident from Figure 3.15, contraction method is capable to reasonably estimate the bending moment induced in the tunnel lining and hence the merit of the proposed grout pressure method is questionable, in particular, there is no exact method that can be used to predetermine the grout pressure to facilitate the prediction of bending moment induced in the tunnel lining.

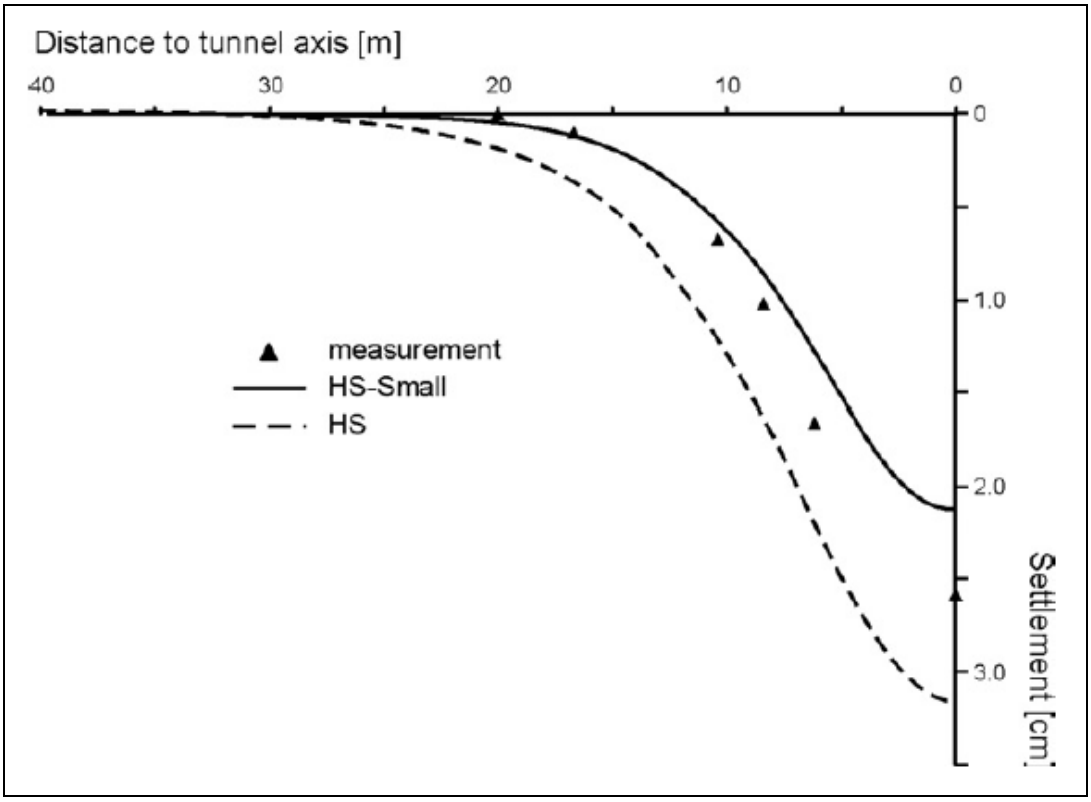

Figure 3.14 Transverse settlement trough of Heinenoord tunnel at four times the tunnel diameter behind the TBM front: Grout pressure method with different constitutive models (after Möller and Vermeer, 2008)

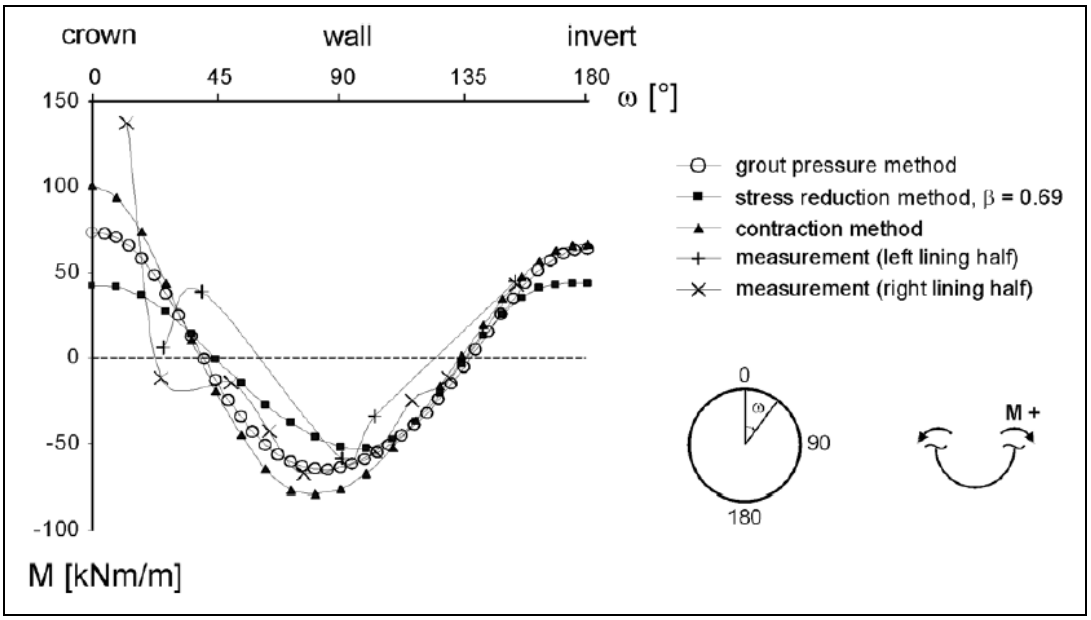

Figure 3.15 Comparison of computed and measured bending moments using the HS-Small model and different installation procedures (after Möller and Vermeer, 2008)

Mroueh and Shahrour (2008) presented a simplified 3D numerical model for the prediction of soil movement induced during tunnel construction using TBM. The homogeneous silty sand was modelled using the Mohr-Coulomb soil model and the coefficient of lateral earth pressure at rest of 0.5 was used. The computation was carried out using the ratio of stress release $\alpha_{dec} = 0.5$, length of unlined zone $L_{dec} = 1D$ and length of the excavated section at each step $L_{lin} = D/3$. The study assumed uniform face pressure equal to $p = \sigma_{ho}$, which refers to the initial axial stress at the tunnel axis. The results indicated that passage of the tunnel caused an approximate 46 per cent of the maximal value of settlement at the tunnel face, which in turn indicated significant difference in terms of the proportion of maximum settlement reported by ITA/AITES Report 2006 (2007). In addition, typical plots of the extension of plasticity also showed different trends of plasticity extension at the tunnel face and behind the tunnel face.

Nunes and Meguid (2009) evaluated the effects of overlying stiff layers above a tunnel excavated in soft ground on the stresses developing in the tunnel lining by conducting laboratory investigation and elastoplastic finite element analyses.

Smaller bending moments were observed to be induced in the tunnel lining as the stiff layer was located closer to the tunnel. For ratio between the stiffness of the upper layer and the saturated clayey soil G_{layer}/G_{soil} of smaller than about 25, the bending moments decrease rapidly with increasing G_{layer}/G_{soil}. For G_{layer}/G_{soil} of greater than about 25, insignificant variation of bending moments with G_{layer}/G_{soil} was observed. It is important to point out that the results between the laboratory measurements and finite element analyses of the effect of the overlying layer thickness on the bending moment at the springline are ambiguous. The former indicated the increase of negative bending moments at the springline with increasing thickness of the stiff layer whereas the latter indicated the decrease of positive bending moments with increasing thickness of the stiff layer. Furthermore, no information on volume loss was indicated.

Osman (2010) presented solutions for the problem of the stability of shallow, unlined twin tunnels embedded within an undrained clay layer. The upper bounds on the loads required to resist collapse are derived and presented in the form of dimensionless stability graphs that account for the variation of shear strength with depth, the embedded depth of tunnels and spacing between tunnels. It was concluded from the dimensionless stability graphs that the spacing between tunnels has a significant influence on their stability. The interaction between tunnels reduces the stability number N_c by up to 35 per cent in shallower tunnels (C/D = 1) where C is the depth of cover and by up to 22 per cent in deeper tunnels (C/D $\geq$ 3). Maximum reduction in tunnel stability occurs when the tunnels are in contact with each other (i.e. s_p = D) if the undrained shear strength varies linearly with depth. Significant reduction in tunnel stability occurs when the distance between centres of tunnels is less than 0.75 times the depth of the tunnel centre below ground surface z_o. It can be assumed that there is no tunnel interaction if the distance between centres of tunnels is greater than 1.5 z_o.

Afifipour et al (2011) analysed the interaction between twin tunnels crossing beneath an underpass using 3D finite element modelling. The results showed that among the TBM operation parameters, the face pressure has more influence on the

underpass movement and the rate of displacement variations, at the tunnel crown was greater than pile toe and underpass surface. It was also observed that the second tunnel construction has led to an increment of approximately 10 per cent in circumferential maximum displacement, axial force, and bending moment of the first tunnel lining. This relatively small influence could be attributed to the sufficient pillar width and little disturbance of EPB shield tunnelling.

Palmer and Mair (2011) presented a simple formula for elastic ground, based on the reciprocal theorem. Comparison between the derived formula and the empirical error function shows the agreement is much closer if K_o is given the lower value of 0.4. They pointed out that although adopting a low value of K_o narrows the settlement trough profile, the observed settlement profile is still narrow for typical K_o of 1.0 or even higher in soils. The plot for the trough width parameter observed in centrifuge tests by Vorster (2005) against the percentage volume indicated the significant variation of trough width parameter with volume loss of smaller than about 4 per cent. They confirmed that the effect of removal of the weight of the soil in the tunnel is not negligible. Although the above analysis applies to unlined tunnels, the same method can be applied to lined tunnels.

Yang and Wang (2011) proposed a simplification to the stochastic medium (SM) theory proposed by Litwiniszyn (1957) to predict the ground surface movements for single circular tunnel and twin circular tunnels. The simplified SM theory is validated by comparisons with the numerical results using the SM theory except for very shallow tunnels.

Zhang et al (2011) presented the displacement controlled boundary integral method for the prediction of the tunnelling-induced ground deformation in homogeneous and non-homogeneous layered soils. The oval-shaped ground deformation pattern is imposed as the boundary condition of the displacement around the tunnel opening to consider non-uniform ground deformation pattern. The applicability of the proposed method is verified with other available published results as well as the displacement controlled finite element analysis. In addition, the results also

indicated that the error obtained by employing the average elastic modulus and average Poisson's ratio based on homogeneous soils converted from layered soils is not negligible. It was also pointed out that the linearity and elasticity assumptions made on the proposed method may underestimate the maximum soil deformations.

Chen et al (2012) analysed the ground surface settlement for twin-tube and quadruple-tube tunnels using both empirical method and 2D finite element analyses. The results showed that the ground surface settlement profile of multi-tube tunnel could be estimated using the Peck (1969)'s empirical equation together with the principle of superposition. It was observed that the width of the ground surface settlement trough obtained from numerical analysis was wider than that obtained from the field data and the empirical equation as a result of the use of a homogeneous modulus within the soil rather than the linear variation in modulus. In addition, it was also pointed out that the analysis conducted for the scenario of "all tunnels excavated simultaneously" produced a better estimate of the ground surface settlement trough than the analysis for tunnels excavated one-by-one, as carried out in the field. As explained, the ground surface settlement trough of multi-tube tunnel obtained through the simulation of a series of tunnels excavation seemed to repeatedly generate undesirable shear strain around the existing tunnels and caused a larger ground loss than that in the "all tunnels excavated simultaneously" analysis. Comparison between the results of the tunnels excavated in the brown-field site, i.e. excavation near an existing tunnel, and the greenfield land indicated the more severe deviation arose from the case involving tunnels excavated one-by-one for the brown-field site.

Mirhabibi and Soroush (2012) conducted finite element analyses to study the effect of surface buildings on ground settlement of twin tunnelling. They concluded that the existence of surface buildings in 2D plane strain led to less settlement as compared to the greenfield condition where the shape and location of trough depends on the combination of geometrical and mechanical parameters of the tunnels and the ground. The parameters involving the stiffness of surface buildings, building width, weight of the buildings, bending stiffness of the buildings, tunnel

depth, centre-to-centre distance of tunnels and surface distance of buildings from centreline of twin tunnels influence the ground settlement. In addition, two modification graphs were developed for predicting the maximum building settlement for preliminary design.

Chakeri et al (2013) investigated the effects of tunnel diameter, surface surcharge and face support pressure on maximum surface settlement. In addition, the results of empirical and numerical methods were compared with observed data. The results indicated that the 3D finite difference model (FDM) predicts well the maximum surface settlement. They concluded that the tunnel diameter, surface surcharge and face support pressure significantly influence the ground surface settlement. It was also pointed out that the value of maximum surface settlement from the Verruijt and Booker (1996) and Loganathan and Poulos (1998) methods are compatible with numerical results for tunnel diameter variations. Although the Herzog (1985) and Schmidt (1969) methods showed significant deviations from the numerical results for tunnel diameter variations, variation of maximum surface settlement with the surface surcharge generated using their methods showed a similar shape to numerical analysis.

Mathew and Lehane (2013) examined the potential for two-dimensional (2D) and three-dimensional (3D) finite element analyses to calculate the ground displacement patterns observed at a greenfield site above two recently completed tunnels in Perth, Western Australia. They observed that the calculated greenfield surface settlement troughs at the same site can vary with the soil stratigraphy and the choice of soil parameters and soil model. They deduced that the generally poor and inconsistent comparisons between the calculations and field observations could be partly attributed to the technique of imposing volumetric contraction at the tunnel location which does not simulate all of the complexities associated with actual tunnelling procedures.

Sahoo and Kumar (2013) performed the analysis of the stability of two long unsupported circular parallel tunnels aligned horizontally in fully cohesive and

cohesive–frictional soils using an upper bound limit analysis in combination with finite elements and linear programming. The stability of tunnels is expressed in terms of a non-dimensional stability number. Their results showed that the stability number reduces substantially with a decrease in the spacing between the two tunnels. However, the stability number increases continuously with an increase in the values of H/D, m and ϕ, where H/D is the tunnel cover to diameter ratio, m is the rate of increase of cohesion with depth for purely cohesive clay and ϕ is the internal friction angle of cohesive-frictional soil. The optimum spacing between the two tunnels required to eliminate the interaction effect increases with an increase in H/D and a decrease in the values of both m and ϕ. The value of the optimum spacing between the two tunnels lies approximately in a range of 1.5D to 3.5D with H/D = 1 and 7D to 12D with H/D = 7. It has also been observed that a rupture zone with the curvilinear boundary, starting from the bottom of the tunnel and extending up to the ground surface, developed in all the cases. The size of this rupture zone was found to increase with an increase in the value of H/D and a decrease in the value of m and ϕ. The results from the analysis compared reasonably well with the different solutions reported in literature.

Tables 3.2 and 3.3 provide a summary of the numerical and analytical studies described in this section for single tunnel and closely spaced tunnels respectively. The tunnel geometry, description of soil/rock at tunnel level, simulation technique and constitutive model, volume loss and summary of finding are listed for each study.

Table 3.2 Parameters and summary of findings for single tunnel

Tunnel Geometry	**Description of Soil/Rock at Tunnel Level**	**Simulation Technique and Constitutive Model**	**Volume Loss**	**Summary of Finding**	**Reference**
Circular lined tunnel Diameter=6.04 m; Depth=12 m to 22 m	Clayey soils and sandy layers (SM, SM/CL, CL)	Optimization technique (conjugate gradient method and gap parameter model)	0.740-3.406 per cent	Identify the angle of the influence zone of ground settlement for clayey soils and sandy layers and effectiveness of back fill grouting. Semi-empirical equations were established and case studies were presented.	Chi et al. (2001)

Table 3.2 Continued

Circular lined tunnel	Stiff to soft clay below the water table	Analytical solution for shallow tunnels in saturated clay immediately after construction	Gap	The location of the bottom boundary of zero vertical deformation should be located at a distance of two tunnel diameters below the tunnel centreline or at the location of a stiff soil layer; Analytical solution cannot substitute detailed numerical analyses where realistic ground properties and construction procedures should be modelled in detail; Reasonable estimates of the gap predicts quite well the magnitude and distribution of the ground settlements.	Chou and Bobet (2002)
Circular tunnel with lining segments	Stiff to hard clay	3D; Mohr-Coulomb model for soils; linear elastic model for grouting material, lining segment and shield machine	3D simulation of shield tunnelling	The comparisons between the results of 2D and 3D analyses with measured ground surface settlements have demonstrated the adequacy of using 2D approach in estimating the ground surface settlement trough if the section considered is far behind the tunnel face as the shield advancing.	Lin et al. (2002)
Circular lined tunnel; EPB shield external diameter is 9.33 m; the cutting wheel diameter, as related to the peripherical bits is 9.38 m; the inner diameter of lining ring is 8.43 m; the thickness is 0.32 m	Brown clay; sandy clay; clayey sand; loamy sand; blue plastic clay; pink plastic clay	3D; linear elastic model; Mohr-Coulomb elastoplastic model; modified Cam clay model	Overexcavation (the void between the ground and the shield); gap (the tailpiece void between soil and liner)	Numerical models should be verified and validated with the help of analytical and empirical models and field data.	Melis et al (2002)
Circular lined tunnel Diameter=9.0 m	Dry ground; saturated ground	2D; 3D; linear elastic	-	An increase of the stresses both in the liner and the ground is observed when the consolidation is taken into account; Difference in radial displacement produced by axisymmetric model and 3D for the case involving lateral stress perpendicular to the tunnel axis of equal to unity and 0.5.	Liakos et al (2003)
Circular jointed tunnel Outer diameter=5.3 m; lining thickness=280 mm; Depth=20 m	Sand layer and clay layer	2D; Elasto-plastic Drucker-Prager yield criterion and the Reyes elasto-plastic matrix	Stress releasing coefficients for the first to the fourth construction stages are chosen to be 0.10, 0.45, 0.3 and 0.15	The adoption of the grout properties that can reflect the state of the grout at each stage as well as the contact condition between the soil and lining that will change with the construction stage by varying stress releasing coefficient show that the proposed numerical procedure can be used to effectively estimate the deformation, stresses and moments experienced by the surrounding soils and concrete	Ding et al (2004)

				lining segments.	

Table 3.2 Continued

Circular lined tunnel Diameter=4.75 m; Depth=30.5 m	London Clay	2D; 3D; Isotropic non-linear elastic pre-yield model; anisotropic non-linear elastic pre-yield model; Mohr-Coulomb model	3.3 Per cent	Neither 3D effects nor elastic soil anisotropy can account for the over-wide settlement curves obtained from finite element tunnel analysis in a high-K_o regime.	Franzius et al (2005)
Circular tunnel; Shotcrete lining; Diameter=9 m; Depth=18 m	London Clay	3D; elastic-perfectly plastic soil model using the Drucker-Prager failure criterion with a nonassociated flow rule	Deactivating the soil elements within the proposed tunnel excavation zone (i.e. incrementally removing body forces of the element)	The surface ground settlements are governed by the combined effects of the stiffness ratio and the coefficient of earth pressure at rest. A three-dimensional stress-transfer mechanism at a tunnel heading is clearly demonstrated by the progressive changes in normal stresses and shear stresses as excavation advances.	Ng and Lee (2005)
Circular tunnel	Uniform clay	Analytical solution for tunnelling-induced undrained ground deformations for shallow and deep tunnels in the soft ground	Apply boundary conditions of the prescribed displacement at the tunnel opening which consist of uniform radial displacement and oval-shaped radial displacement	Oval-shaped radial displacement gives larger surface and maximum subsurface settlements than uniform radial displacement.	Park (2005)
Circular lined tunnel Diameter=6.3 m; Depth=1.5D	Homogeneous, overconsolidated, soft, cohesive soil (the ground water table is assumed to be at the ground surface)	3D; elasto-plastic Cam-Clay model	TBM advance consists of the excavation at the cutting face, the tail void grouting and the erection of a new lining ring during standstill are taken into account	The complexity of the influence of face support pressure, grouting pressure, trailer weight and the length as well as weight and taper of the shield machine on the settlements of the ground surface, the shield movement and the loading of the tunnel lining.	Kasper and Meschke (2006)
Case study 1: Horse shoe shape top heading; Height of top heading=6.2 m; Depth to tunnel invert=22.2 m; Case Study 2: Circular tunnel	Case study 1: Lower Keuper Marl; Case study 2: Sand	Case studies 1 and 2: 2D and 3D; Hardening Soil model with small-strain stiffness (HS-Small); Hardening Soil (HS) model and Mohr-Coulomb	Case study 1: Stress reduction method for 2D analyses; Case study 2: Grout pressure method, contraction method and	The shape of the transverse settlement trough is more affected when applying different installation procedures, i.e. grout pressure method, contraction method and stress reduction method, rather than different constitutive models, i.e. HS-Small, HS and MC models.	Möller (2006)

with segmental linings; External diameter=8.3 m; Thickness of lining ring=0.2 m; Length of lining ring=1.5 m; Depth to tunnel axis=16.65 m		(MC) model	stress reduction method for 2D analyses		

Table 3.2 Continued

Circular lined tunnel Diameter of TBM=3.5 m; Depth is approximately 17.5 m	Marine clay	2D; Multilaminate framework	0 per cent to 2.5 per cent	The shape of the yield surface and the destructuration have an insignificant effect on surface displacement and lining stresses whereas soil bonding and anisotropy have significant effects on surface settlement and lining stresses depending on the OCR value of the natural clay.	Dang and Meguid (2008)
Case study 1: Horse shoe shape top heading; Height of top heading=6.2 m; Depth to tunnel invert=22.2 m; Case Study 2: Circular tunnel with segmental linings; External diameter=8.3 m; Thickness of lining ring=0.2 m; Length of lining ring=1.5 m; Depth to tunnel axis=16.65 m	Case study 1: Lower Keuper Marl; Case study 2: Sand	Case study 1: 2D; Hardening Soil model with small-strain stiffness (HS-Small) and Hardening Soil (HS) model. Mohr-Coulomb (MC) model was adopted for the stiff rock layer below the bottom of the tunnel; Case study 2: 2D; Hardening Soil model with small-strain stiffness (HS-Small) and Hardening Soil (HS) model.	Case study 1: Stress reduction method for 2D analyses; Case study 2: Grout pressure method, contraction method and stress reduction method for 2D analyses	Installation procedures range from open face conventional tunnelling to closed face shield tunnelling are most important to be considered in order to arrive at proper prediction for surface settlement and lining forces. The grout pressure method was proposed for the installation of closed face shield tunnelling. The lining forces are less influenced by the choice of the constitutive model.	Möller and Vermeer (2008)
Circular lined tunnel Outer diameter=7.5 m; lining thickness=0.5 m; Depth=2.5D	Homogeneous silty sand	3D; elastic perfectly-plastic constitutive relation based on the Mohr-Coulomb criterion with a non-associative flow rule	Length of the unlined zone and the partial stress release	A simplified non-linear 3D numerical model is proposed for the determination of the soil movement induced by TBM. Factors considered in the method consist of the length of the unlined zone and the partial stress release.	Mroueh and Shahrour (2008)
Circular lined tunnel; lining radius=0.073 m; thickness=0.00025 m	Coarse sand layer (stiff layer) and clay mix (soft soil)	2D; Mohr-Coulomb failure criterion	Not reported	The response of a tunnel liner was generally affected by the presence of a stiff sand layer above the tunnel.	Nunes and Meguid (2009)
Unlined tunnel	Elastic ground	Reciprocal theorem	Volume loss	The comparison between the derived formula and the empirical error	Palmer and Mair (2011)

				function is encouraging, considering the narrow observed settlement profile for K_o of 1.0 or even higher in soils.	

Table 3.2 Continued

Single circular and twin circular tunnels	Stochastic medium	Simplified stochastic medium theory	Gap parameter	The simplified stochastic medium theory is an effective technique for predicting ground surface movement for single circular tunnel and twin circular tunnels.	Yang and Wang (2011)
Circular lined tunnel	Elastic ground	Modified elastic layered half-space model subjected to arbitrary loads in a Cartesian coordinate system and combined with the method to consider the soil non-homogeneous characters	Oval-shaped non-uniform deformation controlled pattern	The proposed method provides reliable estimates for the ground movements due to tunnelling in multi-layered soils.	Zhang et al (2011)
Circular lined tunnel; Bored diameter=9.14 m; Outer diameter of lining ring=8.85 m; Thickness of lining ring=35 cm; Length of lining ring=1.5 m; Tunnel depth=20.8 m and 23.7 m	Alluvial layers with variable grain size distribution from clay to coarse gravel with cobbles and erratic blocks	3D; Elastic-perfectly plastic constitutional link with a Mohr-Coulomb failure criterion	3D	Factors including tunnel diameter, surface surcharge and face support pressure significantly influence the ground surface settlement. Greater accuracy of Verruijt and Booker (1996) and Loganathan and Poulos (1998) methods in prediction of the effect of tunnel diameter on maximum surface settlement than the Herzog (1985) and Schmidt (1969) methods.	Chakeri et al (2013)

Table 3.3 Parameters and summary of findings for closely spaced tunnels

Tunnel Geometry	**Description of Soil/Rock at Tunnel Level**	**Simulation Technique and Constitutive Model**	**Volume Loss**	**Summary of Finding**	**Reference**
Circular lined tunnels Diameter=4.146 m; Side-by-side; Depth=34 m; spacing=8 m – 32 m and piggyback geometries; Depth=34 m; spacing=10 m to 18 m	London Clay	2D; Non-linear elastic perfectly plastic with Mohr-Coulomb yield surfaces and plastic potentials	1.4 per cent	The magnitude of the interactions expected on any given project will depend on the relevant design volume loss. The influence of tunnel position, tunnel spacing, rest period and sequence of excavation have a varying degree of influence on the surface settlement and the tunnel lining response.	Addenbrooke and Potts (2001)

Table 3.3 Continued

Circular lined tunnel Diameter=4.174 m; Tunnel axes are horizontally aligned; tunnel axes are vertically aligned with second tunnel driven above and below the first respectively	London Clay	2D; elastic-perfectly plastic using the Mohr-Coulomb failure criterion with increasing elastic stiffness with depth	1.4 per cent	Interaction effects for parallel geometry appear to be present up to a pillar width of three to four diameters. Interaction effects for piggy-back geometry where a second tunnel is driven above an already existing one is small at a pillar depth of one diameter. Interaction effects for piggy-back geometry where the lower tunnel is constructed second seem to appear regardless of the depth of the second tunnel. The results obtained fit in with previous studies by Ghaboussi and Ranken (1977), Kim et al (1998), Addenbrooke and Potts and Cooper et al (2002) and demonstrate that economical numerical parametric studies using elasto-plastic soil model.	Koungelis and Augarde (2004)
Oval shape NATM tunnels Equivalent diameter=8.64 m; Depth=25 m; pillar width=1.0D	London Clay	3D; The Taplow Gravel and London Clay were modelled as isotropic and anisotropic elastic-perfectly plastic materials with a modified Drucker-Prager failure criterion and the flow potential	-	Showed the influence of lagging distance between the twin tunnel excavated faces on the tunnel movement and location of the maximum settlement, load-transfer mechanism between the two tunnels and distributions of pore-water pressures.	Ng et al (2004)
Circular lined tunnel; Overburden=60 m – 650 m; pillar width=1.30B – 1.90B where B=tunnel diameter	Rock Formation	Numerical analyses	-	A tunnel interaction assessment criteria was proposed based on the results of numerical analyses for judging the severity of the interactive effect between tunnels. Assessment of tunnel interaction in Hsuehshan Tunnels was conducted using the proposed criterion.	Chern and Hsiao (2005)
Horseshoe tunnel and circular tunnel Diameter = 12 m (main tunnel) and 5 m (pilot tunnel); shotcrete lining; Overburden=300 m	Rock mass	2D; elastic perfect-plastic Mohr-Coulomb model	Rock mass stress release ∑Mstage	The displacements of tunnel excavation and the interaction behaviours of adjacent tunnels are affected by geology, topography, engineering layout and etc.	Lee et al (2005)
Unlined twin circular tunnels	Undrained clay	Upper bound plasticity analysis	Unlined	The upper bounds on the loads required to resist collapse are derived and presented in the form of dimensionless stability graphs that account for the variation of shear strength with depth, the embedded depth of tunnels and spacing between tunnels.	Osman (2010)

Table 3.3 Continued

Circular lined tunnels; Tunnel diameter=6 m; Pillar width=8 m	Dense alluvium formation of different particle size, i.e. gravel with silt and loam admixtures and finer soil being composed by pure silt and loam	3D; Elastoplastic Mohr-Coulomb	-	The face pressure is an important parameter that influences the underpass movement. The second tunnel construction induced an approximately 10 per cent increase in the circumferential maximum displacement, axial force and bending moment of the first tunnel lining.	Afifipour et al (2011)
Circular lined tunnels; Tunnel diameter=6.1 m	Songshan Formation of silty clay and silty sand	2D; Mohr-Coulomb failure criterion	Tunnel contraction parameter	Peck (1969)'s empirical equation together with the principle of superposition could be used to estimate the ground surface settlement profile of multi-tube tunnel. The use of a homogeneous modulus within the soil model led to wider width of the ground surface settlement trough. A better estimate of the ground surface settlement trough was achieved using "all tunnels excavated simultaneously" than the analysis for tunnels excavated one-by-one. More severe deviation was observed for tunnels excavated one-by-one in the brown-field site as compared to the green-field land.	Chen et al (2012)
Circular lined tunnel; TBM cutting wheel diameter=6.9 m; External diameter of shield=6.88 m; Horizontal distance between centreline of the tunnels=13 m to 17 m; Tunnel depth up to 23 m	Lean clay with alternating sandy clay and silt layers	2D; Mohr-Coulomb elastoplastic model	Volume loss control method	The existence of surface buildings in 2D plane strain led to less settlement as compared to the greenfield condition. The parameters involving the stiffness of surface buildings, building width, weight of the buildings, bending stiffness of the buildings, tunnel depth, centre-to-centre distance of tunnels and surface distance of buildings from centreline of twin tunnels influence the ground settlement. Two modification graphs were developed for predicting the maximum building settlement for preliminary design.	Mirhabibi and Soroush (2012)
Circular lined tunnels; Outer diameter of tunnel=6.9 m; Concrete liner thickness=275 mm	North profile: Spearwood Sand; South profile: Alluvium consisting of silty sand (Perth Formation)	2D and 3D; 2D: Elastic Mohr-Coulomb model, Hardening Soil (HS) model and Hardening Soil model with small-strain stiffness (HSsmall); 3D: HS model	2D: Volumetric contraction	The calculated greenfield surface settlement troughs at the same site can vary with the soil stratigraphy and the choice of soil parameters and soil model. The technique of imposing volumetric contraction at the tunnel location does not simulate all of the complexities associated with actual tunnelling procedures and may have led to the generally poor and inconsistent results between the calculations and field observations.	Mathew and Lehane (2013)
Unlined twin circular tunnels	Purely cohesive soil and cohesive-	Upper bound plasticity analysis	Unlined	The variation of stability number has been established as a function of H/D,	Sahoo and Kumar (2013)

	frictional soil			S/D, m and ϕ where S is the clear spacing between tunnels. A rupture zone with the curvilinear boundary, starting from the bottom of the tunnel and extending up to the ground surface, was found to develop in all the cases.	

Table 3.3 Continued

3.5 Recent Field and Laboratory Experimental Studies on Tunnelling

Nomoto et al. (1999) carried out centrifuge model tests for simulating the shield construction process in dry sand using a newly developed 100 mm diameter shield tunnel. A series of "buried-tube-test", "tail void test" and "shield test" were conducted to measure the lining stresses, simulate the process of tail void formation and deal with the complete process of shield construction, respectively. The studies found that the lining stress at the crown elevation was well predicted by Terzaghi's loosening earth pressure. In addition, the results of the tests also confirmed the successful simulation of the shield construction process. Equations proposed for both transverse settlement and longitudinal settlement troughs above the tunnel in sand were found to be in good agreement with the field measurements.

Xu et al. (2003) conducted in-situ static cone penetrometer resistance test to investigate the relationship between the mechanical properties and stress disturbance in a transverse section before and just after tunnelling. The results show an increase in the earth pressure and pore water pressure at shield distance of about 25 m before the measured section and the effect of stress disturbance diminishes at shield distance of about 50 m after the measured section. This observation allows a suitable range of field measured ground surface settlements to be selected for numerical comparison. In addition, the information also enables appropriate boundary dimensions to be determined for 3D numerical analysis.

Lee et al. (2006) conducted a series of centrifuge model tests and numerical modelling to investigate the surface settlement troughs, excess pore water pressure generation, overload factors at collapse for both single and parallel tunnels, as well as arching effects that developed during tunnelling in soft clayey soil. They

proposed positive and negative arching zones for both single tunnel and twin tunnels to serve as references for practising engineers to mitigate possible damages to underground structures due to new adjacent tunnelling. Although the Mohr-Coulomb soil model was adopted to simulate the deformation behaviour of the soft clayey soil due to single and parallel tunnelling, the results generated were in good agreement before tunnel collapse. This observation indicates the suitability of adopting the Mohr-Coulomb soil model for this present research project.

Standing and Burland (2006) investigated the large variations in tunnelling volume loss measured over about 2 km distance between Waterloo, south of the Thames, and the area north of St James's Park. They discussed in detail the factors influencing the volume loss:

1. Influence of geology and lithology where the erosion of the London Clay and material above it has resulted in swelling and softening of the clay and an increase in the soil mass permeability
2. Influence of undrained shear strength where increase in undrained shear strength reduces volume loss
3. Influence of mass permeability where greater ground movement would be expected when tunnelling through ground with higher mass permeability
4. Influence of tunnelling procedures where the degree of face support provided would be crucial to minimising the volume loss. The over-digging ahead of the shield as well as ground disturbance caused by the previous passage of the adjacent tunnels will lead to larger volume loss

It is clear that both geological conditions and workmanship influence the volume loss and in turn, ground movement which may induce damage to the adjacent structures.

Suwansawat and Einstein (2006) used artificial neural networks (ANN) to relate tunnel geometry, geological conditions and shield operation factors to surface settlements data collated for the Bangkok MRTA project. Attempts have been made to correlate each shield operation factor with surface settlement. However, no unique relationship between the operation parameters of TBM and the surface

settlement can be deduced, although some trend was observed for face pressure. This shows the complex interaction between various parameters that influences the magnitude of surface settlement.

Chapman et al. (2007) conducted a series of small scale laboratory model tests on closely space multiple tunnels in Speswhite kaolin clay. The tests produced results that were generally consistent with the ground movement characteristics observed at full scale in the published case studies. The comparison of the results to the Gaussian curve prediction method, however, demonstrate the potential inaccuracy in this approach for predicting ground movements associated with closely spaced multiple tunnels. Modification has been performed on the Gaussian curve prediction method and showed to agree reasonable well with the laboratory data. Since these laboratory tests have been conducted in a very small scale, interrelationships among ground response characteristics and the key operational parameters of the state-of-the-art TBM are not reflected in the test and hence, the proposed method may be experimental specific and may not be readily applied to the real scale tunnelling induced ground settlement.

Chu et al. (2007) conducted a series of model tests of twin circular tunnels in homogeneous material, two-layered formations and three-layered formations subjected to various stress conditions. The study was concerned primarily with the strains and displacements developed around the tunnels. The comparisons of results between model tests and numerical simulation using fictitious stress method (FSM) were found to be in good agreement. The results for two-layered formations suggest that while the settlement at the tunnel crown will be reduced with the presence of a stiffer formation above the formation containing twin tunnels, the presence of a weaker formation above the twin tunnels will lead to an increase in the displacements around the upper tunnel. For three-layered formations, the tunnels were observed to become more stable due to the protection by the upper and lower stiffer formations. However, displacements at the crown and invert will increase as the tunnels are surrounded by weaker formations. It should be pointed out that their

modelling does not include the tunnel liner and hence, all interaction effects may be only attributed to the deformation of the modelled rock mass.

Bilotta (2008) conducted centrifuge tests to investigate the potential of a vertical diaphragm wall in modifying the displacement field induced by tunnel excavation. The diaphragm wall was embedded to one side of the tunnel and the location of the wall, its length, thickness and roughness of the wall-soil interface were varied. Both the results obtained experimentally and numerically suggest that a diaphragm wall can be used in reducing the ground movements where the effectiveness of the wall depends mainly on the length. However, it was pointed out that the effects of wall installation have been completely neglected in the studies where the wall was considered as "wished in place". An efficiency parameter was proposed to quantify the amount by which the wall modifies the reference profile of the settlement. This work explains the unsymmetrical surface settlement profiles reflected in the field data that are commonly observed for urban tunnelling.

Ahmed and Iskander (2011) used transparent soil model tests to investigate the surface settlement profile induced by shield tunnelling and the distribution of soil deformation within the soil mass near the tunnel. The results of the model tests are in agreement with the empirical solution proposed by Peck (1969) in which the surface settlement trough conforms to the normal probability curve. In addition, the measured data also indicated that the settlement trough parameter is independent of the volume loss and linearly proportional to the tunnel depth.

Chen et al (2011) conducted field study of parallel tunnels of 6.2 m diameter constructed using EPB shields in silty soils. They reported that the the pore pressures in the soils showed the zigzag-shape distribution along the distance during shield advancement. The excess pore pressure reached a peak value when the shield injected grouting material into the tail. The settlements indicated upheaval-subsiding behaviour in the longitudinal direction where different magnitudes of upheaval were observed for right line (RL) and left line (LL) tunnel. The trough of the LL tunnel was reported to be more shallow and wider than that of the RL tunnel

where the RL tunnel made the symmetric axis of the final trough of the parallel tunnels incline to the RL tunnel.

Sirivachiraporn and Phienwej (2012) analysed the monitoring data of the first Bangkok subway project excavated by eight EPB shields to evaluate the ground movement characteristics and responses of adjacent buildings. They reported that although most of the maximum ground surface settlements induced by the twin MRT tunnel EPB shield excavation were in a range of 20 mm to 40 mm which corresponds to 0.5 per cent to 2.0 per cent of tunnel volume loss, larger settlements reaching 100 mm were observed for tunnelling through sands or mixed face ground due to certain difficulties such as controlling face pressure and at locations of long duration stoppage. It was pointed out that the relationship between the magnitude of ground surface settlement and shield pressure is not significant with wide scatter of data being observed. For areas of vertically stacked layout of the twin tunnels with larger ground settlements, no clear relationship between the soil properties, tunnel geometry and depth can be observed. They concluded that the predominant controlling factor appears to be the workmanship that was not easy to estimate. The pre-existing building piled foundations and some known and unknown buried utilities and other objects have caused the deviation of the observed shapes of surface settlement troughs from the greenfield Gaussian curve. However, the derived trough width parameter i for those cases that followed the Gaussian curve agrees reasonably with those given by the guidelines by Peck (1969) and Mair et al (1996).

McCabe et al (2012) presented the transverse surface settlement data for 11.77 m, 1.505 m and 2.150 m diameter tunnels from two glacial till (or boulder clay) sites. The measured settlements have been interpreted using a standard Gaussian error function. They concluded that the constant of proportionality which is known as the trough width parameter k' is dependent on the fine or coarse fraction of the till which governs the prediction of volume loss. The values of k' for coarse soils is at the low end of the range given in the Mair and Taylor (1997) database for sands and gravels whereas the k' for fine soils is consistent with the Mair and Taylor (1997)

database for clays. No obvious distinction between the k' values obtained for tunnels in soft and stiff clays was observed. In addition, they also reported that there is no systematic variation in k' with time for glacial till soils and consolidation settlement was not a significant issue. Despite the usefulness of the data in obtaining a preliminary estimate of the volume loss, it was pointed out that the presence of boulders as well as reducing the advance rate can result in high volume losses which are difficult to predict with accuracy.

Divall (2013) carried out a series of plane strain centrifuge tests to investigate the twin tunnelling-induced settlements in overconsolidated clay. The tests were conducted at 100g where the cavities represented two 4 m diameter tunnels at a depth of 10 m at prototype scale. The main variables involved included the spacing between the tunnels, both horizontally and vertically and the magnitude of volume loss. From the results of the centrifuge tests, Divall (2013) concluded that the single tunnel surface and subsurface settlement troughs were well represented by Gaussian distributions. The magnitude of the volume loss from the second tunnel construction increased due to the effect of the first tunnel. This effect decreased with increasing spacing between the tunnels. The settlements between the varying volume losses and spacing between the tunnels have been compared by normalising the vertical displacements against the maximum settlement from the construction of Tunnel A (first tunnel) as shown in Figures 3.16, 3.17 and 3.18. As observed, the wavy surface settlement occurred for the 3D and 4.5D spacing tests. It was also concluded that the surface and subsurface settlement distributions towards the existing tunnel were wider than for a single tunnel.

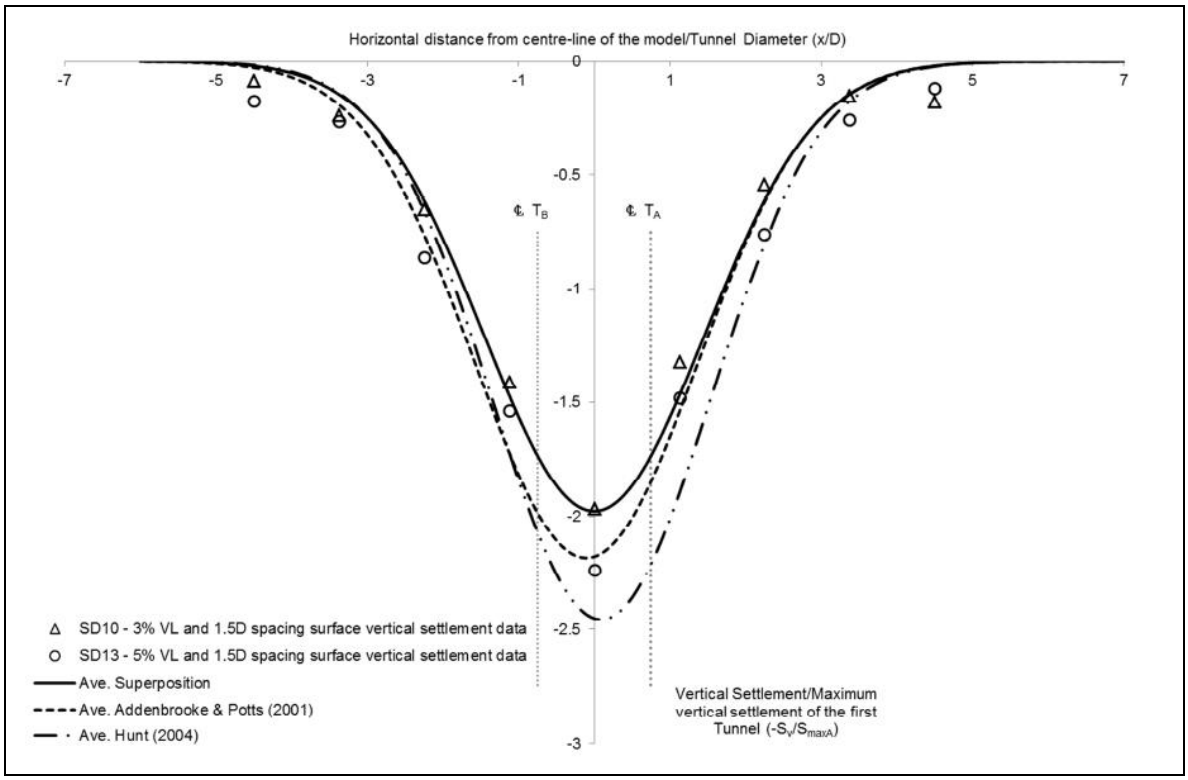

Figure 3.16 Twin-tunnel vertical surface settlement from 1.5D spacing tests (after Divall, 2013)

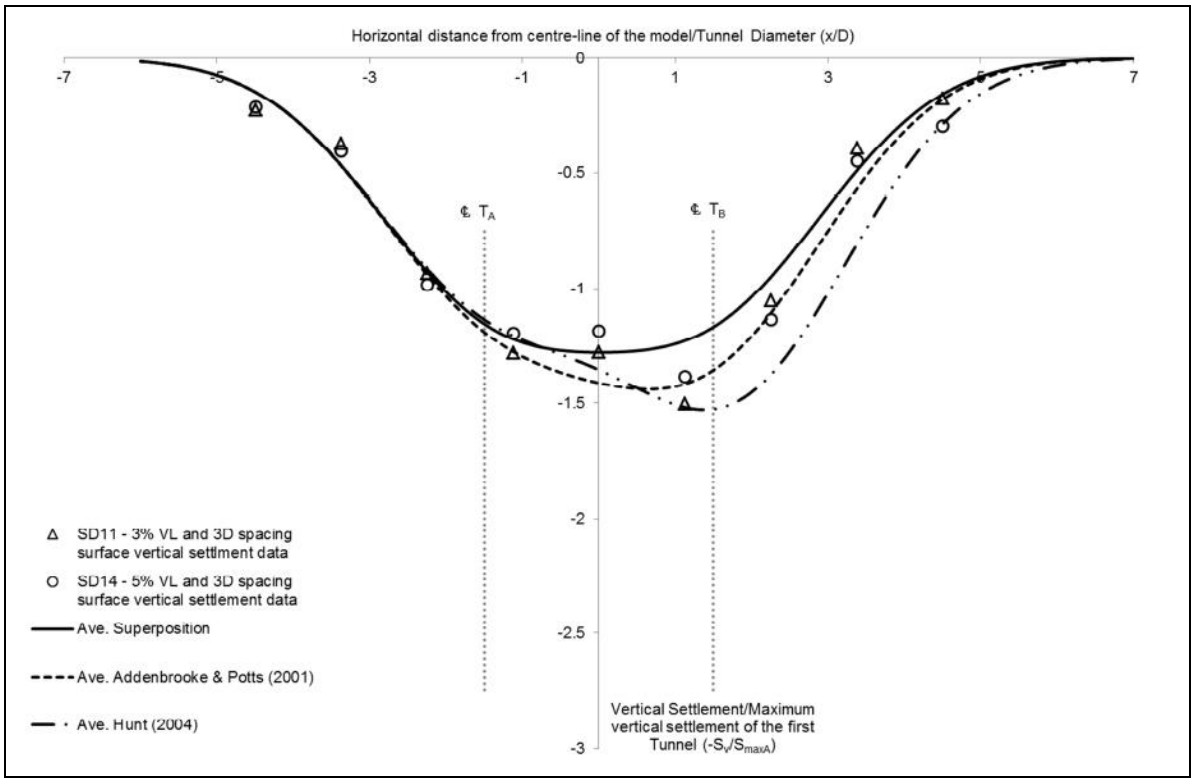

Figure 3.17 Twin-tunnel vertical surface settlement from 3D spacing tests (after Divall, 2013)

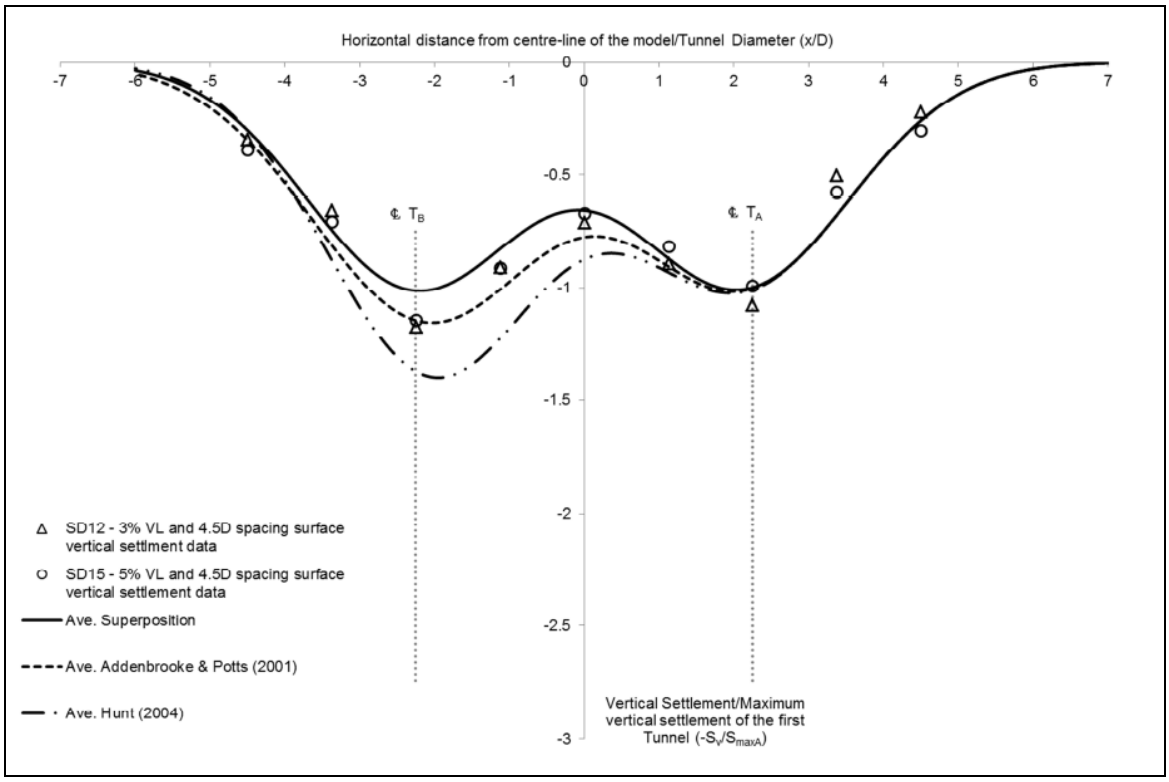

Figure 3.18 Twin-tunnel vertical surface settlement from 4.5D spacing tests (after Divall, 2013)

Standing and Selemetas (2013) studied the ground response to earth pressure balance machine (EPBM) tunnelling at a greenfield site where 8.16 m diameter openings were excavated for two tunnels in London Clay. They reported that the pressurised face of the EPBM and tail-skin grouting led to outward displacements and increases in pore water pressure in the near vicinity of the EPBM, extending about one tunnel diameter from the extrados. Although small degrees of heave were observed above the EPBM temporarily at the surface, the surface and underlying made ground and alluvium generally experienced downward displacements with little vertical straining. The mass settlement of made ground and alluvium layers in conjunction with the upward heave in the London Clay and overlying Terrace Gravels implies that considerable vertical compressive strains occurred within these latter strata. It was also observed that the magnitudes of surface settlements were small for the EPBM tunnelling as compared with those reported for open-face shield tunnelling. They identified the face pressure and tail-skin grouting pressure as factors influencing the ground response. The maximum long-term vertical

displacement of about 16 mm which was essentially complete within a year at the Channel Tunnel Rail Link (CTRL) site was attributed to the A2 unit of London Clay (which is the lowest geological unit of the London Clay Formation) and the relatively impermeable (grouted) lining. Although the surface settlement troughs observed above the tunnels were small and can be modelled using the commonly adopted inverse Gaussian curve, adjustments to the formulation were necessary for the case where heave occurred at the ends of the settlement trough (maybe caused by the concrete slab). In addition, potential asymmetry of the second settlement trough due to the construction of the second tunnel close to the first tunnel also needs to be taken into account. It was also pointed out that the subsurface vertical displacements are generally well predicted using the approach suggested by Mair et al. (1993), but this would not be appropriate for the complex system of heaving and settling subsurface displacements observed with this EPBM case study.

3.6 Summary

A review of published literature in the previous sections reveals that very limited studies have been performed to develop a general method to predict the ground surface settlement induced by closely spaced tunnelling through specific geological setting. It would be useful to develop a method which facilitates rapid estimation of the settlement parameters for field measurements and numerical results. Once a numerical model is calibrated and important factors affecting the magnitude and extent of ground surface settlement trough are identified, empirical equations may be developed with the aim of achieving unification of the bases for predicting the ground surface settlement induced by closely spaced tunnels constructed through specific geological setting. As confidence is gained in the effectiveness of the predictive model, there is the potential for many more empirical equations to be developed for different geological settings based on the adopted methodology.

For interaction between closely spaced tunnels, a narrow range of soil and lining properties was adopted in the past studies. Moreover, some of the previous works were carried out without taking into consideration the effects of volume loss.

Consequently, the range of application of those results for field interpretation is very limited. Furthermore, the interaction effects for cases without considering the volume loss are likely to be underestimated. Hence, it is also the main purpose of the present research to investigate the interaction between two closely spaced bored tunnels that focus on the important parameters that might contribute significantly to the generation of excessive stresses and deformation in the pre-existing tunnel. These parameters include a wide variation of tunnel geometric parameters, soil and lining deformations properties and volume loss.

CHAPTER 4 CIRCLE LINE PROJECT: CONTRACT 856

4.1 Project Background

Circle Line Contract 856 (Stage 5)

The Contract 856 of Circle Line Stage 5 (Figures 4.1 and 4.2) covers construction of the bored tunnel section joining the eastern ventilation shaft (VS) located at the east of Habour Front (HBF) Station with Telok Belangah (TLB), Labrador Park (LBD), Pasir Panjang Cripple Siding (PCS), Pasir Panjang (PPJ) Stations and terminates at West Coast (WCT), i.e. Haw Par Villa Station. There are a total of 10 cross passages constructed using NATM method connecting both inner and outer bound bored tunnels. The total length of East and West Drives is about 5.6 km and the bored tunnelling is divided into 3 EPBM drives as described below:

East Drive

The first outer bound bored tunnelling from Pasir Panjang Cripple Siding to Labrador Park, Telok Belangah and HXO (EPBM East Drive 1) commenced on June 2007, a month slightly earlier than the inner bound bored tunnelling from Pasir Panjang Cripple Siding to HXO (EPBM East Drive 3) and was completed on May and April 2008, respectively. Subsequently, the outer bound bored tunnelling continued its operation from HXO to Harbour Front before terminating at the eastern ventilation shaft.

West Drive

The first inner bound bored tunnelling from Pasir Panjang Cripple Siding to Pasir Panjang and subsequently West Coast commenced on March 2007 and completed its operation on November 2007. The same EPBM Shield was transferred for outer bound bored tunnelling which commenced on January 2008 and terminated on October 2008.

The subsurface conditions along the Contract 856 of Circle Line Stage 5 can be classified into the four major layers consisting of Fill, Kallang Formation, residual

soil and completely weathered rocks of Jurong Formation (SVI and SV) and sedimentary rocks of Jurong Formation (SIV, SIII, SII and SI). They are described in Section 4.4. The engineering geology of Singapore is described in detail in Sharma et al (1999).

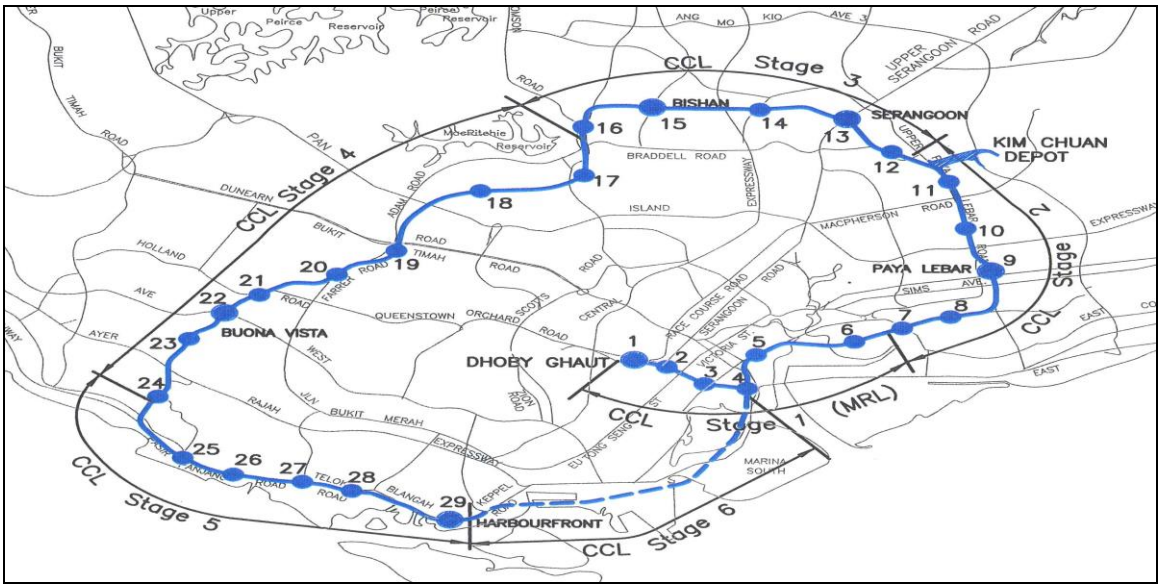

Figure 4.1 Illustration of the Circle Line (CCL) of Singapore

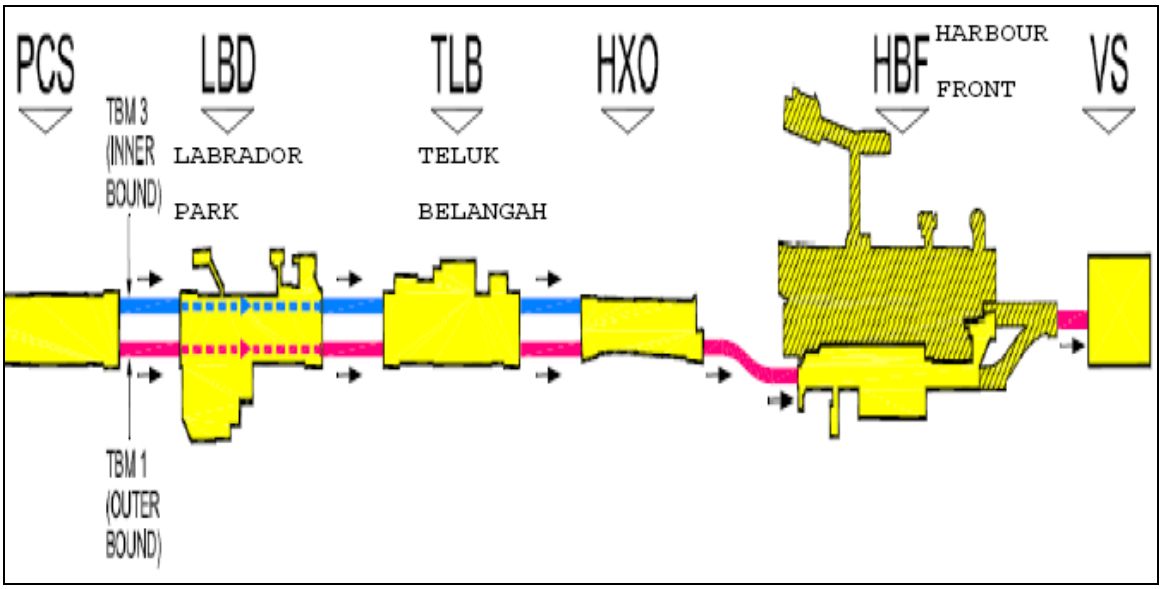

(a)

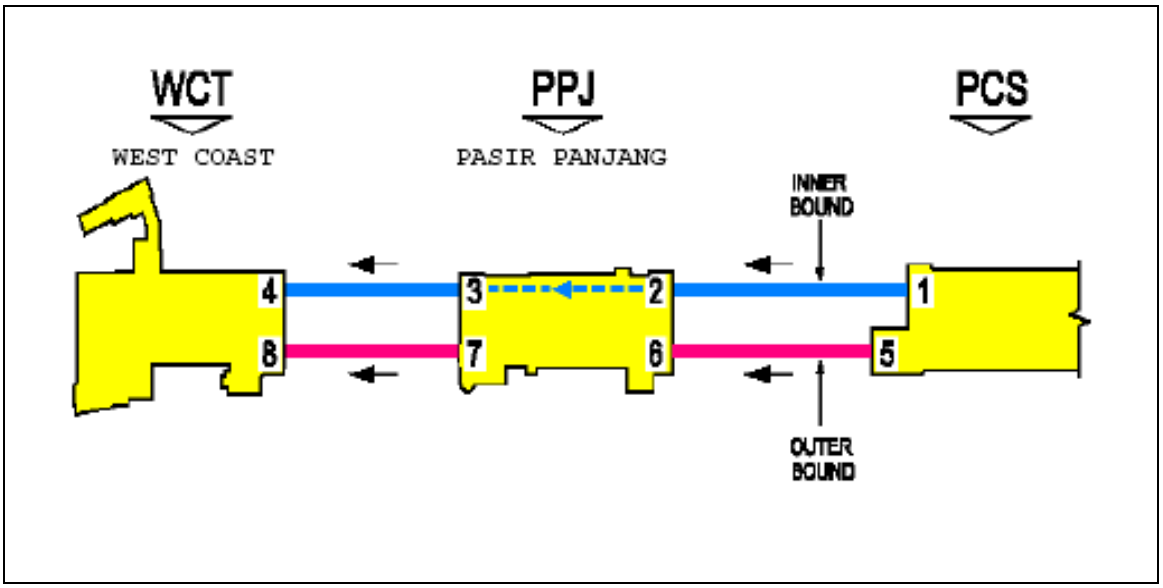

(b)

Figure 4.2 Bored tunnelling for Circle Line Contract 856 (a) Ventilation Shaft (VS) to Pasir Panjang Cripple Siding (PCS); and (b) Pasir Panjang Cripple Siding (PCS) to West Coast (WCT)

4.2 Construction Method of Bored Tunnels

The tunnel was constructed using Earth Pressure Balance Machine (EPBM), as shown in Figure 4.3, at approximately 30 m below the ground surface. The length of the shield is approximately 7900 mm. The outer diameter of the shield is 6600 mm, whereas the cutting wheel has a larger diameter of 6630 mm. The essence of EPBM operation is to have a mixture of soil and water in the excavation chamber under pressure, and to extract it via the screw conveyor. The spoil is then discharged from the end of the screw conveyor on to a conveyor belt. The specification of segmental lining and EPBM is illustrated in Table 4.1.

The segments were erected inside the tailskin of the machine at the position illustrated in Figure 4.4(a). The primary lining consists of 5 precast concrete segments with 1 key segment cover at an angle of 67.5^{o} and 22.5^{o}, respectively, as shown in Figure 4.4(b). The segment is 1400 mm in length and 275 mm thick. The final erected tunnel lining has an inner diameter of 5800 mm. As the machine was

jacked forward off the most recently completed tunnel lining, primary grouting was injected through the tailskin to fill the tail void between the outer diameter of the tunnel lining and the surrounded ground. In addition, secondary grouting may be injected if it is deemed required by the ground condition encountered.

Figure 4.3 Illustration of Earth Pressure Balance Machine (EPBM)

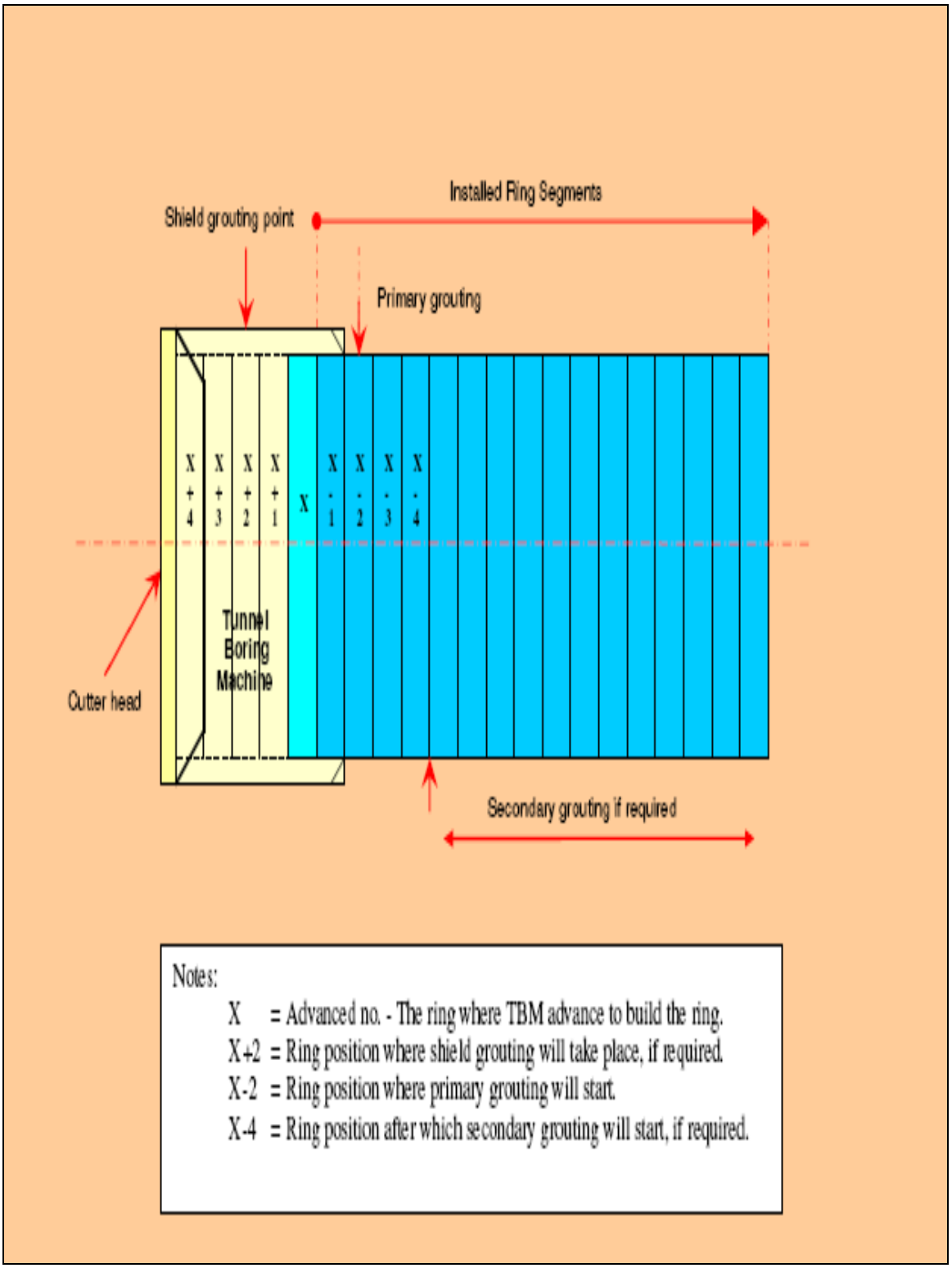
Installed Ring Segments
Shield grouting point
Primary grouting
X+4
X+3
X+2
X+1
X
X-1
X-2
X-3
X-4
Tunnel Boring Machine
Cutter head
Secondary grouting if required
Notes:
X = Advanced no. - The ring where TBM advance to build the ring.
X+2 = Ring position where shield grouting will take place, if required.
X-2 = Ring position where primary grouting will start.
X-4 = Ring position after which secondary grouting will start, if required.

(a)

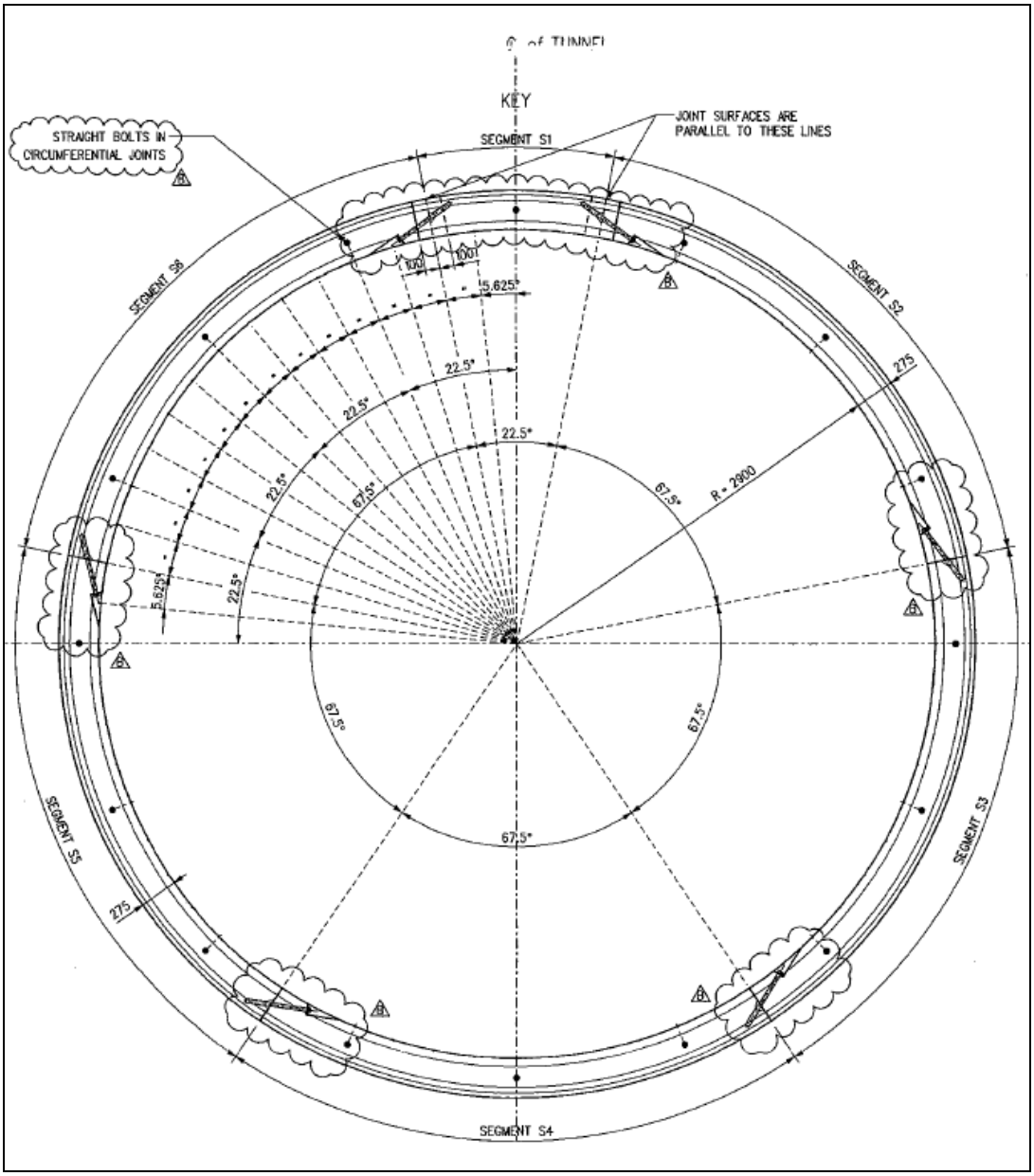

(b)

Figure 4.4 Illustrations of (a) installation position of segmental linings and grouting positions; and (b) dimension of precast concrete segmental lining

Table 4.1 Specification of precast segmental linings and EPBM

Description	Specification
General	
Ring division	5 + key (1x22.5^{o} + 5x67.5^{o})
Segment outer diameter (mm)	6350
Segment inner diameter (mm)	5800
Segment length (m)	1.4
TBM Dimensions	
Length of shield machine (m)	Approximately 7.85
Length of tunnelling equipment (m)	Approximately 70
Cutting Wheel	
Type	Closed type (opening rate 26%)
Diameter (mm)	6630
Direction of rotation	Left and right (two direction for excavation)
Cutting tools	32 single disc cutter 17”
	1 overcutter
	4 twin disc cutters 17”
	72 scrapers
	8 bucket lips
	8 material openings
Number of injection points	5 No. (for foam)
Wear detection device	For 4 scrapers tool
Rotary Union	1 No. (5 lines for foam and 2 lines for hydraulic pipes)
Shield	
Shield type	EPB
Nominal diameter front shield (mm)	6600 (without hardfacing)
Shield length (mm)	Approximately 7900
Operating pressure	4 bar
Earth pressure pick-ups	6 No.
Connecting flange for man lock	1 No. (double lock)
Compressed air regulation device	1 No.
Valves for ventilation pipes	2 No. (in the bulkhead)
Connecting flange for screw conveyor	1 No.
Front gate for the screw conveyor	1 No. (close automatically by power failure)
Pressure wall door	1 No. (600mm)
Probe drilling lines	6 x inclined and 2 x horizontal

Table 4.1 Continued	
Stabilizators	2 No. (Force 540kN or 350 bar per unit)
Dewatering pump	Provided by the job site
Tailskin	
Type	Passive articulation
Diameter (mm)	6580 (end of tailskin)
Seal	3 row wire brush sealing
Spring plates	1 row (bolted at the end of tailskin, 360^{o})
Line of mastic injection	4 x 2No. (ND 25mm)
Line of grout injection	4 No. (ND 50mm single type)
Length (mm)	Approximately 3900
Screw Conveyor	
Type	Screw spiral with shaft (1/2 of the screw front part is wear protected)
Length (mm)	Approximately 11000
Casing	Rotative type
Diameter (mm)	900
Electrical power	315kW
Nominal torque	225kNm
Speed	0 to 22rpm (infinitely adjustable)
Maximum capacity (theoretical)	100% filling
Telescopic stroke (mm)	1000
Discharge gate	1 No. (test pressure 4.5 bar)

4.3 Geotechnical Instrumentation: Ground Surface Settlement Marker

The ground surface settlement markers are installed to monitor surface settlement or heaving of structures and ground. Figures 4.5(a) and (b) illustrate details of the ground surface settlement markers installed on the turf and concrete surfaces, respectively. For installation of ground surface settlement marker on the proposed turf surface, a pit of specified dimension is dug and filled up with cement mortar to form a cement mortar block in the ground. A steel rod with convex top is then installed into the middle of the cement mortar block. For ground surface settlement marker installed on the proposed concrete surface, a hole of specified dimension is

drilled on the proposed location prior to the hole being filled up with cement grout and a stainless steel pin with a plastic grommet is installed on the pavement.

The ground surface settlement markers were placed in arrays at fixed intervals along the ground, as illustrated in Figure 4.6, to provide information on the ground level profile during tunnelling. During measurement, a fixed benchmark is obtained from the Main Contractor prior to the initial reading. The level of all the ground surface settlement markers is subsequently taken using levelling instrument, where all readings including the initial reading were referenced to the pre-agreed benchmark.

The daily monitoring was conducted when the EPBM was at 25 m before as well as after the monitoring point. This monitoring range seems to be in line with the field observations reported by Xu et al. (2003) where their results of cone penetrometer resistance test showed an increase in the earth pressure and pore water pressure at shield distance of about 25 m before the measured section and the effect of stress disturbance diminishes at shield distance of about 50 m after the measured section. The monitoring frequency of ground surface settlement was, however, reduced to thrice a week between 50 m to 300 m behind the EPBM. Weekly monitoring was performed when the EPBM was at distance of greater than 300 m after the monitoring point.

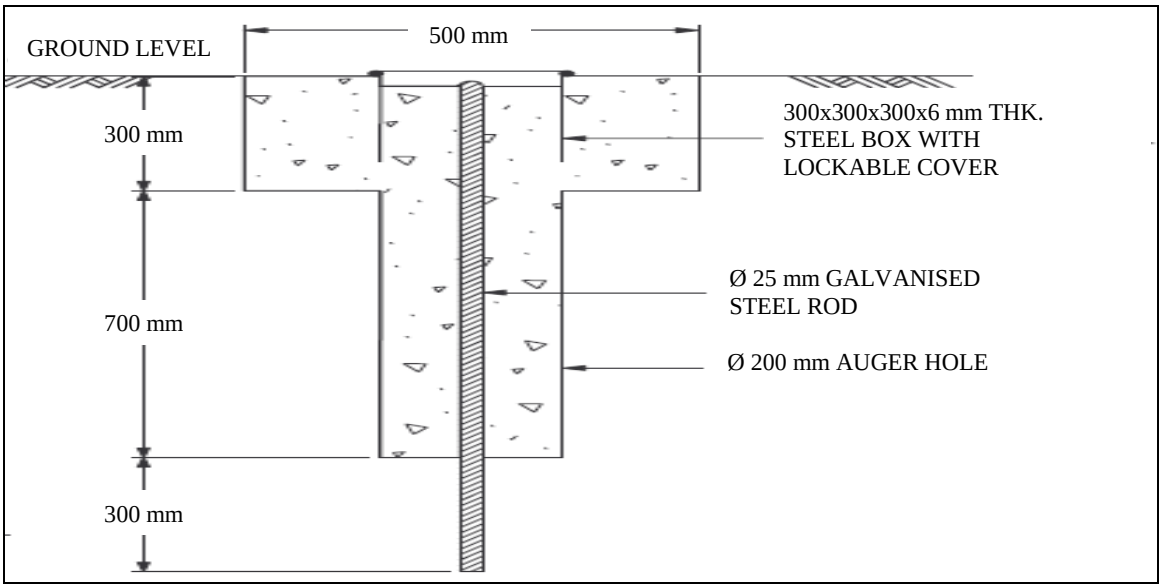

(a)

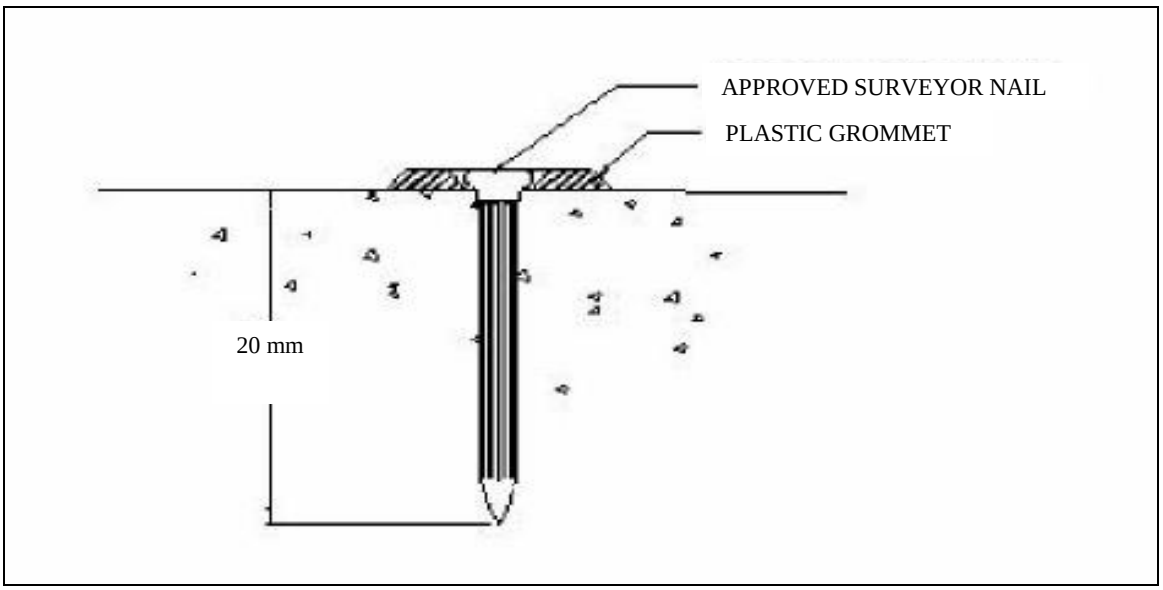

(b)

Figure 4.5 Typical details of ground surface settlement marker on (a) turf surface; and (b) concrete surface

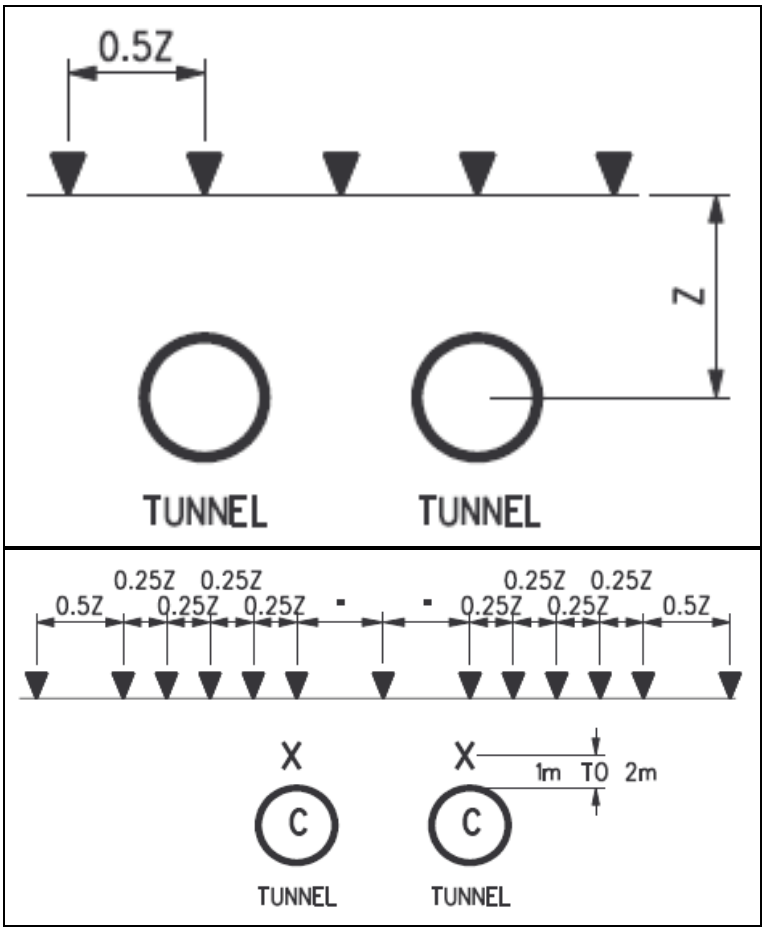

Figure 4.6 Illustration of two different types of monitoring array of ground surface settlement markers installed above bored tunnels

4.4 Ground Characterisation

The subsurface ground conditions have a large influence on the ground movements due to tunnelling. The geological profiles and geotechnical properties of the ground encountered along the alignment of the Circle Line Contract 856 were reported based on soil investigations, in-situ and laboratory tests conducted by the Land Transport Authority (LTA) and the Contractor. Detailed geological profiles and geotechnical properties of various soils and rock types are presented in this chapter.

The tunnel alignment along the Contract 856 of the Circle Line mainly encountered the sedimentary Jurong Formation. Along the East Drive from Pasir Panjang Cripple Siding to eastern ventilation shaft, ground conditions at the tunnel level

predominantly comprise various weathering grades of Jurong Formation, with Kallang Formation intermittently overlying the Jurong Formation. However, mixed face ground of Kallang Formation and Jurong Formation was encountered at some sections along the West Drive from Pasir Panjang Cripple Siding to Pasir Panjang Station. In the remaining section of West Drive from Pasir Panjang Station to West Coast Station, regular ground conditions consisting of Jurong Formation was encountered at tunnel level, with occasionally mixed face condition of various weathering grades of Jurong Formation due to irregular thickness of residual soil and competent rock.

4.4.1 Geological Description of Jurong Formation

The sedimentary rocks of the Jurong Formation consist of sandstones, siltstones, mudstones, conglomerate and limestone that have been subjected to varying degrees of metamorphism. The formation has been severely folded and faulted in the past due to tectonic movements. Table 4.2 illustrates the weathering grade classification for Jurong Formation encountered along the tunnel alignments of the Circle Line Contract 856.

Table 4.2 Description and classification of Jurong Formation (BS 5930:1999 Section 6 Approach 2)

Grade	Classification	Basis for assessment
I	Fresh	Intact strength, unaffected by weathering
II	Slightly weathered	Slightly weakened, slight discolouration, particularly along joint
III	Moderately weathered	Considerably weakened and discoloured, but larger pieces cannot be broken by hand. (RQD is generally > 0, but RQD should not be used as the major criterion for assessment.)
IV	Highly weathered	Core can be broken by hand or consists of gravel size pieces. Generally highly to very highly fractured, but majority of sample consists of lithorelics. (RQD generally = 0, but RQD should not be used as the major guide for assessment). For siltstone, shale, sandstone,

		quartzite and conglomerate, the slake test can be used to differentiate between Grade V (slakes) and Grade IV (does not slake).
V	Completely weathered	Rock weathered down to soil-like material, but bedding intact. Material slakes in water.
VI	Residual soil	Rock degraded to soil in which none of the original bedding remains.

Residual Soil and Completely Weathered Rock (SVI and SV)

Due to weathering, the sedimentary rocks have decomposed into very stiff to hard cohesive soils which include mainly sandy clay and sandy silt as well as very dense coarse-grained soils of silty or clayey sand. The colours of the soils are generally reddish-yellowish brown, brownish yellow and light grey. The residual soil is generally hard or very dense in consistency with SPT N-value up to 100. They are also pockets of moderately weathered rock consists of mainly Sandstone observed in the midst of the residual soil due to its resistance to weathering.

Sedimentary Rocks (SIV to SI)

The highly to moderately weathered zone of sedimentary rocks SIII and SIV is normally found underlying the residual soil and zone of completely weathered rock. These zones mainly consist of bedded Sandstone, Siltstone and Limestone with localized Shale and Mudstone ranging from low strength to high strength. The colours of the rocks vary from greenish to dark grey, reddish purplish and brownish yellow.

The slightly weathered rock and fresh rock SII and SI consist of bedded Sandstone, Limestone, Siltstone and Conglomerate of moderately strength to very high strength with colours vary from greenish-bluish grey to dark grey, reddish purplish brown and mottled white.

4.4.2 Engineering Properties of Residual Soil and Sedimentary Rocks of Jurong Formation

The following summarises the results of site investigations carried out by LTA:

Residual Soil and Completely Weathered Rock (SVI and SV)

The average unit weight of residual soil γ and completely weathered rock (SVI and SV) is 20 kN/m^3. The undrained shear strength c_u estimated based on laboratory triaxial UU test was correlated with SPT N-value as 5N kPa. The initial and secant modulus of undrained compression was observed to increase with increasing SPT N-value. Although the test results proposed correlation of E_u = 0.5N MPa, this value was reported as too conservative and hence such correlation was revised as E_u = 2.0 MPa in accordance to LTA's design value. The suggested engineering properties and geotechnical correlations of residual soil and completely weathered rock of Jurong Formation are summarised in Table 4.3.

Sedimentary Rocks (SIV to SI)

The average unit weight of the sedimentary rocks SIV to SI was 22 kN/m^3. The upper bound, lower bound and average values of the uniaxial compressive strength for Sandstone and Siltstone were 50 MPa, 5 MPa, 20 MPa and 30 MPa, 5 MPa, 20 MPa respectively. Although both Sandstone and Siltstone of SI and SII showed similar upper bound effective cohesion c' of 200 kPa, it is generally expected that the c' for Siltstone of other weathering grades is lower than the Sandstone. The effective friction angle ϕ' for both Sandstone and Siltstone ranges from 38^o to 40^o and 30^o to 35^o respectively. A wide range of initial modulus versus depth was observed for Sandstone and Siltstone. Based on the limited test quantities, the range was generally found to fall within 200 MPa to less than 1000 MPa. The suggested engineering properties of sedimentary rocks SIV to SI are summarised in Table 4.4.

Table 4.3 Engineering properties of residual soil and completely weathered rock of Jurong Formation (SVI and SV) (CPG Consultants Pte. Ltd., 2005)

Type of Materials		**Unit Weight, γ (kN/m^3)**	**SPT N-Value**	**Strength Parameters**			**Modulus of Elasticity, E_u (MPa)**	**Coefficient of Earth Pressure at Rest, K_o**
				Total Stress	**Effective Stress**			
				c_u (kPa)	**c' (kPa)**	**ϕ' (^{o})**		
Jurong Formation S(V) & S(VI)	SPT N<15	20	0~100	5N	5 (clayey) 0 (sandy)	28 (clayey) 32 (sandy)	2.0 N	0.8
	15=<N<30				10 (clayey) 2 (sandy)	28 (clayey) 33 (sandy)		
	30=<N<50				15 (clayey) 5 (sandy)	28 (clayey) 33 (sandy)		
	50=<N<100				15 (clayey) 15 (sandy)	30 (clayey) 34 (sandy)		

Table 4.4 Engineering properties of sedimentary rocks of Jurong Formation (SI to SIV) (CPG Consultants Pte. Ltd., 2005)

Type of Rock		**Unconfined Compressive Strength for Intact Rock (MPa)**	**Unconfined Compressive Strength for Rock Mass (MPa)**	**Modulus of Elasticity, E_u (MPa)**	**Total Stress**	**Effective Stress**	
					c_u (kPa)	**c' (kPa)**	**ϕ' (^{o})**
Sandstone	S(IV)	3 - 30	0.5	1000	2500	40	38
	S(III)	5 - 55	1.5	2000	15000	200	38
	S(II), S(I)	15 - 80	5.0	3000	25000	200	40
Siltstone	S(IV)	12 - 40	0.2	500	1000	20	30
	S(III)	2 - 22	0.5	1000	7500	100	35
	S(II), S(I)	2 - 65	5.0	2000	15000	200	35
Shale	S(IV)	No data available	0.05	200	500	10	30
	S(III)	6 - 32	0.1	300	2000	20	30
	S(II), S(I)	No data available	1.0	600	5000	50	30
Limestone	S(IV)	30	No data available	No data available	4000	50 (Kulhawy and Goodman, 1987)	34 (Wyllie, 1991)
	S(III)	30 - 100			20000		
	S(II), S(I)	70			35000		

4.4.3 Geological Descriptions of Fill and Kallang Formation

Fill

The Fill consists of made deposits of natural earth materials. The thickness of the Fill may vary from 0.5 m to about 10 m. The backfill generally consists of heterogeneous soils frequently mixed with gravels, granite aggregates, rock fragments, bricks, concrete pieces, wood pieces, organic materials and other foreign materials.

Kallang Formation

The Kallang Formation consists of different members including Marine Clay, Estuarine and Fluvial Sediments as described below:

Marine Clay

The consistency of the Marine Clay is generally very soft to medium stiff. The colours of the soil are generally bluish grey and light grey. The soil generally contains shell fragments and traces of peat.

Estuarine

The Estuarine layer consists of soft to very soft peaty clay and peat with partially decomposed wood, vegetation and traces of sand. The colours range from grey, dark grey to black.

Fluvial Sand

The Fluvial Sand consists of gravelly, silty, clayey, fine to coarse grained sand with occasional traces of organic matter and decomposed wood. The colours of soil are generally light brown, whitish grey, grey, reddish brown and yellowish brown. The relative density of the soil generally varies from very loose to medium dense.

Fluvial Clay

The Fluvial Clay predominantly consists of very soft to stiff silty, sandy clay and sandy silt with occasionally decomposed wood, vegetation and organic matter.

4.4.4 Engineering Properties of Fill and Kallang Formation

Fill

The Fill material has an average unit weight γ of 19 kN/m^3. The SPT N-value at depth of less than 6 m can be up to about 25. At the same depth, the undrained shear strength c_u varies from about 10 kPa to 50 kPa. As Fill generally consists of heterogeneous soils of granular and cohesive types, a single set of effective shear strength parameters c' and ϕ' of 0 kPa and 28^o as well as undrained elastic modulus E_u of 10000 kPa are adopted as design values.

Marine Clay

The Marine Clay has an average unit weight γ of 16 kN/m^3. The SPT N-value ranges from 0 to about 10. The undrained shear strength c_u obtained based on field vane test and laboratory triaxial UU test are generally found to vary from 20 kPa to 50 kPa at depths between 5 m to 10 m. The effective shear strength parameters c' and ϕ' are 0 kPa and 22^o whereas the undrained elastic modulus E_u is correlated as $0.2c_u$ MPa.

Estuarine

The Estuarine has an average unit weight γ of 15 kN/m^3. Similar SPT N-value as Marine Clay was encountered for Estuarine which generally fall within the range of 0 to about 10. The undrained shear strength c_u estimated based on laboratory triaxial UU test was found to vary from 10 kPa to 40 kPa for samples collected at depths between 4 m to 7 m. The effective shear strength parameters c' and ϕ' are determined as 0 kPa and 24^o respectively. A smaller undrained elastic modulus E_u of $0.15c_u$ MPa is adopted as compared to Marine Clay.

Fluvial Sand

The Fluvial Sand has an average unit weight γ of 20 kN/m^3. The SPT N-value at depths between 3 m to 15 m ranges from about 0 to 15. The effective shear strength parameters c' and ϕ' were determined as 0 kPa and 30^o respectively. The undrained elastic modulus E_u is correlated with SPT N-value as 2N MPa.

Fluvial Clay

The average unit weight γ for Fluvial Clay is 19 kN/m^3. The SPT N-value at depths between 3 m to 15 m ranges from 0 to 15. The undrained shear strength c_u estimated based on laboratory triaxial UU test indicated the value ranges from 10 kPa to about 50 kPa. The effective shear strength parameters c' and ϕ' are 0 kPa and 27^o respectively. The undrained elastic modulus E_u is correlated as $0.3c_u$ MPa.

The suggested engineering properties of Fill and Kallang Formation are summarised in Table 4.5.

Table 4.5 Engineering properties of Fill and Kallang Formation (CPG Consultants Pte. Ltd., 2005)

Type of Materials	**Unit Weight, γ (kN/m^3)**	**SPT N-Value**	**Strength Parameters**			**Modulus of Elasticity, E_u (MPa)**	**Coefficient of Earth Pressure at Rest, K_o**
			Total Stress	**Effective Stress**			
			c_u (kPa)	**c' (kPa)**	**ϕ' (^{o})**		
Fill	19	0 - 24	20	0	28	10	0.5
Marine Clay	16	0 - 7	10 (z=<4.5m) 25 (4.5<z<8.0m) 35 (z>7.5m)	0	22	0.2 c_u	1.0
Estuarine	15	0 - 7	20 (z=<7.5m) 30 (z>7.5m)	0	24	0.15 c_u	1.0
Fluvial Sand	20	2 - 15	-	0	30	2.0 N	0.7
Fluvial Clay	19	0 - 15	4N	0	27	0.3 c_u	1.0

4.5 Summary

The Circle Line Contract 856 comprised construction of west bored tunnel drives from Pasir Panjang Cripple Siding (PCS) to West Coast (WCT) and east bored tunnel drives from Pasir Panjang Cripple Siding (PCS) to ventilation shaft (VS), which is located at the east of Harbour Front (HBF). The length of the tunnel alignments is about 5.6 km. Along the tunnel alignments, ground surface settlement markers were installed prior to the tunnel construction. Monitoring of ground surface settlement was performed before, during and after EPBM tunnelling.

During EPBM driving, the face pressures, recommended compressed air pressures for interventions into the cutter head and pressures for tail void grout injection system were continuously reviewed based on actual ground conditions encountered and interpretation of monitoring data. The specification of EPBM is shown in Table 4.1.

The geological conditions along the tunnel alignments were broadly classified into Fill, Kallang Formation and Jurong Formation. Fill was observed close to the ground surface in most of the areas along the tunnel alignments. The soil types of Kallang Formation encountered along the tunnel alignments consisted of Marine Clay, Estuarine, Fluvial Sand and Fluvial Clay. The Jurong Formation encountered along the tunnel alignments was grouped into residual soil of SVI, completely weathered rock of SV, highly weathered rock of SIV and moderately weathered rock of SIII. The suggested empirical correlations and engineering properties of Jurong Formation and Kallang Formation are presented in Tables 4.3, 4.4 and 4.5.

CHAPTER 5 FIELD PERFORMANCE OF BORED TUNNELLING THROUGH JURONG FORMATION AND MIXED GROUND OF JURONG FORMATION AND KALLANG FORMATION

5.1 Introduction

As described in Chapter 4, the general geology along the tunnel alignments joining the West Coast Station and ventilation shaft at the east of Harbour Front Station comprises two dominant geological formations. The geological profiles encountered varied from very soft Marine Clay and Fluvial Sediments of Kallang Formation overlying the stiffer and harder Jurong Formation to relatively homogeneous Jurong Formation. The Jurong Formation can be further classified into six weathering classifications ranging from slightly weathered rock and fresh rock (SII and SI) to completely weathered rock and residual soil (SV and SVI), as illustrated in Chapter 4. At tunnel level, mixed-face ground condition consisting of various members of Kallang Formation and Jurong Formation is present at some tunnelling sections. A total of 13 cases were considered. A summary of the ground conditions encountered at the 13 selected ground surface settlement monitoring arrays is presented in Table 5.1. The longitudinal ground surface settlements above the first and second bored tunnels for each of the 13 cases are discussed in this chapter. The transverse surface settlements are presented and discussed in Chapter 6.

Table 5.1 Summary of ground conditions along selected ground surface settlement monitoring arrays

Ground Conditions	First Bored Tunnel	Second Bored Tunnel	Selected Cases
Uniform grade of Jurong Formation (SV)	SV	SV	D35, E9, D34, D7
	Subtotal		4
Mixed grades of Jurong Formation (SIII, SIV and SV)	SIII-SIV-SV	SIII-SIV-SV	D38, D37
	Subtotal		2
	SIV-SV	SIV-SV	D33, D32
	Subtotal		2
Mixed ground of Jurong Formation (SIII, SIV, SV and SVI) and Kallang Formation (Fluvial Sand, Fluvial Clay and Marine Clay)	SIII-SIV-SV-SVI-Fluvial Sand-Marine Clay	SIII-SIV-SV-SVI-Fluvial Sand-Fluvial Clay	E14
	Subtotal		1
	SIII-SIV-SV-SVI	SIII-SV-Fluvial Sand-Fluvial Clay-Marine Clay	D49
	Subtotal		1
	SIV-SV-SVI-Fluvial Clay	SIV-SV-SVI-Fluvial Clay	D47, E10, D46
	Subtotal		3
Total			**13**

5.2 Measured Performance of Bored Tunnelling

As the Earth Pressure Balance Machine (EPBM) parameters are critically dependent on the type of ground, a total of 13 cases of field measurements of longitudinal ground surface settlements due to bored tunnelling through: (a) Uniform grade of Jurong Formation; (b) Mixed grades of Jurong Formation and; (c) Mixed ground of

Jurong Formation and Kallang Formation at the tunnel level are analysed in this section. By reasonably assuming greenfield condition where the effect due to the presence of adjacent buildings or structures on the ground surface settlement is ignored, the relationships between EPBM parameters and magnitude of longitudinal ground surface settlement are assessed.

5.2.1 Uniform Grade of Jurong Formation

Instrumentation Array D35

The location of Instrumentation Array D35 for monitoring ground surface settlements is shown in Figure 5.1. The longitudinal section profiles of Figures 5.2(a) and 5.2(b) summarise the geology along the tunnel alignments. The tunnels were mainly excavated through uniform grade of Jurong Formation (SV). The overlying materials consist of Fluvial Sand and Fill. The longitudinal ground surface settlement profiles corresponding to construction of both the first inner bound and the second outer bound bored tunnels are shown in Figure 5.3(a) and 5.3(b). The longitudinal ground surface settlement recorded by the two ground surface settlement markers of LG1199 and LG1197 installed above the first inner bound and second outer bound bored tunnels are discussed in detail below.

The EPBM on the first inner bound bored tunnel achieved an overall speed of about 50 mm/min. On reaching Array D35 on 01 August 2007, LG1199 started to record settlement of 2.6 mm as shown in Figure 5.3(a). The recorded EPBM earth pressures were from 0.67 bar to 1.76 bar. The assessment made on 02 August 2007 when the EPBM tailskin was beneath LG1199 indicated maximum ground surface settlement of the order of 5 mm. The grout was injected through grout holes in the segments at a volume of 3706 litres and the injection pressures varied between 1.4 bar to 2.2 bar. By the end of the monitoring period, a maximum settlement of up to 11.4 mm was recorded.

The results for the second outer bound bored tunnelling shown in Figure 5.3(b) give a different pattern of longitudinal surface settlement. In this case, virtually no settlement was recorded on early 23 September 2008 for LG1197 until the EPBM face was immediately beneath the monitoring point on 24 September 2008, where measured settlement was initially 7 mm, i.e. larger than the 2.6 mm experienced by the first inner bound bored tunnel and increased to 11 mm during passing of the EPBM tailskin. The EPBM passed LG1197 at a speed of about 36 mm/min. The earth pressure pick-ups in EPBM working chamber recorded 0.9 bar to 1.3 bar earth pressure, i.e. smaller earth pressure than the first inner bound bored tunnelling. This may be also partly attributed to the additional 4.4 mm settlement of the ground at the EPBM face. The grout injection pressure was in a range of 1 bar to 2 bar, with total grout volume of 4032 litres, indicating a comparable grouting pattern produced by first inner bound bored tunnelling. It should be noted that the completion of the grouting seems to have no discernible effect on the associated settlement profiles after 26 September 2008, i.e. no progressive settlement occurred. The settlement marker registered final ground settlement of 15 mm.

Refer to Figures A.1 to A.12 for more information about the EPBM speed, earth pressure and grouting episodes measured at 10 rings before and after the Instrumentation Array D35.

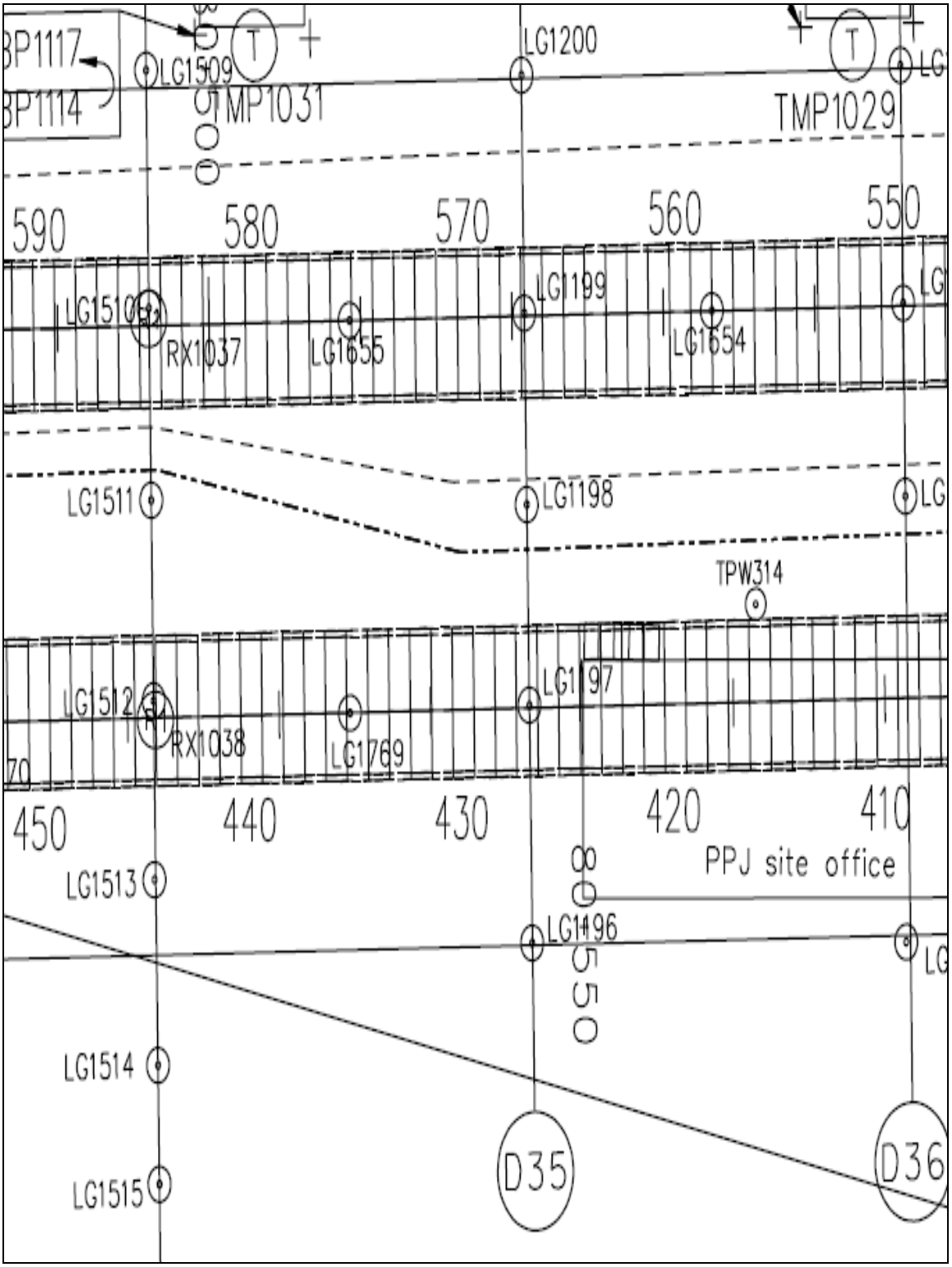

Figure 5.1 Ground surface settlement monitoring array D35

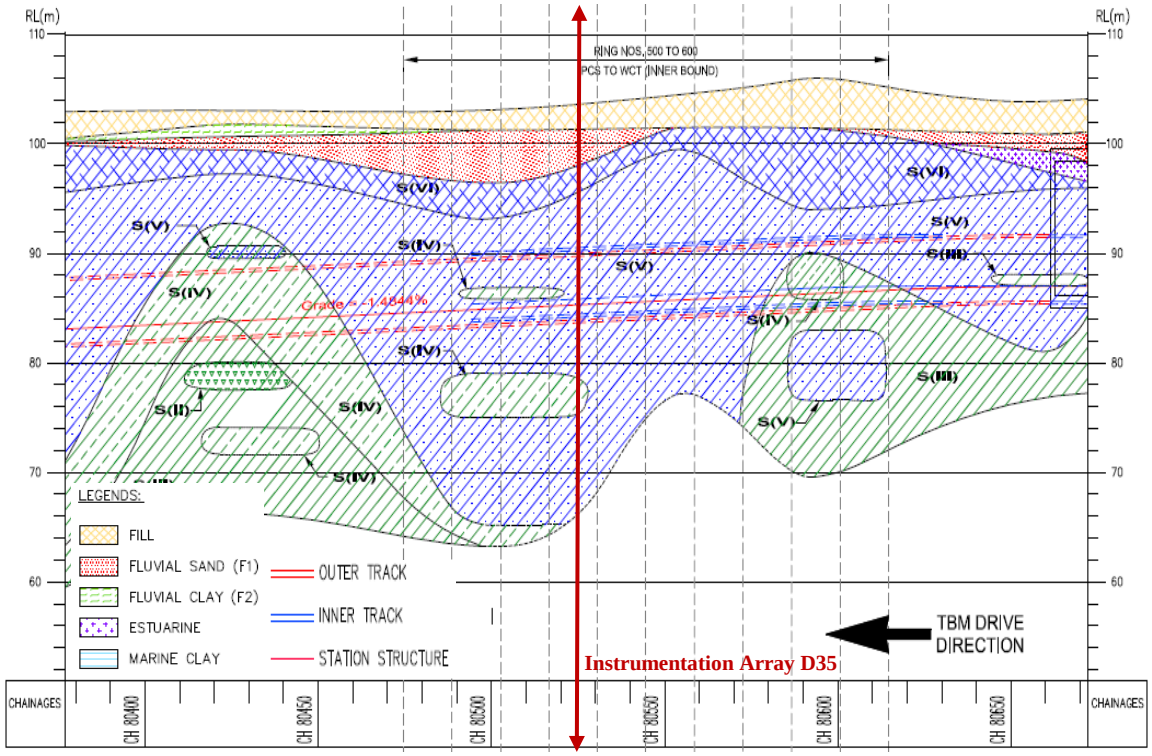

(a)

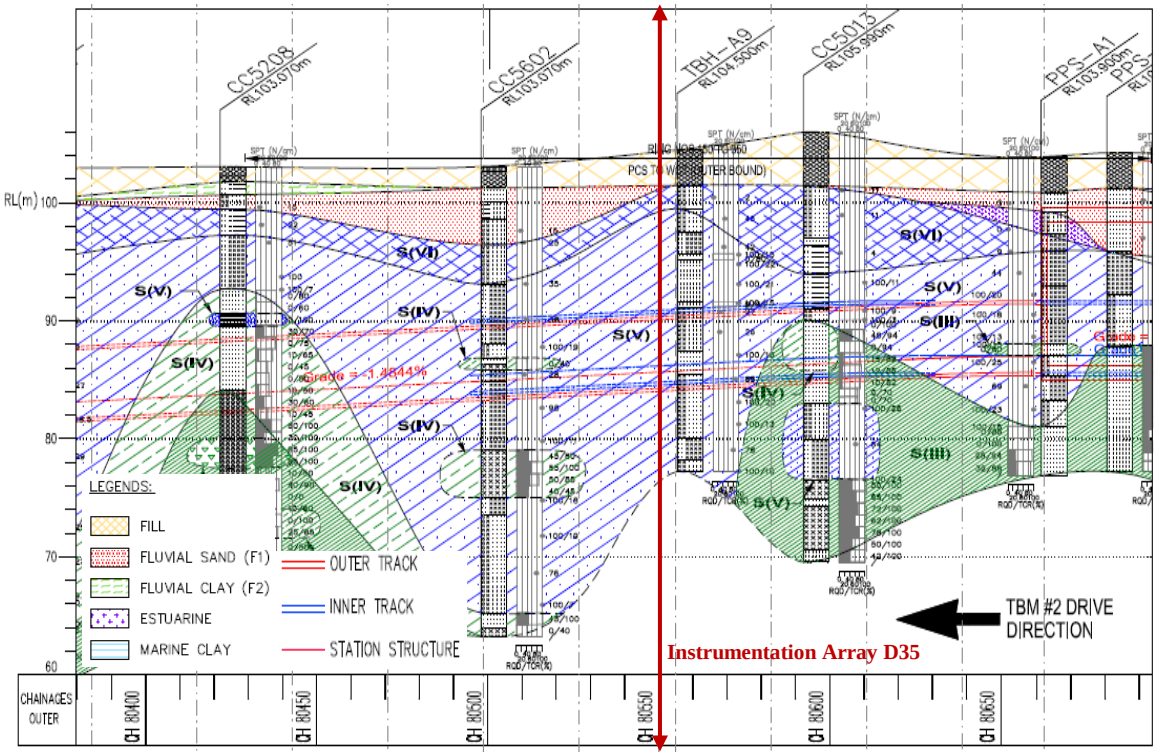

(b)

Figure 5.2 Ground conditions at tunnel level for (a) first inner bound bored tunnel; and (b) second outer bound bored tunnel (Instrumentation Array: D35)

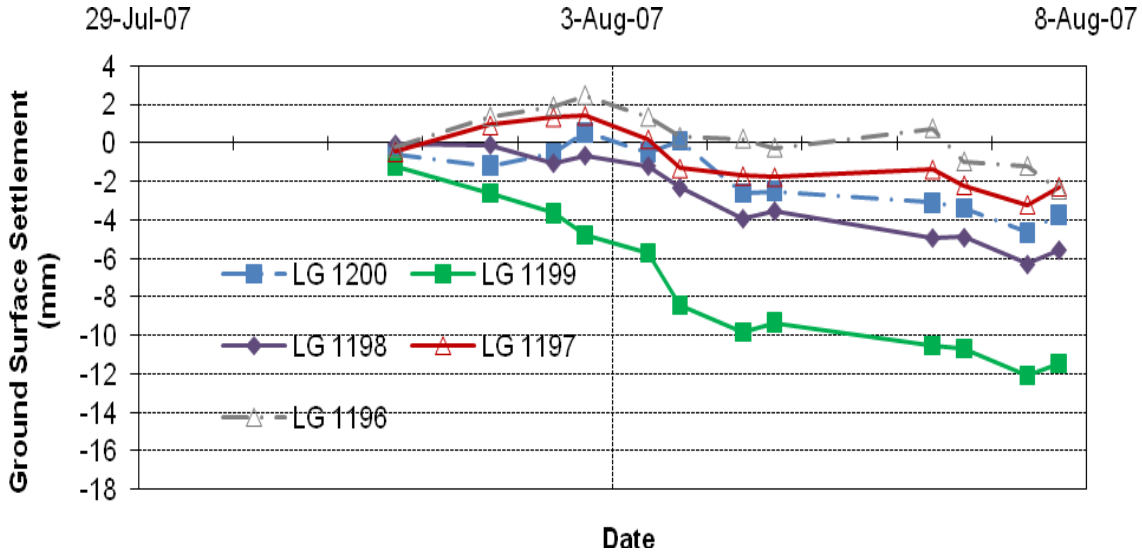

(a)

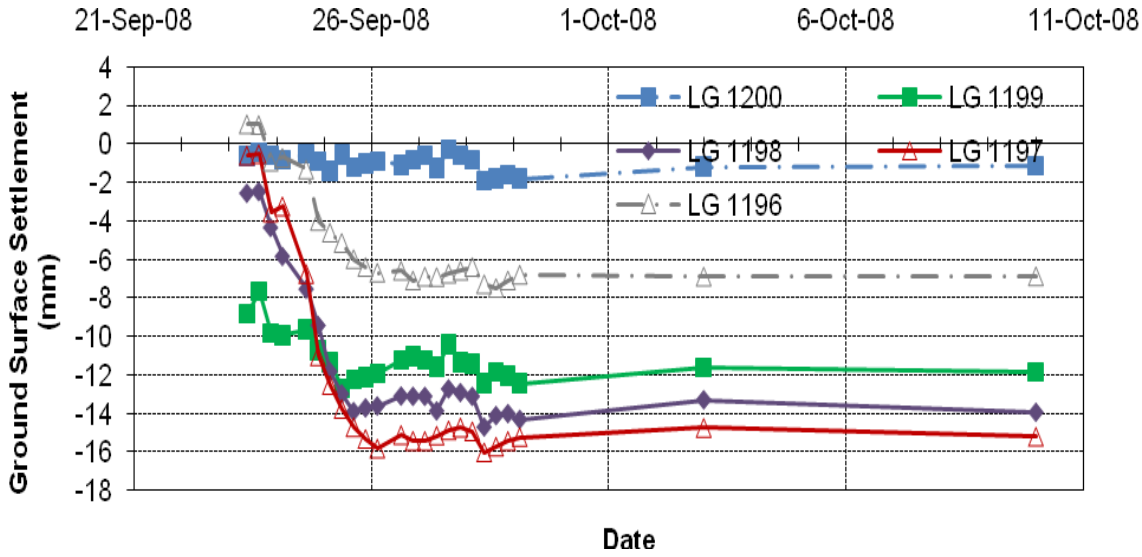

(b)

Figure 5.3 Longitudinal surface settlement profiles (a) after first inner bound bored tunnelling; and (b) after second outer bound bored tunnelling (Instrumentation Array: D35)

Instrumentation Array E9

The location of Instrumentation Array E9 for monitoring ground surface settlements is shown in Figure 5.4. The longitudinal section profiles of Figures 5.5(a) and 5.5(b) summarise the geology along the tunnel alignments. The tunnels were mainly

excavated through uniform grade of Jurong Formation (SV). The overlying materials consist of Fluvial Sand and Fill. The longitudinal ground surface settlement profiles corresponding to construction of both the first inner bound and the second outer bound bored tunnels are shown in Figure 5.6(a) and 5.6(b). The longitudinal ground surface settlement recorded by the two ground surface settlement markers of LG1510 and LG1512 installed above the first inner bound and second outer bound bored tunnels are discussed in detail below.

Examination of Figure A.18 in the Appendix shows that high earth pressure for the first inner bound bored tunnel in a range of 1.98 bar to 2.62 bar as indicated by earth pressure pick-up 5 was exerted when tunnelling between ring number 571 to 575, achieved at a decreasing EPBM speed of 39 mm/min to 34 mm/min. The implication of this is evident from the heave profiles with a maximum magnitude of 1.9 mm recorded by LG1510 on 02 August 2007 where the EPBM was at a distance of approximately 9.8 m (7 rings) to the Array E9. It should be pointed out, however, that other earth pressure pick-ups recorded lower earth pressure in a range of 0.54 bar to 1.5 bar. On 03 August 2007, when the EPBM approached LG1510 at a speed of 38 mm/min with lower earth pressure in a range of 1.49 bar to 1.62 bar, the heave had since settled to 0.9 mm and by the same date, 0.2 mm settlement was recorded. The passing of EPBM tailskin on 04 August 2007 induced maximum ground surface settlement of the order of 5 mm. The grout volume of 3546 litres was injected through grout holes in the segments and the injection pressures varied between 3.5 bar to 3.9 bar. By the end of the monitoring period, a maximum settlement of up to 6.4 mm was recorded. This further ground surface settlement could be due to the shrinkage of the grout.

The results for the second outer bound bored tunnelling give a different pattern of longitudinal surface settlement. In this case, virtually no heave or settlement was recorded on early 25 September 2008. When the EPBM face was immediately beneath the monitoring point LG1512 on the same date, the settlement marker registered 3 mm settlement taking into account the EPBM speed of 30 mm/min and earth pressure in a range of typically 1 bar to 1.76 bar, although substantial earth

pressure of 2.91 bar was experienced by earth pressure pick-up 4. The grout injection pressure was in a range of 1.3 bar to 2.2 bar with total grout volume of 3515 litres when the EPBM tailskin passed LG1512. The lower grout injection pressure could have led to larger maximum settlement of up to 12 mm. The ground surface settlement appeared to increase to 14 mm on 28 September 2007. There is clear evidence, however, that the secondary grouting has led to less settlement of the order of 12 mm after the date mentioned.

Refer to Figures A.13 to A.24 for more information about the EPBM speed, earth pressure and grouting episodes measured at 10 rings before and after the monitoring array.

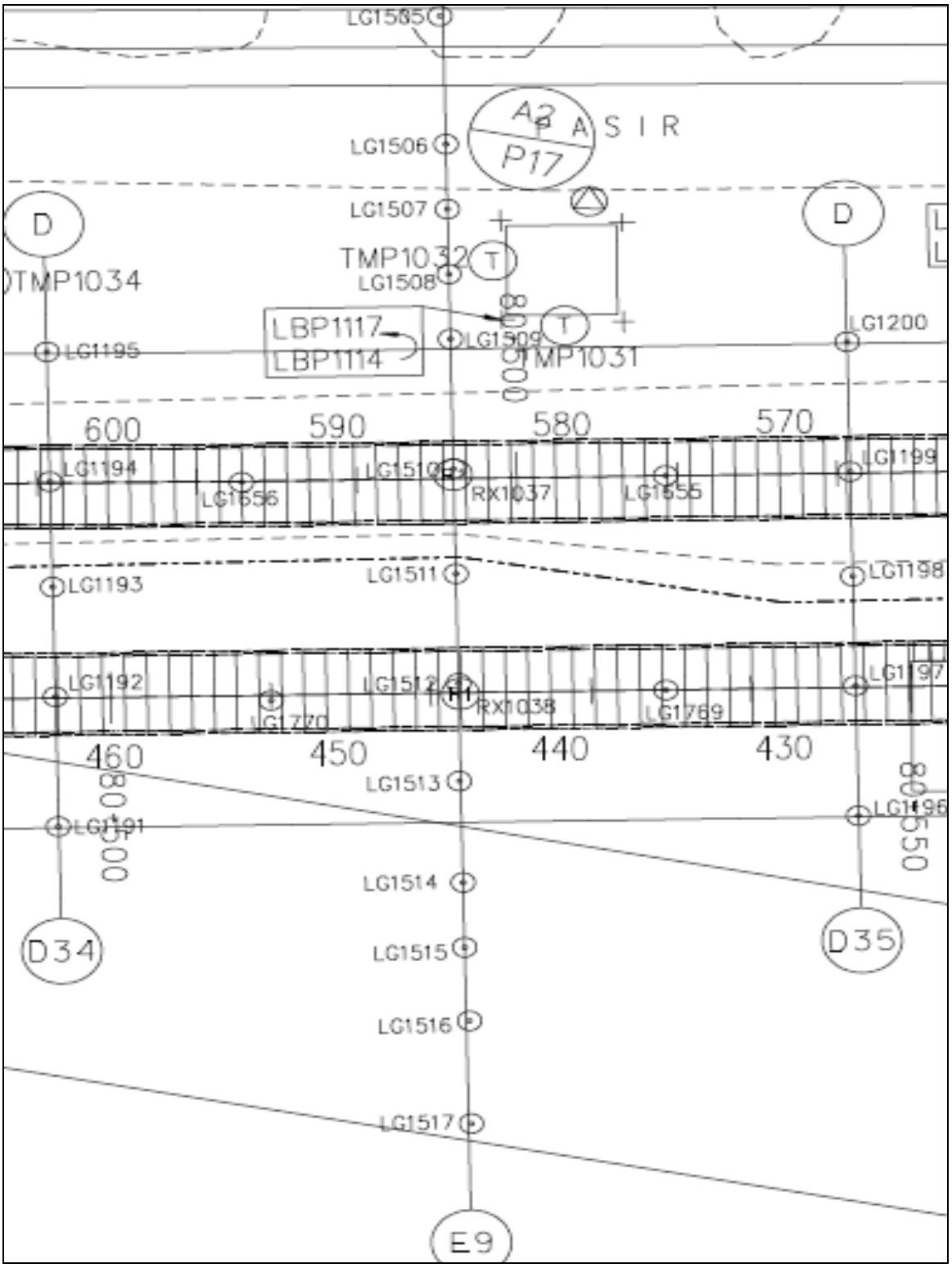

Figure 5.4 Ground surface settlement monitoring array E9

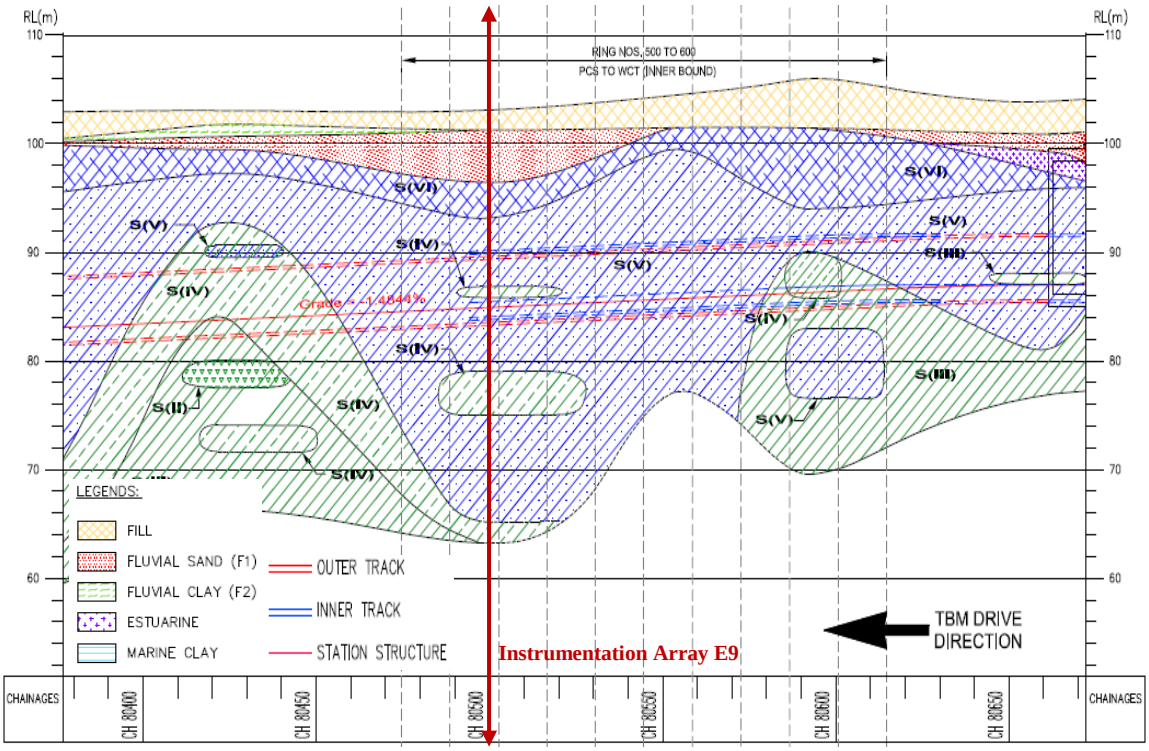

(a)

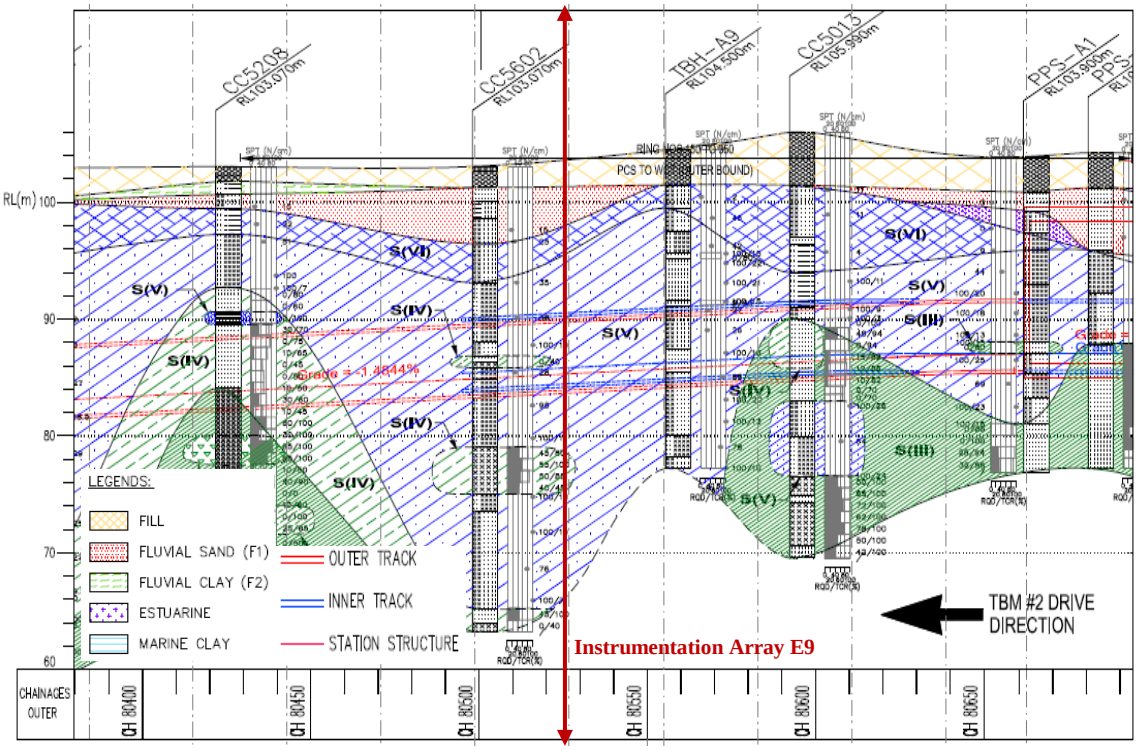

(b)

Figure 5.5 Ground conditions at tunnel level for (a) first inner bound bored tunnel; and (b) second outer bound bored tunnel (Instrumentation Array: E9)

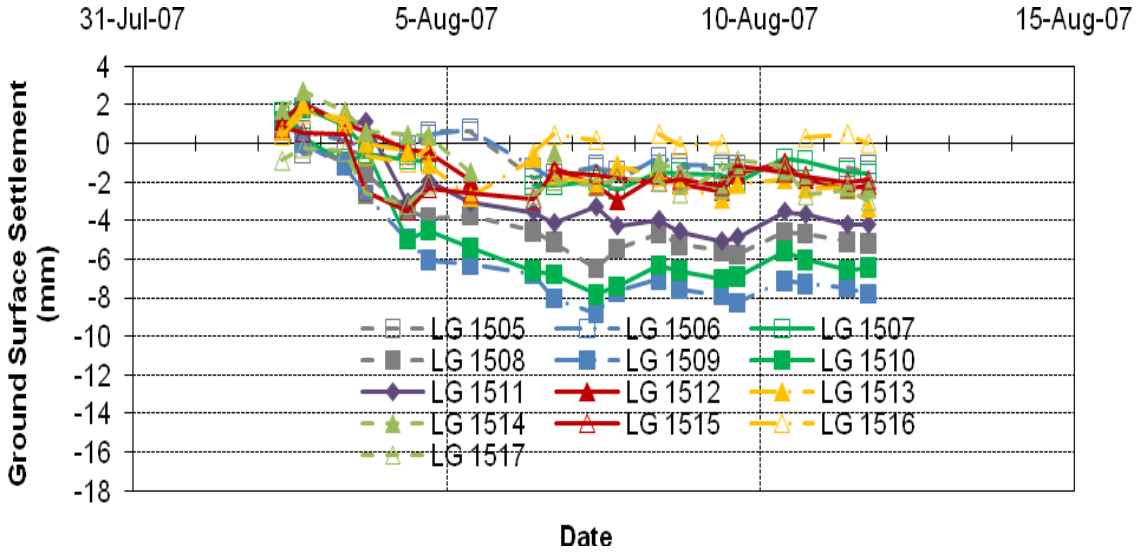

(a)

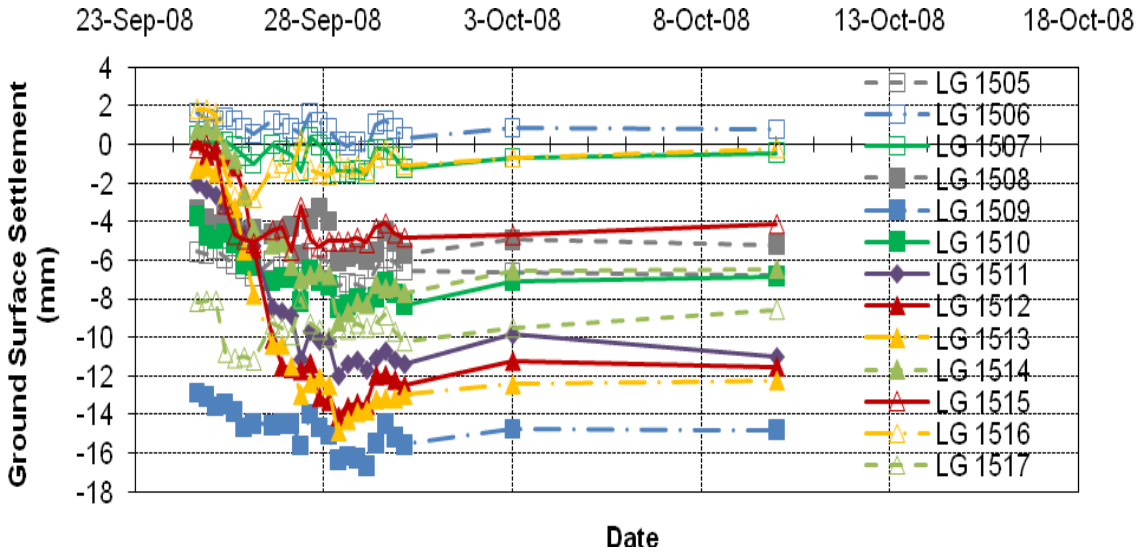

(b)

Figure 5.6 Longitudinal surface settlement profile (a) after first bored tunnelling; and (b) after second bored tunnelling (Instrumentation Array: E9)

Instrumentation Array D34

The location of Instrumentation Array D34 for monitoring ground surface settlements is shown in Figure 5.7. The longitudinal section profiles of Figures 5.8(a) and 5.8(b) summarise the geology along the tunnel alignments. The tunnels were mainly excavated through uniform grade of Jurong Formation (SV). The

overlying materials consist of Fluvial Sand and Fill. The longitudinal ground surface settlement profiles corresponding to construction of both the first inner bound and the second outer bound bored tunnels are shown in Figure 5.9(a) and 5.9(b). The longitudinal ground surface settlement recorded by the two ground surface settlement markers of LG1194 and LG1192 installed above the first inner bound and second outer bound bored tunnels are discussed in detail below.

The ground surface heave of 1 mm between 03 and 04 August 2007 prior to EPBM approaching Array D34 can be inferred from the high earth pressure in a range of 0.95 bar to 2.41 bar as detected by earth pressure pick-up 5 during erection of ring number 589 to 591 (see Figure A.30(a)) at decreasing EPBM speed of 50 mm/min to 37 mm/min, even though the EPBM was approximately 12.6 m (9 rings) from the Array D34. It should be pointed out, however, other earth pressure pick-ups recorded lower earth pressure in a range of 0.52 bar to 1.21 bar. On reaching Array D34 on 06 August 2007 at speed of 35 mm/min, LG1194 recorded 1 mm ground surface settlement. The measured EPBM earth pressure was in the range of 0.45 bar to 1.34 bar, except earth pressure pick-up 5 recorded higher earth pressure of 3.16 bar. It should also be pointed out that the ground surface settlement of 1 mm indicates that it was only evident for the ground surface heave to occur over a distance above the EPBM face. The assessment made on 07 August 2007 when the EPBM tailskin passed LG1194 indicated maximum ground surface settlement of the order of 7 mm. The grout was injected at a volume of 3861 litres at injection pressure in a range of 1.3 bar to 1.7 bar. The shrinkage of grout that took place after 07 August 2007 could have led to greater maximum ground surface settlement of 9 mm recorded on 09 August 2007. By the end of the monitoring period, a smaller maximum settlement of 6 mm was recorded. The fact that the secondary grouting could have been applied should not be neglected.

Reference should be made to Figure 5.33(a) for the pre-existing 2.2 mm ground surface settlement recorded by LG1192. It can therefore be deduced from Figure 5.9(b) that the first inner bound bored tunnelling has induced approximately 2 mm ground surface settlement above the pre-construct second outer bound bored tunnel.

In this case, settlement of 5.6 mm was observed (derived 3.4 mm) on 27 September 2008 where the EPBM face was immediately beneath the monitoring point LG1192. The EPBM passed the LG1192 at a speed of 47 mm/min. The earth pressure pick-ups in EPBM working chamber recorded about typically 0.72 bar to 1.06 bar earth pressure, except earth pressure pick-up 4 recorded substantially lower pressure of 0.03 bar. When the EPBM tailskin passed LG1192 on 27 September 2008, maximum ground surface settlement of 11.7 mm was observed (derived 9.5 mm). The grout injection pressure was in a range of 1.3 bar to 2 bar, with total grout volume of 4014 litres. The subsequent monitoring frequency on 28 September 2007 indicated an increase of maximum ground surface settlement to 16.8 mm (derived 14.6 mm). It was believed that secondary grouting was then carried out which reduced the maximum ground surface settlement to 12.1 mm at the end of period of monitoring (derived 9.9 mm).

Refer to Figures A.25 to A.36 for more information about the EPBM speed, earth pressure and grouting episodes measured at 10 rings before and after the monitoring array.

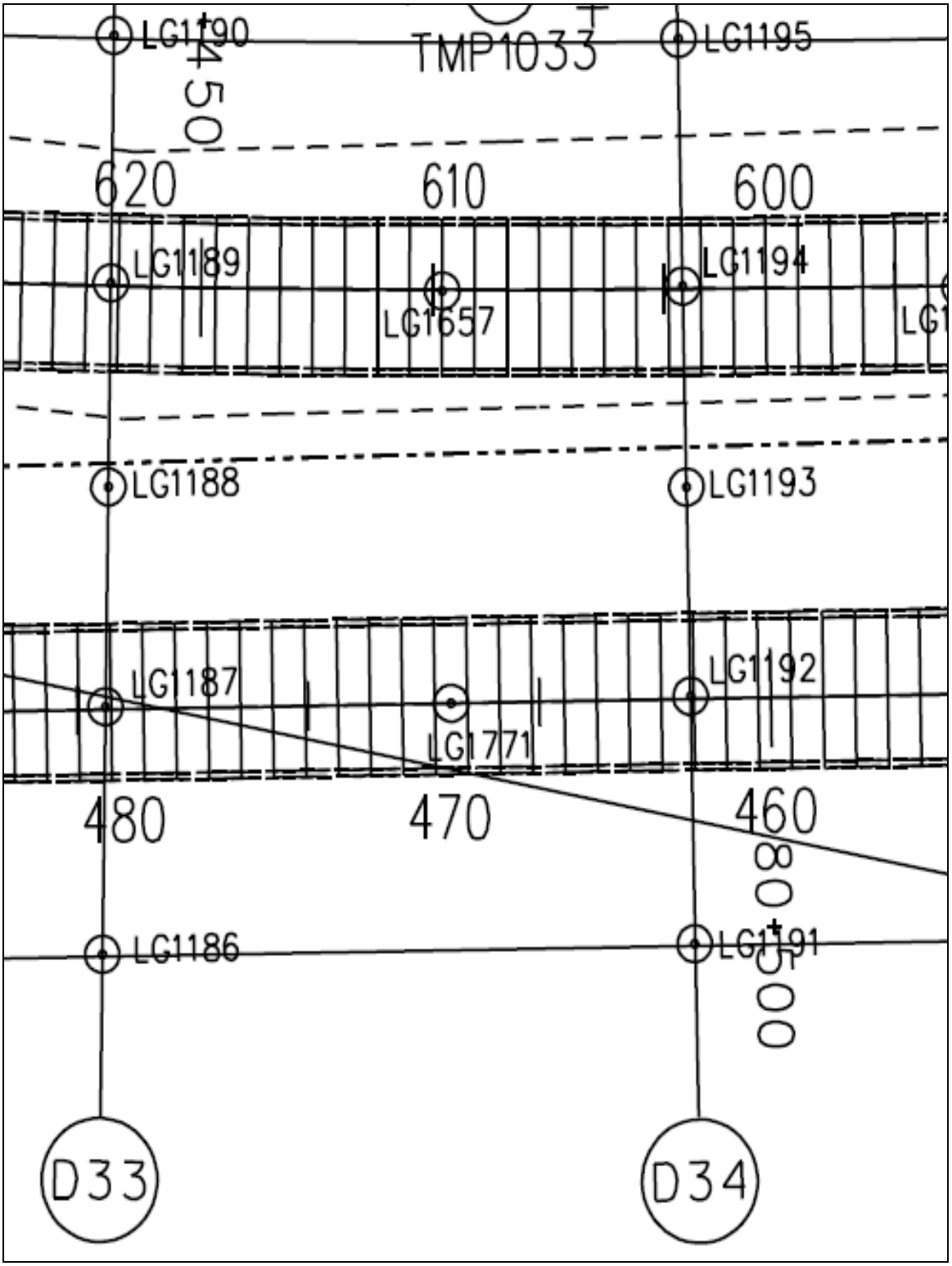

Figure 5.7 Ground surface settlement monitoring array D34

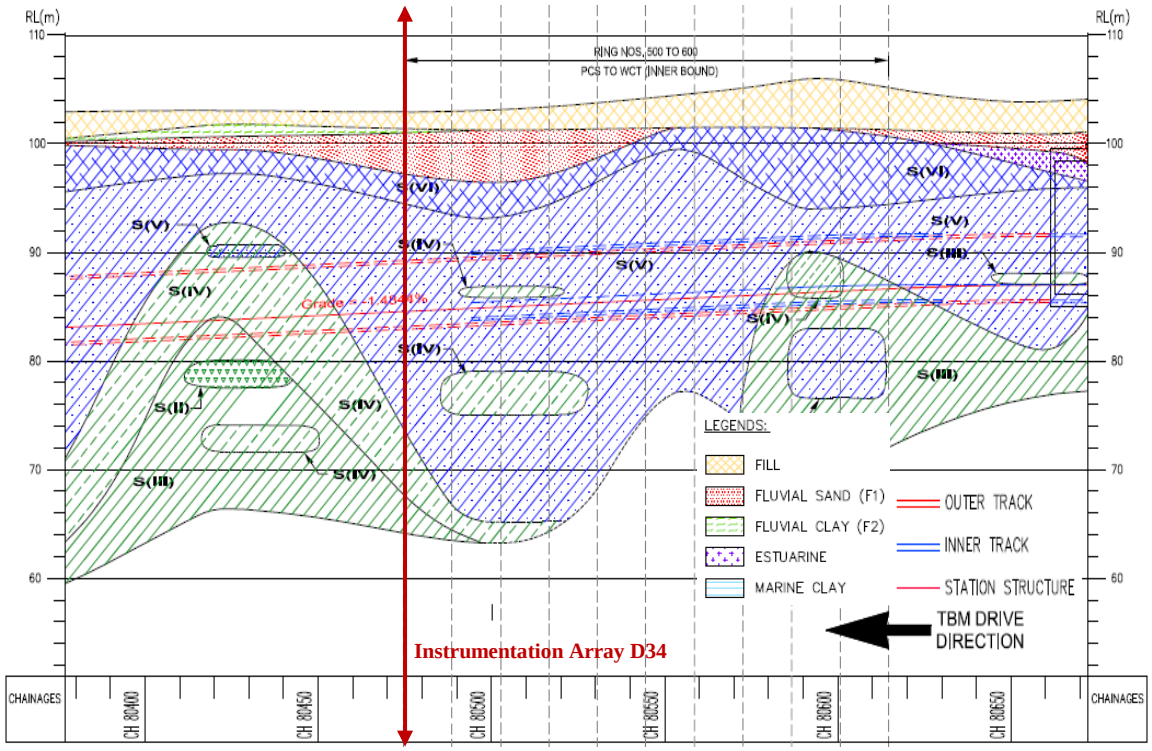

(a)

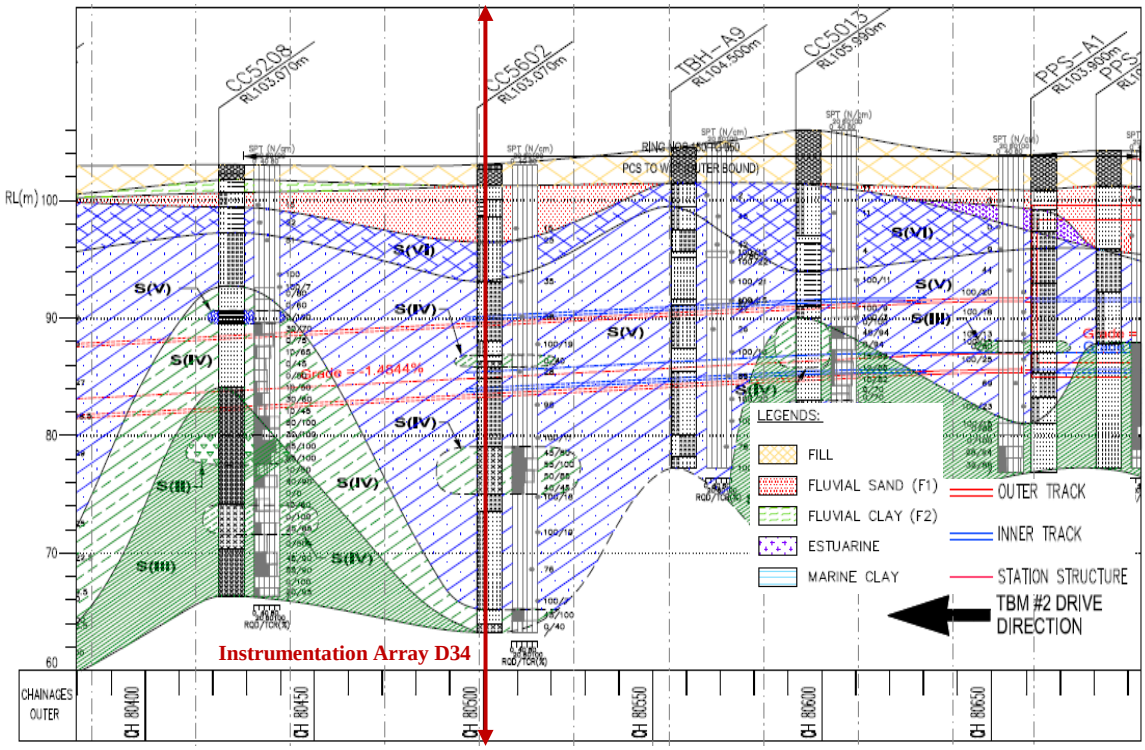

(b)

Figure 5.8 Ground conditions at tunnel level for (a) first inner bound bored tunnel; and (b) second outer bound bored tunnel (Instrumentation Array: D34)

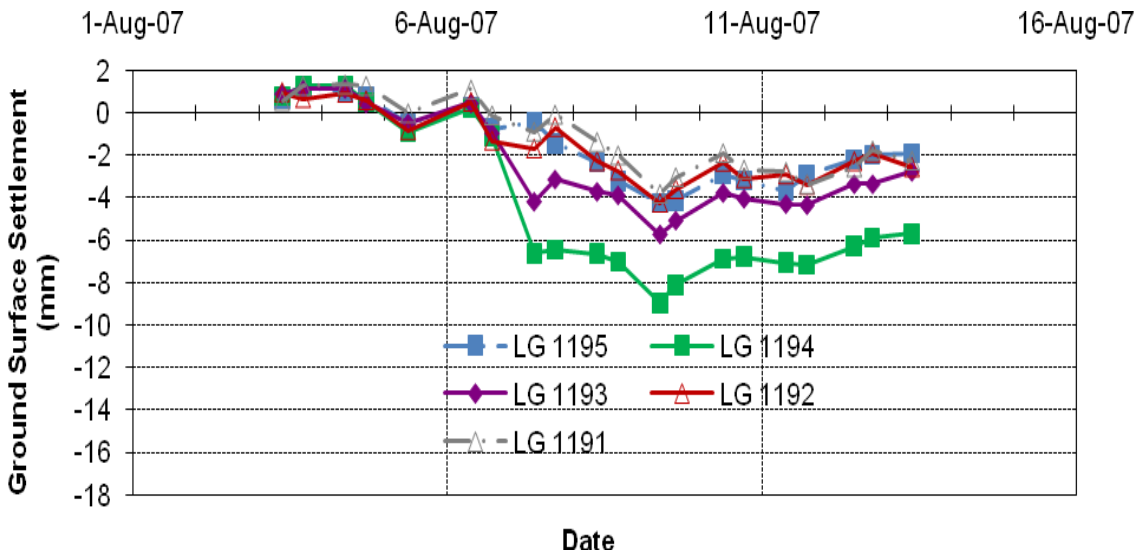

(a)

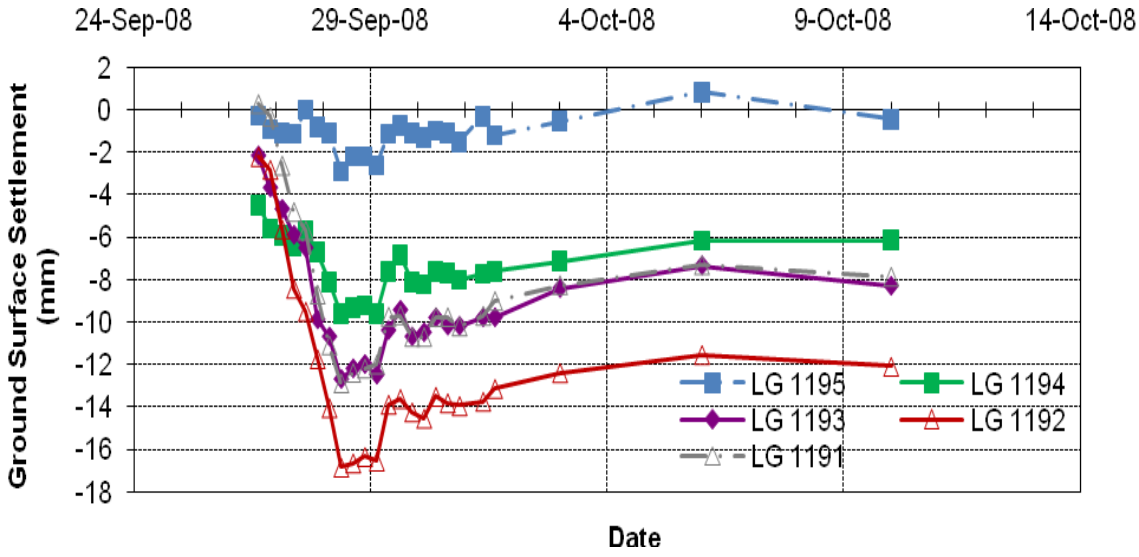

(b)

Figure 5.9 Longitudinal surface settlement profile (a) after first bored tunnelling; and (b) after second bored tunnelling (Instrumentation Array: D34)

Instrumentation Array D7

The location of Instrumentation Array D7 for monitoring ground surface settlements is shown in Figure 5.10. The longitudinal section profiles of Figures 5.11(a) and 5.11(b) summarise the geology along the tunnel alignments. The tunnels were mainly excavated through Jurong Formation (SV). The overlying materials

consist of Jurong Formation (SVI) and Fill. The longitudinal ground surface settlement profiles corresponding to construction of both the first inner bound and the second outer bound bored tunnels are shown in Figure 5.12(a) and 5.12(b). The longitudinal ground surface settlement recorded by the two ground surface settlement markers of LG1275 and LGA1277 installed above the first inner bound and second outer bound bored tunnels are discussed in detail below.

The ground surface heave of 3 mm recorded on early 24 October 2007 prior to EPBM approaching Array D7 can be inferred from the increasing EPBM speed from 40 mm/min to 70 mm/min (see Figure A.37(a)) and high earth pressure in a range of 2.16 bar to 2.47 bar as indicated by earth pressure pick-up 5 during erection of ring number 1189 to 1193 (see Figure A.42(a)). It should be pointed out, however, that other earth pressure pick-ups recorded lower earth pressure in a range of 1.46 bar to 2.1 bar. During that period, the EPBM face was at a distance of approximately 9.8m (7 rings) from Array D7. When EPBM approached LG1275 on the same date at a decreasing speed of 42 mm/min and earth pressure in the range of 1.48 bar to 1.77 bar, the magnitude of ground surface heave has decreased to 2 mm. The assessment made by the end of 24 October 2007 when the EPBM tailskin passed LG1275 indicated maximum ground surface heave was of the order of 1 mm. The grout was injected at a volume of 3346 litres at injection pressure in a range of 2.3 bar to 3.2 bar. Zero ground settlement was recorded on early 25 October 2007. A progressive settlement of LG1275 to 3 mm was recorded at a later stage on 25 October 2007. Maximum settlement amounted to 4 mm was recorded on 26 October 2007. By the end of the monitoring period on 27 October 2007, settlement of 4 mm was initially recorded with final settlement recorded as 6 mm on the same date.

In the case of the second outer bound bored tunnelling, initial ground surface settlement of the order of 1 mm was recorded before 03 December 2008. Upon approach of the EPBM beneath LGA1277 at an increasing speed of 40 mm/min on 03 December 2008, a maximum settlement of 5.3 mm was recorded. The measured EPBM earth pressure was in the range of 1.06 bar to 3.05 bar. The EPBM tailskin

passed LGA1277 on 04 December 2008 with grout injection pressure in a range of 2.2 bar to 2.8 bar and at a volume of 3857 litres, where maximum ground surface settlement of 8.3 mm was recorded. The maximum ground surface settlement recorded by the end of the monitoring period on 10 December 2008 was 8.8 mm.

Refer to Figures 5.109 to 5.120 for more information about the EPBM speed, earth pressure and grouting episodes measured at 10 rings before and after the monitoring array.

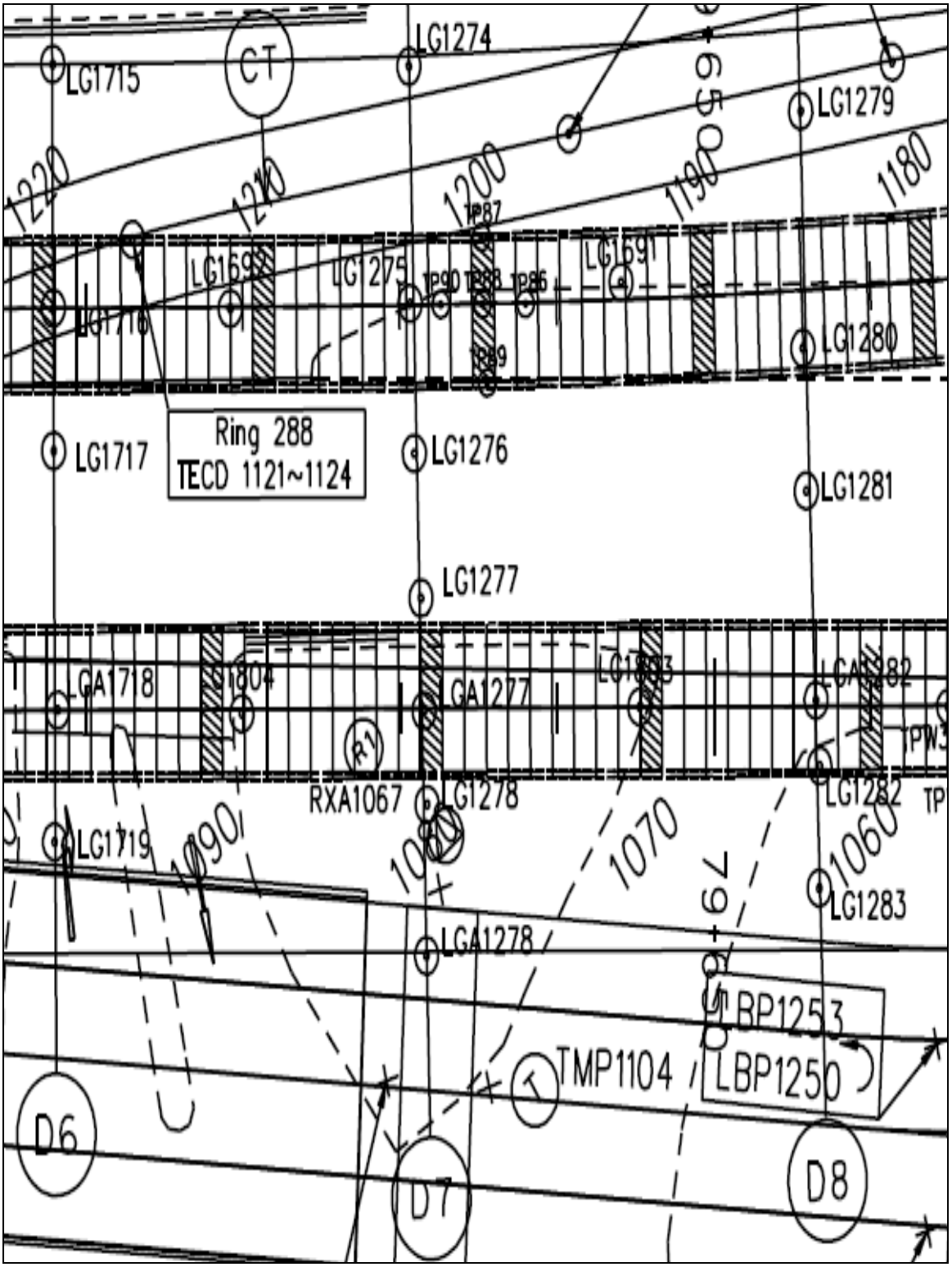

Figure 5.10 Ground surface settlement monitoring array D7

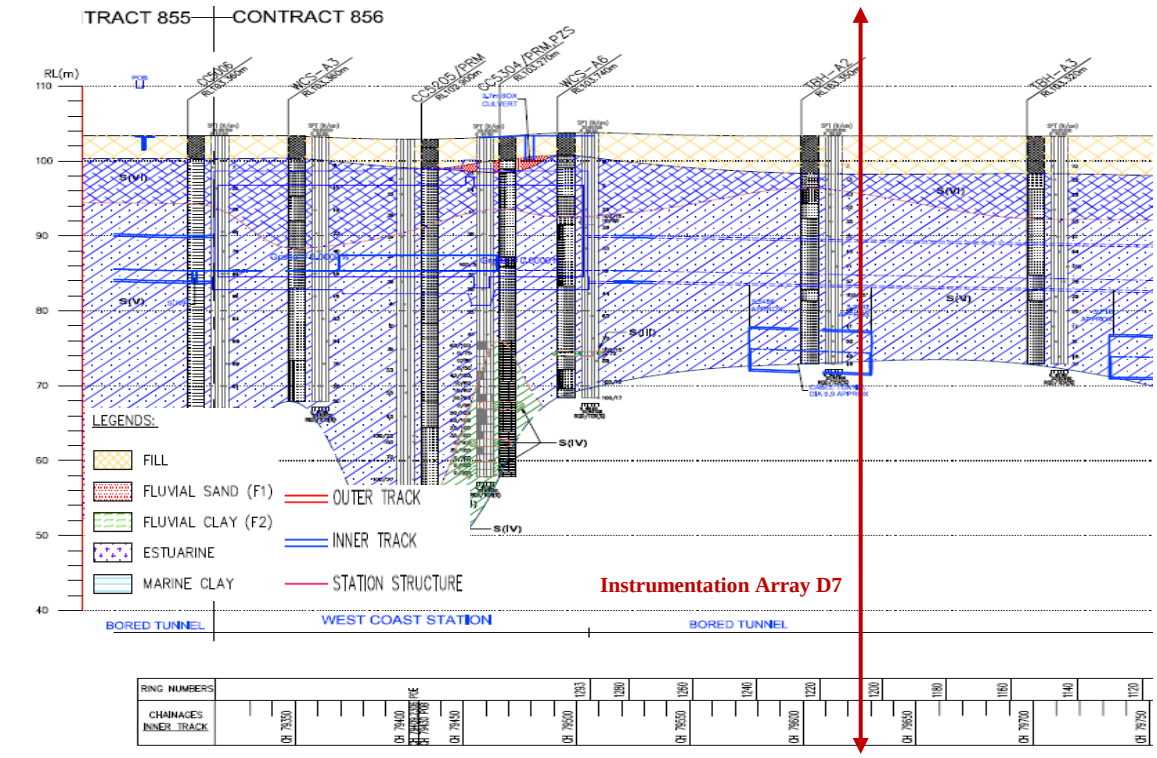

(a)

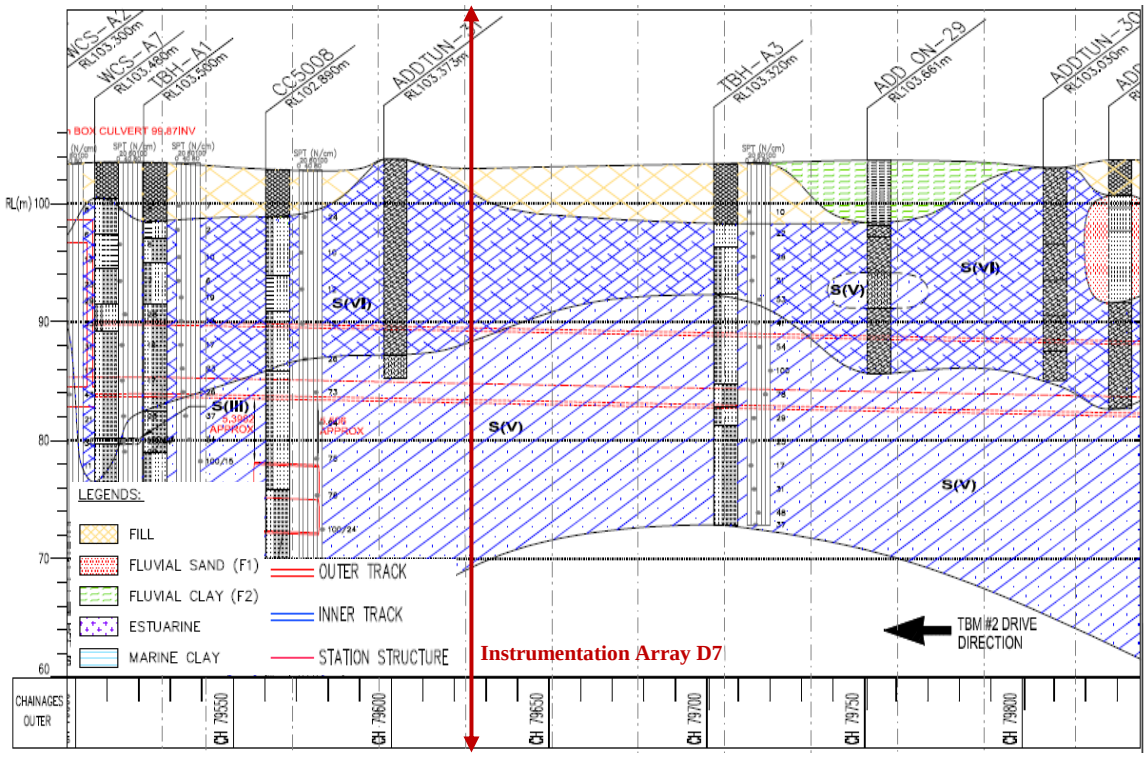

(b)

Figure 5.11 Ground conditions at tunnel level for (a) first inner bound bored tunnel; and (b) second outer bound bored tunnel (Instrumentation Array: D7)

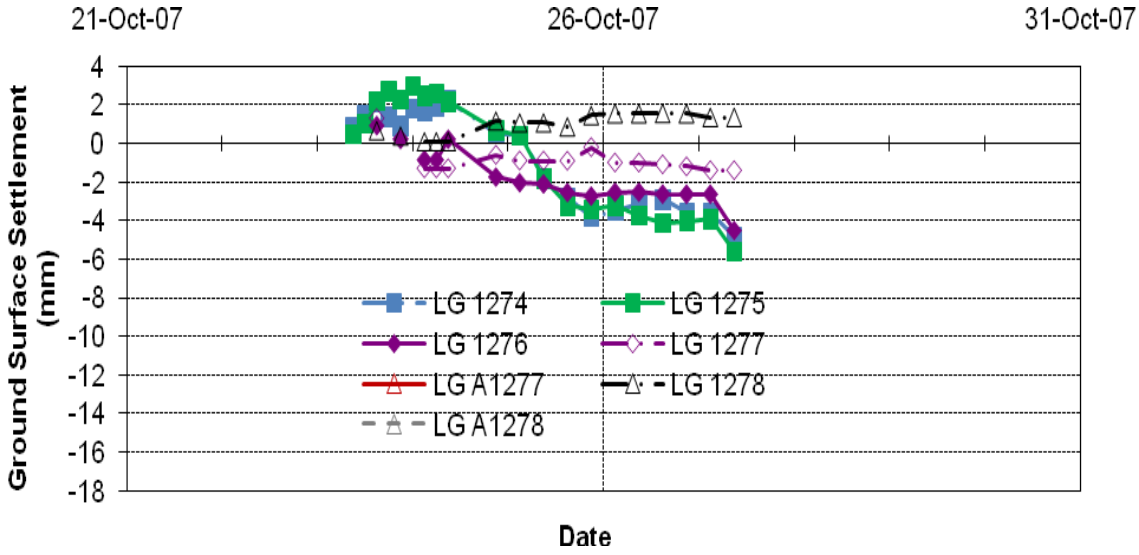

(a)

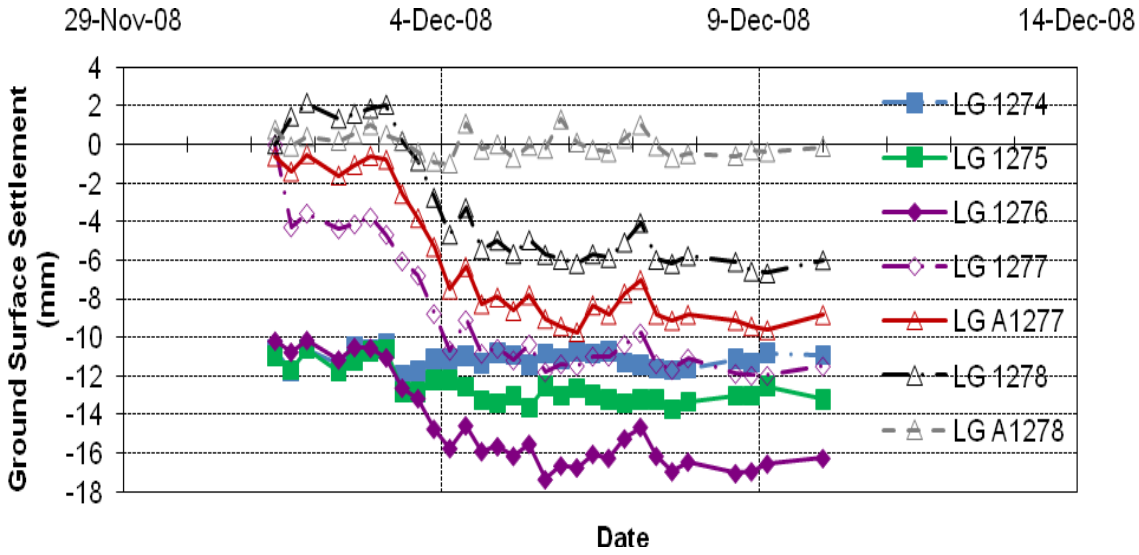

(b)

Figure 5.12 Longitudinal surface settlement profile (a) after first bored tunnelling; and (b) after second bored tunnelling (Instrumentation Array: D7)

5.2.2 Mixed Grades of Jurong Formation

Instrumentation Array D38

The location of Instrumentation Array D38 for monitoring ground surface settlements is shown in Figure 5.13. The longitudinal section profiles of Figures

5.14(a) and 5.14(b) summarise the geology along the tunnel alignments. The tunnels were mainly excavated through mixed grades of Jurong Formation (SIII, SIV and SV). The overlying materials consist of Jurong Formation (SVI), Fluvial Sand and Fill. The longitudinal ground surface settlement profiles corresponding to construction of both the first inner bound and the second outer bound bored tunnels are shown in Figure 5.15(a) and 5.15(b). The longitudinal ground surface settlement recorded by the two settlement markers of LG1213 and LG1211 installed above the first inner bound and second outer bound bored tunnels are discussed in detail below.

Upon EPBM reaching Array D38 on 27 July 2007 at speed of 31 mm/min, LG1213 recorded 5.2 mm ground surface settlement. The measured EPBM earth pressure was in the range of 0.39 bar to 1.04 bar. The assessment made on 28 July 2007 when the EPBM tailskin passed LG1213 indicated maximum ground surface settlement of the order of 8 mm. The grout was injected at a volume of 3624 litres at injection pressure in a range of 1.5 bar to 2.2 bar. By the end of the monitoring period, a smaller maximum settlement of 7.2 mm was recorded.

The first inner bound bored tunnelling has induced approximately 4 mm ground surface settlement above the pre-construct second outer bound bored tunnel. In this case, settlement of 3.3 mm was computed on 20 September 2008 where the EPBM face was immediately beneath the monitoring point LG1211. The EPBM passed the LG1211 at speed of 27 mm/min. The earth pressure pick-ups in EPBM working chamber recorded about typically 0.83 bar to 1.58 bar earth pressure, except earth pressure pick-up 4 recorded substantially higher pressure of 4.73 bar. When the EPBM tailskin passed LG1192 on 20 September 2008, maximum ground surface settlement of 14.5 mm was recorded (derived 10.5mm). The grout injection pressure was in a range of 1.2 bar to 3.4 bar, with total grout volume of 4076 litres. The subsequent monitoring on 22 September 2008 indicated an increase of maximum ground surface settlement to 18.8 mm (derived 14.8 mm). Apart from some minor fluctuations, the maximum ground surface settlement approached the same 18.8 mm (derived 14.8 mm) by the end of the monitoring period.

Refer to Figures A.49 to A.60 for more information about the EPBM speed, earth pressure and grouting episodes measured at 10 rings before and after the monitoring array.

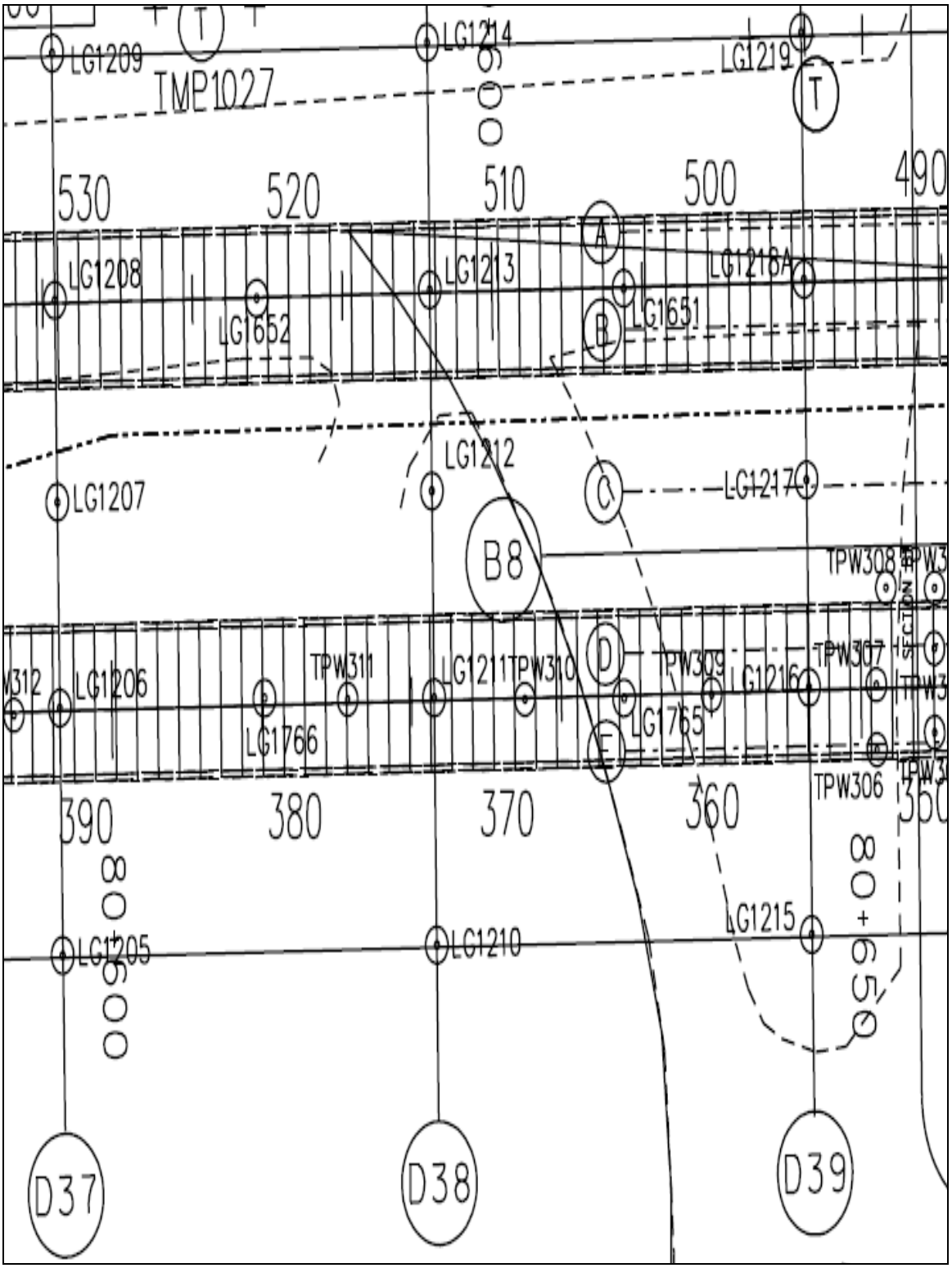

Figure 5.13 Ground surface settlement monitoring array D38

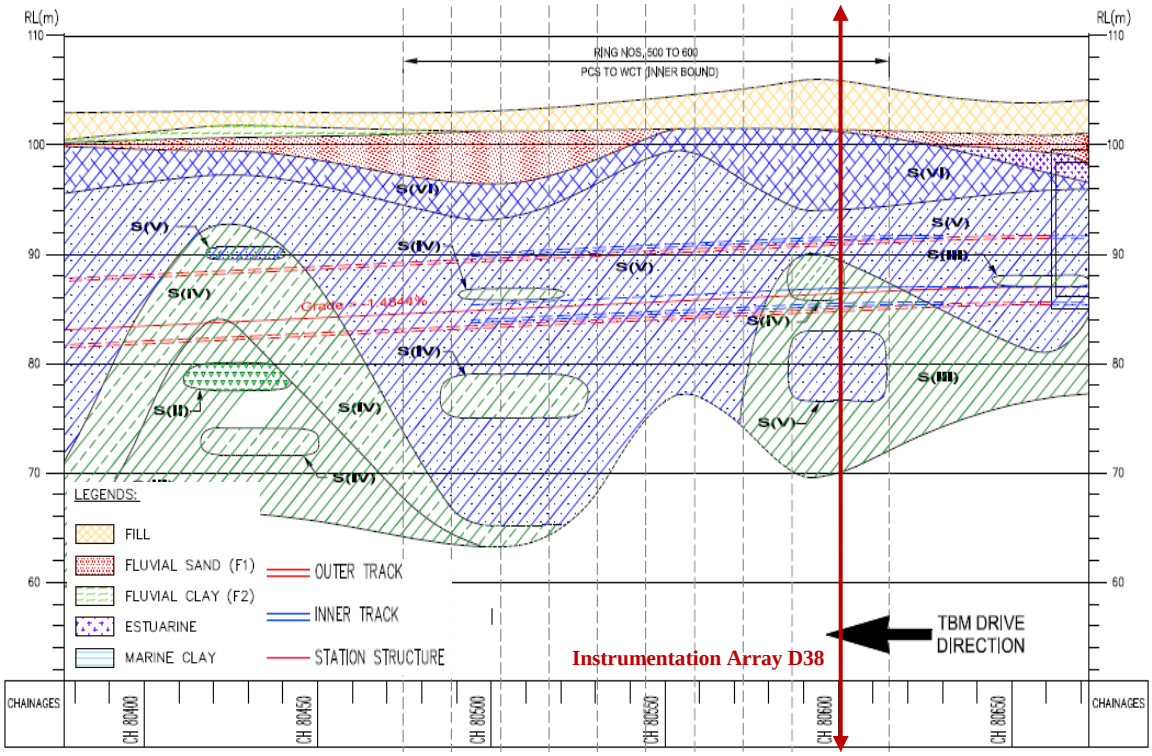

(a)

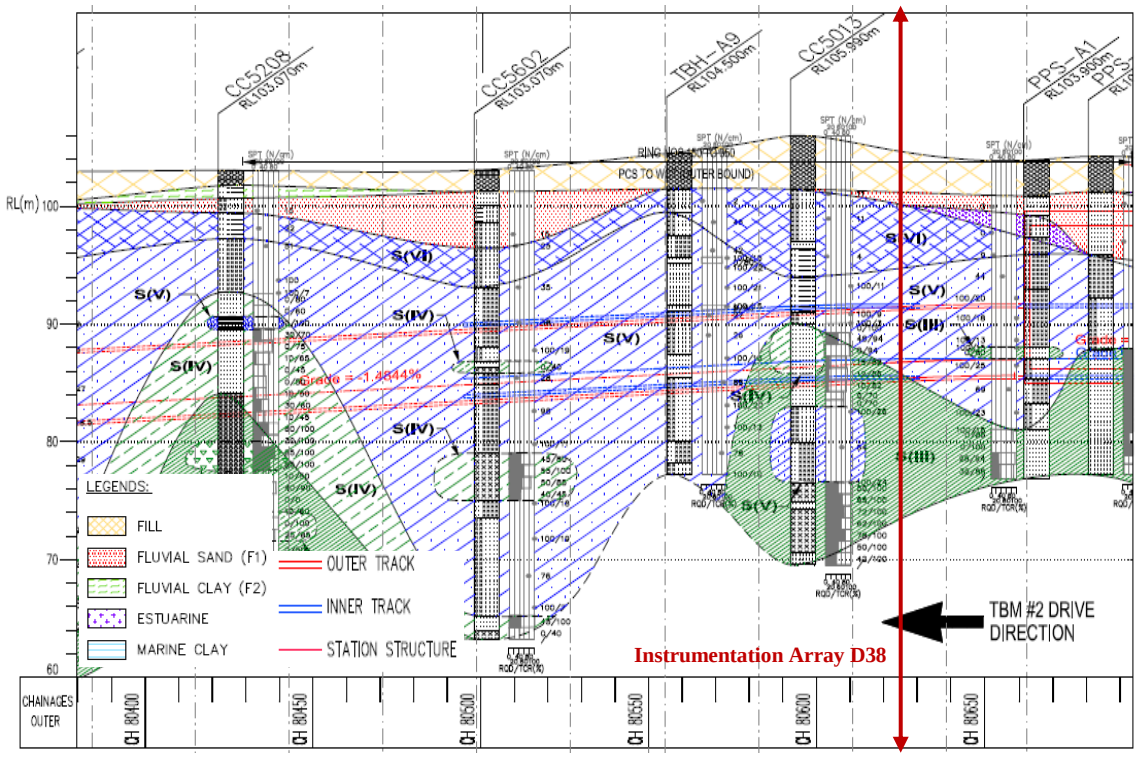

(b)

Figure 5.14 Ground conditions at tunnel level for (a) first inner bound bored tunnel; and (b) second outer bound bored tunnel (Instrumentation Array: D38)

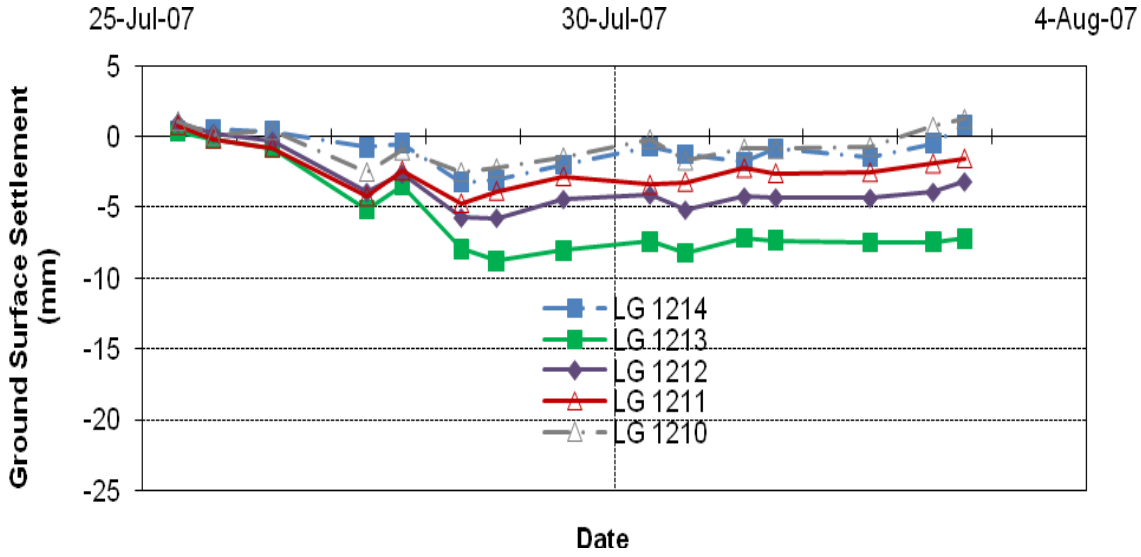

(a)

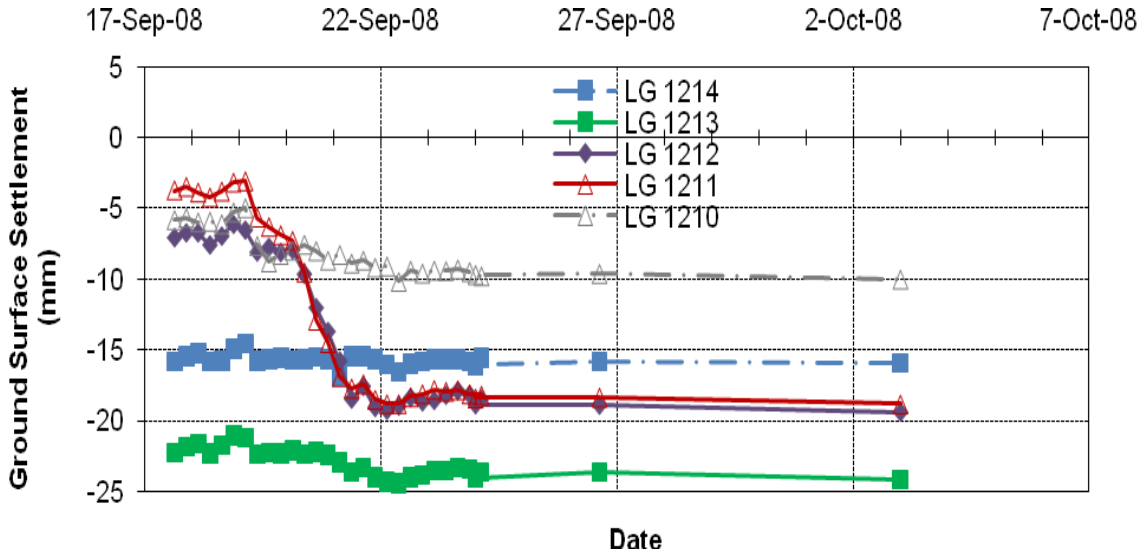

(b)

Figure 5.15 Longitudinal surface settlement profile (a) after first bored tunnelling; and (b) after second bored tunnelling (Instrumentation Array: D38)

Instrumentation Array D37

The location of Instrumentation Array D37 for monitoring ground surface settlements is shown in Figure 5.16. The longitudinal section profiles of Figures 5.17(a) and 5.17(b) summarise the geology along the tunnel alignments. The tunnels were mainly excavated through mixed grades of Jurong Formation (SIII, SIV and

SV). The overlying materials consist of Jurong Formation (SVI), Fluvial Sand and Fill. The longitudinal ground surface settlement profiles corresponding to construction of both the first inner bound and the second outer bound bored tunnels are shown in Figure 5.18(a) and 5.18(b). The longitudinal ground surface settlement recorded by the two ground surface settlement markers of LG1208 and LG1206 installed above the first inner bound and second outer bound bored tunnels are discussed in detail below.

There was an apparent 2.1 mm settlement of LG1208 on 28 July 2007, prior to the approach of the EPBM. The significantly lower EPBM earth pressure of less than 1 bar (except earth pressure pick-ups 5 and 6 which show a reduce trend from higher earth pressure) when erecting ring 517 to 524 was likely to be a contributing factor. Upon EPBM approaching Array D37 on 29 July 2007 at speed of 43 mm/min, LG1208 recorded 2.5 mm ground surface settlement. The measured EPBM earth pressure was in the range of 0.64 bar to 1.15 bar. The assessment made on 30 July 2007 when the EPBM tailskin passed LG1208 indicated maximum ground surface settlement of the order of 25 mm. The grout was injected at a volume of 3654 litres at injection pressure in a range of 2 bar to 3.5 bar. The maximum ground surface settlement remained approximately constant until the end of the monitoring period on 04 August 2007.

In the case of the second outer bound bored tunnelling, initial ground surface settlement of 3 mm was recorded on 21 September 2008, upon the approach of the EPBM beneath LG1206. Ground surface settlement increased to 13.4 mm on the same date. The EPBM passed LG1206 at speed of 46 mm/min. The earth pressure pick-ups in EPBM working chamber recorded about typically 0.22 bar to 1.88 bar earth pressure. When the EPBM tailskin passed LG1206 on 22 September 2008, maximum ground surface settlement of 36.5 mm was recorded. The grout injection pressure was in a range of 1.4 bar to 2.9 bar, with total grout volume of 3714 litres. The maximum ground surface settlement approached 39.1 mm by the end of the monitoring period. In referring to the EPBM earth pressure for a ring prior to EPBM face approaching LG1206, there was an abrupt drop in the EPBM earth

pressure from higher range of 1.7 bar to 3.26 bar (Figures A.62(b) to A.67(b)). Thus illustrate effectively the corresponding larger ground surface settlement as compared to the first inner bound bored tunnel. This resulted in 0.56 per cent and 34.27 per cent of the total settlement occurring at the EPBM face during first inner bound and second outer bound tunnelling respectively.

Refer to Figures A.61 to A.72 for more information about the EPBM speed, earth pressure and grouting episodes measured at 10 rings before and after the monitoring array.

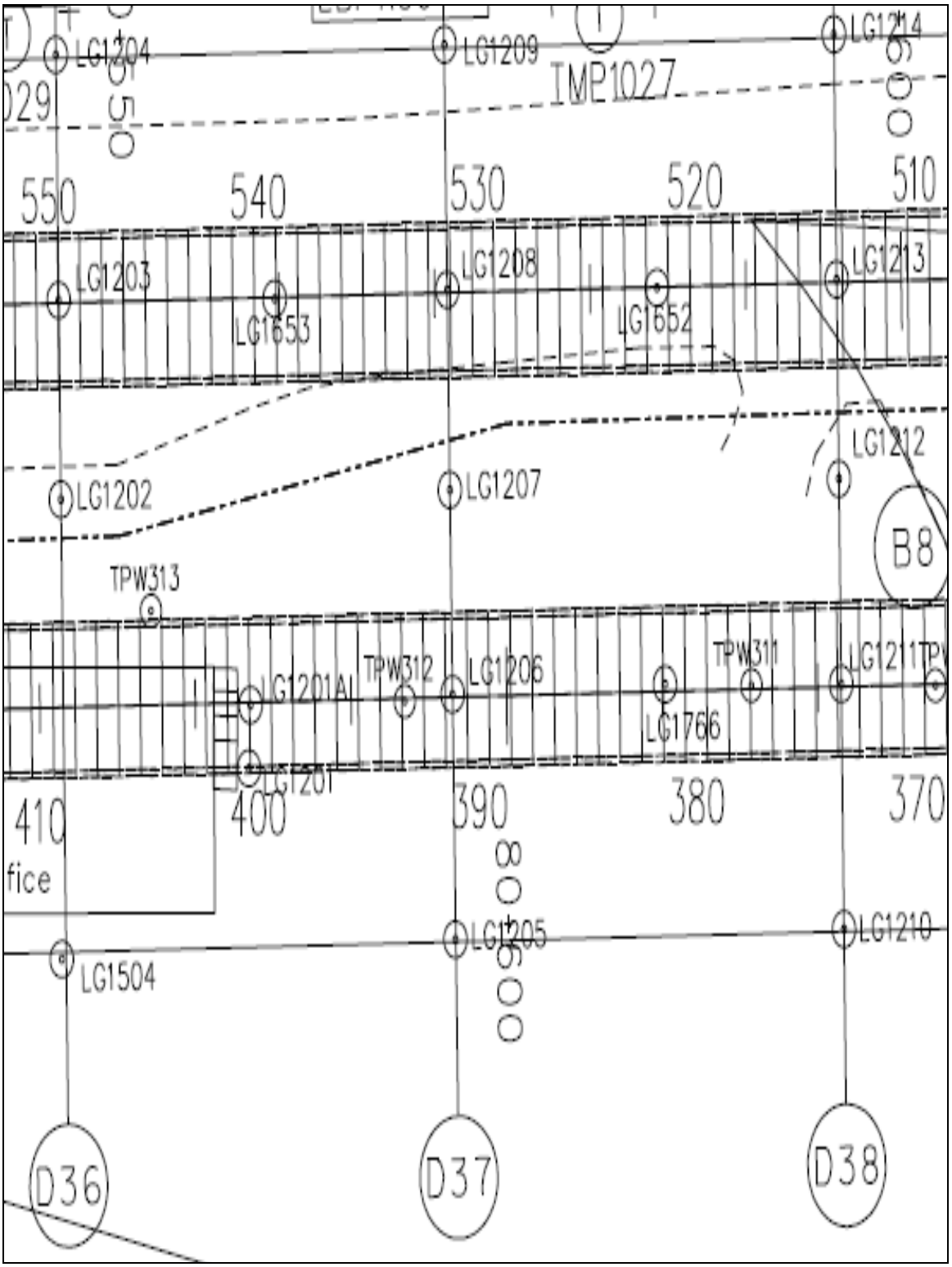

Figure 5.16 Ground surface settlement monitoring array D37

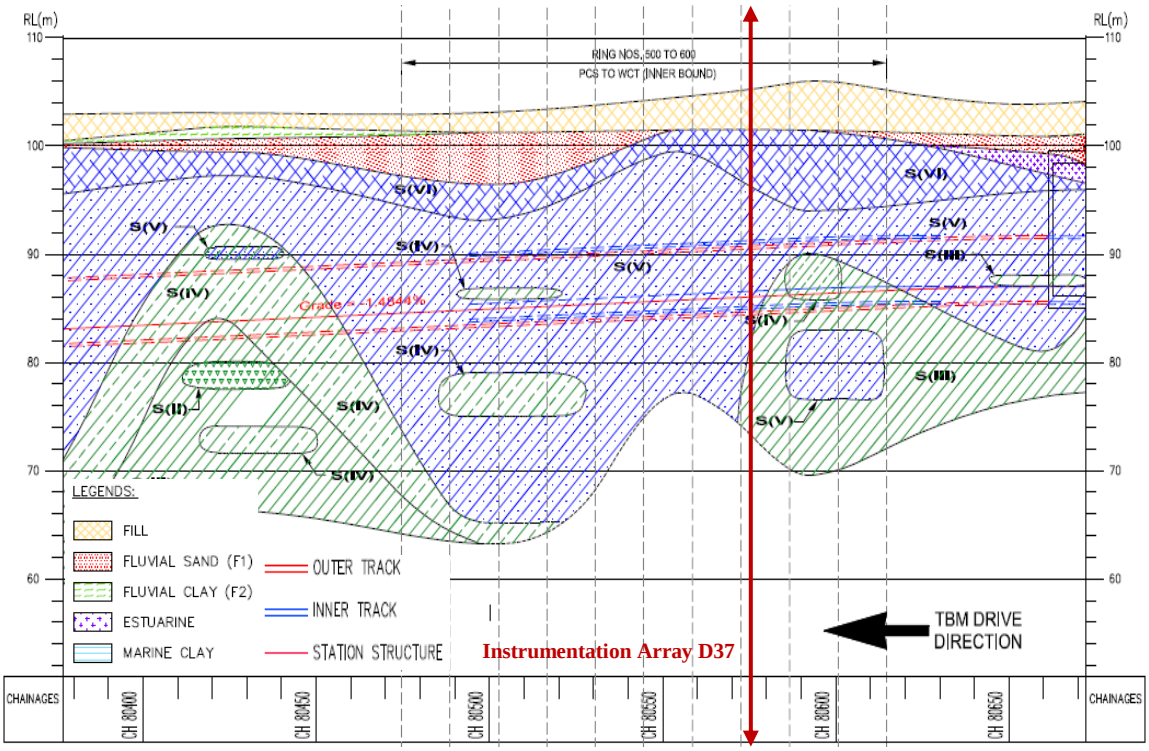

(a)

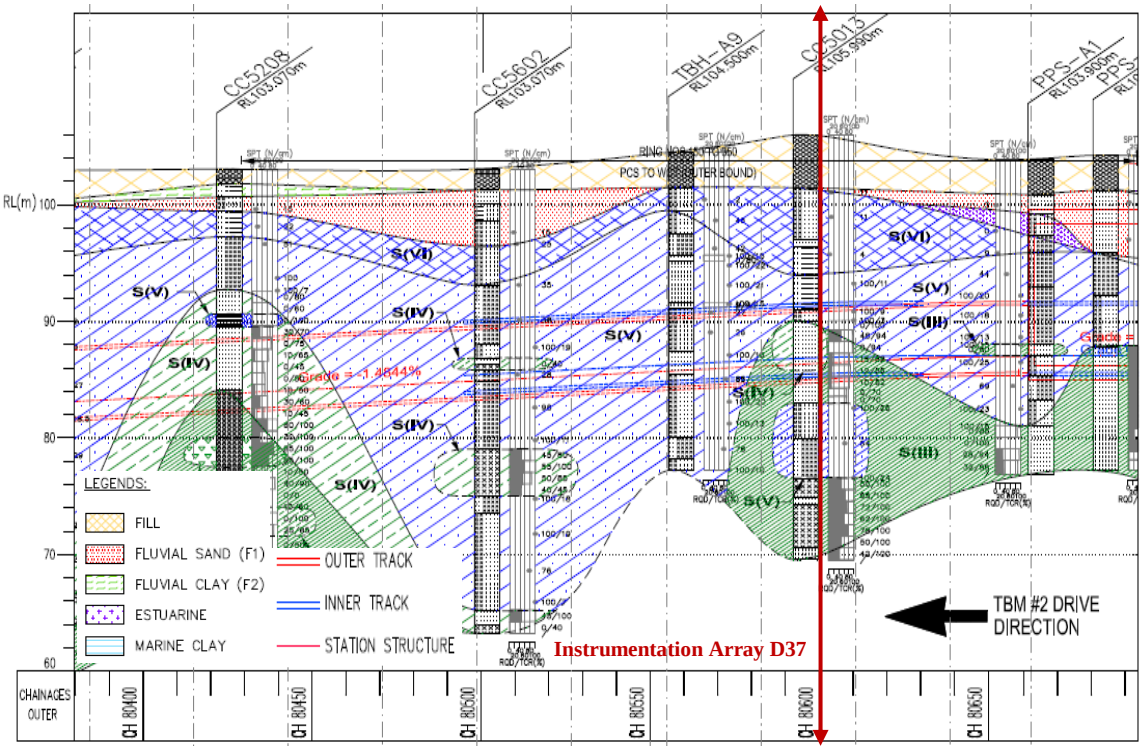

(b)

Figure 5.17 Ground conditions at tunnel level for (a) first inner bound bored tunnel; and (b) second outer bound bored tunnel (Instrumentation Array D37)

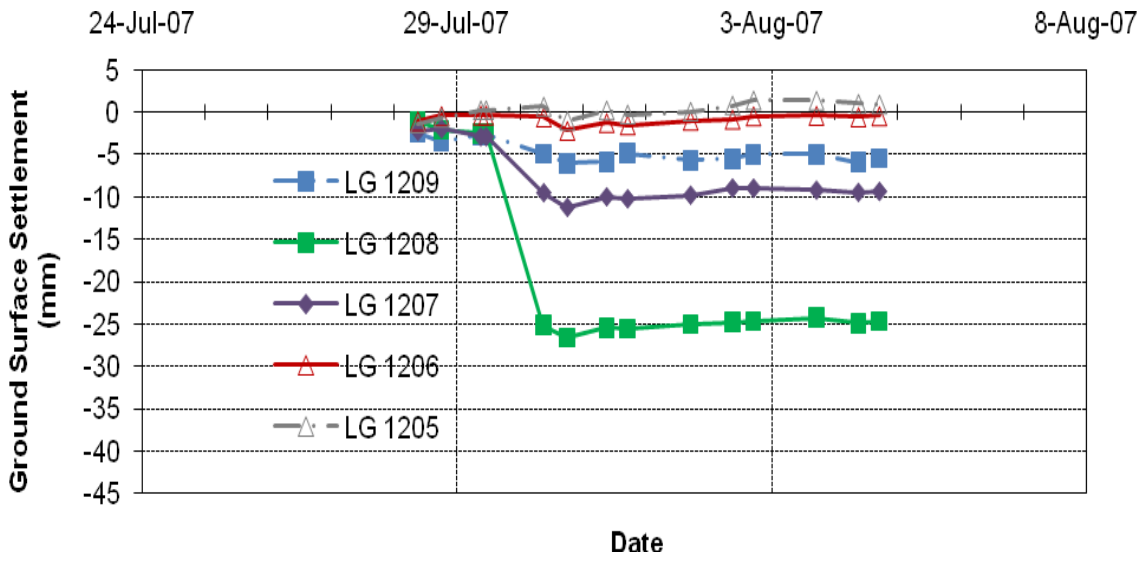

(a)

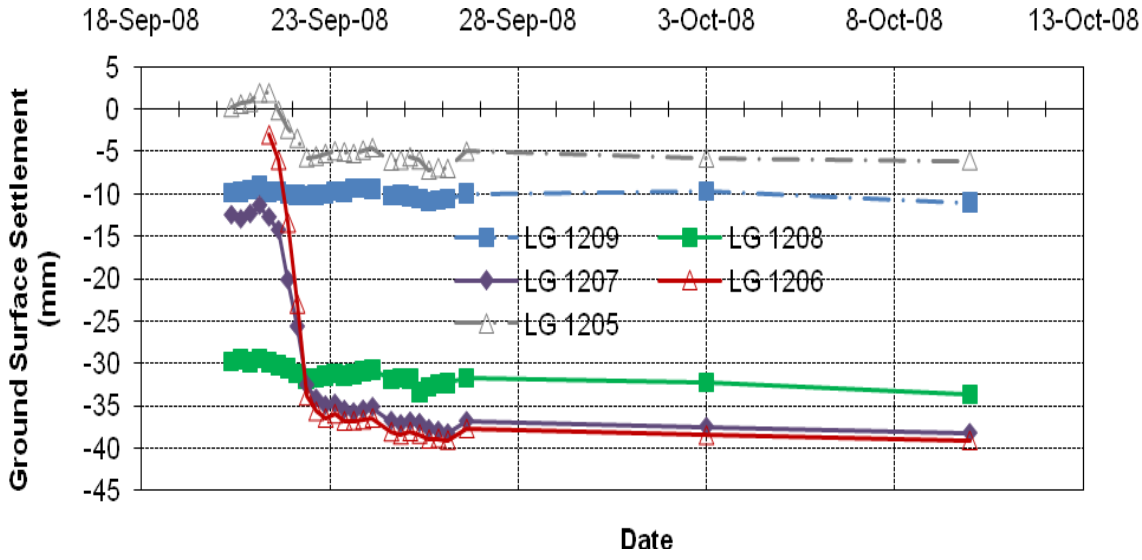

(b)

Figure 5.18 Longitudinal surface settlement profile (a) after first bored tunnelling; and (b) after second bored tunnelling (Instrumentation Array: D37)

Instrumentation Array D33

The location of Instrumentation Array D33 for monitoring ground surface settlements is shown in Figure 5.19. The longitudinal section profiles of Figures 5.20(a) and 5.20(b) summarise the geology along the tunnel alignments. The tunnels were mainly excavated through mixed grades of Jurong Formation (SIV and SV).

The overlying materials consist of Jurong Formation (SVI), Fluvial Sand and Fill. The longitudinal ground surface settlement profiles corresponding to construction of both the first inner bound and the second outer bound bored tunnels are shown in Figure 5.21(a) and 5.21(b). The longitudinal ground surface settlement recorded by the two ground surface settlement markers of LG1189 and LG1187 installed above the first inner bound and second outer bound bored tunnels are discussed in detail below.

The ground surface heave of 2 mm and the subsequent settlement of 5 mm were recorded by LG1189 between 07 August and 09 August 2007, prior to the approach of the EPBM. Figures A.74(a) to A.79(a) in the Appendix show comparable plots of the variation of EPBM earth pressure for this effect (ring number 606 to 613), although the effect is not so marked, where Figure A.79(a) involves fluctuation of EPBM earth pressure between 1 bar to 1.5 bar. Upon the EPBM approaching Array D33 on 10 August 2007 at speed of 34 mm/min, LG1189 recorded 4 mm ground surface settlement. The measured EPBM earth pressure was in the range of 0.7 bar to 1.4 bar, with exceptionally high earth pressure recorded by earth pressure pick-up 3 bar of 2.37 bar. The assessment made on 10 August 2007 when the EPBM tailskin passed LG1189 indicated maximum ground surface settlement of the order of 5 mm. The grout was injected at a volume of 3612 litres at injection pressure in a range of 1.4 bar to 2.1 bar. Maximum ground settlement from 10 August to 11 August 2007 was up to 8 mm. A progressively decrease in the maximum ground surface settlement to 4 mm by the end of the monitoring period could be caused by the significantly higher P1 line of grout injection pressure of 5.6 bar when erecting ring number 623 from 10 August to 11 August 2007, compared with 2.1 bar, 1.5 bar and 2.7 bar for P2, P3 and P4 line of grout injection respectively.

In the case of the second outer bound bored tunnelling, initial ground surface settlement of 2.9 mm was recorded on 29 September 2008, upon approach of the EPBM beneath LG1187 at speed of 48 mm/min. The measured EPBM earth pressure was in the range of 1.09 bar to 1.2 bar. Ground surface settlement of 3.8 mm was recorded on the same date when the EPBM tailskin passed LG1187 with

grout injection pressure in a range of 1.4 bar to 2 bar and at a volume of 3781 litres. The maximum ground surface settlement approached 7 mm on 30 September and decreased to 4.3 mm by the end of the monitoring period on 10 October 2008.

Refer to Figures A.73 to A.84 for more information about the EPBM speed, earth pressure and grouting episodes measured at 10 rings before and after the monitoring array.

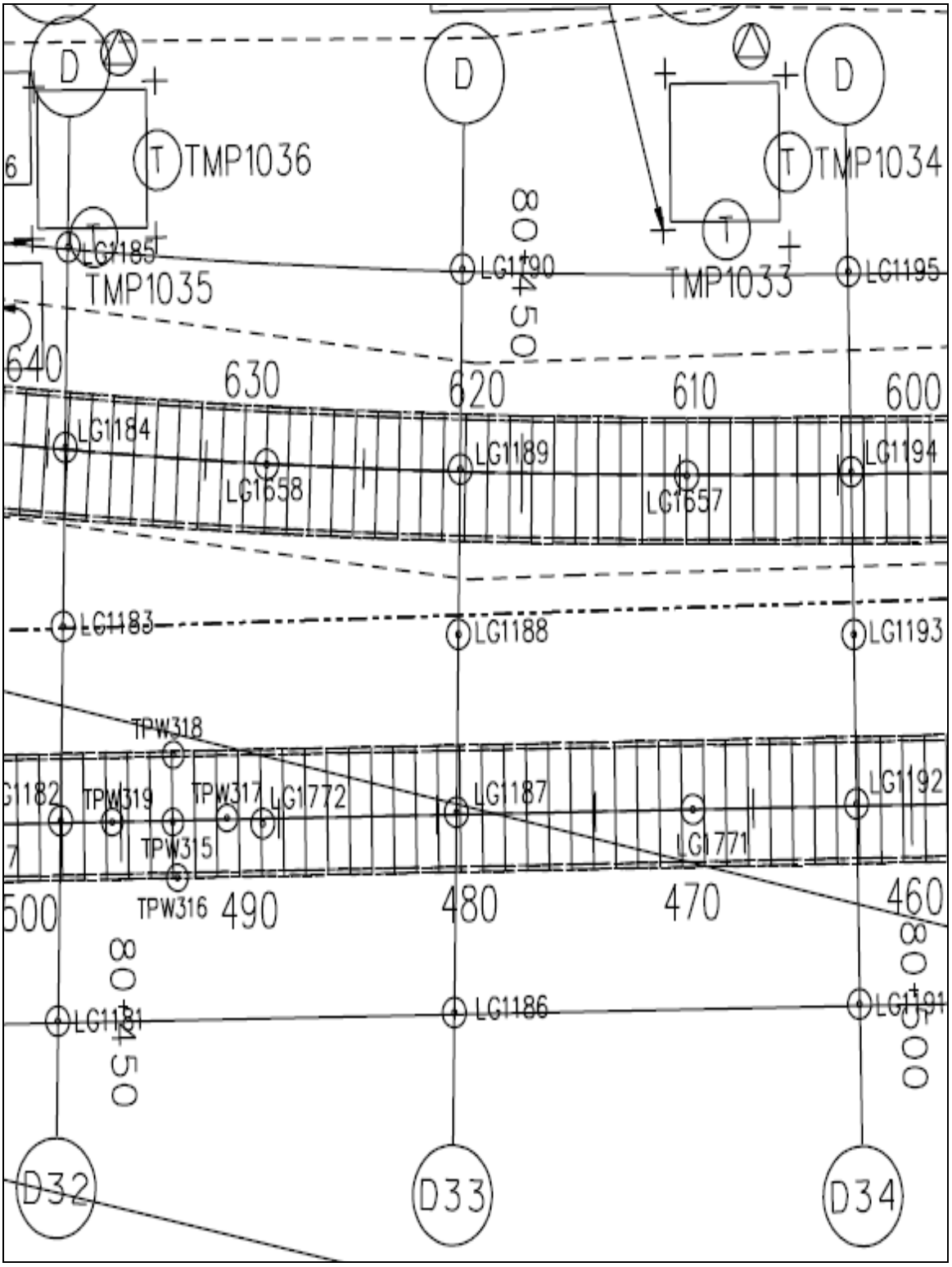

Figure 5.19 Ground surface settlement monitoring array D33

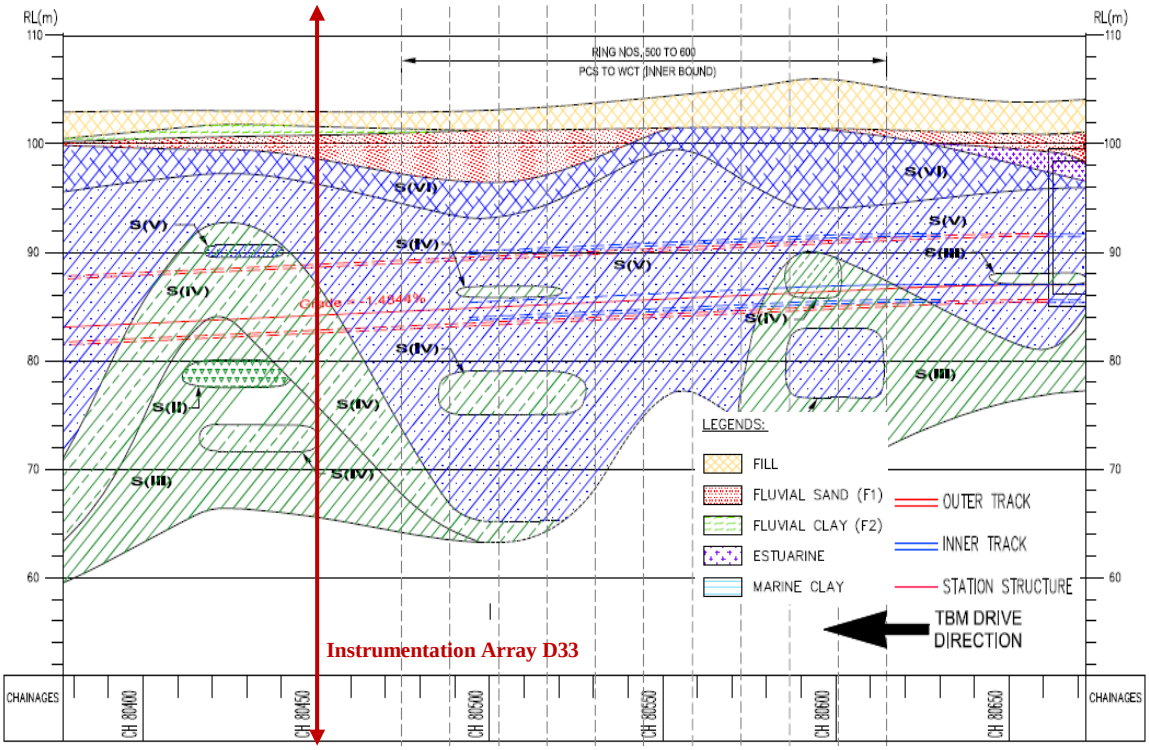

(a)

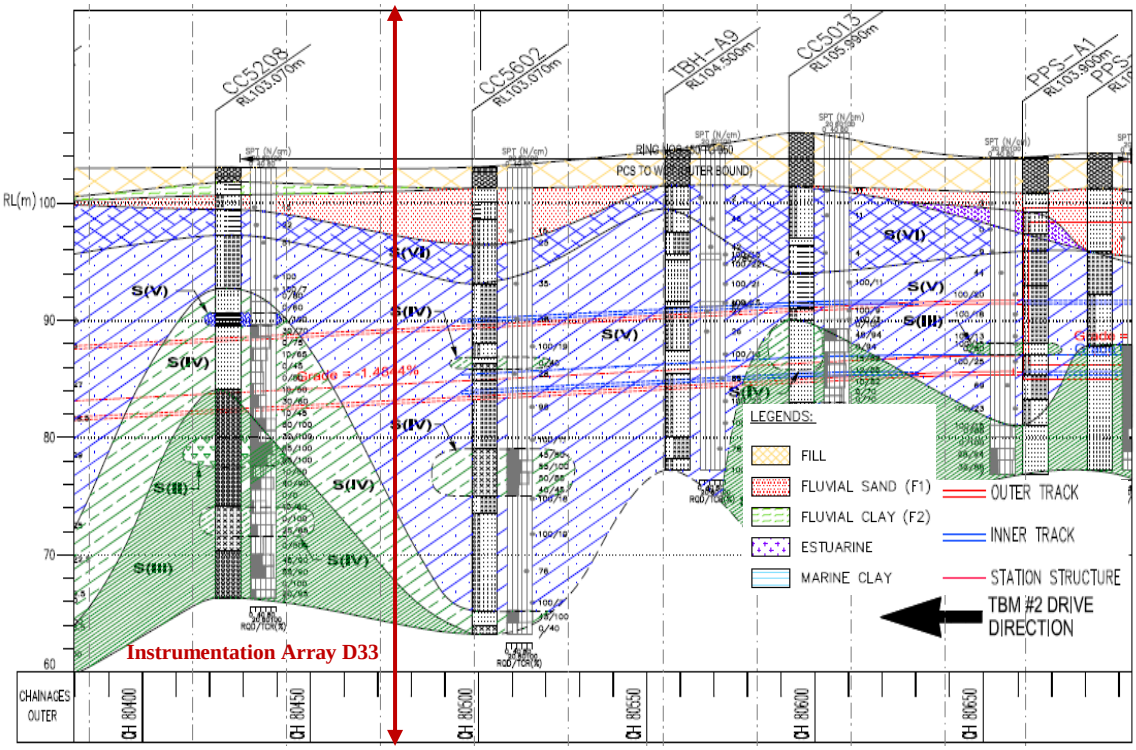

(b)

Figure 5.20 Ground conditions at tunnel level for (a) first inner bound bored tunnel; and (b) second outer bound bored tunnel (Instrumentation Array: D33)

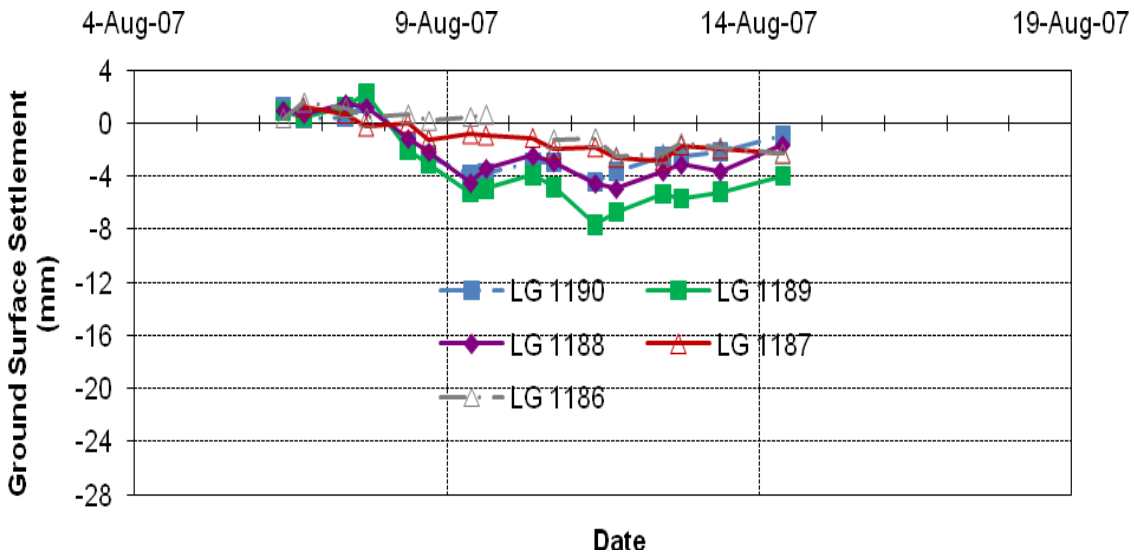

(a)

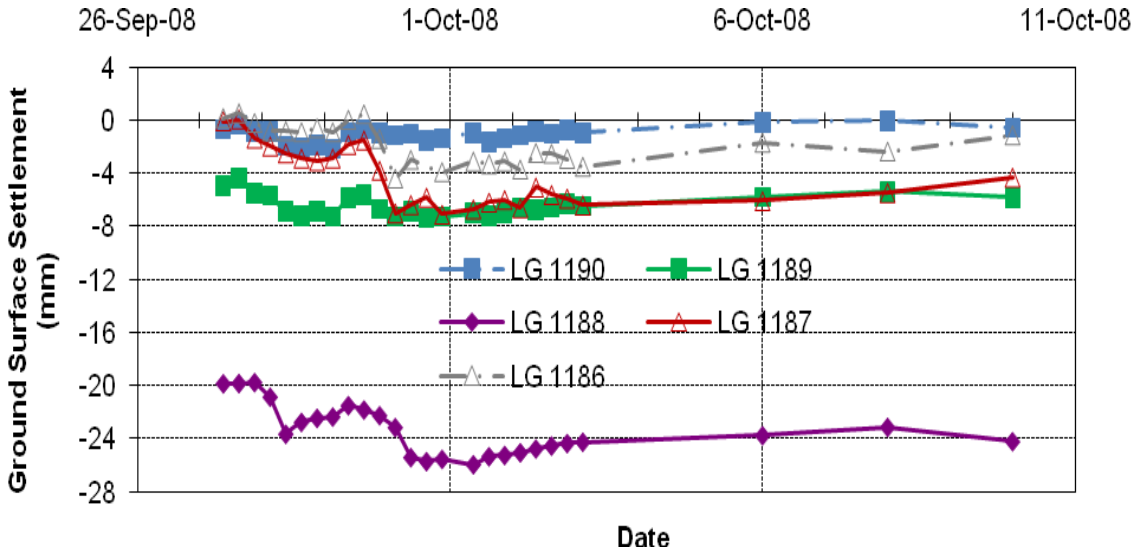

(b)

Figure 5.21 Longitudinal surface settlement profile (a) after first bored tunnelling; and (b) after second bored tunnelling (Instrumentation Array: D33)

Instrumentation Array D32

The location of Instrumentation Array D32 for monitoring ground surface settlements is shown in Figure 5.22. The longitudinal section profiles of Figures 5.23(a) and 5.23(b) summarise the geology along the tunnel alignments. The tunnels were mainly excavated through mixed grades of Jurong Formation (SIV and SV).

The overlying materials consist of Jurong Formation (SVI), Fluvial Sand, Fluvial Clay and Fill. The longitudinal ground surface settlement profiles corresponding to construction of both the first inner bound and the second outer bound bored tunnels are shown in Figure 5.24(a) and 5.24(b). The longitudinal ground surface settlement recorded by the two ground surface settlement markers of LG1184 and LG1182 installed above the first inner bound and second outer bound bored tunnels are discussed in detail below.

A maximum ground surface settlement of 3 mm was recorded on 09 August 2007 when the EPBM face was 29.4 m (21 rings) before LG1184. On 10 August 2007, settlement was recorded as 1 mm. This indicates that the accuracy of the instrument was about ± 2 mm. An assessment of the EPBM speed revealed a significant decrease in rate from 36 mm/min to 10 mm/min on 11 August 2007 when erecting ring number 630 and 631. A reduction in the EPBM earth pressure was also observed. This could possibly explain the increase in ground surface settlement to 4 mm on the same date. Upon EPBM approaching at a speed of 40 mm/min on 12 August 2007, LG1189 recorded 5 mm ground surface settlement. The measured EPBM earth pressure was in the range of 0.48 bar to 1.67 bar. The assessment made on 12 August 2007 when the EPBM tailskin passed LG1184 indicated maximum ground surface settlement of the order of 6 mm. The grout was injected at a volume of 3715 litres at injection pressure in a range of 1.4 bar to 2.7 bar. A small decrease in the maximum ground surface settlement to 4 mm by the end of the monitoring period on 14 August 2007 was recorded.

In the case of the second outer bound bored tunnelling, initial ground surface settlement of 1.5 mm was recorded on 29 September 2008. Upon approach of the EPBM beneath LG1182 at speed of 46 mm/min on 30 September 2008, a maximum settlement of 3.2 mm was recorded. The measured EPBM earth pressure was in the range of 0.65 bar to 0.94 bar. No data was recorded between 30 September and 03 October 2008 where the EPBM tailskin passed LG1182 on 02 October 2008 with grout injection pressure in a range of 1.1 bar to 1.4 bar and at a volume of 3708 litres. The lower grout injection pressure range could have led to 12.9 mm ground

surface settlement recorded on 03 October 2008. The maximum ground surface settlement decreased to 11.8 mm by the end of the monitoring period on 10 October 2008.

Refer to Figures A.85 to A.96 for more information about the EPBM speed, earth pressure and grouting episodes measured at 10 rings before and after the monitoring array.

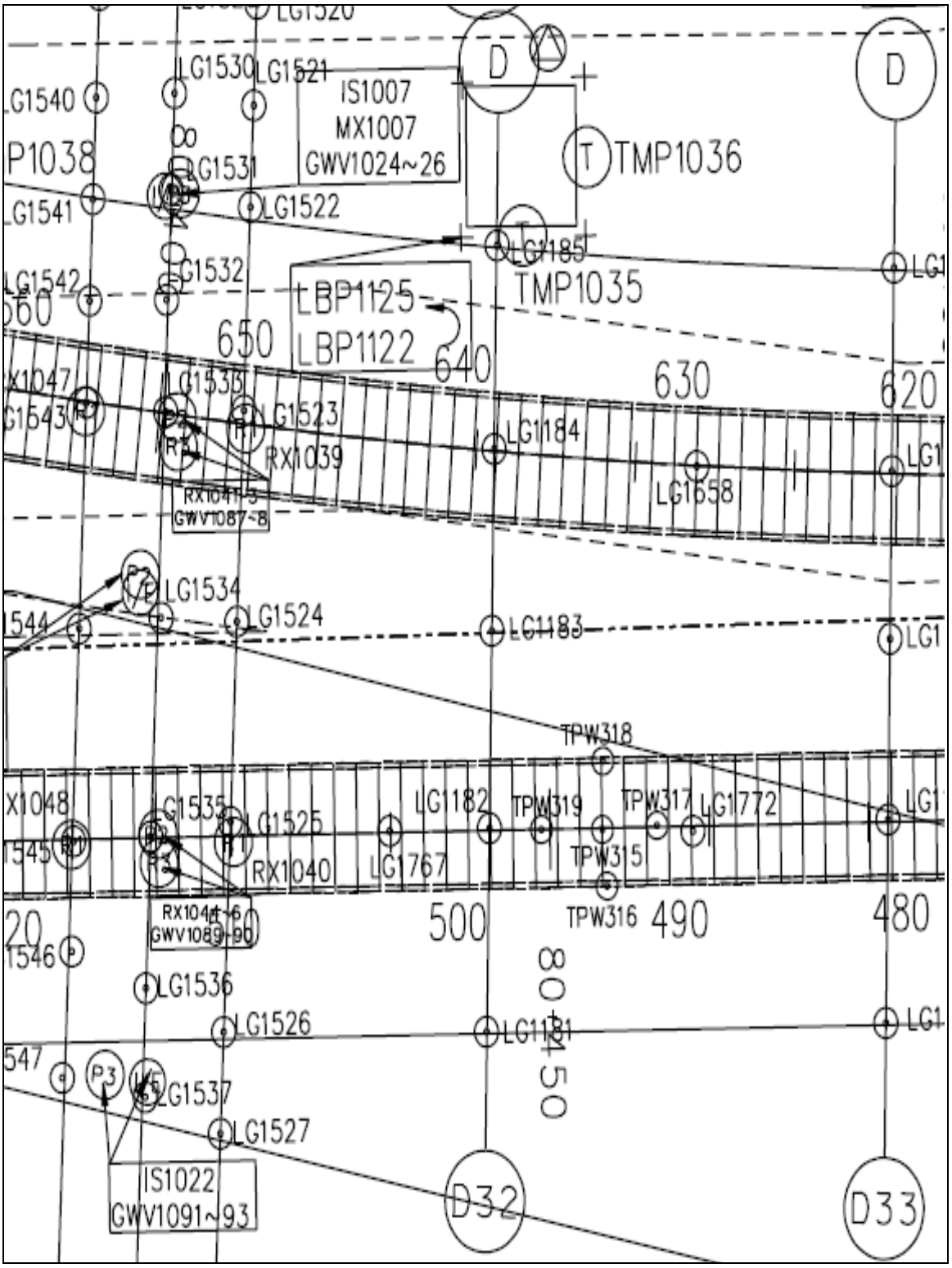

Figure 5.22 Ground surface settlement monitoring array D32

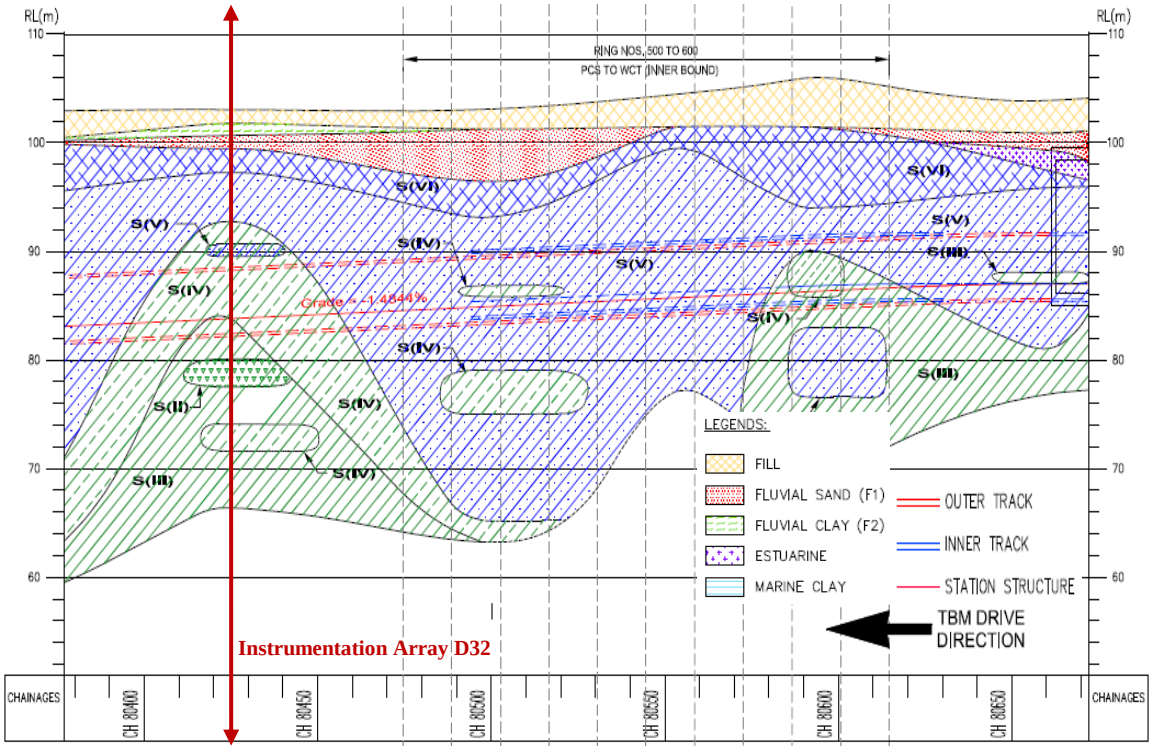

(a)

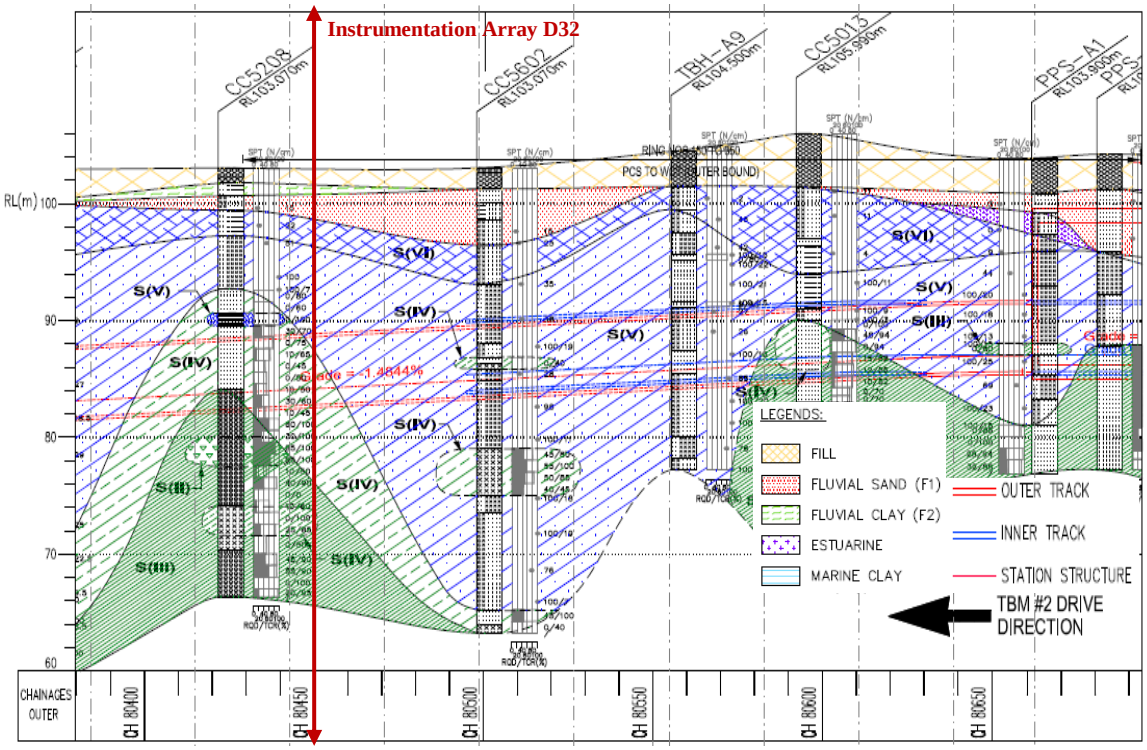

(b)

Figure 5.23 Ground conditions at tunnel level for (a) first inner bound bored tunnel; and (b) second outer bound bored tunnel (Instrumentation Array: D32)

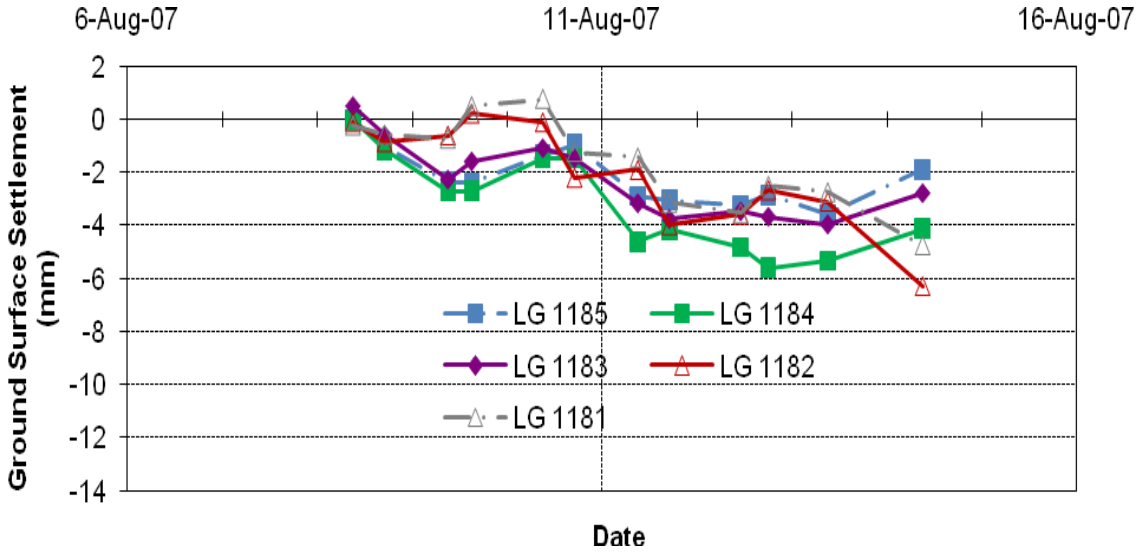

(a)

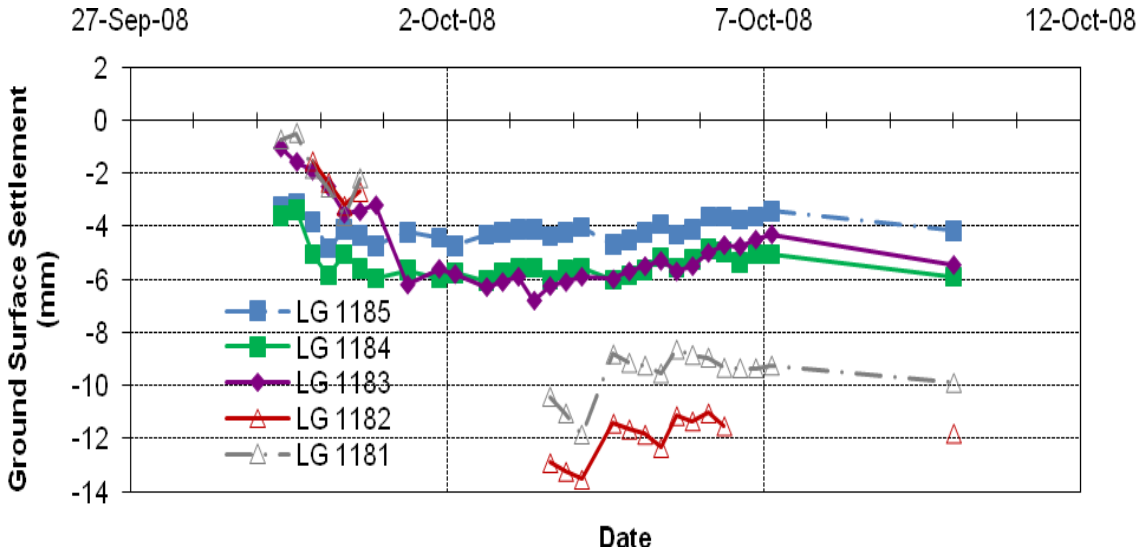

(b)

Figure 5.24 Longitudinal surface settlement profile (a) after first bored tunnelling; and (b) after second bored tunnelling (Instrumentation Array: D32)

5.2.3 Mixed Ground of Jurong Formation and Kallang Formation

Instrumentation Array E14

The location of Instrumentation Array E14 for monitoring ground surface settlements is shown in Figure 5.25. The longitudinal section profiles of Figures

5.26(a) and 5.26(b) summarise the geology along the tunnel alignments. The tunnels were mainly excavated through mixed ground of Jurong Formation (SIII, SIV, SV and SVI) and Kallang Formation (Fluvial Sand, Fluvial Clay and Marine Clay). The overlying materials consist of Fluvial Sand, Marine Clay, Estuarine and Fill. The longitudinal ground surface settlement profiles corresponding to construction of both the first inner bound and the second outer bound bored tunnels are shown in Figure 5.27(a) and 5.27(b). The longitudinal ground surface settlement recorded by the two ground surface settlement markers of LG1477 and LG1734 installed above the first inner bound and second outer bound bored tunnels are discussed in detail below.

There was virtually no settlement recorded on 31 March 2007 until the EPBM face was beneath the vicinity of LG1477 at a speed of 26 mm/min on 01 April 2007 where ground surface settlement was initially recorded as 7 mm. This significant increase in ground surface settlement was probably a result of considerable reduction in EPBM speed from over 40 mm/min to the present rate. The maximum ground surface settlement increased to 9 mm on 02 April 2007 when the EPBM face was immediately beneath LG1477. The EPBM speed increased to 32 mm/min and earth pressure was in the range of 1.43 bar to 2.06 bar. The passing of the EPBM shield on 02 April 2007 induced significant ground surface settlement of up to 35 mm. The assessment made on 03 April 2007 when the EPBM tailskin passed LG1477 indicated maximum ground surface settlement of the order of 37 mm. The grout was injected at a volume of 4057 litres at injection pressure in a range of 2.2 bar to 4.3 bar. A progressive settlement occurred over a short period from 03 April to 04 April 2007 where maximum ground surface settlement approached 48 mm. By the end of the monitoring period on 09 April 2007, ground surface settlement was recorded as 46 mm. This indicates that no ground consolidation settlement has taken place.

In the case of the second outer bound bored tunnelling, initial ground surface heave recorded before 26 January 2008 was of the order of 1 mm, probably a result of higher EPBM earth pressure of over 3 bar as recorded by earth pressure pick-up 3.

Upon approach of the EPBM face beneath LGA1734 at speed of 31 mm/min on 26 January 2008, a maximum heave of 2.2 mm was recorded. The measured EPBM earth pressure was in the range of 1.66 bar to 2.63 bar. The EPBM tailskin passed LG1734 on 26 January 2008 with grout injection pressure in a range of 1.9 bar to 2.3 bar and at a volume of 3598 litres, where maximum ground surface settlement of 2.8 mm was recorded. The maximum ground surface settlement increased progressively to 11.1 mm on 27 January 2007. By the end of the monitoring period on 01 February 2008, the maximum ground surface settlement was 12.5 mm. There was no clear indication that ground consolidation settlement has taken place.

Refer to Figures A.97 to A.108 for more information about the EPBM speed, earth pressure and grouting episodes measured at 10 rings before and after the monitoring array.

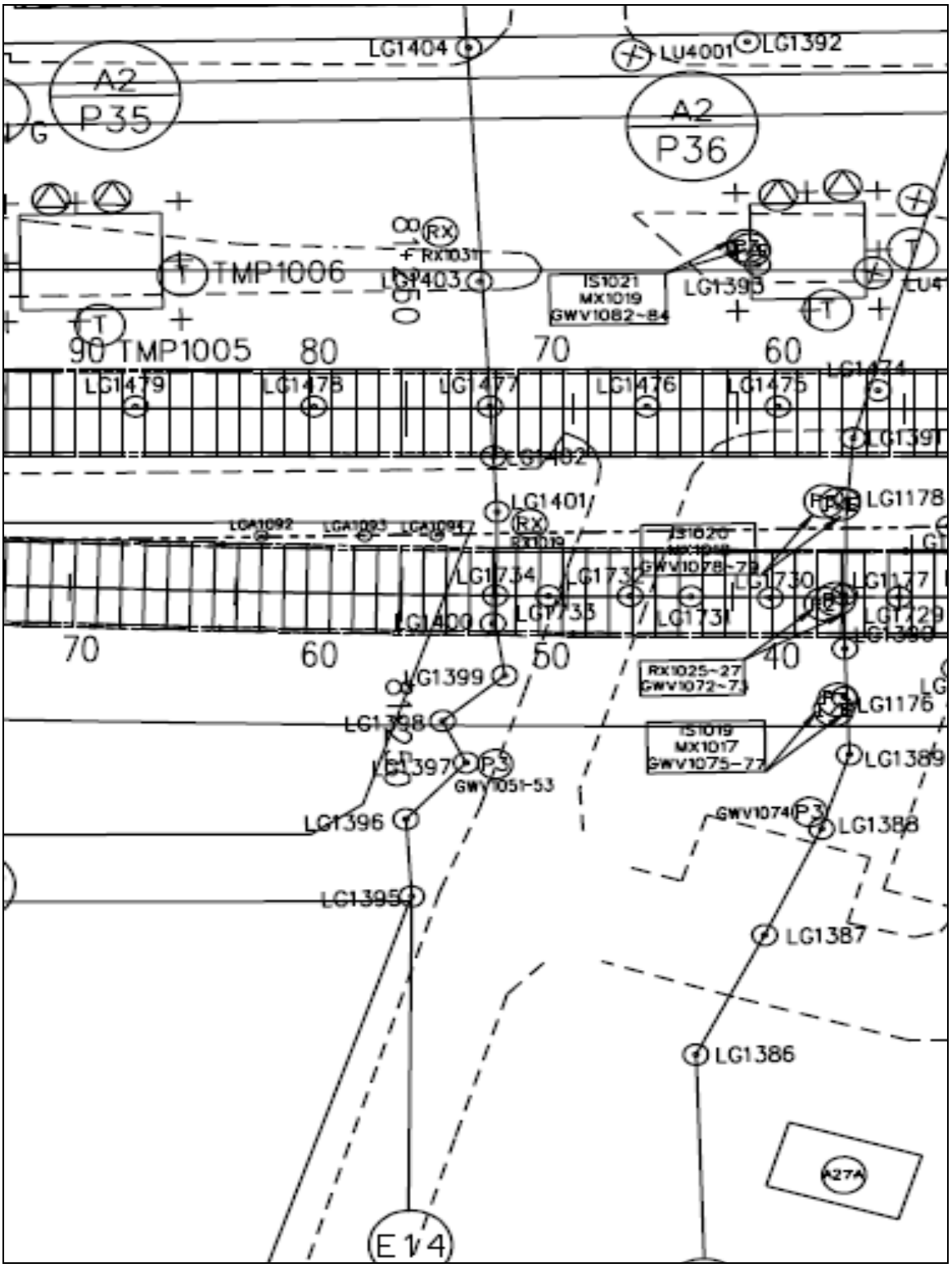

Figure 5.25 Ground surface settlement monitoring array E14

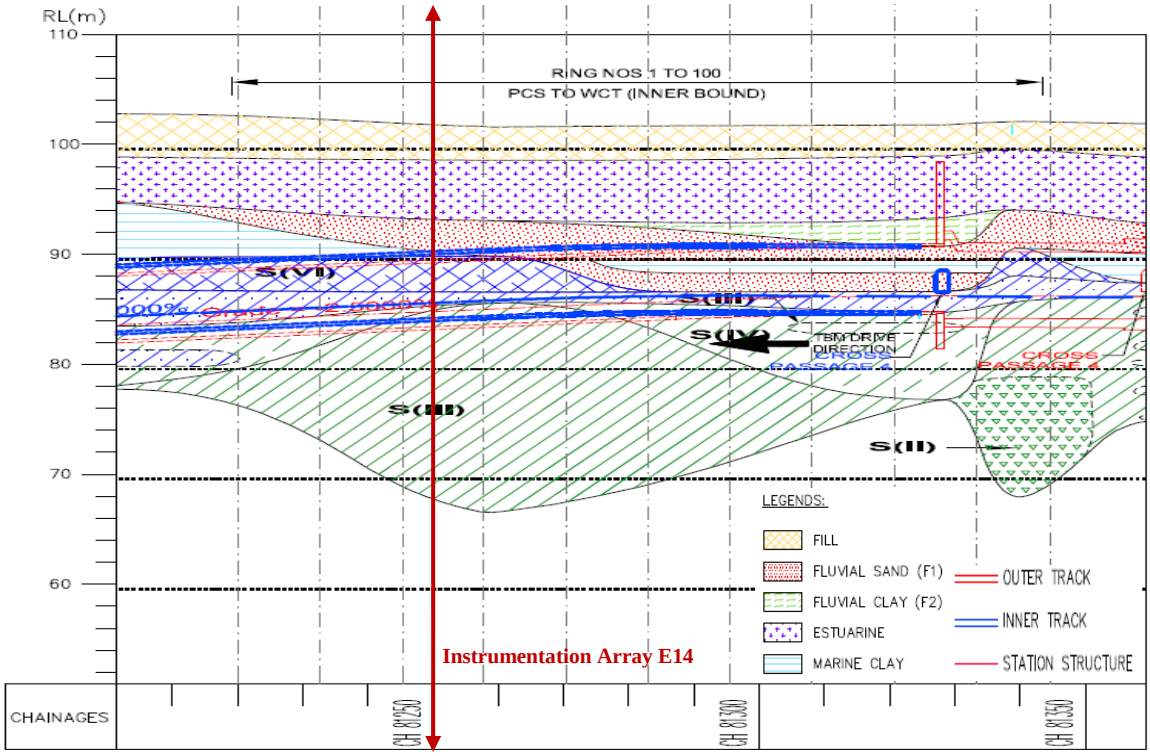

(a)

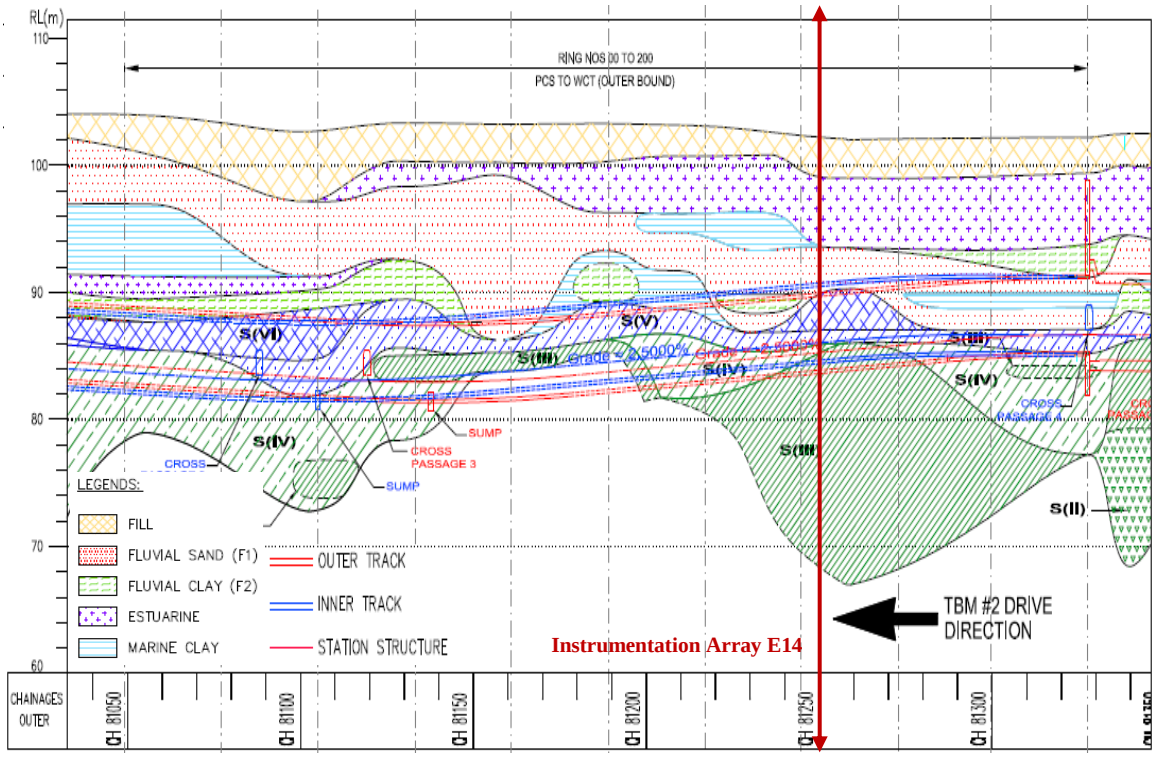

(b)

Figure 5.26 Ground conditions at tunnel level for (a) first inner bound bored tunnel; and (b) second outer bound bored tunnel (Instrumentation Array: E14)

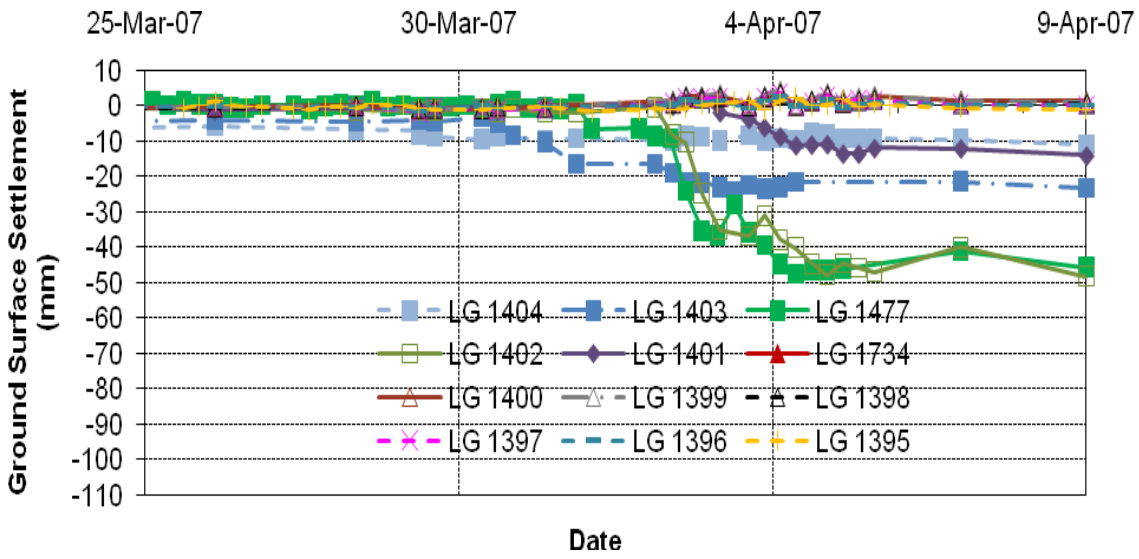

(a)

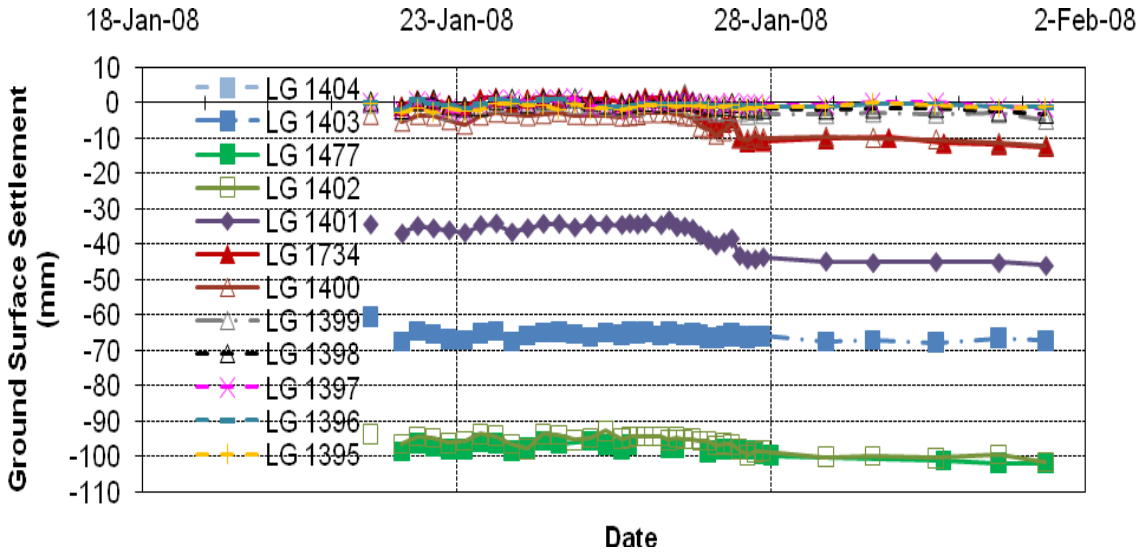

(b)

Figure 5.27 Longitudinal surface settlement profile (a) after first bored tunnelling; and (b) after second bored tunnelling (Instrumentation Array: E14)

Instrumentation Array D49

The location of Instrumentation Array D49 for monitoring ground surface settlements is shown in Figure 5.28. The longitudinal section profiles of Figures 5.29(a) and 5.29(b) summarise the geology along the tunnel alignments. The tunnels were mainly excavated through mixed ground of Jurong Formation (SIII, SIV, SV

and SVI) and Kallang Formation (Fluvial Sand, Fluvial Clay and Marine Clay). The overlying materials consist of Fluvial Sand, Fluvial Clay, Marine Clay, Estuarine and Fill. The longitudinal ground surface settlement profiles corresponding to construction of both the first inner bound and the second outer bound bored tunnels are shown in Figure 5.30(a) and 5.30(b). The longitudinal ground surface settlement recorded by the two ground surface settlement markers of LG1408 installed above the first inner bound bored tunnel and LG1170 installed adjacent to the second outer bound bored tunnel are discussed in detail below.

The EPBM face approached LG1408 at a speed of 36 mm/min on 11 April 2007 where ground surface settlement was recorded as 1 mm. The earth pressure was in the range of 1.73 bar to 1.81 bar. A maximum ground surface settlement of 20 mm was recorded a day after the passing of EPBM tailskin on 11 April 2007. When the EPBM tailskin was beneath LG1408, grouting at a volume of 3910 litres and at injection pressure in a range of 3.2 bar to 3.8 bar was performed. A progressive settlement occurred over a longer period from 12 April to 23 April 2007 where maximum ground surface settlement approached 31 mm. By the end of the monitoring period on 30 April 2007, similar ground surface settlement of 31 mm was recorded, indicating the end of ground consolidation settlement.

In the case of the second outer bound bored tunnelling, initial ground surface settlement recorded on 29 January 2008 was 34 mm, showing significant difference from the final settlement of 17 mm recorded on 30 April 2007 during EPBM tunnelling of the first inner bound bored tunnel. The reason for the large difference is not clear as inspection of the plot indicated no further ground consolidation settlement has taken place after 24 April 2007. Upon approach of the EPBM face beneath Instrumentation Array D49 at speed of 29 mm/min on 01 February 2008, a maximum settlement of 37 mm was initially recorded. Hence, the derived maximum ground surface settlement due to the EPBM face position is 3 mm after considering the initial settlement. The measured EPBM earth pressure was in the range of 1.87 bar to 3.08 bar. The EPBM tailskin passed Instrumentation Array D49 on 01 February 2008 with grout injection pressure in a range of 1.4 bar to 3.3 bar

and at a significantly large grout volume of 6766 litres, where maximum ground surface settlement of 13 mm was derived. Inspection of the EPBM parameter plots for EPBM speed, earth pressure pick-up 3 and total grout indicates slower EPBM speed of typically less than 30 mm/min at higher earth pressure of 4.32 bar was achieved at the later stage. In addition, quantity of grout of generally over 6000 litres was also used when erecting the subsequent few rings. Comparison of the longitudinal section profile of Figure 5.137(b) revealed the presence of Fluvial Sand at the tunnel level and hence, suggesting flowing or slowly ravelling ground condition could have been taken place during EPBM tunnelling. Despite progressively increase of maximum ground surface settlement was observed, no measurement was made after 03 February 2008 where the final maximum ground surface settlement was derived as 24 mm.

Refer to Figures A.109 to A.120 for more information about the EPBM speed, earth pressure and grouting episodes measured at 10 rings before and after the monitoring array.

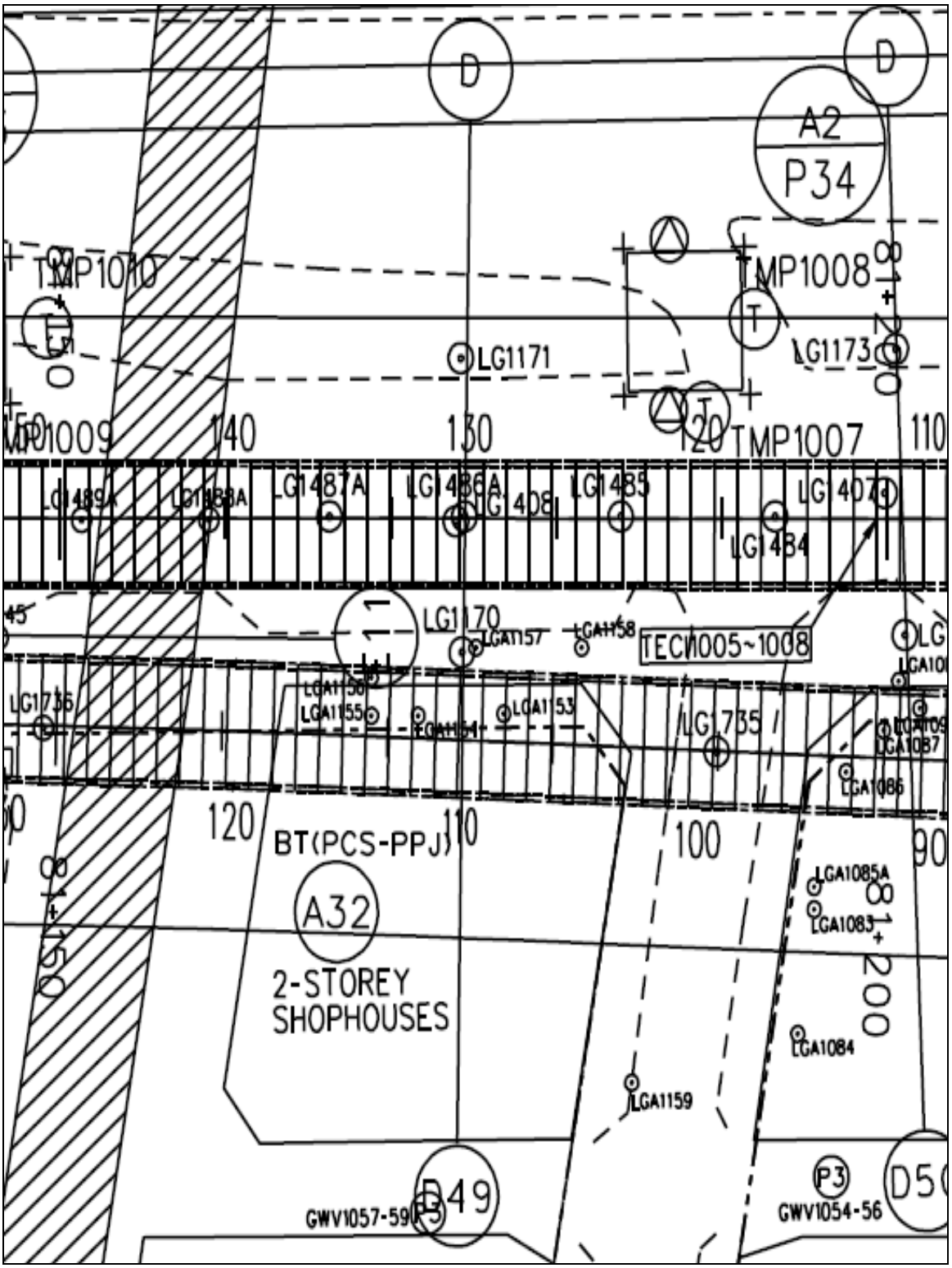

Figure 5.28 Ground surface settlement monitoring array D49

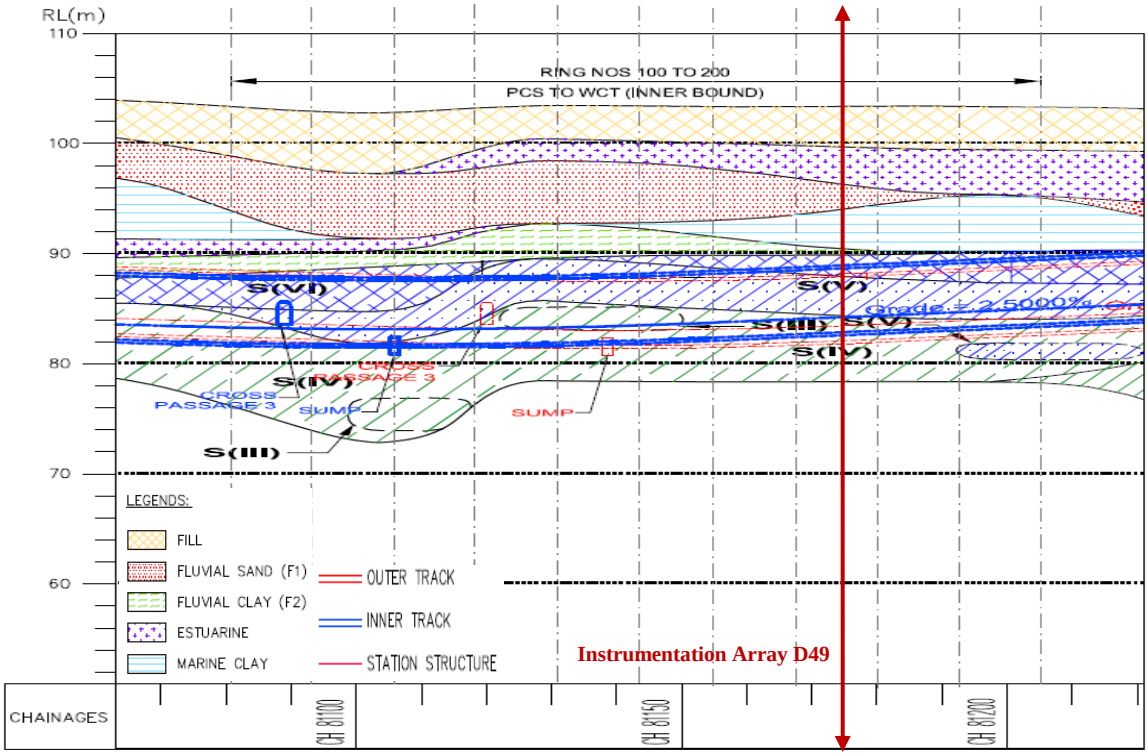

(a)

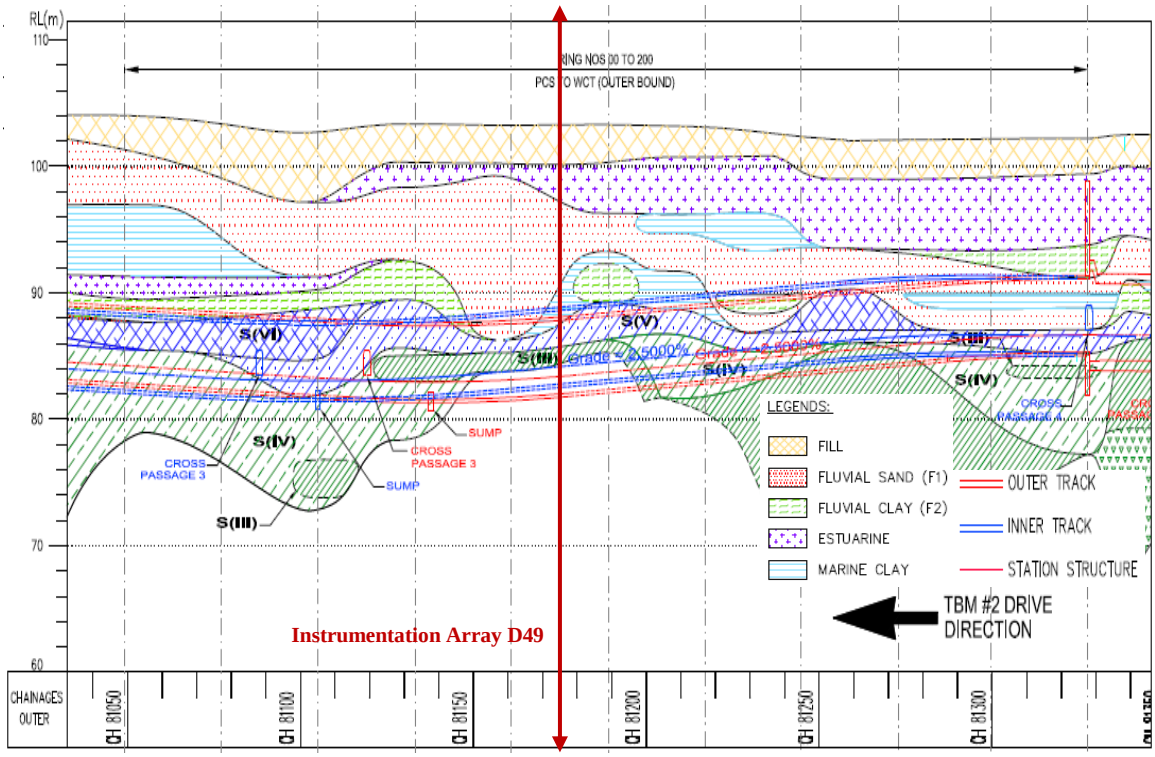

(b)

Figure 5.29 Ground conditions at tunnel level for (a) first inner bound bored tunnel; and (b) second outer bound bored tunnel (Instrumentation Array: D49)

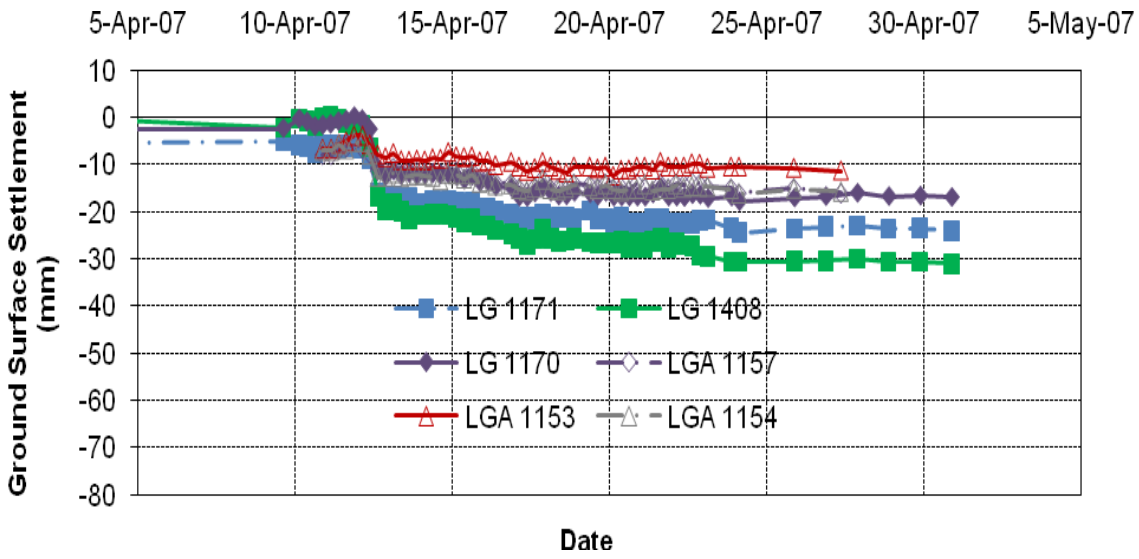

(a)

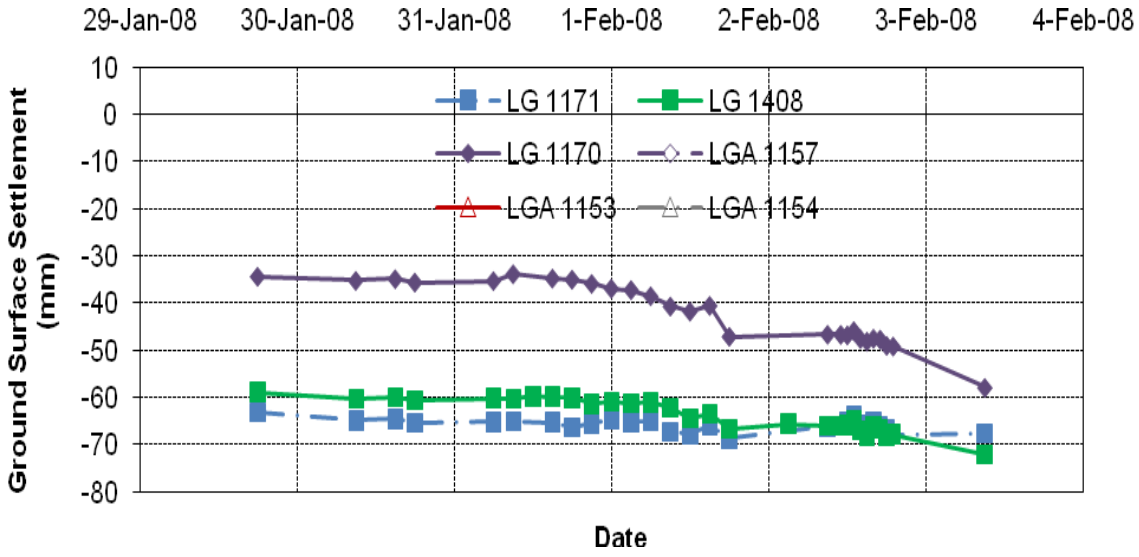

(b)

Figure 5.30 Longitudinal surface settlement profile (a) after first bored tunnelling; and (b) after second bored tunnelling (Instrumentation Array: D49)

Instrumentation Array D47

The location of Instrumentation Array D47 for monitoring ground surface settlements is shown in Figure 5.31. The longitudinal section profiles of Figures 5.32(a) and 5.32(b) summarise the geology along the tunnel alignments. The tunnels were mainly excavated through mixed ground of Jurong Formation (SIV, SV and

SVI) and Kallang Formation (Fluvial Clay). The overlying materials consist of Fluvial Clay, Estuarine, Marine Clay, Fluvial Sand and Fill. The longitudinal ground surface settlement profiles corresponding to construction of both the first inner bound and the second outer bound bored tunnels are shown in Figure 5.33(a) and 5.33(b). The longitudinal ground surface settlement recorded by the two ground surface settlement markers of LG1421 and LG1163 installed above the first inner bound and second outer bound bored tunnels are discussed in detail below.

The erection of ring number 188 was performed at EPBM speed of 19 mm/min with earth pressure in a range of 1.98 bar to 2.94 bar on 05 May 2007. However, an extremely large quantity of total grout of 34622 litres was used with grout injection pressure in a range of 1.4 bar to 3 bar. There was then a stoppage of EPBM tunnelling from 05 May to 21 May 2007 for corrective actions to be taken. During this period, ground surface settlement of the order of 1 mm was recorded by LG1421, indicating no significant ground loss due to the EPBM stoppage. The EPBM face approached LG1421 at a speed of 21 mm/min between 23 May and early 24 May 2007 where ground surface settlement increased from 1.8 mm to 6.9 mm respectively. The earth pressure was in the range of 2.03 bar to 3.29 bar. A maximum ground surface settlement of 28.3 mm was recorded during the passing of EPBM tailskin on 24 May 2007. When the EPBM tailskin was beneath LG1421, grouting at a volume of 5038 litres and at injection pressure in a range of 2.1 bar to 2.7 bar was performed. Observation of LG1165 and LG1164 indicated no ground consolidation settlement has taken place after passing of EPBM. Thus, it could be concluded that the slight increase in ground surface settlement from 28.3 mm to over 32 mm between 24 May and 27 May 2007 was possibly due to the shrinkage of large quantity of grout as mentioned earlier. By the end of the monitoring period on 02 June 2007, ground surface settlement of 34.9 mm was recorded.

In the case of the second outer bound bored tunnelling, initial ground surface settlement recorded on 15 February 2008 was 22.4 mm, showing significant difference from the final settlement of 9.8 mm recorded on 02 June 2007 during EPBM tunnelling of the first inner bound bored tunnel. The reason for the large

difference is not clear as inspection of the plot indicated no ground consolidation settlement has taken place. There was a gradual increase in the maximum ground surface settlement from 22.4 mm recorded on 15 February 2008 to 27 mm recorded on 18 February 2008. This could possibly be due to the decrease of EPBM earth pressure from over 4 bar as indicated by earth pressure pick-up 6 to 2.45 bar prior to increasing to over 3 bar. Upon approach of the EPBM face beneath LG1163 at speed of 18 mm/min on 19 February 2008, a maximum settlement of 29.9 mm was initially recorded. Taking into account the maximum ground surface settlement of 22.4 mm recorded on 15 February 2008, the initial derived maximum ground surface settlement due to approaching of the EPBM face is 7.5 mm. The maximum ground surface settlement increased to 42.8 mm (derived 20.4 mm) on the same date. The measured EPBM earth pressure was in the range of 1.87 bar to 2.62 bar. Another EPBM stoppage occurred from 20 February to 21 February 2008 during erection of ring number 180. The stoppage was attributed to the extremely large quantity of total grout of 23399 litres being used. During this period, maximum ground surface settlement increased from 53.2 mm to 63.8 mm (derived 30.8 mm to 41.4 mm). Other EPBM parameters were within the expected range of 13 mm/min for EPBM speed, 1.96 bar to 2.48 bar for EPBM earth pressure and 1.9 bar to 2.3 bar for grout injection pressure. The EPBM tailskin passed LG1163 on 21 February 2008 with grout injection pressure in a range of 2.1 bar to 2.3 bar and at a grout volume of 3754 litres, where initial maximum ground surface settlement of 65.6 mm (derived 43.2 mm) was recorded. The maximum ground surface settlement increased to 70.4 mm (derived 48 mm) on early 22 February 2007. It should be pointed out that there was an abrupt increase in the maximum ground surface settlement from 79.7 to 121.7 mm (derived 57.3 to 99.3 mm) between end of 22 February and early 23 February 2008. The measurement remained approximately constant until the end of the monitoring period on 24 February 2008.

Refer to Figures A.121 to A.132 for more information about the EPBM speed, earth pressure and grouting episodes measured at 10 rings before and after the monitoring array.

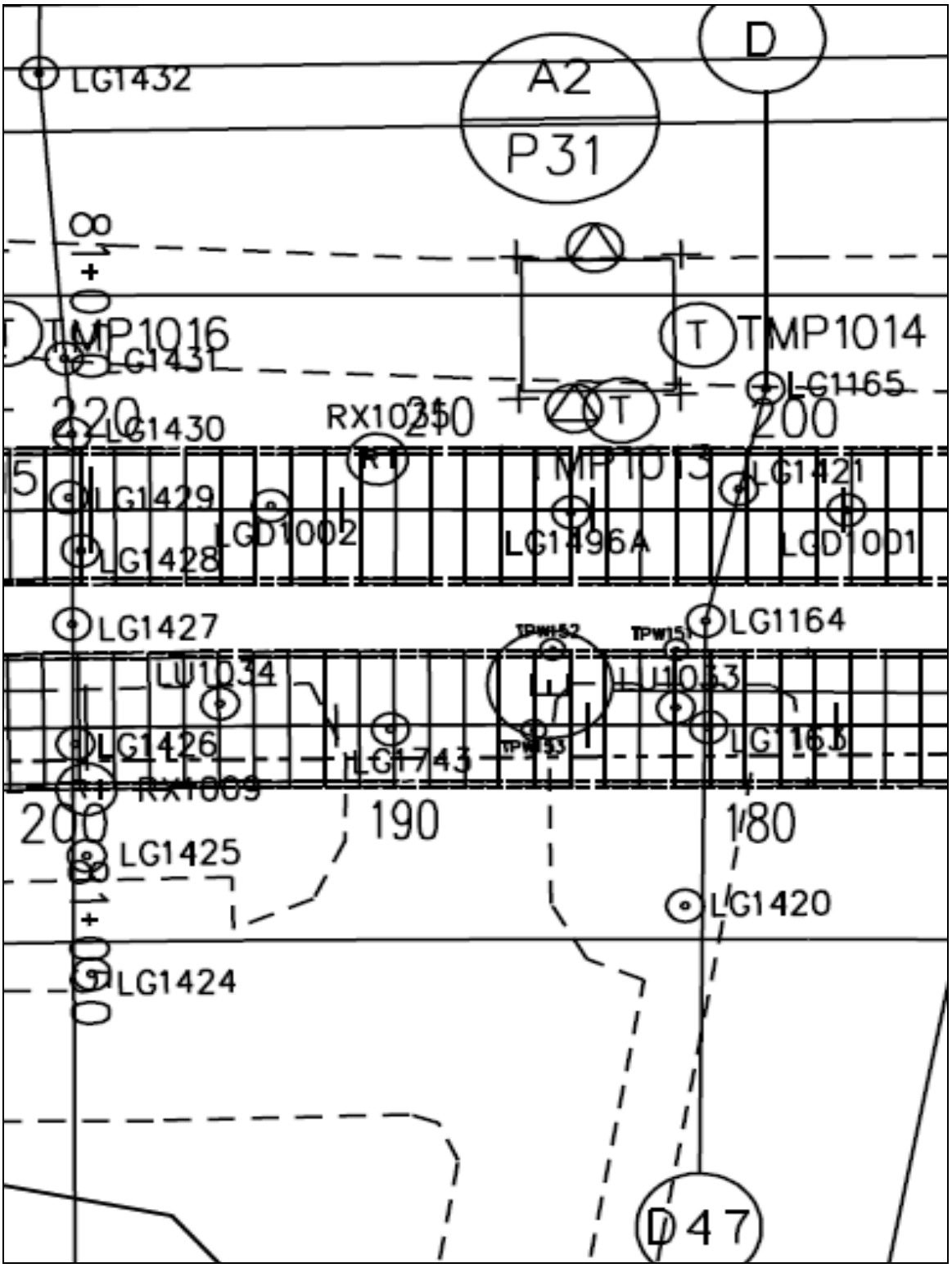

Figure 5.31 Ground surface settlement monitoring array D47

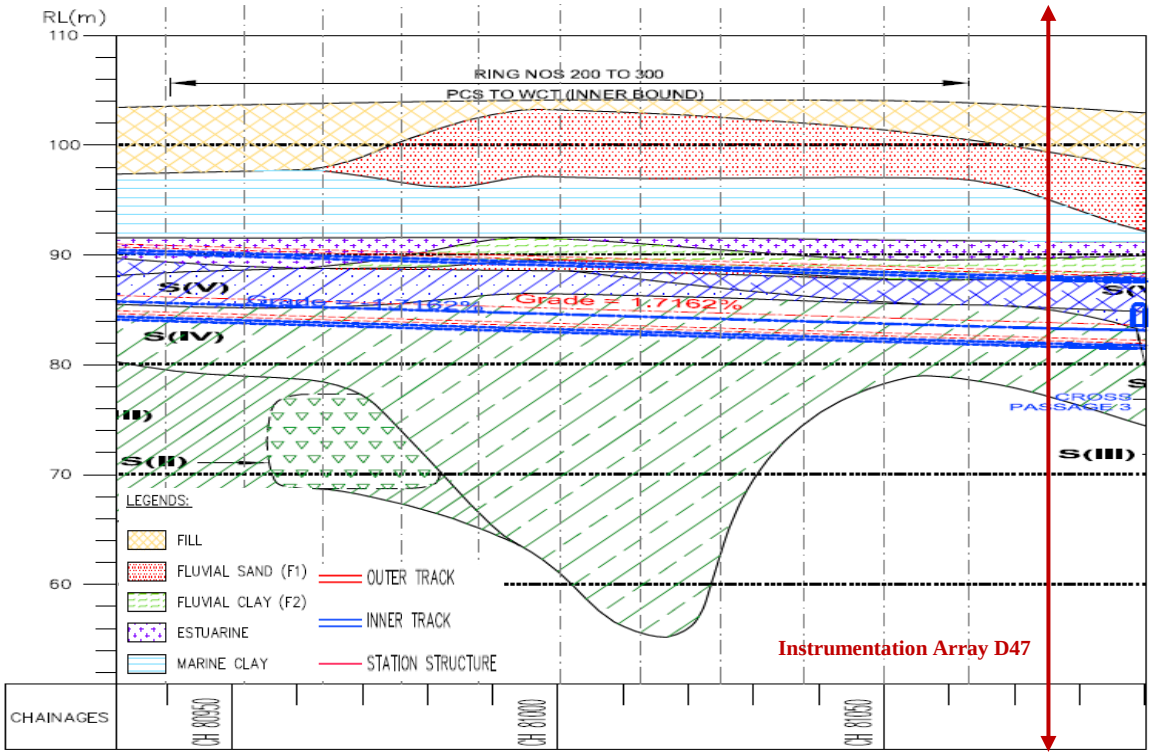

(a)

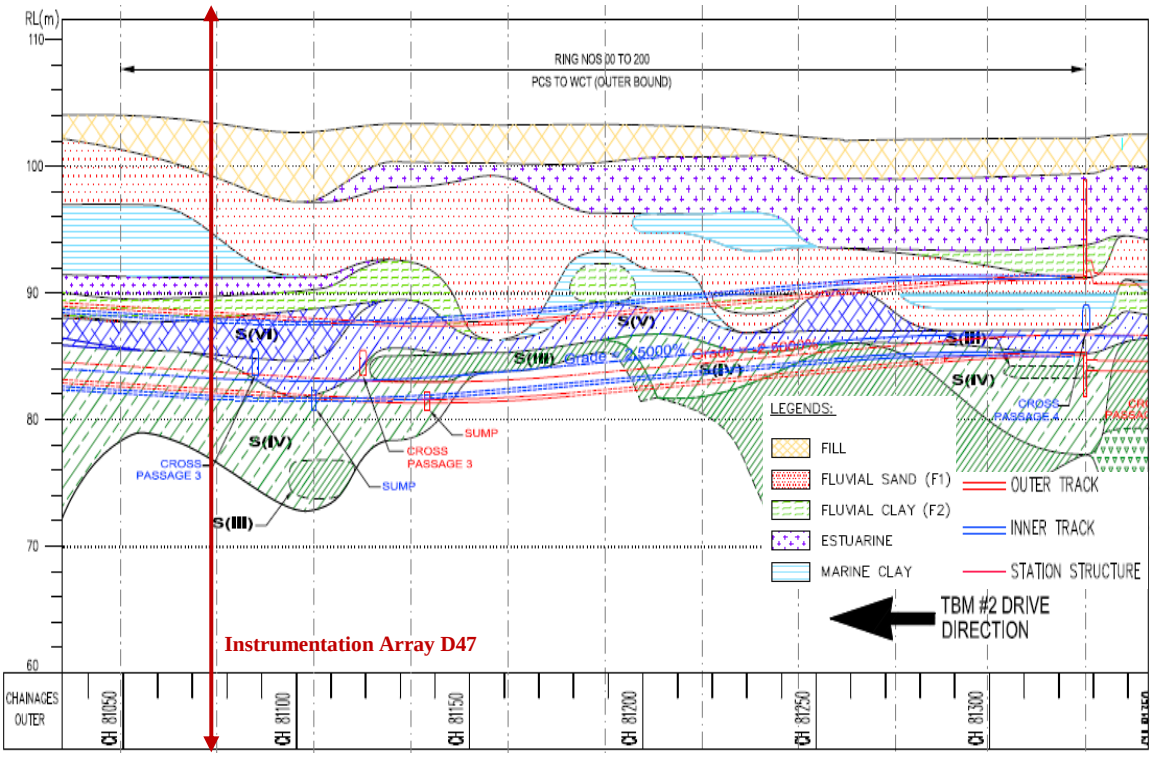

(b)

Figure 5.32 Ground conditions at tunnel level for (a) first inner bound bored tunnel; and (b) second outer bound bored tunnel (Instrumentation Array: D47)

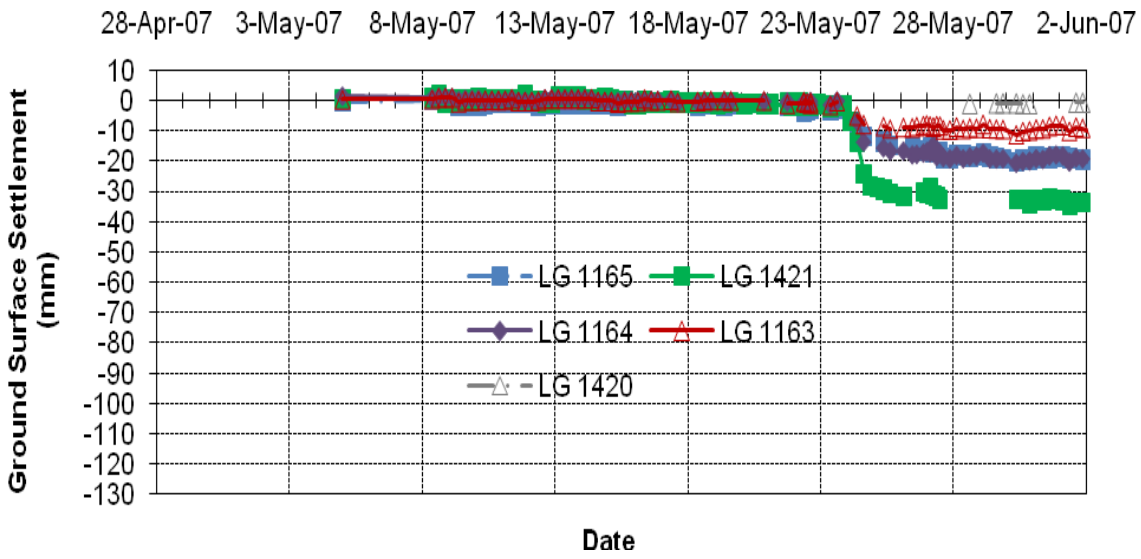

(a)

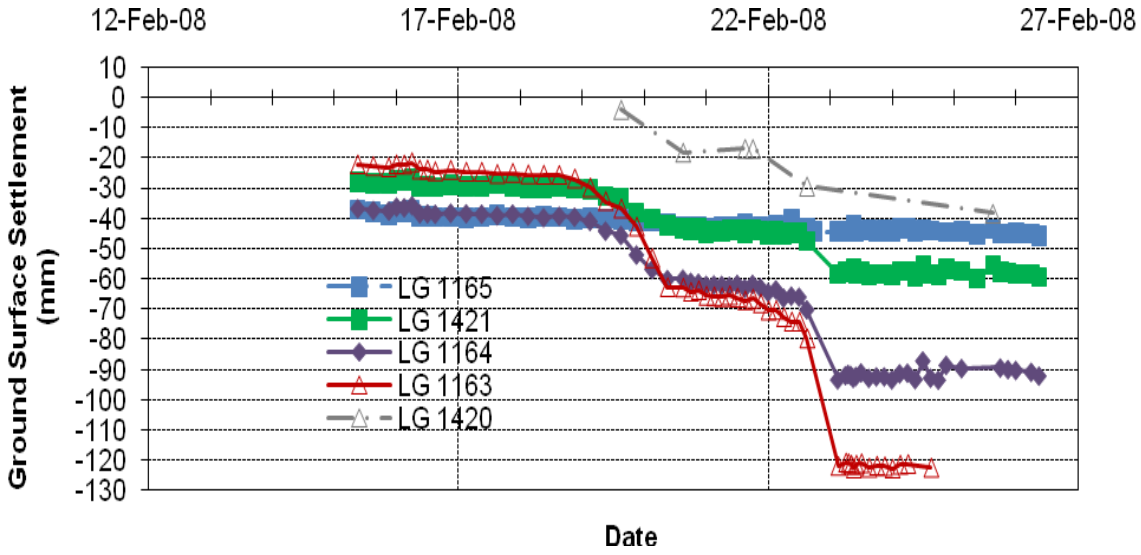

(b)

Figure 5.33 Longitudinal surface settlement profile (a) after first bored tunnelling; and (b) after second bored tunnelling (Instrumentation Array: D47)

Instrumentation Array E10

The location of Instrumentation Array E10 for monitoring ground surface settlements is shown in Figure 5.34. The longitudinal section profiles of Figures 5.35(a) and 5.35(b) summarise the geology along the tunnel alignments. The tunnels were mainly excavated through mixed ground of Jurong Formation (SIV, SV and

SVI) and Kallang Formation (Fluvial Clay). The overlying materials consist of Fluvial Clay, Estuarine, Marine Clay, Fluvial Sand and Fill. The longitudinal ground surface settlement profiles corresponding to construction of both the first inner bound and the second outer bound bored tunnels are shown in Figure 5.36(a) and 5.36(b). The longitudinal ground surface settlement recorded by the two ground surface settlement markers of LG1429 and LG1426 installed above the first inner bound and second outer bound bored tunnels are discussed in detail below.

An initial ground surface heave of about 2 mm was recorded on 25 May 2007. This was followed by a maximum ground surface settlement of 4.6 mm recorded on the same date. During this period, the EPBM speed was generally between 25 mm/min to 31 mm/min. A gradual decrease in earth pressure (as indicated by earth pressure pick-ups 1 to 5) as EPBM progressed from ring number 206 to 209 could be the reason for the corresponding ground surface response. The measured results showed that an increase in EPBM earth pressure when erecting ring number 211 and 212 reduced the ground surface settlement to 2.9 mm on early 26 May 2007. When the EPBM face approached LG1429 at a speed of 20 mm/min on 26 May 2007 the ground surface settlement increased from 2.9 mm to 11.3 mm. The earth pressure was in the range of 1.95 bar to 2.97 bar. A slightly decrease in the maximum ground surface settlement from 11.3 mm to 10.6 mm was recorded during the passing of EPBM tailskin beneath LG1429 between 26 May and 27 May 2007, although subsequent increase in the maximum ground surface settlement to 14.8 mm was observed on 27 May 2007. The relatively small magnitude of ground surface settlement developed over the tailskin could be attributed to the larger EPBM grouting volume of 4338 litres performed at the higher injection pressure in a range of 2 bar to 3.7 bar. Despite further increase in the ground surface settlement, no ground consolidation settlement was observed. By the end of the monitoring period on 06 June 2007, ground surface settlement of 18 mm was recorded.

In the case of the second outer bound bored tunnelling, initial ground surface settlement recorded on 19 February 2008 was 19 mm, showing significant difference from the final settlement of 13.3 mm recorded on 06 June 2007 during

EPBM tunnelling of the first inner bound bored tunnel. The reason for the large difference is not clear as inspection of the plot indicated no ground consolidation settlement has taken place. There was a gradual increase in the maximum ground surface settlement from 19 mm (defined as datum) recorded on 19 February 2008 to 23.1 mm (derived 4.1 mm) recorded on 22 February 2008. There was then a decrease in the maximum ground surface settlement to 19.6 mm (derived 0.6 mm) before a final ground surface settlement of 22.1 mm (derived 3.1 mm) was recorded on 22 February 2008. This small settlement and heave condition is not discussed as it was necessary to use data from a slightly earlier ring number to illustrate effectively the corresponding ground surface response for EPBM tunnelling through very soft soils of Kallang Formation immediately above the tunnel level. Upon approach of the EPBM face beneath LG1426 at speed of 30 mm/min on 23 February 2008, a maximum settlement of 25.1 mm (derived 6.1 mm) was initially recorded. The maximum ground surface settlement increased to 31.8 mm (derived 12.8 mm) on the same date. The measured EPBM earth pressure was in the range of 1.92 bar to 2.47 bar. The EPBM tailskin passed LG1426 on 24 February 2008 with grout injection pressure in a range of 2.7 bar to 3.1 bar and at a grout volume of 5662 litres, where initial maximum ground surface settlement of 32.4 mm (derived 13.4 mm) was recorded. A further increase in the maximum ground surface settlement to 57.8 mm (derived 38.8 mm) was recorded on 25 February 2008. This was followed by a gradual increase in the maximum ground surface settlement to about 63 mm (derived 44 mm), probably due to the shrinkage of the large quantity of grout. The measurement remained approximately constant till the end of the monitoring period on 29 February 2008.

Refer to Figures A.133 to A.144 for more information about the EPBM speed, earth pressure and grouting episodes measured at 10 rings before and after the monitoring array.

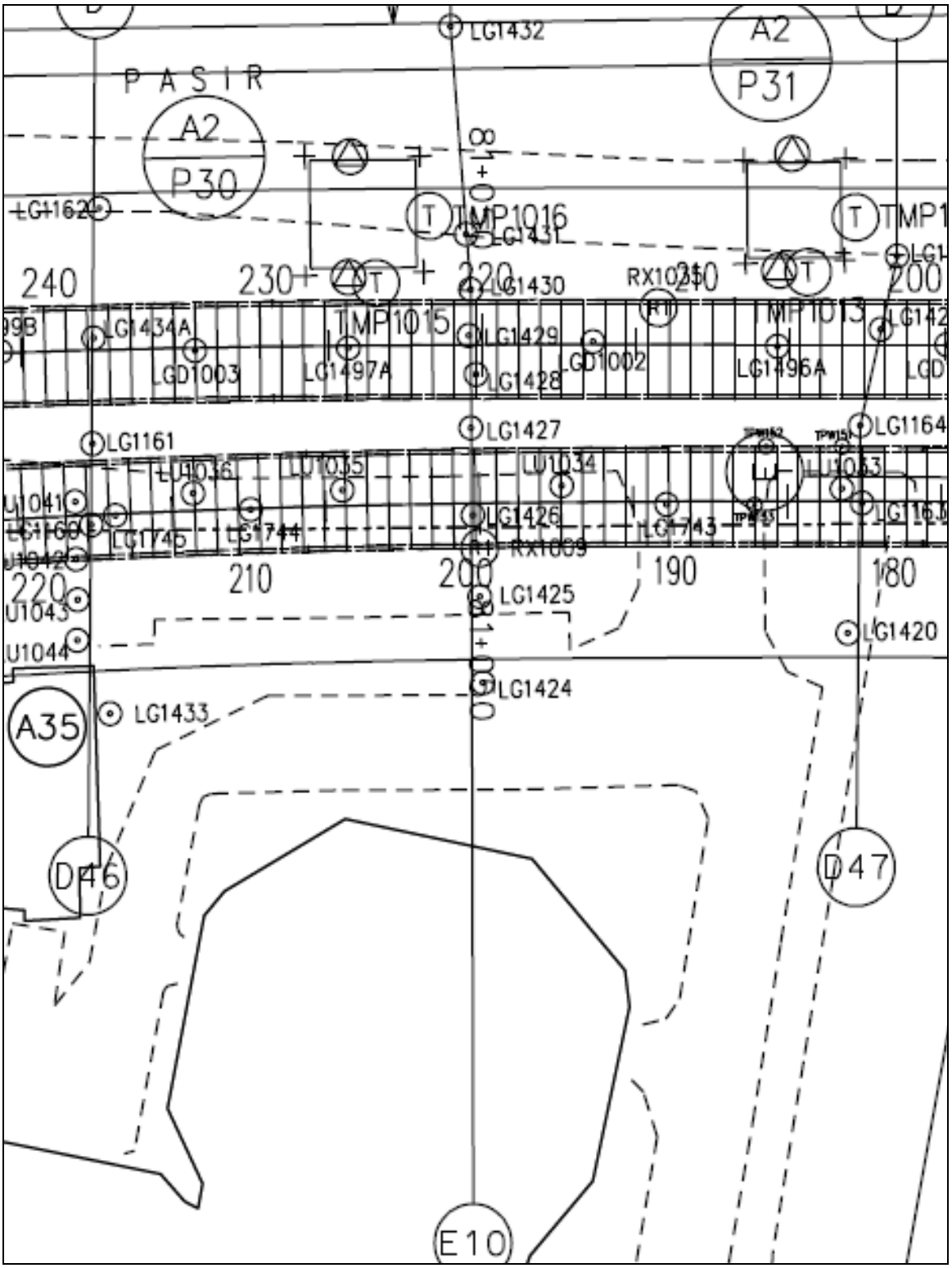

Figure 5.34 Ground surface settlement monitoring array E10

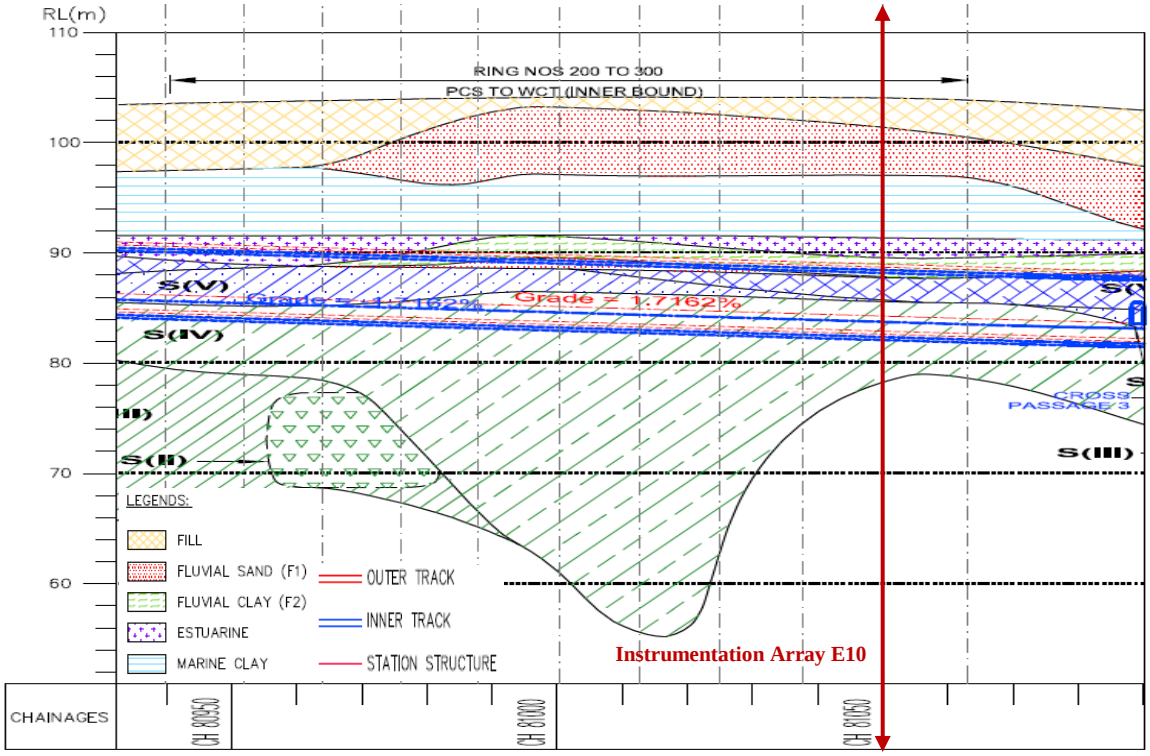

(a)

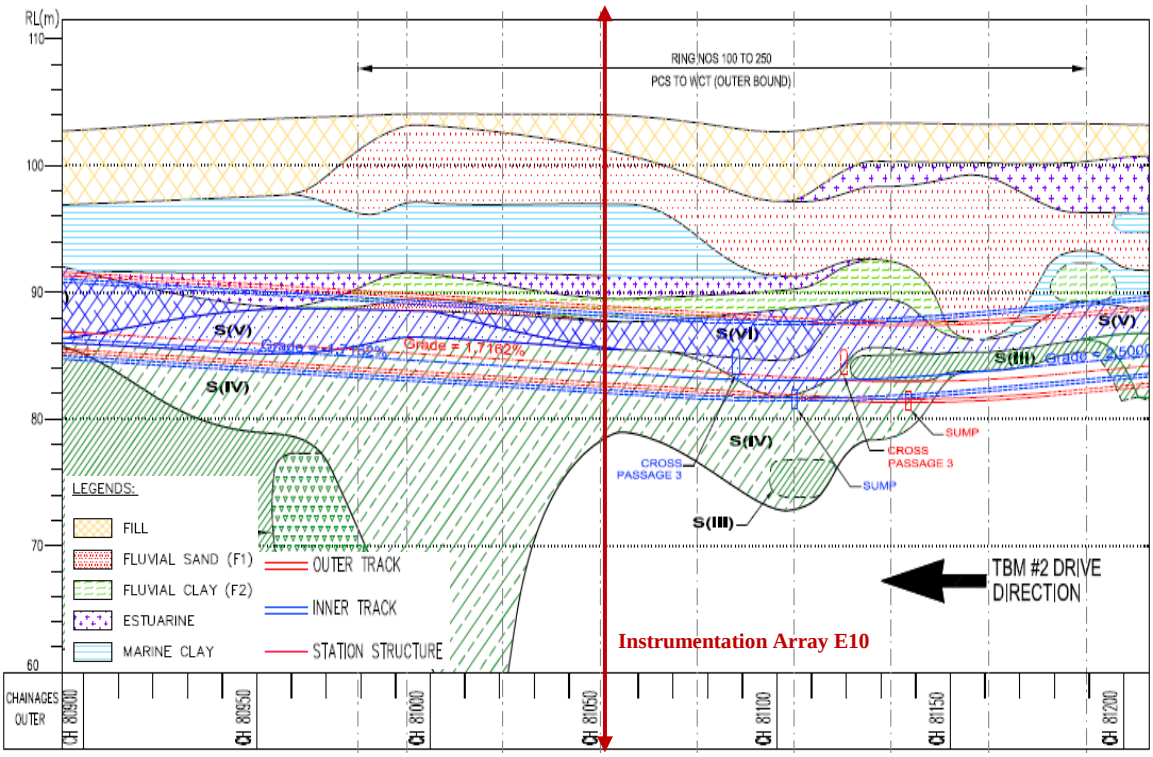

(b)

Figure 5.35 Ground conditions at tunnel level for (a) first inner bound bored tunnel; and (b) second outer bound bored tunnel (Instrumentation Array: E10)

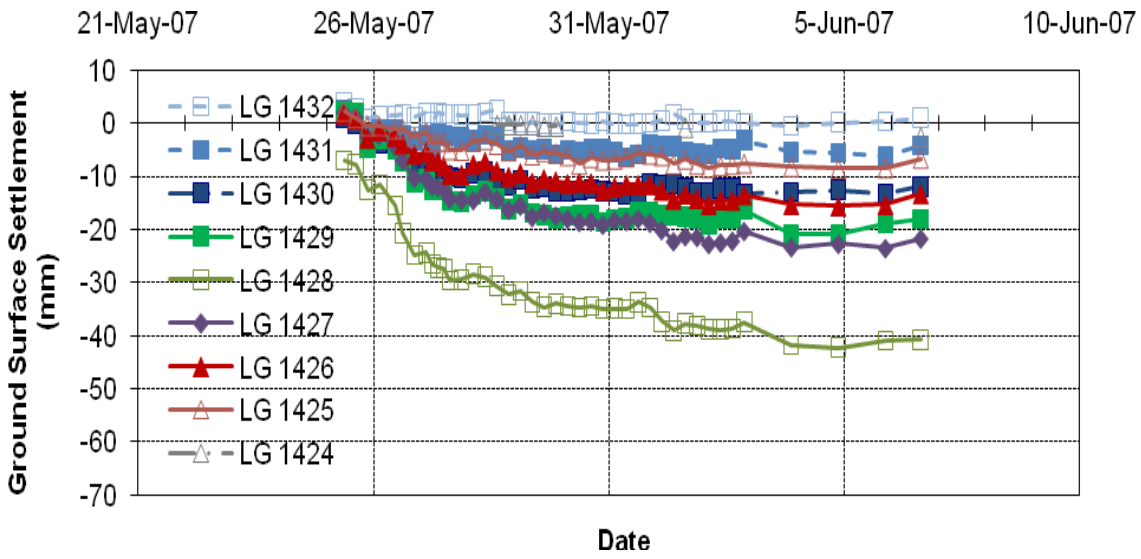

(a)

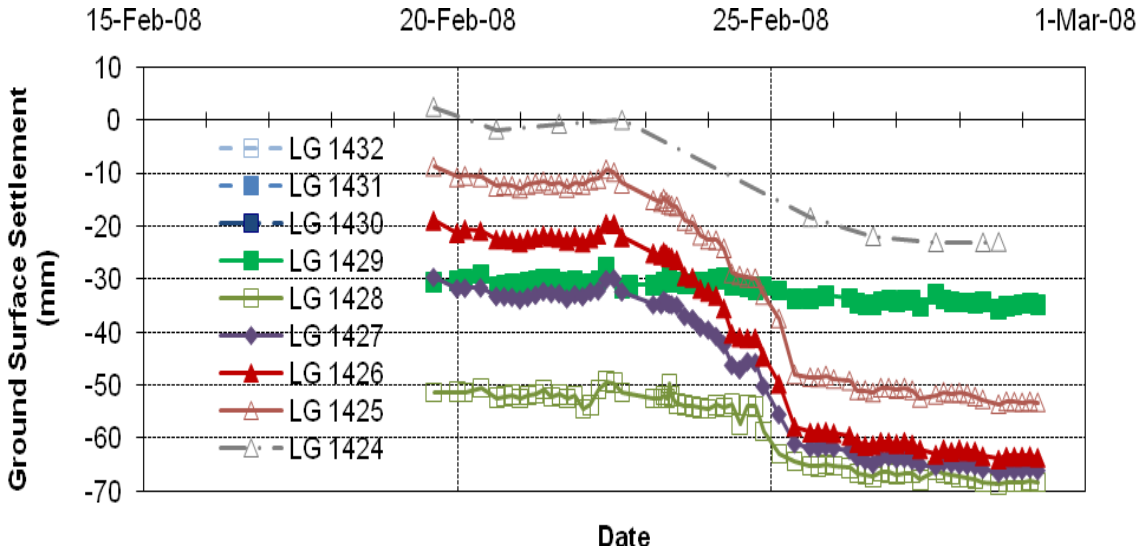

(b)

Figure 5.36 Longitudinal surface settlement profile (a) after first bored tunnelling; and (b) after second bored tunnelling (Instrumentation Array: E10)

Instrumentation Array D46

The location of Instrumentation Array D46 for monitoring ground surface settlements is shown in Figure 5.37. The longitudinal section profiles of Figures 5.38(a) and 5.38(b) summarise the geology along the tunnel alignments. The tunnels were mainly excavated through mixed ground of Jurong Formation (SIV, SV and

SVI) and Kallang Formation (Fluvial Clay). The overlying materials consist of Fluvial Clay, Estuarine, Marine Clay, Fluvial Sand and Fill. The longitudinal ground surface settlement profiles corresponding to construction of both the first inner bound and the second outer bound bored tunnels are shown in Figure 5.39(a) and 5.39(b). The longitudinal ground surface settlement recorded by the two ground surface settlement markers of LG1434A and LG1160 installed above the first inner bound and second outer bound bored tunnels are discussed in detail below.

Generally 1.5 mm to 2.5 mm of ground surface settlement had taken place prior to the approach of the EPBM beneath LG1434A. This indicates the longer zone of influence of the settlement of Fluvial Clay encountered along the tunnel route. When the EPBM face approached LG1434A at a speed of 44 mm/min on 01 June 2007 the ground surface settlement increased from 2.1 mm to 7.1 mm. The earth pressure was in the range of 2.05 bar to 2.44 bar. A further increase in the maximum ground surface settlement from 12.3 mm to 20.5 mm was recorded during passing of the EPBM tailskin beneath LG1434A on early 02 June 2007. There was subsequently an abrupt increase in the maximum ground surface settlement to 40.2 mm on the same date. This significantly large magnitude of ground surface settlement occurred over a short period of time indicates squeezing of Fluvial Clay at the tail void. There was no improvement observed in the EPBM grout injection parameters when the EPBM grouting was performed at about a similar volume of 4481 litres at injection pressure in a range of 2.1 bar to 4.2 bar as the earlier tunnelling stage. Again, there was no ground consolidation settlement observed. By the end of the monitoring period on 08 June 2007, ground surface settlement of 37.6 mm was recorded.

In the case of the second outer bound bored tunnelling, initial ground surface settlement recorded by LG1160 on 22 February 2008 was 11.6 mm, showing considerable difference from the final settlement of approximately 8 mm recorded between 03 June and 06 June 2007 during EPBM tunnelling of the first inner bound bored tunnel. The reason for the small magnitude of maximum ground surface settlement of 2.4 mm recorded by LG1160 on 08 June 2007 is not clear and should

be cautiously viewed. There was a gradual increase in the maximum ground surface settlement from 11.6 mm (defined as datum) recorded on 22 February 2008 to 15.1 mm (derived 3.5 mm) recorded on 24 February 2008. Upon approach of the EPBM face beneath LG1160 at speed of 25 mm/min on 25 February 2008, a maximum settlement of 14.1 mm (derived 2.5 mm) was initially recorded. The maximum ground surface settlement increased to 25.6 mm (derived 14 mm) on the same date. The measured EPBM earth pressure was in the range of 1.25 bar to 2.06 bar. The EPBM tailskin passed LG1160 on 26 February 2008 where maximum ground surface settlement increase from 25.8 mm (derived 14.2 mm) to 38.8 mm (derived 27.2 mm). The grout injection pressure was in a range of 0.7 bar to 3.2 bar and at a grout volume of 3728 litres. This induced a gradual decrease in the maximum ground surface settlement to 35.6 mm (derived 24 mm) on the same date. LG1160 recorded a progressive increase in the maximum ground surface settlement from 36.1 mm (derived 24.5 mm) on 27 February 2008 to 46.8 mm (derived 35.2 mm) on 01 March 2008. This could be attributed to the squeezing of the Fluvial Clay into the insufficiently grouted tail void. The maximum ground surface settlement remained approximately constant till the end of the monitoring period on 01 March 2008.

Refer to Figures A.145 to A.156 for more information about the EPBM speed, earth pressure and grouting episodes measured at 10 rings before and after the monitoring array.

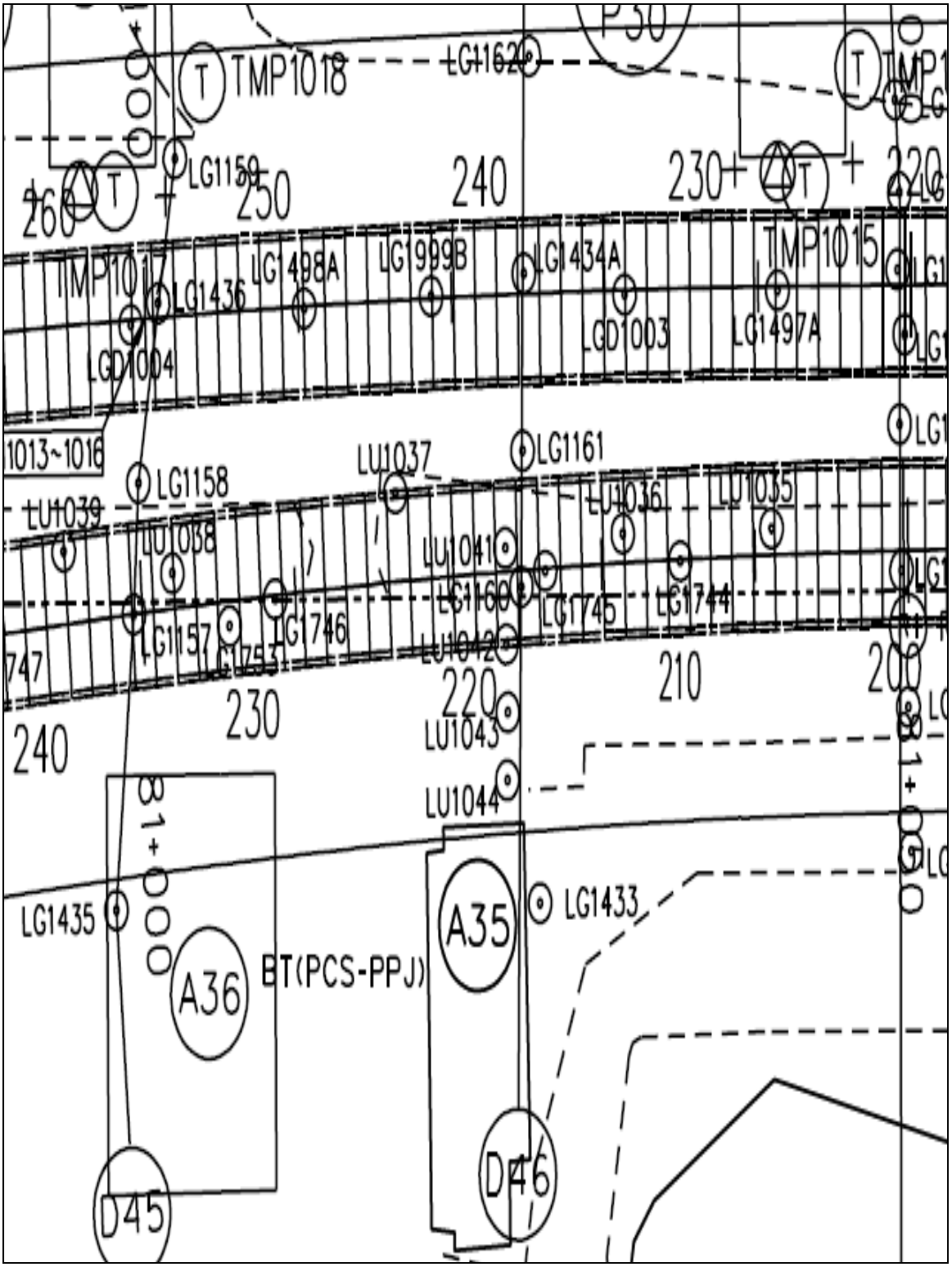

Figure 5.37 Ground surface settlement monitoring array D46

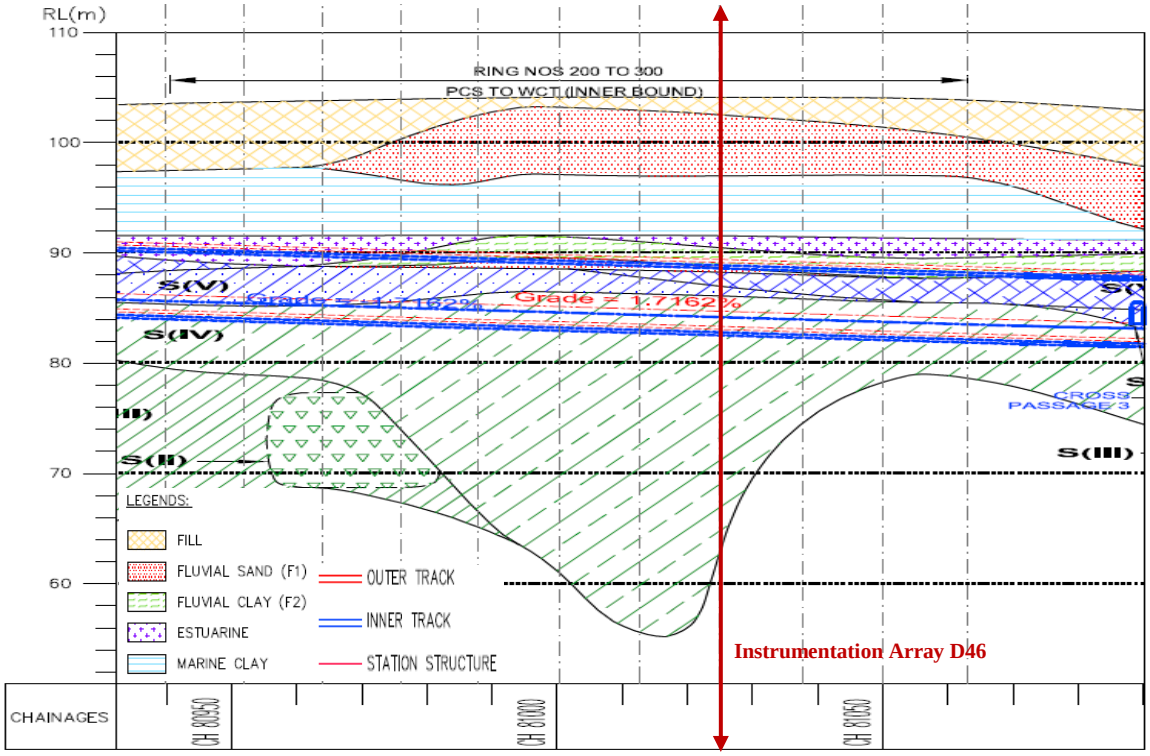

(a)

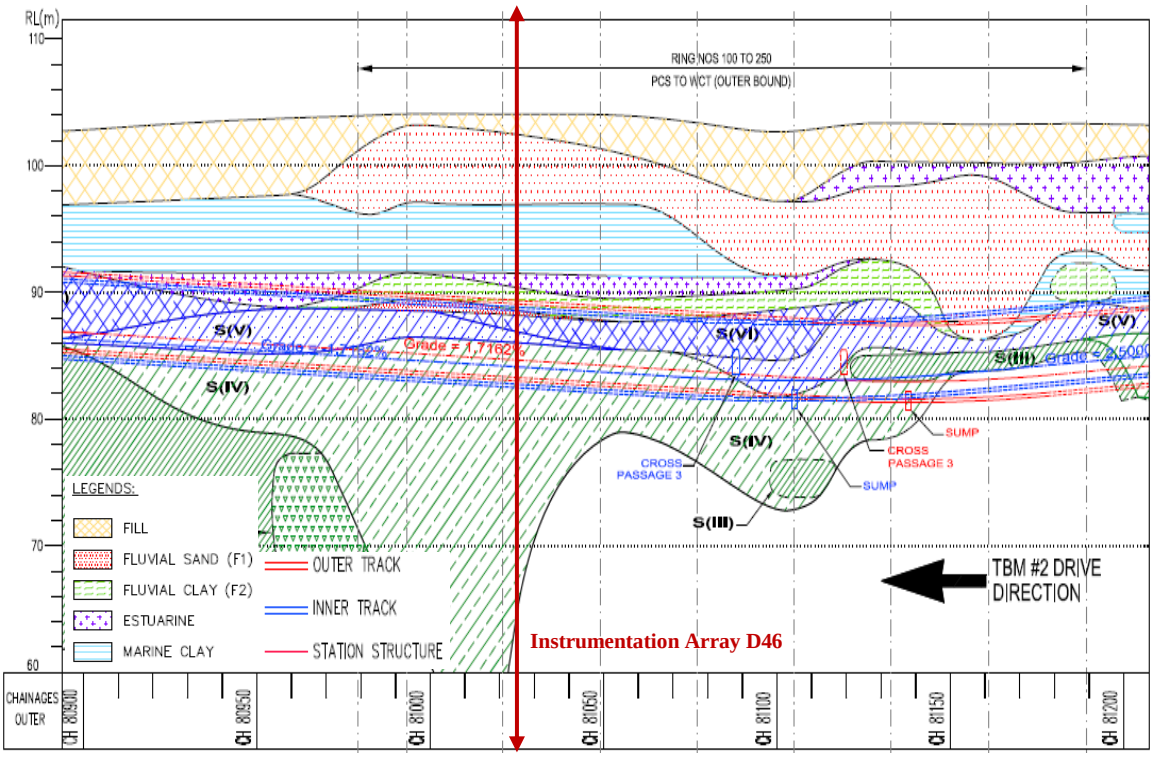

(b)

Figure 5.38 Ground conditions at tunnel level for (a) first inner bound bored tunnel; and (b) second outer bound bored tunnel (Instrumentation Array: D46)

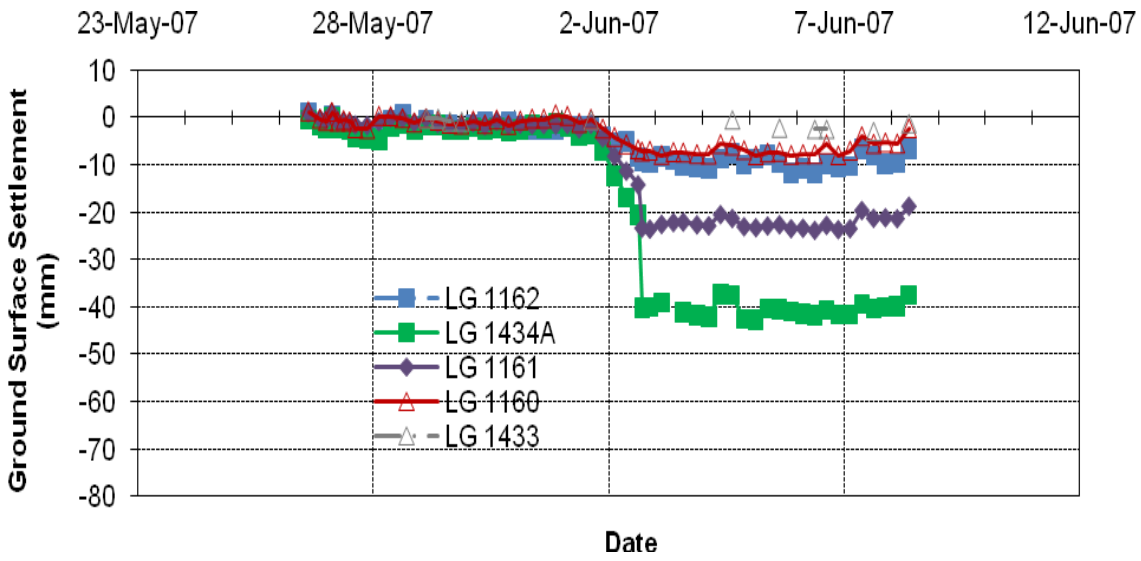

(a)

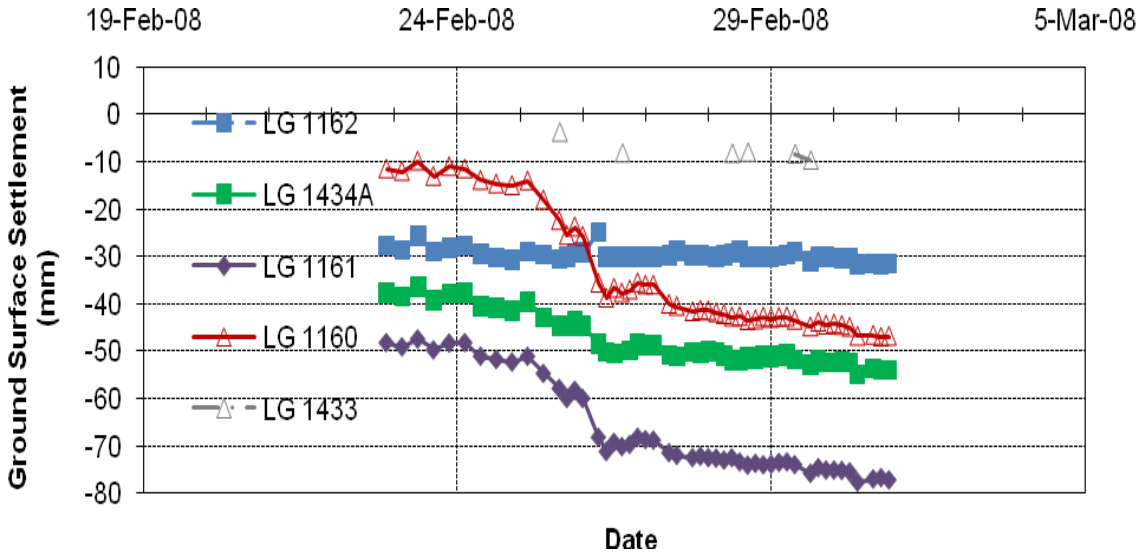

(b)

Figure 5.39 Longitudinal surface settlement profile (a) after first bored tunnelling; and (b) after second bored tunnelling (Instrumentation Array: D46)

5.3 Summary

The longitudinal ground surface settlement profiles measured above the first inner bound and second outer bound bored tunnels constructed through uniform grade of Jurong Formation, mixed grades of Jurong Formation and mixed ground of Jurong

Formation and Kallang Formation for Circle Line Contract 856 were studied. The following conclusions can be drawn:

1. For Instrumentation Array D35, given similar EPBM earth pressure of 0.67 to 1.76 bar and 0.9 to 1.3 bar for the first inner bound and second outer bound bored tunnelling, the slower EPBM speed of 36 mm/min for the second outer bound bored tunnelling as compared to the 50 mm/min for first inner bound bored tunnelling had led to additional 4.4 mm maximum ground surface settlement observed above the EPBM face for the second outer bound bored tunnel. This suggests a considerable influence of the EPBM speed on the magnitude of the maximum ground surface settlement above EPBM face for tunnelling through uniform grade of Jurong Formation.
2. As observed for Instrumentation Array E9, EPBM tunnelling through uniform grade of Jurong Formation at high earth pressure in a range of 1.98 to 2.62 bar as measured by one of the earth pressure pick-ups induced ground surface heave of 1.9 mm at a distance of approximately 7 rings in front of the EPBM face, despite the decrease in EPBM speed from 39 to 34 mm/min. The Instrumentation Array D34 showed ground surface heave of 1 mm at a distance of approximately 9 rings in front of EPBM face where EPBM tunnelling was at a decreasing speed of 50 to 37 mm/min with earth pressure in a range of 0.95 to 2.41 bar measured by one of the earth pressure pick-ups. Observation for Instrumentation Array D7 involved ground surface heave of 3 mm at a distance of approximately 7 rings in front of EPBM face where EPBM speed increased from 40 to 70 mm/min at high earth pressure in a range of 2.16 to 2.47 bar as measured by one of the earth pressure pick-ups. These observations highlighted the influence of EPBM speed on the ground surface heave.
3. The initial occurrence of ground surface heave may lead to smaller resultant ground surface settlement upon approach of the EPBM face. Corresponding evidence was observed for Instrumentation Array E9 and D34. The former with the EPBM speed of 38 mm/min at earth pressure in a range of 1.49 to 1.62 bar had induced a change in the initial ground surface heave of 1.9 mm to ground surface settlement of 0.2 mm. The latter showed a change in the ground surface heave of 1 mm to ground surface settlement of the same magnitude, taking into

account of EPBM speed of 35 mm/min and earth pressure in a range of 0.45 to 1.34 bar, except gauge 5 recorded a higher earth pressure of 3.16 bar. The net settlement of 2 mm was achieved above the EPBM face.

4. The presence of mixed grades of Jurong Formation along the tunnel route may lead to significant differences in the magnitude of the ground surface settlement measured between the first and second constructed bored tunnels. Hence, sufficient ground investigation is required along each tunnel route for better planning on the appropriate range of EPBM parameters to be used during tunnelling to minimise the ground surface response.
5. For the first EPBM tunnelling (Instrumentation Arrays D33 and D32) through mixed grades of Jurong Formation SIV and SV, EPBM grout injection pressure in a range of 1.4 to 2.7 bar at volume of 3612 to 3715 litres could minimise the maximum ground surface settlement to below 10 mm. It should, however, be expected for a significantly larger magnitude of final ground surface settlement to occur during the second EPBM tunnelling along the adjacent route.
6. For EPBM tunnelling through mixed ground of Jurong Formation and Kallang Formation, an inefficiency of grouting over the EPBM shield and tail void may induce significantly larger final settlement due to flowing and squeezing of Fluvial Sand and Fluvial Clay over a short period of time.
7. EPBM negotiates through mixed ground of Jurong Formation and Kallang Formation at a slower speed, higher earth pressure, larger grout injection pressure and volume as compared to uniform grade of Jurong Formation.

The comparative study indicates qualitatively that, to some extent, there is a quantitative interrelationship between the EPBM parameters and the ground surface response. The information gathered from Circle Line Contract 856 should be useful for other bored tunnelling projects constructed through similar ground conditions.

CHAPTER 6 FINITE ELEMENT ANALYSIS OF GROUND SURFACE SETTLEMENTS INDUCED BY CLOSELY SPACED BORED TUNNELS

6.1 Introduction

An assessment of longitudinal ground surface settlements utilising Earth Pressure Balance Machine (EPBM) parameters in Chapter 5 has provided insight into the performance of EPBM tunnelling through Jurong Formation and mixed ground of Jurong Formation and Kallang Formation. Following from this, it is also necessary to be able to estimate the extent and magnitude of the ground surface settlement. A total of 13 back analyses have been performed in this chapter using two-dimensional (2D) finite element method program PLAXIS. Comparisons have been made between the field measurements of Circle Line Contract 856 and results generated using PLAXIS for the transverse surface settlements above single bored tunnel and closely spaced bored tunnels. The main reasons for not considering the three-dimensional (3D) finite element simulation were explained in Sections 3.2 and 3.4 as follows:

a. Lin et al. (2002) in Figures 3.7 and 3.8 pointed out that a 2D analysis can be performed in place of the 3D analysis for estimation of transverse surface settlement if the section considered is far behind the tunnel face as the shield advances.
b. Möller (2006) in Figures 3.9 and 3.13 has shown the adequacy of 2D numerical analysis to produce comparable results with 3D numerical analysis for ground surface settlements.
c. Although the effects of Tunnel Boring Machine (TBM) face pressure can be studied using 3D numerical analyses where it is well known that increasing TBM face pressure reduces the volume loss, reference should be made to the findings of Shirlaw (2002) as illustrated in Figure 3.3 that for tunnelling through weathered rocks of the Jurong Formation with no Kallang Formation soils above tunnel, the settlements were observed to be uniformly low and independent of the face pressure.

All these references indicate that it is not as critical to conduct 3D numerical analyses in this research involving bored tunnels constructed through weathered rocks of the Jurong Formation.

For numerical modelling, careful selection of the relevant soil model and its representative soil properties is essential for achieving good quality result. It is generally appreciated that tunnelling involves unloading and reloading of its surrounding soils. Hence, deformation properties for unloading and reloading should be considered in numerical analysis where the Hardening Soil model was adopted for assessing the ground surface settlement. The Mohr-Coulomb model has also been used to facilitate comparison between the results of the two different soil models. The framework for evaluating the soil properties are presented first, followed by the finite element modelling procedures and the results of the back analyses.

6.2 Mohr-Coulomb (MC) Model for Sand

For the Fluvial Sand, the correlation for the undrained Young's modulus E_u is shown in Table 4.5. The drained Young's modulus E' is obtained from elastic theory where

$$G = \frac{E'}{2(1+\nu_d)} = \frac{E_u}{2(1+\nu_u)} \tag{6.1}$$

Assuming drained Poisson's ratio $\nu_d = 0.3$ and undrained Poisson's ratio $\nu_u = 0.5$,

$$E' = \frac{E_u}{1.15} \tag{6.2}$$

Schmertmann (1978) proposed correlations between ϕ' and D_r for uniform or well-graded fine, medium and coarse sand as shown in Equations 6.3 to 6.5.

Uniform fine sand: $\phi' = 28^o + 0.14D_r$ (6.3)

Uniform medium or well-graded fine sand: $\phi' = 31.5^o + 0.12D_r$ (6.4)

Uniform coarse or well-graded medium sand: $\phi' = 35^o + 0.10D_r$ (6.5)

Chu et al. (2000) conducted a laboratory study to characterise the engineering properties of the Fluvial Sand. The in situ relative density was calculated to be 26.9 per cent which indicates the sand was at a loose state (Terzaghi and Peck, 1948). Hence, Equation 6.3 is adopted for calculation of effective friction angle for Fluvial Sand with $c' = 0$ kPa.

6.3 Mohr-Coulomb (MC) Model for Clay

The correlations between undrained Young's modulus and undrained shear strength with Standard Penetration Test (SPT) N value for residual soil (SVI) and completely weathered rock of Jurong Formation (SV) are presented in Table 4.3. The Geotechnical Interpretative Report by CPG Consultants Pte. Ltd. (2005) for Circle Line Contract 856 recommended E_u = 2.0N MPa for residual soil and completely weathered rock of Jurong Formation.

Leong et al. (2003) reported a trend showing SPT N value increasing with depth z through the residual soils of Jurong Formation. A considerable scatter in the SPT N value plotted with depth z from several boreholes is shown Figure 6.1. It was highlighted by Leong et al. (2003) that more valuable information can be obtained when the SPT N value is plotted against depth z from the top of the Jurong Formation. Based on the correlations developed for each lower bound and upper bound SPT N value against depth z, an average correlation of N as 1.5z which appeared to fit the lower bound correlation for typical SPT N value with depth z from top of Jurong Formation as indicated in Figure 6.2 is obtained. As the folding nature of the Jurong Formation may complicate the process to determine the depth of its top surface, the practical way is to adopt the correlation where the depth is determined from the ground surface from where the borehole is sunk. Thus, the average correlation as shown in Equation 6.6 is assumed for the back analysis.

$$N = 1.5z \tag{6.6}$$

Based on recent extensive pressuremeter testing implemented for the land transport infrastructure construction in Singapore, empirical relationships between SPT N value and pressuremeter modulus E_p for different types of soils in Singapore were recommended by Goh et al. (2012), as shown in Table 6.1. Referring to the proposed normalised stiffness degradation curve for retaining walls, foundations and tunnels (see Figure 6.3), Atkinson and Sallfors (1991) and Mair (1993) indicated that the shear strain for tunnelling was in a range of about 0.05 per cent to 1 per cent. Consequently, 0.5 per cent radial strain was adopted as the basis for estimating the reload modulus given by Equation 6.7 for residual soil and completely weathered rock of Jurong Formation.

$$E_p = 2.8N = E_u \tag{6.7}$$

The corresponding plot for correlation of SPT N value with undrained shear strength c_u obtained from unconsolidated undrained triaxial tests for residual soil and completely weathered rock of Jurong Formation was presented by Leong et al. (2003), suggesting c_u in a range of N to 8N (see Figure 6.4). It was also pointed out by Leong et al (2003) that Stroud's (1974) correlation of c_u as 5N kPa (Equation 6.8) provides a reasonable average for the Singapore residual soils and is adopted in this study.

$$c_u = 5N \tag{6.8}$$

For the soft clays of Kallang Formation, the corresponding correlations for undrained Young's modulus E_u and undrained shear strength c_u shown in Table 4.5 were assumed in the numerical analysis. The variation of undrained shear strength c_u with depth from ground surface as shown in Figure 6.5 was also used as a guideline in determining the undrained shear strength c_u for the Marine Clay.

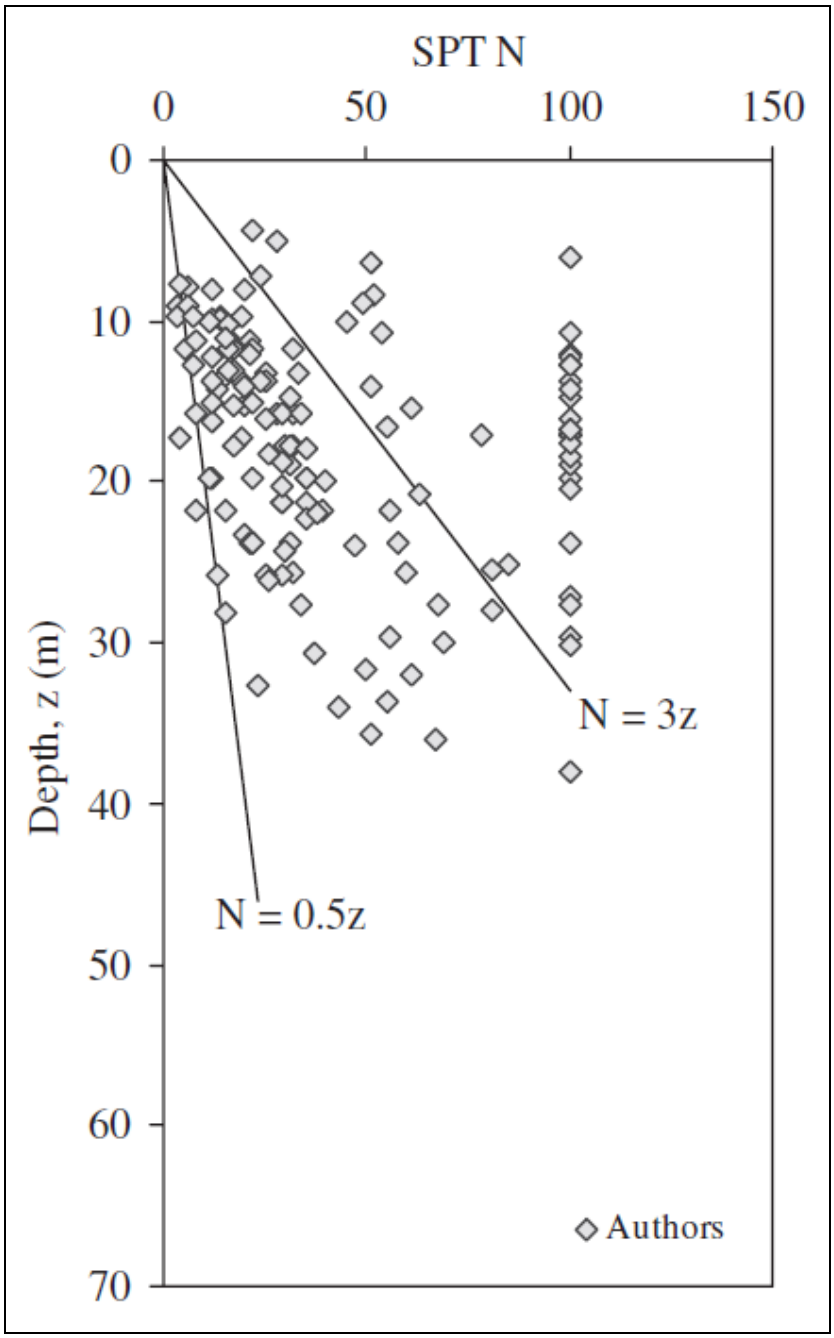

Figure 6.1 Typical SPT results with depth for Jurong Formation residual soils (after Leong et al., 2003)

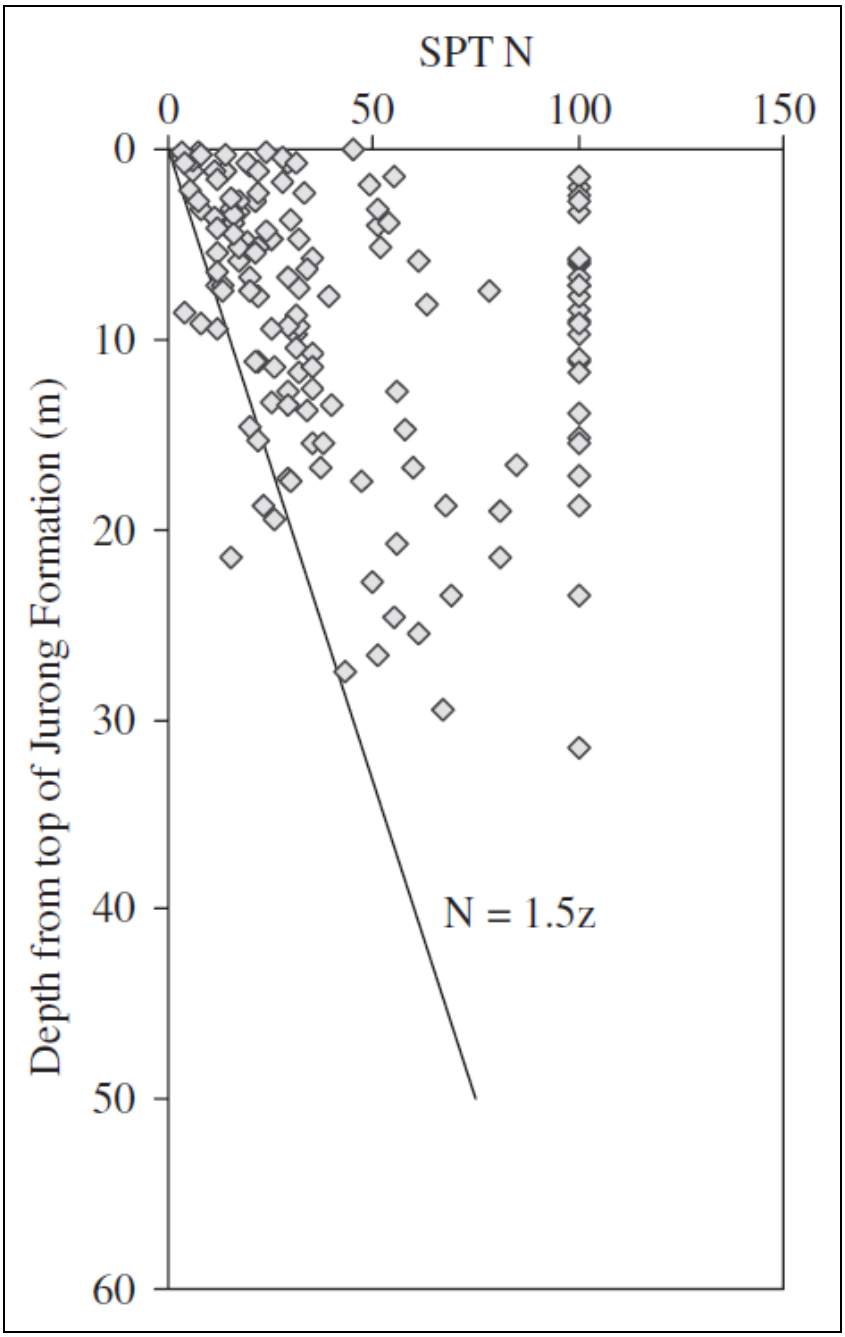

Figure 6.2 Typical SPT results with depth from top of formation for Jurong Formation residual soils (after Leong et al., 2003)

Table 6.1 Pressuremeter modulus for different types of soils in Singapore (after Goh et al., 2012)

	Elastic modulus interpreted from reload portion of pressuremeter curve		
	Reload modulus at 1% radial strain	Reload modulus at 0.5% radial strain	Reload modulus at 0.1% radial strain
	Pressuremeter moduli correlated to SPT-N (in MPa)		
Soils of Bukit Timah Granite (GV, GVI)	1.8*N	3.0*N	7.8*N
Old Alluvium of various grades of weathering	2.5*N	3.7*N	9.6*N
Soils of Jurong Formation (SV, SVI)	1.6*N	2.8*N	8.4*N

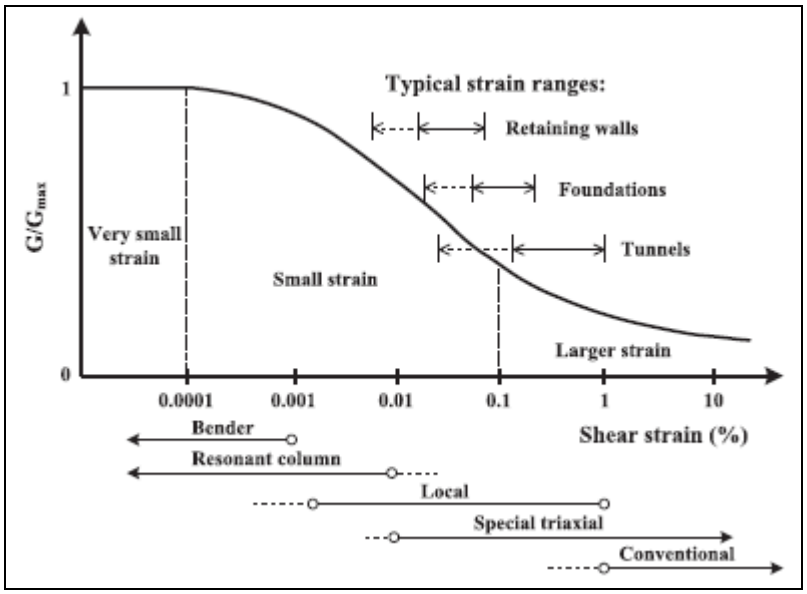

Figure 6.3 Normalised stiffness degradation curve (after Atkinson and Sallfors, 1991; Mair, 1993)

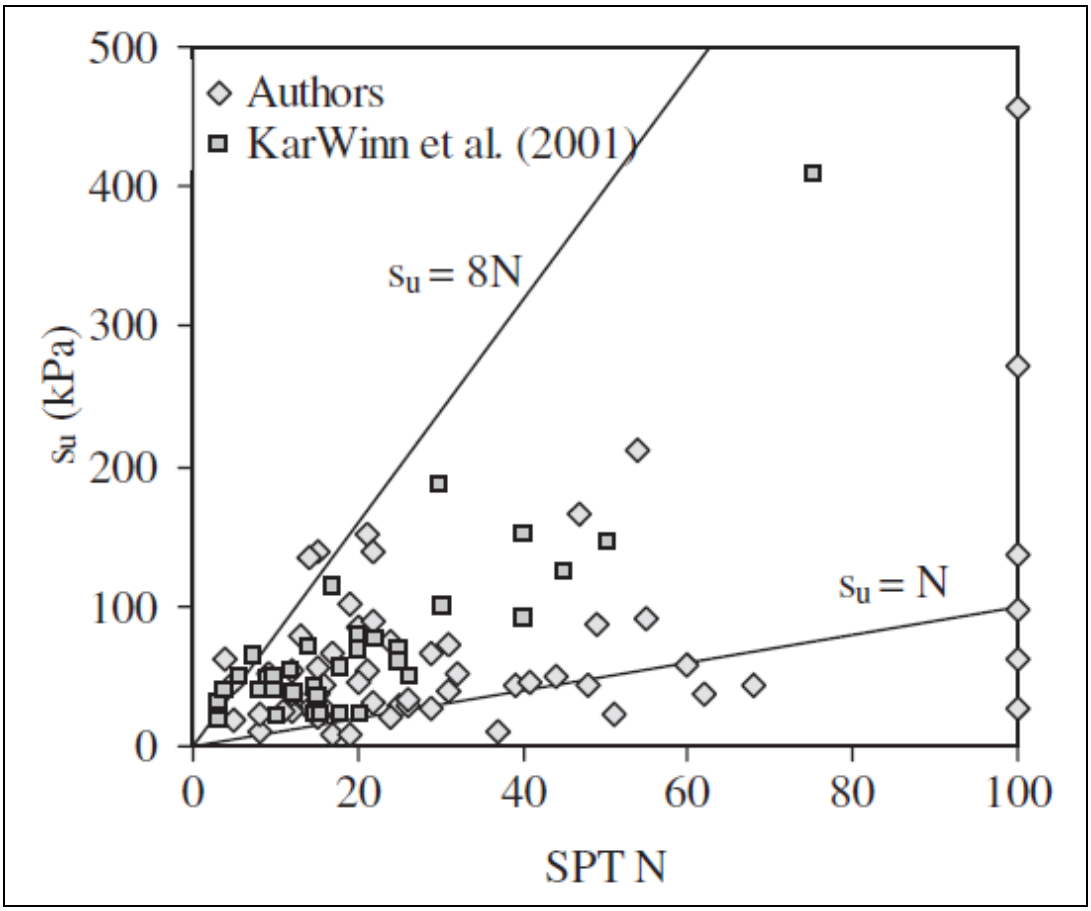

Figure 6.4 Correlation of SPT N with c_u (indicated as s_u) from UU tests for Jurong Formation residual soils (Leong et al., 2003)

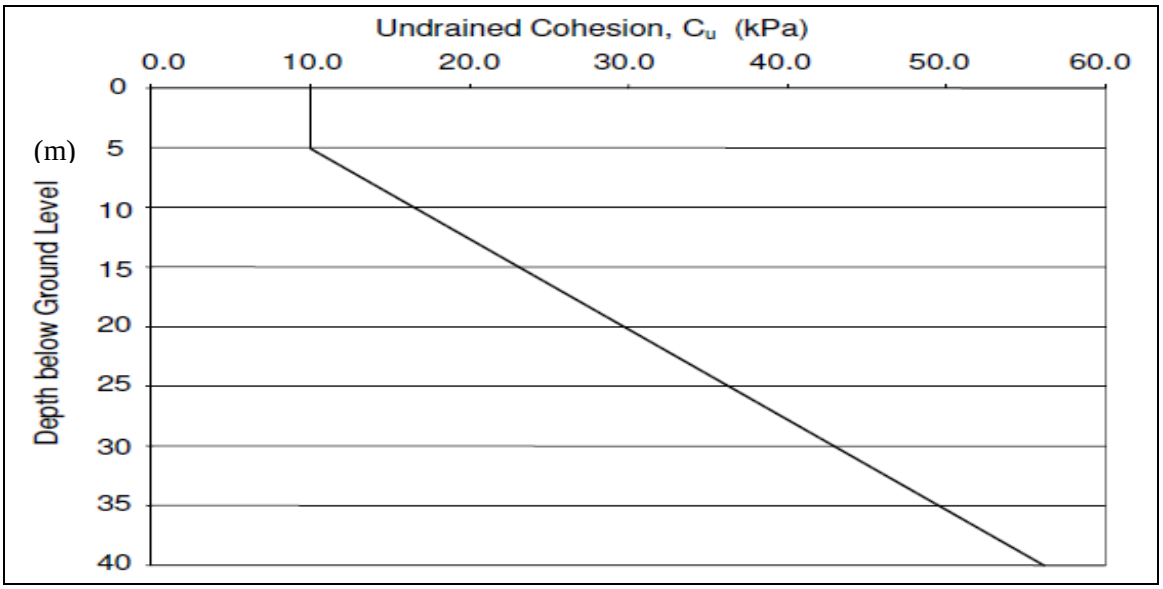

Figure 6.5 Undrained cohesion of the normally or slightly over-consolidated Marine Clay (after Land Transport Authority, 2010)

6.4 Hardening Soil (HS) Model for Firm to Hard Clay

The Hardening Soil (HS) model (Schanz et al., 1999) is a hyperbolic soil model for simulating the behaviour of different soil types from loose sand to various clays. The model was based on the classical theory of plasticity using stress-dependent stiffness. The plastic strains were calculated by introducing a multi-surface yield criterion. The hardening law was assumed to be isotropic depending both on the plastic shear strains and volumetric strains. The model involved frictional hardening characteristics to model plastic shear strains in deviatoric loading and cap hardening characteristics to model plastic volumetric strains in primary compression. The failure mechanism was defined by means of the Mohr-Coulomb failure criterion.

Figure 6.6 shows the stress-strain relationship of the HS model which is implemented in PLAXIS. In the figure, the parameter E_{50} is the confining stress dependent stiffness modulus for primary loading and is given by the Equation 6.9. The amount of stress dependency is given by the power m. As observed from laboratory tests of many clay soils, the power m = 1.0 is recommended.

For unloading and reloading stress paths, another stress-dependent stiffness modulus E_{ur} is used and defined as Equation 6.12.

The failure parameters c', ϕ' and ψ of the Hardening Soil model coincide with those of the Mohr-Coulomb model. The basic parameters for soil stiffness are as follows:

Secant stiffness in standard drained triaxial test (E_{50}^{ref})

In this research, the Hardening Soil model with Undrained B is used to model the undrained or short-term material behaviour. The stiffness is defined in terms of effective stress properties and strength is defined in terms of undrained shear strength c_u. Since $\phi_u = 0$, E_{50} and E_{ur} are constants and no longer increasing with confining stress, σ'_3.

$$E_{50} = E_{50}^{ref} \left(\frac{c_u \cos\phi_u - \sigma_3^{'} \sin\phi_u}{c_u \cos\phi_u + p^{ref} \sin\phi_u}\right)^m = E_{50}^{ref} = const. \quad (6.9)$$

where p^{ref}=100 kPa

$$E_{50} = 0.7E_u \text{ (see Figure 6.7)} \quad (6.10)$$

Tangent stiffness for primary oedometer loading (E_{oed}^{ref})

The default recommendation from PLAXIS is

$$E_{oed}^{ref} = E_{50}^{ref} \quad (6.11)$$

Unloading / reloading stiffness (E_{ur}^{ref})

$$E_{ur} = E_{ur}^{ref} \left(\frac{c_u \cos\phi_u - \sigma_3^{'} \sin\phi_u}{c_u \cos\phi_u + p^{ref} \sin\phi_u}\right)^m = E_{ur}^{ref} = const. \quad (6.12)$$

The default recommendation from PLAXIS is

$$E_{ur} = 3E_{50} \quad (6.13)$$

The other parameters are as follows:

Poisson's ratio for unloading-reloading (ν_{ur})

The default recommendation from PLAXIS is

$\nu_{ur} = 0.2$

K_o-value for normal consolidation (K_o^{nc})

$$K_o^{nc} = 1 - \sin\phi^{'} \quad (6.14)$$

Failure ratio (R_f)

$$R_f = \frac{q_f}{q_a} \quad (6.15)$$

The default recommendation from PLAXIS is $R_f = 0.9$ (see Figure 6.6).

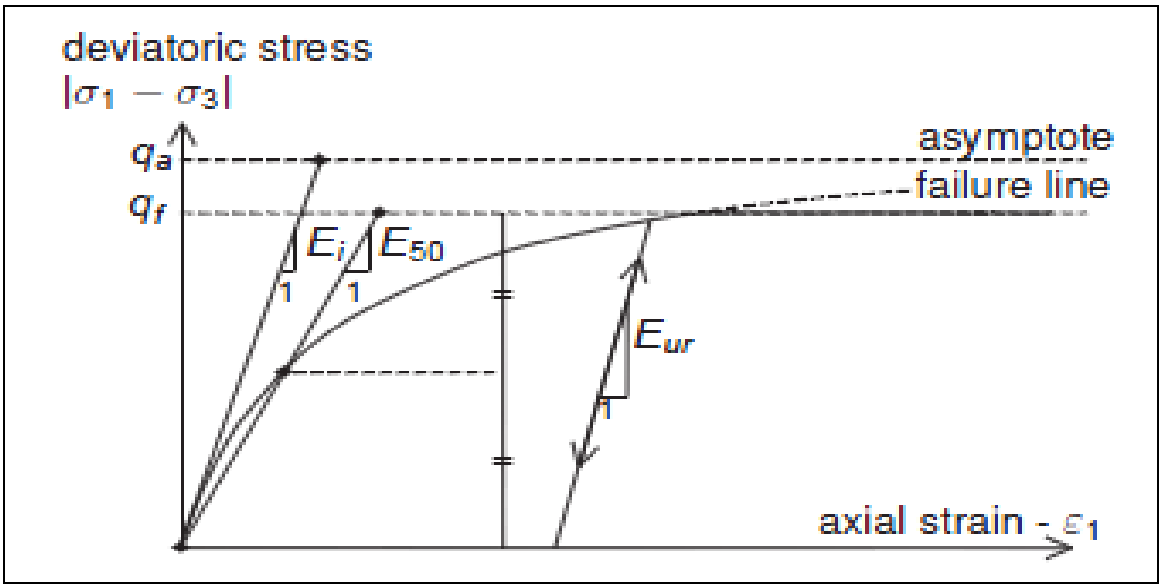

Figure 6.6 Hyperbolic stress-strain relation in primary loading for a standard drained triaxial test (after Brinkgreve et al., 2012)

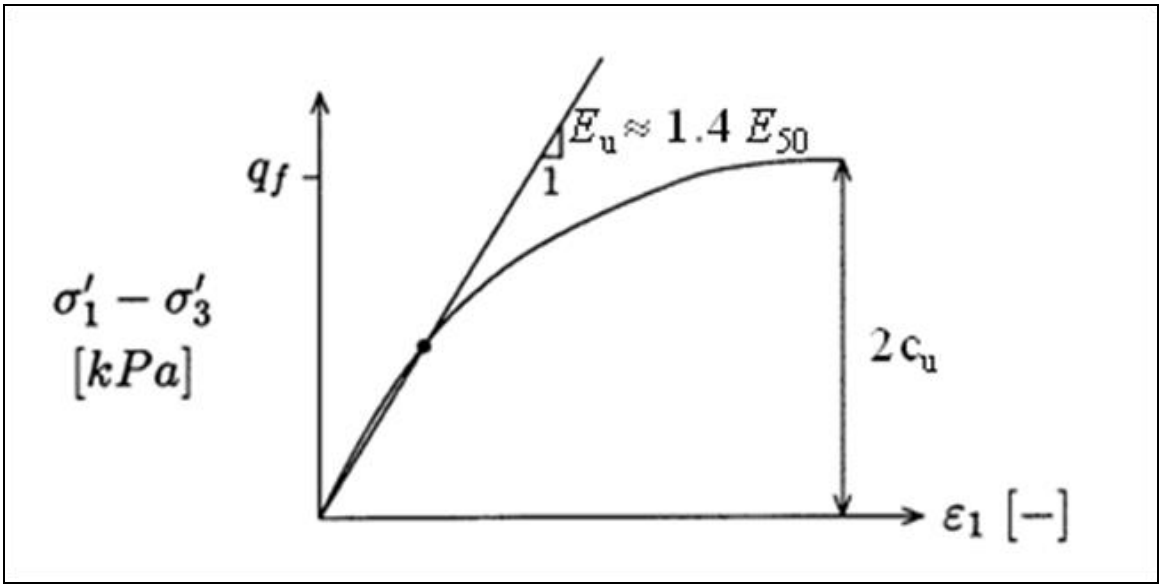

Figure 6.7 Hyperbolic stress-strain relation in primary loading for a standard drained triaxial test (after Sture, 2004)

The correlations used for the back analyses are summarised in Tables 6.2 and 6.3 for the HS and MC models respectively. For the Jurong Formation, both the HS and MC models were considered. For the Marine Clay and Fluvial Sand, only the MC model was considered.

Table 6.2 Hardening Soil (HS) model

Soil property	Symbol	Suggested Equation	Unit
Undrained shear strength for Jurong Formation	c_u	5N	kPa
Secant Young's modulus	E_{50}	$0.7E_u$ (with E_u=2.8N)	MPa

Table 6.3 Mohr-Coulomb (MC) model

Soil Property	Symbol	Suggested Equation	Unit
Undrained shear strength for Jurong Formation	c_u	5N	kPa
Undrained shear strength for Marine Clay	c_u	See Table 4.5	kPa
Effective friction angle for Fluvial Sand	ϕ'	$28^o+0.14D_r$	^{o}
Undrained Young's modulus for Jurong Formation	E_u	2.8N	MPa
Undrained Young's modulus for Marine Clay	E_u	$0.2c_u$	MPa
Drained Young's modulus for Fluvial Sand	E'	$E_u/1.15$	MPa

6.5 Finite Element Modelling

The finite element method program, PLAXIS, was adopted to model the first inner bound (I.B.) and second outer bound (O.B.) bored tunnels constructed through Jurong Formation and mixed ground of Jurong Formation and Kallang Formation. Both the Hardening Soil (HS) model and Mohr-Coulomb (MC) model were used to simulate the soil behaviour. The simulation was performed using 15-node triangular elements. All tunnels which have the same outer and inner diameter of 6350 mm

and 5800 mm were modelled using 5-node plate elements. The linear elastic parameters of tunnel lining are summarised in Table 6.4. The standard fixities option in PLAXIS which imposes no horizontal displacement along the vertical boundaries and no displacement along the bottom horizontal boundary was selected to represent the displacement boundary conditions. The generation of the mesh was performed using global coarseness of very fine mesh with subsequent local refinement of the uppermost geometry line to achieve acceptable accuracy on the numerical results.

Table 6.4 Material properties of the tunnel lining

Property	**Symbol**	**Value**	**Unit**
Thickness	t	0.275	m
Unit weight	γ_l	24	kN/m^3
Deformation modulus	E_l	30000	MPa
Poisson's ratio	ν_l	0.25	-

The staged construction simulation involved the following steps:

Initial phase: Perform initial stress analysis using K_o procedure;

Phase 1: Construction of the first tunnel by deactivating the soil and activating the tunnel lining;

Phase 2: Applying contraction of a tunnel lining to simulate soil volume loss (VL) due to construction of a bored tunnel;

Phase 3: Repetition of steps in Phase 1 for second tunnel;

Phase 4: Repetition of step in Phase 2 for second tunnel.

6.5.1 Boundaries and Mesh Size

A sensitivity analysis was carried out to determine the optimal boundaries and mesh size prior to the back analysis. The tunnel was fixed at a depth below the ground surface H of 3 times the diameter of the tunnel D. As the ground surface settlement will be affected by the distance of the horizontal bottom boundary below the tunnel axis H', numerical calibration was performed based on field measurements. Given the accuracy achieved in predicting the ground surface settlements resulting from

the construction of each single bored tunnel and closely spaced bored tunnels as shown in Figure 6.8, it is reasonable to fix the horizontal bottom boundary at a distance of 1D below the tunnel axis for analysis involving tunnel constructed in stiff soil. Both the vertical boundaries were increased at an increment of 5D from the tunnel axis for cases involving medium mesh, fine mesh and very fine mesh until there was no change in the maximum ground surface settlement and edge settlement, as shown in Figures 6.9 and 6.10. Figure 6.11 shows the finite element model with very fine mesh and minimum required distance of 30D between vertical boundaries with tunnel axis that was adopted to minimise the influence of vertical boundaries on the ground surface settlement. The enlarged view of 15-node triangular elements and 5-node plate elements is shown in Figure 6.12.

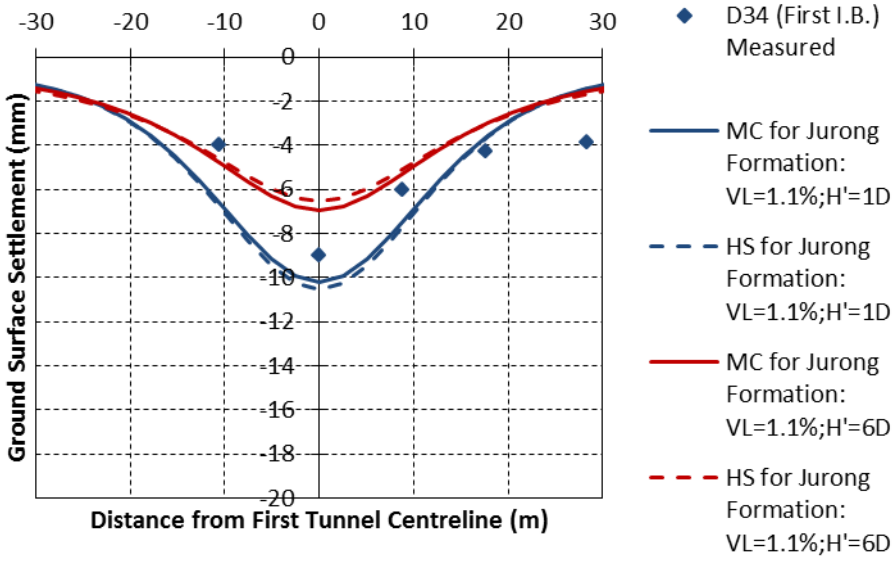

(a) D34 (First I.B.)

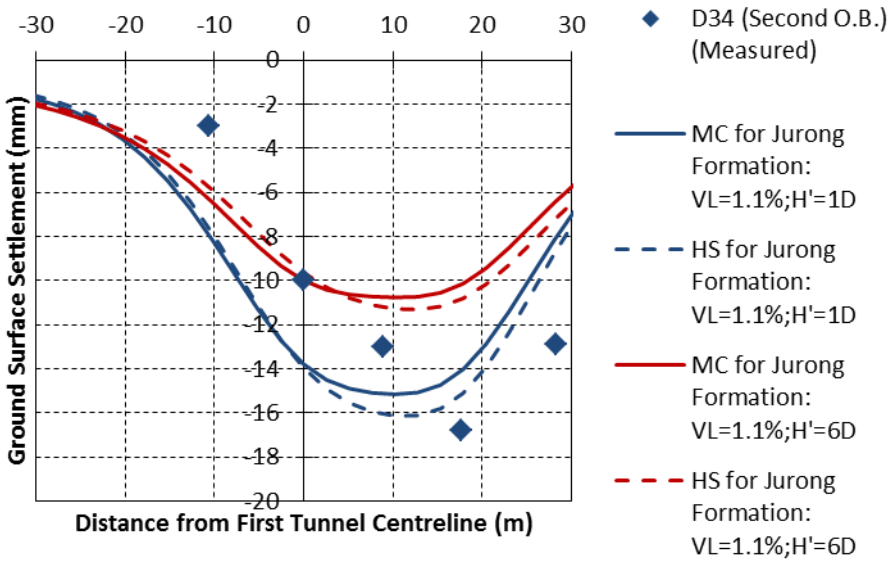

(b) D34 (Second O.B.)

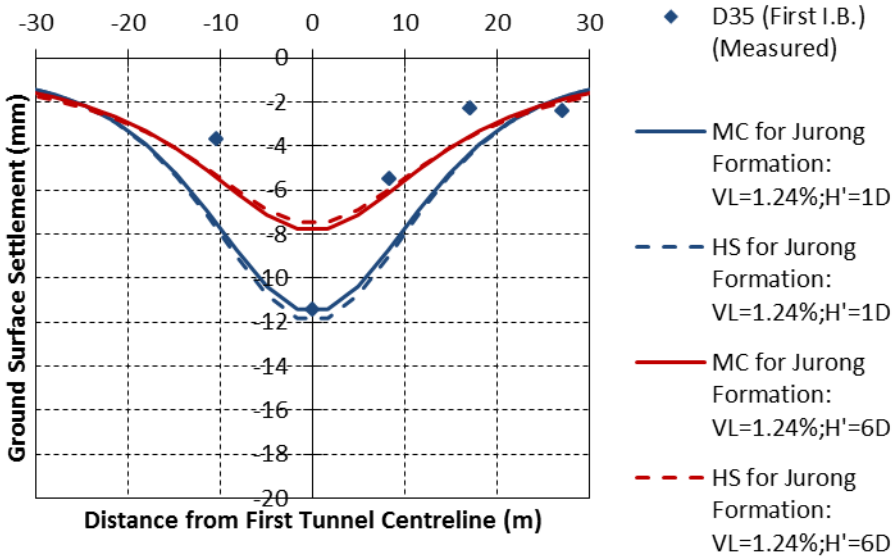

(c) D35 (First I.B.)

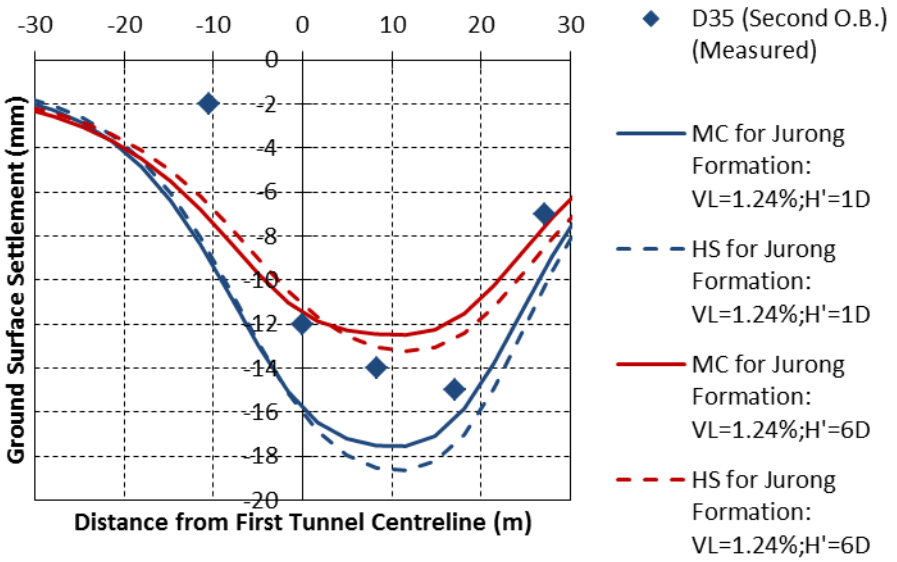

(d) D35 (Second O.B.)

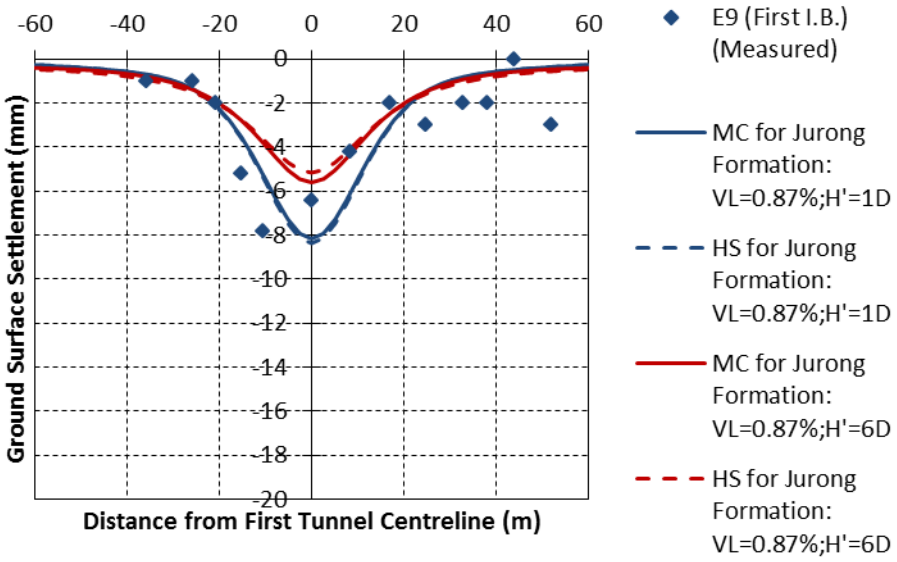

(e) E9 (First I.B.)

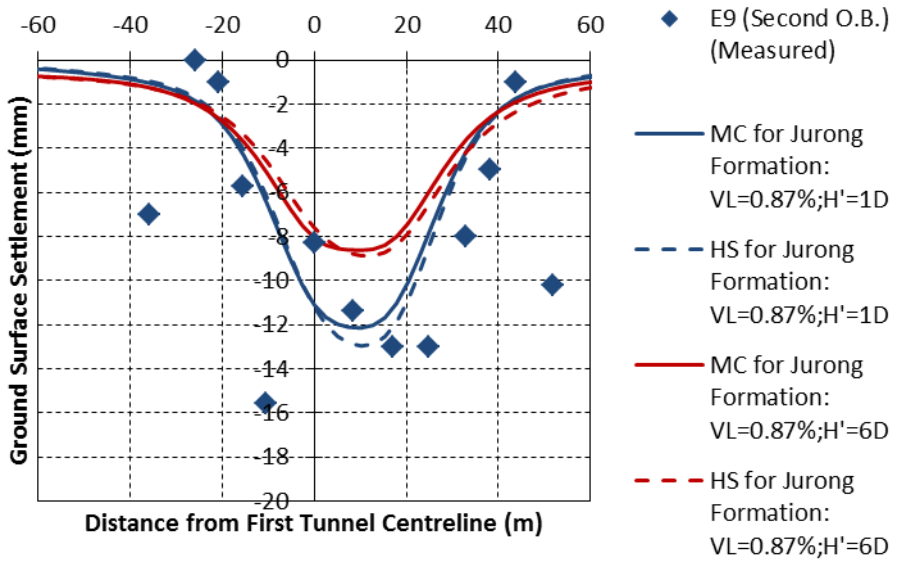

(f) E9 (Second O.B.)

Figure 6.8 Predicted ground surface settlements based on two different distance of horizontal bottom boundary below the tunnel axis for Instrumentation Arrays (a) D34 (First I.B.); (b) D34 (Second O.B.); (c) D35 (First I.B.); (d) D35 (Second O.B.); (e) E9 (First I.B.); and (f) E9 (Second O.B.)

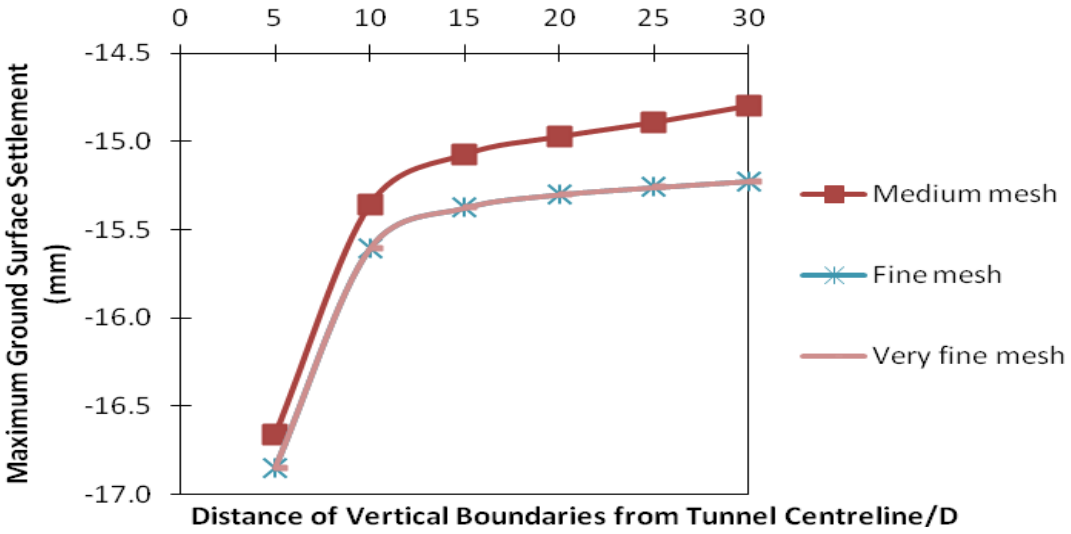

Figure 6.9 Variation of maximum ground surface settlement with normalised distance of vertical boundaries from tunnel centreline

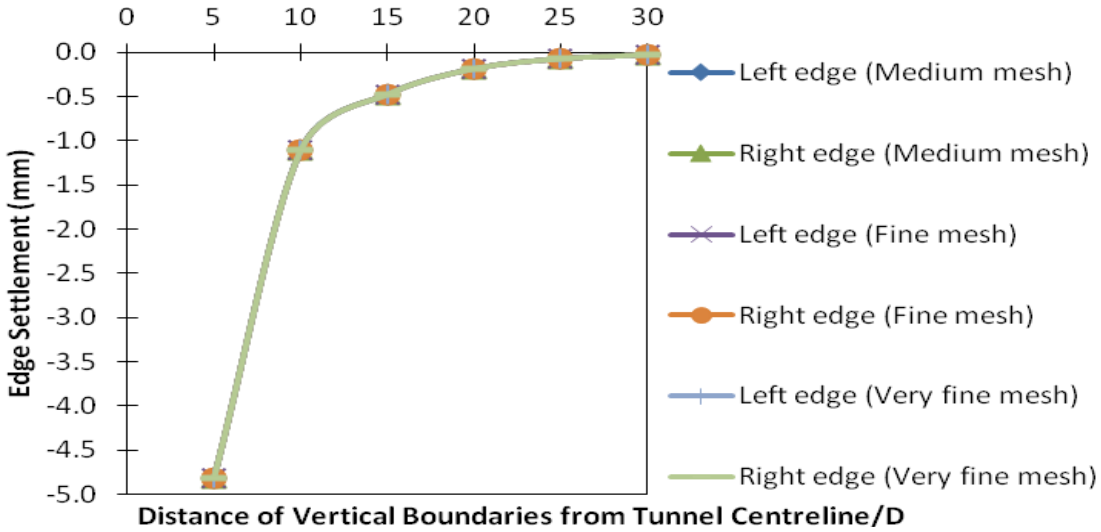

Figure 6.10 Variation of edge settlement with normalised distance of vertical boundaries from tunnel centreline

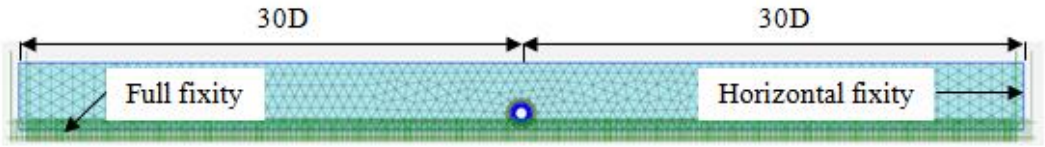

Figure 6.11 Finite element model with very fine mesh as well as minimum required distance between vertical boundaries and tunnel axis

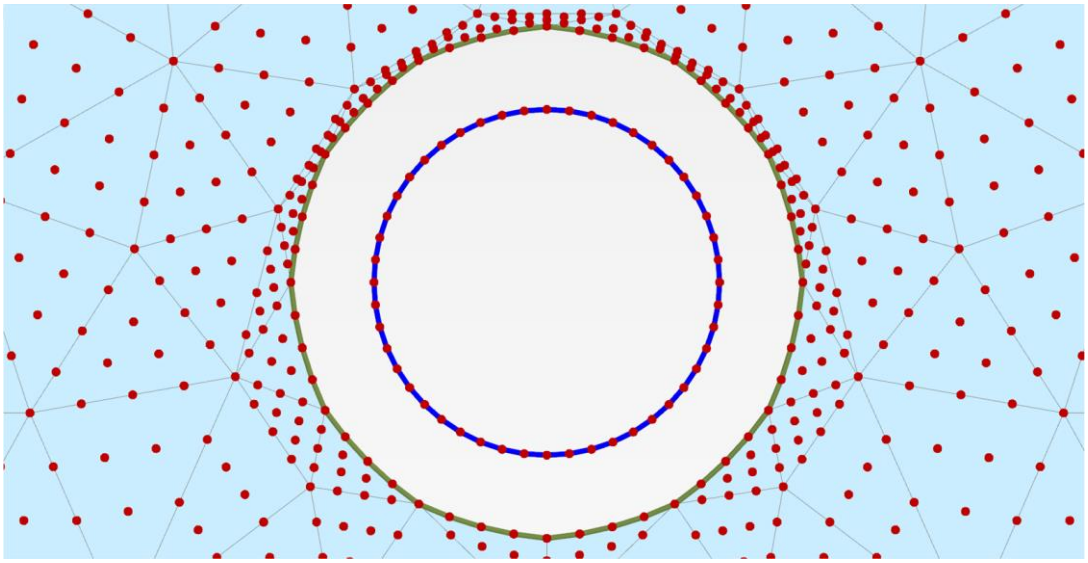

Figure 6.12 Enlarged view of 15-node triangular elements and 5-node plate elements

6.6 Case Studies

This section presents the results of the 13 back analyses on single and closely spaced bored tunnels based on the empirical correlations of soil parameters for both Hardening Soil (HS) model and Mohr-Coulomb (MC) model presented in Sections 6.2, 6.3 and 6.4. They comprise: (i) 4 cases involving uniform grade of Jurong Formation; (ii) 4 cases involving mixed grades of Jurong Formation; and (iii) 5 cases involving mixed ground of Jurong Formation and Kallang Formation. The pillar widths of the closely spaced bored tunnels ranges from 4.8 m to 12.3 m. Assessments have been made on the difference in transverse surface settlement determined using the HS model and MC model where the former has the capability of simulating the non-linearity and unloading effects of soil. The results of both models are compared with the field measurements.

6.6.1 Instrumentation Array D35

The installation of Instrumentation Array D35 facilitated monitoring of the transverse surface settlement due to the closely spaced bored tunnelling through uniform grade of Jurong Formation. Part of the finite element mesh used for the study is shown in Figure 6.13. Also shown in this figure are the strata with their thickness (see Table 6.5). The parameters assumed in the analyses are summarised in Table 6.5. Both first inner bound and second outer bound bored tunnels have axis of 17.1 m below the ground level at a pillar width of 10.5 m. Figure 6.14 shows the computed and measured transverse surface settlement after the first inner bound bored tunnelling. The corresponding computed and measured transverse surface settlement following the second outer bound bored tunnelling are shown in Figure 6.15.

As shown in Figure 6.14 for analysis of a single bored tunnel, a simulated volume loss VL of 1.24 per cent yielded good agreement with the measured maximum settlement and edge settlement. Despite a slightly larger maximum settlement

generated using the HS model, both HS and MC models gave similar settlement profiles towards both left and right edges.

As shown in Figure 6.15, the analysis for the closely spaced bored tunnels simulated using similar volume loss of 1.24 per cent yielded identical trend of transverse surface settlement for both the HS and MC models. At a distance of approximately 30 m away from the centreline of the first inner bound bored tunnel, the measured settlement for the right arm is larger than the left arm. This indicates shifting of the transverse surface settlement trough towards the second outer bound bored tunnel where the maximum settlement was drawn towards the second outer bound bored tunnel. Both Figures 6.14 and 6.15 indicate some differences in the computed transverse surface settlement using the HS and MC models with slightly larger maximum settlement being observed for the former.

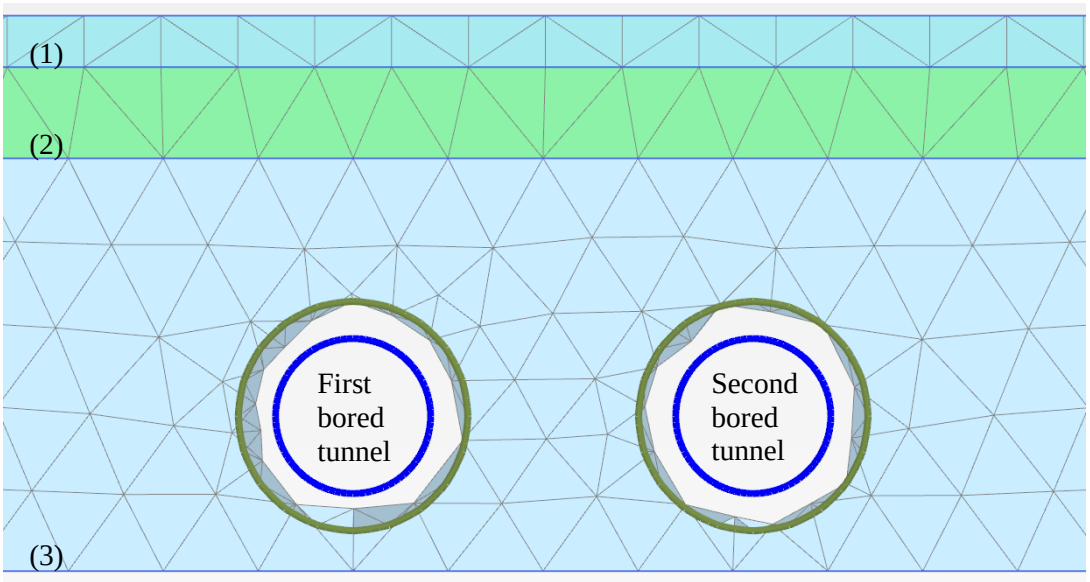

Figure 6.13 Partial finite element mesh in vicinity of bored tunnels (Instrumentation Array D35)

Table 6.5 Soil Properties (Instrumentation Array D35)

(Numbering) Strata	Strata Thickness (m)	γ_{sat} (kN/m^3)	c_u (kPa)	c' (kPa)	ϕ' (^{o})	E' (kPa)	MC		HS	
							E_u (kPa)	ν	E_{50} (kPa)	ν_{ur}
(1) Fill	2.2	19	20	-	-	-	10000	0.495	-	-
(2) Fluvial Sand	4.4	20	-	0	30	14783	-	0.3	-	-
(3) Jurong Formation	17.1	20	150	-	-	-	84000	0.495	58800	0.2

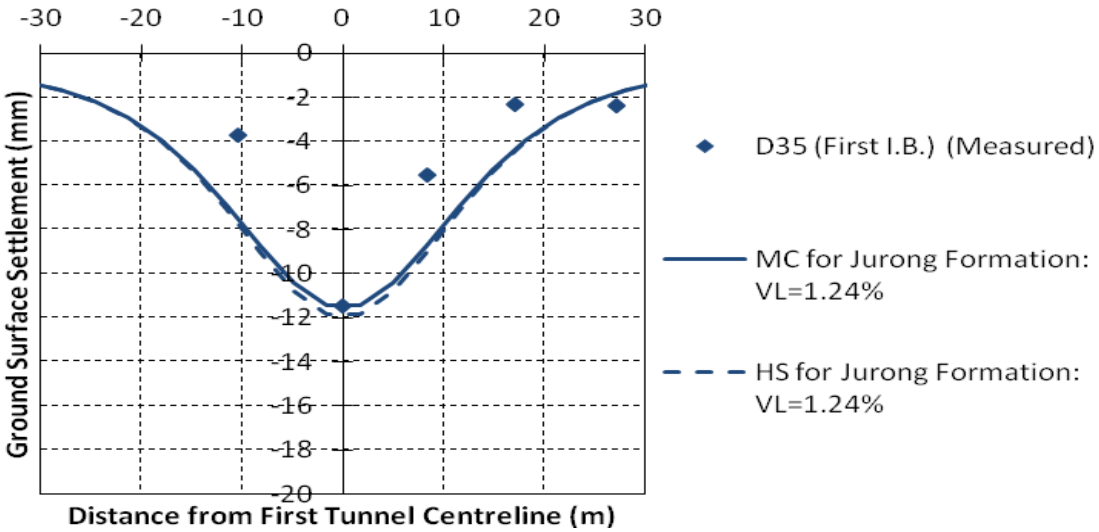

Figure 6.14 Transverse surface settlement after first inner bound bored tunnelling (Instrumentation Array D35)

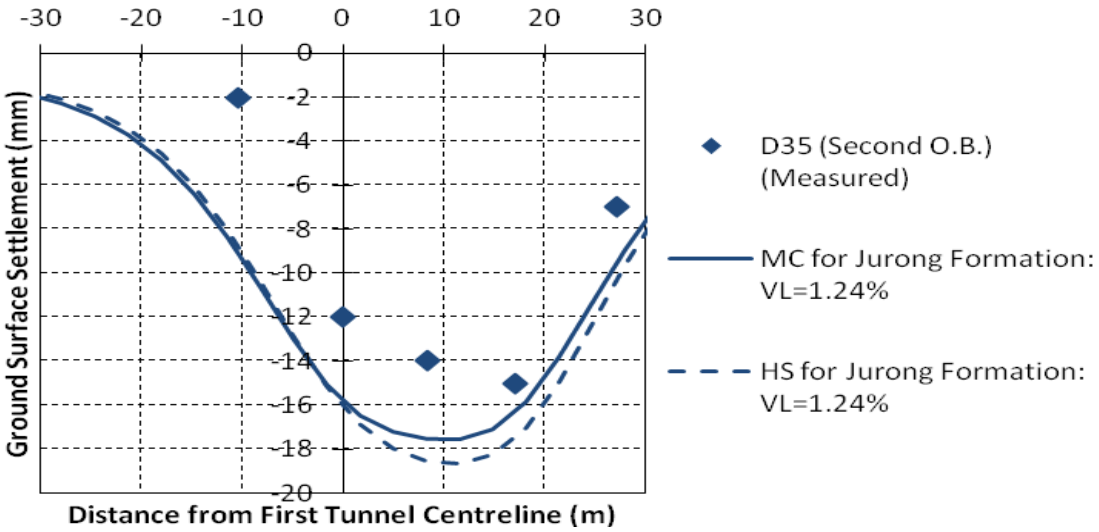

Figure 6.15 Transverse surface settlement after second outer bound bored tunnelling (Instrumentation Array D35)

6.6.2 Instrumentation Array E9

The installation of Instrumentation Array E9 facilitated monitoring of transverse surface settlement due to the closely spaced bored tunnelling through uniform grade of Jurong Formation. Part of the finite element mesh used for the study is shown in Figure 6.16. Also shown in this figure are the strata with their thickness (see Table 6.6). The parameters assumed in the analyses are summarised in Table 6.6. Both first inner bound and second outer bound bored tunnels have axis of 17.1 m below the ground level at a pillar width of 10.5 m. Figure 6.17 shows the computed and measured transverse surface settlement after the first inner bound bored tunnelling. The corresponding computed and measured transverse surface settlement following the second outer bound bored tunnelling are shown in Figure 6.18.

As shown in Figure 6.17, the measured surface settlements above the first inner bound bored tunnel were in close agreement with the transverse surface settlement computed using HS and MC models, for volume loss of 0.87 per cent. A very slight difference in the maximum settlement was computed for the HS and MC models because of the small volume loss assumed.

As shown in Figure 6.18, for the more complex situation involving closely spaced bored tunnels, there was considerable scatter in the measured surface settlement. It should be noted that using HS model marginally improves the estimation of the maximum settlement while similar edge settlements of left and right arms were obtained for both the HS and MC models. Inspection of the transverse surface settlement trough indicates that the maximum settlement was drawn towards the second outer bound bored tunnel where slightly larger edge settlement can be observed at a distance of 60 m to the right of the centreline of the first inner bound bored tunnel.

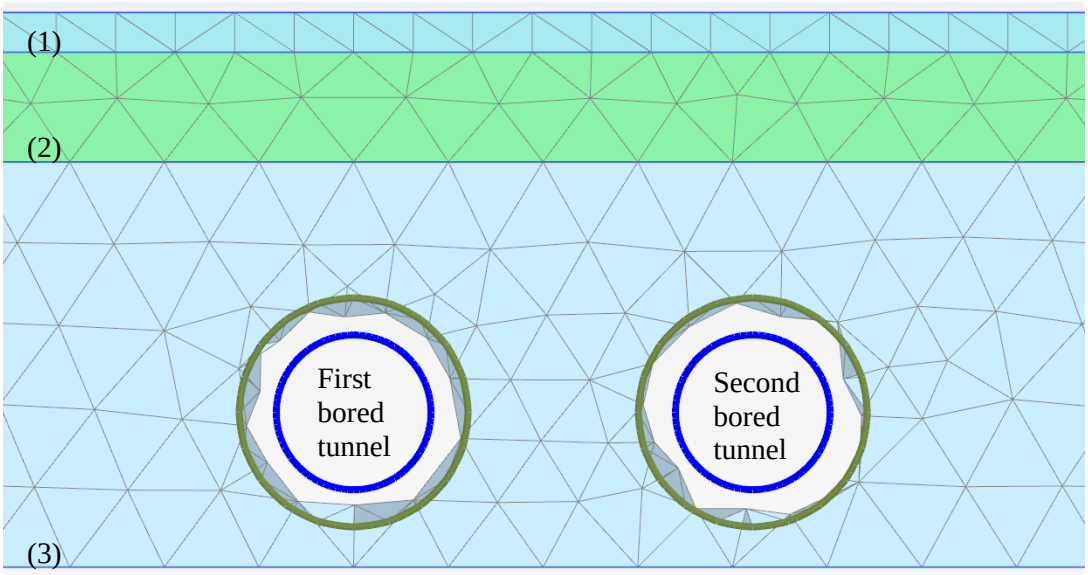

Figure 6.16 Partial finite element mesh in vicinity of bored tunnels (Instrumentation Array E9)

Table 6.6 Soil Properties (Instrumentation Array E9)

(Numbering) Strata	**Strata Thickness (m)**	**γ_{sat} (kN/m^3)**	**c_u (kPa)**	**c' (kPa)**	**ϕ' (^{o})**	**E' (kPa)**	**MC**		**HS**	
							E_u (kPa)	**ν**	**E_{50} (kPa)**	**ν_{ur}**
(1) Fill	1.7	19	20	-	-	-	10000	0.495	-	-
(2) Fluvial Sand	4.7	20	-	0	30	14783	-	0.3	-	-
(3) Jurong Formation	17.4	20	150	-	-	-	84000	0.495	58800	0.2

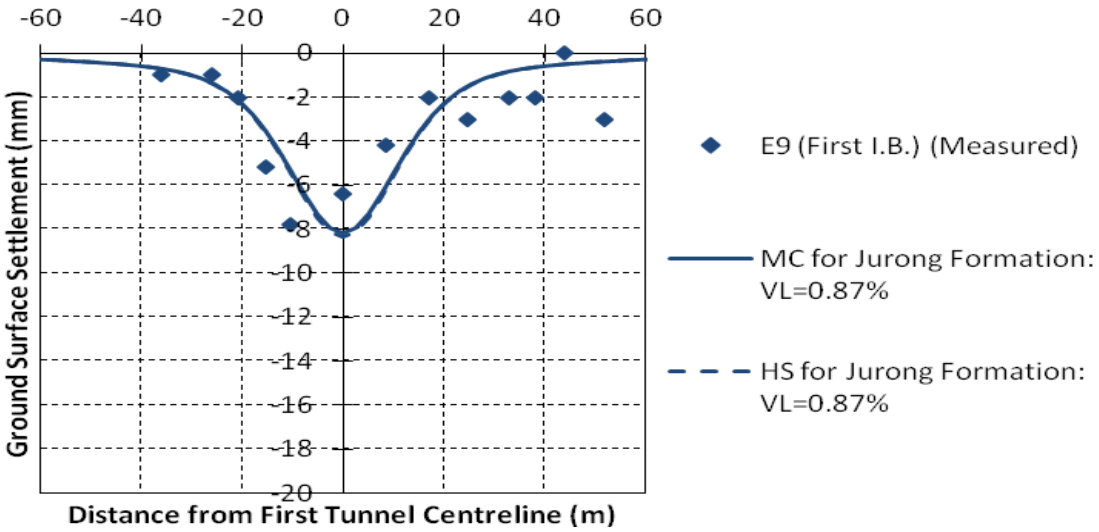

Figure 6.17 Transverse surface settlement after first inner bound bored tunnelling (Instrumentation Array E9)

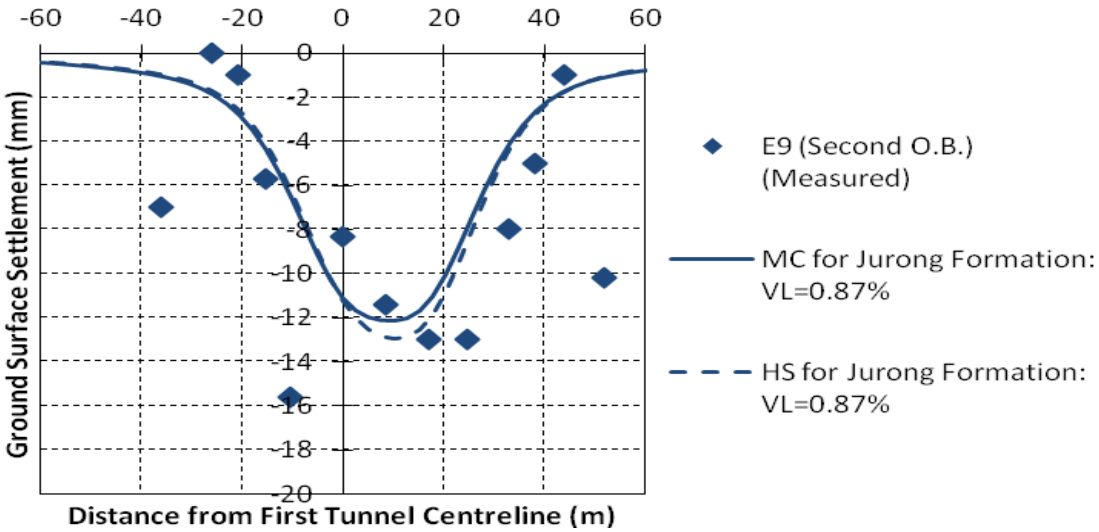

Figure 6.18 Transverse surface settlement after second outer bound bored tunnelling (Instrumentation Array E9)

6.6.3 Instrumentation Array D34

The installation of Instrumentation Array D34 facilitated monitoring of transverse surface settlement due to the closely spaced bored tunnelling through uniform grade of Jurong Formation. Part of the finite element mesh used for the study is shown in

Figure 6.19. Also shown in this figure are the strata with their thickness (see Table 6.7). The parameters assumed in the analyses are summarised in Table 6.7. Both first inner bound and second outer bound bored tunnels have axis of 17.7 m below the ground level at a pillar width of 11.1 m. Figure 6.20 shows the computed and measured transverse surface settlement after the first inner bound bored tunnelling. The corresponding computed and measured transverse surface settlement following the second outer bound bored tunnelling are shown in Figure 6.21.

As shown in Figure 6.20, while the measured maximum settlement was slightly less than those computed using both HS and MC models, the opposite trend was observed for the edge settlement of the right arm, for the first inner bound bored tunnel. For a volume loss of 1.1 per cent, there is minimal difference between the maximum settlement computed using HS model and MC model.

As shown in Figure 6.21, the HS model resulted in a slightly closer agreement of the shape of transverse surface settlement above closely spaced bored tunnels as compared to the MC model. The smaller discrepancy of the HS model in defining the location of the maximum settlement drawn towards the second outer bound bored tunnel should also be highlighted.

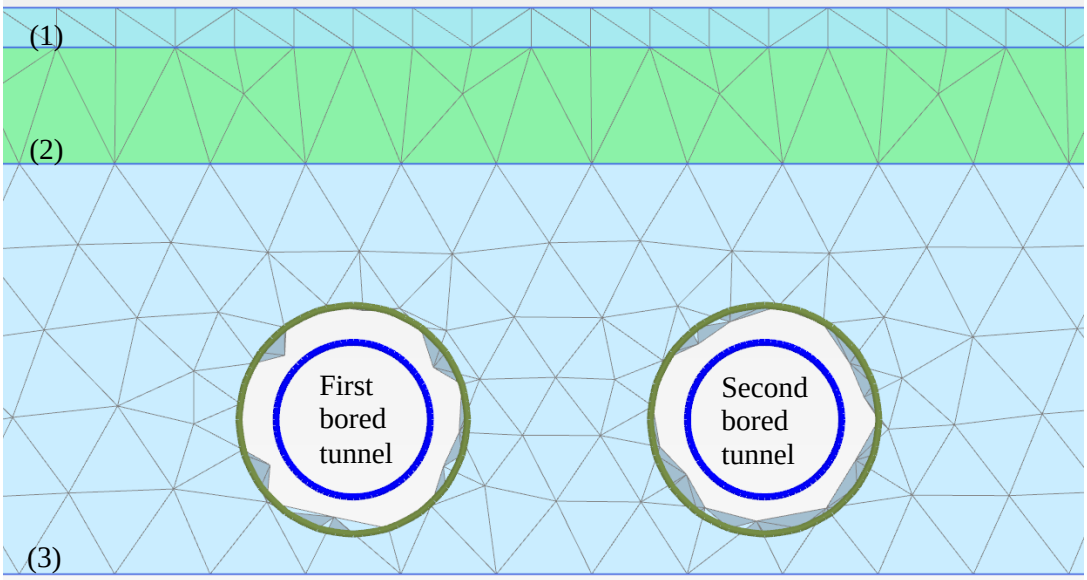

Figure 6.19 Partial finite element mesh in vicinity of bored tunnels (Instrumentation Array D34)

Table 6.7 Soil Properties (Instrumentation Array D34)

(Numbering) Strata	Strata Thickness (m)	γ_{sat} (kN/m^3)	c_u (kPa)	c' (kPa)	ϕ' (^{o})	E' (kPa)	MC		HS	
							E_u (kPa)	ν	E_{50} (kPa)	ν_{ur}
(1) Fill	1.7	19	20	-	-	-	10000	0.495	-	-
(2) Fluvial Sand	5.0	20	-	0	30	14783	-	0.3	-	-
(3) Jurong Formation	17.7	20	150	-	-	-	84000	0.495	58800	0.2

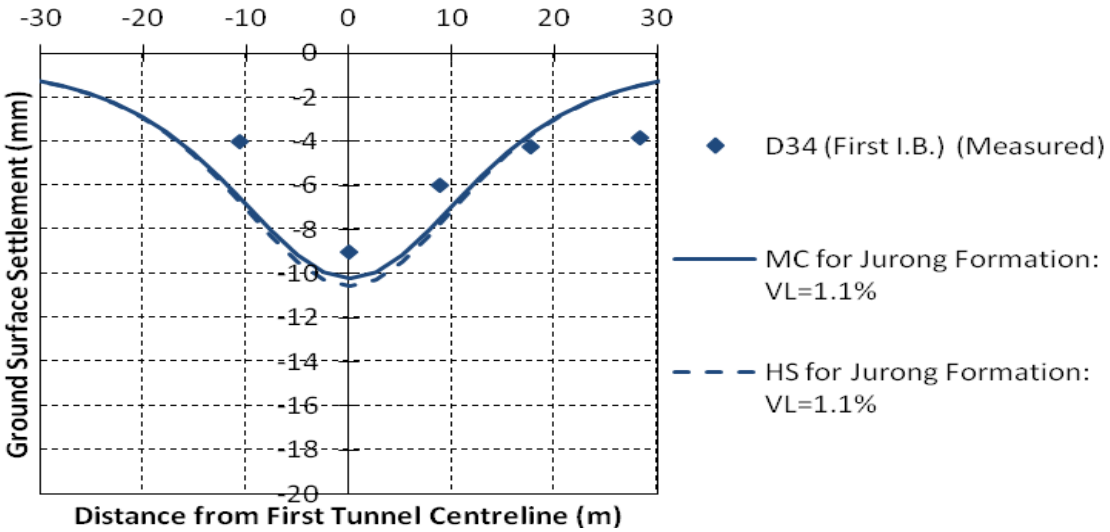

Figure 6.20 Transverse surface settlement after first inner bound bored tunnelling (Instrumentation Array D34)

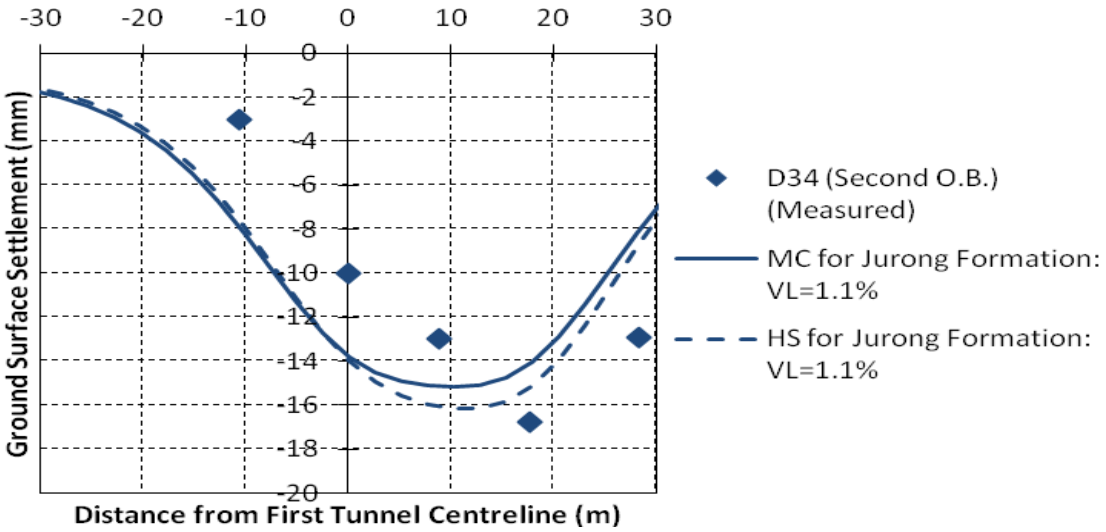

Figure 6.21 Transverse surface settlement after second outer bound bored tunnelling (Instrumentation Array D34)

6.6.4 Instrumentation Array D7

The installation of Instrumentation Array D7 facilitated monitoring of transverse surface settlement due to the closely spaced bored tunnelling through uniform grade of Jurong Formation. Part of the finite element mesh used for the study is shown in Figure 6.22. Also shown in this figure are the strata with their thickness (see Table 6.8). The parameters assumed in the analyses are summarised in Table 6.8. Both first inner bound and second outer bound bored tunnels have axis of 17.1 m below the ground level at a pillar width of 10.1 m. Figure 6.23 shows the computed and measured transverse surface settlement after the first inner bound bored tunnelling. The corresponding computed and measured transverse surface settlement following the second outer bound bored tunnelling are shown in Figure 6.24.

As shown in Figure 6.23, a maximum settlement of 3 mm was measured above the first inner bound bored tunnel. One point representing the measured surface settlement at the left arm seemed to differ from the general trend observed for the transverse surface settlement possibly due to measurement error. In contrast, the right arm appeared to have been experienced a small heave. For the small volume loss of 0.21 per cent there was no discernible difference in the computed transverse

surface settlement for both the HS and MC models. Both models were in reasonably agreement with the measured results.

As shown in Figure 6.24, greater settlement was observed around the first inner bound cored tunnel after the second outer bound bored tunnelling. Inspection of EPBM performance illustrated in Chapter 5 revealed significantly higher earth pressure of 3.05 bar and grout volume of 3857 litres were achieved during the second outer bound bored tunnelling, as compared to earth pressure of 1.77 bar and grout volume of 3346 litres for the first inner bound bored tunnelling. Hence, pre-disturbed soil around the first inner bound bored tunnel experienced greater disturbance during the second outer bound bored tunnelling which resulted in larger volume loss around the first inner bound bored tunnel. Increasing volume loss to 1.47 per cent (denoted by the symbol VL(1) in Figure 6.24) for the first inner bound bored tunnel resulted in reasonably good estimation for the computed settlements at the right arm. This pattern of developing volume loss has drawn the computed maximum settlement towards the first inner bound bored tunnel as a result of the smaller volume loss (denoted by the symbol VL(2) in Figure 6.24) simulated for the second outer bound bored tunnel. The HS model generally showed a slight improvement in estimating the transverse surface settlement over the MC model.

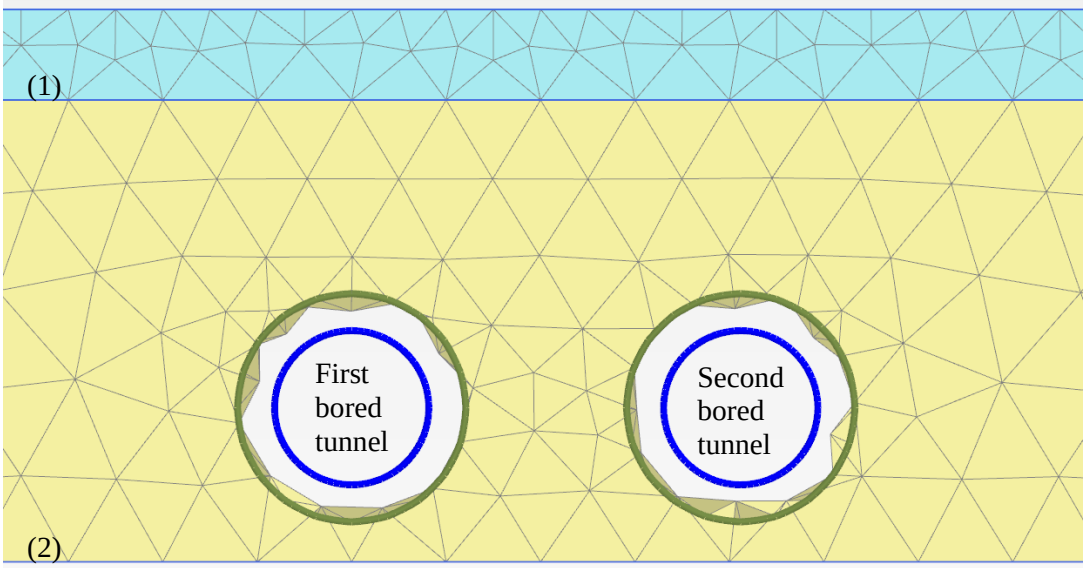

Figure 6.22 Partial finite element mesh in vicinity of bored tunnels (Instrumentation Array D7)

Table 6.8 Soil Properties (Instrumentation Array D7)

(Numbering) Strata	Strata Thickness (m)	γ_{sat} (kN/m^3)	c_u (kPa)	c' (kPa)	ϕ' (^{o})	E' (kPa)	MC		HS	
							E_u (kPa)	ν	E_{50} (kPa)	ν_{ur}
(1) Fill	3.9	19	20	-	-	-	10000	0.495	-	-
(2) Jurong Formation	19.9	20	150	-	-	-	84000	0.495	58800	0.2

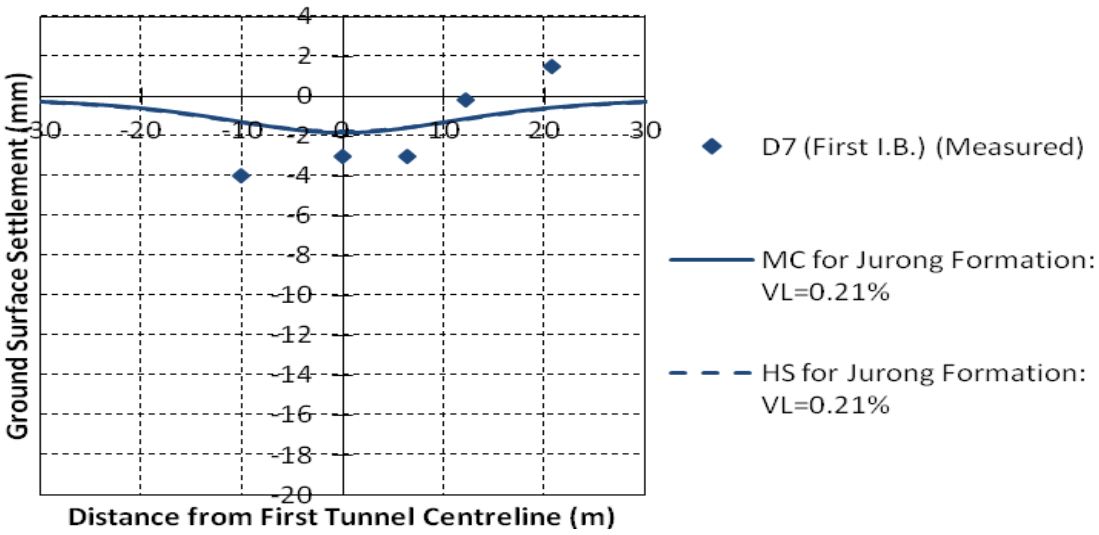

Figure 6.23 Transverse surface settlement after first inner bound bored tunnelling (Instrumentation Array D7)

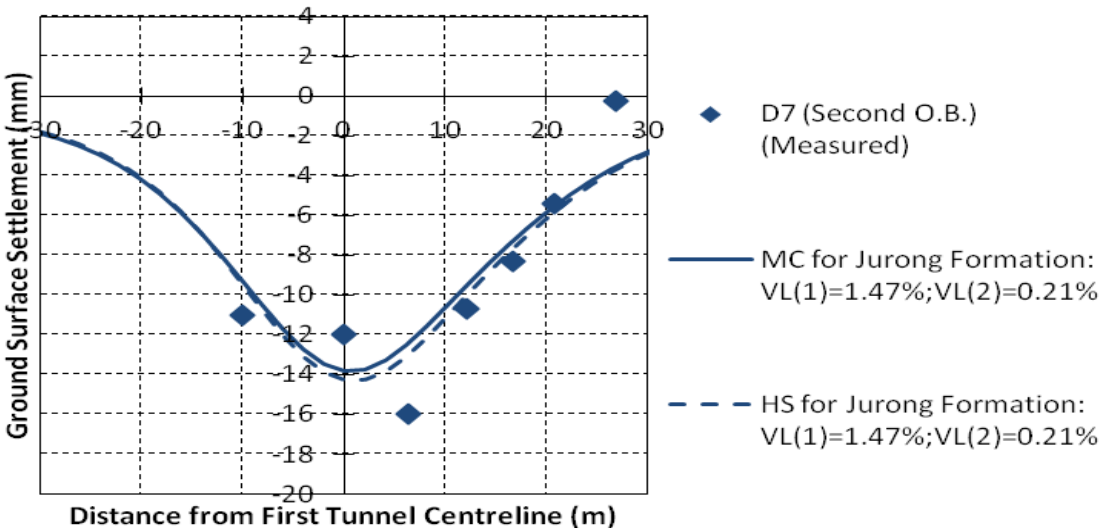

Figure 6.24 Transverse surface settlement after second outer bound bored tunnelling (Instrumentation Array D7)

6.6.5 Instrumentation Array D38

The installation of Instrumentation Array D38 facilitated monitoring of transverse surface settlement due to the closely spaced bored tunnelling through mixed grades of Jurong Formation. Part of the finite element mesh used for the study is shown in Figure 6.25. Also shown in this figure are the strata with their thickness (see Table 6.9). The parameters assumed in the analyses are summarised in Table 6.9. Both first inner bound and second outer bound bored tunnels have axis of 17.7 m below the ground level at a pillar width of 11.1 m. Figure 6.26 shows the computed and measured transverse surface settlement after the first inner bound bored tunnelling. The corresponding computed and measured transverse surface settlement following the second outer bound bored tunnelling are shown in Figure 6.27.

As shown in Figure 6.26, the computed results for both the HS and MC models were in reasonable agreement with the measured right arm transverse surface settlement for volume loss of 1.04 per cent. However, the measured surface settlement at 10.6 m leftward from the centreline of the first tunnel was significantly less than the computed greenfield surface settlement for single bored tunnel.

As shown in Figure 6.27, the computed results for closely spaced bored tunnels showed an excellent agreement with the right arm measured transverse surface settlement. However, significant discrepancy between the computed and measured results was observed for the left arm of the transverse surface settlement. This is likely to be due to measurement errors in the left arm. The additional volume loss of 0.52 per cent, representing half the percentage of the volume loss incurred in the first inner bound bored tunnel (VL(1) = 1.04 per cent) was used for the second outer bound bored tunnel (VL(2) = 1.56 per cent) after considering the approximately similar order of magnitude of the EPBM parameters being adopted for the first inner bound and second outer bound bored tunnelling. Hence, this additional 0.52 per cent of volume loss adopted for the second outer bound bored tunnel could be attributed to the effect of ground disturbance during second outer bound bored tunnelling.

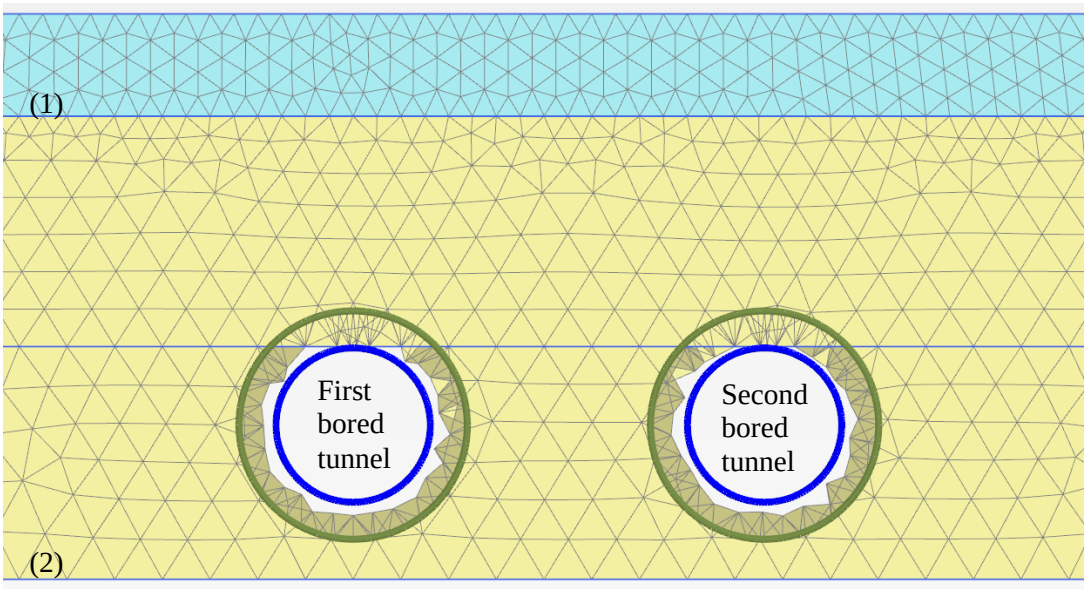

Figure 6.25 Partial finite element mesh in vicinity of bored tunnels (Instrumentation Array D38)

Table 6.9 Soil Properties (Instrumentation Array D38)

(Numbering) Strata	Strata Thickness (m)	γ_{sat} (kN/m^3)	c_u (kPa)	c' (kPa)	ϕ' (^{o})	E' (kPa)	MC		HS	
							E_u (kPa)	ν	E_{50} (kPa)	ν_{ur}
(1) Fill	4.4	19	20	-	-	-	10000	0.495	-	-
(2) Jurong Formation	19.9	20	150	-	-	-	84000	0.495	58800	0.2

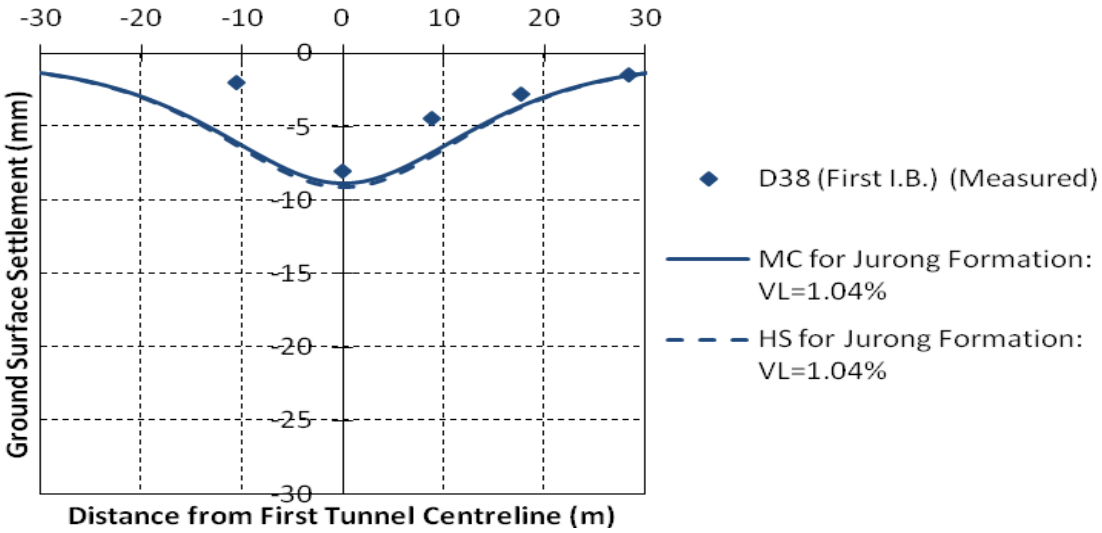

Figure 6.26 Transverse surface settlement after first inner bound bored tunnelling (Instrumentation Array D38)

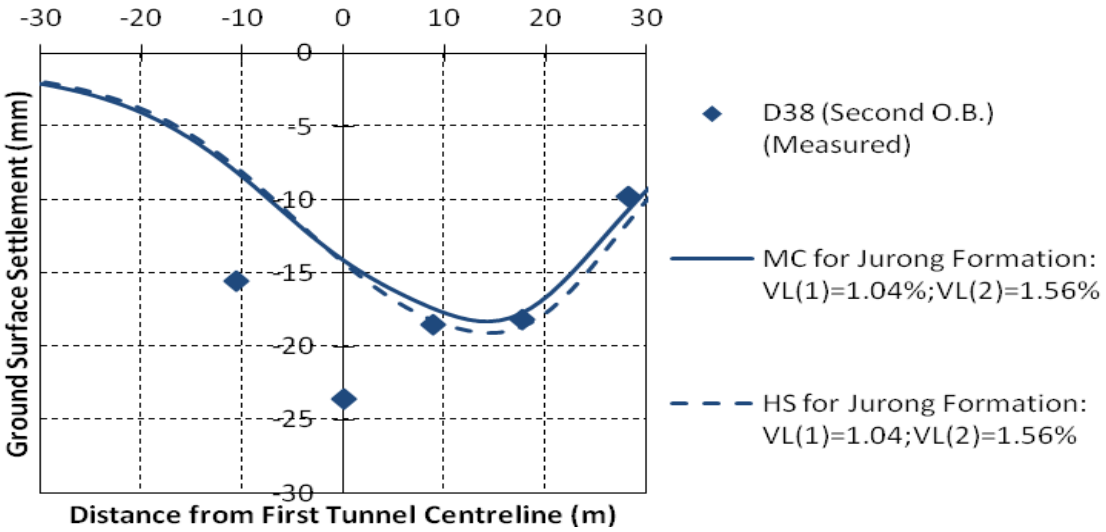

Figure 6.27 Transverse surface settlement after second outer bound bored tunnelling (Instrumentation Array D38)

6.6.6 Instrumentation Array D37

The installation of Instrumentation Array D37 facilitated monitoring of transverse surface settlement due to the closely spaced bored tunnelling through mixed grades of Jurong Formation. Part of the finite element mesh used for the study is shown in Figure 6.28. Also shown in this figure are the strata with their thickness (see Table 6.10). The parameters assumed in the analyses are summarised in Table 6.10. Both first inner bound and second outer bound bored tunnels have axis of 17.4 m below the ground level at a pillar width of 11.1 m. Figure 6.29 shows the computed and measured transverse surface settlement after the first inner bound bored tunnelling. The corresponding computed and measured transverse surface settlement following the second outer bound bored tunnelling are shown in Figure 6.30.

Figure 6.29 shows that for a volume loss of 2.50 per cent, both HS and MC models slightly underestimate the maximum settlement while overestimating the edge settlements above the first inner bound bored tunnel. The measured transverse surface settlement appeared to be narrower than that of the computed results. The results also show that the HS model yields slightly better agreement with the maximum settlement above the single bored tunnel.

Figure 6.30 shows reasonably agreement between the computed and measured settlement for the two bored tunnels. In this case, the HS model gives slightly better estimates of the maximum settlement for both the single bored tunnel and closely spaced bored tunnels. In addition, there is reasonable estimation of the edge settlement at the left arm for both HS and MC models. The smaller measured edge settlement at the right arm may be due to field measurement errors.

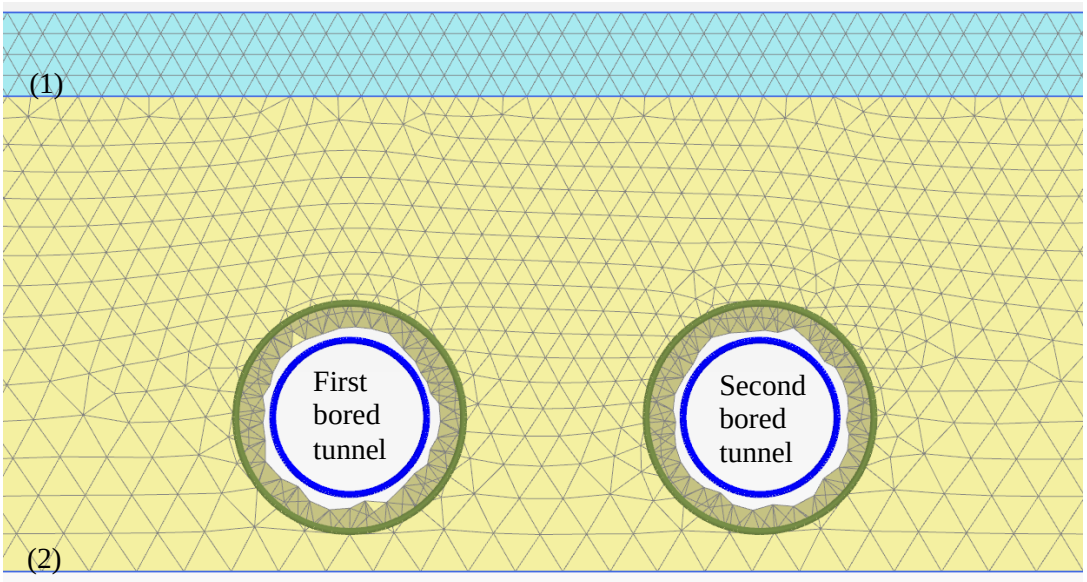

Figure 6.28 Partial finite element mesh in vicinity of bored tunnels (Instrumentation Array D37)

Table 6.10 Soil Properties (Instrumentation Array D37)

(Numbering) Strata	**Strata Thickness (m)**	**γ_{sat} (kN/m^3)**	**c_u (kPa)**	**c' (kPa)**	**ϕ' (^{o})**	**E' (kPa)**	**MC**		**HS**	
							E_u (kPa)	**ν**	**E_{50} (kPa)**	**ν_{ur}**
(1) Fill	3.6	19	20	-	-	-	10000	0.495	-	-
(2) Jurong Formation	20.4	20	150	-	-	-	84000	0.495	58800	0.2

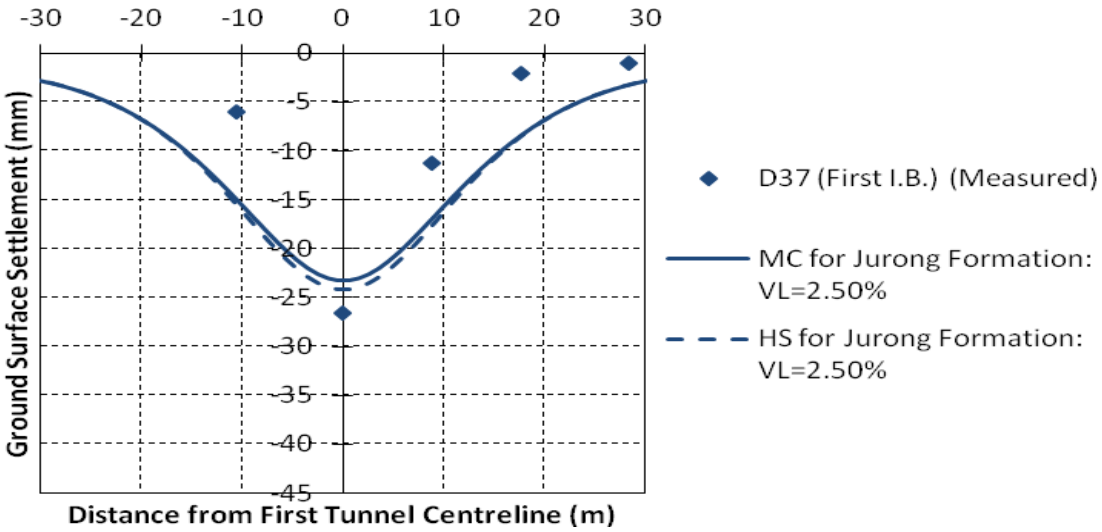

Figure 6.29 Transverse surface settlement after first inner bound bored tunnelling (Instrumentation Array D37)

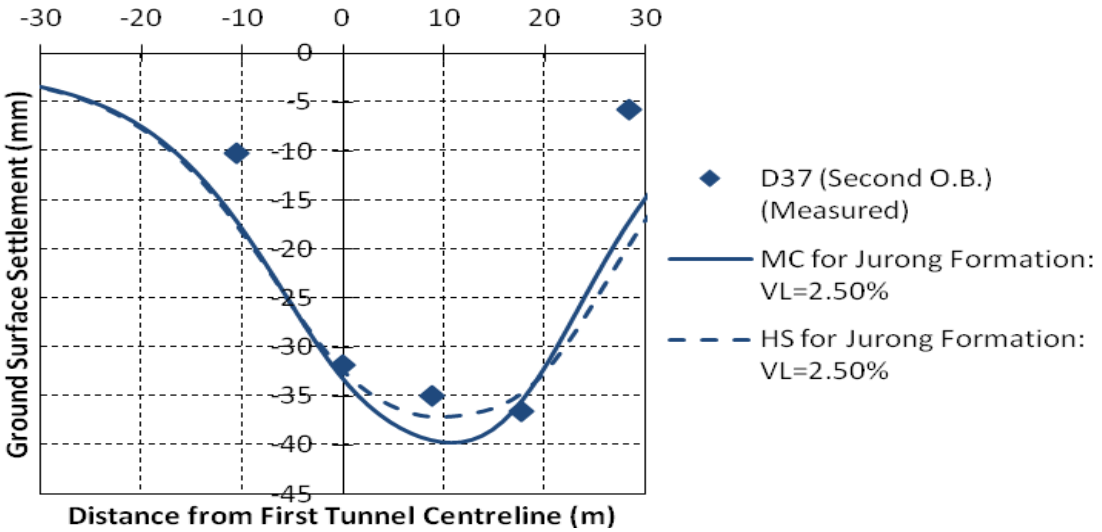

Figure 6.30 Transverse surface settlement after second outer bound bored tunnelling (Instrumentation Array D37)

6.6.7 Instrumentation Array D33

The installation of Instrumentation Array D33 facilitated monitoring of transverse surface settlement due to the closely spaced bored tunnelling through mixed grades of Jurong Formation. Part of the finite element mesh used for the study is shown in

Figure 6.31. Also shown in this figure are the strata with their thickness (see Table 6.11). The parameters assumed in the analyses are summarised in Table 6.11. Both first inner bound and second outer bound bored tunnels have axis of 17.4 m below the ground level at a pillar width of 10.9 m. Figure 6.32 shows the computed and measured transverse surface settlement after the first inner bound bored tunnelling. The corresponding computed and measured transverse surface settlement following the second outer bound bored tunnelling are shown in Figure 6.33.

As shown in Figure 6.32 for the single bored tunnel, although the measured maximum settlement was slightly less than that computed using the HS and MC models, the measured edge settlement was in agreement with the computed profiles. It is reasonable to assume that the volume loss of 1.10 per cent adopted for the analysis is correct.

As shown in Figure 6.33, the measured transverse surface settlement for closely spaced bored tunnels, however, differed significantly from the Gaussian normal probability curve. However, the computed maximum settlement using the HS and MC models with volume loss of 1.65 per cent was in close agreement with the measured results.

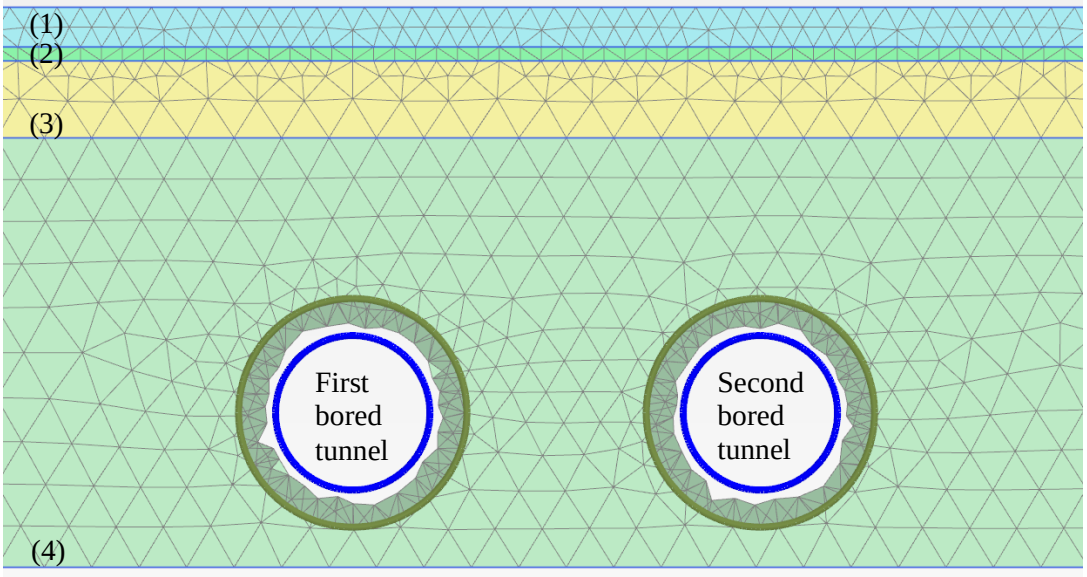

Figure 6.31 Partial finite element mesh in vicinity of bored tunnels (Instrumentation Array D33)

Table 6.11 Soil Properties (Instrumentation Array D33)

(Numbering) Strata	Strata Thickness (m)	γ_{sat} (kN/m^3)	c_u (kPa)	c' (kPa)	ϕ' (^{o})	E' (kPa)	MC		HS	
							E_u (kPa)	ν	E_{50} (kPa)	ν_{ur}
(1) Fill	1.7	19	20	-	-	-	10000	0.495	-	-
(2) Fluvial Clay	0.6	19	30	-	-	-	9000	0.495	-	-
(3) Fluvial Sand	3.3	20	-	0	30	14783	-	0.3	-	-
(4) Jurong Formation	18.5	20	150	-	-	-	84000	0.495	58800	0.2

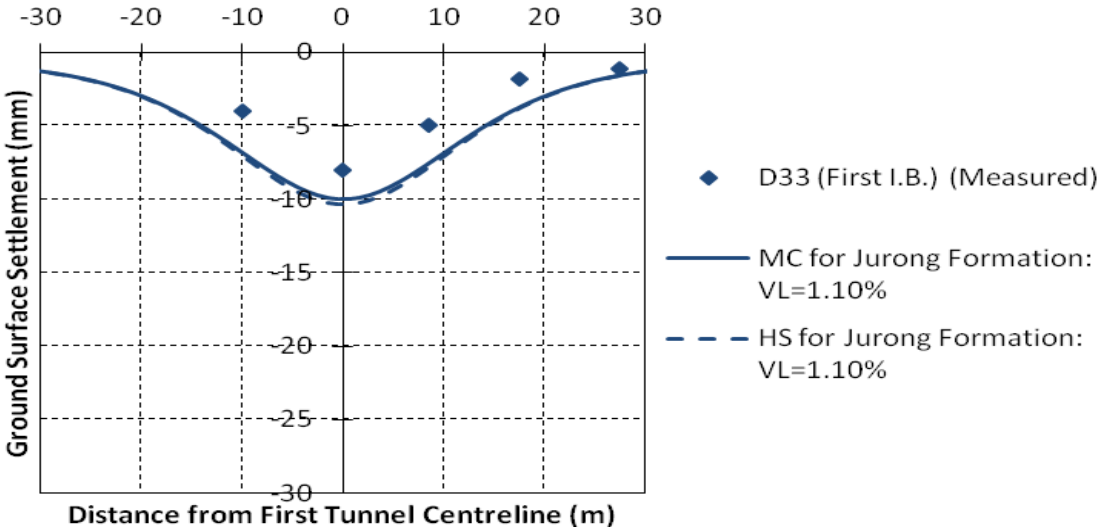

Figure 6.32 Transverse surface settlement after first inner bound bored tunnelling (Instrumentation Array D33)

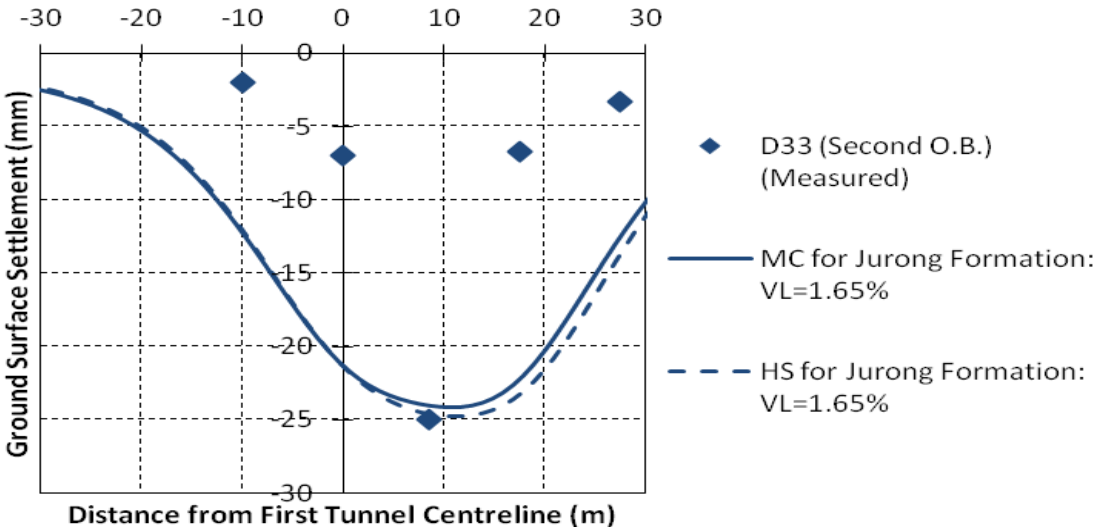

Figure 6.33 Transverse surface settlement after second outer bound bored tunnelling (Instrumentation Array D33)

6.6.8 Instrumentation Array D32

The installation of Instrumentation Array D32 facilitated monitoring of transverse surface settlement due to the closely spaced bored tunnelling through mixed grades of Jurong Formation. Part of the finite element mesh used for the study is shown in Figure 6.34. Also shown in this figure are the strata with their thickness (see Table 6.12). The parameters assumed in the analyses are summarised in Table 6.12. Both first inner bound and second outer bound bored tunnels have axis of 17.7 m below the ground level at a pillar width of 12.3 m. Figure 6.35 shows the computed and measured transverse surface settlement after the first inner bound bored tunnelling. The corresponding computed and measured transverse surface settlement following the second outer bound bored tunnelling are shown in Figure 6.36.

As shown in Figure 6.35 for the single bored tunnel, although both HS and MC models show reasonable agreement with the measured transverse surface settlement, they generally underestimate the measured transverse surface settlement especially the edge settlement. As observed, the measured transverse surface settlement trough conformed closely to the Gaussian normal probability curve as represented by the

computed results using the HS and MC models assuming volume loss of 0.48 per cent.

As shown in Figure 6.36 for transverse surface settlement above closely spaced bored tunnels, using HS model with volume loss of 0.96 per cent improves the estimation of the maximum settlement and edge settlement. The measured transverse surface settlement, however, seemed to depart significantly from the Gaussian normal probability curve. Inspection of the EPBM parameters indicated that the magnitude of EPBM parameters for first inner bound bored tunnelling is generally greater than the second outer bound bored tunnelling. This observation could have explained the incremental of the volume loss of the first inner bound bored tunnelling from 0.48 per cent to doubly of its value of 0.96 per cent during second outer bound bored tunnelling, attributed to the larger zone of influence during second outer bound bored tunnelling which led to an increase in the ground surface settlement, i.e. volume loss, adjacent to the first inner bound bored tunnel.

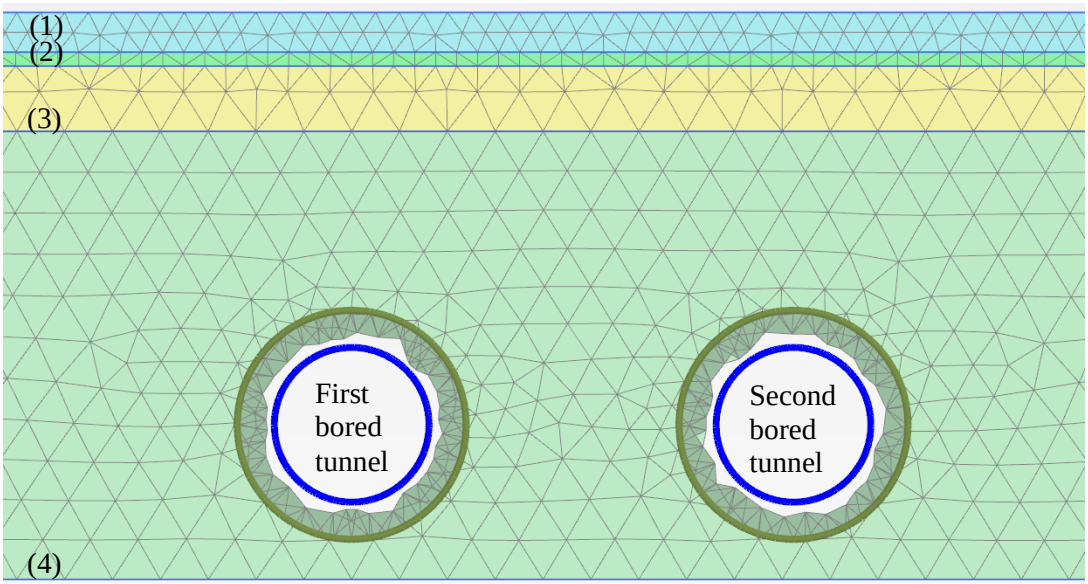

Figure 6.34 Partial finite element mesh in vicinity of bored tunnels (Instrumentation Array D32)

Table 6.12 Soil Properties (Instrumentation Array D32)

(Numbering) Strata	Strata Thickness (m)	γ_{sat} (kN/m^3)	c_u (kPa)	c' (kPa)	ϕ' (^{o})	E' (kPa)	MC		HS	
							E_u (kPa)	ν	E_{50} (kPa)	ν_{ur}
(1) Fill	1.7	19	20	-	-	-	10000	0.495	-	-
(2) Fluvial Clay	0.6	19	30	-	-	-	9000	0.495	-	-
(3) Fluvial Sand	2.8	20	-	0	30	14783	-	0.3	-	-
(4) Jurong Formation	19.3	20	150	-	-	-	84000	0.495	58800	0.2

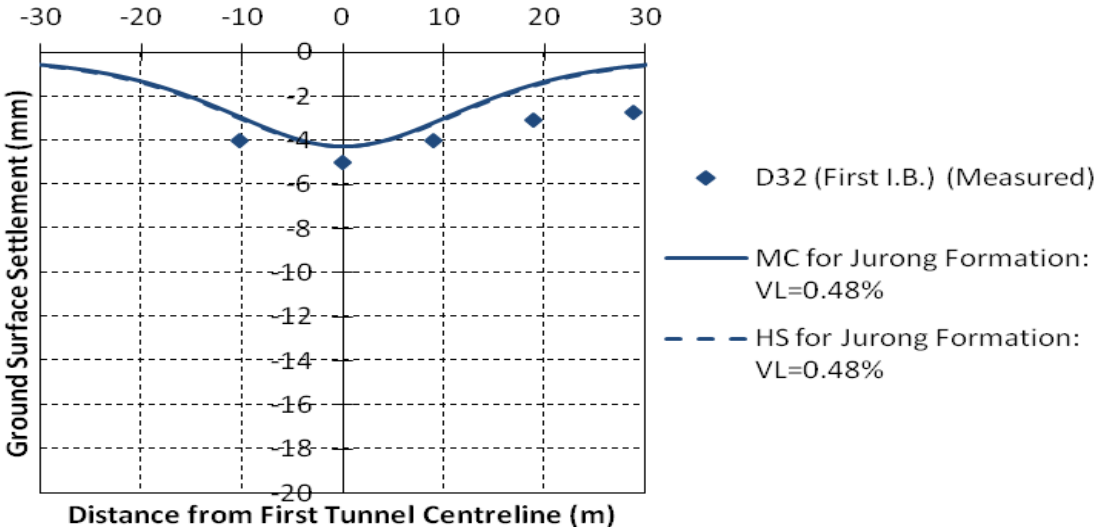

Figure 6.35 Transverse surface settlement after first inner bound bored tunnelling (Instrumentation Array D32)

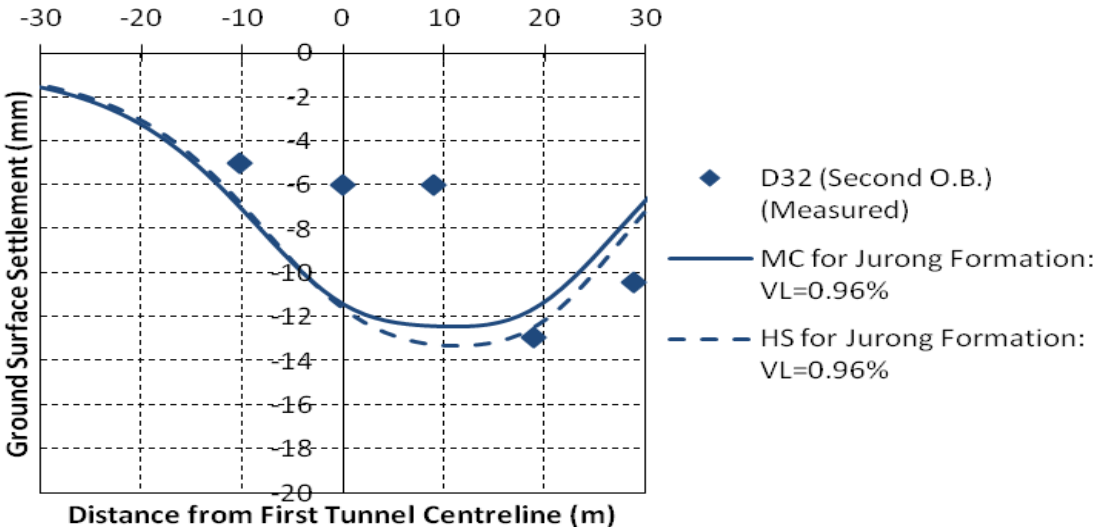

Figure 6.36 Transverse surface settlement after second outer bound bored tunnelling (Instrumentation Array D32)

6.6.9 Instrumentation Array E14

The installation of Instrumentation Array E14 facilitated monitoring of transverse surface settlement due to the closely spaced bored tunnelling through mixed ground of Jurong Formation and Kallang Formation. Part of the finite element mesh used for the study is shown in Figure 6.37. Also shown in this figure are the strata with their thickness (see Table 6.13). The parameters assumed in the analyses are summarised in Table 6.13. Both first inner bound and second outer bound bored tunnels have axis of 14.7 m below the ground level at a pillar width of 7.2 m. Figure 6.38 shows the computed and measured transverse surface settlement after the first inner bound bored tunnelling. The corresponding computed and measured transverse surface settlement following the second outer bound bored tunnelling are shown in Figure 6.39.

As shown in Figure 6.38, both the measured and computed transverse surface settlements using the HS and MC models show good agreement for the case of single bored tunnel. Better estimation using volume loss of 4.06 per cent was obtained for the left arm of the transverse surface settlement as compared to the right arm.

As shown in Figure 6.39, similarly, reasonably good agreement was observed for the measured and computed transverse surface settlements using the HS and MC models, for closely spaced bored tunnels. However, using HS model slightly underestimates the maximum settlement and edge settlement. It should be highlighted that the smaller volume loss for the second outer bound bored tunnel could be attributed to the higher EPBM earth pressure of 2.63 bar exerted on the tunnel face, which has substantially minimised the measured settlement above the EPBM face. As mentioned in Section 5.2.3, in this case, settlement above the EPBM face was 2.2 mm as compared to the 9 mm above the first inner bound bored tunnel with maximum EPBM earth pressure of 2.06 bar. In addition, a much smaller quantity of grout injection volume of 3598 litres adopted during the second outer bound bored tunnelling as compared to 4057 litres during the first inner bound bored tunnelling could have led to an increasing volume loss of the first inner bound bored tunnel from 4.06 per cent to 6.09 per cent, resulting from volume loss at the tail void of the second outer bound bored tunnelling.

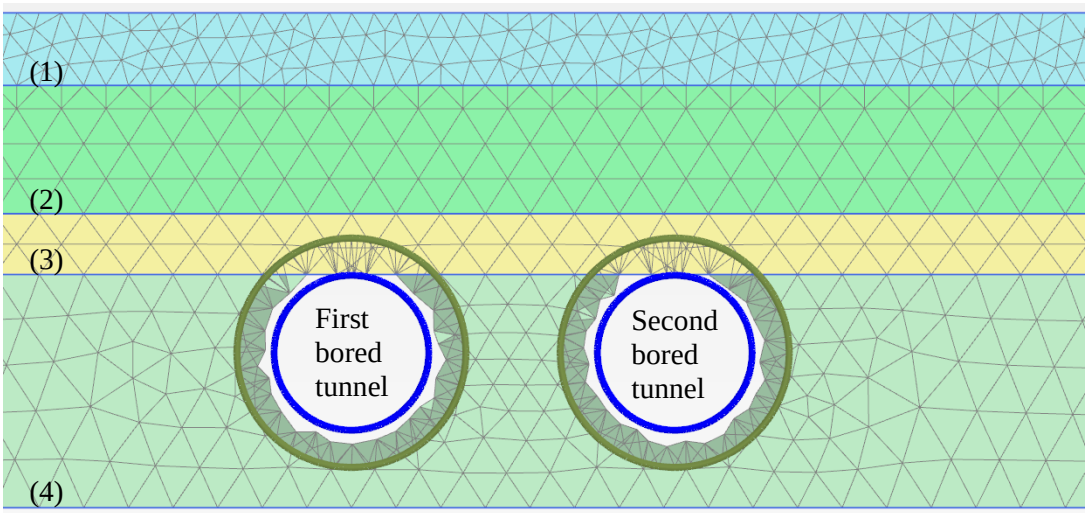

Figure 6.37 Partial finite element mesh in vicinity of bored tunnels (Instrumentation Array E14)

Table 6.13 Soil Properties (Instrumentation Array E14)

(Numbering) Strata	Strata Thickness (m)	γ_{sat} (kN/m^3)	c_u (kPa)	c' (kPa)	ϕ' (^{o})	E' (kPa)	MC		HS	
							E_u (kPa)	ν	E_{50} (kPa)	ν_{ur}
(1) Fill	3.1	19	20	-	-	-	10000	0.495	-	-
(2) Estuarine	5.5	15	30	-	-	-	4500	0.495	-	-
(3) Fluvial Sand	2.6	20	-	0	30	14783	-	0.3	-	-
(4) Jurong Formation	10.1	20	150	-	-	-	84000	0.495	58800	0.2

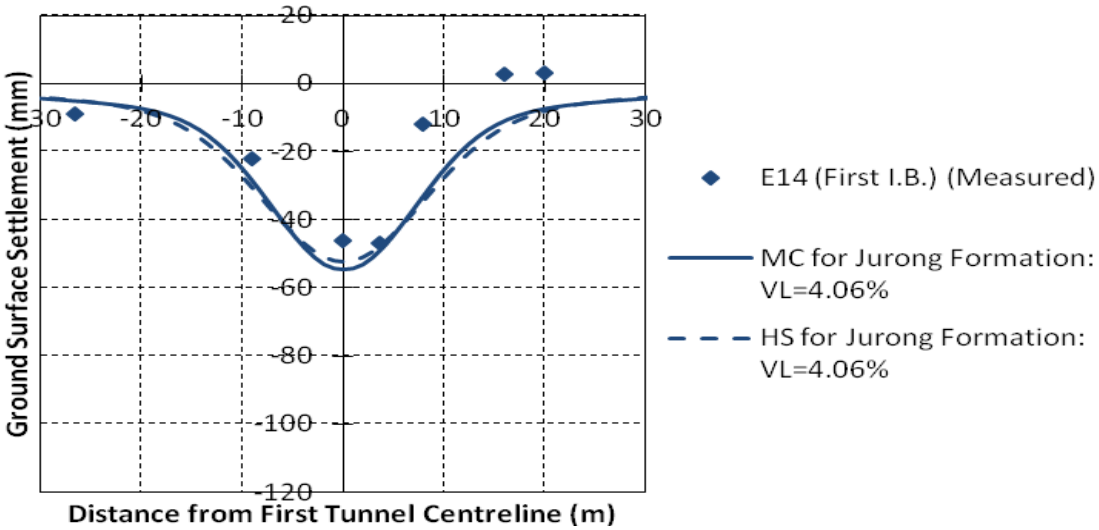

Figure 6.38 Transverse surface settlement after first inner bound bored tunnelling (Instrumentation Array E14)

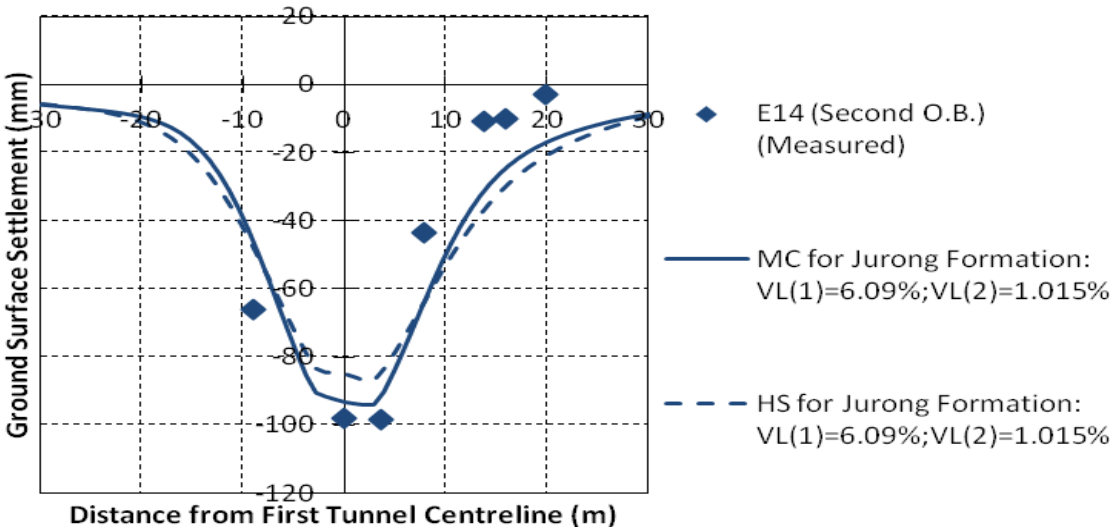

Figure 6.39 Transverse surface settlement after second outer bound bored tunnelling (Instrumentation Array E14)

6.6.10 Instrumentation Array D49

The installation of Instrumentation Array D49 facilitated monitoring of transverse surface settlement due to the closely spaced bored tunnelling through mixed ground of Jurong Formation and Kallang Formation. Part of the finite element mesh used for the study is shown in Figure 6.40. Also shown in this figure are the strata with their thickness (see Table 6.14). The parameters assumed in the analyses are summarised in Table 6.14. Both first inner bound and second outer bound bored tunnels have axis of 18.2 m below the ground level at a pillar width of 5.5 m. Figure 6.41 shows the computed and measured transverse surface settlement after the first inner bound bored tunnelling. The corresponding computed and measured transverse surface settlement following the second outer bound bored tunnelling are shown in Figure 6.42.

Figure 6.41 shows that the HS model gives very good agreement with the measured magnitude and shape of the transverse surface settlement for single bored tunnel for volume loss of 2.54 per cent. The shape of the transverse surface settlement computed using the MC model also shows similar shape as the HS model, except that a slightly smaller maximum settlement was computed.

Figure 6.42 shows the computed results above closely spaced bored tunnels were in good agreement with the maximum settlement. However, significant discrepancy between the computed and measured results were observed for the two measured surface settlement points above the first inner bound bored tunnel and left arm of the transverse surface settlement respectively, possibly as a result of measurement errors.

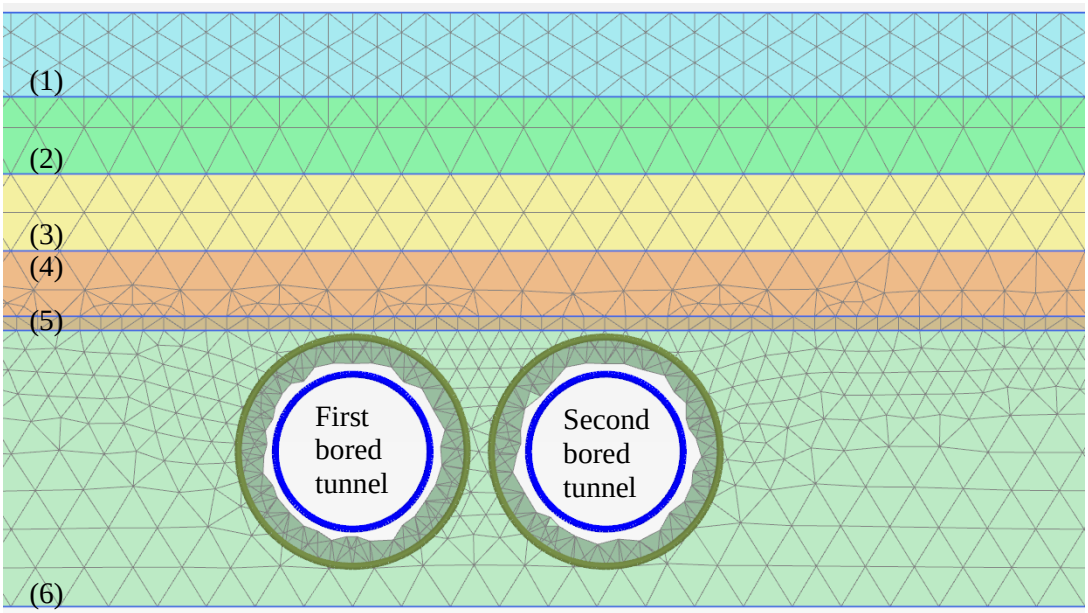

Figure 6.40 Partial finite element mesh in vicinity of bored tunnels (Instrumentation Array D49)

Table 6.14 Soil Properties (Instrumentation Array D49)

(Numbering) Strata	**Strata Thickness (m)**	**γ_{sat} (kN/m^3)**	**c_u (kPa)**	**c' (kPa)**	**ϕ' (^{o})**	**E' (kPa)**	**MC**		**HS**	
							E_u (kPa)	**ν**	**E_{50} (kPa)**	**ν_{ur}**
(1) Fill	3.6	19	20	-	-	-	10000	0.495	-	-
(2) Estuarine	3.3	15	30	-	-	-	4500	0.495	-	-
(3) Fluvial Sand	3.3	20	-	0	30	14783	-	0.3	-	-
(4) Marine Clay	2.8	16	35	-	-	-	7000	0.495	-	-
(5) Fluvial Clay	0.6	19	30	-	-	-	9000	0.495	-	-
(6) Jurong Formation	11.9	20	150	-	-	-	84000	0.495	58800	0.2

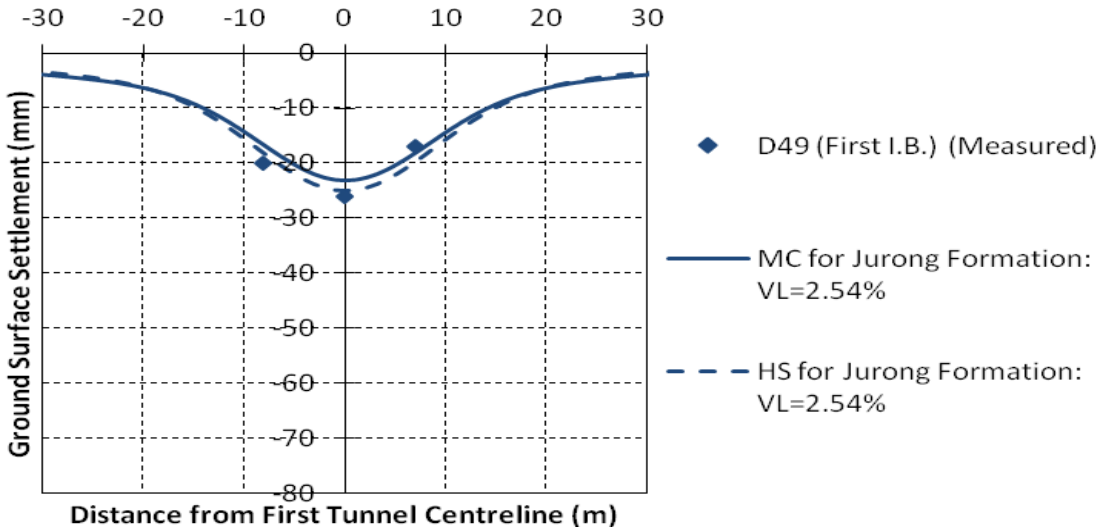

Figure 6.41 Transverse surface settlement after first inner bound bored tunnelling (Instrumentation Array D49)

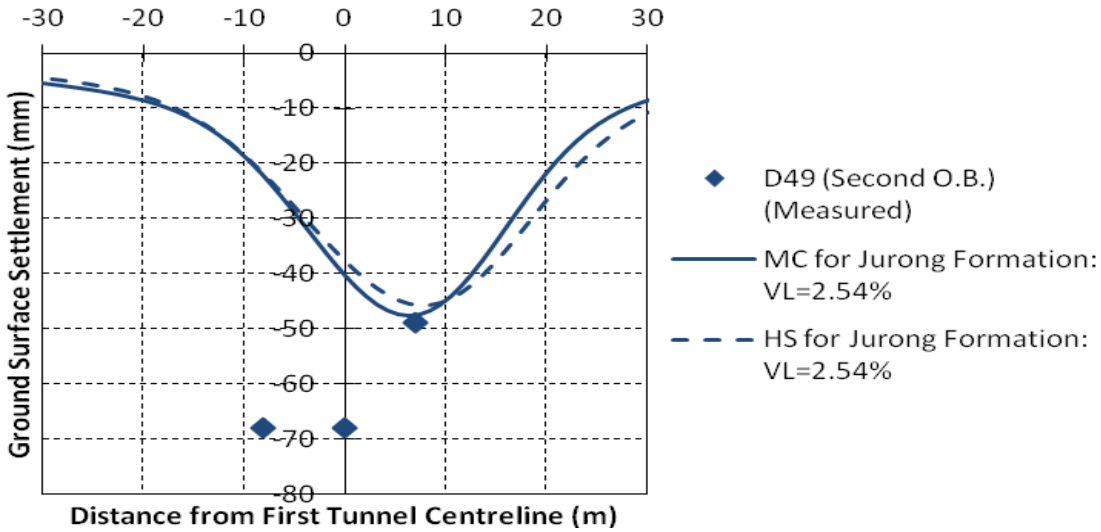

Figure 6.42 Transverse surface settlement after second outer bound bored tunnelling (Instrumentation Array D49)

6.6.11 Instrumentation Array D47

The installation of Instrumentation Array D47 facilitated monitoring of transverse surface settlement due to the closely spaced bored tunnelling through mixed ground of Jurong Formation and Kallang Formation. Part of the finite element mesh used

for the study is shown in Figure 6.43. Also shown in this figure are the strata with their thickness (see Table 6.15). The parameters assumed in the analyses are summarised in Table 6.15. Both first inner bound and second outer bound bored tunnels have axis of 19.3 m below the ground level at a pillar width of 4.8 m. Figure 6.44 shows the computed and measured transverse surface settlement after the first inner bound bored tunnelling. The corresponding computed and measured transverse surface settlement following the second outer bound bored tunnelling are shown in Figure 6.45.

As shown in Figure 6.44, the computed results using the HS and MC models are in reasonable agreement with the measured transverse surface settlement above single bored tunnel for a volume loss of 3.18 per cent. An important difference between these computed and measured result is that a wider transverse surface settlement trough was generated using the HS and MC models as compared to measured values.

The adoption of a lower range of EPBM earth pressure, grout injection pressure and grout volume during second outer bound bored tunnelling as compared to first inner bound bored tunnelling led to significantly larger volume loss being observed for the former. As shown in Figure 6.45, the analyses using a volume loss combination of 3.18 per cent for the first inner bound bored tunnel and 7.62 per cent for the second outer bound bored tunnel gave good agreement with the measured transverse surface settlement for closely spaced bored tunnels.

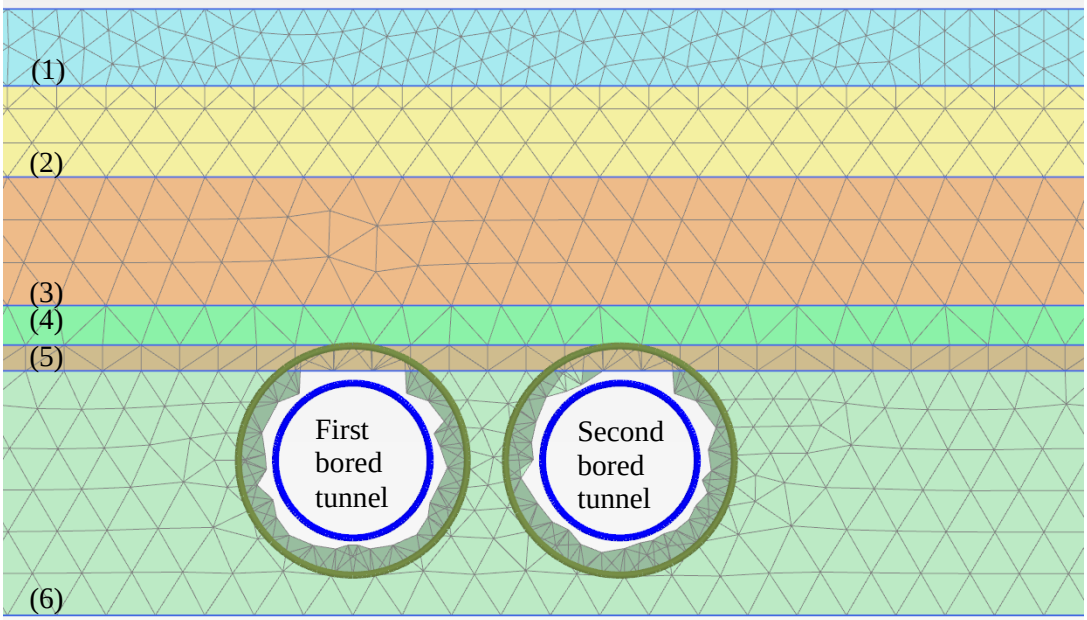

Figure 6.43 Partial finite element mesh in vicinity of bored tunnels (Instrumentation Array D47)

Table 6.15 Soil Properties (Instrumentation Array D47)

(Numbering) Strata	**Strata Thickness (m)**	**γ_{sat} (kN/m^3)**	**c_u (kPa)**	**c' (kPa)**	**ϕ' (^{o})**	**E' (kPa)**	**MC**		**HS**	
							E_u (kPa)	**ν**	**E_{50} (kPa)**	**ν_{ur}**
(1) Fill	3.3	19	20	-	-	-	10000	0.495	-	-
(2) Fluvial Sand	3.9	20	-	0	30	14783	-	0.3	-	-
(3) Marine Clay	5.5	16	35	-	-	-	7000	0.495	-	-
(4) Estuarine	1.7	15	30	-	-	-	4500	0.495	-	-
(5) Fluvial Clay	1.1	19	30	-	-	-	9000	0.495	-	-
(6) Jurong Formation	10.5	20	150	-	-	-	84000	0.495	58800	0.2

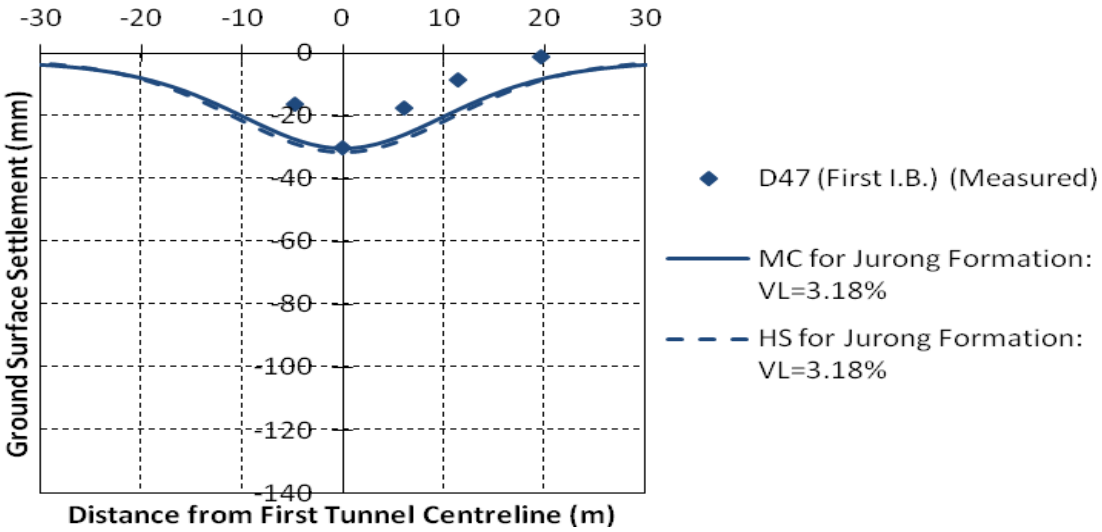

Figure 6.44 Transverse surface settlement after first inner bound bored tunnelling (Instrumentation Array D47)

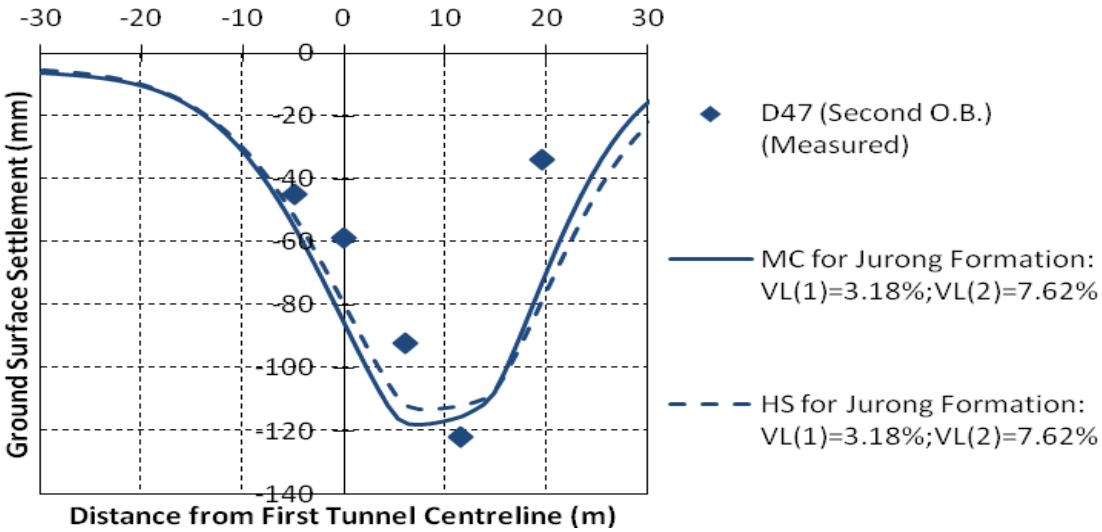

Figure 6.45 Transverse surface settlement after second outer bound bored tunnelling (Instrumentation Array D47)

6.6.12 Instrumentation Array E10

The installation of Instrumentation Array E10 facilitated monitoring of transverse surface settlement due to the closely spaced bored tunnelling through mixed ground of Jurong Formation and Kallang Formation. Part of the finite element mesh used

for the study is shown in Figure 6.46. Also shown in this figure are the strata with their thickness (see Table 6.16). The parameters assumed in the analyses are summarised in Table 6.16. Both first inner bound and second outer bound bored tunnels have axis of 18.8 m below the ground level at a pillar width of 5.0 m. Figure 6.47 shows the computed and measured transverse surface settlement after the first inner bound bored tunnelling. The corresponding computed and measured transverse surface settlement following the second outer bound bored tunnelling are shown in Figure 6.48.

It is generally agreed that the Gaussian normal probability curve can be used to estimate the transverse surface settlement above single bored tunnel with the maximum settlement located above the single bored tunnel. As shown in Figure 6.47, the measured transverse surface settlement seemed to depart significantly from the Gaussian normal probability curve. However, both the results computed using HS and MC models were in reasonable agreement with the measured transverse surface settlement to the right of the tunnel centreline of the first inner bound bored tunnel for a volume loss of 3.36 per cent. The significant difference in the measured transverse surface settlement to the left of the tunnel centreline of the first inner bound bored tunnel as compared with those estimated using HS and MC models can be inferred from the damage of monitoring instruments which is shown as the loss of three measurement points in Figure 6.48.

As shown in Figure 6.48, corresponding estimations for transverse surface settlement above closely spaced bored tunnels using HS and MC models show good agreement with the measurement. Given similar magnitude of volume loss for first inner bound and second outer bound bored tunnels, the maximum settlement generated seems to drawn towards the second outer bound bored tunnel due to greater soil disturbance after second outer bound bored tunnelling.

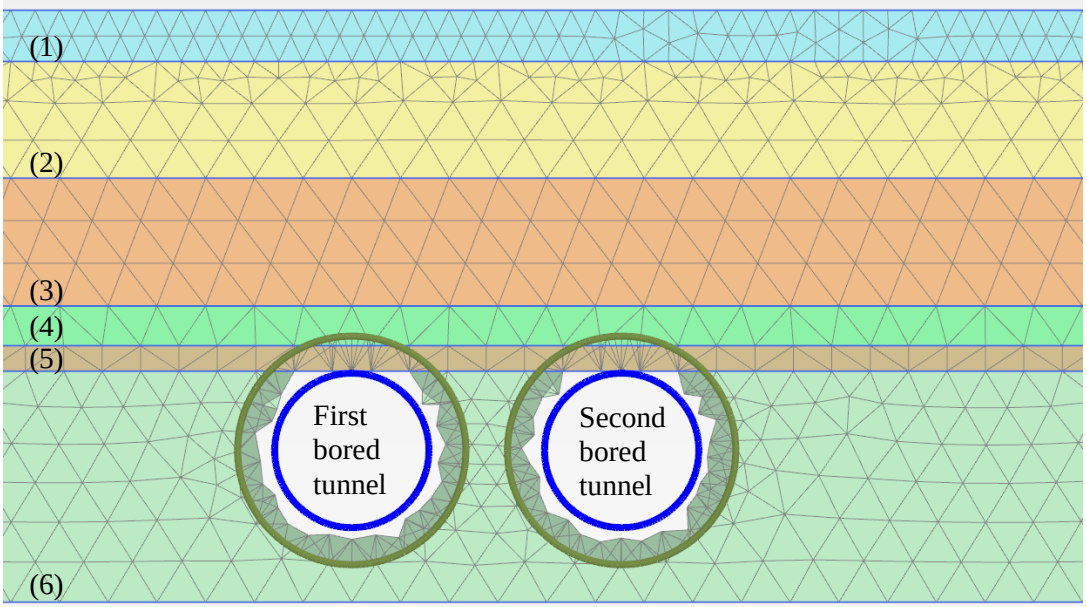

Figure 6.46 Partial finite element mesh in vicinity of bored tunnels (Instrumentation Array E10)

Table 6.16 Soil Properties (Instrumentation Array E10)

(Numbering) Strata	**Strata Thickness (m)**	γ_{sat} **(kN/m^3)**	c_u **(kPa)**	c' **(kPa)**	ϕ' **(^{o})**	E' **(kPa)**	**MC**		**HS**	
							E_u **(kPa)**	**ν**	E_{50} **(kPa)**	ν_{ur}
(1) Fill	2.2	19	20	-	-	-	10000	0.495	-	-
(2) Fluvial Sand	5.0	20	-	0	30	14783	-	0.3	-	-
(3) Marine Clay	5.5	16	35	-	-	-	7000	0.495	-	-
(4) Estuarine	1.7	15	30	-	-	-	4500	0.495	-	-
(5) Fluvial Clay	1.1	19	30	-	-	-	9000	0.495	-	-
(6) Jurong Formation	9.9	20	150	-	-	-	84000	0.495	58800	0.2

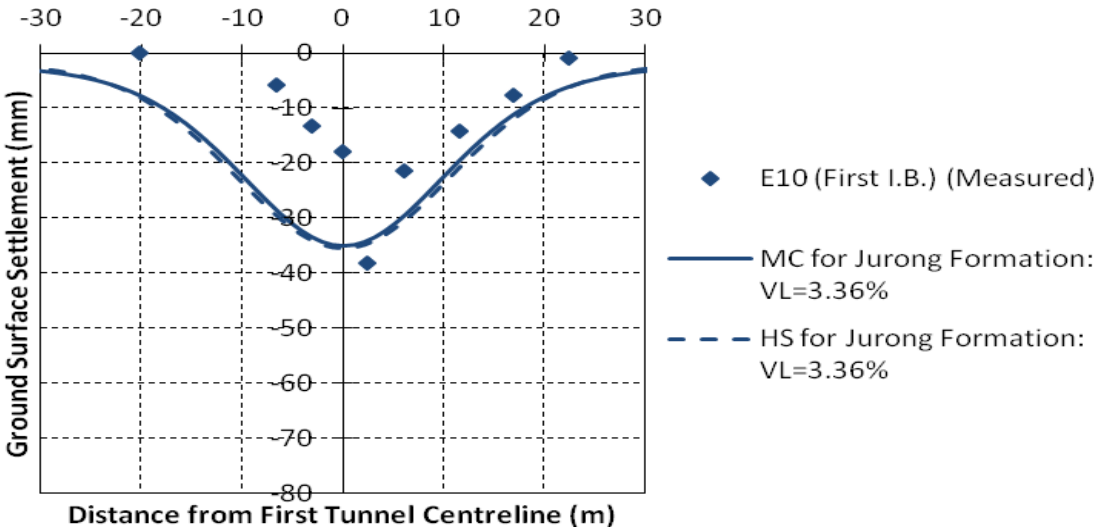

Figure 6.47 Transverse surface settlement after first inner bound bored tunnelling (Instrumentation Array E10)

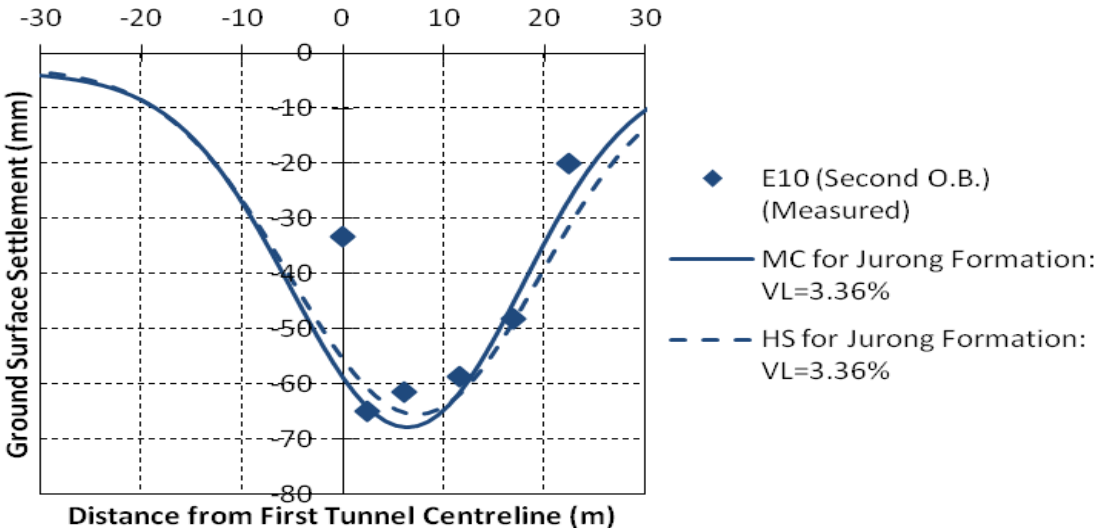

Figure 6.48 Transverse surface settlement after second outer bound bored tunnelling (Instrumentation Array E10)

6.6.13 Instrumentation Array D46

The installation of Instrumentation Array D46 facilitated monitoring of transverse surface settlement due to the closely spaced bored tunnelling through mixed ground of Jurong Formation and Kallang Formation. Part of the finite element mesh used

for the study is shown in Figure 6.49. Also shown in this figure are the strata with their thickness (see Table 6.17). The parameters assumed in the analyses are summarised in Table 6.17. Both first inner bound and second outer bound bored tunnels have axis of 18.2 m below the ground level at a pillar width of 5.5 m. Figure 6.50 shows the computed and measured transverse surface settlement after the first inner bound bored tunnelling. The corresponding computed and measured transverse surface settlement following the second outer bound bored tunnelling are shown in Figure 6.51.

It is easier to match the maximum settlement above single bored tunnel. However, it is more difficult to obtain a good match of the overall shape of the transverse surface settlement. As shown in Figure 6.50, the computed results from both the HS and MC models were in reasonable agreement with the measured transverse surface settlement at volume loss of 3.46 per cent.

As shown in Figure 6.51, the computed results for the left arm transverse surface settlement agreed well with the measured results. However, both HS and MC models overestimate the magnitude of the right arm transverse surface settlement. Such overestimation may be due to measurement errors such as the deviation between the exact locations of field instruments as compared to those stipulated on the drawing. However, there is no evidence to validate this argument.

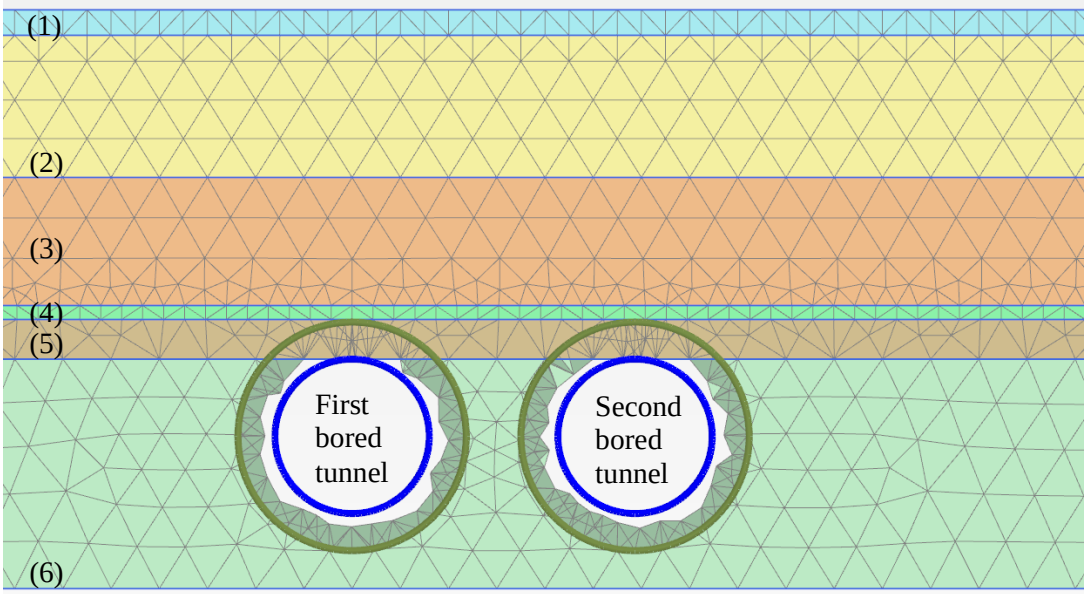

Figure 6.49 Partial finite element mesh in vicinity of bored tunnels (Instrumentation Array D46)

Table 6.17 Soil Properties (Instrumentation Array D46)

(Numbering) Strata	**Strata Thickness (m)**	**γ_{sat} (kN/m^3)**	**c_u (kPa)**	**c' (kPa)**	**ϕ' (^{o})**	**E' (kPa)**	**MC**		**HS**	
							E_u (kPa)	**ν**	**E_{50} (kPa)**	**ν_{ur}**
(1) Fill	1.1	19	20	-	-	-	10000	0.495	-	-
(2) Fluvial Sand	6.1	20	-	0	30	14783	-	0.3	-	-
(3) Marine Clay	5.5	16	35	-	-	-	7000	0.495	-	-
(4) Estuarine	0.6	15	30	-	-	-	4500	0.495	-	-
(5) Fluvial Clay	1.7	19	30	-	-	-	9000	0.495	-	-
(6) Jurong Formation	9.9	20	150	-	-	-	84000	0.495	58800	0.2

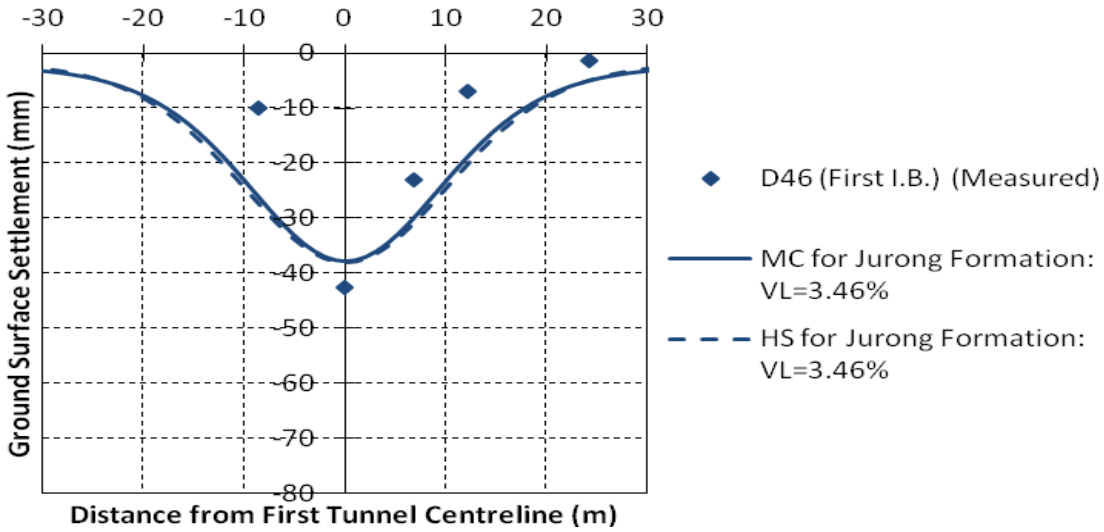

Figure 6.50 Transverse surface settlement after first inner bound bored tunnelling (Instrumentation Array D46)

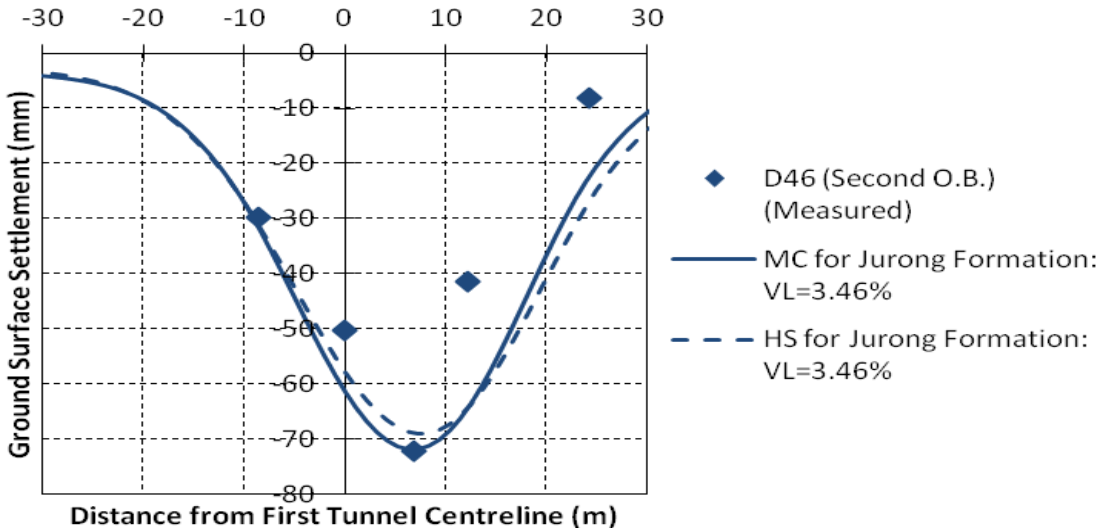

Figure 6.51 Transverse surface settlement after second outer bound bored tunnelling (Instrumentation Array D46)

6.7 Summary

The first inner bound and second outer bound bored tunnels were constructed from Pasir Panjang Cripple Siding to West Coast. Due to close proximity of both tunnels, similar ground conditions were encountered along the tunnelling routes which

mainly consist of uniform grade of Jurong Formation, mixed grades of Jurong Formation and mixed ground of Jurong Formation and Kallang Formation. The finite element analyses using HS model and MC model have been adopted to back analyse the transverse surface settlement above single bored tunnel and closely spaced bored tunnels for a total of 13 case studies. The input soil parameters were determined based on a number of empirical correlations where shear strength and deformation parameters of HS model and MC model for Jurong Formation were determined based on SPT blow counts.

For the case involving closely spaced bored tunnels, the HS model generally resulted in larger computed maximum settlement as compared to the MC model for the cases with smaller volume loss. However, the opposite trend was observed for the cases with larger volume loss. In most cases analyses using both HS and MC models show good agreement with the measured transverse surface settlement and the location of maximum settlement for the case involving closely spaced bored tunnels.

Depending on the EPBM performance of the second bored tunnelling, the maximum settlement may draw towards the second bored tunnel or the first bored tunnel due to greater soil disturbance experienced around the bored tunnel for the case of closely spaced bored tunnels. In this case, appropriate estimation of volume loss is necessary to achieve better estimation of the transverse surface settlement. Figure 6.52 summarises the variation of volume loss induced in the second outer bound bored tunnel with normalised pillar width. As observed, decreasing pillar width increases volume loss due to greater soil disturbance experienced by the second outer bound bored tunnel.

Besides adopting the appropriate soil properties for estimating transverse surface settlement, good quality field measurements are also required for good calibration of the numerical model. In this case, the presence of adjacent aboveground structures, heterogeneous soil profiles in the field as well as inaccuracy of field measurements as a result of disturbance or damage of the monitoring instruments

may lead to the difference between computed and measured values which increase the difficulty of achieving perfect agreement. Hence, achieving as closely as possible a consistent settlement shape should be given priority.

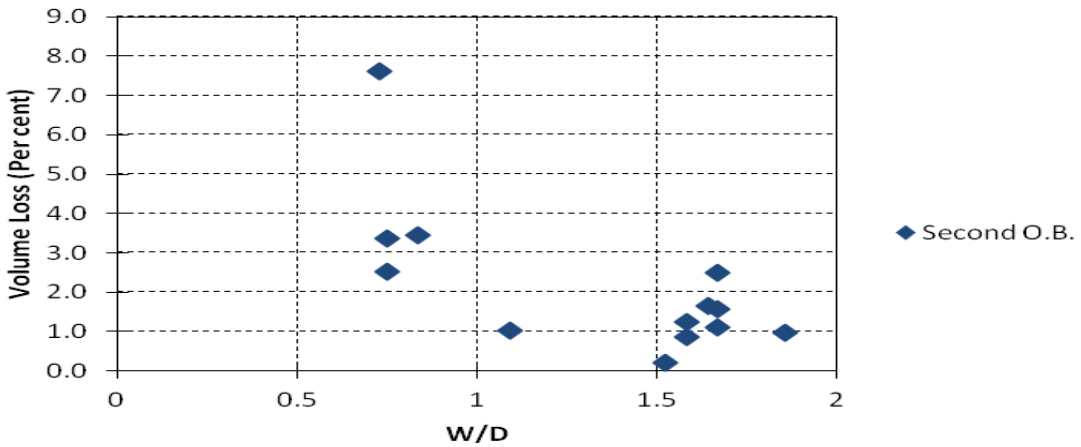

Figure 6.52 Variation of volume loss induced in second outer bound bored tunnel with dimensionless pillar width

CHAPTER 7 DETERMINATION OF SETTLEMENT PARAMETERS FOR SINGLE BORED TUNNEL AND CLOSELY SPACED BORED TUNNELS

7.1 Introduction

As discussed in Chapter 3, Peck (1969) showed that the pattern of surface settlements for single or two closely spaced tunnels can be approximated by a Gaussian probability curve. The surface settlement S at a distance x from the tunnel centreline is given by Equation 3.1, where the surface settlement is $0.61S_{max}$ at a distance i from either side of the tunnel centreline. In this chapter, the shape and extent of the surface settlements is established by estimating the trough width parameter i and the location of maximum surface settlement Loc S_{max} for the 13 cases presented in Chapter 6. This is achieved using the Excel spreadsheet built-in optimisation routine Solver to minimise the error between the computed and measured settlement. The computed trough width parameter i is also compared with the recommendations by Peck (1969), O'Reilly and New (1982) and Mair and Taylor (1997).

7.2 Spreadsheet Computation

The automated spreadsheet search algorithm is used to perform the minimisation procedure to determine the trough width parameter i and location of maximum surface settlement Loc S_{max}. The back analysis is based on the minimisation of the error function D_i that represents the squared of the discrepancy between the measured transverse surface settlement and the corresponding computed result obtained from the Gaussian probability curve given by Equation 7.1.

$$S(x)_G = A\frac{1}{\sqrt{2\pi}\sigma}[-e^{\frac{-(x-\mu)^2}{2\sigma^2}}] \tag{7.1}$$

where σ is the standard deviation of the Gaussian probability curve representing the trough width parameter i, x is the coordinate and μ is the mean representing the location of the maximum surface settlement Loc S_{max}.

Both the unknown trough width parameter i and location of maximum surface settlement Loc S_{max} are obtained using the Excel spreadsheet built-in optimisation routine Solver. Figure 7.1 shows a typical spreadsheet setup. The Solver works with a group of cells that are related, either directly or indirectly, to the formula in one cell and uses techniques from the operation search to find the optimal solution. For example, cells H5 to H9 in Figure 7.1 represent the x-coordinate of the ground surface settlement and cells I5 to I9 represent the magnitude of the measured ground surface settlement. The D_i (cells K5 to K9) value is obtained by subtracting the magnitude of the Gaussian probability curve defined by Equation 7.1 (cells J5 to J9) with the magnitude of the measured ground surface settlement and squaring the value, as shown in Equation 7.2. Set Objective (cell B10) consists of the summation of cell K5 to cell K9. Minimisation of the error function in the Set Objective is carried out using the Solver by changing cell C5 (trough width parameter i), cell B5 (Loc S_{max}) and cell D5 (trough area). Prior to invoking the Solver search algorithm, the unknown trough width parameter i, location of maximum surface settlement Loc S_{max} and trough area are randomly set in the preliminary range. Iterative numerical derivatives and directional search for these unknown values are automatically carried out in the spreadsheet environment.

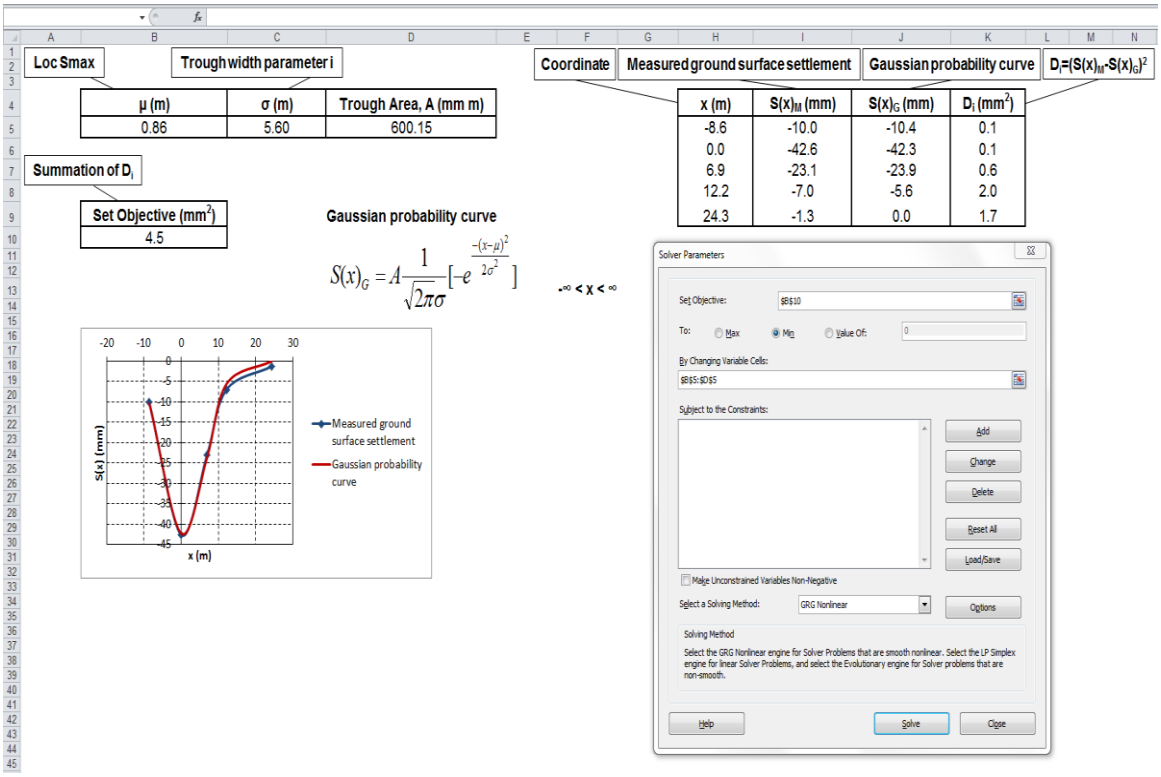

Figure 7.1 Example of Excel spreadsheet to determine i and Loc S_{max}

$$D_i = (S(x)_M - S(x)_G)^2 \tag{7.2}$$

7.3 Accuracy Assessment

Using the approach outlined in Section 7.2, the following presents the computed trough width parameter i and location of maximum surface settlement Loc S_{max} values for all the 13 measured instrumentation arrays that were discussed in Chapter 6.

Instrumentation Array D35

Figures 7.2 and 7.3 show the measured settlement and the corresponding computed Gaussian probability curve for single bored tunnel and closely spaced bored tunnels respectively, for Instrumentation Array D35. The distance to the point of inflection i has been determined as 7.45 m for single bored tunnel and 12.40 m for closely spaced bored tunnels. The location of maximum surface settlement Loc S_{max} is

offset at 0.23 m from the tunnel axis of single bored tunnel. Table 7.1 indicates that the value of i for single tunnel computed from this analysis compares reasonably well with the recommendations by Peck (1969), O'Reilly and New (1982) and Mair and Taylor (1997).

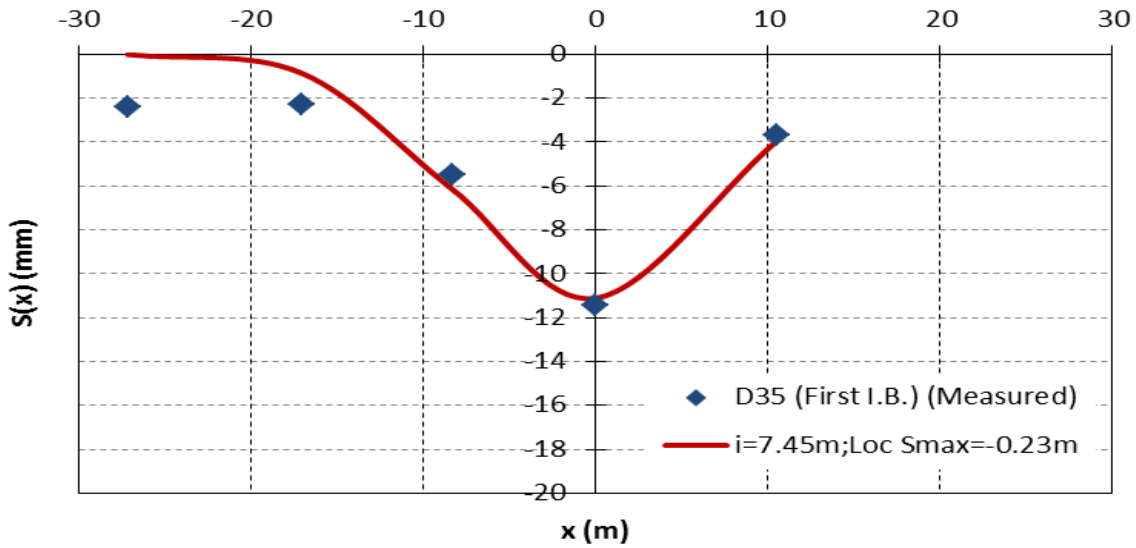

Figure 7.2 Gaussian probability curve for single bored tunnel (Instrumentation Array D35)

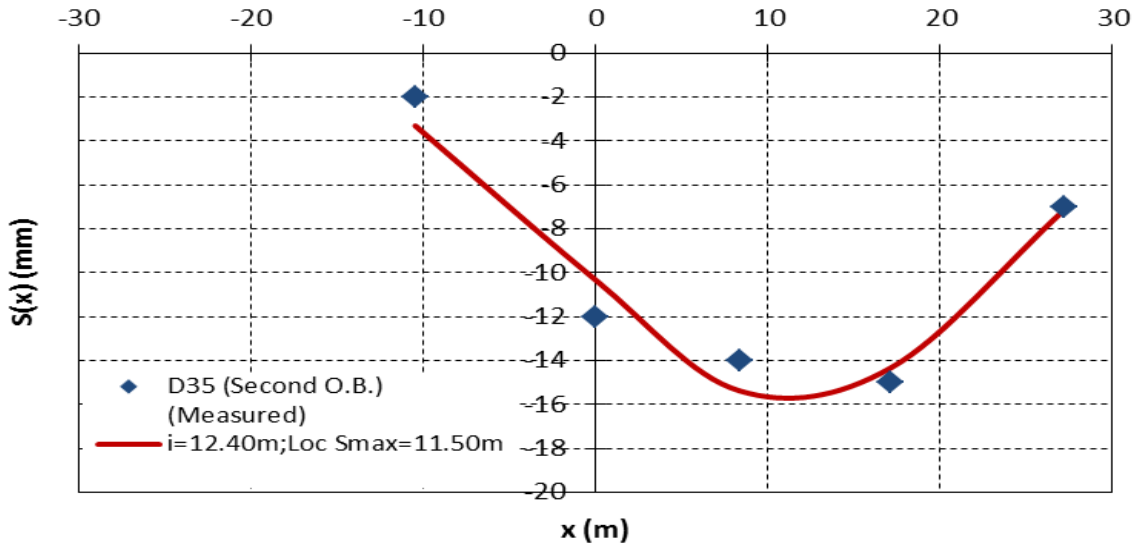

Figure 7.3 Gaussian probability curve for closely spaced bored tunnels (Instrumentation Array D35)

Table 7.1 Comparison of trough width parameter i above single tunnel as recommended by various researchers (Instrumentation Array D35)

Researchers	i (m)
Peck (1969)	7.02 – 8.56
O'Reilly and New (1982)	8.46
Mair and Taylor (1997)	8.56
This study	7.45

Instrumentation Array E9

Figures 7.4 and 7.5 show the measured settlement and the corresponding computed Gaussian probability curve for single bored tunnel and closely spaced bored tunnels respectively, for Instrumentation Array E9. The distance to the point of inflection i has been determined as 15.37 m for single bored tunnel and 25.28 m for closely spaced bored tunnels. The location of maximum surface settlement Loc S_{max} is offset at 2.59 m from the tunnel axis of single bored tunnel. Table 7.2 indicates that there is a significant deviation of the computed value of i for single tunnel compared with the recommendations by Peck (1969), O'Reilly and New (1982) and Mair and Taylor (1997).

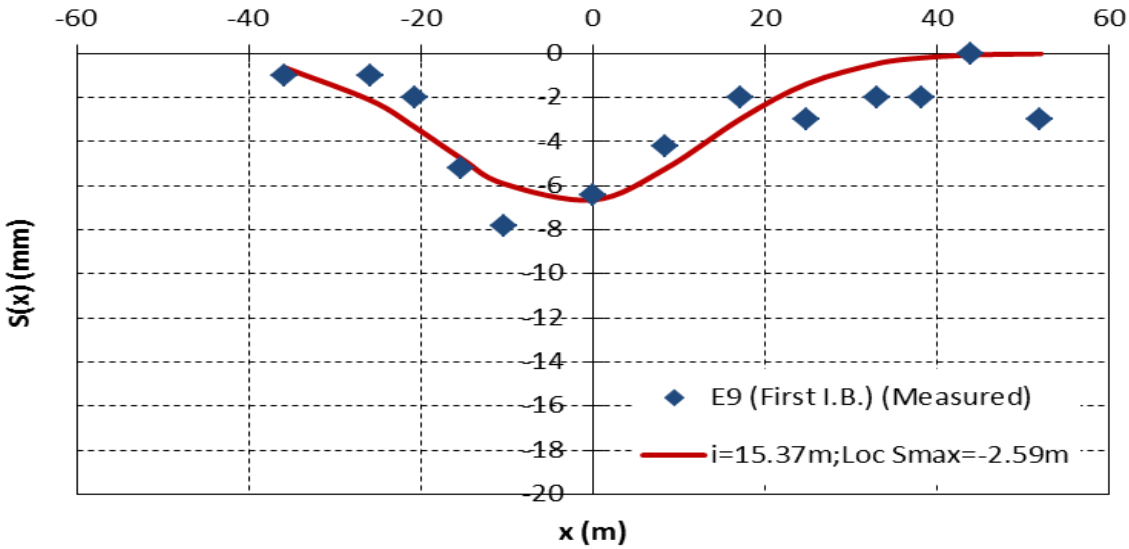

Figure 7.4 Gaussian probability curve for single bored tunnel (Instrumentation Array E9)

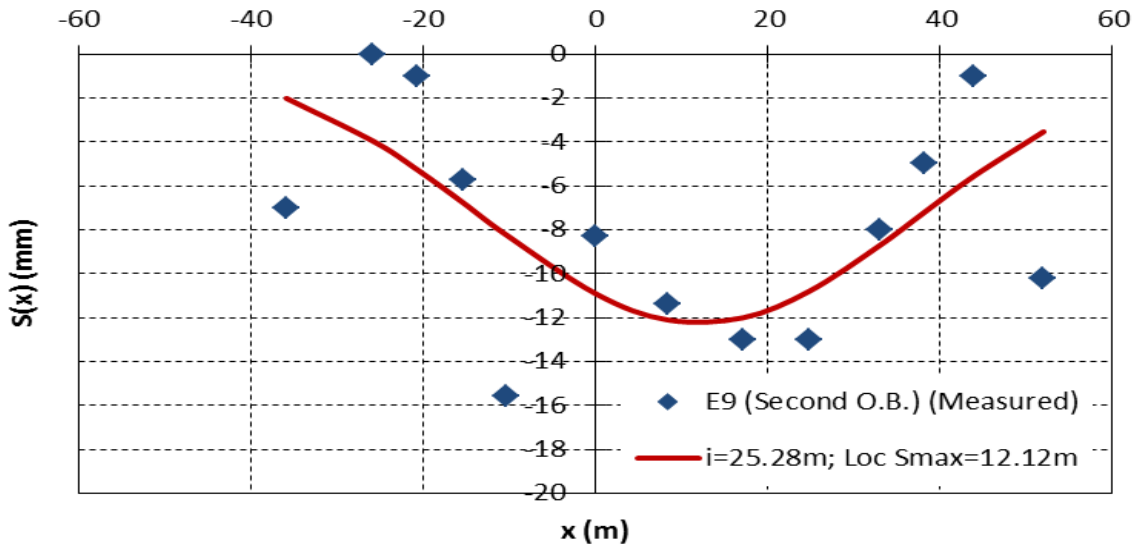

Figure 7.5 Gaussian probability curve for closely spaced bored tunnels (Instrumentation Array E9)

Table 7.2 Comparison of trough width parameter i above single tunnel as recommended by various researchers (Instrumentation Array E9)

Researchers	i (m)
Peck (1969)	7.02 – 8.56
O'Reilly and New (1982)	8.46
Mair and Taylor (1997)	8.56
This study	15.37

Instrumentation Array D34

Figures 7.6 and 7.7 show the measured settlement and the corresponding computed Gaussian probability curve for single bored tunnel and closely spaced bored tunnels respectively, for Instrumentation Array D34. The distance to the point of inflection i has been determined as 16.83 m for single bored tunnel and 16.16 m for closely spaced bored tunnels. The location of maximum surface settlement Loc S_{max} is offset at 3.93 m from the tunnel axis of single bored tunnel. Table 7.3 indicates that there is a significant deviation of the computed value of i for single tunnel

compared with the recommendations by Peck (1969), O'Reilly and New (1982) and Mair and Taylor (1997).

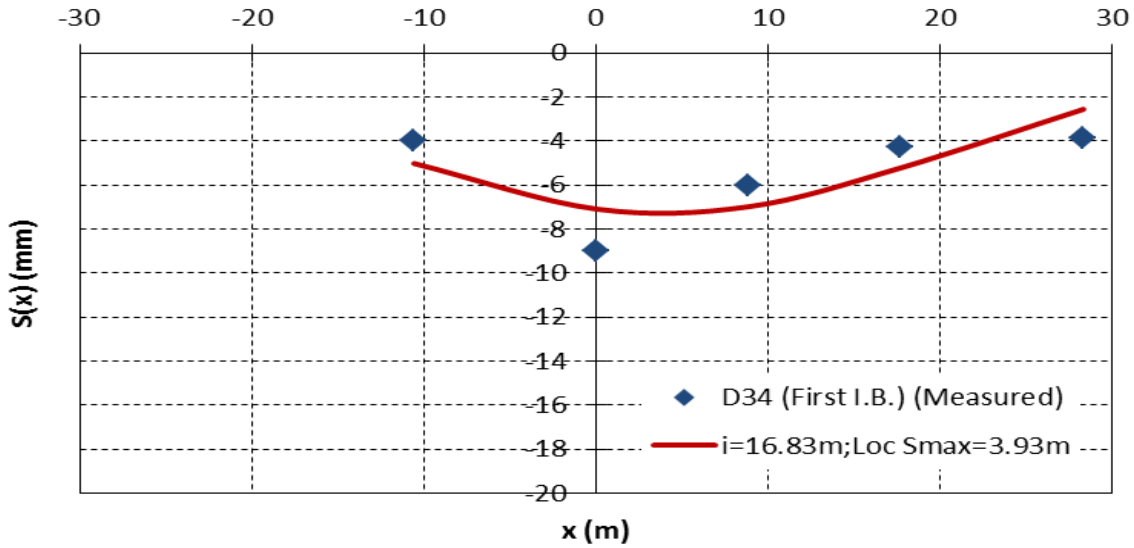

Figure 7.6 Gaussian probability curve for single bored tunnel (Instrumentation Array D34)

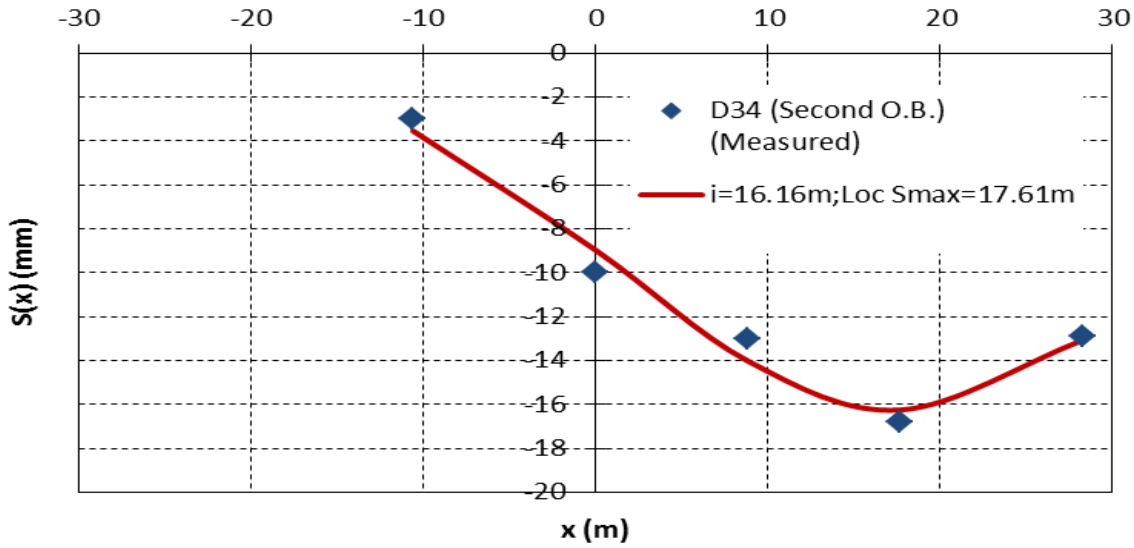

Figure 7.7 Gaussian probability curve for closely spaced bored tunnels (Instrumentation Array D34)

Table 7.3 Comparison of trough width parameter i above single tunnel as recommended by various researchers (Instrumentation Array D34)

Researchers	i (m)
Peck (1969)	7.20 – 8.84
O'Reilly and New (1982)	8.70
Mair and Taylor (1997)	8.84
This study	16.83

Instrumentation Array D7

Figures 7.8 and 7.9 show the measured settlement and the corresponding computed Gaussian probability curve for single bored tunnel and closely spaced bored tunnels respectively, for Instrumentation Array D7. The distance to the point of inflection i has been determined as 9.71 m for single bored tunnel and 13.13 m for closely spaced bored tunnels. The location of maximum surface settlement Loc S_{max} is offset at 5.88 m from the tunnel axis of single bored tunnel. Table 7.4 indicates that there is a deviation of the computed value of i for single tunnel compared with the recommendations by Peck (1969), O'Reilly and New (1982) and Mair and Taylor (1997).

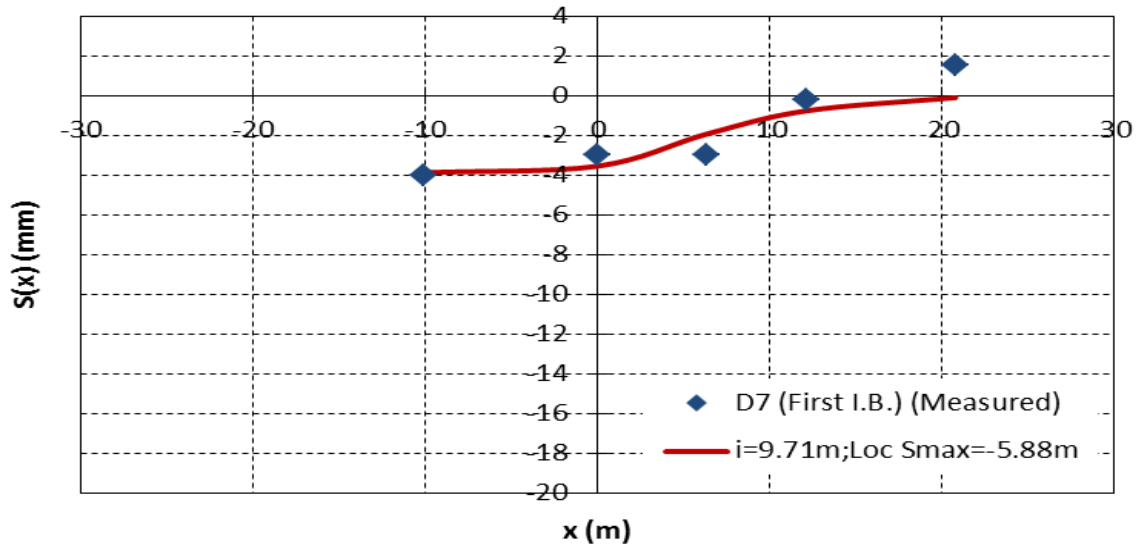

Figure 7.8 Gaussian probability curve for single bored tunnel (Instrumentation Array D7)

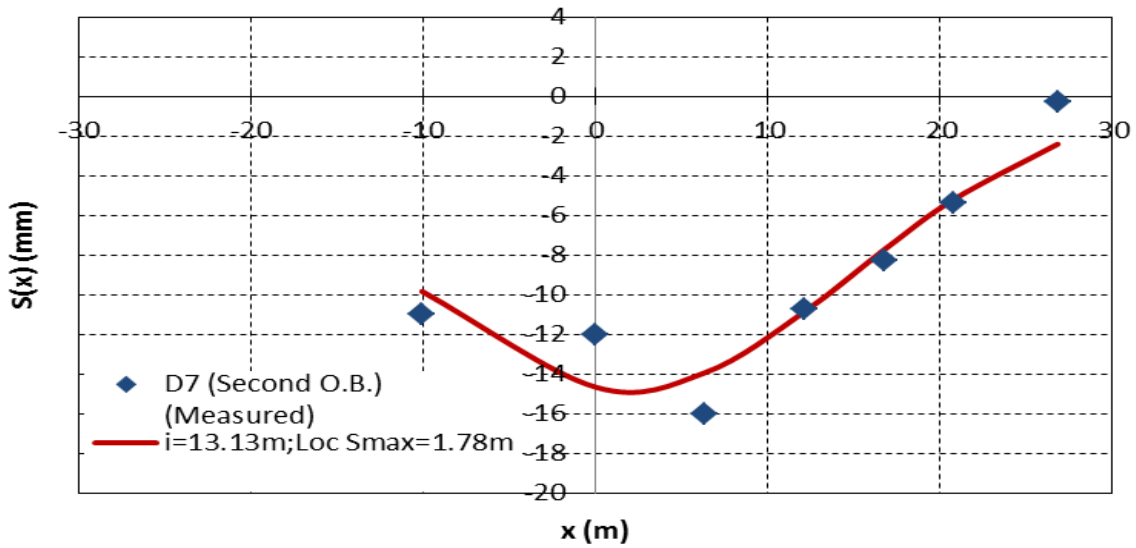

Figure 7.9 Gaussian probability curve for cosely spaced bored tunnels (Instrumentation Array D7)

Table 7.4 Comparison of trough width parameter i above single tunnel as recommended by various researchers (Instrumentation Array D7)

Researchers	i (m)
Peck (1969)	7.02 – 8.56
O'Reilly and New (1982)	8.46
Mair and Taylor (1997)	8.56
This study	9.71

Instrumentation Array D38

Figures 7.10 and 7.11 show the measured settlement and the corresponding computed Gaussian probability curve for single bored tunnel and closely spaced bored tunnels respectively, for Instrumentation Array D38. The distance to the point of inflection i has been determined as 8.93 m for single bored tunnel and 19.29 m for closely spaced bored tunnels. The location of maximum surface settlement Loc S_{max} is offset at 2.16 m from the tunnel axis of single bored tunnel. Table 7.5 indicates similar order of magnitude of computed value of i for single tunnel as

compared to the recommendations by Peck (1969), O'Reilly and New (1982) and Mair and Taylor (1997).

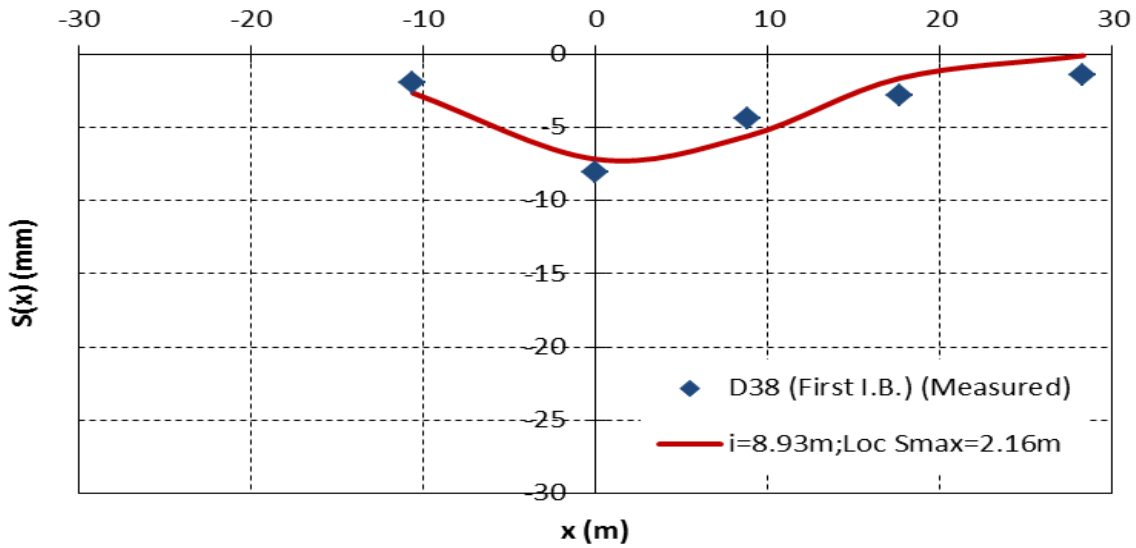

Figure 7.10 Gaussian probability curve for single bored tunnel (Instrumentation Array D38)

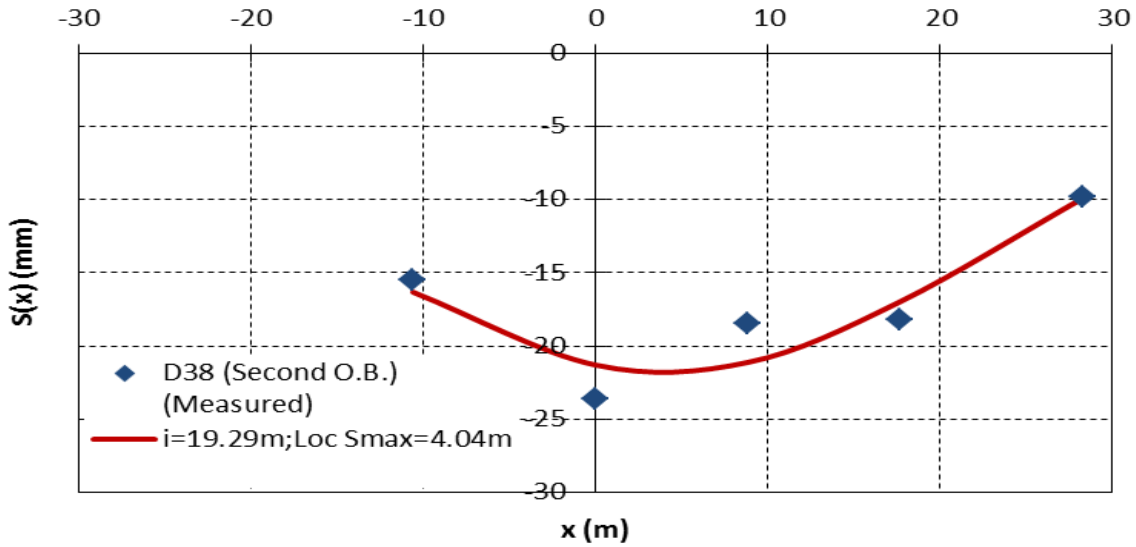

Figure 7.11 Gaussian probability curve for closely spaced bored tunnels (Instrumentation Array D38)

Table 7.5 Comparison of trough width parameter i above single tunnel as recommended by various researchers (Instrumentation Array D38)

Researchers	i (m)
Peck (1969)	7.20 – 8.84
O'Reilly and New (1982)	8.70
Mair and Taylor (1997)	8.84
This study	8.93

Instrumentation Array D37

Figures 7.12 and 7.13 show the measured settlement and the corresponding computed Gaussian probability curve for single bored tunnel and closely spaced bored tunnels respectively, for Instrumentation Array D37. The distance to the point of inflection i has been determined as 6.46 m for single bored tunnel and 11.83 m for closely spaced bored tunnels. The location of maximum surface settlement Loc S_{max} is offset at 0.46 m from the tunnel axis of single bored tunnel. Table 7.6 indicates minor deviation of the computed value of i as compared to the recommendation by Peck (1969) for single tunnel. However, relatively larger deviation of computed value of i for single tunnel was noted as compared to the recommendations by O'Reilly and New (1982) and Mair and Taylor (1997).

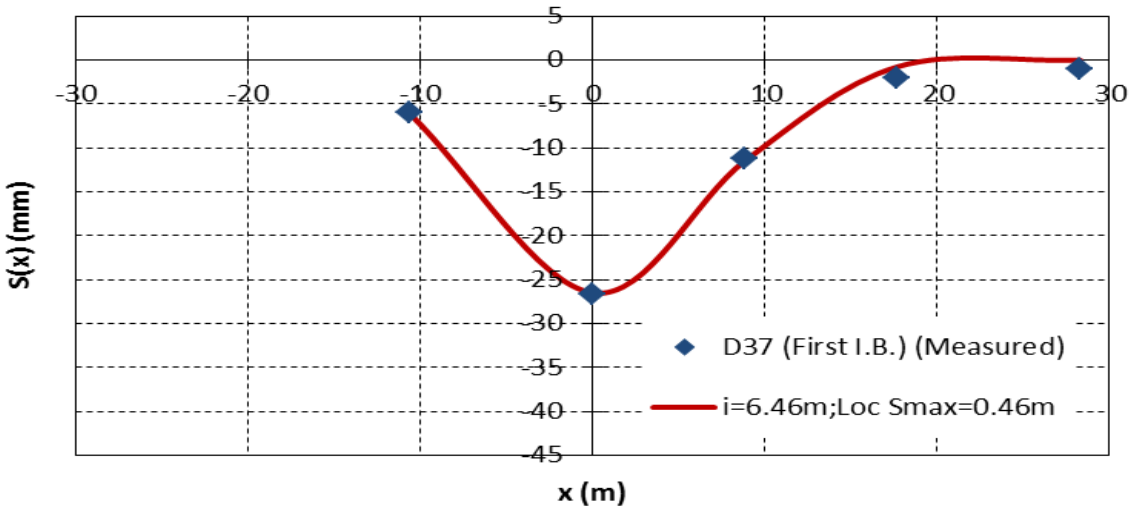

Figure 7.12 Gaussian probability curve for single bored tunnel (Instrumentation Array D37)

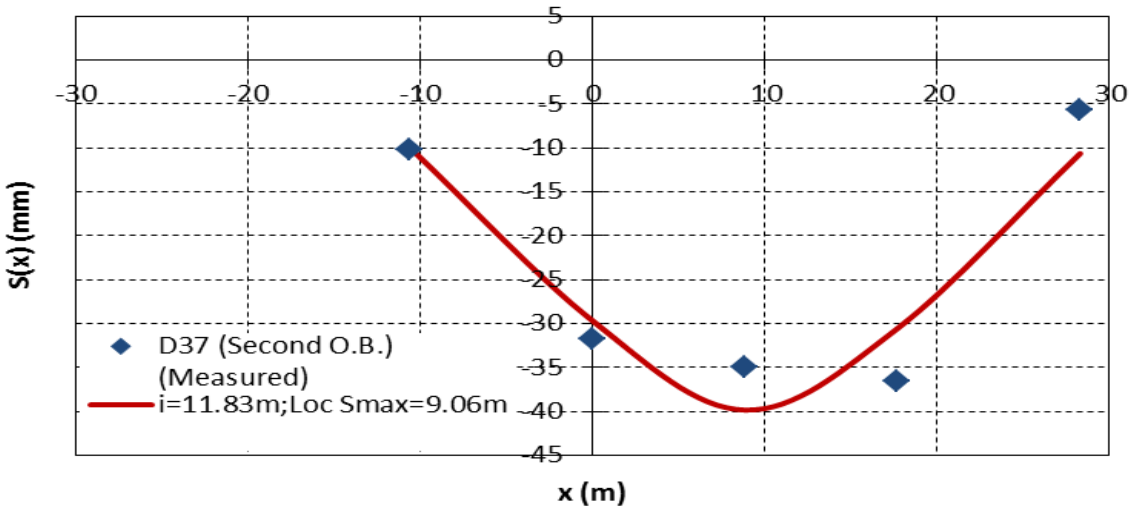

Figure 7.13 Gaussian probability curve for closely spaced bored tunnels (Instrumentation Array D37)

Table 7.6 Comparison of trough width parameter i above single tunnel as recommended by various researchers (Instrumentation Array D37)

Researchers	i (m)
Peck (1969)	7.11 – 8.70
O'Reilly and New (1982)	8.58
Mair and Taylor (1997)	8.70
This study	6.46

Instrumentation Array D33

Figures 7.14 and 7.15 show the measured settlement and the corresponding computed Gaussian probability curve for single bored tunnel and closely spaced bored tunnels respectively, for Instrumentation Array D33. The distance to the point of inflection i has been determined as 9.42 m for single bored tunnel and 5.48 m for closely spaced bored tunnels. The location of maximum surface settlement Loc S_{max} is offset at 0.52 m from the tunnel axis of single bored tunnel. Table 7.7 indicates minor deviation of the computed value of i for single tunnel as compared to the recommendations by Peck (1969), O'Reilly and New (1982) and Mair and Taylor (1997).

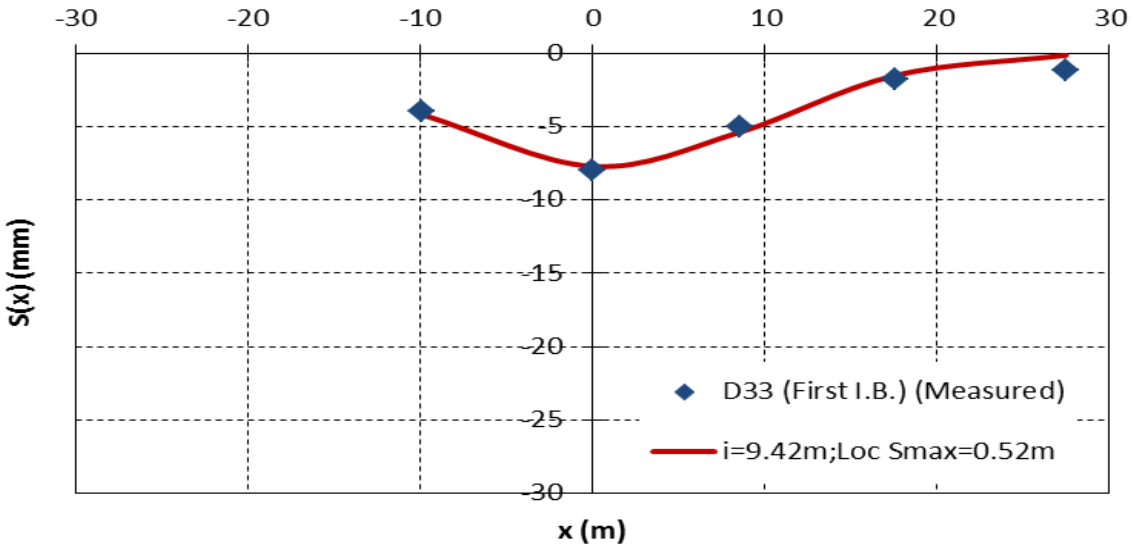

Figure 7.14 Gaussian probability curve for single bored tunnel (Instrumentation Array D33)

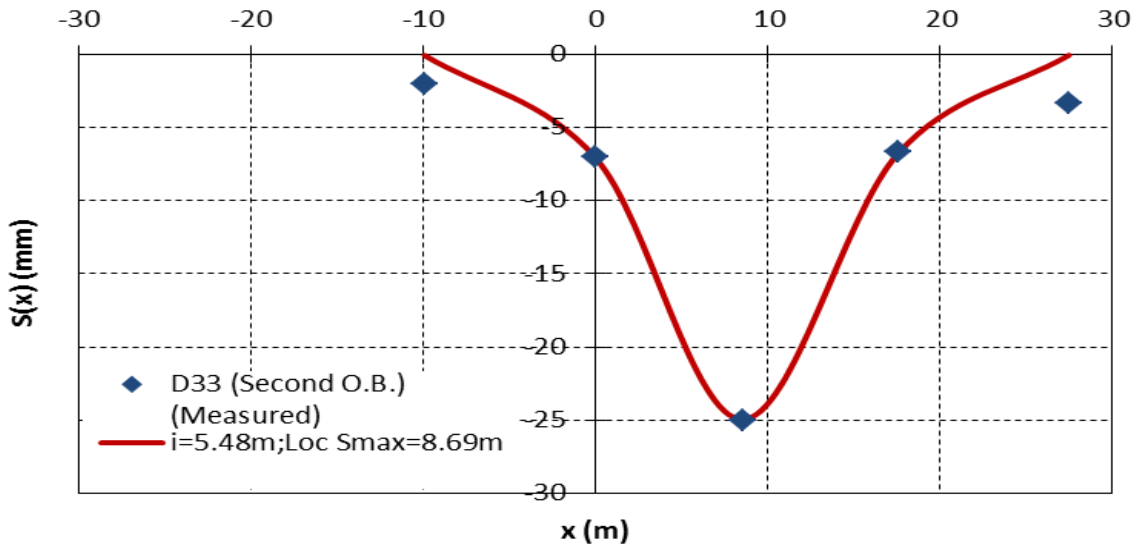

Figure 7.15 Gaussian probability curve for closely spaced bored tunnels (Instrumentation Array D33)

Table 7.7 Comparison of trough width parameter i above single tunnel as recommended by various researchers (Instrumentation Array D33)

Researchers	i (m)
Peck (1969)	7.11 – 8.70
O'Reilly and New (1982)	8.58
Mair and Taylor (1997)	8.70
This study	9.42

Instrumentation Array D32

Figures 7.16 and 7.17 show the measured settlement and the corresponding computed Gaussian probability curve for single bored tunnel and closely spaced bored tunnels respectively, for Instrumentation Array D32. The distance to the point of inflection i has been determined as 26.52 m for single bored tunnel and 29.14 m for closely spaced bored tunnels. The location of maximum surface settlement Loc S_{max} is offset at -0.66 m from the tunnel axis of single bored tunnel. Table 7.8 indicates significantly larger deviation of computed value of i for single tunnel as

compared to the recommendations by Peck (1969), O'Reilly and New (1982) and Mair and Taylor (1997).

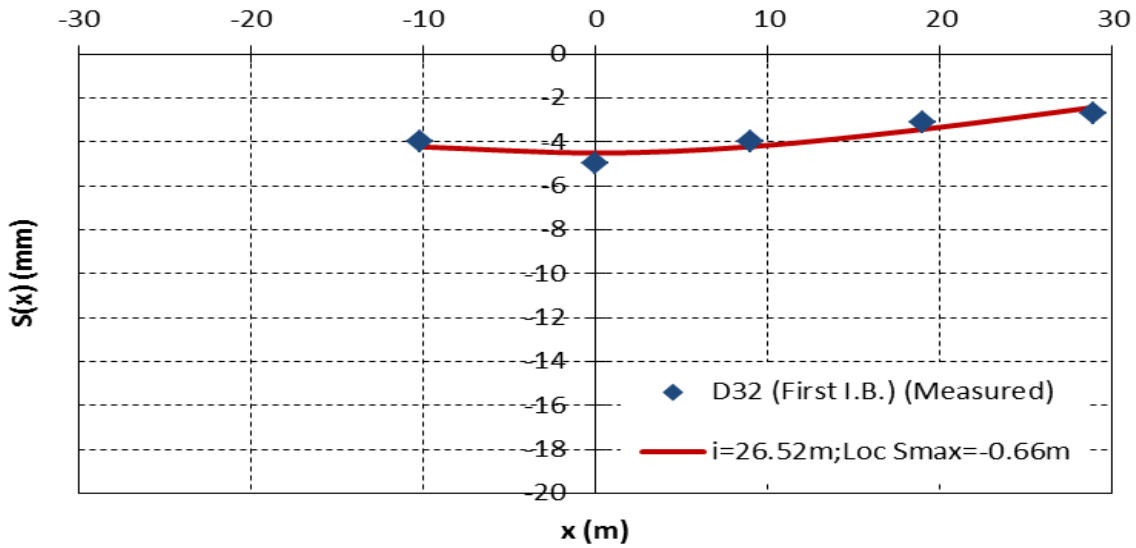

Figure 7.16 Gaussian probability curve for single bored tunnel (Instrumentation Array D32)

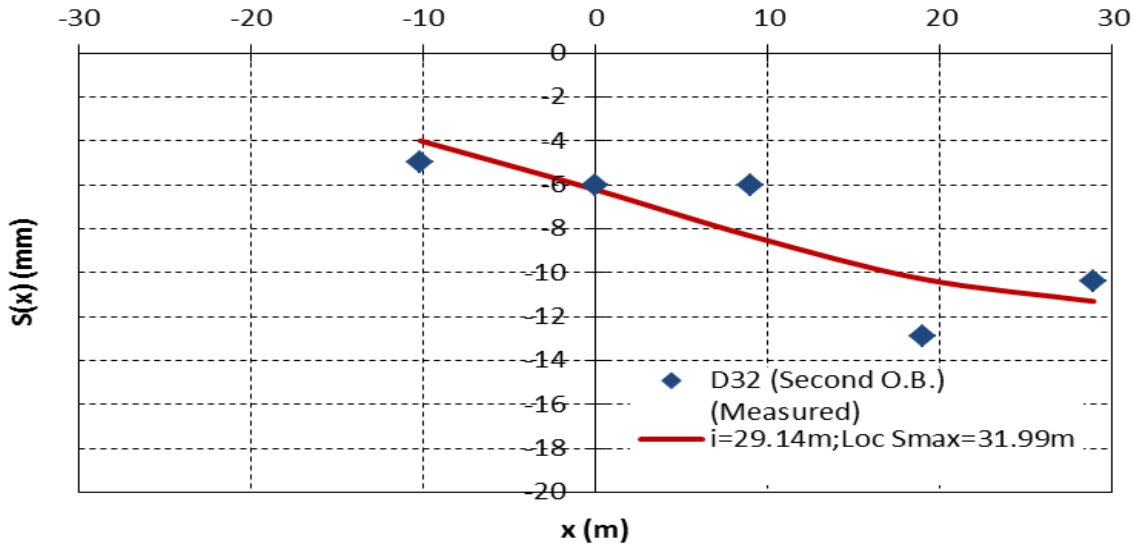

Figure 7.17 Gaussian probability curve for closely spaced bored tunnels (Instrumentation Array D32)

Table 7.8 Comparison of trough width parameter i above single tunnel as recommended by various researchers (Instrumentation Array D32)

Researchers	i (m)
Peck (1969)	7.20 – 8.84
O'Reilly and New (1982)	8.70
Mair and Taylor (1997)	8.84
This study	26.52

Instrumentation Array E14

Figures 7.18 and 7.19 show the measured settlement and the corresponding computed Gaussian probability curve for single bored tunnel and closely spaced bored tunnels respectively, for Instrumentation Array E14. The distance to the point of inflection i has been determined as 5.96 m for single bored tunnel and 7.52 m for closely spaced bored tunnels. The location of maximum surface settlement Loc S_{max} is offset at -0.90 m from the tunnel axis of single bored tunnel. Table 7.9 indicates a good comparison between the computed value of i for single tunnel and the recommendation by Peck (1969). However, larger value of i were recommended by O'Reilly and New (1982) and Mair and Taylor (1997).

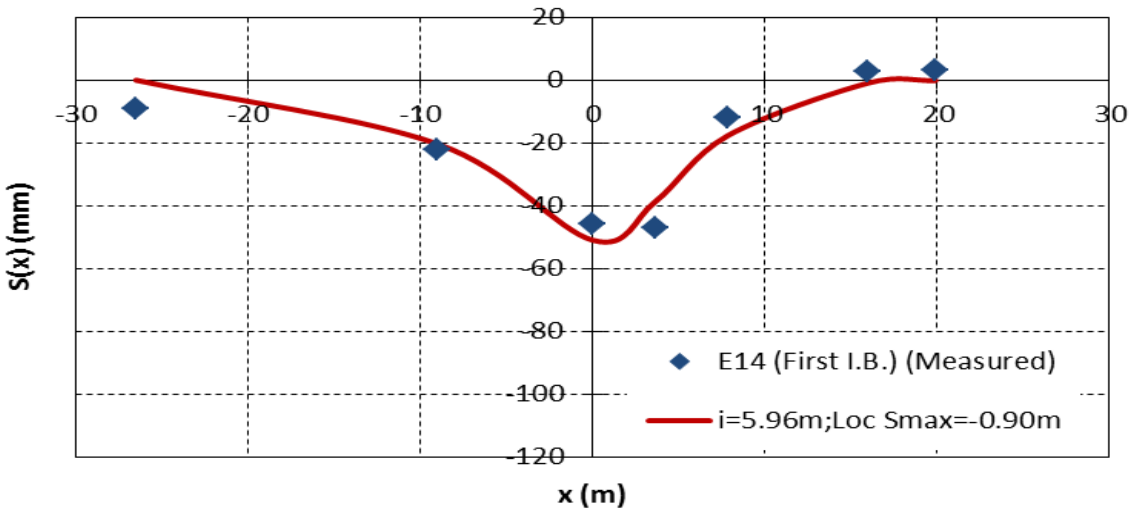

Figure 7.18 Gaussian probability curve for single bored tunnel (Instrumentation Array E14)

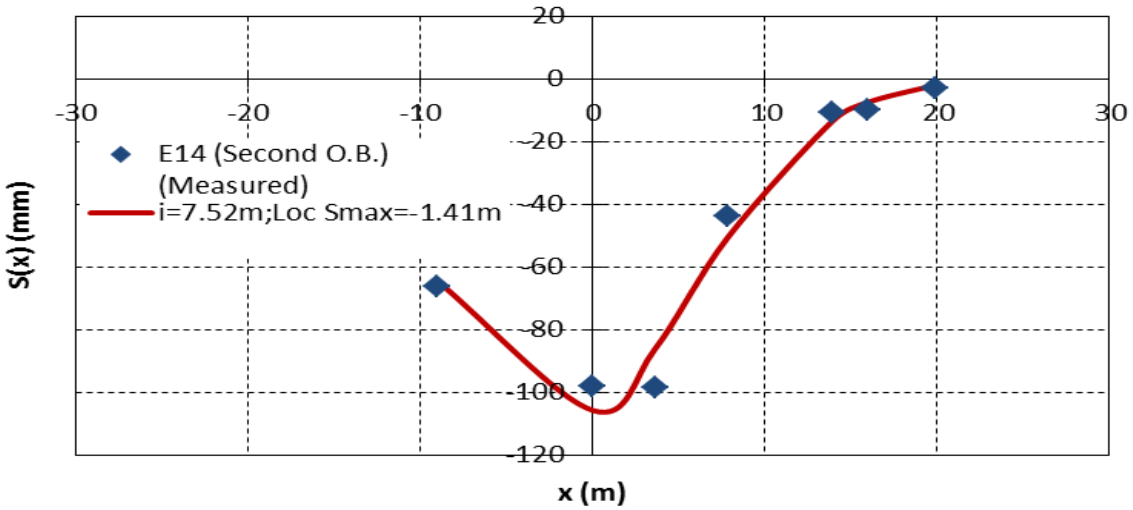

Figure 7.19 Gaussian probability curve for closely spaced bored tunnels (Instrumentation Array E14)

Table 7.9 Comparison of trough width parameter i above single tunnel as recommended by various researchers (Instrumentation Array E14)

Researchers	i (m)
Peck (1969)	6.23 – 7.37
O'Reilly and New (1982)	7.44
Mair and Taylor (1997)	7.37
This study	5.96

Instrumentation Array D49

Figures 7.20 and 7.21 show the measured settlement and the corresponding computed Gaussian probability curve for single bored tunnel and closely spaced bored tunnels respectively, for Instrumentation Array D49. The distance to the point of inflection i has been determined as 8.97 m for single bored tunnel and 12.62 m for closely spaced bored tunnels. The location of maximum surface settlement Loc S_{max} is offset at -1.47 m from the tunnel axis of single bored tunnel. Table 7.10 indicates good agreement between the computed value of i for single tunnel and recommendation by Peck (1969). In addition, similar order of magnitude of

computed value of i was noted as compared to the recommendations by O'Reilly and New (1982) and Mair and Taylor (1997).

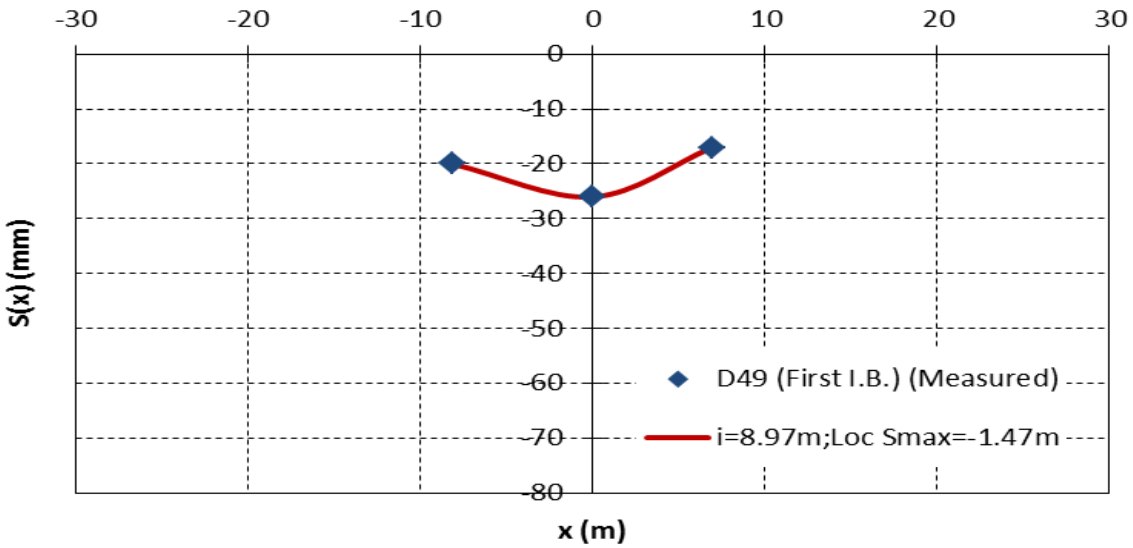

Figure 7.20 Gaussian probability curve for single bored tunnel (Instrumentation Array D49)

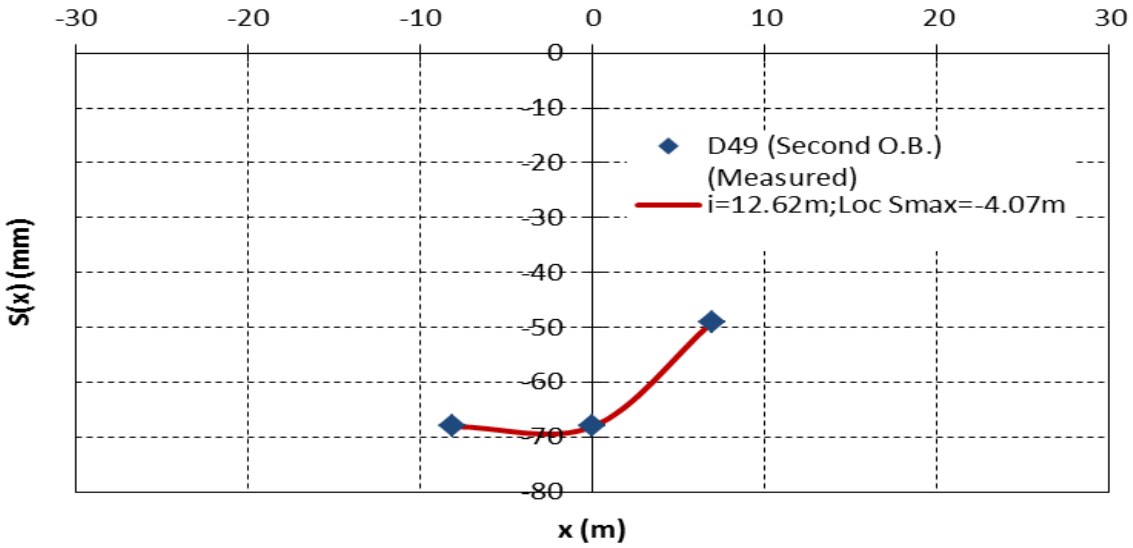

Figure 7.21 Gaussian probability curve for closely spaced bored tunnels (Instrumentation Array D49)

Table 7.10 Comparison of trough width parameter i above single tunnel as recommended by various researchers (Instrumentation Array D49)

Researchers	i (m)
Peck (1969)	7.56 – 9.39
O'Reilly and New (1982)	9.18
Mair and Taylor (1997)	9.39
This study	8.97

Instrumentation Array D47

Figures 7.22 and 7.23 show the measured settlement and the corresponding computed Gaussian probability curve for single bored tunnel and closely spaced bored tunnels respectively, for Instrumentation Array D47. The distance to the point of inflection i has been determined as 5.76 m for single bored tunnel and 8.19 m for closely spaced bored tunnels. The location of maximum surface settlement Loc S_{max} is offset at 0.98 m from the tunnel axis of single bored tunnel. Table 7.11 indicates larger deviation of the computed value of i for single tunnel as compared to the recommendations by Peck (1969), O'Reilly and New (1982) and Mair and Taylor (1997).

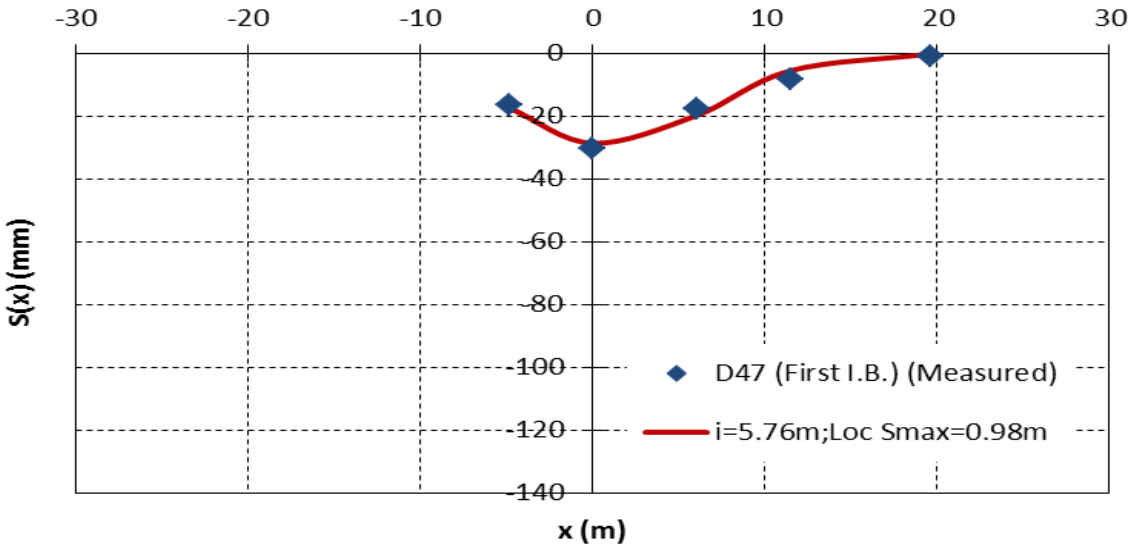

Figure 7.22 Gaussian probability curve for single bored tunnel (Instrumentation Array D47)

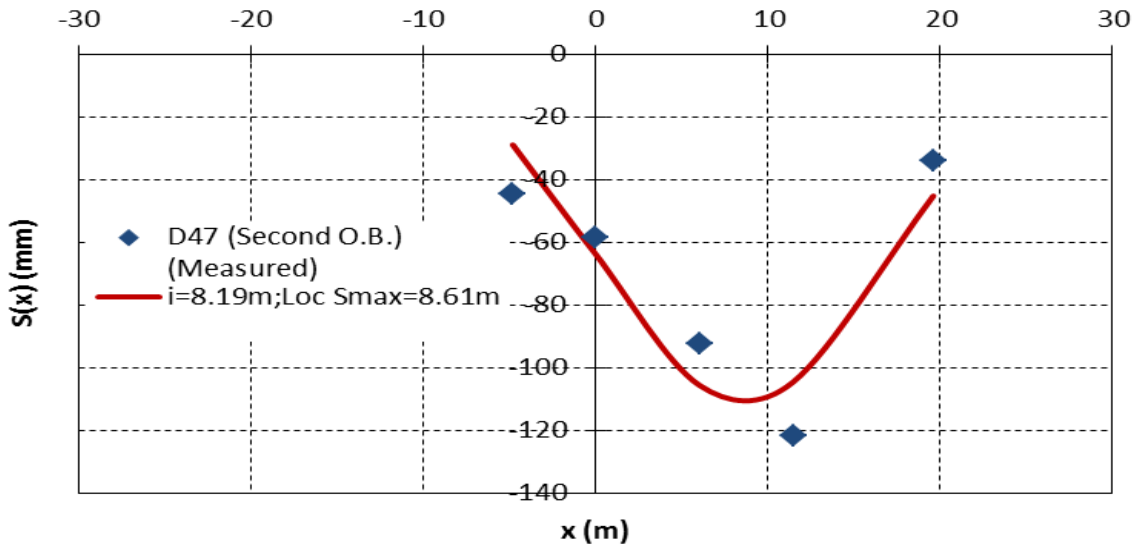

Figure 7.23 Gaussian probability curve for closely spaced bored tunnels (Instrumentation Array D47)

Table 7.11 Comparison of trough width parameter i above single tunnel as recommended by various researchers (Instrumentation Array D47)

Researchers	i (m)
Peck (1969)	7.74 – 9.67
O'Reilly and New (1982)	9.42
Mair and Taylor (1997)	9.67
This study	5.76

Instrumentation Array E10

Figures 7.24 and 7.25 show the measured settlement and the corresponding computed Gaussian probability curve for single bored tunnel and closely spaced bored tunnels respectively, for Instrumentation Array E10. The distance to the point of inflection i has been determined as 6.06 m for single bored tunnel and 9.08 m for closely spaced bored tunnels. The location of maximum surface settlement Loc S_{max} is offset at 4.21 m from the tunnel axis of single bored tunnel. Table 7.12 indicates larger deviation of the computed value of i for single tunnel as compared to the

recommendations by Peck (1969), O'Reilly and New (1982) and Mair and Taylor (1997).

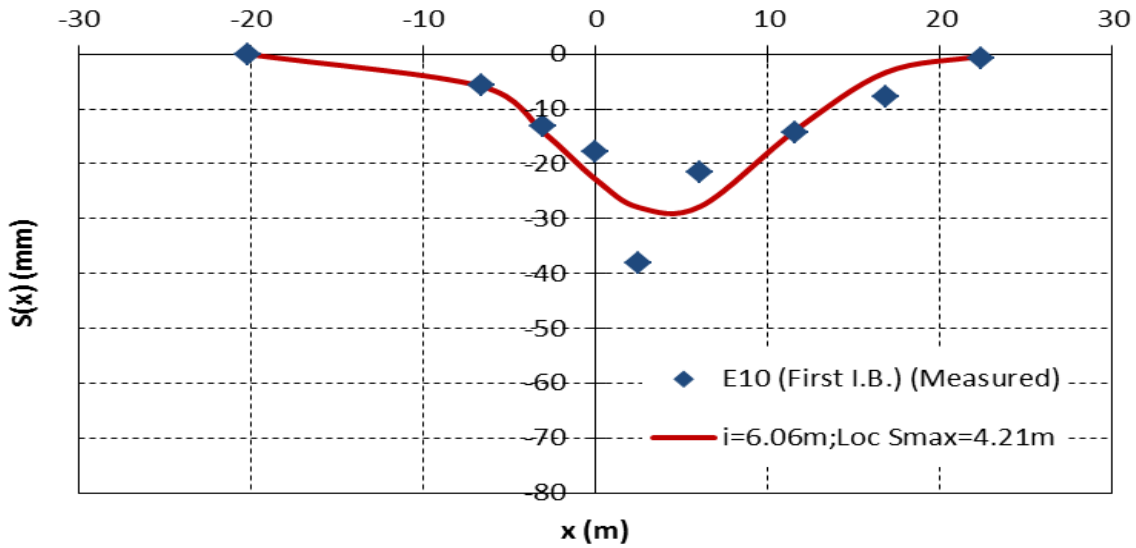

Figure 7.24 Gaussian probability curve for single bored tunnel (Instrumentation Array E10)

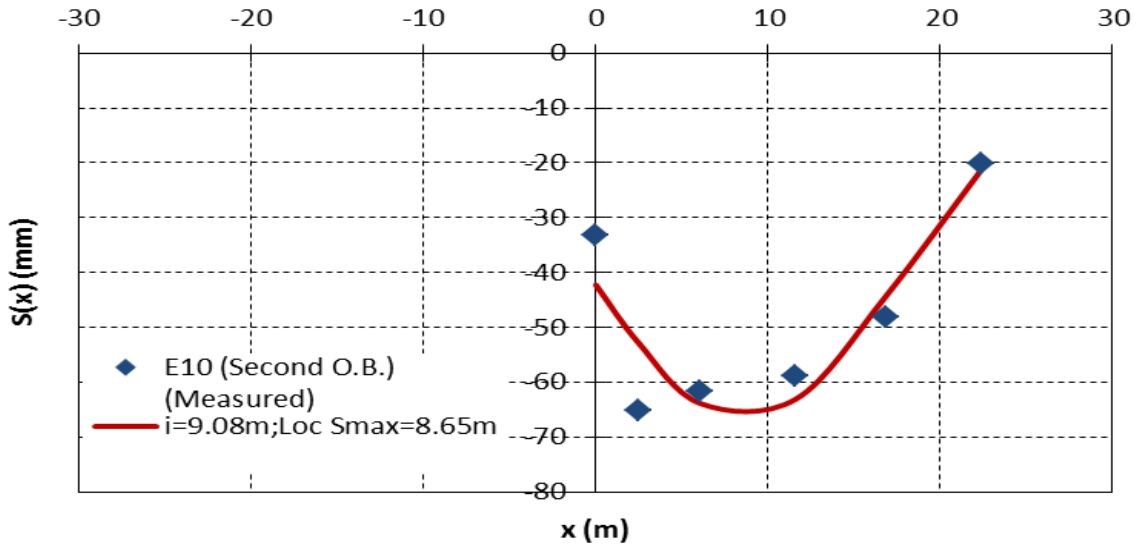

Figure 7.25 Gaussian probability curve for closely spaced bored tunnels (Instrumentation Array E10)

Table 7.12 Comparison of trough width parameter i above single tunnel as recommended by various researchers (Instrumentation Array E10)

Researchers	i (m)
Peck (1969)	7.56 – 9.39
O'Reilly and New (1982)	9.18
Mair and Taylor (1997)	9.39
This study	6.06

Instrumentation Array D46

Figures 7.26 and 7.27 show the measured settlement and the corresponding computed Gaussian probability curve for single bored tunnel and closely spaced bored tunnels respectively, for Instrumentation Array D46. The distance to the point of inflection i has been determined as 5.60 m for single bored tunnel and 9.54 m for closely spaced bored tunnels. The location of maximum surface settlement Loc S_{max} is offset at 0.86 m from the tunnel axis of single bored tunnel. Table 7.13 indicates larger deviation of the computed value of i for single tunnel as compared to the recommendations by Peck (1969), O'Reilly and New (1982) and Mair and Taylor (1997).

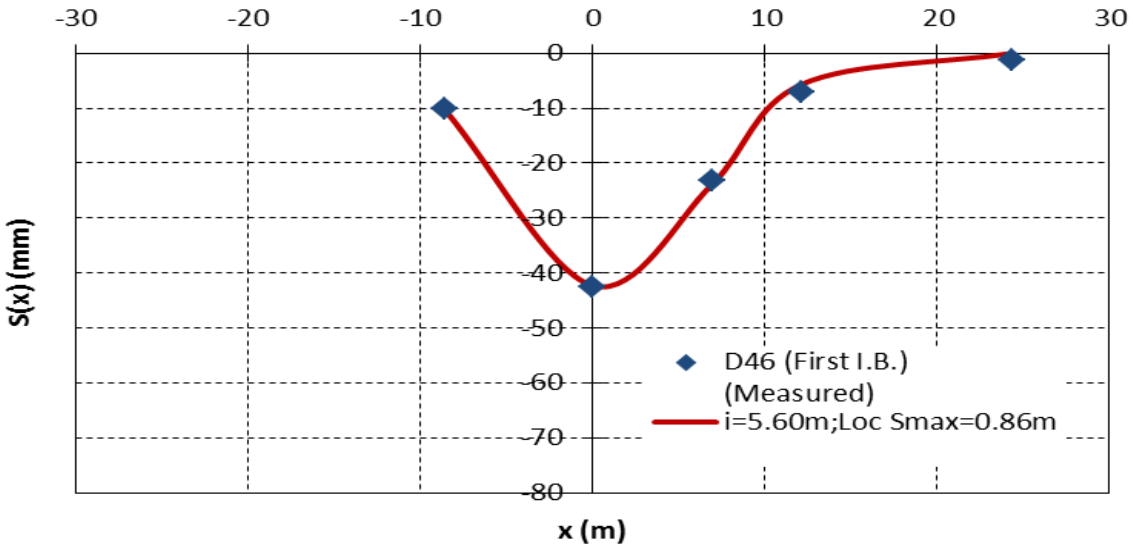

Figure 7.26 Gaussian probability curve for single bored tunnel (Instrumentation Array D46)

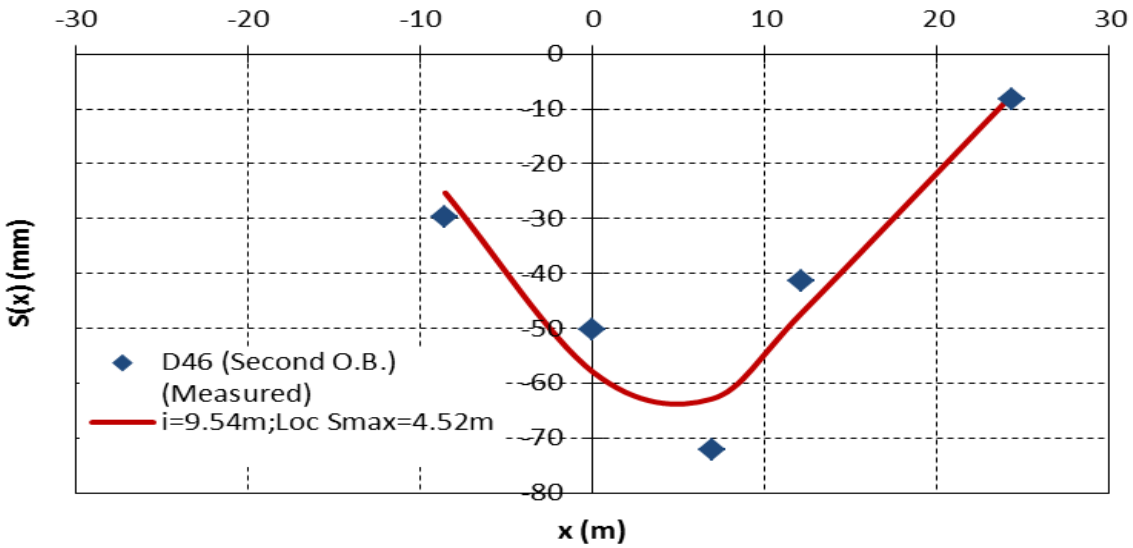

Figure 7.27 Gaussian probability curve for closely spaced bored tunnels (Instrumentation Array D46)

Table 7.13 Comparison of trough width parameter i above single tunnel as recommended by various researchers (Instrumentation Array D46)

Researchers	i (m)
Peck (1969)	7.38 – 9.12
O'Reilly and New (1982)	8.94
Mair and Taylor (1997)	9.12
This study	5.60

7.4 Summary

From the comparison made between the measured transverse surface settlement and the computed Gaussian probability curve, the following conclusions can be drawn:

1. For bored tunnelling through uniform grade of Jurong Formation, the estimated trough width parameter i for Instrumentation Array D35 fall within the range recommended by Peck (1969). The location of the maximum surface settlement Loc S_{max} shows negligible offset from the tunnel axis.

2. For bored tunnelling through mixed grades of Jurong Formation, larger volume loss observed for Instrumentation Array D37 (as mentioned in Section 6.6.6) as compared to Instrumentation Array D33 (as mentioned in Section 6.6.7) due to EPBM performance could have led to a wide variation of trough width parameter i being estimated as compared to those recommended by various researchers. In addition, the large discrepancy between the shape of the measured transverse surface settlement and the Gaussian probability curve could possibly be due to measurement error.
3. For bored tunnelling through mixed ground of Jurong Formation and Kallang Formation, the estimated trough width parameter i are generally found to be approximately 6 m for Instrumentation Arrays E14, D47 and D46. This value is below the range recommended by various researchers.
4. The trough width parameter i determined for closely spaced bored tunnels are generally greater than those for single bored tunnel. The location of maximum surface settlement Loc S_{max} is also found to be offset from the tunnel axis.
5. The Excel spreadsheet built-in optimisation routine Solver can be adequately adopted to estimate the trough width parameter i and location of maximum surface settlement Loc S_{max} for both single bored tunnel and closely spaced bored tunnels provided good quality field measurements are available.
6. If the other points of the measured transverse surface settlement for single bored tunnel are significantly deviate from the Gaussian probability curve despite the location of maximum surface settlement is above the tunnel axis, the Excel spreadsheet built-in optimisation routine Solver will compute the trough width parameter i and location of maximum surface settlement Loc S_{max} based on generating the best fit Gaussian probability curve among the deviated measurements. This may result in computing a significantly larger or smaller trough width parameter i and location of maximum surface settlement Loc S_{max}.
7. For poor quality field measurements, it is necessary to either manually or use some numerical techniques to establish the initial shape of transverse surface settlement prior to using the Excel spreadsheet built-in optimisation routine Solver for subsequent determination of trough width parameter i and location of

maximum surface settlement Loc S_{max} in order to improve accuracy of estimation.

8. The Excel spreadsheet built-in optimisation routine Solver could be used to estimate the trough width parameters i and location of maximum surface settlement Loc S_{max} for closely spaced bored tunnels where the latter becomes one of the important parameters to be determined due to the shifting of the location of maximum surface settlement Loc S_{max} from the tunnel axis as a result of soil disturbance between the two adjacent bored tunnels.

CHAPTER 8 EMPIRICAL EQUATIONS FOR PREDICTING SETTLEMENT PARAMETERS FOR CLOSELY SPACED BORED TUNNELS

8.1 Introduction

The development of the Excel spreadsheet built-in optimisation routine Solver to estimate the trough width parameter i and location of maximum surface settlement Loc S_{max} in Chapter 7 requires good quality field measurements to obtain reliable results. Furthermore, this method can only be used as a tool for back analysis. In this chapter, numerical parametric study for closely spaced bored tunnels for a wide range of tunnel geometric parameters as well as shear strength and deformation parameters of soil was first carried out. Subsequently, based on the computed settlement profiles, the Excel spreadsheet was used to determine the trough width parameter i and location of maximum surface settlement Loc S_{max}. Simplified empirical equations were then developed for estimating trough width parameter i and location of maximum surface settlement Loc S_{max} for practical usage.

8.2 Range of Application

The numerical parametric study for closely spaced bored tunnels involved two different ground types: (i) Jurong Formation; and (ii) mixed ground of Jurong Formation and Marine Clay.

Despite the presence of mixed grades of Jurong Formation, the analysis in Chapter 6 adopted only a single homogeneous layer of Jurong Formation of not less than 12 m in thickness to represent the corresponding stratum. This simplification was shown to give reasonable estimates of the transverse surface settlements for bored tunnelling through mixed grades of Jurong Formation and is therefore also assumed in this parametric study. Examples for the finite element mesh used for the cases involving closely spaced bored tunnels constructed through Jurong Formation are shown in Figures 8.1 and 8.2, for depth of burial of bored tunnels (diameter D of 6

m) of 2D and 6D respectively. Various depth of burial of closely spaced bored tunnels varying from 2D, 3D, 4D, 5D to a maximum of 6D for each tunnel diameter of 4 m, 6 m, 8 m, 10 m and 12 m were considered. In addition, pillar width was also varied at 1/6D, 1/2D, 1D and 2D for each case of tunnel diameter and tunnel depth. For each stratum, both the shear strength and deformation properties of soil were determined as discussed in Chapter 6, taking into account of variation of undrained shear strength and deformation modulus with depth. Similar assumptions were used for cases involving mixed ground of Jurong Formation and Marine Clay. Examples of the finite element mesh used for the cases involving mixed ground of Jurong Formation and Marine Clay are shown in Figures 8.3 and 8.4. It should be pointed out that the undrained shear strength of Marine Clay was determined at similar 12 m depth intervals for up to a maximum of 40 m depth, depending on the depth of burial of the closely spaced bored tunnels. For example, bored tunnels with diameter of 4 m, 6 m, 8 m, 10 m and 12 m have maximum Marine Clay thickness of up to 24 m, 36 m, 40 m, 40 m and 36 m above the respective tunnel level. The undrained modulus of Marine Clay was defined using E_u as $0.2c_u$ MPa, where the c_u value was obtained from Figure 6.5. Similar tunnel lining parameters adopted in Chapter 6 were used in this study. In short, numerical simulations for closely spaced bored tunnels constructed through Jurong Formation and mixed ground of Jurong Formation and Marine Clay were performed as closely as possible to the real ground conditions with varying shear strength and deformation properties of soil with thickness in multiples of 12 m. In all the analyses, the HS model was used for the Jurong Formation and the MC model for the Marine Clay. The properties considered in the parametric study are listed in Table 8.1.

Table 8.1 Summary of properties for parametric study

Parameter	**Symbol**	**Value**	**Unit**
Tunnel diameter	D	4, 6, 8, 10 and 12	m
Dimensionless depth of burial	H/D	2, 3, 4, 5 and 6	-
Dimensionless pillar width	W/D	1/6, 1/2, 1 and 2	-
Strata thickness for Jurong Formation (interval)	H_{JF}	12	m
Secant Young's modulus for Jurong Formation (12 m interval)	E_{50}	$0.7E_u$ where $E_u=2.8N$ and $N=1.5z$	MPa
Undrained shear strength for Jurong Formation (12 m interval)	c_u	$5N$ and $N=1.5z$	kPa
Strata thickness for Marine Clay (interval)	H_{MC}	12	m
Secant Young's modulus for Marine Clay (12 m interval)	E_{50}	$0.7E_u$ where $E_u=0.2c_u$ (see Figure 6.7 and Table 4.5)	MPa
Undrained shear strength for Marine Clay (12 m interval)	c_u	(see Figure 6.5)	kPa

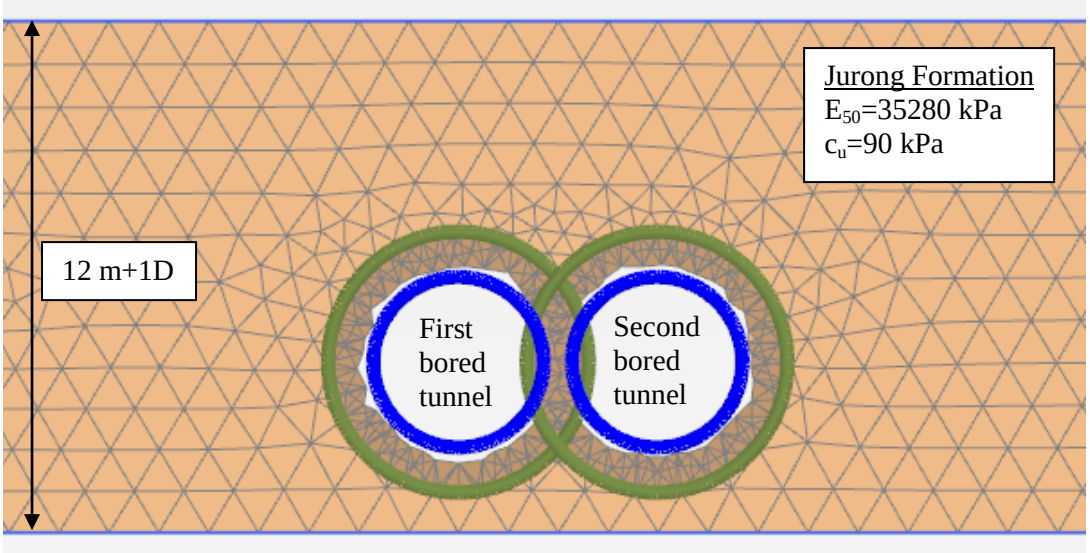

Figure 8.1 Partial finite element mesh for D=6 m bored tunnels at minimum depth of burial of 2D (Jurong Formation)

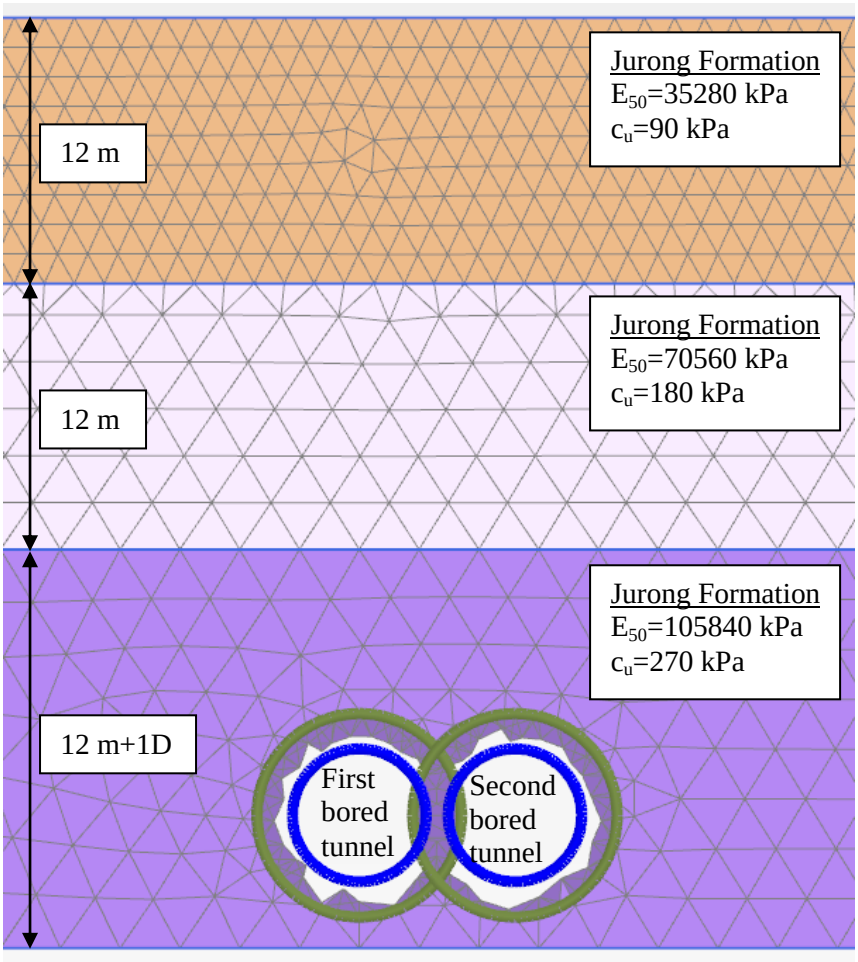

Figure 8.2 Partial finite element mesh for D=6 m bored tunnels at maximum depth of burial of 6D (Jurong Formation)

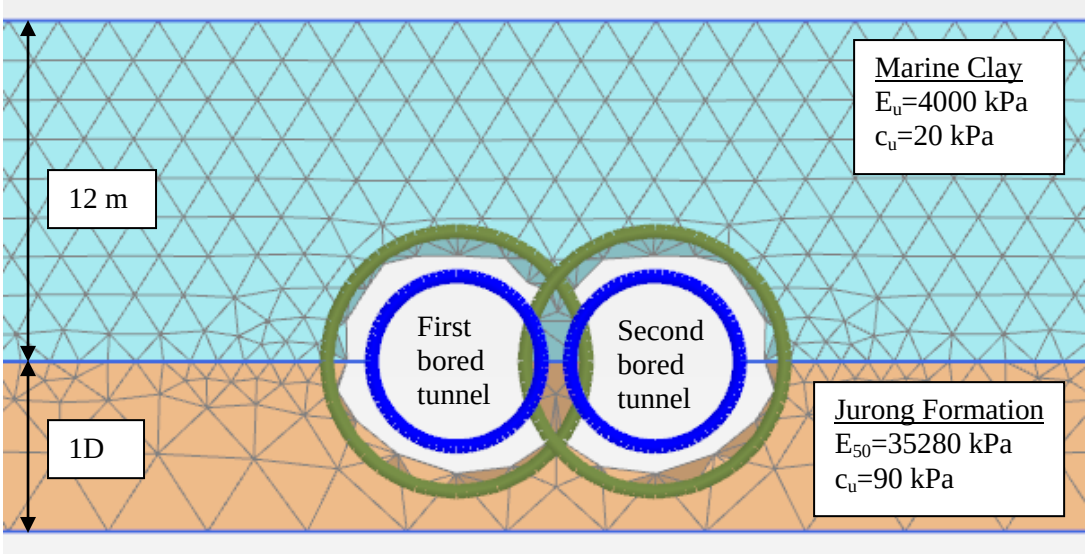

Figure 8.3 Partial finite element mesh for D=6 m bored tunnels at minimum depth of burial of 2D (mixed ground of Jurong Formation and Marine Clay)

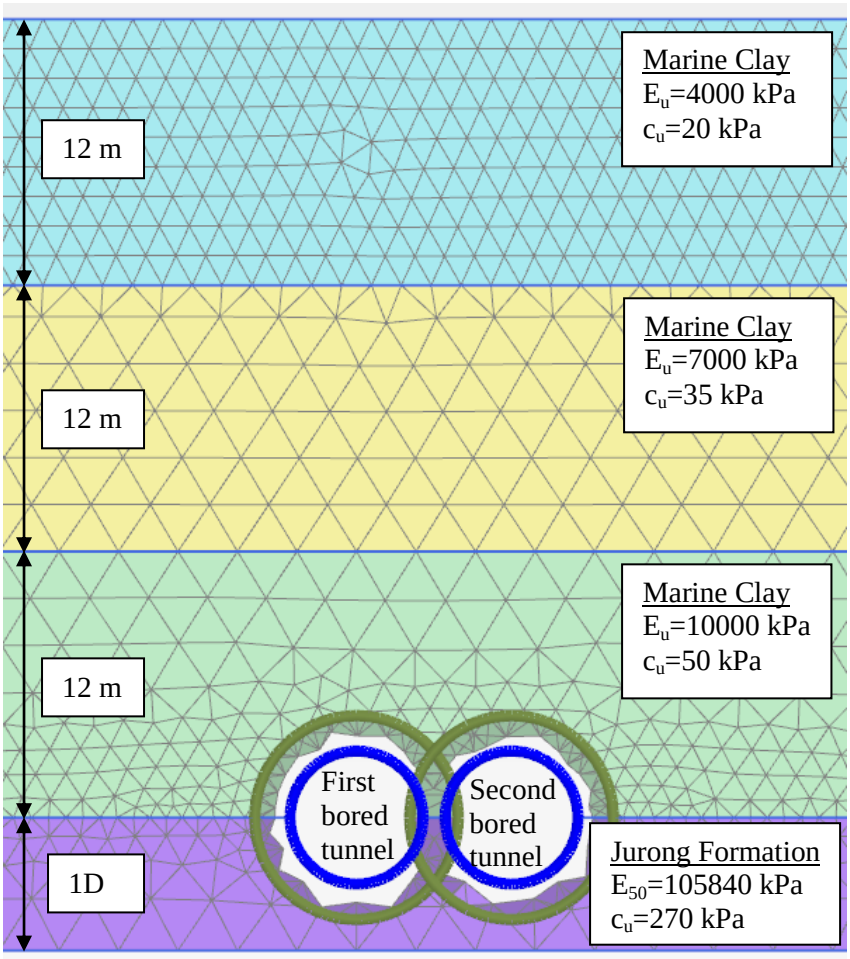

Figure 8.4 Partial finite element mesh for D=6 m bored tunnels at maximum depth of burial of 6D (mixed ground of Jurong Formation and Marine Clay)

8.3 Influence of Tunnel Geometric Parameters

The effects of tunnel geometric parameters including tunnel diameter, pillar width and tunnel depth were investigated using volume loss of 0.5 per cent and 5 per cent respectively. These values represent the approximate lower bound and upper bound volume loss encountered in the back analysis in Chapter 6. The results are summarised in Appendix B.

For brevity, only the results for closely spaced bored tunnels of 6 m diameter constructed through Jurong Formation (Figures 8.5 to 8.9) and mixed ground of Jurong Formation and Marine Clay (Figures 8.10 and 8.11) are compared and discussed as follows:

1. Given the same tunnel diameter D and tunnel depth H, maximum ground surface settlement increases with decreasing pillar width W as shown in Figure 8.5. At the largest pillar width of 2D, a relatively flatter maximum surface settlement can be observed for volume loss of 0.5 per cent whereas the maximum surface settlement for volume loss of 5 per cent appears as wavy. These observed surface settlement profiles are similar to the surface settlement profiles obtained by Divall (2013) for twin-tunnel vertical surface settlement from 3D spacing (centre-to-centre spacing of the tunnels) tests as shown in Figure 3.8. All cases (see Figure 8.5) show maximum surface settlements drawn towards the second bored tunnel.

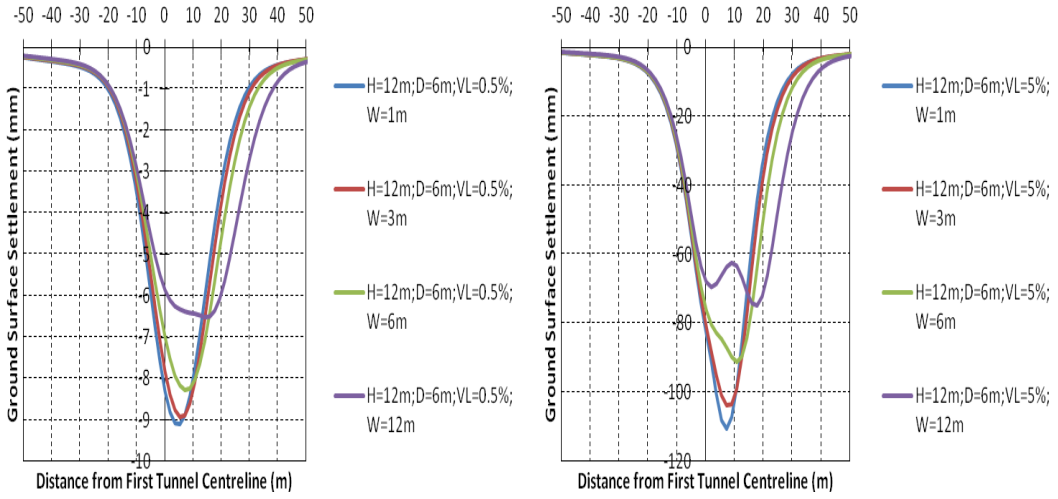

(a) (b)

Figure 8.5 Variation of ground surface settlement for closely spaced bored tunnels (D=6 m; H=12 m) with pillar width, for volume loss of (a) 0.5%; and (b) 5% (Jurong Formation)

2. Comparison between closely spaced bored tunnels for tunnel depth of 12 m (see Figure 8.5) and 18 m (see Figure 8.6) indicates a gradually smoother shape of the maximum surface settlement for the deeper bored tunnels.

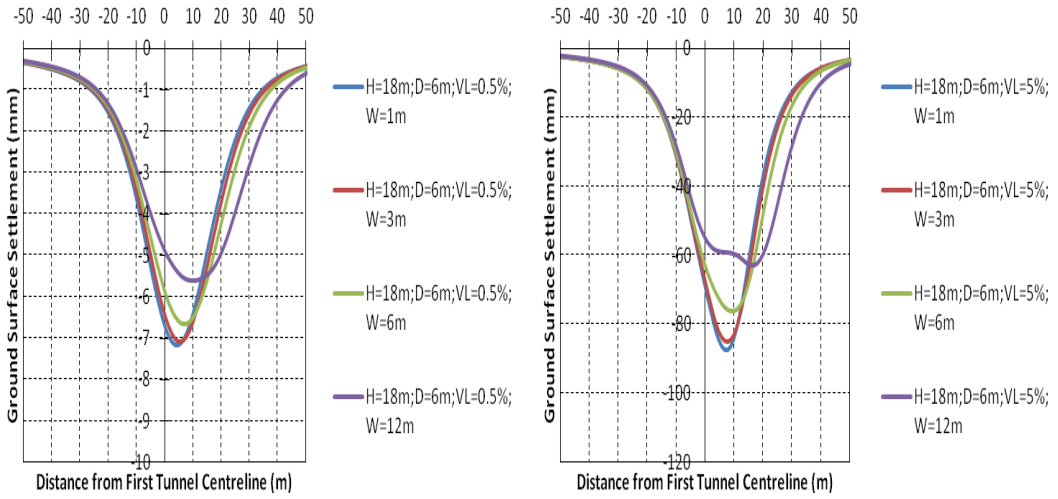

(a) (b)

Figure 8.6 Variation of ground surface settlement for closely spaced bored tunnels (D=6 m; H=18 m) with pillar width, for volume loss of (a) 0.5%; and (b) 5% (Jurong Formation)

3. Both the flatter and wavy shape of maximum surface settlements were not observed for H≥4D, as shown in Figures 8.7, 8.8 and 8.9. It is important to highlight that similar trends were observed for closely spaced 12 m diameter bored tunnels. These plots are presented in Appendix B, for brevity.

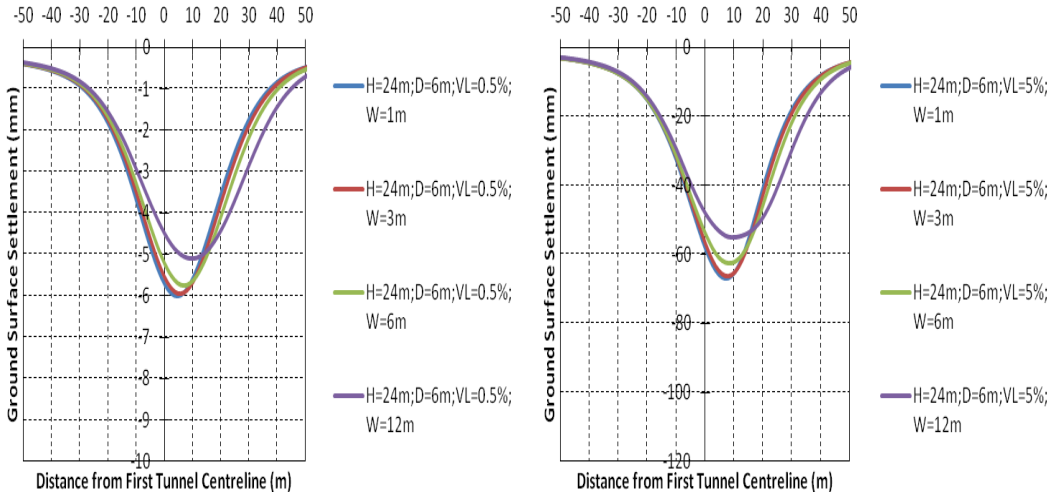

(a) (b)

Figure 8.7 Variation of ground surface settlement for closely spaced bored tunnels (D=6 m; H=24 m) with pillar width, for volume loss of (a) 0.5%; and (b) 5% (Jurong Formation)

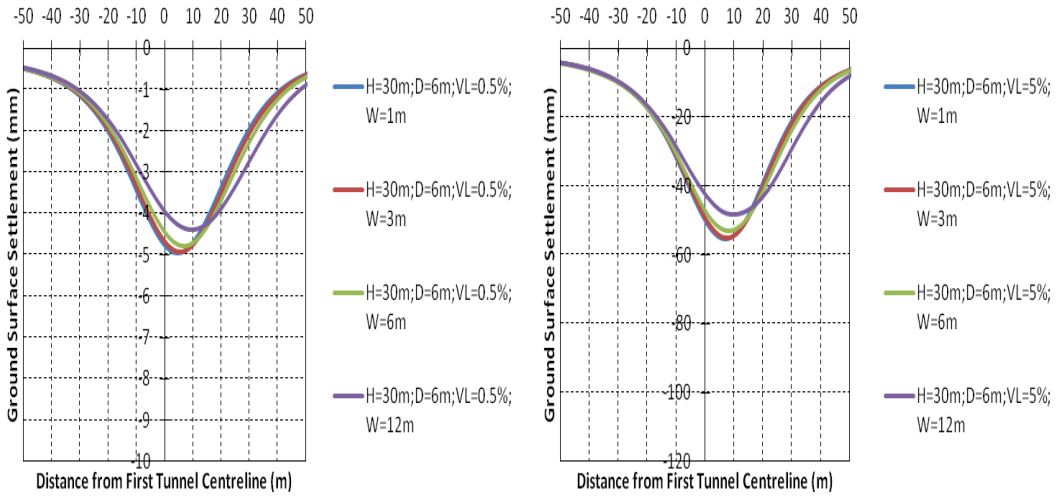

(a) (b)

Figure 8.8 Variation of ground surface settlement for closely spaced bored tunnels (D=6 m; H=30 m) with pillar width, for volume loss of (a) 0.5%; and (b) 5% (Jurong Formation)

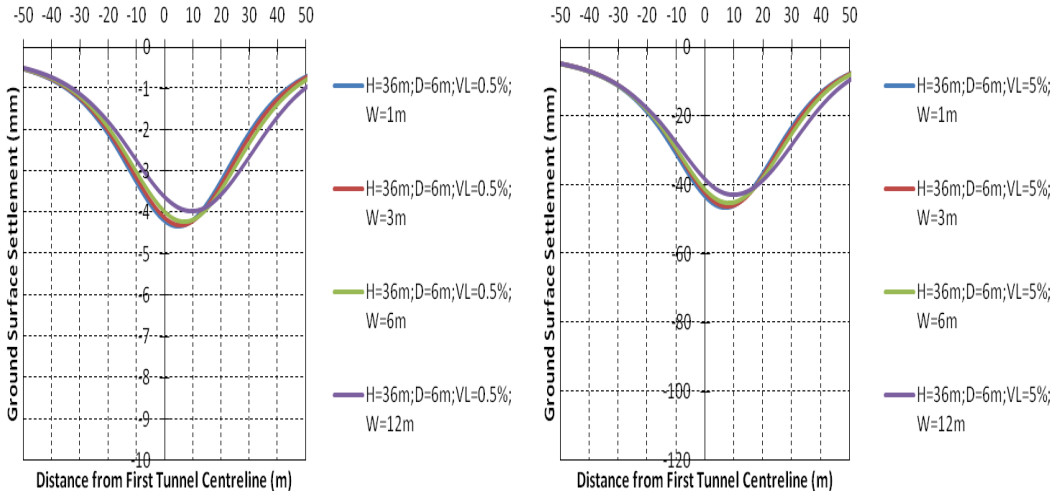

(a) (b)

Figure 8.9 Variation of ground surface settlement for closely spaced bored tunnels (D=6 m; H=36 m) with pillar width, for volume loss of (a) 0.5%; and (b) 5% (Jurong Formation)

4. Figures 8.5 to 8.9 indicate the magnitude of maximum surface settlement decreases with increasing tunnel depth, for cases involving volume loss of 0.5 per cent and 5 per cent. It should also be pointed out that the trough width parameter i increasing with tunnel depth.
5. Regarding the shape and extent of transverse surface settlement trough, there was significant shifting of the transverse surface settlement trough towards the second bored tunnel for the case involving pillar width of 2D. Comparison of the curves indicates that larger ground surface settlement was observed for pillar width of 2D as compared to pillar width of 1/6D, at any identical distance for the right arm of transverse surface settlement trough, for both volume loss of 0.5 per cent and 5 per cent. However, no significant difference can be seen for pillar width of 1/2D, 1D and 1/6D. In contrast, smaller ground surface settlement was observed for pillar width of 2D for the left arm of transverse surface settlement trough in particular, around the location of the maximum surface settlement as compared to other pillar widths.

6. As shown in Figures 8.7, 8.8 and 8.9, increasing tunnel depth has led to gradual convergence of the ground surface settlement curves, regardless of difference in pillar width.
7. For closely spaced bored tunnels constructed through mixed ground of Jurong Formation and Marine Clay, the wavy shape of the maximum surface settlement occurred at volume loss of 0.5 per cent (see Figure 8.10(a)), but was not observed for closely spaced bored tunnels constructed through Jurong Formation (see Figure 8.5(a)) at the same volume loss condition. For volume loss of 5 per cent, the wavy shape of the maximum surface settlement for the former (see Figure 8.10(b)) was also observed to be more prominent as compared to the latter (see Figure 8.5(b)).

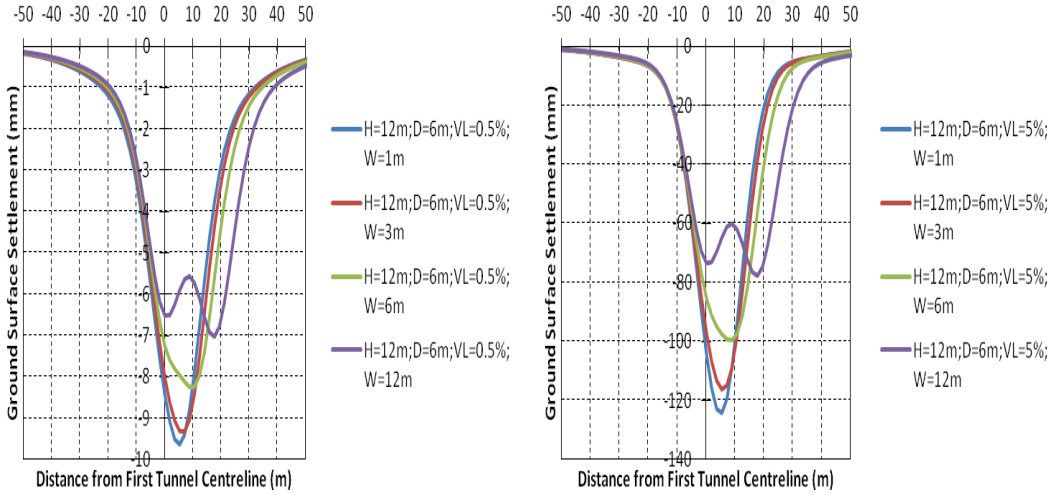

(a) (b)

Figure 8.10 Variation of ground surface settlement for closely spaced bored tunnels (D=6 m; H=12 m) with pillar width, for volume loss of (a) 0.5%; and (b) 5% (mixed ground of Jurong Formation and Marine Clay)

8. For the mixed ground, as with the cases involving closely spaced bored tunnel constructed through Jurong Formation, the wavy shape of the maximum surface settlement subsided at tunnel depth of 3D, as shown in Figure 8.11 and this shape was not observed for H≥4D.

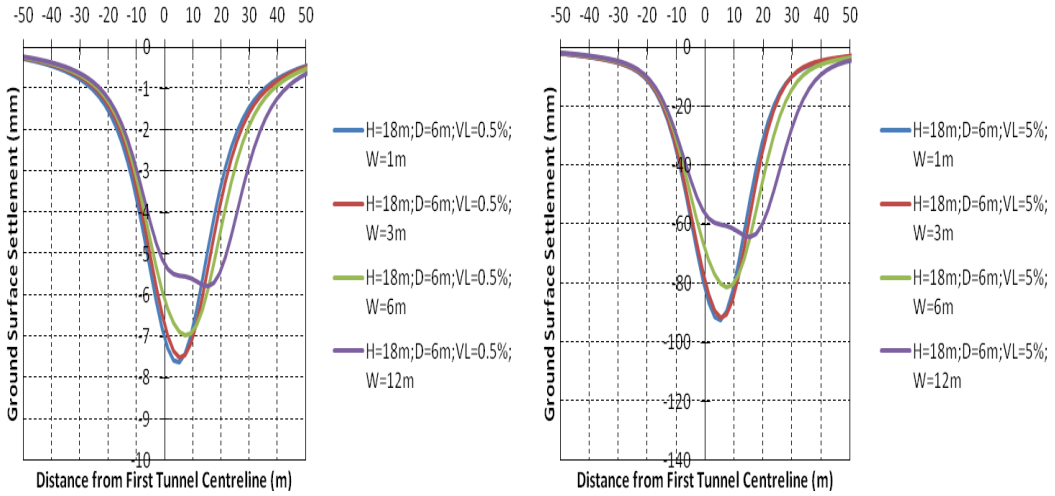

(a) (b)

Figure 8.11 Variation of ground surface settlement for closely spaced bored tunnels (D=6 m; H=18 m) with pillar width, for volume loss of (a) 0.5%; and (b) 5% (mixed ground of Jurong Formation and Marine Clay)

9. Each volume loss of 0.5 per cent and 5 per cent induced larger magnitude of the maximum surface settlement for closely spaced bored tunnels constructed through mixed ground of Jurong Formation and Marine Clay as compared to closely spaced bored tunnel constructed through Jurong Formation. Apart from the magnitude of the maximum surface settlement, similar trends were generally observed for the two different ground types.
10. The results of analyses involving tunnel depth of 4 m, 8 m, 10 m and 12 m show similar trends and therefore, for brevity, are presented in Appendix B.

8.4 Regression Models

The results from parametric study described in the preceding section and summarised in Appendix B provide a platform for developing a series of design charts for determining the trough width parameter i and location of maximum surface settlement Loc S_{max}. This is achieved by plotting the trough width parameter i with dimensionless pillar width W/D and location of maximum surface settlement Loc S_{max} with dimensionless pillar width respectively, for a defined range of tunnel

diameter (D) and dimensionless depth of burial (H/D), for volume loss of 0.5 per cent and 5 per cent. Subsequently, using regression analysis (see Figure B.48), Equations 8.1 to 8.4 were developed for cases involving residual soil ground type and Equations 8.5 to 8.8 for cases involving mixed soils (residual soil with overlying Marine Clay) ground type.

The Equations 8.1 to 8.4 enable determination of trough width parameter i and location of maximum surface settlement Loc S_{max} as follows:

For trough width parameter i (residual soil with volume loss of 0.5 per cent):

$$
\begin{aligned}
i_{R0.5} = {} & [(0.0023(\frac{H}{D})^3 - 0.0194(\frac{H}{D})^2 - 0.017(\frac{H}{D}) + 0.6277)(D) \\
& + (-0.0044(\frac{H}{D})^4 + 0.0401(\frac{H}{D})^3 - 0.0499(\frac{H}{D})^2 - 0.2807(\frac{H}{D}) - 0.1244)](\frac{W}{D}) \\
& + [0.0055(\frac{H}{D})^3 - 0.0318(\frac{H}{D})^2 + 0.6344(\frac{H}{D}) + 0.6311](D) \\
& + [-0.0581(\frac{H}{D})^3 + 0.5087(\frac{H}{D})^2 - 1.8614(\frac{H}{D}) + 1.6195]
\end{aligned}
\tag{8.1}
$$

where the subscript R denotes residual soil and 0.5 denotes the volume loss.

Figure 8.12 shows the comparison of the trough width parameter i computed using $i_{R0.5}$ with the value obtained from the finite element analysis i_{FEM}, with a coefficient of determination R^2=0.9988.

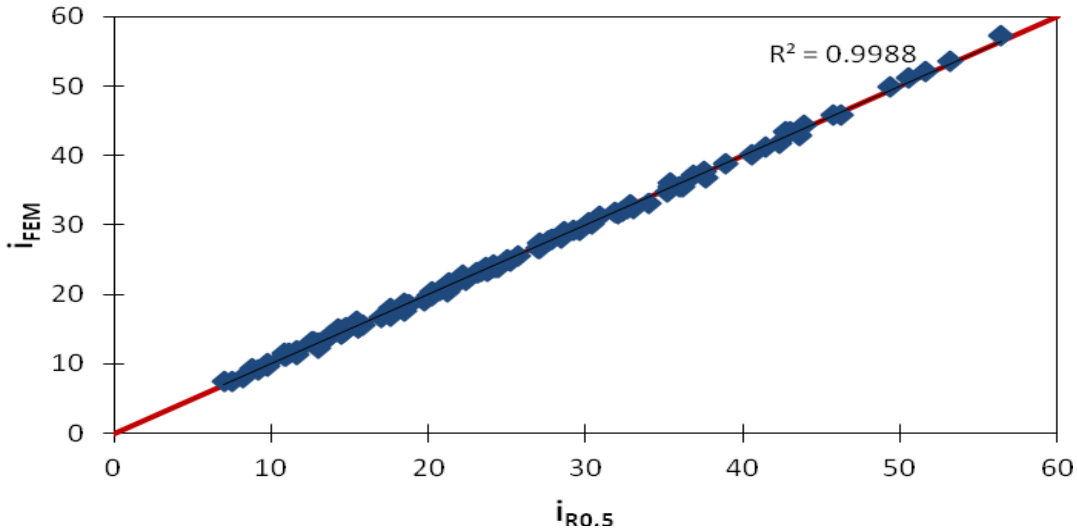

Figure 8.12 Comparison of $i_{R0.5}$ with i_{FEM}

For trough width parameter i (residual soil with volume loss of 5 per cent):

$$i_{R5.0} = [(-0.0016(\frac{H}{D})^4 + 0.0232(\frac{H}{D})^3 - 0.1244(\frac{H}{D})^2 + 0.2493(\frac{H}{D}) + 0.4525)(D)$$
$$+ 0.0129(\frac{H}{D})^4 - 0.2054(\frac{H}{D})^3 + 1.2105(\frac{H}{D})^2 - 3.2504(\frac{H}{D}) + 2.2997](\frac{W}{D})$$
$$+ [0.0073(\frac{H}{D})^4 - 0.1133(\frac{H}{D})^3 + 0.6791(\frac{H}{D})^2 - 1.2742(\frac{H}{D}) + 1.9409](D)$$
$$- 0.0456(\frac{H}{D})^4 + 0.7182(\frac{H}{D})^3 - 4.1844(\frac{H}{D})^2 + 10.351(\frac{H}{D}) - 8.2795 \quad (8.2)$$

where the subscript R denotes residual soil and 5.0 denotes the volume loss.

Figure 8.13 shows the comparison of the trough width parameter i computed using $i_{R5.0}$ with the value obtained from the finite element analysis i_{FEM}, with a coefficient of determination R^2=0.999.

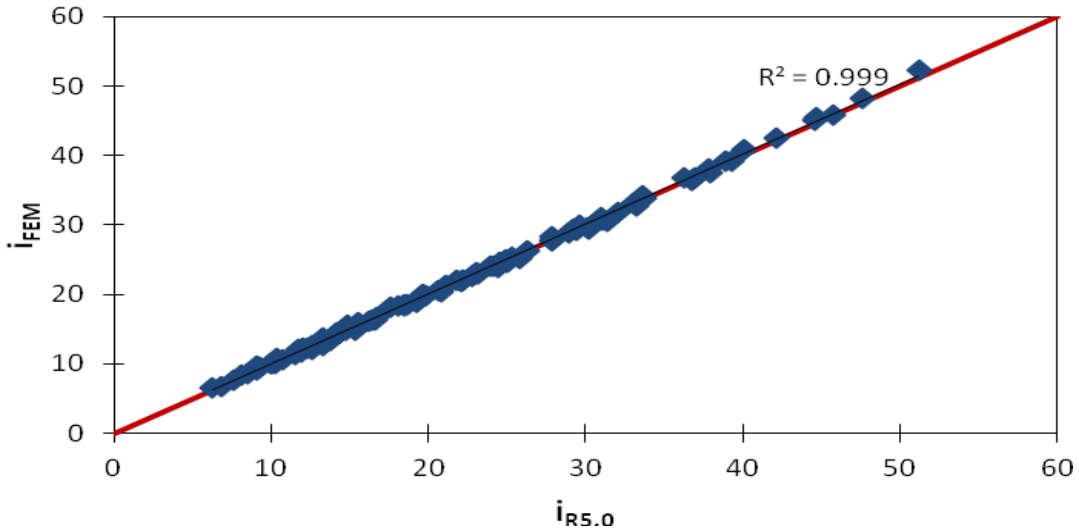

Figure 8.13 Comparison of $i_{R5.0}$ with i_{FEM}

For location of maximum surface settlement Loc S_{max} (residual soil with volume loss of 0.5 per cent):

$$Loc \quad S_{\max R0.5} = [(-0.0019(\frac{H}{D})^4 + 0.0316(\frac{H}{D})^3 - 0.1977(\frac{H}{D})^2 + 0.4759(\frac{H}{D}) + 0.1364)(D)$$
$$+ 0.0139(\frac{H}{D})^4 - 0.2413(\frac{H}{D})^3 + 1.5042(\frac{H}{D})^2 - 3.7199(\frac{H}{D}) + 2.9371](\frac{W}{D})$$
$$+ [0.0031(\frac{H}{D})^4 - 0.0509(\frac{H}{D})^3 + 0.3136(\frac{H}{D})^2 - 0.8122(\frac{H}{D}) + 1.4018](D)$$
$$- 0.0126(\frac{H}{D})^4 + 0.2504(\frac{H}{D})^3 - 1.7692(\frac{H}{D})^2 + 5.0308(\frac{H}{D}) - 4.8674 \qquad (8.3)$$

where subscript R denotes residual soil and 0.5 denotes the volume loss.

Figure 8.14 shows the comparison of the location of maximum surface settlement Loc S_{max} computed using Loc $S_{max\ R0.5}$ with the value obtained from the finite element analysis Loc $S_{max\ FEM}$, with a coefficient of determination R^2= 0.997.

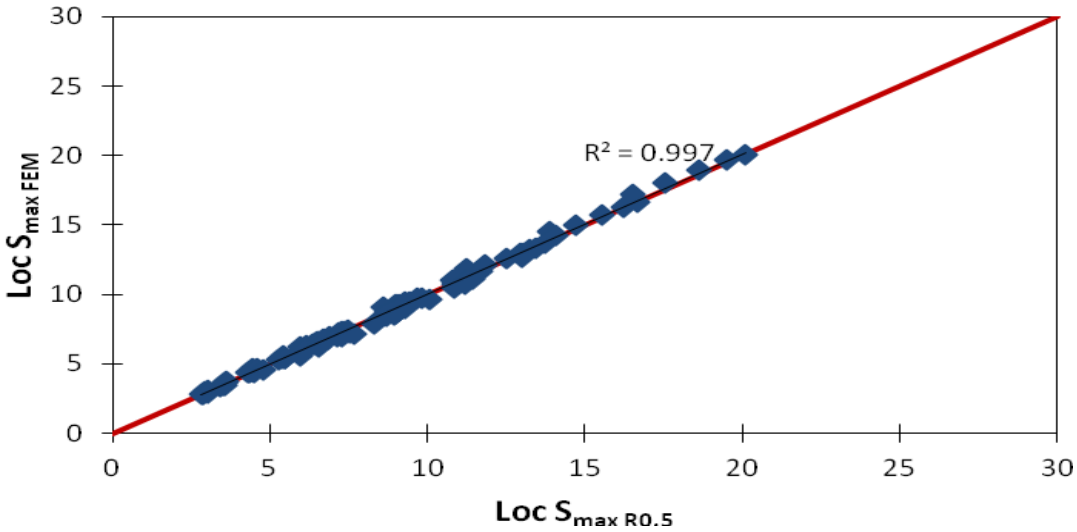

Figure 8.14 Comparison of Loc $S_{max\ R0.5}$ with Loc $S_{max\ FEM}$

For location of maximum surface settlement Loc S_{max} (residual soil with volume loss of 5 per cent):

$$Loc \quad S_{\max R5.0} = [(0.0065(\frac{H}{D})^3 - 0.0923(\frac{H}{D})^2 + 0.2939(\frac{H}{D}) + 0.3239)(D)$$
$$- 0.0054(\frac{H}{D})^4 + 0.0491(\frac{H}{D})^3 + 0.0304(\frac{H}{D})^2 - 0.6757(\frac{H}{D}) - 0.0815](\frac{W}{D})$$
$$+ [-0.01(\frac{H}{D})^3 + 0.1562(\frac{H}{D})^2 - 0.6265(\frac{H}{D}) + 1.295](D)$$
$$+ 0.0185(\frac{H}{D})^4 - 0.1916(\frac{H}{D})^3 + 0.2283(\frac{H}{D})^2 + 1.9693(\frac{H}{D}) - 2.3402 \qquad (8.4)$$

where subscript R denotes residual soil and 5.0 denotes volume loss.

Figure 8.15 shows the comparison of the location of maximum surface settlement Loc S_{max} computed using Loc $S_{max\ R5.0}$ with the value obtain from the finite element analysis Loc $S_{max\ FEM}$, with a coefficient of determination R^2= 0.9941.

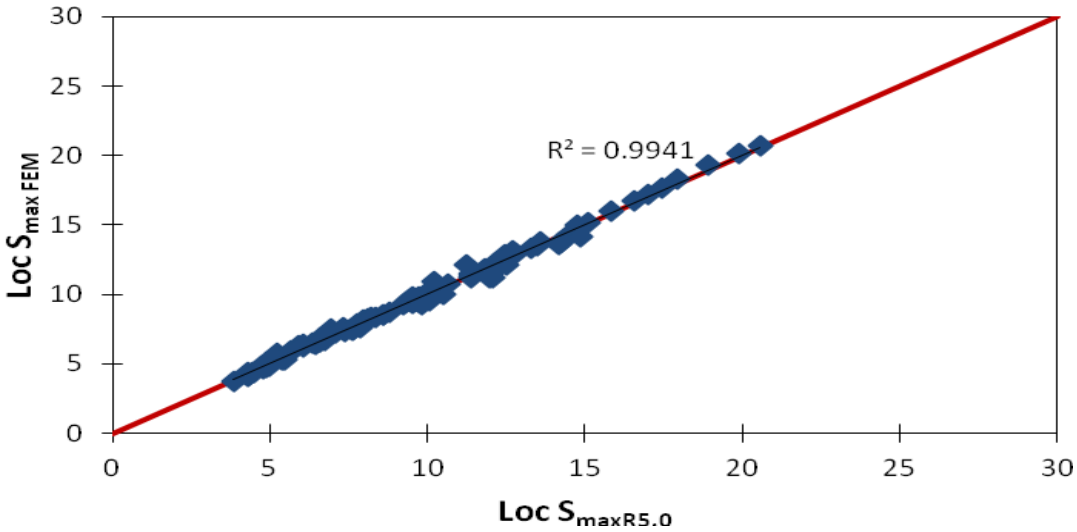

Figure 8.15 Comparison of Loc $S_{max\ R5.0}$ with Loc $S_{max\ FEM}$

Similarly for the mixed soils, for trough width parameter i (mixed soils with volume loss of 0.5 per cent):

$$i_{M0.5} = [(0.0023(\frac{H}{D})^4 - 0.0349(\frac{H}{D})^3 + 0.192(\frac{H}{D})^2 - 0.5043(\frac{H}{D}) + 1.0065)(D)$$
$$- 0.0177(\frac{H}{D})^4 + 0.2687(\frac{H}{D})^3 - 1.393(\frac{H}{D})^2 + 2.8435(\frac{H}{D}) - 2.3015](\frac{W}{D})$$
$$+ [-0.0169(\frac{H}{D})^4 + 0.2768(\frac{H}{D})^3 - 1.5918(\frac{H}{D})^2 + 4.2149(\frac{H}{D}) - 2.422](D)$$
$$+ 0.115(\frac{H}{D})^4 - 1.9082(\frac{H}{D})^3 + 11.143(\frac{H}{D})^2 - 26.761(\frac{H}{D}) + 22.676 \quad (8.5)$$

where subscript M denotes mixed soils and 0.5 denotes the volume loss.

Figure 8.16 shows the comparison of the trough width parameter i computed using $i_{M0.5}$ with the value obtained from the finite element analysis i_{FEM}, with a coefficient of determination R^2=0.9976.

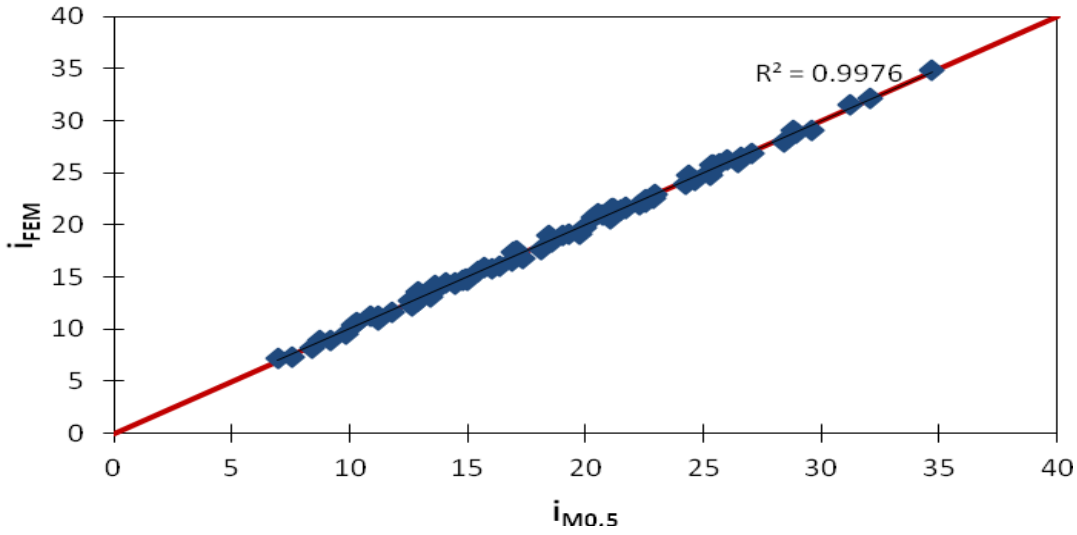

Figure 8.16 Comparison of $i_{M0.5}$ with i_{FEM}

For trough width parameter i (mixed soils with volume loss of 5 per cent):

$$i_{M5.0} = [(-0.0012(\frac{H}{D})^4 + 0.0215(\frac{H}{D})^3 - 0.1289(\frac{H}{D})^2 + 0.2212(\frac{H}{D}) + 0.5639)(D)$$
$$+ 0.0013(\frac{H}{D})^4 - 0.0579(\frac{H}{D})^3 + 0.5757(\frac{H}{D})^2 - 1.9733(\frac{H}{D}) + 1.6612](\frac{W}{D})$$
$$+ [-0.0101(\frac{H}{D})^4 + 0.1585(\frac{H}{D})^3 - 0.8588(\frac{H}{D})^2 + 2.3604(\frac{H}{D}) - 1.226](D)$$
$$+ 0.0968(\frac{H}{D})^4 - 1.5307(\frac{H}{D})^3 + 8.4824(\frac{H}{D})^2 - 19.455(\frac{H}{D}) + 15.901 \quad (8.6)$$

where subscript M denotes mixed soils and 5.0 denotes the volume loss.

Figure 8.17 shows the comparison of the trough width parameter i computed using $i_{M5.0}$ with the value obtained from the finite element analysis i_{FEM}, with a coefficient of determination R^2=0.9958.

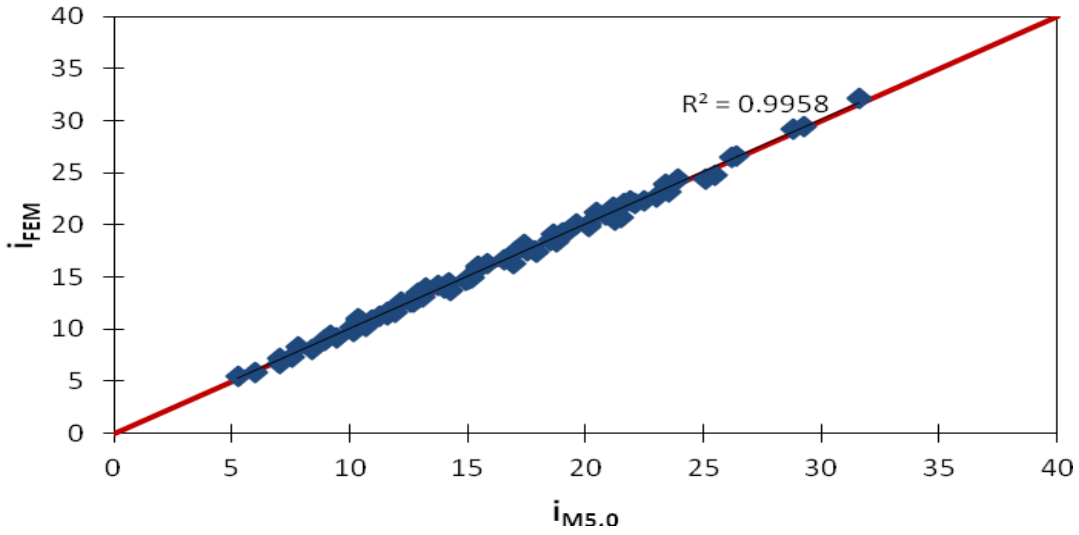

Figure 8.17 Comparison of $i_{M5.0}$ with i_{FEM}

For location of maximum surface settlement Loc S_{max} (mixed soils with volume loss of 0.5 per cent):

$$Loc \quad S_{\max M0.5} = [(-0.0038(\frac{H}{D})^4 + 0.0552(\frac{H}{D})^3 - 0.291(\frac{H}{D})^2 + 0.6924(\frac{H}{D}) - 0.0267)(D)$$
$$+ 0.0164(\frac{H}{D})^4 - 0.2442(\frac{H}{D})^3 + 1.3435(\frac{H}{D})^2 - 3.3496(\frac{H}{D}) + 2.5458](\frac{W}{D})$$
$$+ [0.0008(\frac{H}{D})^4 - 0.0028(\frac{H}{D})^3 - 0.021(\frac{H}{D})^2 + 0.0372(\frac{H}{D}) + 0.5142](D)$$
$$+ 0.008(\frac{H}{D})^4 - 0.1661(\frac{H}{D})^3 + 1.0499(\frac{H}{D})^2 - 2.1799(\frac{H}{D}) + 2.2241 \qquad (8.7)$$

where subscript M denotes mixed soils and 0.5 denotes the volume loss.

Figure 8.18 shows the comparison of the location of maximum surface settlement Loc S_{max} computes using Loc $S_{max\ M0.5}$ with the value obtained from the finite element analysis Loc $S_{max\ FEM}$, with a coefficient of determination R^2= 0.9961.

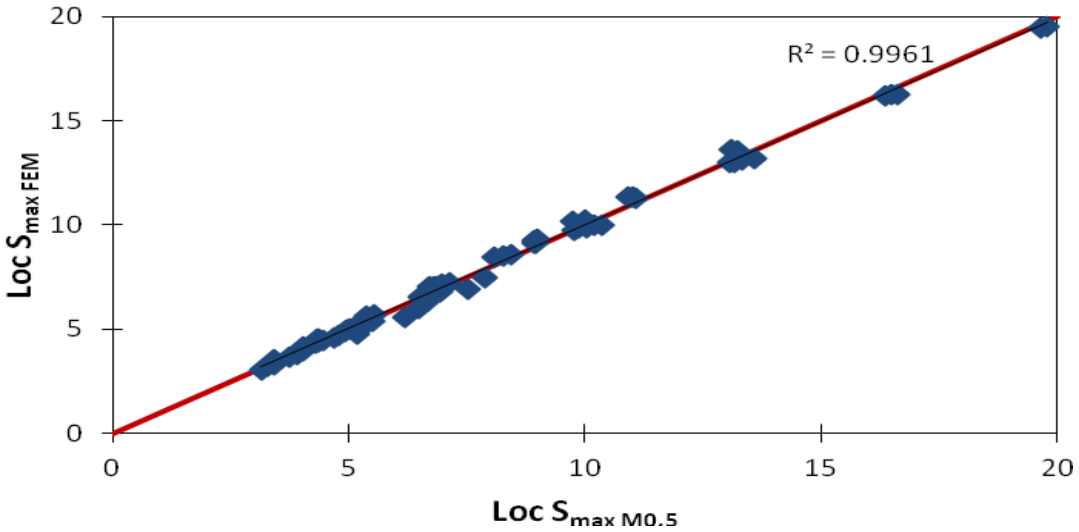

Figure 8.18 Comparison of Loc $S_{max\ M0.5}$ with Loc $S_{max\ FEM}$

For location of maximum surface settlement Loc S_{max} (mixed soils with volume loss of 5 per cent):

$$Loc \quad S_{\max M5.0} = [(-0.0048(\frac{H}{D})^4 + 0.0728(\frac{H}{D})^3 - 0.3987(\frac{H}{D})^2 + 0.9564(\frac{H}{D}) - 0.2436)(D)$$
$$+ 0.0127(\frac{H}{D})^4 - 0.2135(\frac{H}{D})^3 + 1.3242(\frac{H}{D})^2 - 3.543(\frac{H}{D}) + 2.7551](\frac{W}{D})$$
$$+ [-0.0004(\frac{H}{D})^4 + 0.0105(\frac{H}{D})^3 - 0.0564(\frac{H}{D})^2 + 0.0151(\frac{H}{D}) + 0.6059](D)$$
$$+ 0.0418(\frac{H}{D})^4 - 0.6305(\frac{H}{D})^3 + 3.2175(\frac{H}{D})^2 - 6.2605(\frac{H}{D}) + 4.64 \qquad (8.8)$$

where subscript M denotes mixed soils and 5.0 denotes the volume loss.

Figure 8.19 shows the comparison of the location of maximum surface settlement Loc S_{max} computes using Loc $S_{max\ M5.0}$ with the value obtained from the finite element analysis Loc $S_{max\ FEM}$, with a coefficient of determination R^2= 0.9973.

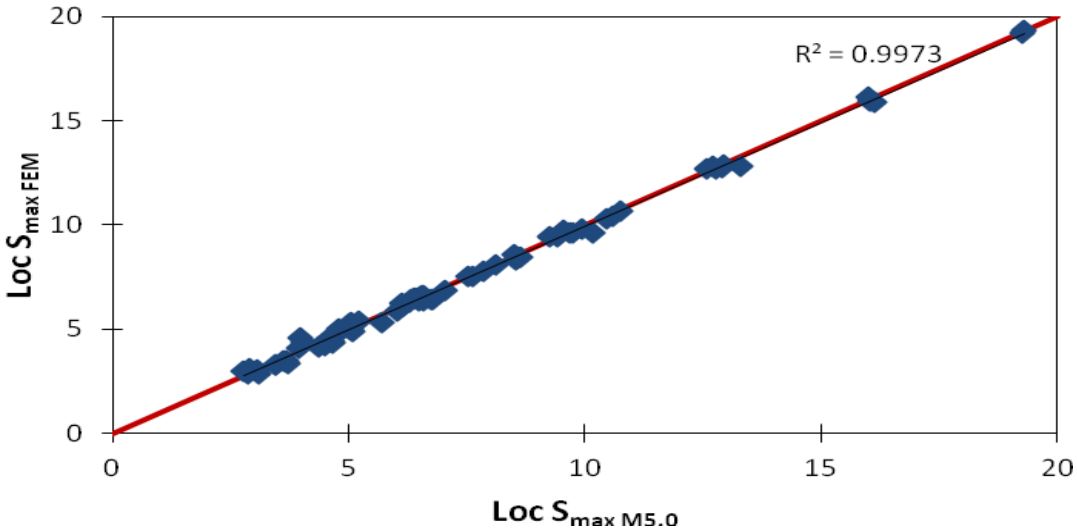

Figure 8.19 Comparison of Loc $S_{max\ M5.0}$ with Loc $S_{max\ FEM}$

The Equations 8.1 to 8.8 suggests that both the trough width parameter i and location of maximum surface settlement Loc S_{max} is dependent on tunnel diameter, dimensionless depth of burial and dimensionless pillar width and are applicable within their range of application as defined in Table 8.1.

8.5 Guidelines for Mass Rapid Transit (MRT) Tunnels

The construction of Mass Rapid Transit (MRT) tunnels usually involves bored tunnelling of approximately 6 m in diameter carried out at depth of about 18 m below the ground surface. As such, Figures 8.20 and 8.21 are prepared to facilitate the interpretation of trough width parameter i and location of maximum surface settlement Loc S_{max} associated with construction of closely spaced bored tunnels.

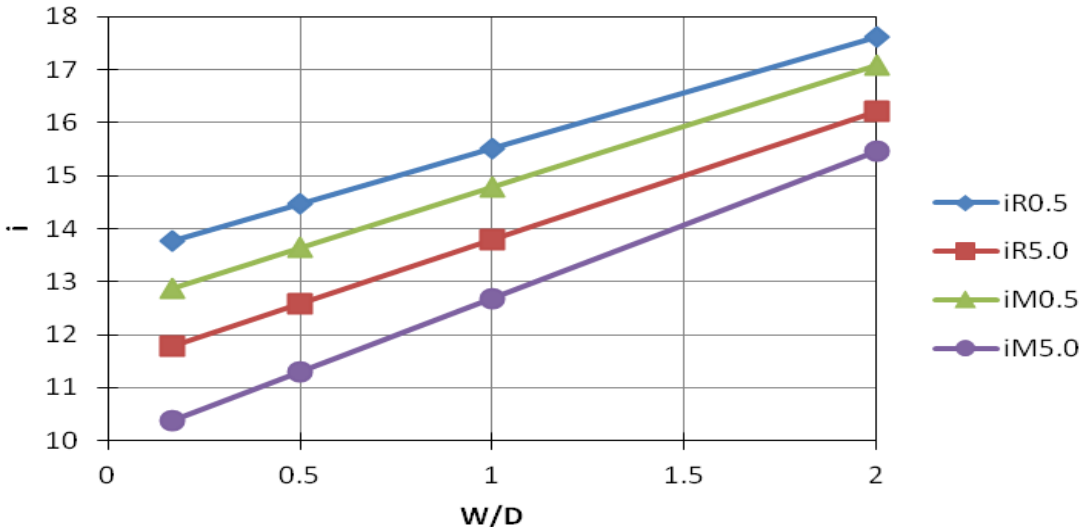

Figure 8.20 Variation of i with W/D (H/D=3 and D=6 m)

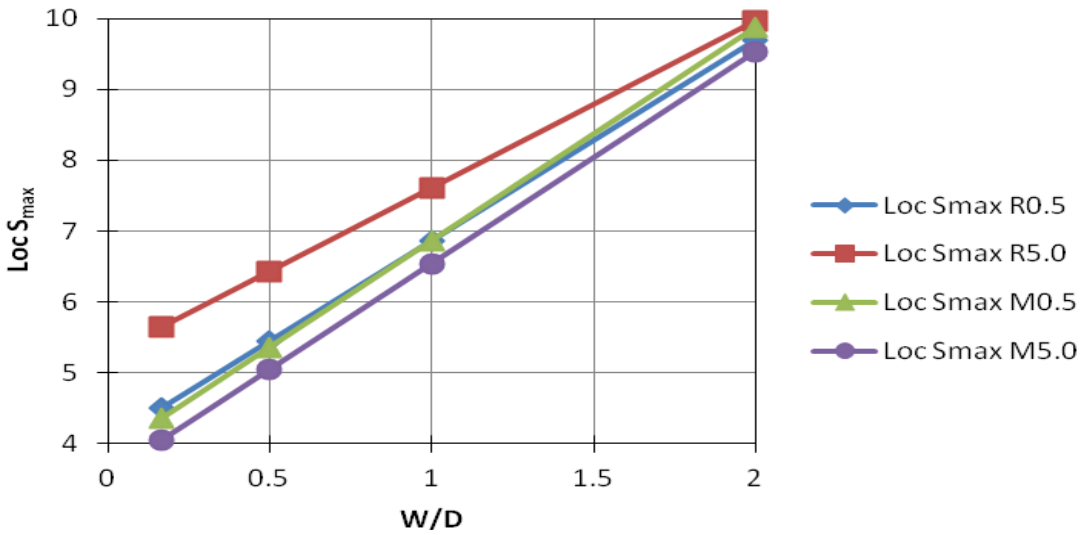

Figure 8.21 Variation of Loc S_{max} with W/D (H/D=3 and D=6 m)

8.6 Numerical Verification

The results obtained from Equations 8.1 to 8.8 are compared with the results of additional finite element analyses for cases involving residual soils and cases involving mixed soils, i.e. residual soils with overlying Marine Clay. These cases were not considered in the development of the equations in Section 8.4, and serve as additional validation of the empirical equations. Each of the analyses consists of

H/D varying from 2.5, 3.5 4.5 to 5.5 at W/D of 1.5, for volume loss of 0.5 per cent and 5 per cent. As indicated in Figures 8.22, 8.23, 8.24 and 8.25, the difference in the results computed using Equations 8.1 to 8.8 and the finite element results are minimal.

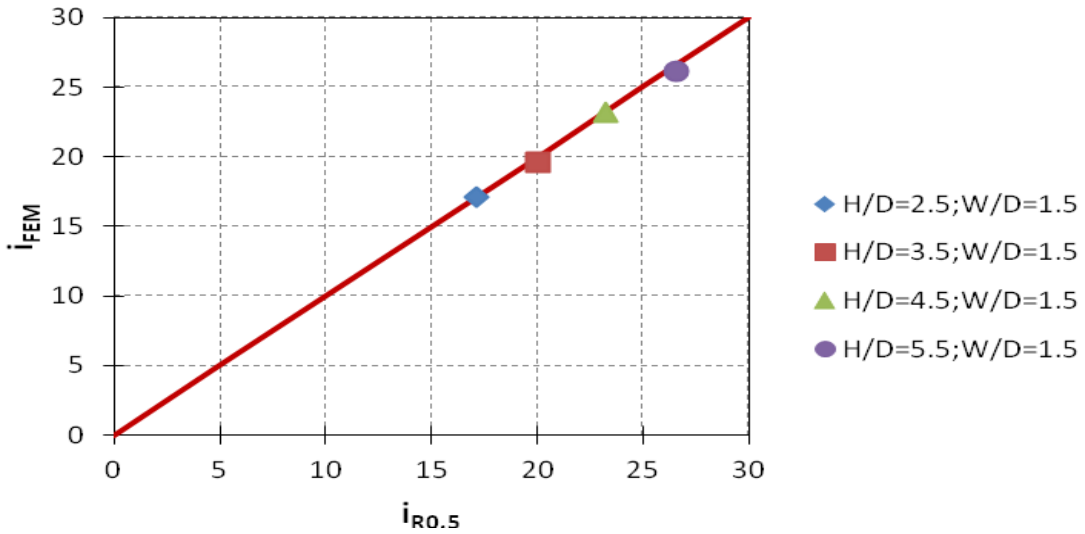

(a)

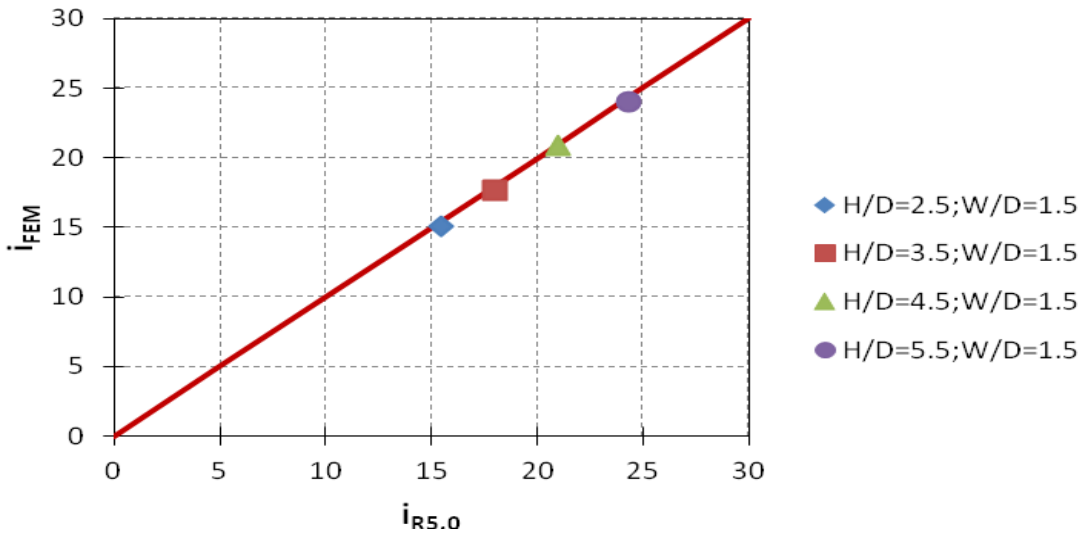

(b)

Figure 8.22 Comparison between i_R and i_{FEM} for residual soil for (a) VL=0.5%; and (b) VL=5%

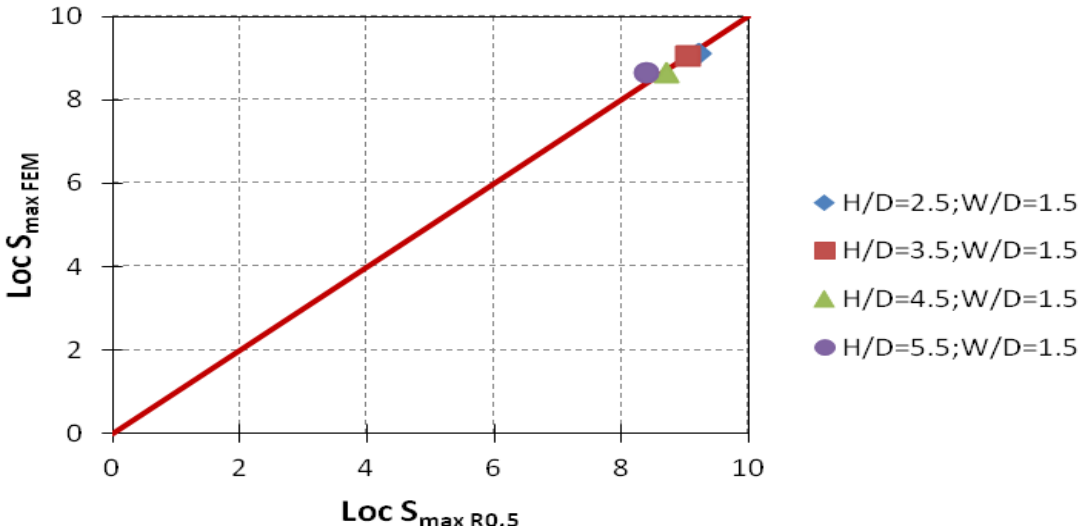

(a)

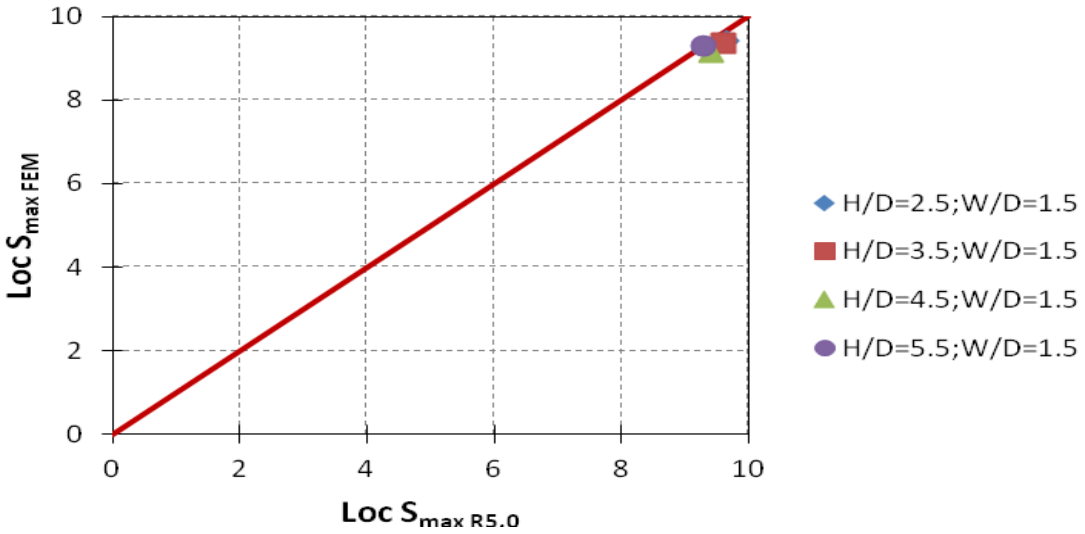

(b)

Figure 8.23 Comparison between Loc $S_{max\ R}$ and Loc $S_{max\ FEM}$ for residual soil for (a) VL=0.5%; and (b) VL=5%

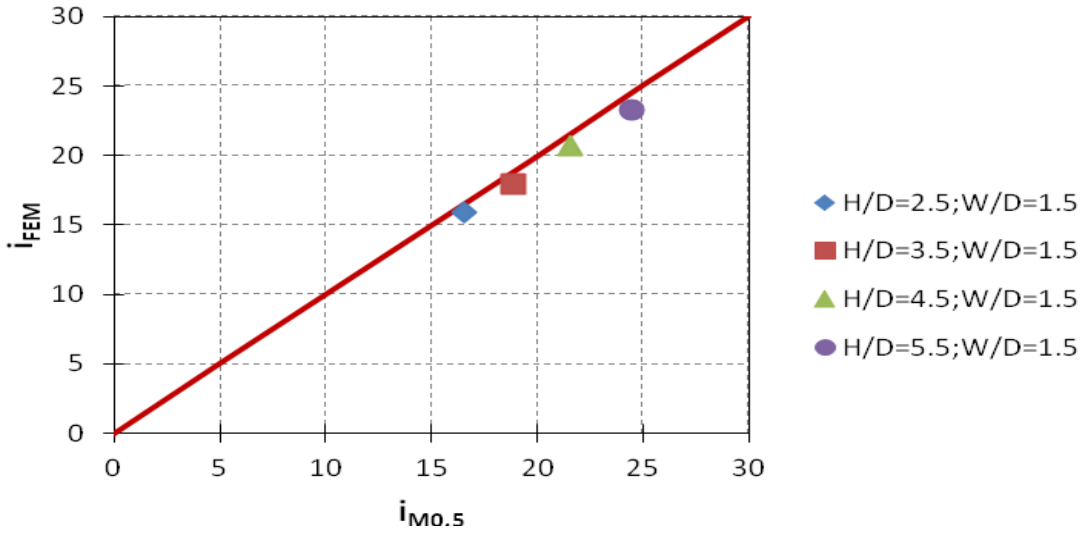

(a)

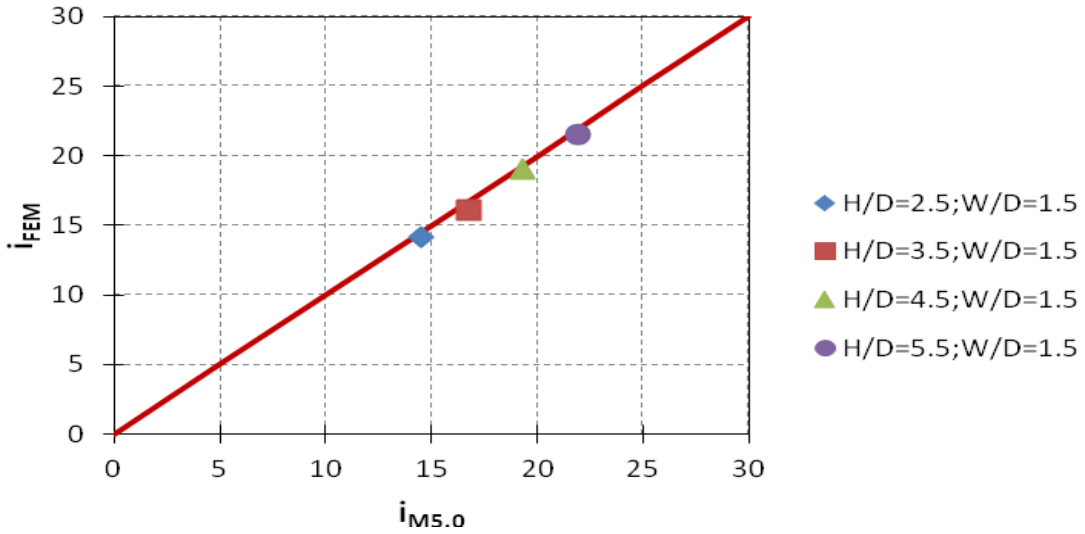

(b)

Figure 8.24 Comparison between i_M and i_{FEM} for mixed soils for (a) VL=0.5%; and (b) VL=5%

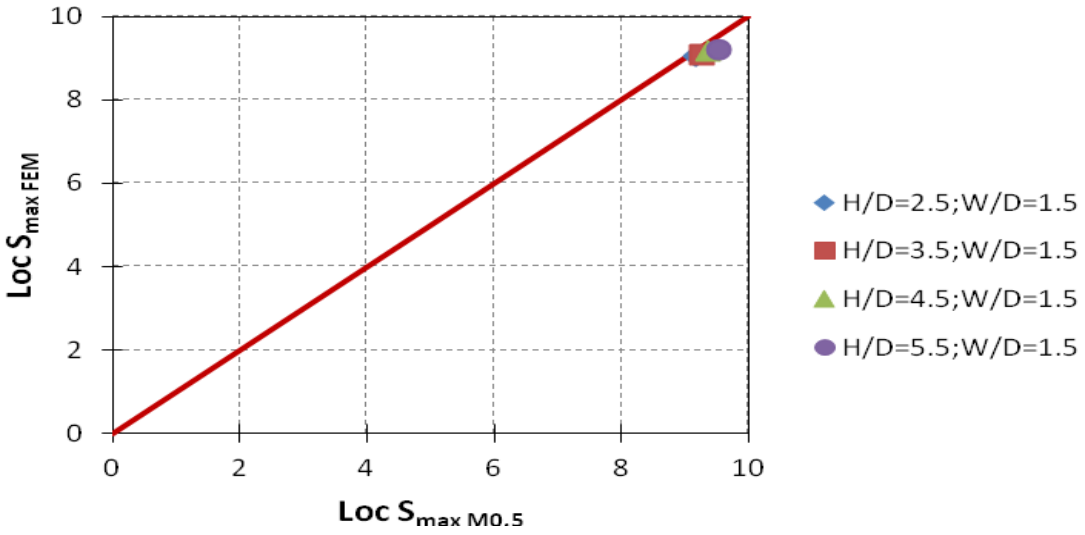

(a)

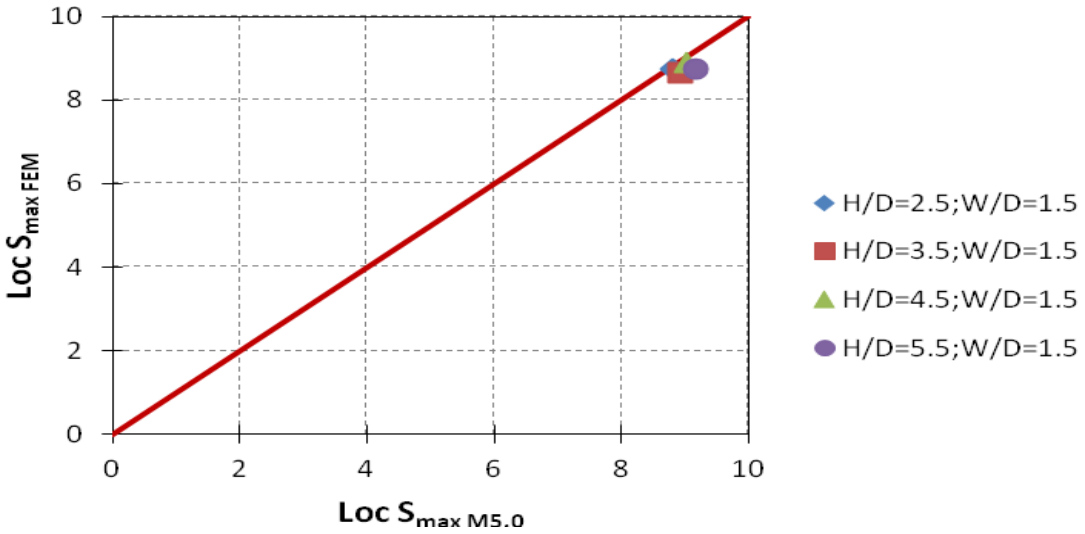

(b)

Figure 8.25 Comparison between Loc $S_{max\ M}$ and Loc $S_{max\ FEM}$ for mixed soils for (a) VL=0.5%; and (b) VL=5%

8.7 Case Studies

Validation of Equations 8.1 to 8.8 was also carried out by comparison with some of the FEM back analysed data reported previously in Chapter 6. These data are denoted by the symbols $i_{FEM\ (Field)}$ and Loc $S_{max\ FEM\ (Field)}$. Four cases were selected, i.e. Instrumentation Arrays D37 and D38 involving residual soil at the tunnel level,

and D46 and E10 involving mixed ground of residual soil and Marine Clay at the tunnel level, after considering the similarity of the volume loss developed in both the first and second bored tunnels. It should be highlighted that the trough width parameter $i_{FEM\ (Field)}$ for Instrumentation Arrays D46 and E10 show better agreement with $i_{M5.0}$ (Equation 8.6) compared with $i_{M0.5}$ (Equation 8.5), as shown in Figures 8.26(b) and 8.26(a) respectively. This is attributed to the larger volume loss of 3.46 and 3.36 per cent for Instrumentation Array D46 and E10 respectively, which is close to the volume loss of 5 per cent. Since the comparisons were made using the idealised results of finite element analyses which give a more consistent shape of transverse surface settlement compared with the field measurements, and also partly because the Loc $S_{max\ R0.5}$ (Equation 8.3) and Loc $S_{max\ R5.0}$ (Equation 8.4) and Loc $S_{max\ M0.5}$ (Equation 8.7) and Loc $S_{max\ M5.0}$ (Equation 8.8) for volume loss of 0.5 per cent and 5 per cent give relatively similar results of location of maximum surface settlement Loc S_{max}, good estimations of location of maximum surface settlement Loc S_{max} for Instrumentation Arrays D37, D46 and E10 using these equations are obtained, as shown in Figures 8.27(a) and 8.27(b). In addition, the sensitivity of the Loc $S_{max\ R0.5}$ (Equation 8.3) and Loc $S_{max\ R5.0}$ (Equation 8.4) to the difference in volume loss of first and second bored tunnel should be noted, resulting in slightly larger differences for D38 (see Figure 8.27) compared with the other cases.

Figures 8.28 and 8.29 reiterate the appreciable difference between the trough with parameter i generated using $i_{R0.5}$ (Equation 8.1) and $i_{R5.0}$ (Equation 8.2) for Instrumentation Arrays D37 and D38 and $i_{M0.5}$ (Equation 8.5) and $i_{M5.0}$ (Equation 8.6) for Instrumentation Arrays D46 and E10 as compared to the marginally difference between the location of maximum surface settlement Loc S_{max} generated using Loc $S_{max\ R0.5}$ (Equation 8.3) and Loc $S_{max\ R5.0}$ (Equation 8.4) for Instrumentation Arrays D37 and D38 and Loc $S_{max\ M0.5}$ (Equation 8.7) and Loc $S_{max\ M5.0}$ (Equation 8.8) for Instrumentation Arrays D46 and E10 for 0.5 per cent and 5 per cent of volume loss respectively. The expression of VL(1,2) in Figures 8.26 to 8.29 denotes similar volume loss induced in the first and second bored tunnels.

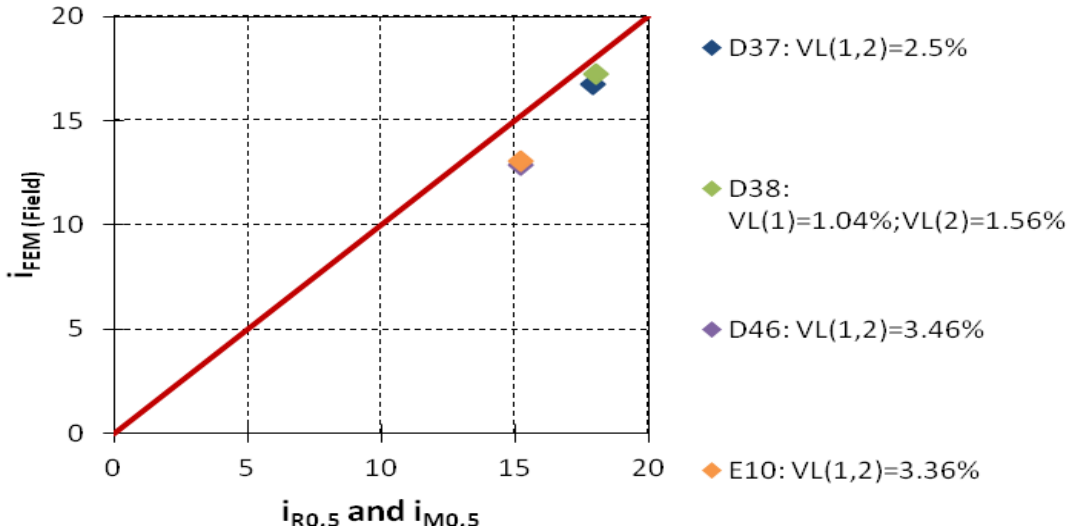

(a)

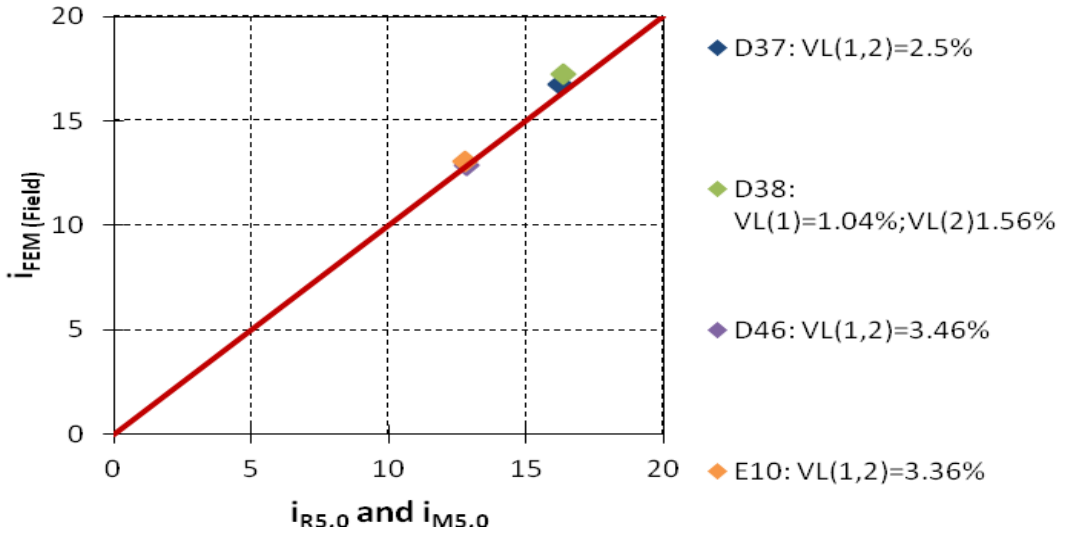

(b)

Figure 8.26 Comparison between $i_{R0.5}$, $i_{M0.5}$, $i_{R5.0}$, $i_{M5.0}$ and the $i_{FEM\ (Field)}$ for (a) VL=0.5%; and (b) VL=5%

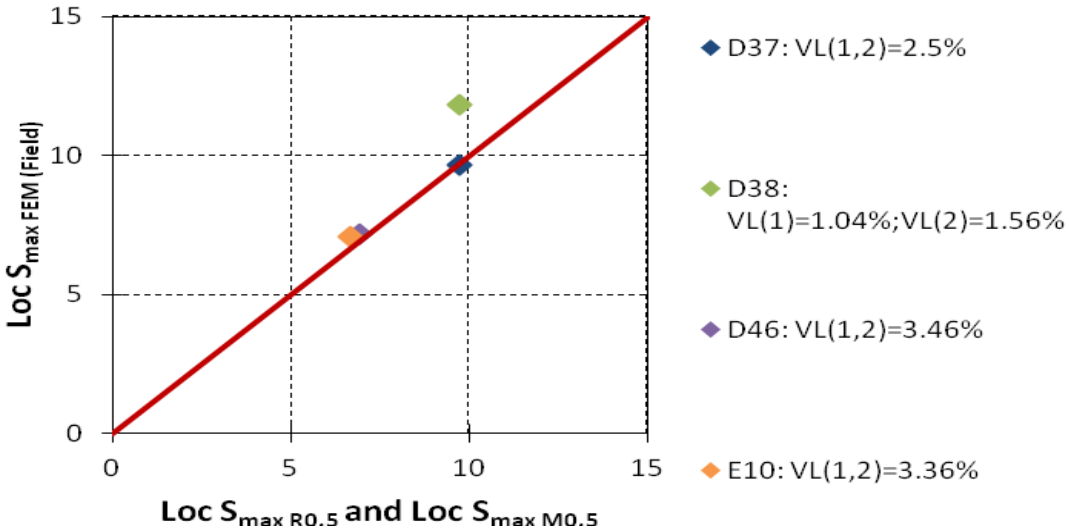

(a)

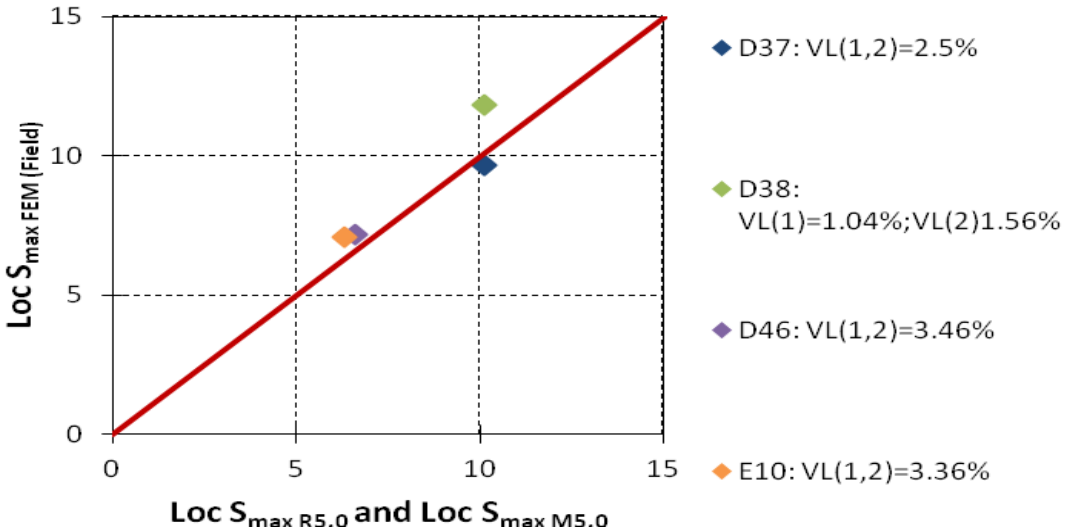

(b)

Figure 8.27 Comparison between Loc $S_{max\ R0.5}$, Loc $S_{max\ M0.5}$, Loc $S_{max\ R5.0}$, Loc $S_{max\ M5.0}$ and Loc $S_{max\ FEM\ (Field)}$ for (a) VL=0.5%; and (b) VL=5%

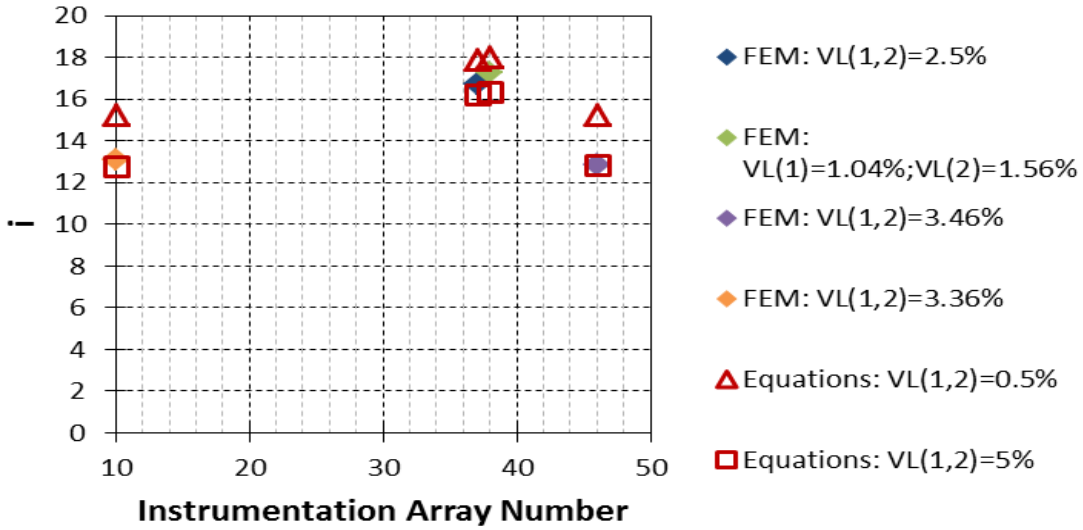

Figure 8.28 Comparison between the empirical equations and $i_{FEM\ (Field)}$ for Instrumentation Array E10, D37, D38 and D46

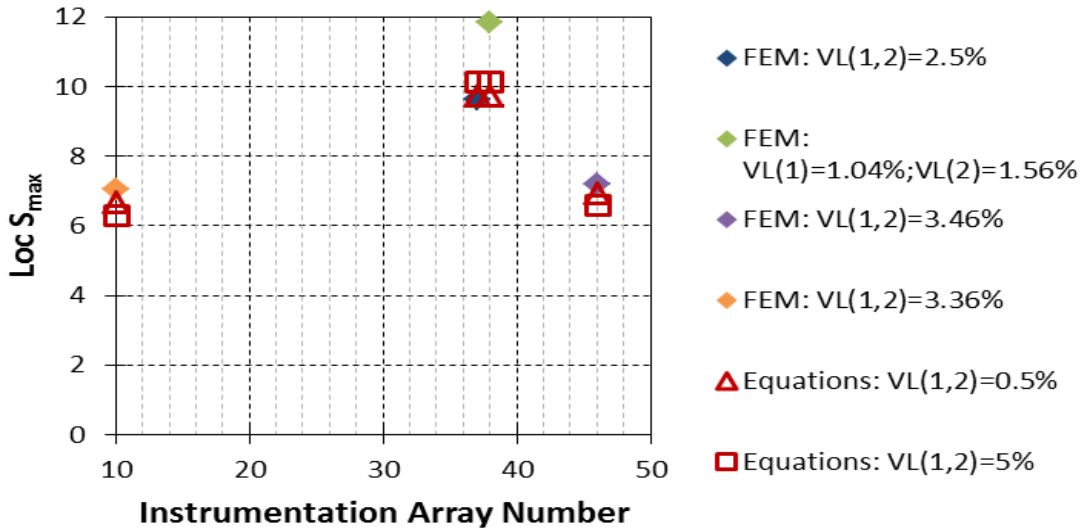

Figure 8.29 Comparison between the empirical equations and Loc $S_{max\ FEM\ (Field)}$ for Instrumentation Array E10, D37, D38 and D46

8.8 Summary

Based on the results of comprehensive parametric studies, regression analysis were performed to develop empirical equations for estimating the trough width parameter i and location of maximum surface settlement Loc S_{max}, for volume loss of 0.5 per cent and 5 per cent respectively. While notable difference was observed between trough width parameter estimated using $i_{R0.5}$ and $i_{R5.0}$ for Jurong Formation as well as $i_{M0.5}$ and $i_{M5.0}$ for mixed ground of Jurong Formation and Kallang Formation, marginal difference was noted for location of maximum surface settlement estimated using Loc $S_{max\ R0.5}$ and Loc $S_{max\ R5.0}$ as well as Loc $S_{max\ M0.5}$ and Loc $S_{max\ M5.0}$ for volume loss of 0.5 per cent and 5 per cent respectively. The adoption of these empirical equations enables a rapid estimation of the trough width parameter i and location of maximum surface settlement Loc S_{max} (both lower bound and upper bound for cases involving volume loss of 0.5 per cent and 5 per cent), which is required to generate the Gaussian curve of ground surface settlement for engineering analysis. In addition, the necessity for routine numerical analyses to be performed can also be avoided.

CHAPTER 9 EFFECTS OF TUNNEL INTERACTION ON STRESSES AND DISPLACEMENTS INDUCED IN THE PRE-EXISTING BORED TUNNEL

9.1 Introduction

In many large cities such as Singapore, rapid development of land has indirectly increased the congestion of the underground space. As a result, both site constraints and construction risks have become major challenges faced by many practising engineers in selecting the optimum tunnel alignment to accommodate future underground transportation system, communication and utility networks such as electric cable systems and sewerage systems. During construction of closely spaced underground tunnels, careful evaluation of the effects of constructing the new tunnel on the adjacent pre-existing tunnel must be considered.

Hence, the main purpose of this chapter is to investigate the interaction effects between the two adjacent bored tunnels with focus on the major variables that contribute significantly to the excessive stresses and deformation induced in the pre-existing tunnel. The parameters investigated included a variation of tunnel geometric parameters, soil and lining deformations properties and volume loss. In addition, the study also investigates independently the three fundamental interaction effects, namely primary effect, volume loss effect of pre-existing tunnel and volume loss effect of new adjacent tunnel as well as their roles in affecting overall interaction effects between closely spaced bored tunnels.

9.2 Finite Element Modelling

As in Chapter 6, the two-dimensional (2D) finite element method program, PLAXIS was adopted for the numerical study. The tunnel lining was modelled using plate consisting of 5-node beam elements, where 15-node triangular elements were adopted in simulating the soil medium. The very fine mesh was used and local refinement was also performed on the tunnel lining to improve the accuracy of the

computed results. As the analyses presented in this chapter exclude the ground surface settlement, smaller vertical boundaries and horizontal boundary of 6.5D and 7.5D from the tunnel centreline were assumed.

Full-face excavations of the pre-existing and new adjacent bored tunnels with linings supporting the tunnels immediately after the excavations were modelled. In addition, the method of contraction, defined as the ratio of the area reduction to the original outer tunnel cross section area (in percentage), was adopted to model the volume loss that occurs during the tunnel installation process.

The validity of using a linear elastic model for soil in estimating the stresses and displacements induced in the pre-existing bored tunnel after interaction with the new adjacent bored tunnel was first explored by conducting a case study and will be discussed in Section 9.3. Furthermore, Peck et al.'s (1972) solutions for stresses and displacements induced in the tunnel lining also assumed both lining and ground behave linearly elastic.

9.3 Case Study: Mass Rapid Transit (MRT) Tunnels, Singapore (Lo et al., 1987)

The effectiveness of the 2D finite element analysis utilising a linear elastic soil model in estimating the stresses and deformation involving tunnel interactions was evaluated with reference to a published case history of the Singapore MRT System reported by Lo et al. (1987). The case history involved four interweaving tunnels of 5850 mm diameter, constructed between Raffles Place and City Hall Stations from February 1985 to September 1986 using the mechanical shield tunnelling method. The paper reported the measured thrust, moment and deformation induced in the southbound (SB) tunnel due to the construction of the eastbound (EB) tunnel.

Figure 9.1 illustrates the orientation of four tunnels and the simplified soil profiles at the tunnel section, i.e. section A-A as reported in the case history. It was reported by Lo et al (1987) that the initial deeper SB followed by EB headings were entirely

advanced within the Old Alluvium deposit, whereas the shallower westbound (WB) followed by northbound (NB) tunnels were partially and totally constructed through the buried channel of Kallang Formation. Due to limited published data, the deformation properties of the Old Alluvium are assumed based on the corresponding SPT N-value reported in the case history. The average of the correlations derived by Orihara and Khoo (1998) for the deformation modulus of Old Alluvium as shown in Equations 9.1 and 9.2 were adopted. Table 9.1 summarises the deformation properties of Old Alluvium. The lining parameters assumed in the analysis are presented in Table 6.4. A volume loss of 0.5 percent that represents a typical volume loss measured during tunnelling through Old Alluvium (Shirlaw, 2002) was adopted for both SB and EB tunnels.

Thrust induced in the pre-existing tunnel as a result of additional external imposed load due to tunnel interaction was measured using total pressure cell. The flexibility of the tunnel lining controls its deformation which was measured using tape extensometer. The incremental bending moment due to deformation of the pre-existing tunnel after interaction with the new adjacent tunnel was measured using stress meter. Comparisons of the computed thrust, moment and deformation induced in the SB tunnel with the measured data reported by Lo et al. (1987) are presented in Table 9.2. It can be concluded that the computed thrust, moment and deformation based on the 2D finite element modelling are in good agreement with the reported field measurements. Therefore, the general validity of the proposed modelling methodology was affirmed for subsequent parametric studies.

$E_p = 1N(MPa)$ For first cycle of pressuremeter test (9.1)

$E_p = 2N(MPa)$ For second cycle of pressuremeter test (9.2)

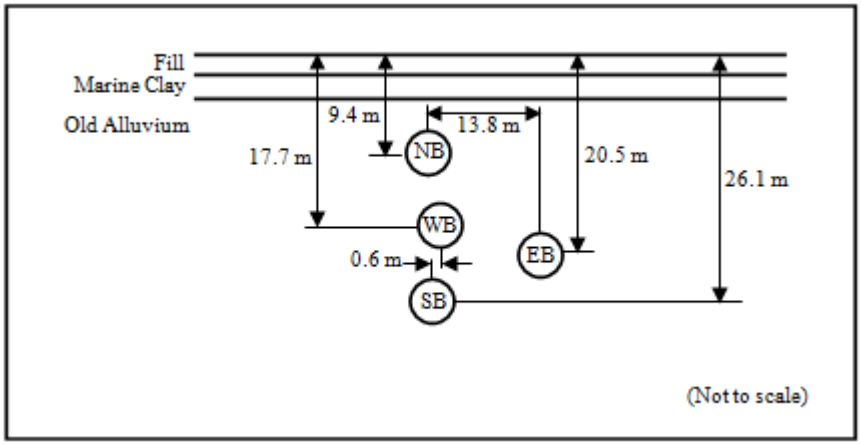

Figure 9.1 Orientation of four tunnels and simplified soil profiles at Section A-A (after Lo et al., 1987)

Table 9.1 Soil properties of Old Alluvium

Property	**Symbol**	**Value**	**Unit**
Unit weight	γ_s	21	kN/m^3
Undrained Young's modulus	E_u	120	MPa
Poisson's ratio	ν	0.495	-
Coefficient of earth pressure at rest	K_o	1.0	-
SPT N-value	-	80	blow count

Table 9.2 Comparison of computed and measured thrust, moment and lining deformation in SB tunnel

Parameter	**This Study**	**Measured**	**Unit**
Thrust	830.74	625	kN
Bending moment	26.53	30	kNm
Deformation	0.00095	0.0015	m

9.4 PARAMETRIC STUDIES

A series of parametric studies was performed to investigate the influence of the major variables on the maximum thrust, bending moment and deformation induced in the pre-existing bored tunnel after interaction with the new adjacent bored tunnel. The variables were classified into two broad categories: (1) Tunnel geometric parameters; and (2) soil and lining deformation parameters.

9.4.1 Reference Case

In this reference case, the interaction between the pre-existing and the new adjacent bored tunnels at various tunnel angular relative positions is considered. Figure 9.2 illustrates the general characteristics of the reference case. It consists of two closely spaced bored tunnels of 6.0 m diameter with a dimensionless depth of burial H/D of 3.5 for the pre-existing bored tunnel. The angular relative position was measured by an angle θ between the centre-to-centre line of the pre-existing and new adjacent bored tunnels and the crown-invert line of the pre-existing bored tunnel. An angle θ of 0^o represents a new adjacent bored tunnel excavated directly above the crown of a pre-existing bored tunnel, whereas an angle θ of 90^o represents a new adjacent bored tunnel excavated at the springline level of the pre-existing bored tunnel. The dimensionless pillar width W/D of 0.25 and 1.0 were adopted to study the tunnel interaction. Two values of relative stiffness, i.e. E_s/E_l of 0.0003 and 0.03 where E_s is the soil modulus, corresponding to flexibility ratio F of 0.5 and 50 as defined by Peck et al. (1972) were adopted. Since the deformation modulus of the elastic tunnel lining shown in Table 6.4 was used as the E_l value in computing the relative stiffness, both E_s/E_l = 0.0003 and 0.03 can therefore be considered as representative relative stiffness for cases involving concrete tunnel lining constructed in soft and stiff ground, respectively. The E_s/E_l of 0.0003 was termed as stiff lining, whereas E_s/E_l of 0.03 was termed as flexible lining in this study. Two different coefficients of earth pressure at rest, i.e. K_o = 0.5 and 1.5, were considered to represent normally consolidated and overconsolidated ground. A volume loss of 2 per cent, which represents an upper bound for 93 per cent of the volume loss measured during the

construction of North East Line (NEL) of Singapore MRT System (Shirlaw et al., 2001), was adopted throughout the analysis. It is also important to point out that values of negative incremental maximum bending moment represents tension on the exterior interaction face of the tunnel lining, which in turn results in lengthening of the diameter at the interaction face of the pre-existing bored tunnel, while positive incremental maximum bending moment represents tension on the exterior face. The interface strength is defined by the parameter R_{inter} in PLAXIS 2D (Brinkgreve et al., 2012) and is assumed as R_{inter} = 1.0 throughout the analyses.

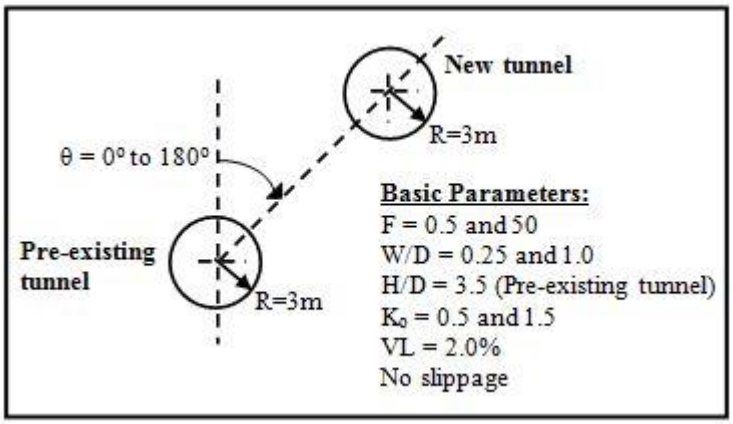

Figure 9.2 General characteristics of the reference case

9.4.2 Tunnel Geometric Parameters

Angular Relative Position

Figure 9.3 shows the maximum thrust, maximum bending moment and total displacements induced in the pre-existing bored tunnel before and after interaction with the new adjacent bored tunnel, for angular relative position θ varying from 0^o to 180^o, for the two different lining flexibility and K_o values with W/D of 0.25. Figure 9.3(a) shows that for the stiff lining case, excavation of new bored tunnel adjacent to the crown, springline or invert of the pre-existing bored tunnel has significant influence on the maximum thrust induced in the pre-existing bored tunnel, as compared to other angular relative positions. For instance, the pre-existing bored tunnel experienced a decrease in the maximum thrust when the new bored tunnel is excavated directly adjacent to the crown and springline of the pre-

existing bored tunnel, for K_o of 0.5 and 1.5 respectively. This can be attributed to the decrease in the dominant vertical stresses acting on the pre-existing bored tunnel for K_o of 0.5 due to the removal of soil mass above the bored tunnel. However, excavation of a new bored tunnel adjacent to the springline of pre-existing bored tunnel reduces the dominant horizontal stresses acting on the pre-existing bored tunnel, for K_o of 1.5. In general, excavation of an adjacent new bored tunnel around the shoulder and haunch of the pre-existing bored tunnel with stiff lining has minimal influence on the maximum thrust induced in the pre-existing bored tunnel. The variation of the maximum thrust with tunnel angular relative position for the flexible lining case is shown in Figure 9.3(b) for K_o of 0.5 and 1.5. It should be noted that the maximum thrust induced in the flexible lining are significantly larger than the stiff lining, for single bored tunnel. The interaction effects lead to considerable incremental maximum thrust in the pre-existing bored tunnel for both K_o. This suggests allowance should be made for the effect of additional loading for closely spaced bored tunnels. In addition, the incremental maximum thrust for K_o of 0.5 is more sensitive to relative position as compared to K_o of 1.5. For the flexible lining, the larger maximum thrust occurs at tunnel angular relative position of 90^o as compared to 0^o and 180^o for both K_o of 0.5 and 1.5 indicates that the total vertical stresses dominate the incremental maximum thrust in the pre-existing bored tunnel after interaction with the new adjacent bored tunnel.

Figure 9.3(c) shows the significant influence of the angular relative position of a new adjacent bored tunnel on the maximum bending moment induced in the pre-existing bored tunnel for the stiff lining case. A decrease in the maximum bending moment in the pre-existing bored tunnel after interaction with the new adjacent bored tunnel at certain relative positions can be identified. These interaction effects were found to be significantly dependent on the K_o. It should, however, be noted in Figure 9.3(d) that while the maximum bending moment in the pre-existing bored tunnel increases significantly at any angular relative position of the new adjacent bored tunnel for the flexible lining case, the influence of K_o on the maximum bending moment is minimal. For the stiff lining case with K_o of 0.5, a decrease in the maximum bending moment in the pre-existing bored tunnel is observed when

the new adjacent bored tunnel is excavated above the pre-existing bored tunnel for relative positions varying from 0^o to about 30^o. This can be attributed to the decrease in dominant vertical stresses acting on the pre-existing bored tunnel after the new bored tunnel is excavated. However, the maximum bending moment induced in the pre-existing bored tunnel increases when the new adjacent bored tunnel is excavated at relative positions of about 45^o to 157.5^o, i.e. when the new adjacent bored tunnel is excavated relatively close to the springline of the pre-existing bored tunnel. The maximum increase in bending moment is about 25 per cent as compared to before constructing the new adjacent bored tunnel. This is attributed to the decrease in horizontal stresses after excavating the new bored tunnel close to the springline of the pre-existing bored tunnel. The reduction of the horizontal stresses increases the deformation of the pre-existing bored tunnel and hence, the maximum bending moment increases. Besides, the excavation of a new bored tunnel below the pre-existing bored tunnel may also lead to significant decreases in the maximum bending moment for K_o of 0.5. This is due to the decrease in the ground stiffness in the vertical direction which leads to less invert support to the pre-existing bored tunnel and hence, the maximum bending moment decreases. The observed variation in maximum bending moment for this case is about 20 per cent lesser than that before interaction with the new adjacent tunnel. In general, the results presented in Figures 9.3(a) to 9.3(d) indicate that the excavation of new adjacent bored tunnel at the location where dominant total stresses are acting on the pre-existing bored tunnel leads to the favourable interaction effects for the stiff lining case. However, variation of interaction effects with tunnel angular relative position is unfavourable for the flexible lining case, due to the larger thrust and maximum bending moment induced in the pre-existing bored tunnel after interaction with the new adjacent bored tunnel.

The variation of total displacements with tunnel angular relative position are shown in Figures 9.3(e) and 9.3(f) for the stiff lining case and flexible lining case respectively. It must be pointed out that the decrease in total displacements of the pre-existing bored tunnel after interaction with the new adjacent bored tunnel for K_o of 0.5 at tunnel angular relative position of 180^o implies the influence of the invert

support on the total displacements for stiff lining case. The comparative study of the result for K_o of 1.5 has affirmed the validity of the interpretation, where smaller total displacements as compared to the tunnel angular relative position of 0^o was observed. The small difference in the total displacements between K_o of 0.5 and 1.5 for the flexible lining case indicates the minimal influence of K_o on the total displacements.

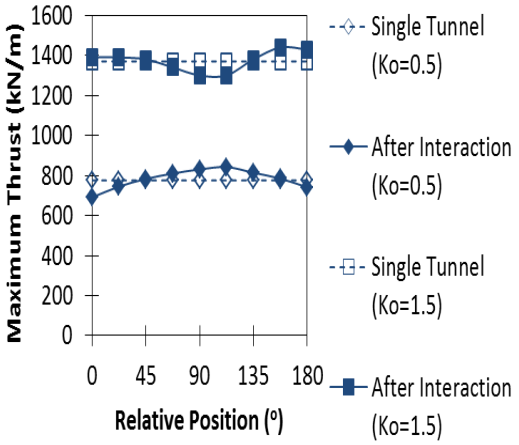

(a) Stiff Lining

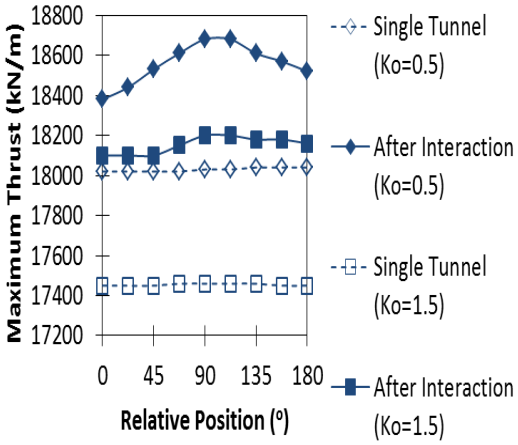

(b) Flexible Lining

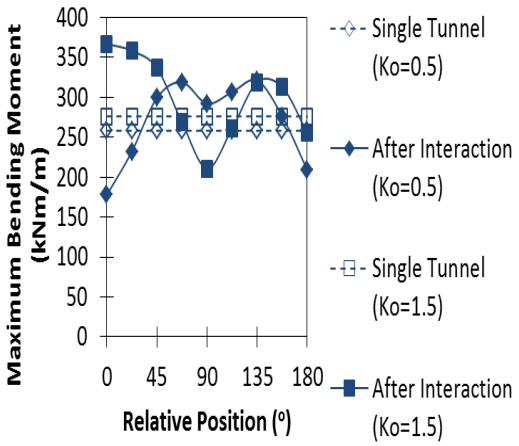

(c) Stiff Lining

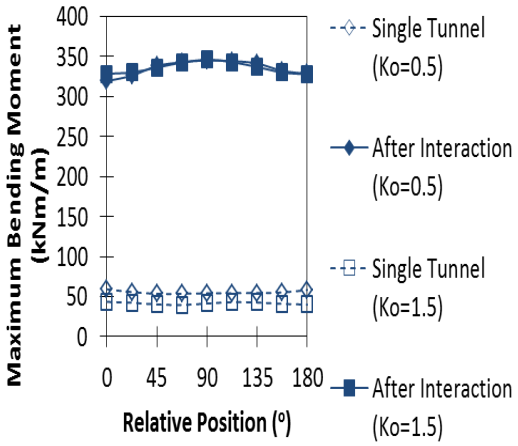

(d) Flexible Lining

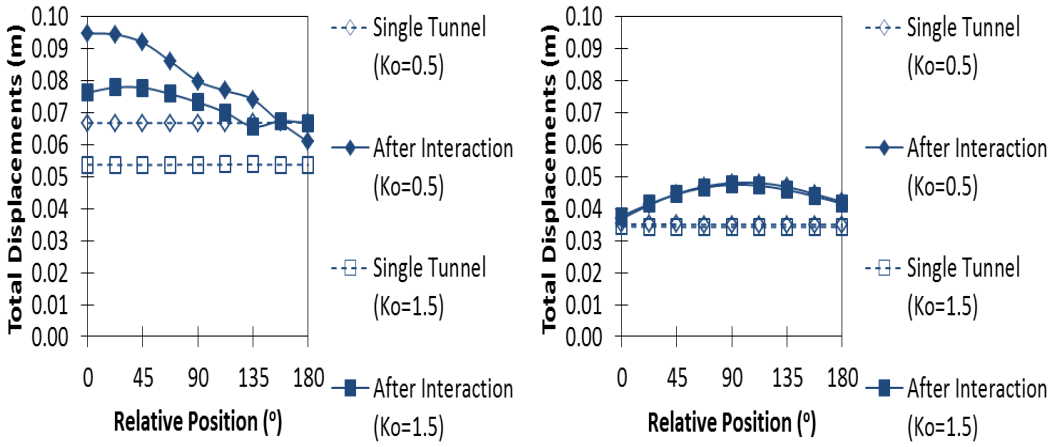

(e) Stiff Lining (f) Flexible Lining

Figure 9.3 Variations of maximum thrust, maximum bending moment and total displacements with angular relative positions (W/D=0.25)

Tunnel Proximity

An investigation into the influence of tunnel proximity on the incremental maximum bending moment and diameter change in the pre-existing bored tunnel was performed. Two values of dimensionless pillar width, i.e. W/D = 0.25 and 1.0, were considered in the analysis. Results of the study are presented in Figure 9.4. It should be pointed out that only the results for horizontal diameter change were presented in this study as the vertical diameter change shares similar but opposite deformation trends as compared to the horizontal diameter change.

Figure 9.4 shows significant influence of the tunnel proximity on tunnel interaction for the flexible lining case, as compared to the stiff lining case. For example, there is a larger increase in the maximum bending moment and horizontal diameter for the flexible lining case when distance between the two bored tunnels decreases from W/D = 1.0 to 0.25. However, variation of the incremental maximum bending moment to tunnel angular relative position and K_o are found to be minimal for the flexible lining case.

For K_o of 0.5, the results for the stiff lining case indicate that excavation of a new adjacent bored tunnel in very close proximity, i.e. W/D = 0.25, at locations above

the pre-existing bored tunnel with angular relative positions varying from about 0^o to 22.5^o may lead to substantial increase in the maximum bending moment and horizontal diameter of the pre-existing bored tunnel, as shown in Figure 9.4. The interaction effects decrease with increasing tunnel proximity and approach the single tunnel case at W/D = 1.0, in particular when the new bored tunnel was excavated close to the springline of the pre-existing bored tunnel for K_o of 0.5. This indicates that the required tunnel proximity for the stiff lining is dependent on the tunnel angular relative position and K_o. For K_o of 0.5 and 1.5, the interactions between adjacent bored tunnels for the stiff lining case approaches the single tunnel condition at smaller tunnel proximity as compared to the flexible lining. As a result of the differences in the stress distribution of the pre-existing bored tunnel after excavating a new adjacent bored tunnel at an angular relative position above and below the pre-existing bored tunnel, an important difference in the incremental maximum bending moment and horizontal diameter change between θ of 0^o and 180^o can be observed in Figure 9.4, for K_o of 1.5.

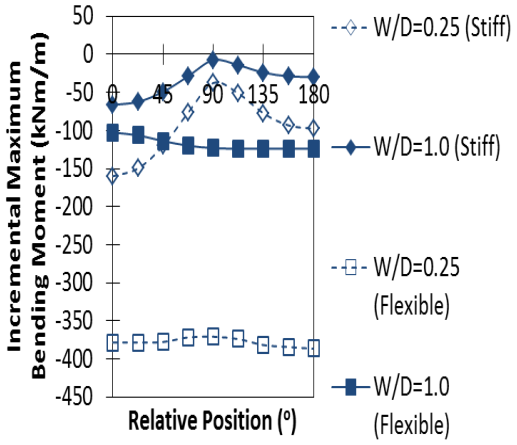

(a) K_o = 0.5

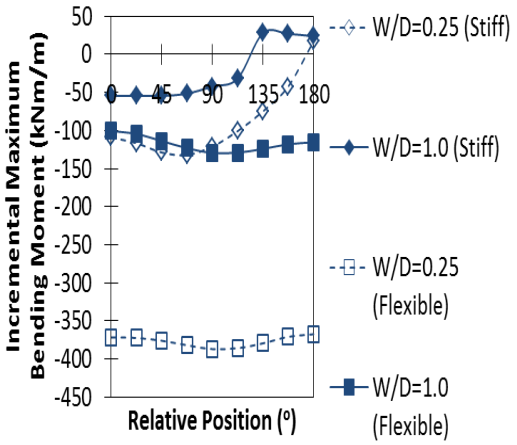

(b) K_o = 1.5

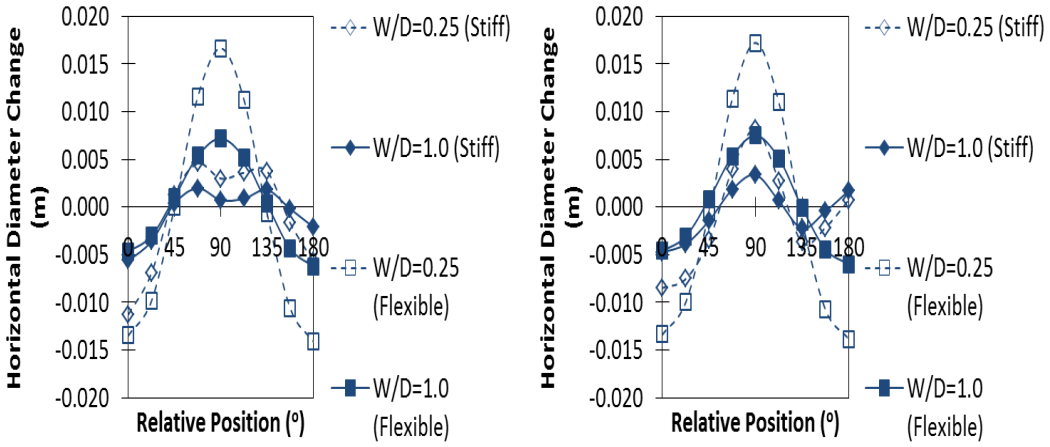

(c) K_o = 0.5 (d) K_o = 1.5

Figure 9.4 Variations of incremental maximum bending moment and horizontal diameter change with tunnel proximity

9.4.3 Soil and Lining Deformation Parameters

Relative Stiffness

Both soil and lining stiffness are important parameters governing the soil-structure interaction between adjacent bored tunnels. A study of the influence of the relative stiffness E_s/E_l on the interaction effects of closely spaced bored tunnels was performed in this section. The results of E_s/E_l = 0.0003 and 0.03 corresponding to stiff and flexible lining cases for W/D of 0.25 are presented in Figure 9.5.

The previous plots in Figures 9.3(c) and 9.3(d) suggest the inverse relationship between E_s/E_l and maximum bending moment for single bored tunnel. Increasing E_s/E_l from 0.0003 to 0.03 leads to a reduction in the maximum bending moment induced in the tunnel lining. This is attributed to the capability of the flexible lining to deform and redistribute the unbalanced stresses acting on the tunnel. However, Figure 9.5 shows that for the interaction between two adjacent bored tunnels, increasing E_s/E_l from 0.0003 to 0.03 resulted in significant increase in the maximum bending moment and horizontal diameter change of the pre-existing bored tunnel. Moreover, the flexible lining case produced practically similar magnitude of incremental maximum bending moment, regardless of tunnel angular relative position and K_o, whereas the opposite behaviour was observed for the stiff lining

case. This significant difference in the interaction behaviour between stiff and flexible lining case highlights the limitation of performing the tunnel interaction analysis using a single lining flexibility value. Hence, the findings obtained from the analysis might not be applicable to cases involving different lining flexibility.

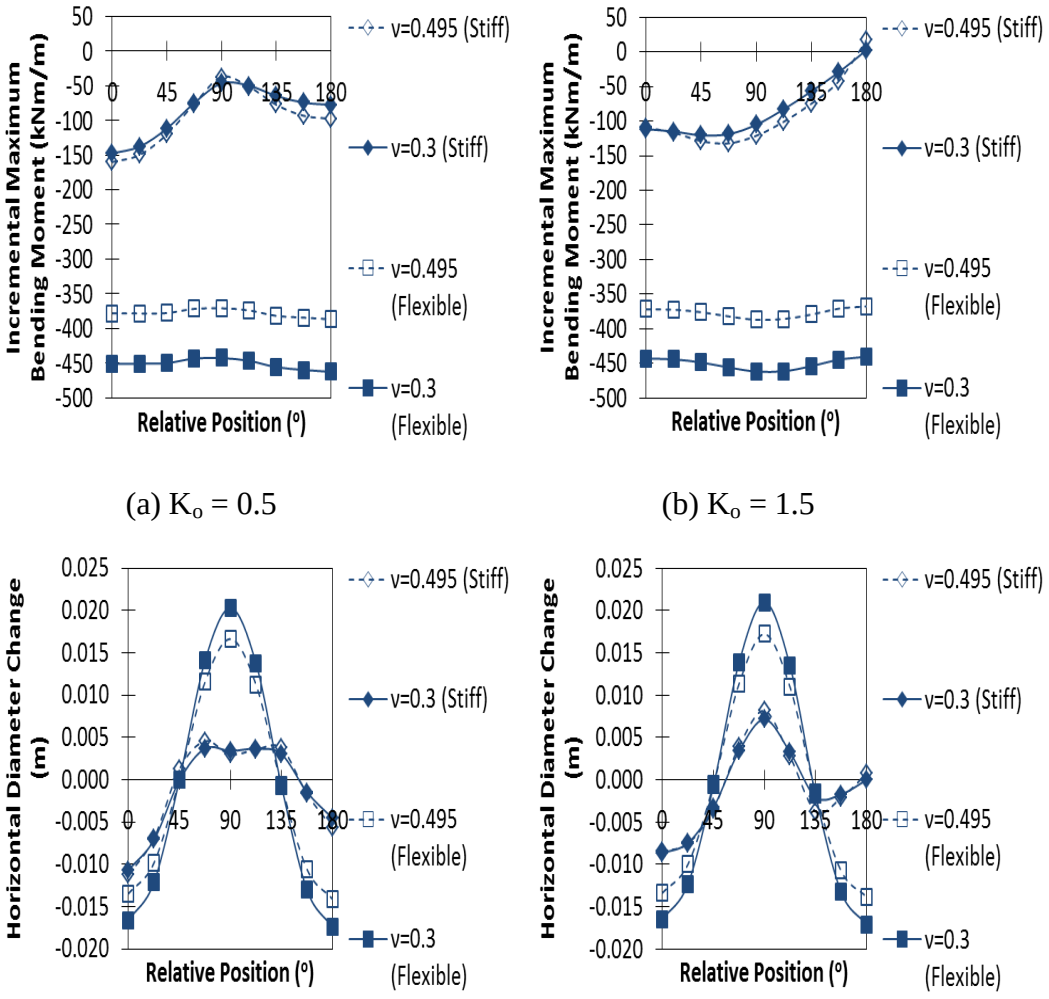

(a) K_o = 0.5 (b) K_o = 1.5

(c) K_o = 0.5 (d) K_o = 1.5

Figure 9.5 Variations of incremental maximum bending moment and horizontal diameter change with Poisson's ratio (W/D=0.25)

Poisson's Ratio

Figure 9.5 illustrates the sensitivity of the incremental maximum bending moment and horizontal diameter change induced in the pre-existing bored tunnel to the Poisson's ratio of soil ν. The study focused on ν of 0.495 and 0.30, i.e.

corresponding to typical ν adopted for short-term (undrained behaviour) and long-term interaction (drained behaviour), respectively.

As observed, the influence of ν on the tunnel interaction for the stiff lining case is minimal. However, interaction effects for ν of 0.3 are more significant as compared to ν of 0.495, for the flexible lining case. An average increase of about 20 per cent in maximum bending moment and 22 per cent in horizontal diameter change were observed for the flexible lining case when reducing ν from 0.495 to 0.3. These observations are in good agreement with one of the experimental findings by Kim (1996) who reported that the measured long-term interaction effects for lining with flexibility ratio F greater than 68, i.e. classified as flexible lining case in this study, were in the order of 20 per cent greater than the corresponding short-term values. The result suggests for the flexible lining case, the short-term interaction effects are more crucial as the additional magnitude of interaction effects that developed over the long-term are small.

9.5 Comparison of Stiff Lining and Flexible Lining

Based on the numerical analyses in Section 9.4, the following phenomena were observed:

1 The interaction effects between the stiff and flexible lining cases show a significant difference in trends. The variation of incremental maximum bending moment and horizontal diameter change with tunnel angular relative positions and K_o are more significant for the stiff lining case, compared with the flexible lining case.
2 The observed plots for incremental maximum bending moment and also symmetrical plots for horizontal diameter change at θ of 90^o for the flexible lining case indicate similar tunnel interaction behaviour regardless of the angular relative position of the new adjacent bored tunnel above or below the axis level of the pre-existing bored tunnel.
3 The interaction effects for the stiff lining case approach the single tunnel case at smaller W/D as compared to the flexible lining case.

The observed phenomenon 1 demonstrates the significant difference in the nature of interaction mechanisms between the stiff and flexible lining cases. In addition, phenomenon 2 reveal the mechanisms of interaction for the flexible lining case are mainly controlled by stress relief associated with the volume loss of the new adjacent tunnel. Hence, both the tunnel angular relative position and K_o does not contribute significantly to the overall interaction effects. Besides, the dependency of the interaction effects on tunnel angular relative position and K_o for the stiff lining case also implies that the nature of interaction mechanisms are mainly governed by lining deformation of the new adjacent bored tunnel, which subsequently alter the soil stresses and in turn, stresses and deformation of the pre-existing bored tunnel. However, for the flexible lining case, this effect is minimal since a stiff ground would result in smaller deformation of the new adjacent bored tunnel. As expected intuitively, the interaction effects due to the alteration of soil stresses acting onto the pre-existing bored tunnel resulting from the lining deformation of the new adjacent bored tunnel for stiff lining case would diminish significantly with increasing tunnel proximity as compared to stress relief due to volume loss that mainly control the interaction mechanisms for the flexible lining case. Therefore, phenomenon 3 is explained. These observations demonstrate the importance of evaluating the significant contributions of each fundamental interaction effect, termed here as primary effect, volume loss effect of pre-existing bored tunnel and volume loss effect of new adjacent bored tunnel on the complex tunnel interaction between closely spaced bored tunnel, for the stiff and flexible lining cases. These effects are considered in the next section.

9.6 Assessment of Fundamental Interaction Effects

The following steps illustrate the procedures involved to determine the complex interaction effects between closely spaced bored tunnels:

For determining the magnitude of the primary effect, the staged construction simulation involves the following steps:

Initial phase: Perform initial stress analysis using K_o procedure;

Phase 1*: Construction of the first tunnel by deactivating the soil and activating the tunnel lining;

Phase 2*: Construction of the second tunnel by deactivating the soil and activating the tunnel lining;

The required magnitude of the primary effect is then obtained by subtracting Phase 1* from Phase 2*.

The required magnitude of volume loss effect of the new adjacent bored tunnel is obtained by subtracting Phase 3 (refer to Section 6.5) from Phase 4 (refer to Section 6.5).

The required magnitude of volume loss effect of pre-existing bored tunnel is obtained by subtracting Phase 2 (refer to Section 6.5) and magnitude of primary effect from Phase 3 (refer to Section 6.5).

Phase 4 (refer to Section 6.5) – Phase 2 (refer to Section 6.5) = magnitude of primary effect + magnitude of volume loss effect of new adjacent bored tunnel + magnitude of volume loss effect of pre-existing bored tunnel

9.6.1 Primary Effect

As explained in Section 9.5, the primary effect is defined as the interaction effect governing soil-lining interaction behaviour in the absence of volume loss. It can be seen from Table 9.3 that the nature of the interaction mechanisms for the primary effect is dependent on the tunnel angular relative position, K_o of soil and lining flexibility. The mechanisms of interaction involved the lining deformation of the new adjacent bored tunnel which leads to the alteration of soil stresses between the two bored tunnels and subsequently influence the stresses and deformation of the pre-existing bored tunnel.

As shown in Table 9.3, the primary effect induces significantly smaller incremental maximum bending moment and horizontal diameter change for the flexible lining

case as compared to the stiff lining case. This is intuitively expected since a stiff ground would result in smaller deformation of the new adjacent bored tunnel. As a result, the resultant change in soil stresses acting on the interaction face of the pre-existing bored tunnel is small. This subsequently induces less deformation of the lining and consequently smaller incremental maximum bending moment in the pre-existing bored tunnel.

In addition, the results for the horizontal diameter change for the stiff lining case in Table 9.3 also indicate the influence of K_o on the deformation pattern of the pre-existing bored tunnel after interaction with the new adjacent bored tunnel. For K_o of 0.5, the horizontal diameter of the pre-existing bored tunnel decreases (shown as negative value in Table 9.3) when the new bored tunnel is excavated around the springline, i.e. θ of 90^o, of the pre-existing bored tunnel. The reduction of the horizontal diameter indicates less squatting of the pre-existing bored tunnel after interaction with the new adjacent bored tunnel. In addition, it is important to point out that the positive incremental maximum bending moment which corresponds to compression on the exterior interaction face of the pre-existing bored tunnel can be observed in Table 9.3. In contrast, squatting of the pre-existing bored tunnel is more significant for K_o of 1.5. This behaviour is represented by the increase in the horizontal diameter (shown as positive value in Table 9.3) and the negative incremental maximum bending moment which represents tension on the exterior interaction face of the pre-existing bored tunnel after interaction with the new adjacent bored tunnel.

The interaction mechanisms for primary effect confirm the finding by Ghaboussi and Ranken (1977) in which the deformation of the pillar springline decreases as the pillar width is reduced for K_o of 0.5. However, it should be emphasized that the observation made by Ghaboussi and Ranken (1977) only constitutes part of the overall interaction effects as proposed in this study. Therefore, this primary effect can be considered as an ideal tunnel interaction case without volume loss incurred.

Table 9.3 Primary effect on tunnel interaction (W/D=0.25)

Angular Relative Positions (^{o})	Stiff Lining		Flexible Lining	
	Incremental Maximum Bending Moment (kNm/m)		Incremental Maximum Bending Moment (kNm/m)	
	K_o=0.5	K_o=1.5	K_o=0.5	K_o=1.5
0	-82.9	-32.1	-8.8	-2.3
90	46.1	-36.5	4.7	-11.5
180	-17.0	97.6	-10.8	8.3
Angular Relative Positions (^{o})	**Stiff Lining**		**Flexible Lining**	
	Horizontal Diameter Change (mm)		**Horizontal Diameter Change (mm)**	
	K_o=0.5	**K_o=1.5**	**K_o=0.5**	**K_o=1.5**
0	-6.1	-3.3	-0.3	-0.2
90	-3.2	2.0	-0.1	0.4
180	-0.2	6.2	-0.2	0.1

9.6.2 Volume Loss Effect of New Adjacent Bored Tunnel

In addition to the primary effect, the interaction between closely spaced bored tunnels is also influenced by the volume loss developed during construction of the new adjacent bored tunnel, termed as volume loss effect of new adjacent bored tunnel. This interaction effect excludes volume loss in the pre-existing bored tunnel. The interaction mechanisms involve the reduction of total stress acting on the interaction face of the pre-existing bored tunnel due to volume loss in the new adjacent bored tunnel. This stress relief leads to additional deformation and bending moment induced in the pre-existing bored tunnel. As the stress relief is controlled by the volume loss in the new adjacent bored tunnel, increasing volume loss increases stress relief which in turn increases the magnitude of interaction effects of the pre-existing bored tunnel.

For interaction between two adjacent bored tunnels at θ of 90^o, the volume loss effect of new adjacent bored tunnel leads to an increase in the horizontal diameter of the pre-existing bored tunnel, as shown in Table 9.4. This squatting behaviour is due to the reduction of the total horizontal stress acting on the springline of the pre-existing bored tunnel as a result of volume loss in the new adjacent bored tunnel. However, the opposite behaviour involving decrease in the horizontal diameter is observed for the interaction between tunnels at θ of 0^o and 180^o. This is attributed to the reduction of the total vertical stress acting on the pre-existing bored tunnel. As can be seen from Table 9.4, the magnitude of interaction effects involving θ of 90^o

is relatively larger compared to θ of 0^o and 180^o. This suggests that the effects due to lateral stress relief are relatively larger than vertical stress relief. In addition, it should be highlighted that similar magnitude of interaction effects were observed at θ of 0^o, 90^o and 180^o, for K_o of 0.5 and 1.5. The larger deformation of the pre-existing tunnel with flexible lining towards the newly excavated adjacent tunnel also lead to the much greater incremental maximum bending moment for the flexible lining case as compared to the stiff lining case.

Table 9.4 Volume loss effect of new adjacent bored tunnel on tunnel interaction (W/D=0.25)

Angular Relative Positions (^{o})	**Stiff Lining**		**Flexible Lining**	
	Incremental Maximum Bending Moment (kNm/m)		**Incremental Maximum Bending Moment (kNm/m)**	
	K_o=0.5	**K_o=1.5**	**K_o=0.5**	**K_o=1.5**
0	-83.4	-83.4	-667.4	-667.4
90	-90.5	-91.6	-681.9	-681.9
180	-87.2	-87.2	-674.3	-674.3
Angular Relative Positions (^{o})	**Stiff Lining**		**Flexible Lining**	
	Horizontal Diameter Change (mm)		**Horizontal Diameter Change (mm)**	
	K_o=0.5	**K_o=1.5**	**K_o=0.5**	**K_o=1.5**
0	-5.5	-5.5	-16.1	-16.1
90	6.6	6.6	24.2	24.2
180	-5.8	-5.8	-16.9	-16.9

9.6.3 Volume Loss Effect of Pre-Existing Bored Tunnel

The volume loss developed during the construction of the pre-existing bored tunnel may influence the stresses and deformation of its tunnel lining after interaction with the new adjacent bored tunnel. This interaction effect is termed as volume loss effect of pre-existing bored tunnel. It is important to note that this effect excludes volume loss in the new adjacent bored tunnel and shows a reverse relationship as compared to the volume loss effect of new adjacent bored tunnel. The interaction mechanism involved the reduction of soil stresses acting on the interaction face of the new adjacent bored tunnel due to volume loss in the pre-existing bored tunnel. This stress relief induced additional deformation in the new adjacent bored tunnel which in turn leads to an increase in soil stresses acting on the pre-existing bored tunnel. These interaction mechanisms subsequently influence the stresses and deformation of the pre-existing bored tunnel.

Comparison of results in Tables 9.4 and 9.5 indicate that the contribution of volume loss effect of new adjacent bored tunnel towards the overall interaction effects is more significant as compared to volume loss effect of pre-existing bored tunnel. It is clear that the former is due to the immediate influence of stress relief as a result of volume loss of the new adjacent bored tunnel while the latter is due to the indirect influence of the deformation of the new adjacent bored tunnel on the stresses and deformation induced in the pre-existing bored tunnel.

Table 9.5 Volume loss effect of pre-existing bored tunnel on tunnel interaction (W/D=0.25)

Angular Relative Positions (^{o})	**Stiff Lining**		**Flexible Lining**	
	Incremental Maximum Bending Moment (kNm/m)		**Incremental Maximum Bending Moment (kNm/m)**	
	K_o=0.5	**K_o=1.5**	**K_o=0.5**	**K_o=1.5**
0	5.9	5.9	296.1	296.1
90	6.5	6.5	304.5	304.5
180	6.1	6.1	296.6	296.6
Angular Relative Positions (^{o})	**Stiff Lining**		**Flexible Lining**	
	Horizontal Diameter Change (mm)		**Horizontal Diameter Change (mm)**	
	K_o=0.5	**K_o=1.5**	**K_o=0.5**	**K_o=1.5**
0	0.3	0.3	2.8	2.8
90	-0.4	-0.4	-7.4	-7.4
180	0.3	0.3	2.9	2.9

9.7 Practical Implications on Peck et al.'s (1972) Equations

As discussed in Section 9.6, the nature of the interaction mechanisms between primary effect and volume loss effects is significantly different. Hence, the application of a single normalised moment, defined as $\Delta M_{max}/\gamma HR^2$, and normalised deformation, defined as $\Delta D_{H/V}M_c/D\gamma H$, by Peck et al. (1972) for a single tunnel case to interprete the magnitude of complex interaction effects for closely spaced bored tunnels might not be effective. In the above expressions ΔM_{max} is the incremental maximum bending moment, γH is the overburden pressure acting at tunnel level and R is the tunnel radius, $\Delta D_{H/V}$ is the horizontal (H) or vertical (V) diameter change (positive value corresponds to increase in tunnel diameter; negative value corresponds to the decrease in tunnel diameter), D is the initial tunnel diameter and M_c is the constrained modulus which is assumed as 5/3 times the value of Young's modulus of soil E_s. This is attributed to the fact that the

volume loss factor, which contributes significantly to tunnel interaction, is not considered in the normalised equations proposed by Peck et al. (1972) for a single tunnel case. Hence, these observations in Section 9.6 show the importance of separating the complex interaction effects into primary effect, volume loss effect of new adjacent bored tunnel and volume loss effect of pre-existing bored tunnel to facilitate a new normalised moment and deformation to be proposed in Chapter 10 for the interpretation of volume loss effects while adopting the normalised moment and deformation definitions proposed by Peck et al. (1972) for the interpretation of primary effect. The magnitude of overall interaction effects can be obtained by the summation of the moment and deformation computed separately from volume loss effects and primary effect. These findings open up the possibility of developing a series of design charts in Chapter 10 for determination of the incremental maximum bending moment and deformation induced in the pre-existing bored tunnel after interaction with the new adjacent parallel bored tunnel.

9.8 Summary

A series of analyses to investigate the interaction between closely spaced bored tunnels has been performed in this chapter. Observations of the results demonstrate the interaction effects between closely spaced bored tunnels are significantly influenced by tunnel geometric parameters, soil and lining deformation properties and volume loss. In addition, the studies also identify the significant difference in the interaction mechanisms between stiff and flexible lining. The separation of the complex interaction effects into three fundamental interaction effects reveals the deficiency of applying the normalised moment and deformation expressions proposed by Peck et al. (1972) in the interpretation of incremental maximum bending moment and deformation for closely spaced bored tunnels. This limitation indicates the importance of establishing new normalised moment and deformation charts in the interpretation of volume loss effects. This is discussed further in Chapter 10.

CHAPTER 10 DESIGN CHARTS FOR ESTIMATING MAGNITUDE OF INTERACTION EFFECTS FOR CLOSELY SPACED TUNNELS

10.1 Introduction

The need for relatively simple design charts that could aid in the evaluation of the likely interaction effects between closely spaced parallel tunnels was established in Chapter 9, particularly for preliminary design purpose. These design charts must be able to account for the most significant parameters that influence the tunnel interaction behaviour and at the same time allow those parameters to be interpreted rapidly and accurately.

Peck (1969) proposed some general guidelines considering the ring load, bending moment and lining distortion of the first tunnel resulting from the passage of an adjacent second tunnel. However, the field measurements presented only accounted for certain lining stiffness and tunnel spacing. Soliman et al. (1993) introduced the diagrams of the relative changes in moment and displacements for parallel closely spaced double-tube tunnels in comparison with a single tunnel case. However, their solutions did not include the effects of volume loss and hence, the magnitude of interaction effects tend to be underestimated. Although a general review of the previous works in Chapter 3 demonstrates an extensive amount of field measurements and numerical analyses have been conducted for closely spaced tunnels, much of these results are difficult to correlate due to the site specific nature of the projects. Hence, the present research aims at developing a series of comprehensive design charts for estimating the magnitude of interaction effects induced in the pre-existing tunnel associated with the construction of a new adjacent parallel tunnel. Based on the following reasons, linear elastic model was adopted in generating the design charts:

1. Peck et al. (1972) plotted the results of the finite element calculation generated using linear elastic model in terms of thrust coefficient, moment coefficient and dimensionless diameter change for single shallow tunnel.

2. Kim (1996) adopted linear elastic model to generate results for comparison with results obtained from physical model tests for closely spaced tunnels in clay, where reasonably good agreements were observed.
3. Möller and Vermeer (2008) pointed out that the structural forces are less influenced by the choice of the constitutive model based on comparison made between the measured lining stresses and results of 2D numerical analyses for single tunnel.

The proposed design charts take into consideration of volume loss effects, tunnel geometric parameters as well as soil and lining deformation properties. Furthermore, the practicality of the design charts is explored by verifying the predicted results against seven published case histories.

10.2 Development of Design Charts

The proposed design charts were classified into two categories of interaction effects, namely, design charts for primary effect and design charts for volume loss effects. The former category of interaction effect is solely related with the deformation of tunnel lining, without considering the effects of volume loss whereas the latter is essentially related to the stress relief resulting from the volume loss that occurred during tunnel construction. Each category of design charts was normalised with representative parameters, as shown in Equations 10.1 to 10.4, to facilitate the interpretation of incremental maximum bending moment and lining deformation due to each interaction effect. It should be emphasized that the classification of design charts into two different categories for determining the incremental maximum bending moment and lining deformation is necessary (as discussed in Chapter 9) owing to the significant difference in the nature of interaction mechanisms between the two interaction effects.

Equations 10.1 and 10.2 were adopted in computing the incremental maximum bending moment ΔM_p as well as the change in the vertical and horizontal diameter ΔD_p resulting from the primary effect, where the interaction mechanisms are mainly governed by the deformation of two closely spaced parallel tunnels. It should be

noted that these parameters are consistent with those presented in the literature by Peck et al. (1972) for the single tunnel case. However, Equations 10.3 and 10.4 were proposed to account for the incremental maximum bending moment ΔM_{VL} as well as the change in the vertical and horizontal diameter ΔD_{VL} due to the volume loss effects, where the interaction mechanisms are governed by stress relief due to volume loss that occurred in both the pre-existing and new adjacent tunnels. The relative stiffness of the ground to the tunnel lining, defined as flexibility ratio (Peck et al., 1972), is shown in Equation 10.5.

Primary effect:

$$\Delta M_p = \frac{\Delta M_{\max}}{\gamma_s H R^2} \tag{10.1}$$

$$\Delta D_p = \frac{\Delta D_{H/V} M_c}{D \gamma_s H} \tag{10.2}$$

Volume loss effects:

$$\Delta M_{VL}(VL) = \frac{\Delta M_{\max} D}{E_l t^3} \tag{10.3}$$

$$\Delta D_{VL}(VL) = \frac{\Delta D_{H/V}}{D} \tag{10.4}$$

Flexibility ratio:

$$F = \frac{\frac{E_s}{(1+\nu)}}{\frac{6E_l I_l}{(1-\nu_l^2)} \frac{1}{R^3}} \tag{10.5}$$

In the above expressions, ΔM_P is the incremental maximum moment coefficient for primary effect; ΔD_p is the deformation coefficient for primary effect; ΔM_{VL} is the incremental maximum moment coefficient per unit volume loss for volume loss effects; ΔD_{VL} is the diameter change coefficient per unit volume loss for volume loss effects; F is the flexibility ratio; ΔM_{max} is the incremental maximum bending moment (positive sign corresponds to compression on the lining exterior; negative

sign corresponds to tension on the lining exterior); $\Delta D_{H/V}$ is the vertical (V) or horizontal (H) diameter change (positive value corresponds to an increase in tunnel diameter whereas negative value corresponds to the decrease in tunnel diameter); $\gamma_s H$ is the overburden pressure at tunnel level; R is the tunnel radius; D is the tunnel diameter; M_c is the constrained modulus which is assumed as 5/3 times the value of deformation modulus of soil, E_s (Peck et al., 1972); E_l is the deformation modulus of tunnel lining; t is the thickness of tunnel lining; VL is the volume loss in percentage; ν is the Poisson's ratio of the soil; ν_l is the Poisson's ratio of the tunnel lining; and I_l is the moment of inertia of the cross section per unit length along the axis of the tunnel.

10.3 Numerical Verification for Variation of Volume Loss

Comparisons of the results for incremental maximum bending moment, vertical and horizontal diameter change estimated using Equations 10.3 and 10.4 with the finite element computed results (FEM), for a range of volume loss cases varying from 0 per cent to 6 per cent are shown in Figure 10.1. An excellent agreement is observed for all the results and hence, affirms the validity of the proposed Equations 10.3 and 10.4 to determine the interaction effects of volume loss.

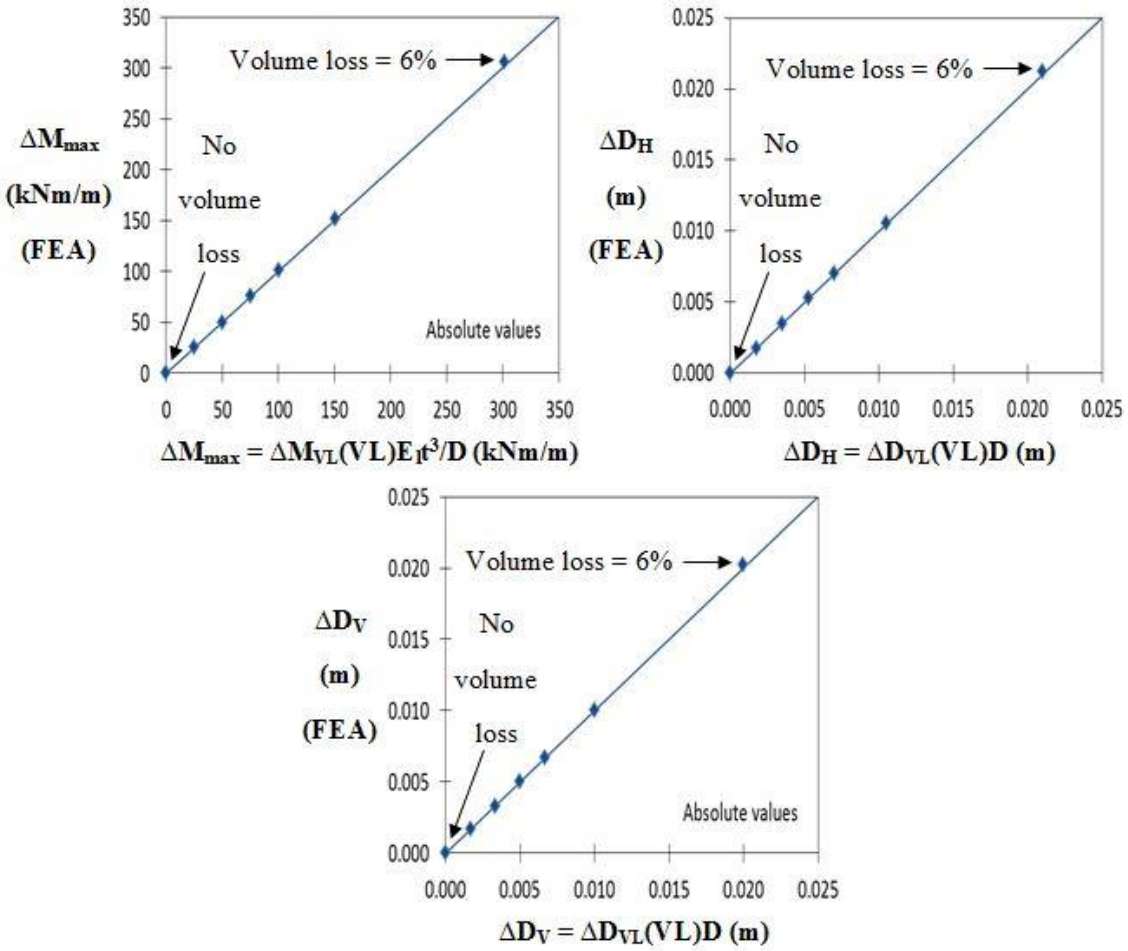

Figure 10.1 Comparison of (a) incremental maximum bending moment; (b) horizontal diameter change; and (c) vertical diameter change between FEM and Equations 10.3 and 10.4

10.4 Limiting Conditions for Design Charts

A series of finite element sensitivity analyses using the geometry shown in Figure 10.2 was conducted to define the limiting conditions for a range of parameters adopted in the design charts. From the results shown in Figure 10.3, the following are observed:

1. Figure 10.3(a) shows that both incremental maximum bending moment ΔM_{max} and diameter change $\Delta D_{H/V}$ increases as the dimensionless pillar width W/D between the two tunnels decreases. The critical W/D below which the ΔM_{max} and $\Delta D_{H/V}$ increases significantly is about 1.0, particularly for the flexible lining case.

2. The approximately linear trendline for ΔM_{max} and $\Delta D_{H/V}$ for dimensionless depth of burial H/D $\geq$ 2.0 in Figure 10.3(b) implies that the tunnel interactions have occurred in a fully buried condition. Hence, the adoption of H/D = 6.0 as the upper limiting boundary to account for the effect of depth factor is considered reasonable.
3. The relative stiffness, E_s/E_l was adopted to investigate the effects of lining flexibility on the magnitude of interaction effects. Increasing E_s/E_l increases ΔM_{max} and $\Delta D_{H/V}$ as shown in Figure 10.3(c). However, this variation becomes minimal once E_s/E_l is greater than 0.10. Therefore, it can be concluded that the adoption of E_s/E_l = 0.24, which corresponding to F = 400 to represent a perfectly flexible lining case in the design charts is sufficient.
4. As shown in Figure 10.3(d), increasing ν from 0.3 to 0.495 decreases the magnitude of interaction effects by about 20 percent for the flexible lining. This indicates that the long-term interaction effects for closely spaced parallel tunnels induce relatively larger ΔM_{max} and $\Delta D_{H/V}$ in the pre-existing tunnel as compared to the short-term interaction effects. However, the small variation of ΔM_{max} and $\Delta D_{H/V}$ with ν in Figure 10.3(d) reveals that the incremental interaction effects over the short-term are more critical as compared to the additional interaction effects that are generated over the long-term, for both the stiff and flexible lining cases. This observation is consistent with one of the experimental findings by Kim (1996). Hence, the design charts presented in this research only focus on the short-term interaction effects.
5. Both ΔM_{max} and $\Delta D_{H/V}$ are linearly related to K_o as shown in Figure 10.3(e). The formation of design charts based on K_o = 0.5 and 1.5, representing normally consolidated and overconsolidated ground as stated by (Peck et al., 1972), for primary effect enables ΔM_{max} and $\Delta D_{H/V}$ for other K_o to be estimated using linear interpolation.

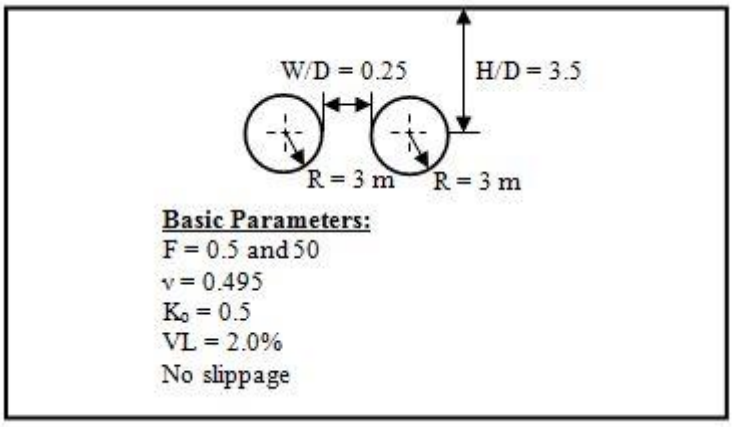

Figure 10.2 Illustrations of numerical model (reference case)

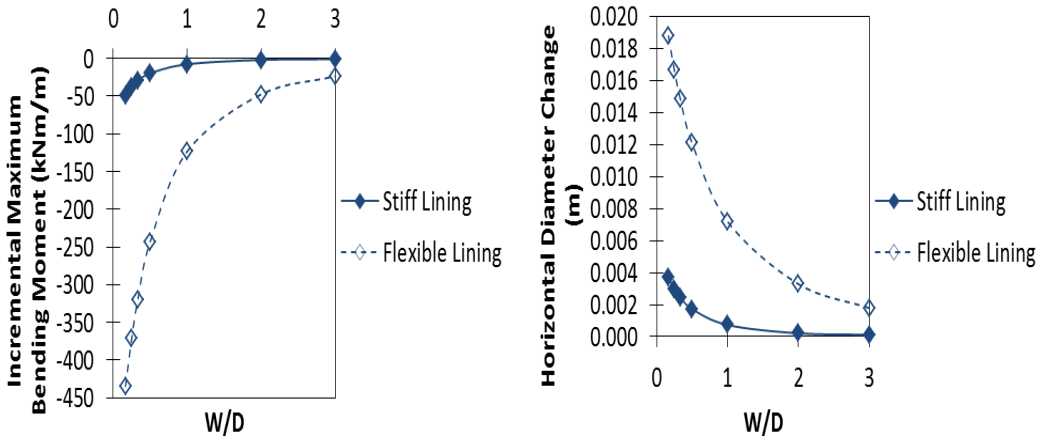

(a) Dimensionless pillar width (W/D)

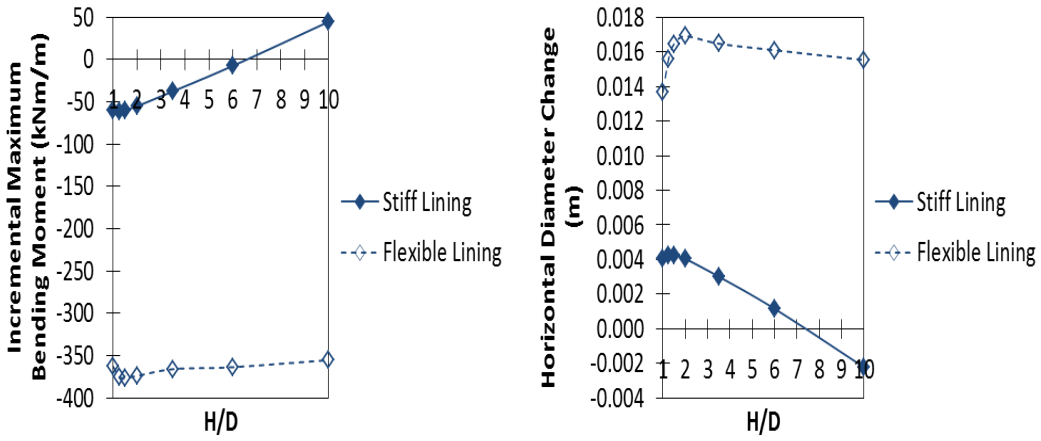

(b) Dimensionless depth of burial (H/D)

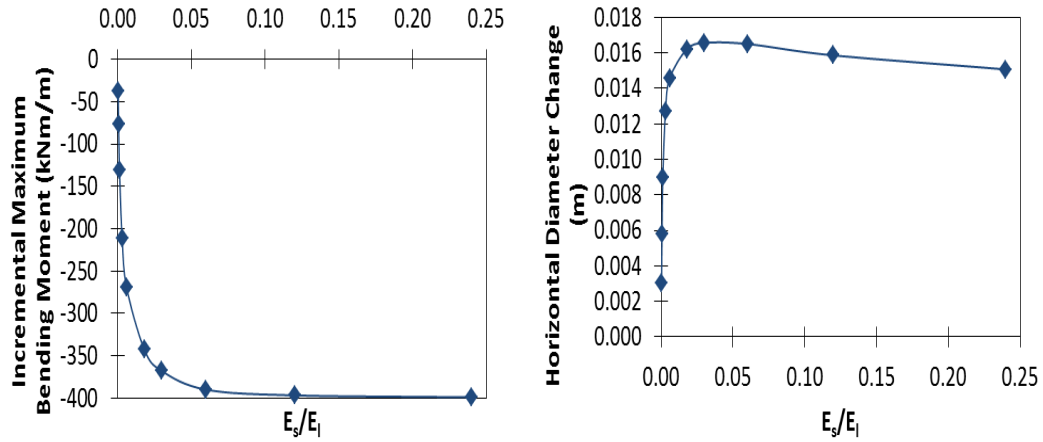

(c) Relative stiffness (E_s/E_l)

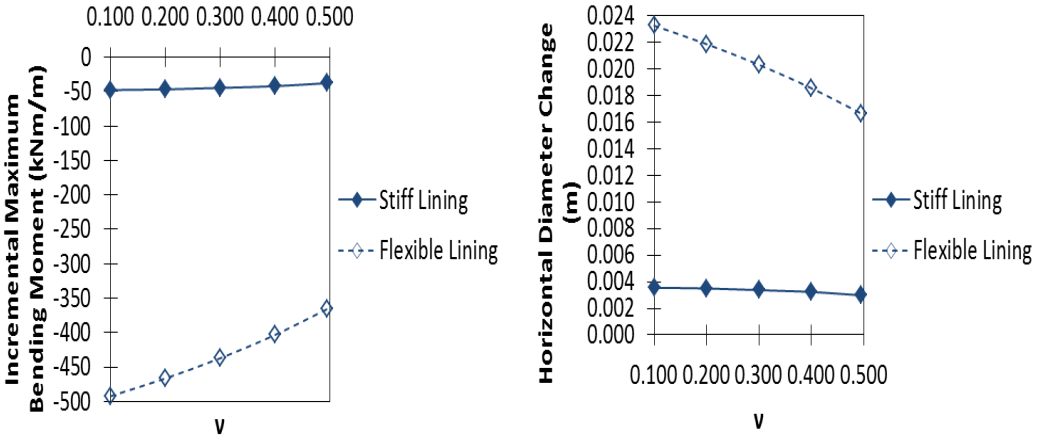

(d) Poisson's ratio of soil (ν)

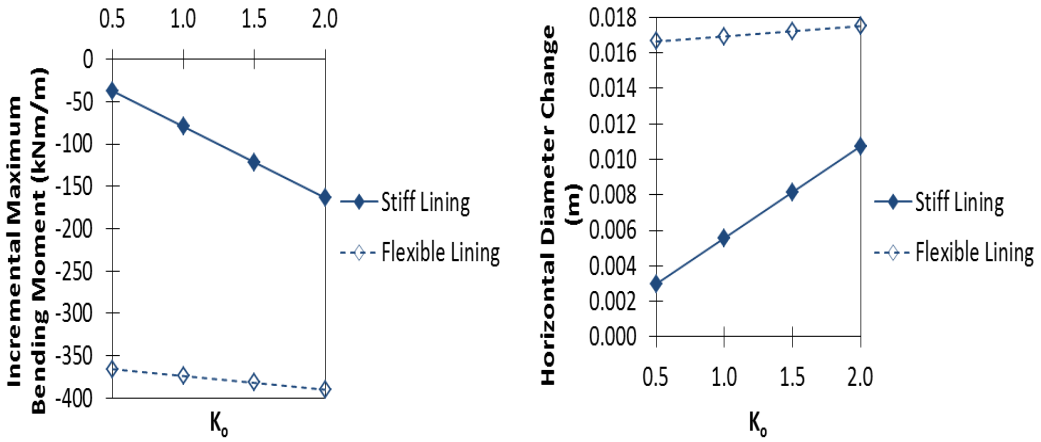

(e) K_o

Figure 10.3 Variations of magnitude of interaction effects with various factors (a) dimensionless pillar width (W/D); (b) dimensionless depth of burial (H/D); (c) relative stiffness (E_s/E_l); (d) Poisson's Ratio of Soil (ν); and (e) K_o

10.5 Design Charts

Based on the sensitivity analyses in Section 10.4, a series of design charts shown in Figures 10.4 to 10.9 (see Appendix C for more details) were established to determine the incremental maximum bending moment as well as vertical and horizontal diameter change of the pre-existing tunnel after interaction with the new adjacent parallel tunnel. The following points are highlighted in relation to the practicality of the design charts:

1. The design charts are given as a function of tunnel geometric parameters, soil and lining deformation properties as well as volume loss. The charts were prepared for F ranging from 0.5 to 400, W/D from 1/6 to 1.0, H/D from 1.0 to 6.0 and K_o of 0.5 and 1.5. These limiting boundaries cover the entire range of most practical combinations of the parameters for tunnel interaction.
2. The design charts for estimating the incremental maximum bending moment and diameter change due to volume loss effects are generated in terms of per unit volume loss in percentage. By applying Equations 10.3 and 10.4, both ΔM_{max} and $\Delta D_{H/V}$ due to volume loss effects can be calculated for any given

volume loss. This eliminates the need to generate a large number of design charts to account for different values of volume loss.

3. The design charts associated with volume loss effects are further classified into two subcategories, namely, design charts for volume loss effect of pre-existing tunnel and design charts for volume loss effect of new adjacent tunnel. This is practically important as it allows the possibility of assuming different workmanship quality and consequently different volume loss condition for each pre-existing and new adjacent tunnels. The total ΔM_{max} and $\Delta D_{H/V}$ due to volume loss effects for both pre-existing and new adjacent tunnels are equivalent to the summation of ΔM_{max} and $\Delta D_{H/V}$ computed from each subcategory using Equations 10.3 and 10.4.
4. The overall ΔM_{max} and $\Delta D_{H/V}$ induced in the lining of the pre-existing tunnel after interaction with the new adjacent tunnel are equivalent to the summation of each ΔM_{max} and $\Delta D_{H/V}$ computed from primary effect and volume loss effects.
5. To account for the three-dimensional (3D) effects of tunnel interaction, it would be a coherent approach to consider only the partial contribution of primary effect on the overall interaction effects. It is of interest to note in subsequent case studies that considerably encouraging agreements were achieved by assuming the realization of only 2/3 of the primary effect.

Primary Effect

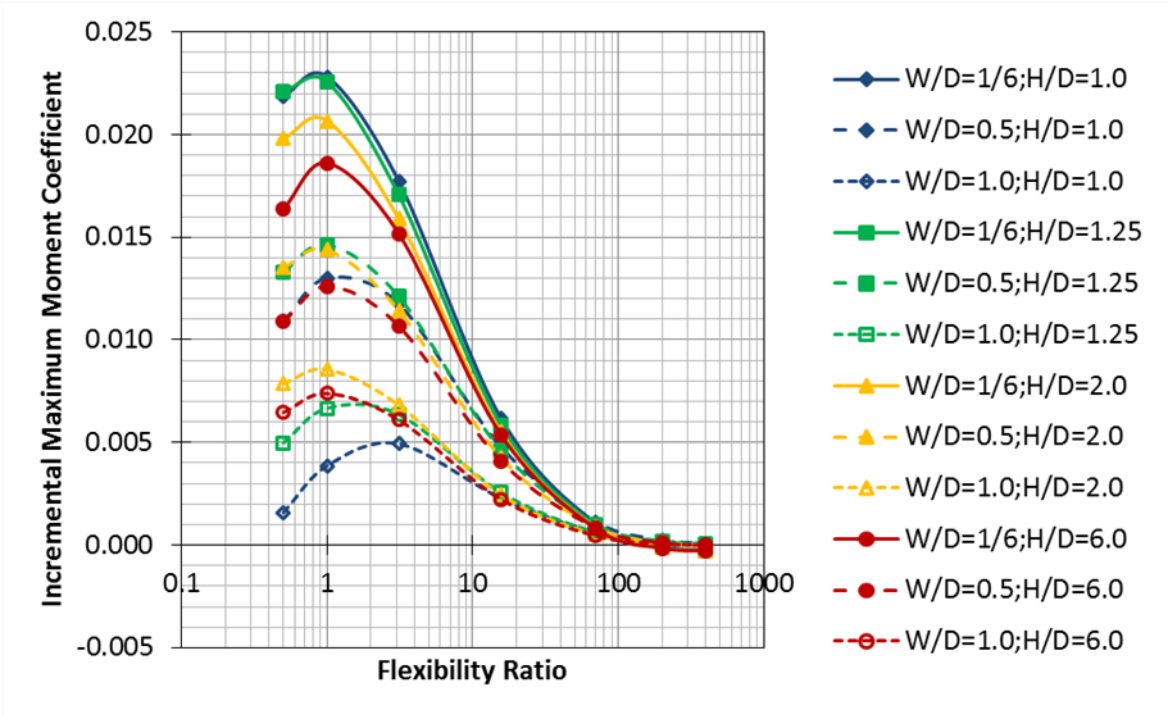

(a) K_o=0.5

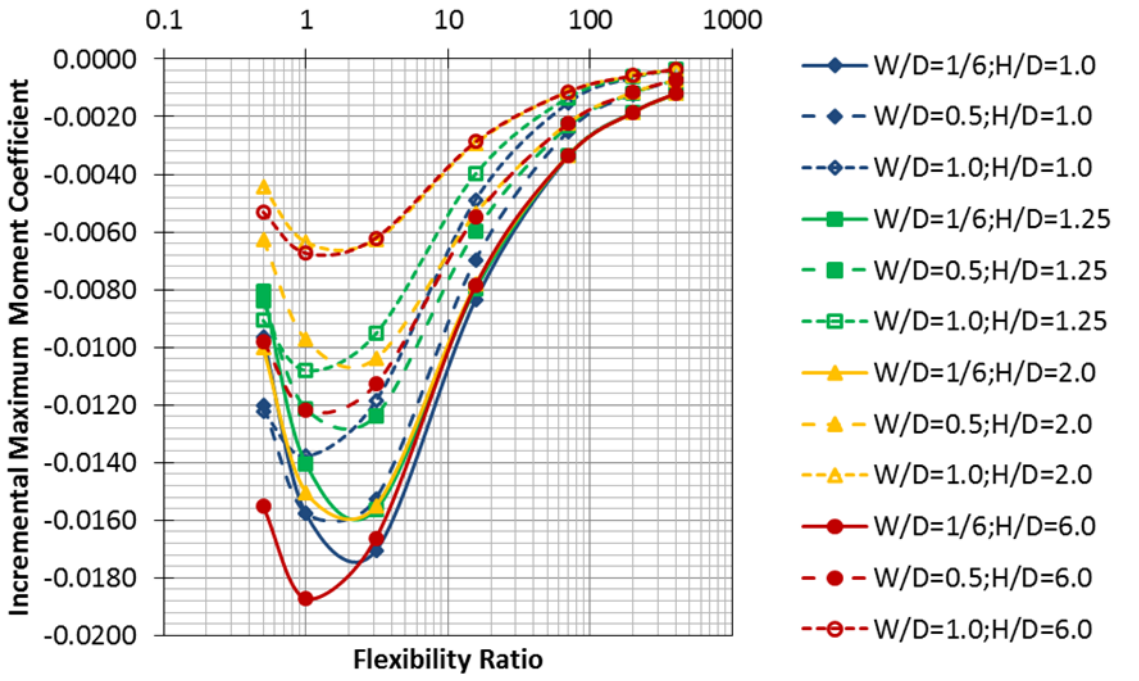

(b) K_o=1.5

Figure 10.4 Incremental maximum moment coefficient for primary effect ΔM_p

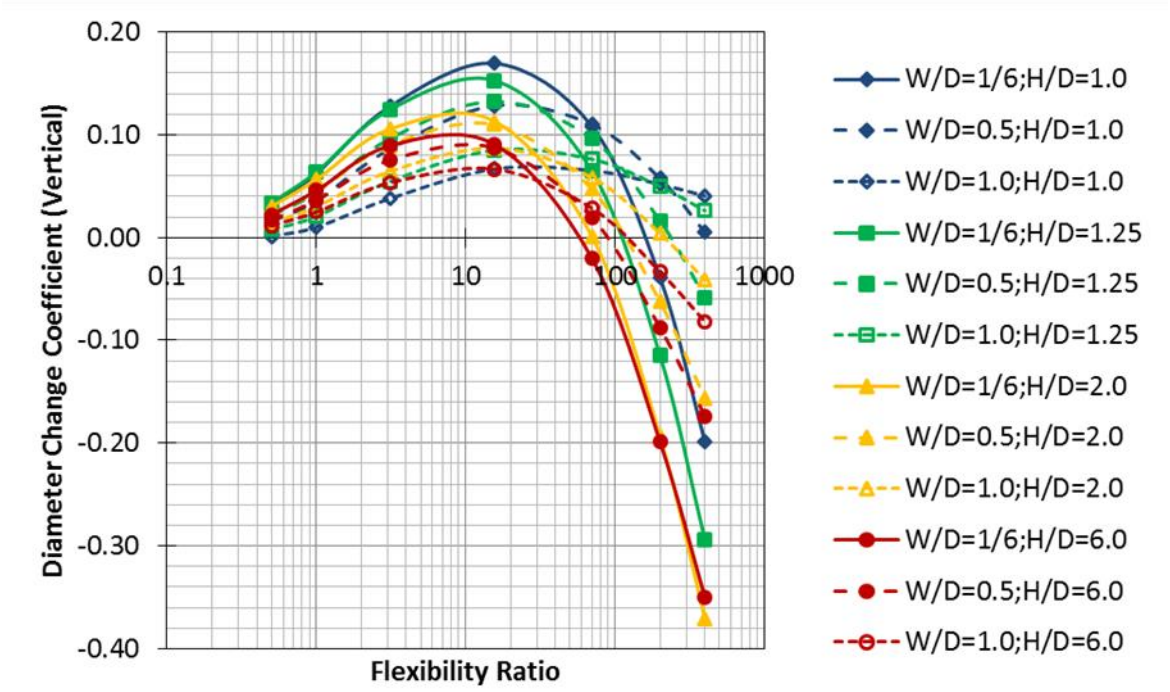

(a) K_o=0.5

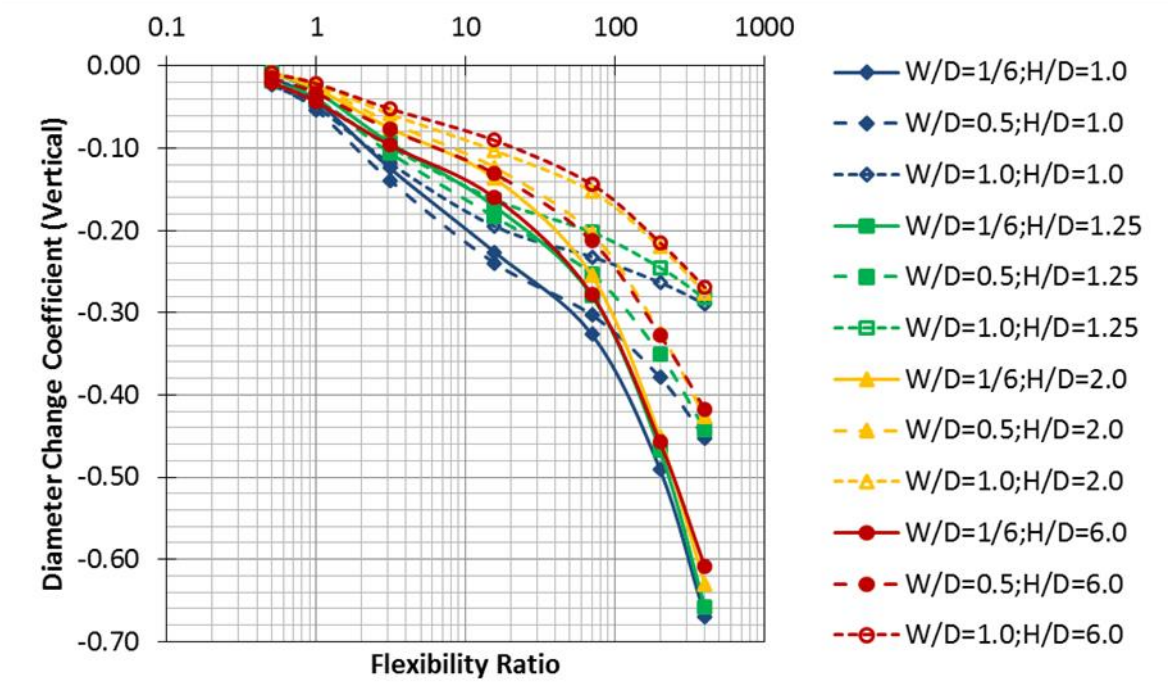

(b) K_o=1.5

Figure 10.5 Vertical diameter change coefficient for primary effect ΔD_p

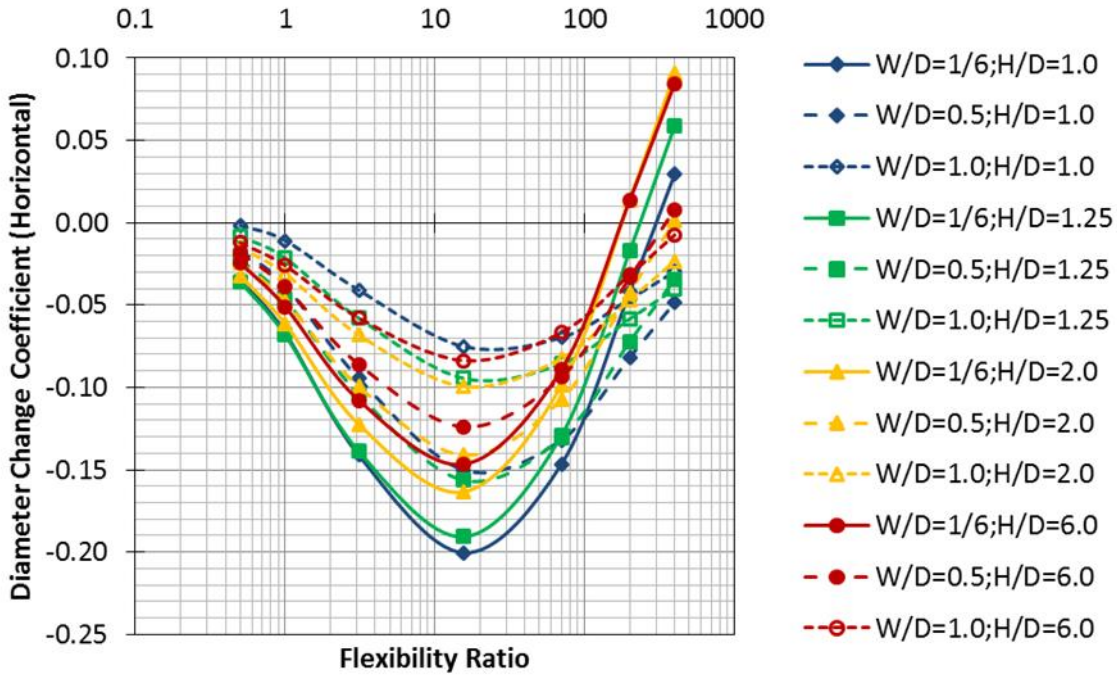

(a) K_o=0.5

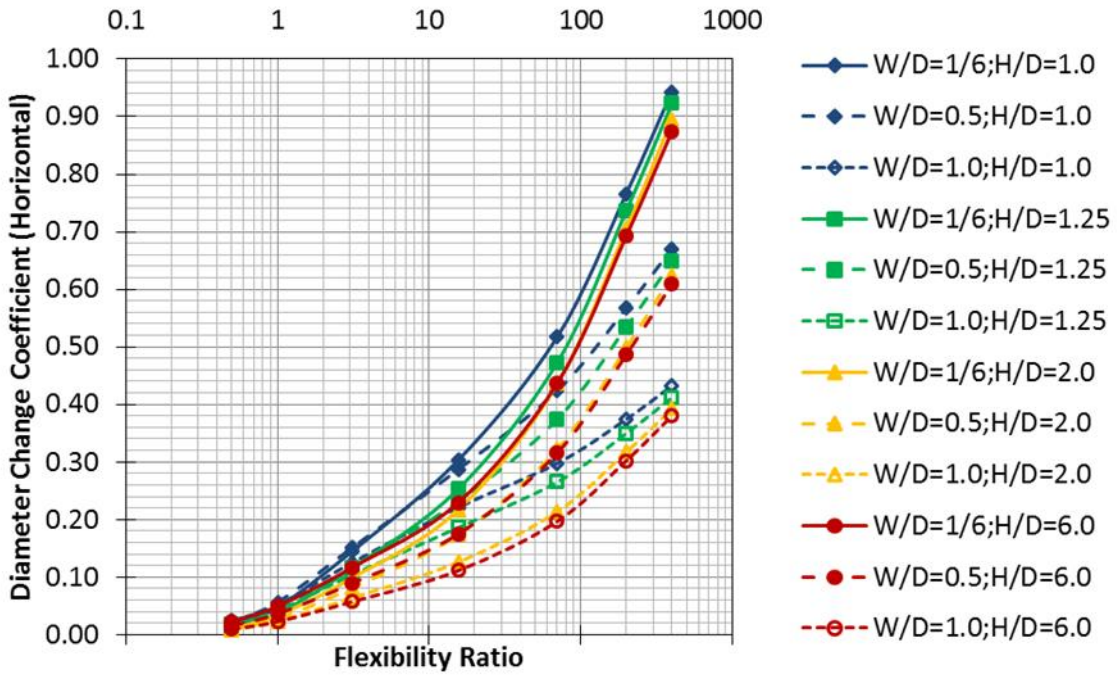

(b) K_o=1.5

Figure 10.6 Horizontal diameter change coefficient for primary effect ΔD_p

Volume Loss Effects

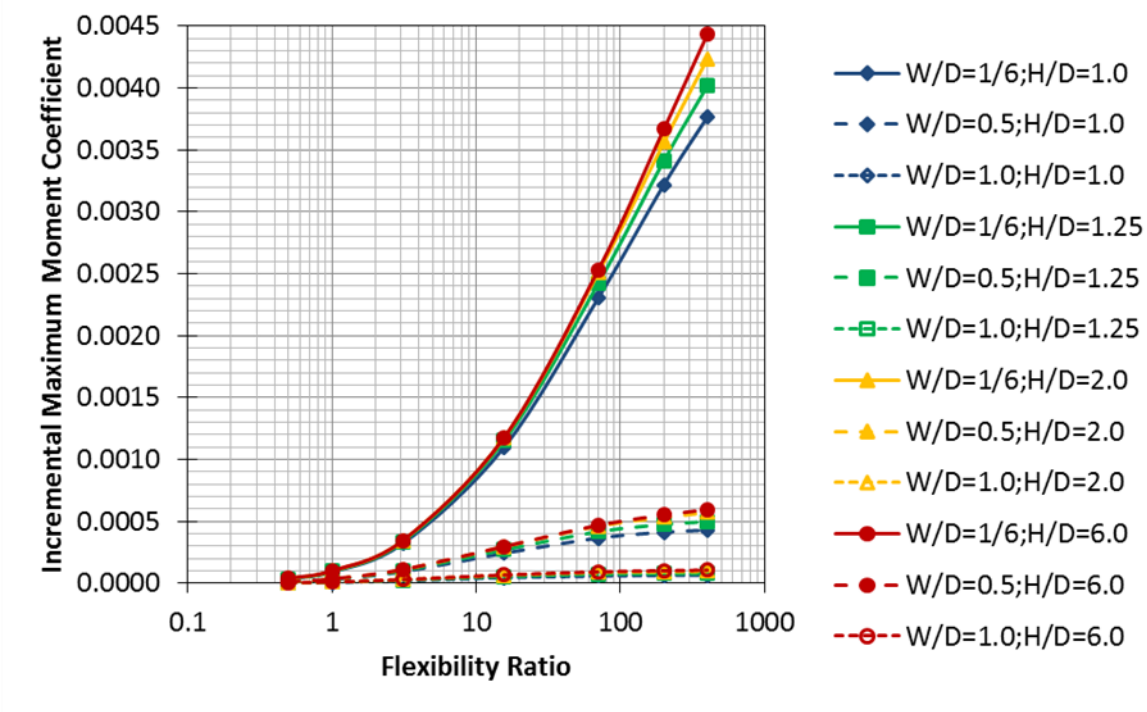

(a) Volume loss effect of pre-existing tunnel

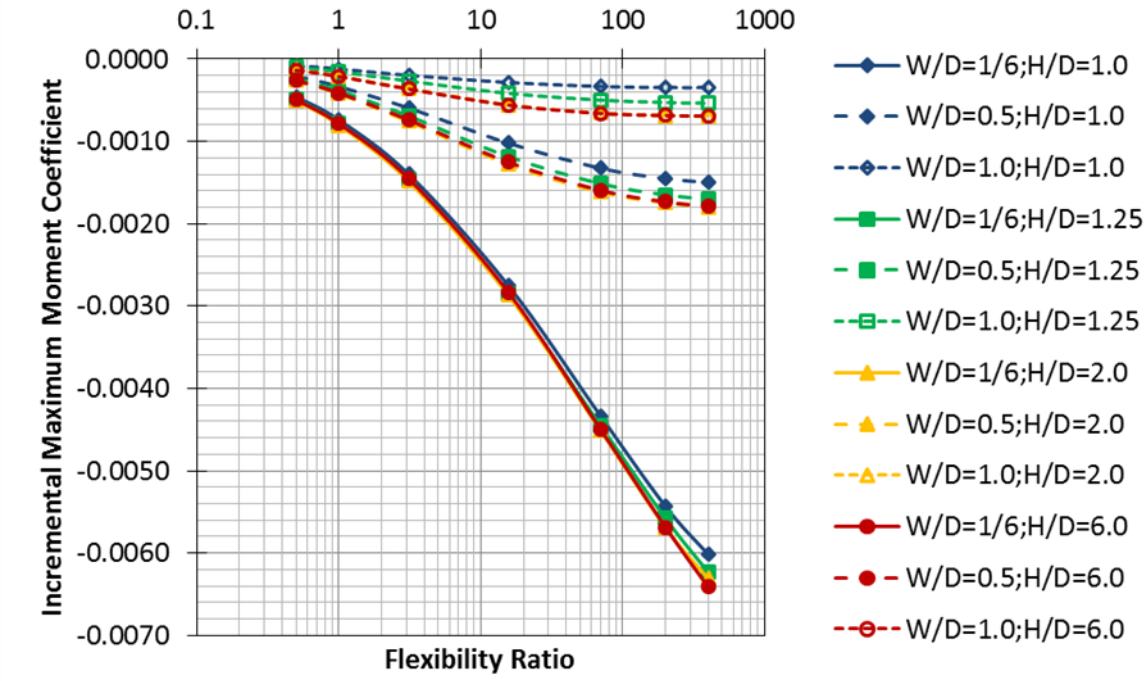

(b) Volume loss effect of new adjacent tunnel

Figure 10.7 Incremental maximum moment coefficient for volume loss effects ΔM_{VL}

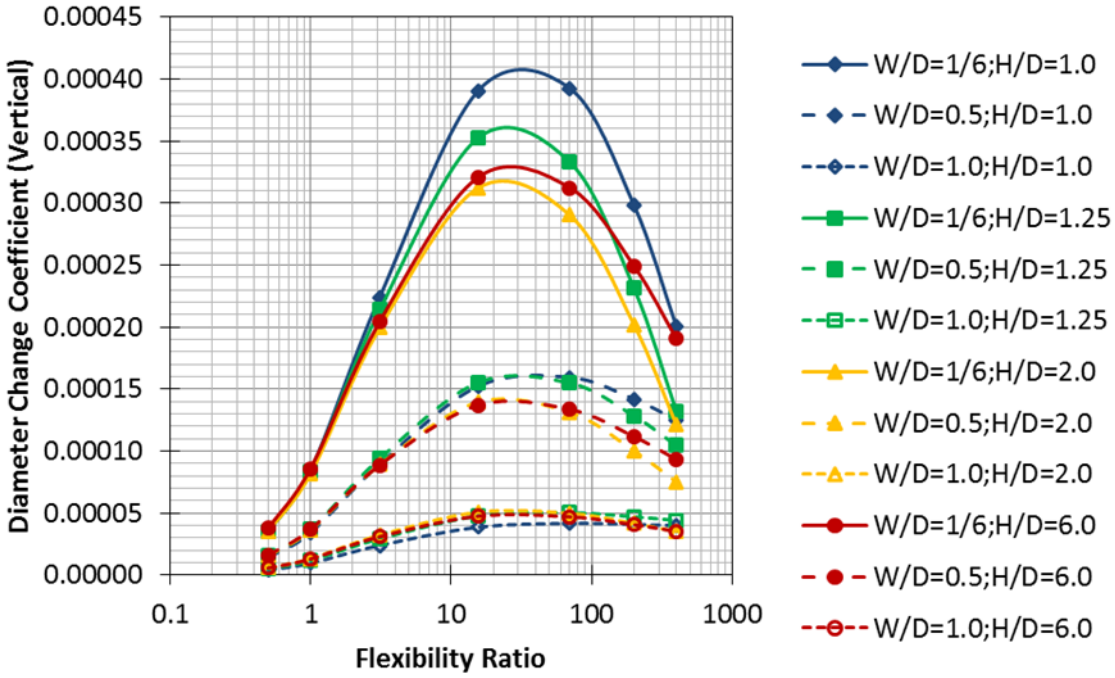

(a) Volume loss effect of pre-existing tunnel

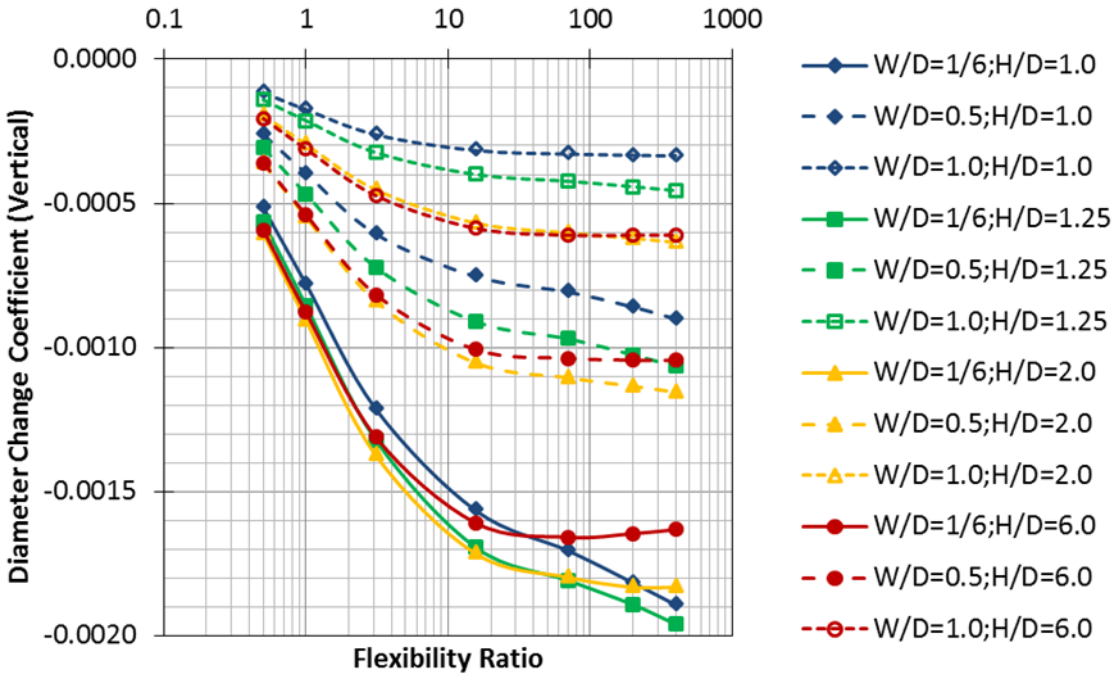

(b) Volume loss effect of new adjacent tunnel

Figure 10.8 Vertical diameter change coefficient for volume loss effects ΔD_{VL}

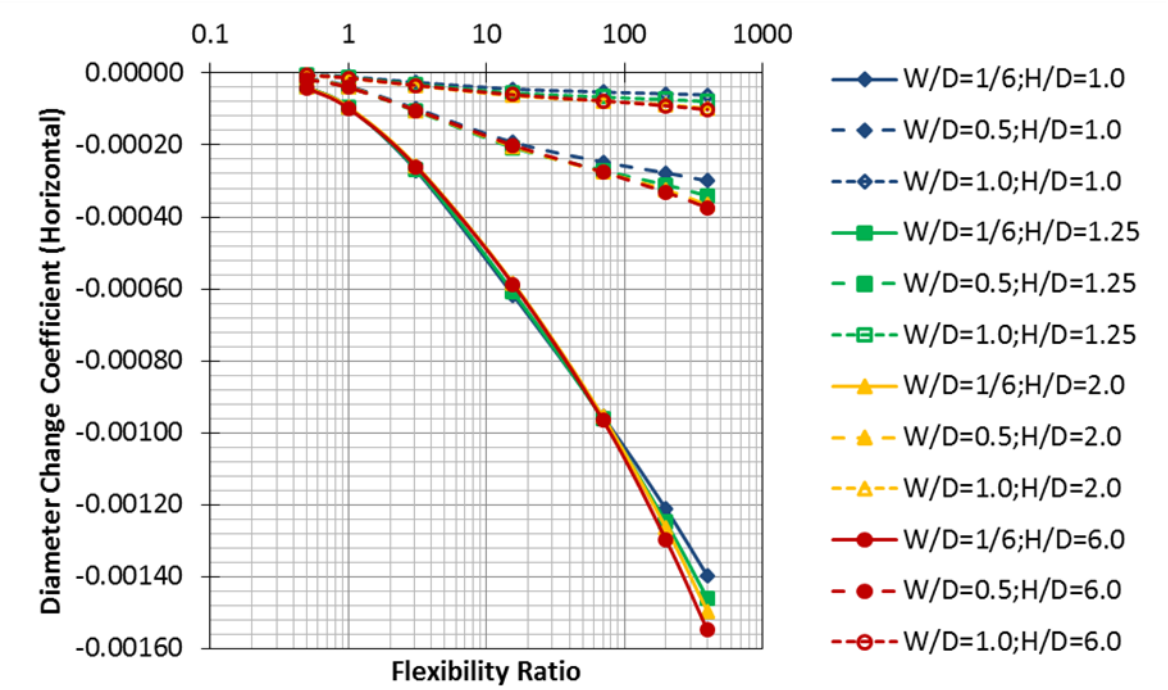

(a) Volume loss effect of pre-existing tunnel

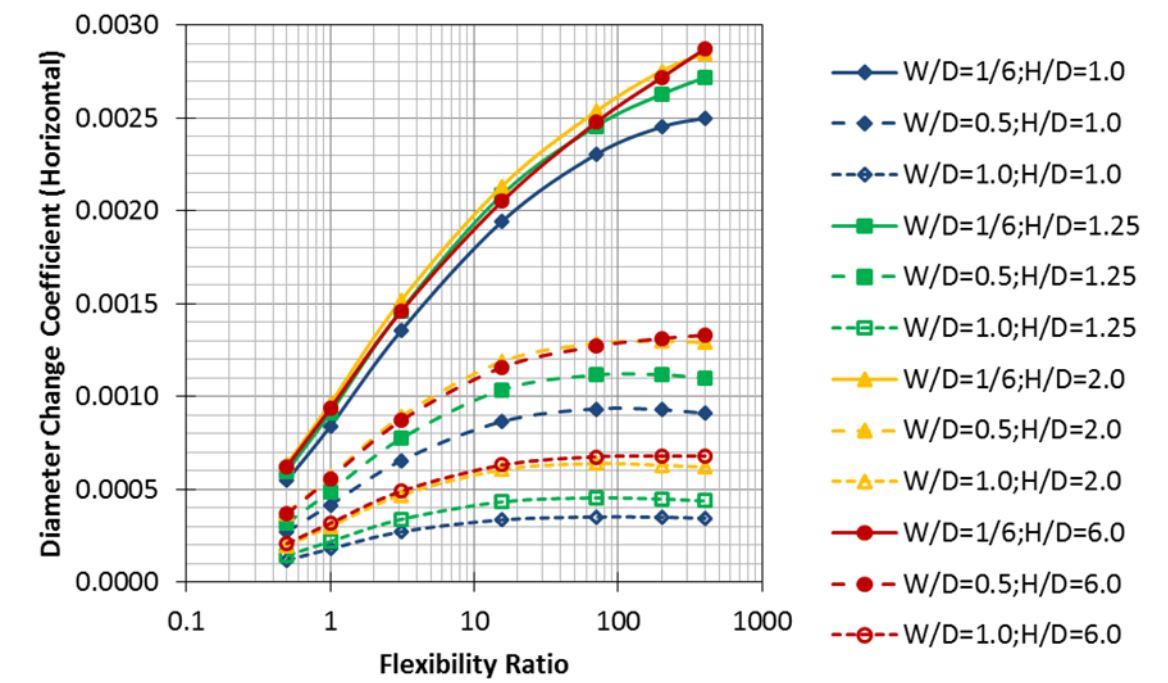

(b) Volume loss effect of new adjacent tunnel

Figure 10.9 Horizontal diameter change coefficient for volume loss effects ΔD_{VL}

10.6 Case Studies

The applicability of the proposed design charts was validated through evaluation of a total of seven published case histories including laboratory scale model test. These case histories encompass a significant range of volume loss, lining flexibility, W/D and H/D ratios as summarised in Table 10.1. The predicted and measured horizontal and vertical diameter changes as well as incremental maximum bending moment induced in the pre-existing tunnel after interaction with the new adjacent tunnel are compared in Figures 10.10 to 10.14.

Table 10.1 Summary of case histories

Cases	Tunnel Geometric Parameters		Lining Properties		Soil Properties		Volume Losses (%)	References
	H/D	W/D	t (m)	E_l (MPa)	γ_s (kN/m^3)	E_s (MPa)		
Victoria Line, U.K. (Grey iron)	24 / 4.04	0.61 / 4.04	0.0616	89635	20	130	1.0 - 1.4	Ward (1969)
Victoria Line, U.K. (Ductile iron)	24 / 4.04	0.61 / 4.04	0.0452	165480	20	130	1.0 - 1.4	Ward (1969)
Victoria Line, U.K. (Cut ductile iron)	24 / 4.04	0.61 / 4.04	0.0285	165480	20	130	1.0 - 1.4	Ward (1969)
Victoria Line, U.K. (Concrete)	26 / 4.04	2.4 / 4.04	0.23	37922.5	20	130	1.0 - 1.4	Ward and Thomas (1965)
NATM Trial Tunnel, U.K.	28 / 5.35	5 / 5.35	0.15	25000	20	100	0.5 - 1.1	Kimmance et al. (1996)
Northern Line Tunnel, U.K.	21 / 7.0	5.8 / 7.0	0.11	170000	20	100	0.5 - 1.1	Kimmance et al. (1996)
Parallel Tunnel Test PS3	5.57 (With surcharge) / 0.07	0.028 / 0.07 0.070 / 0.07	0.000356	210000	16.7	12.42	≈ 6	Kim (1996)

10.6.1 Case 1: Victoria Line, U.K. (Ward, 1969; Ward and Thomas, 1965)

Cast Iron Segments

A full scale experiment to compare the structural performance of tunnel linings of different flexibility during the construction of Victoria Line at Brixton was reported by Ward (1969). The properties of the three different cast iron linings are summarised in Table 10.1. The running tunnels of 4.04 m diameter were parallel to

each other at a pillar width of about 0.6 m and the depth of the tunnels was approximately 24 m in the London Clay. The average unloading Young's modulus of London Clay at Site O as reported by Ward et al. (1959) was adopted in this case study. This Young's modulus is chosen after considering the unloading mechanisms involved during tunnelling and the originally very stiff nature of the London Clay. In addition, the K_o value of 1.5 was assumed for the London Clay. This value was from the upper-bound profile given by Hight and Higgins (1995) for London Clay between 10 m and 30 m below the ground surface, as reported in the literature by Franzius et al (2005).

Ward (1969) reported that the ground loss estimated from the underground observations at another section of the Victoria Line at Brixton was about 0.18 m^2, equivalent to volume loss of 1.4 per cent for a 4.04 m diameter tunnel. However, the ground loss obtained from the surface observations near to the above underground observations were about 0.13 m^2 and 0.47 m^2, equivalent to volume loss of 1.0 per cent and 3.7 per cent respectively. After considering the possible errors due to the disturbance on the natural reference points in the streets (Ward, 1969), a more representative lower bound of the volume loss values of 1.0 per cent and 1.4 per cent were adopted as a range in predicting the lining deformations of the pre-existing tunnel due to the volume loss effect of new adjacent tunnel and volume loss effect of pre-existing tunnel.

Figure 10.10 shows the predicted and measured lining deformations for various types of tunnel lining. The measured and predicted horizontal diameter changes of the pre-existing tunnel were generally in good agreement, except for the lining that was made of grey iron, where the horizontal diameter change was slightly overpredicted by the proposed design charts. In addition, a relatively conservative predicted vertical diameter changes as compared to field measurements are also observed, but the trends for both the predicted and measured profiles are very similar.

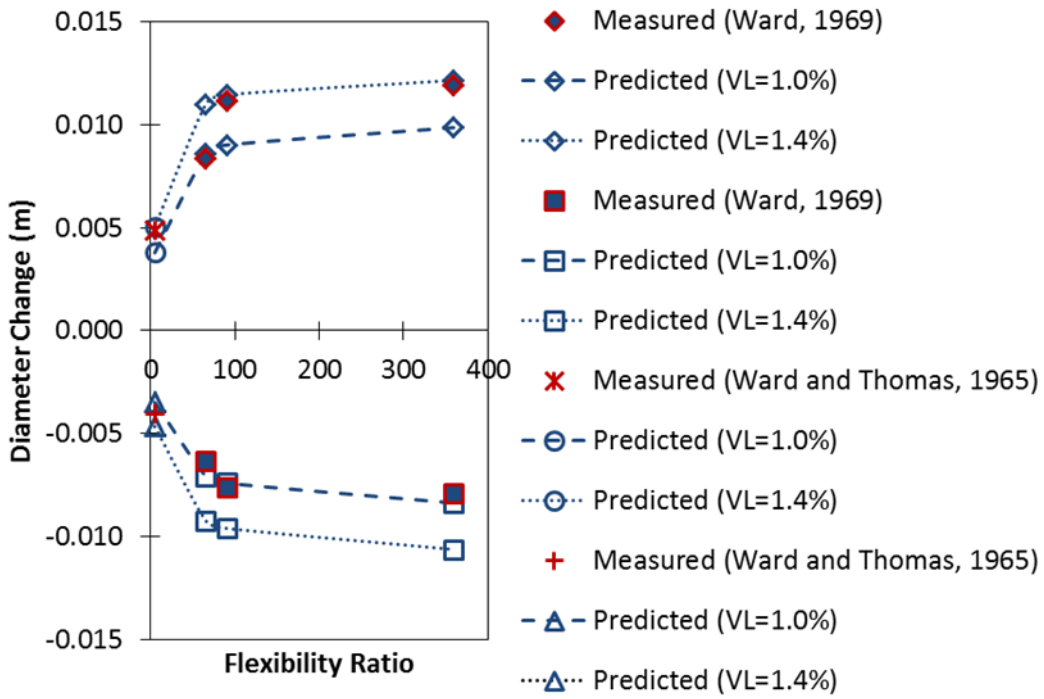

Figure 10.10 Measured and predicted horizontal and vertical diameter change for Victoria Line, U.K. (Ward, 1969; Ward and Thomas, 1965)

Concrete Segments

Ward and Thomas (1965) reported the field measurements observed from another experimental portion of the Victoria Line. These particular tunnels were lined with precast concrete segments with the properties of the concrete lining summarised in Table 10.1. The running tunnels of 4.04 m diameter were parallel to each other at a pillar width of about 2.4 m and the depth of the tunnels were approximately 26 m in the London Clay. The average unloading Young's modulus of the London Clay at Site O (Ward et al., 1959) was adopted in this study owing to the similarity of the London Clay properties to those at Site O (Ward and Thomas, 1965). In addition, the K_o value of 1.5 was assumed for the London Clay.

The volume losses similar to those reported for the cast iron linings were adopted to predict the deformations in the precast concrete lining after interaction with the new adjacent parallel tunnel. It can be seen from Figure 10.10 that the predicted lining deformations of the precast concrete lining are in very good agreement with the field measurements.

10.6.2 Case 2: Contract 104 - London Bridge Station, U.K. (Kimmance et al., 1996)

NATM Trial and Jubilee Line Extension (JLE) West Bound Tunnels

Kimmance et al. (1996) reported the deformations developed in closely spaced tunnels for Contract 104, London Bridge Station of the Jubilee Line Extension (JLE). The JLE West Bound Tunnel was constructed at a pillar width of about 5 m with the NATM Trial Tunnel at a depth of approximately 28 m in the London Clay, as summarised in Table 10.1. These tunnels were 5.35 m in average diameter and had a thickness of about 0.15 m. The Young's modulus for shotcrete and London Clay were 25 GPa and 0.1 GPa respectively as suggested by Kimmance et al. (1996). In addition, the K_o value of 1.5 was assumed for the London Clay.

Two volume losses, i.e. VL of 0.5 per cent and 1.1 per cent, were adopted to predict the lining deformations due to the volume loss effect of the newly excavated adjacent JLE West Bound Tunnel and volume loss effect of the pre-existing NATM Trial Tunnel. These values correspond to the lower and upper bound of the typical volume losses estimated from the surface observations during the construction of JLE running tunnels using NATM/SCL method (Standing and Selman, 2001).

The predicted lining deformations based on the proposed design charts are shown in Figure 10.11, together with those measured and predicted by Kimmance et al. (1996) using a simplified approach developed by Soliman et al. (1993). As shown in Figure 10.11, the predicted horizontal diameter change using the proposed design charts is in good agreement with the field measurement, although the vertical diameter change is slightly underpredicted based on an average volume loss of 0.8 per cent.

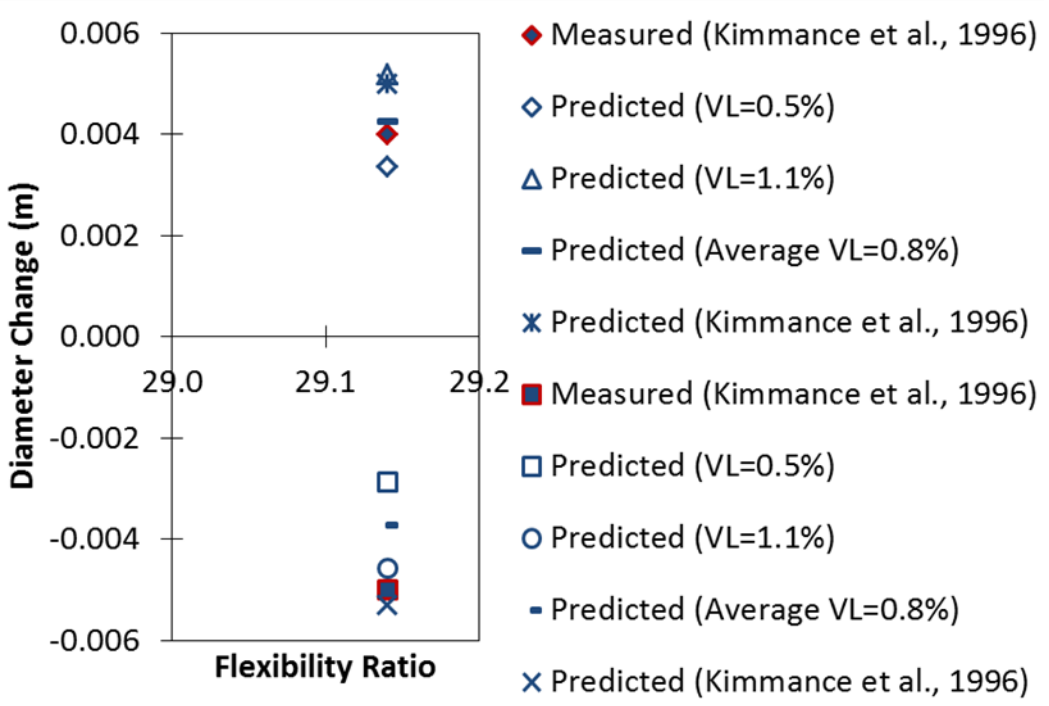

Figure 10.11 Measured and predicted horizontal and vertical diameter change for NATM Trial Tunnel (Kimmance et al., 1996)

Northern Line Tunnels

The JLE Project at London Bridge also involved the excavation of a new Northern Line Tunnel at a pillar width of about 5.8 m parallel to the existing Northern Line Tunnel. The depth of the tunnels was approximately 21 m in the London Clay, with the properties summarised in Table 10.1. The pre-existing Northern Line Tunnel of 7 m diameter was lined with cast iron lining with an effective thickness of 0.11 m and Young's modulus of 170 GPa (Kimmance et al., 1996) while the spheroidal graphite iron (SGI) lining with Young's modulus of approximately 170 GPa was adopted for the new 8 m diameter tunnel. In addition, the K_o value of 1.5 was assumed for the London Clay.

Figure 10.12 compares the measured and predicted lining deformations using the proposed design charts, together with the predictions made by Kimmance et al. (1996) based on the approach developed by Soliman et al. (1993). The small difference between the measured and predicted results suggests that a good estimation of the lining deformation is achieved using the proposed design charts.

In addition, it is worth noting that the present proposed method of prediction using the design charts differs significantly from the approach developed by Soliman et al. (1993). Observations of the predicted results published by Kimmance et al. (1996) demonstrate that the horizontal diameter changes predicted for closely spaced tunnels are generally smaller than those predicted for single tunnel, which is contrary to the finding by Soliman et al. (1993) that the lateral outward deformation of the first tunnel caused by driving the second tunnel are much larger than in case of a single tunnel. Furthermore, the approach developed by Soliman et al. (1993) which does not consider the effects of volume loss also excludes the effects of K_o and hence imposing restrictions on the determination of the magnitude of interaction effects.

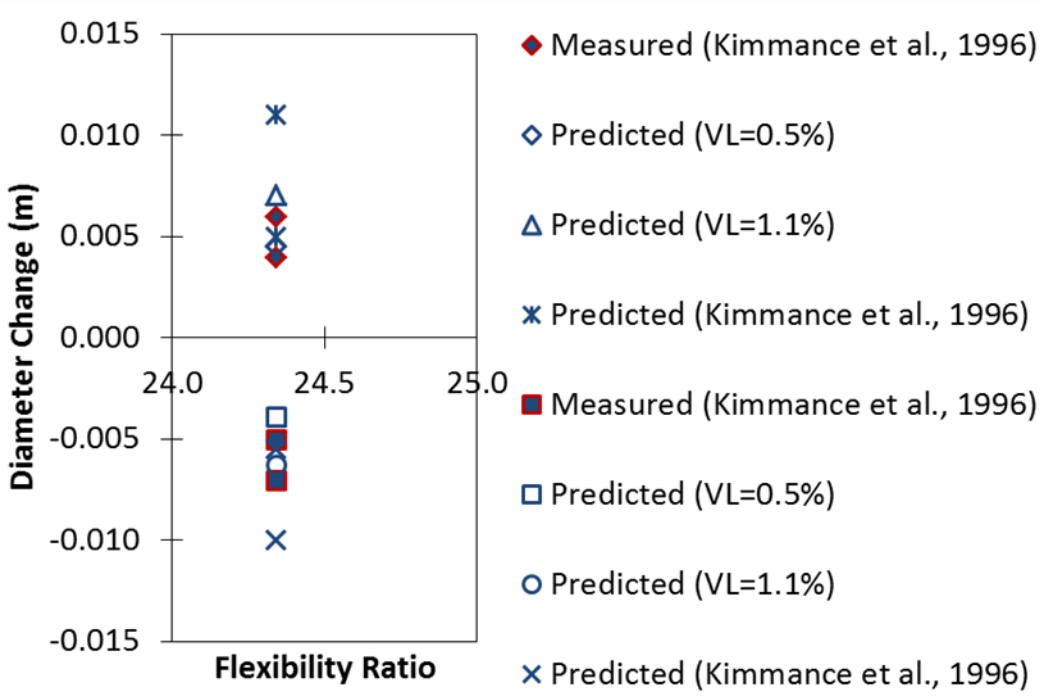

Figure 10.12 Measured and predicted horizontal and vertical diameter change for pre-existing Northern Line Station Tunnel (Kimmance et al., 1996)

10.6.3 Case 3: Physical Model Test (Kim, 1996)

Parallel Tunnels Test (PS3)

Kim (1996) conducted a laboratory scale physical model test to investigate the interaction between closely spaced parallel tunnels in clay. A set of five parallel tunnel tests, i.e. PS1, PS2, PS3, PS4 and PS3R were carried out using samples of kaolin clay in a plane strain setup. However, comparisons between measured and predicted results were mainly focused on test PS3, as highlighted in the literature by Kim et al. (1996).

The clay samples were prepared by consolidating the kaolin slurry within the test rig. A surcharge was applied to a stress-controlled boundary on top of the clay sample to provide the required OCR value of 1.0 for test PS3 as well as to simulate the behaviour of a tunnel that is distant from the ground surface. The tunnel linings consisted of plain steel tubes of approximately 0.07 m in diameter with thickness of 0.000356 m. All the geometric parameters as well as soil and lining properties for test PS3 are summarised in Table 10.1.

It should be noted that three tunnels were installed in test PS3. The ‘distant’ (second) tunnel and subsequently ‘close’ (third) tunnel were positioned at a pillar width of 1.0D and 0.4D respectively away from the first tunnel. Kim (1996) assumed that the interaction effects measured during the installation of ‘close’ tunnel were unaffected by the previous installation of the ‘distant’ tunnel. In addition, all tunnels were installed using a model tunnelling machine that was designed to simulate the construction of a full scale shield tunnel. The rotary cutting head of the tunnelling machine was oversized slightly to produce a volume loss of approximately 6 per cent.

The predicted lining deformations and incremental maximum bending moment for test PS3 are shown in Figures 10.13 and 10.14 respectively, together with the test measurements and results of finite element back analyses as reported by Kim

(1996). The test measurements and the predicted lining deformations using the proposed design charts are generally in good agreement, as shown in Figure. 10.13.

Figure 10.14 shows that the proposed design charts underpredicted the incremental maximum bending moment for the 'close' tunnel case. Similarly, a less satisfactory prediction is observed for the 'distant' tunnel case, although the agreement between the predicted and result of finite element back analysis (Kim, 1996) is encouraging. This underprediction may be possibly due to the disagreement between the volume loss of approximately 6 per cent (Kim, 1996) adopted in the predictions and the actual volume loss occurred during the test. This explanation is reasonable due to the fact that all the test measurements for the 'distant' tunnel case are consistently larger than those predicted, as shown in Figures 10.13 and 10.14.

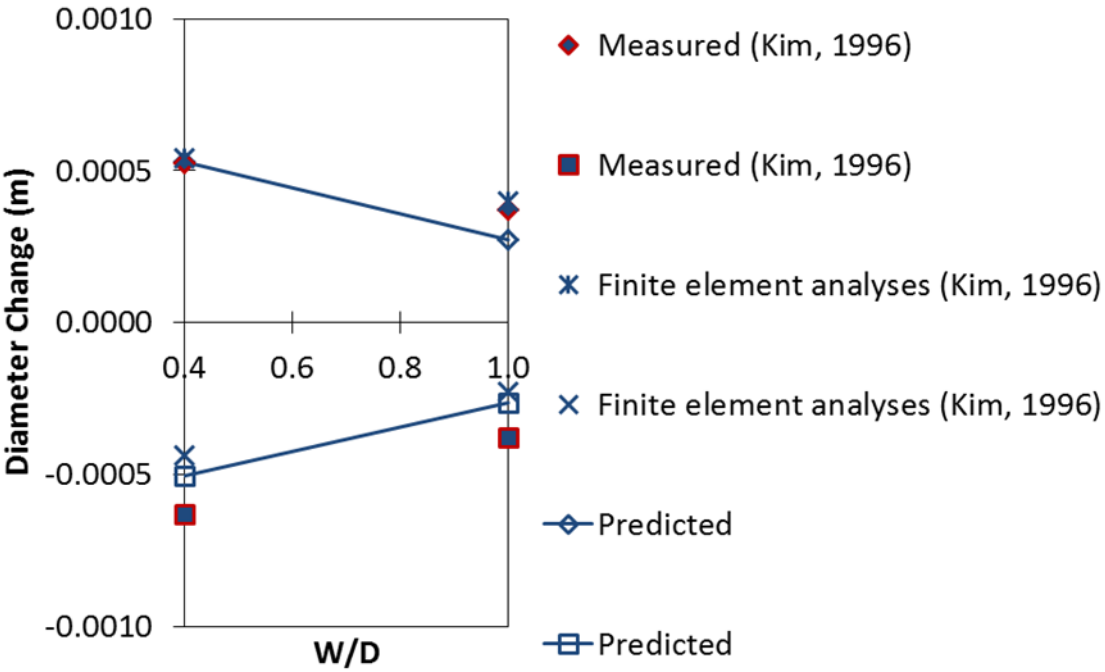

Figure 10.13 Measured and predicted horizontal and vertical diameter change for PS3 (Kim, 1996)

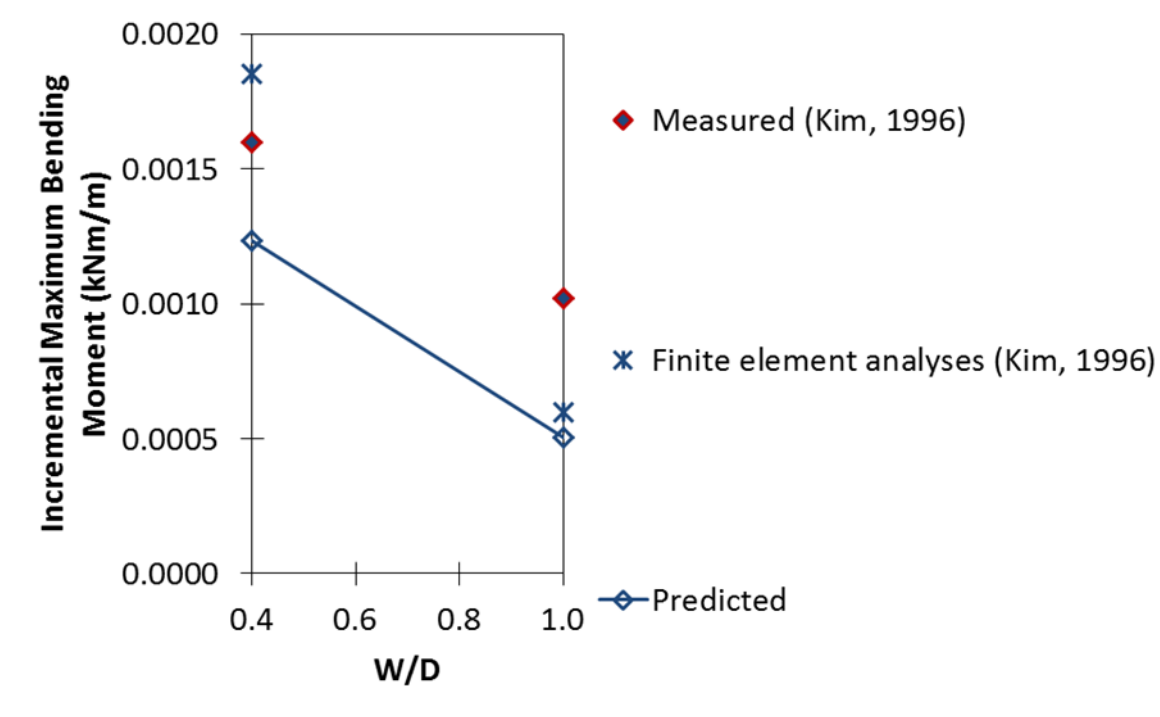

Figure 10.14 Measured and predicted incremental maximum bending moment for PS3 (Kim, 1996)

10.7 Summary

A series of design charts have been developed to determine the incremental maximum bending moment and lining deformation of the pre-existing tunnel after interaction with the new adjacent tunnel. The design charts are classified into primary effect and volume loss effects and are able to account for the significant difference in interaction mechanisms. The design charts for volume loss effects, together with the proposed dimensionless parameters allow the determination of incremental maximum bending moment and lining deformation due to any given volume loss. In addition, the further separation of the design charts for volume loss effects into volume loss effect of pre-existing tunnel and volume loss effect of new adjacent tunnel allows different volume loss to be practically assumed for each tunnel excavation. The adoption of the flexibility ratio to account for various lining flexibility also bridges the gap between a perfectly rigid and a perfectly flexible lining adopted for tunnel interaction analysis. The good agreement between the predicted results and the field measurements from a total of seven published case

histories has affirmed the general validity of the proposed design charts. Validation of the case studies also justifies the simplifying assumption that the soil is linear elastic will give reasonable results. Hence, the proposed design charts are believed to be useful as a rapid and inexpensive tool for preliminary design considerations as well as for interpretation of field monitoring results.

CHAPTER 11 ANALYSIS OF JOINTED TUNNEL LINING

11.1 Introduction

The precast segmental lining is used as ground support in many bored tunnelling projects. However, the influence of joints between the lining segments on the stresses induced in the tunnel lining is often neglected. In most cases, a continuous tunnel lining is assumed in the design of the segmental tunnel lining. This may lead to an overestimation of the stresses induced in the lining, which in turn may affect the construction costs. In this chapter, previous research relevant to the study of stresses induced in both the continuous and jointed tunnel lining are first reviewed. The results of finite element analyses in which the joints are modelled are then presented.

11.2 Morgan's Design Method

Morgan (1961) proposed a method of analysis that relates the effects of stiffness of the lining to the characteristics of the ground. His theoretical study considered the state of stress around the tunnel due to its construction and its influence on the elliptical deformation and bending moment of the tunnel lining, as shown in Figure 11.1. For permanent support to the ground consisting of granular soil, he suggested that the design active loading on the flexible arch of a tunnel may be calculated by taking into account the effect of arching in the ground. For a circular tunnel in clay, the equilibrium pressure between the clay and the lining will tend to approach the swelling pressure of the clay and is modified by local release due to lining deformation. The state of stress about a circular tunnel in rock is considered by assuming the ground is an elastic body obeying Hooke's law. The maximum distortions and hence the maximum bending moment occur at points on the springline, crown and invert. Equations are developed for calculating the incremental radial loading against the extrados of the lining for the case where the ground is continuous for a long distance along the line of the tunnel and assuming no strain occurs in this direction; bending moment in the lining due to passive

loading against ground; bending moment in the lining due to active loading; and relationship between the maximum bending moments in the continuous lining of constant section and the assumed active loading were established. In addition, hoop load at axis and crown of the lining may be evaluated for the cases in which the ground surrounding the existing tunnel is subjected to a variation in external loading. The stability of the articulating linings was considered where the external pressure between ground and lining and at the state of collapse of a tunnel can be calculated through an equation incorporating the mean elastic modulus of soil. It should be pointed out that the larger modulus of elasticity of the ground will lead to lower stress induced in the lining for single tunnel case and hence, saving in the cost of the lining could be achieved. However Morgan's analysis omitted the shear stresses between the lining and the ground.

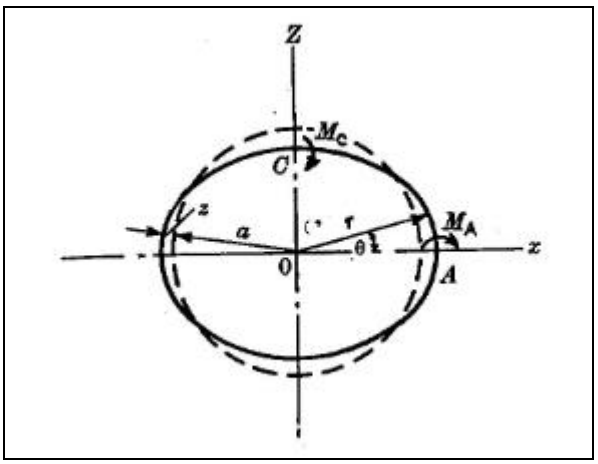

Figure 11.1 Elliptical deformation of a circular tunnel lining (after Morgan, 1961)

11.3 Muir Wood's Design Method

Muir Wood (1975) modified Morgan's method and corrected the error assumed by Morgan (1961) that the plane strain entailed plane stress which led to higher value for the coefficient of ground reaction. A modified equation for maximum bending moment was established. The incorporation of the stiffness ratio (Muir Wood, 1975) representing the ratio of the stiffness of the tunnel lining (to deformation in the 'elliptical' mode) to that of the surrounding ground led to the reduction in bending moment to be carried by the lining. In addition, the introduction of the

shear force between the ground and the lining by Muir Wood also leads to a further reduction in the maximum bending moment in the lining. Corresponding to the direct compression of the lining, Muir Wood proposed that the stress in elastic ground around a circular tunnel would cause a change in uniform normal ground/lining pressure and thus the radial deflection, would give rise to compression in the lining. The compressibility factor is defined as the compressibility of the tunnel in relation to that of the surrounding ground. It was pointed out that this compressibility factor is not the same as the compressibility ratio of Peck et al. (1972) (see Equation 11.2) which considers the cylinder of ground displaced by the tunnel. A high compressibility factor reduces the loading on the tunnel lining. A general guideline has also been proposed by Muir Wood for the determination of initial state of stress, in particular, by adopting the intermediate between the intact and perforated condition of the surrounding earth pressure.

In addition, Muir Wood also proposed that for a lining that is composed of equal segments, n_e, the effective moment of inertia, I_e can be expressed as:

$$I_e = I_j + (\frac{4}{n_e})^2 I_l \qquad (I_e \leq I_l,\ n_e > 4) \qquad (11.1)$$

where I_e is the effective value of I_l; I_j is the second moment of area at the joint; and n_e is the number of equal segments and that $I_j << I_l$ for an expanded and articulating lining. The I_e is used to calculate the stiffness ratio.

Since Muir Wood assumed that the initial earth pressure acting around a tunnel is of an ‘elliptical’ shape, as illustrated in Figure 11.2, the load around the tunnel will have two maxima and two minima. For four or fewer segments, Muir Wood suggested that the existence of joints may not affect the ring stiffness. However, for an increasing number of equal segments n_e, the I_j may be appreciably less than I_l and thus reducing the bending moment of the lining.

The bending moments in a lining are related to the effects of shear forces between ground and lining, the stiffness ratio and the effects of joints in a lining whereas direct radial loading of a tunnel is related to its compressibility factor. Considering these factors may lead to a reduction of stresses induced in the tunnel lining.

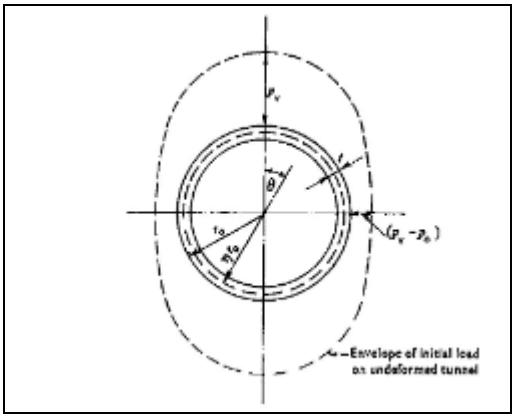

Figure 11.2 Reference diagram for initial loading on tunnel prior to deformation (after Muir Wood, 1975)

11.4 Peck et al.'s Design Method

Peck et al. (1972) suggested that a flexible liner interacts with the surrounding soil in such a way that the pressure distribution on the liner and the corresponding deflected shape result in negligible bending moment at all points in the lining whereas a rigid liner is one which deflects insignificantly under the load imposed by the soil and thus there is very little soil-structure interaction. They pointed out that the magnitude of the thrust and moment is affected by the stiffness of the lining relative to that of the soil medium and to the depth of the tunnel.

According to Peck et al. (1972), flexible liners do not have to be designed for moments consistent with the initial stress distribution in the soil. But the liner must be designed to accommodate the diameter changes and the corresponding bending moments. For rigid liners, the coefficient of earth pressure at rest is usually estimated and the bending moments and thrusts are calculated on the assumption of no interaction between the soil and the liner. They suggested that the tunnel liners

of intermediate stiffness must consider the soil-structure interaction and must yield design moments and design thrusts as functions of liner stiffness.

Both compressibility ratio C_r and flexibility ratio F were introduced and are used in Peck et al.'s equations for the preliminary design of deep tunnel. The compressibility ratio is a measure of the extensional stiffness of the medium relative to that of the liner as shown in Equation 11.2. Flexibility ratio is a measured of the flexural stiffness of the medium relative to that of the liner as shown in Equation 10.5.

$$C_r = \frac{\dfrac{E_s}{(1+\nu)(1-2\nu)}}{\dfrac{E_l t}{(1-\nu_l^{\,2})}\dfrac{1}{R}} \tag{11.2}$$

where E_s is the deformation modulus of soil, ν is the Poisson's ratio of soil, E_l is the deformation modulus of tunnel lining, t is the thickness of tunnel lining, ν_l is the Poisson's ratio of tunnel lining and R is the tunnel radius.

The moment coefficient is proposed by Peck et al. (1972) in the interpretation of moment for two values of K_o. The moment coefficient is a function of the flexibility ratio and it was found that the decrease of moment coefficient is very substantial for a flexibility ratio of less than 10 and hence, indicates that the liner behaves relatively flexible with respect to the soil medium for flexibility ratio greater than about 10.

The proposed thrust coefficient as by Peck et al. (1972) is found to be relatively insensitive to the flexibility ratio but is sensitive to the initial value of K_o. It was also observed that the thrust coefficient is practically the same for all flexibility ratios greater than 10 which indicates that the tunnel liners with flexibility ratio greater than 10 as flexible liner. The thrust coefficient decreases as the compressibility ratio increases.

The diameter changes of the tunnel are primarily a function of the flexibility ratio, the difference in the free-field principal stresses and the modulus of the soil medium and are influenced to a minor extent by the compressibility ratio. Dimensionless diameter change as shown in Equation 10.2 was proposed by Peck et al. (1972) to interprete diameter changes for two values of K_o at various flexibility ratios. It was also observed that the diameter changes approach constant values when the flexibility ratio exceeds 10 which indicate that the deformations are primarily governed by the soil and are very little influenced by the structural liner and thus concluded that tunnel liners with flexibility ratio greater than 10 acts as flexible liners.

For shallow tunnel, the results of the finite element calculation that are plotted in terms of thrust coefficient, moment coefficient and dimensionless diameter change are shown in Figure 11.3. Peck et al. (1972) showed in Figure 11.3(a) that the maximum thrust coefficient occurs at the springline and is relatively insensitive to the flexibility and compressibility ratios for a K_o value of 0.5. The thrust coefficient increases as the depth of burial increases and approaches the fully buried condition at a dimensionless depth of burial H/D of 1.5. For a K_o value of 2.0, the thrust coefficient at the invert is sensitive to the stiffness of the tunnel lining and the thrust coefficient decreases as the dimensionless depth of burial increases. The fully buried condition occurs at a dimensionless depth of burial of about 1.5.

Referring to Figure 11.3(b), Peck et al. (1972) showed that the moment coefficient is a function of the flexibility of the tunnel liner for a K_o value of 0.5. The moment coefficient increases with dimensionless depth of burial and approaches fully buried condition at a dimensionless depth of burial of about 1.5. The difference observed for a K_o value of 2.0 is that the moment coefficient decreases as the dimensionless depth of burial increases. In addition, the moment coefficient is more sensitive to the stiffness of the tunnel liner. However, the moment coefficient reaches the same fully buried condition at a dimensionless depth of burial of about 1.5.

For the dimensionless displacement coefficient from the finite element solutions versus the dimensionless depth of burial as shown in Figure 11.3(c), Peck et al. (1972) showed that the largest diameter change takes place on the horizontal diameter and increases with increasing dimensionless depth of burial to a constant value for dimensionless depth of burial greater than 1.5, for a K_o value of 0.5. However, the largest diameter change takes place on the vertical diameter for a K_o value of 2.0 and the dimensionless displacement decreases as the dimensionless depth of burial increases.

These solutions that can account for the interaction between the soil and the liner have led to a reduction in stresses in the lining.

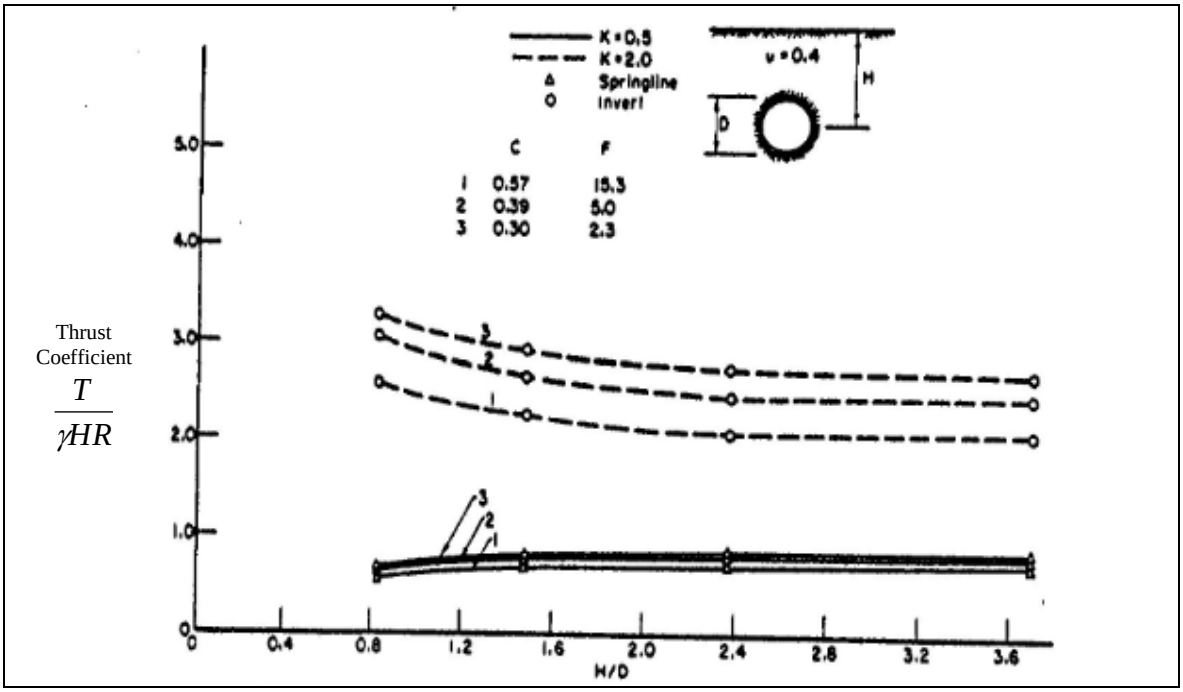

(a)

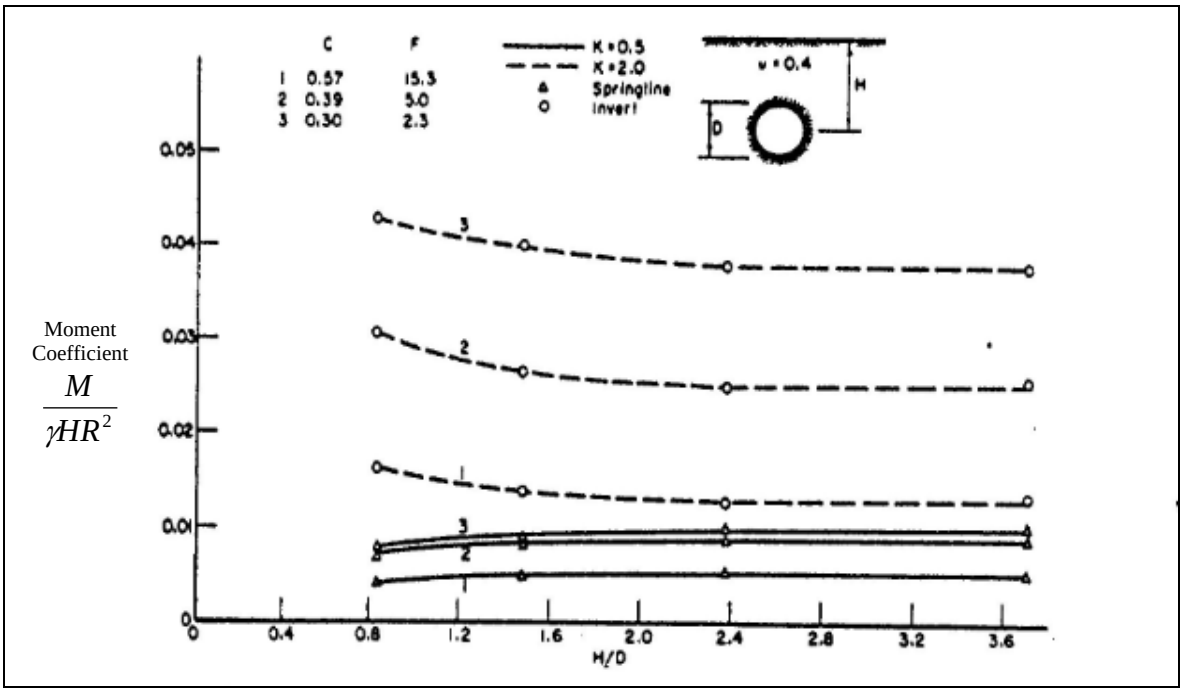

(b)

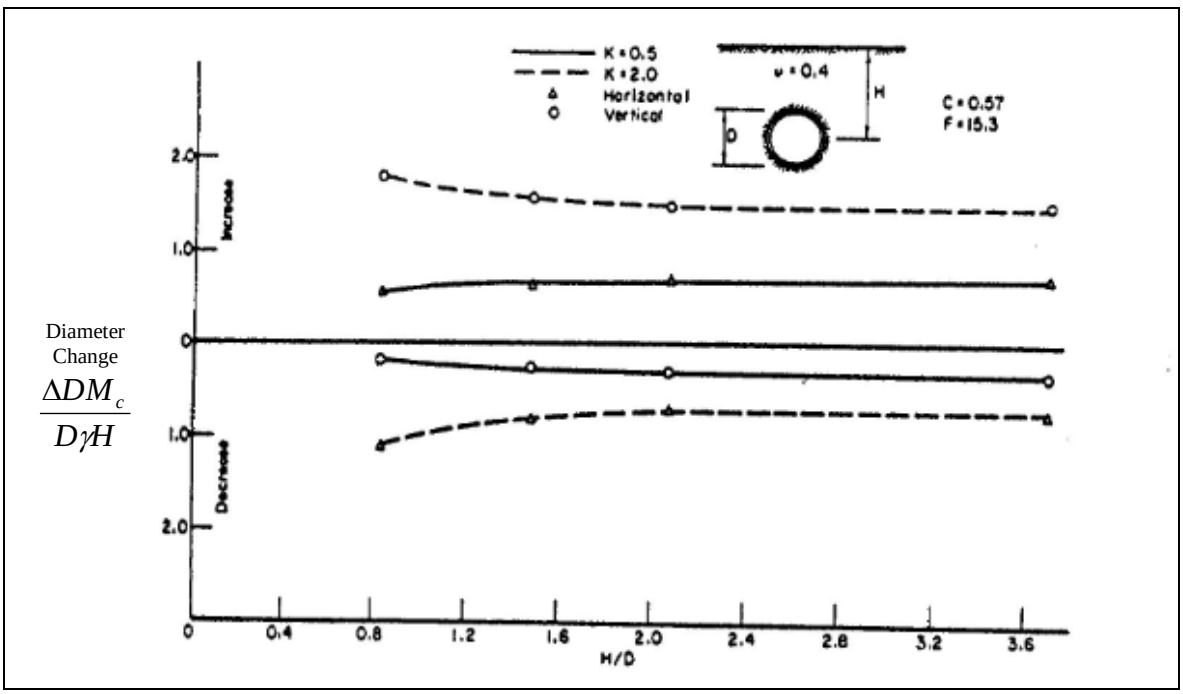

(c)

Figure 11.3 Variation of (a) thrust coefficient; (b) moment coefficient; and (c) diameter change with depth of burial (after Peck et al., 1972)

11.5 Lee et al and Lee and Ge's Design Method

Lee et al (2001) presented an analytical solution for the prediction of internal forces and displacements of a jointed segmental precast circular tunnel lining. The force method is used to determine the internal forces and displacements of the jointed tunnel lining. Lee and Ge (2001) presented a new method of determining the correction factor to approximate a jointed, shield-driven tunnel lining as a continuous ring structure under plane strain conditions. In the proposed model as illustrated in Figure 11.4, the tunnel lining is thus considered as a continuous ring with a discounted rigidity by applying a reduction factor η to the bending rigidity of the actual tunnel lining E_lI_l as shown in Equation 11.3.

$$\eta = \frac{(E_l I_l)_e}{E_l I_l} \tag{11.3}$$

where $(E_lI_l)_e$ is the effective bending rigidity of the equivalent continuous tunnel.

The main factors affecting the effective rigidity ratio are joint stiffness, soil resistance, joint distribution, number of joints and tunnel geometry and are summarised in Table 11.1. Inspection of this table indicates that both joint stiffness ratio and number of joints have significant influence on the effective rigidity ratio. While increasing joint stiffness ratio will result in an increase in the effective rigidity ratio and thus an increase in the bending moment induced in the tunnel lining, the opposite is true if the number of joints were to increase. Other than the joint distribution, the soil resistance coefficient of less than 30000 kN/m^3 has also been found to have an insignificant influence on the bending moment induced in the tunnel lining. The tunnel geometry is a basic parameter to be considered in design. Depending on the total number of joints, the selection of the relevant thickness is crucial since a reduction in thickness may lead to an increase in the bending moment for a 3-joint tunnel whereas the favourable reverse response may be observed for a 4-joint tunnel. In addition, it has also been observed that the bending moment induced in the tunnel lining increases with increasing radius of the tunnel.

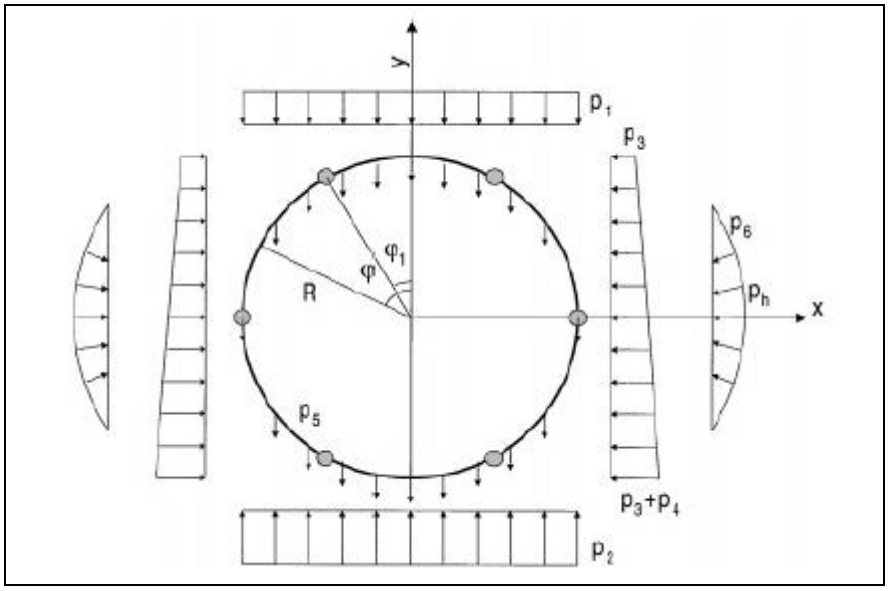

Figure 11.4 Model diagram of a jointed tunnel lining (after Lee et al., 2001)

Table 11.1 Main factors affecting the effective rigidity ratio $(E_lI_l)_e/(E_lI_l)$ (after Lee and Ge, 2001)

Factor	**$(E_lI_l)_e/(E_lI_l)$**
Joint stiffness ratio $K_\theta l/E_lI_l$ (↑)	Sensitive (↑)
Coefficient of soil resistance K_s (↑)	Not sensitive if $K_s < 30000$ kN/m^3 (↑)
Joint distribution (uniform, →)	Not sensitive (↓)
No. of joints (↑)	Sensitive (↓)
Geometry	
Thickness (↓)	Depends on total number of joints (↑ when 3 joints; ↓ when 4 joints)
Radius (↑)	Sensitive (↑)
Joint stiffness reduction	Sensitive (↓)

Note: The arrows indicate a tendency to increase (↑), decrease (↓), or remain uniform (→).

11.6 Summary of Some Previous Research

Although many insights have been gained from the methods discussed in Sections 11.2 to 11.5, some shortcomings restrict their usefulness. In a discussion to

Morgan's Paper, Muir Wood (1975) pointed out some errors and suggested modifications of Morgan's expressions. However, the Muir Wood approach did not take into consideration of structural effects such as the tunnel geometry, joint stiffness and joint arrangement as indicated by Lee and Ge (2001). It must be pointed out that although Lee and Ge (2001) took these factors into consideration, their design method often requires a rather long iterative process. In practical situations, Peck et al.'s design approach allows a fairly quick estimation of the stresses and diameter changes of the tunnel lining. However, their approach does not take into account the effects of joints. The finite element method provides an alternative approach and hence, in the following section a numerical study of the effects of joints on the stresses and deformation induced in the tunnel lining, in particular for tunnel interaction, is presented.

11.7 Problem Background

The 4-joint+key segmental linings (see Figure 4.4) are adopted in the construction of bored tunnels for Circle Line Contract 856. Hence, in the present research the behaviour of 4-joint+key, 5-joint and non-jointed tunnel lining were compared to assess the differences in each approach.

11.8 Finite Element Modelling

Figure 11.5 illustrates the 4-joint+key, 5-joint and non-jointed tunnel lining adopted in this study. The study was performed using two-dimensional (2D) finite element method program, PLAXIS. The tunnel lining parameters as summarised in Table 6.4 was adopted in this study. The main analysis focused on a 6.35 m diameter tunnel constructed at depth of 18 m below the ground surface where SPT N value of 27 was determined using Equation 6.6. The computed E_p of 75600 kPa was determined using Equation 6.7. The soil is assumed to be linear elastic as explained in Section 10.1.

The lining segments were modelled by defining a number of joints within the lining. The orientations of the joints were defined using the hinge and rotation spring where zero spring stiffness was assumed for all the joints. In this study, a reference joint is defined as a joint that is initially located at the tunnel crown. The orientation of the reference joint is measured at an angle θ_j in the clockwise direction from the tunnel crown. For a 4-joint +key segmental lining, two closely spaced joints (with key) at an initial angle of -11.25^o and $+11.25^o$ were used as reference joints whereas for a 5-joint segmental lining only a single joint (without key) is used as a reference joint. In this case, an angle θ_j of 0^o represents a reference joint being positioned at the tunnel crown, while an angle of θ_j of 11.25^o and 12^o represent the first orientation of the reference joint rotating in the clockwise direction towards the tunnel shoulder for a 4-joint+key segmental lining and a 5-joint segmental lining respectively. Similar steps as described in Chapter 6 were subsequently followed to model the staged construction.

A general modelling procedure has been developed for the analysis of closely spaced bored tunnels of 1.5 m pillar width. In this case, the reference joint of the second closely spaced parallel bored tunnel will be oriented in the same direction as the reference joint of the first bored tunnel. As an example, if the reference joint of the first bored tunnel is to be rotated in the clockwise direction, the reference joint of the second bored tunnel will be rotated in the same clockwise direction alongside the first bored tunnel. Taking the same orientation of the first bored tunnel and the second closely spaced parallel bored tunnels into account, the behaviour of the first bored tunnel will be investigated.

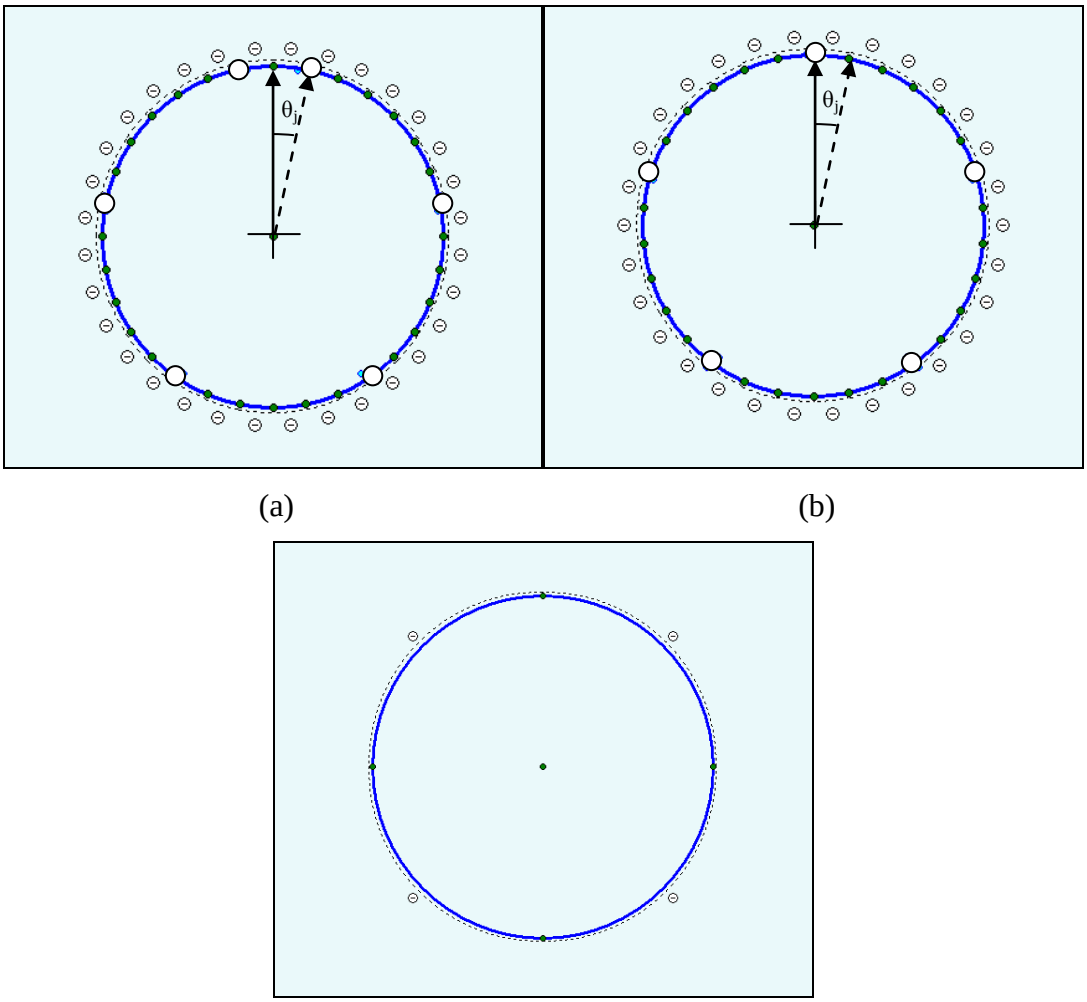

(a) (b)

(c)

Figure 11.5 Illustrations of (a) 4-joint+key; (b) 5-joint; and (c) non-jointed tunnel lining

11.9 Analyses for Single Bored Tunnel

A series of analyses was conducted to investigate the effects of K_o, volume loss and orientation of reference joint on the maximum bending moment, minimum bending moment, thrust and total displacement induced in the 4-joint+key, 5-joint and non-jointed tunnel lining of a single bored tunnel. The analyses involved using K_o of 0.5, 1.0 and 1.5. Comparisons were also carried out between cases of no volume loss and cases involving volume loss of 2.5 per cent. The orientation of reference joint for the 4-joint +key will be varied in a range from 0^o to 180^o at an interval of

11.25^o whereas the 5-joint has orientation of reference joint ranging from 0^o to 72^o at an interval of 12^o.

The results of the maximum bending moment are plotted in Figure 11.6. As observed, the jointed tunnel lining generally induced smaller maximum bending moment as compared to the non-jointed tunnel lining. This is attributed to the fact that the span of the structural member is shorter with prescribed number of joints which in turn, induced lower bending moments in the lining. For K_o of 0.5, the volume loss of 2.5 per cent in both jointed and non-jointed single bored tunnels resulted in larger maximum bending moment generated in the tunnel lining as compared to cases involving no volume loss. The opposite trend is observed for K_o of 1.5. Regardless of volume loss, the 5-joint induced larger maximum bending moment as compared to the 4-joint+key. This indicates a tendency of the key segment to improve the flexibility of the tunnel lining. As a result of the equal total vertical and horizontal stresses acting on the jointed and non-jointed tunnel lining, K_o of 1.0 induced significantly lower maximum bending moment in both the jointed and non-jointed tunnel lining as compared to K_o of 0.5 and 1.5. A comparative study carried out for the minimum bending moment also showed similar trends as the maximum bending moment for K_o of 0.5 and 1.5 and the results are presented in Figure 11.7. For K_o of 1.0, it should be noted from Figure 11.7(b) that cases involving volume loss of 2.5 per cent for jointed and non-jointed tunnel lining induced smaller minimum bending moment as compared to cases involving no volume loss, which is contrary to the observation for maximum bending moment as shown in Figure 11.6(b). These observations demonstrate the different mode of deformation of the tunnel lining for cases involving volume loss and no volume loss. The former involves tension (smaller minimum bending moment) of the tunnel lining at the springline suggesting the squatting of the single bored tunnel whereas the latter is essentially due to ovaling of the single bored tunnel, i.e. compression (smaller maximum bending moment) at the tunnel springline.

For the same volume loss condition, Figure 11.8 shows negligible variation of maximum thrust with orientation of reference joint for the 4-joint+key and 5-joint.

In addition, similar maximum thrust was observed for both the jointed and non-jointed tunnel lining. Comparison between cases involving volume loss of 2.5 per cent and no volume loss indicates that cases with volume loss of 2.5 per cent generated the largest maximum thrust for K_o of 0.5 and the smallest maximum thrust for K_o of 1.5 whereas cases without volume loss exhibited the opposite response. The occurrence of volume loss results in positive maximum thrust whereas no volume loss results in negative maximum thrust. For cases involving no volume loss, it is apparent that the maximum thrust induced in the tunnel lining is governed by the K_o. However, lateral stress relief occurs as the volume loss was assumed in all analyses. In this case, the maximum thrust induced in the tunnel lining is mainly controlled by the total vertical stresses (overburden pressure), with total horizontal stresses acting as a limiting condition for mobilisation. The smaller total horizontal stresses for K_o of 0.5 as compared to K_o of 1.5 has led to larger direct compression of the lining for the former which in turn, induced larger maximum thrust in the tunnel lining. It can be seen that the results of minimum thrust are similar in form to the maximum thrust, as shown in Figure 11.9.

The influence of K_o and volume loss on total displacements induced in each 4-joint+key, 5-joint and non-jointed tunnel lining are presented in Figure 11.10. It was generally observed for both the jointed and non-jointed tunnel lining that the total displacements for cases involving no volume loss is significantly smaller than cases involving 2.5 per cent volume loss. For K_o of 0.5 and 1.5, relatively larger total displacements was observed for the 4-joint+key and the 5-joint as compared to the non-jointed tunnel lining, for all conditions of volume loss. However, no difference in total displacements was observed between jointed and non-jointed tunnel lining for K_o of 1.0, for each case of volume loss. Clearly, this is attributed to the same total vertical stresses and total horizontal stresses acting on the tunnel lining. The influence of orientation of reference joint on the total displacements induced in the 4-joint+key and the 5-joint is similar, depending on the K_o and the volume loss.

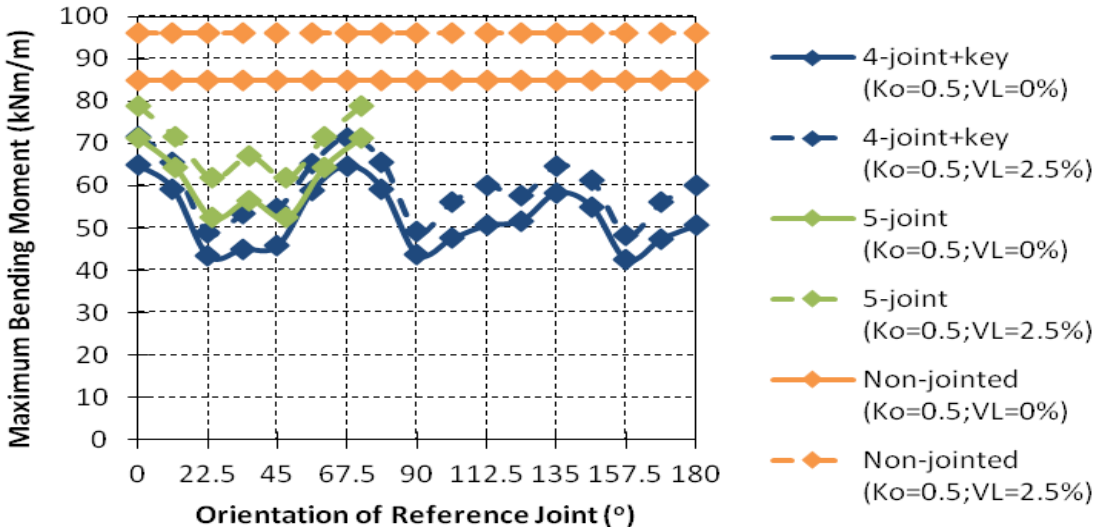
Maximum Bending Moment (kNm/m)
100
90
80
70
60
50
40
30
20
10
0
0 22.5 45 67.5 90 112.5 135 157.5 180
Orientation of Reference Joint (°)
4-joint+key (Ko=0.5;VL=0%)
4-joint+key (Ko=0.5;VL=2.5%)
5-joint (Ko=0.5;VL=0%)
5-joint (Ko=0.5;VL=2.5%)
Non-jointed (Ko=0.5;VL=0%)
Non-jointed (Ko=0.5;VL=2.5%)

(a)

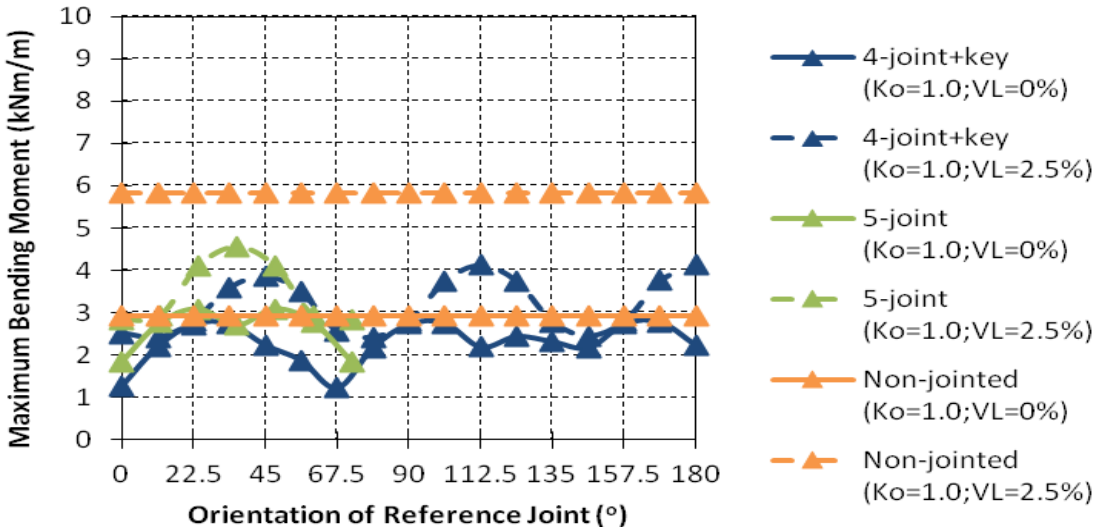
Maximum Bending Moment (kNm/m)
10
9
8
7
6
5
4
3
2
1
0
0 22.5 45 67.5 90 112.5 135 157.5 180
Orientation of Reference Joint (°)
4-joint+key (Ko=1.0;VL=0%)
4-joint+key (Ko=1.0;VL=2.5%)
5-joint (Ko=1.0;VL=0%)
5-joint (Ko=1.0;VL=2.5%)
Non-jointed (Ko=1.0;VL=0%)
Non-jointed (Ko=1.0;VL=2.5%)

(b)

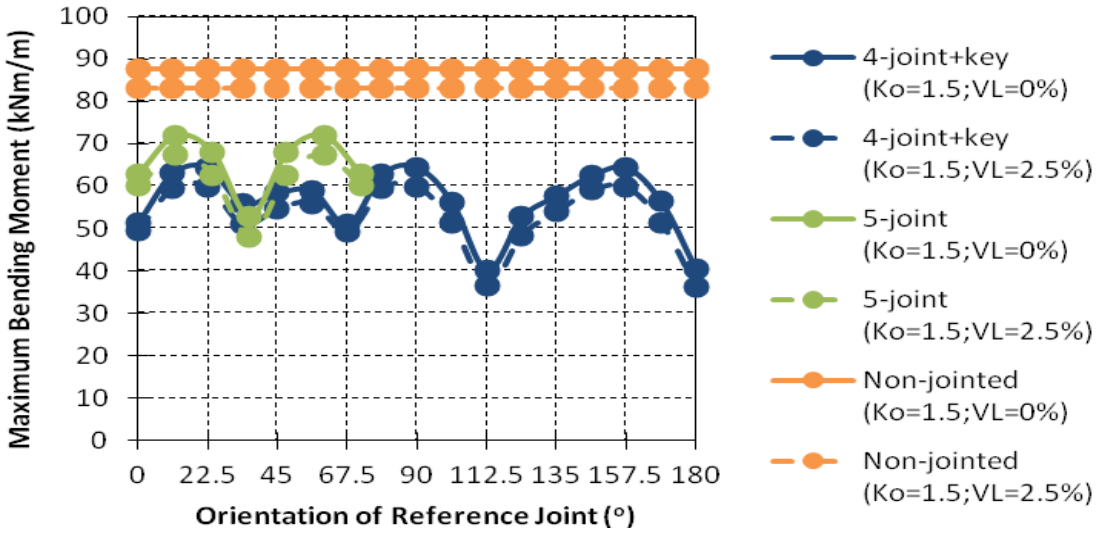

(c)

Figure 11.6 Variation of maximum bending moment with orientation of reference joint for (a) K_o=0.5; (b) K_o=1.0; and (c) K_o=1.5

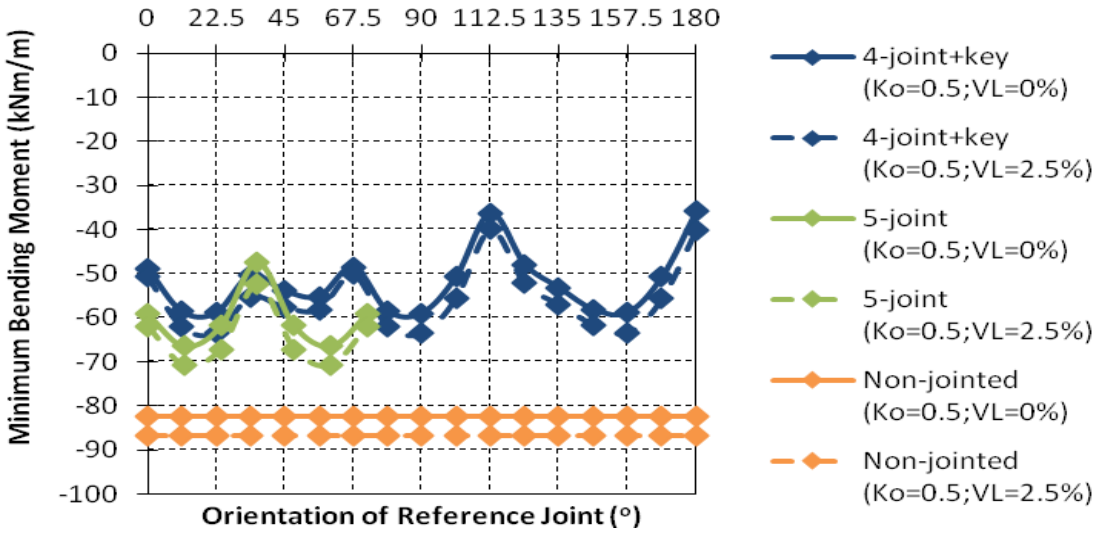

(a)

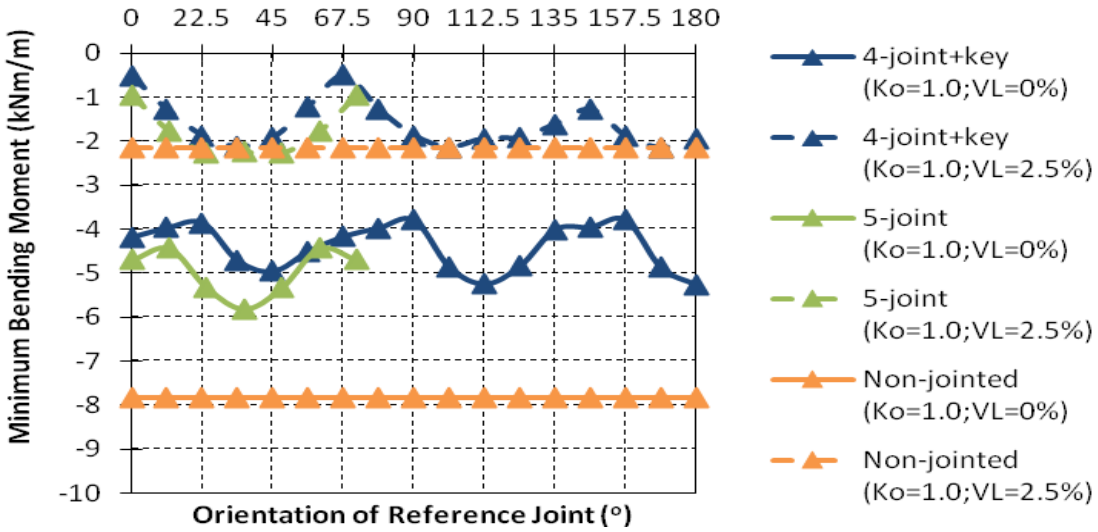

(b)

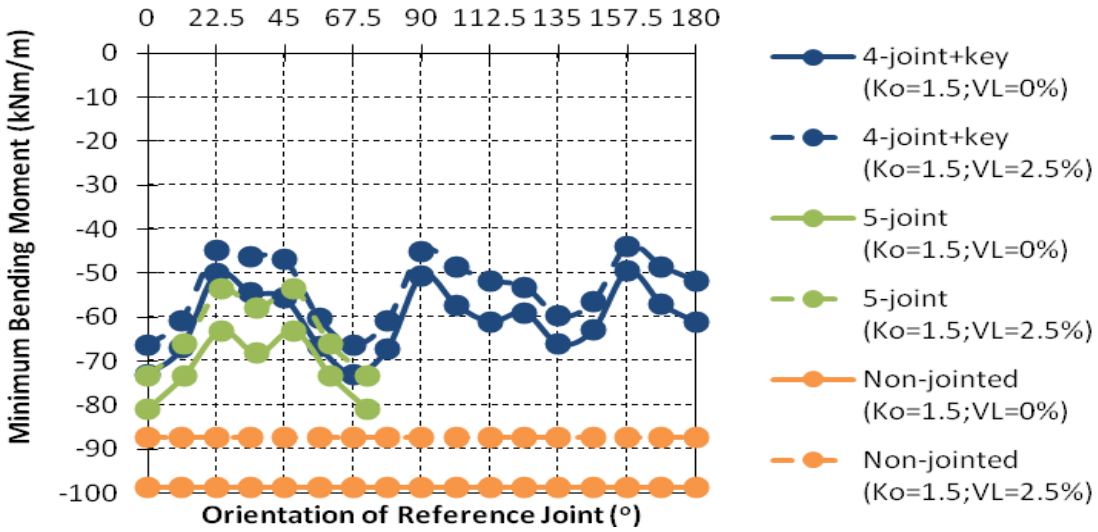

(c)

Figure 11.7 Variation of minimum bending moment with orientation of reference joint for (a) K_o=0.5; (b) K_o=1.0; and (c) K_o=1.5

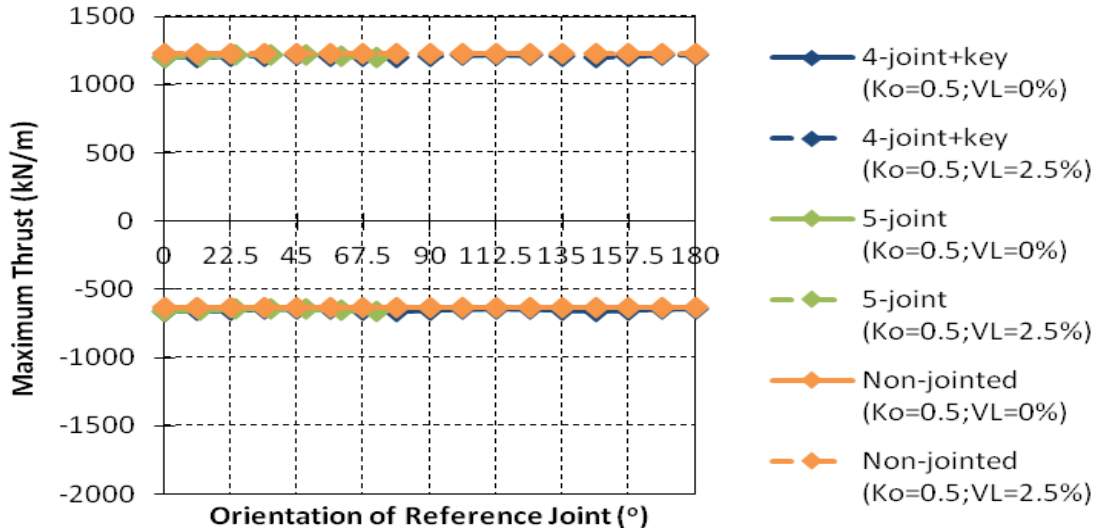
1500
1000
500
0
-500
-1000
-1500
-2000
0 22.5 45 67.5 90 112.5 135 157.5 180
Maximum Thrust (kN/m)
Orientation of Reference Joint (°)
4-joint+key (Ko=0.5;VL=0%)
4-joint+key (Ko=0.5;VL=2.5%)
5-joint (Ko=0.5;VL=0%)
5-joint (Ko=0.5;VL=2.5%)
Non-jointed (Ko=0.5;VL=0%)
Non-jointed (Ko=0.5;VL=2.5%)

(a)

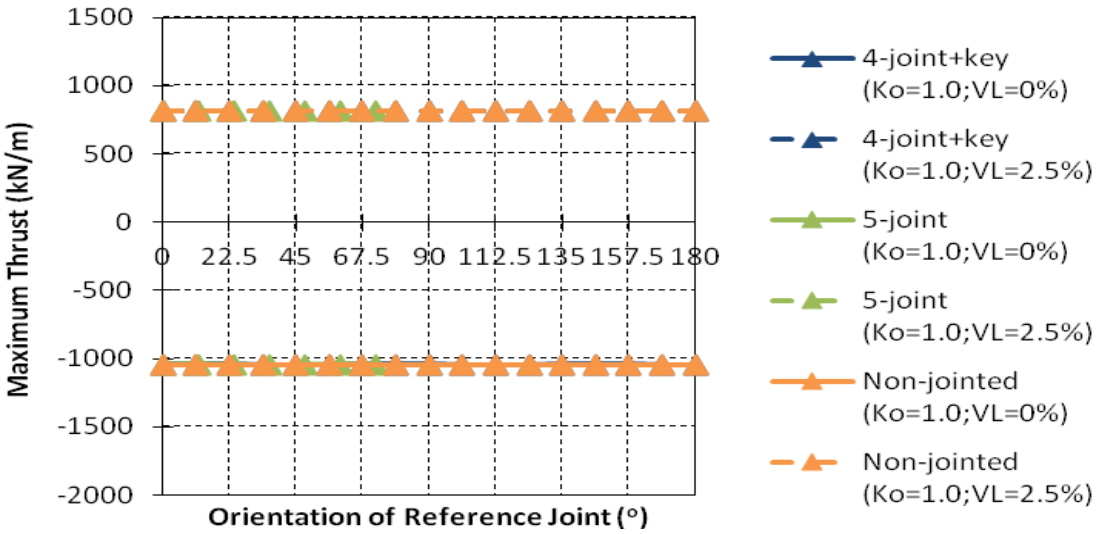
1500
1000
500
0
-500
-1000
-1500
-2000
0 22.5 45 67.5 90 112.5 135 157.5 180
Maximum Thrust (kN/m)
Orientation of Reference Joint (°)
4-joint+key (Ko=1.0;VL=0%)
4-joint+key (Ko=1.0;VL=2.5%)
5-joint (Ko=1.0;VL=0%)
5-joint (Ko=1.0;VL=2.5%)
Non-jointed (Ko=1.0;VL=0%)
Non-jointed (Ko=1.0;VL=2.5%)

(b)

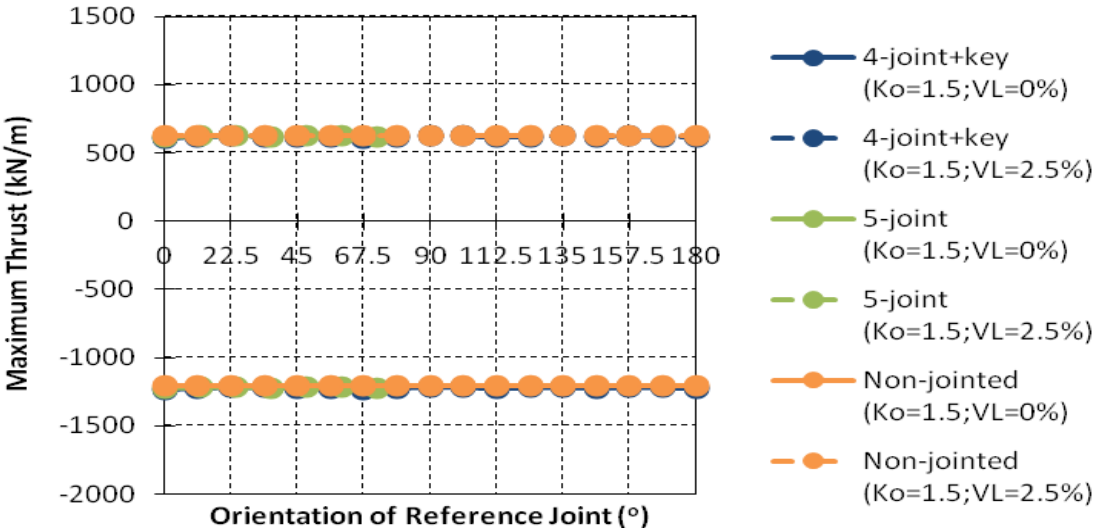

(c)

Figure 11.8 Variation of maximum thrust with orientation of reference joint for (a) K_o=0.5; (b) K_o=1.0; and (c) K_o=1.5

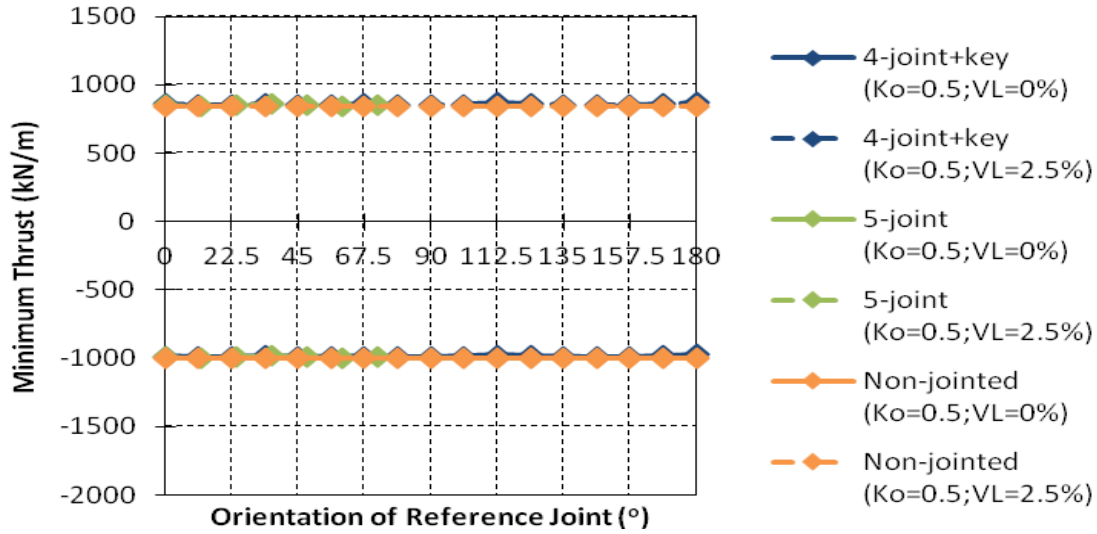

(a)

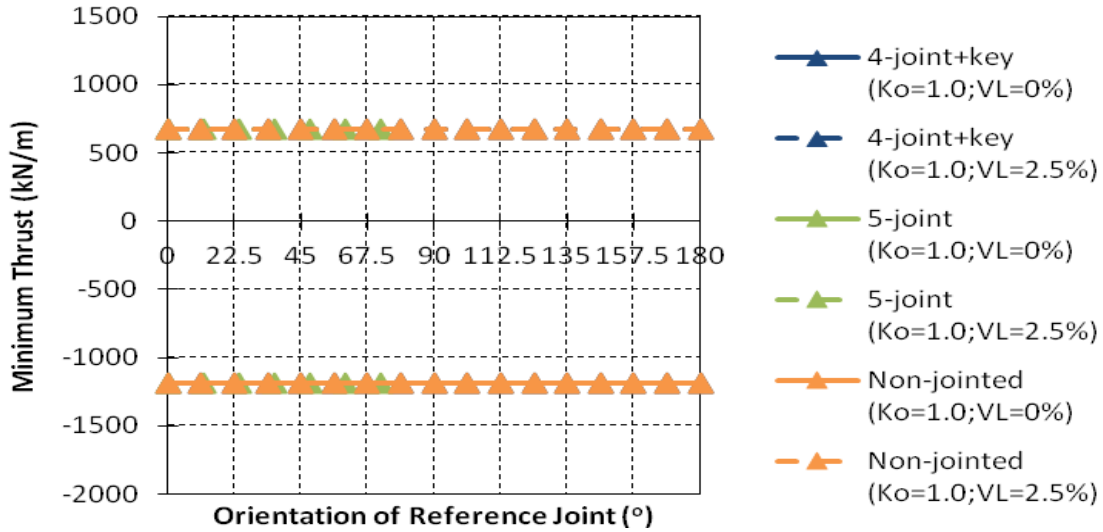

(b)

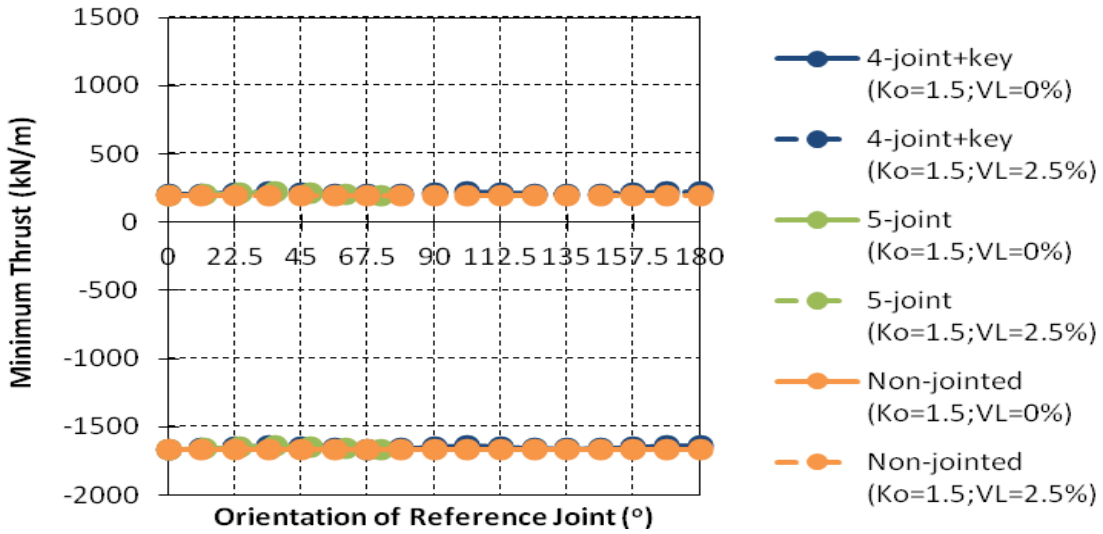

(c)

Figure 11.9 Variation of minimum thrust with orientation of reference joint for (a) K_o=0.5; (b) K_o=1.0; and (c) K_o=1.5

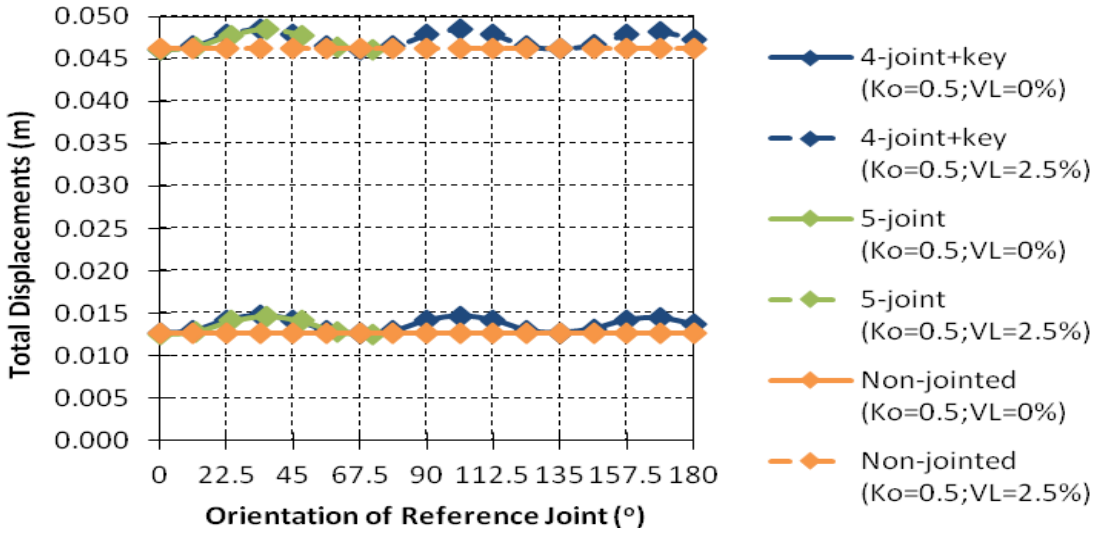
0.050
0.045
0.040
0.035
0.030
0.025
0.020
0.015
0.010
0.005
0.000
Total Displacements (m)
0 22.5 45 67.5 90 112.5 135 157.5 180
Orientation of Reference Joint (°)
4-joint+key (Ko=0.5;VL=0%)
4-joint+key (Ko=0.5;VL=2.5%)
5-joint (Ko=0.5;VL=0%)
5-joint (Ko=0.5;VL=2.5%)
Non-jointed (Ko=0.5;VL=0%)
Non-jointed (Ko=0.5;VL=2.5%)

(a)

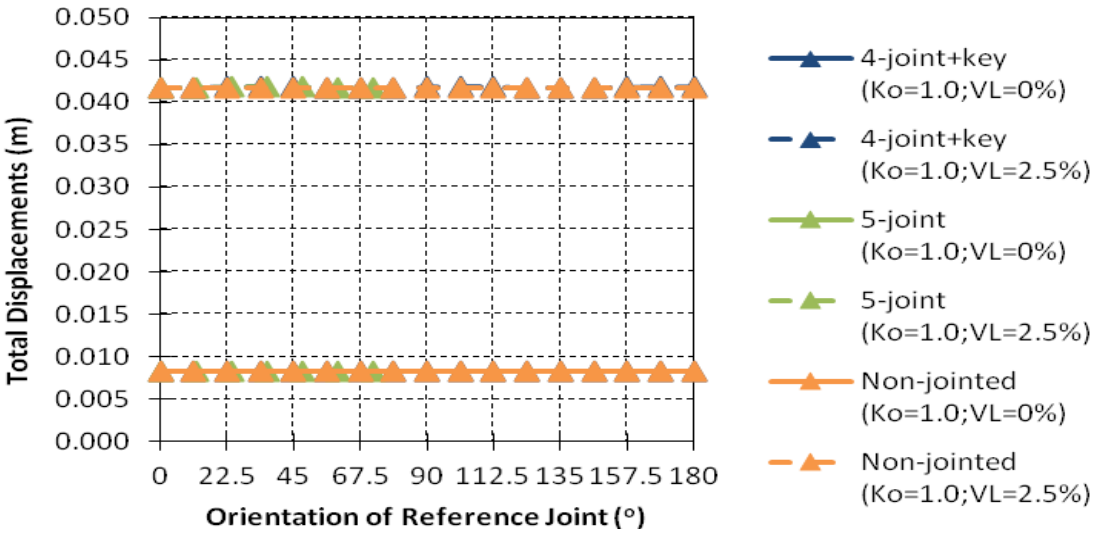
0.050
0.045
0.040
0.035
0.030
0.025
0.020
0.015
0.010
0.005
0.000
Total Displacements (m)
0 22.5 45 67.5 90 112.5 135 157.5 180
Orientation of Reference Joint (°)
4-joint+key (Ko=1.0;VL=0%)
4-joint+key (Ko=1.0;VL=2.5%)
5-joint (Ko=1.0;VL=0%)
5-joint (Ko=1.0;VL=2.5%)
Non-jointed (Ko=1.0;VL=0%)
Non-jointed (Ko=1.0;VL=2.5%)

(b)

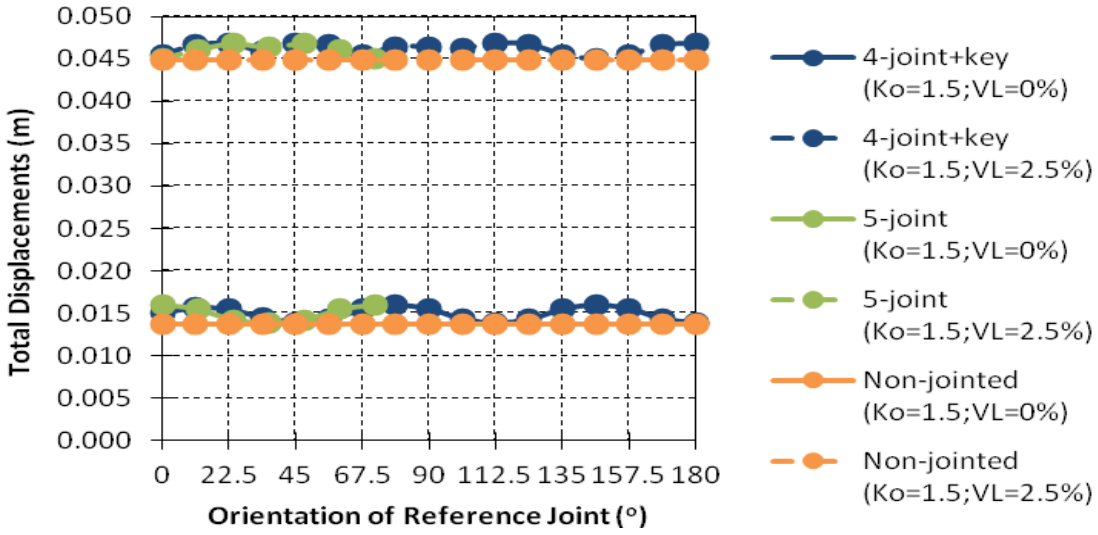

(c)

Figure 11.10 Variation of total displacements with orientation of reference joint for (a) K_o=0.5; (b) K_o=1.0; and (c) K_o=1.5

11.10 Analyses for Closely Spaced Parallel Bored Tunnels

In the analysis of tunnel interaction, the volume loss is an important parameter. The volume loss induced in the second closely spaced parallel bored tunnel will influence the stresses and displacement of the adjacent first bored tunnel. Hence, a volume loss of 2.5 per cent that represents the average volume loss computed from the construction of Circle Line Contract 856 will be adopted in the investigation.

Clockwise Orientation of Reference Joint

The interaction between closely spaced parallel bored tunnels has led to significant maximum bending moment induced in the first bored tunnel, for K_o of 1.0 as shown in Figure 11.11. This observation is in contrast to the small maximum bending moment induced in the single bored tunnel for K_o of 1.0 as shown in Figure 11.6(b). Figures 11.11(a) and 11.11(b) for K_o of 0.5 and 1.0 indicate that larger maximum bending moment was induced in the non-jointed tunnel lining of the first bored tunnel whereas for K_o of 1.5 (see Figure 11.11(c)) approximately the same order of maximum bending moment was induced in the first bored tunnel involving the 5-joint and the non-jointed tunnel lining respectively. In this case, the effect of larger

stress relief for K_o of 1.5 on the total displacements (see Figure 11.14(c)) and thus the maximum bending moment induced in the first bored tunnel is clearly evident. Generally, the maximum bending moment induced in the 5-joint can be considered as the equivalent upper bound for the 4-joint+key, regardless of the clockwise orientation of the reference joint. Figure 11.12 shows a close consistent trend between the minimum bending moment induced in the 4-joint+key and the 5-joint. Despite consistency in the trend, the minimum bending moment induced in the 5-joint may consist of an equivalent upper or lower bound for the 4-joint+key, depending on the clockwise orientation of reference joint. For K_o of 0.5, 1.0 and 1.5, the non-jointed tunnel lining provides a reasonable equivalent upper bound for the maximum and minimum bending moments induced in the 4-joint+key.

Figure 11.13 shows the variation of maximum thrust with clockwise orientation of reference joint for the 4-joint+key, the 5-joint and the non-jointed tunnel lining. The difference between the maximum thrust induced in the 4-joint+key and 5-joint is marginal, regardless of the clockwise orientation of reference joint. The results for K_o of 0.5, 1.0 and 1.5 indicate the slightly larger maximum thrust induced in the non-jointed tunnel lining as compared to the 4-joint+key and the 5-joint. This observation suggests the possibility of adopting the maximum thrust induced in the non-jointed tunnel lining to estimate the maximum thrust induced in the 4-joint+key and the 5-joint. Intuitively it is reasonable to idealise the maximum thrust induced in the 4-joint+key and the 5-joint as a constant value, regardless of the orientation of the reference joint.

The presence of joints increases the flexibility of the tunnel lining and hence, larger total displacements were observed for the 4-joint+key and the 5-joint as compared to the non-jointed tunnel lining, as shown in Figures 11.14(a) and 11.14(b) for K_o of 0.5 and 1.0 respectively. It is interesting to note that the 5-joint provides relatively similar total displacements as the 4-joint+key. In addition, similar total displacements were also observed between the 4-joint+key, the 5-joint and the non-jointed tunnel lining for K_o of 1.5. This indicates that the total displacements are not sensitive to the clockwise orientation of the reference joint for K_o of 1.5.

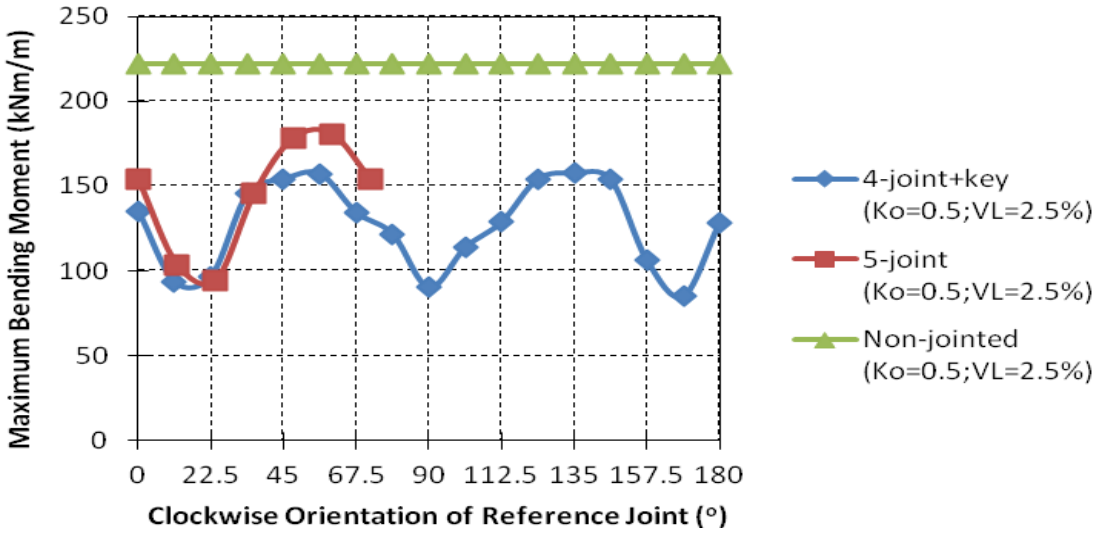
Maximum Bending Moment (kNm/m)
250
200
150
100
50
0
0 22.5 45 67.5 90 112.5 135 157.5 180
Clockwise Orientation of Reference Joint (°)
4-joint+key (Ko=0.5;VL=2.5%)
5-joint (Ko=0.5;VL=2.5%)
Non-jointed (Ko=0.5;VL=2.5%)

(a)

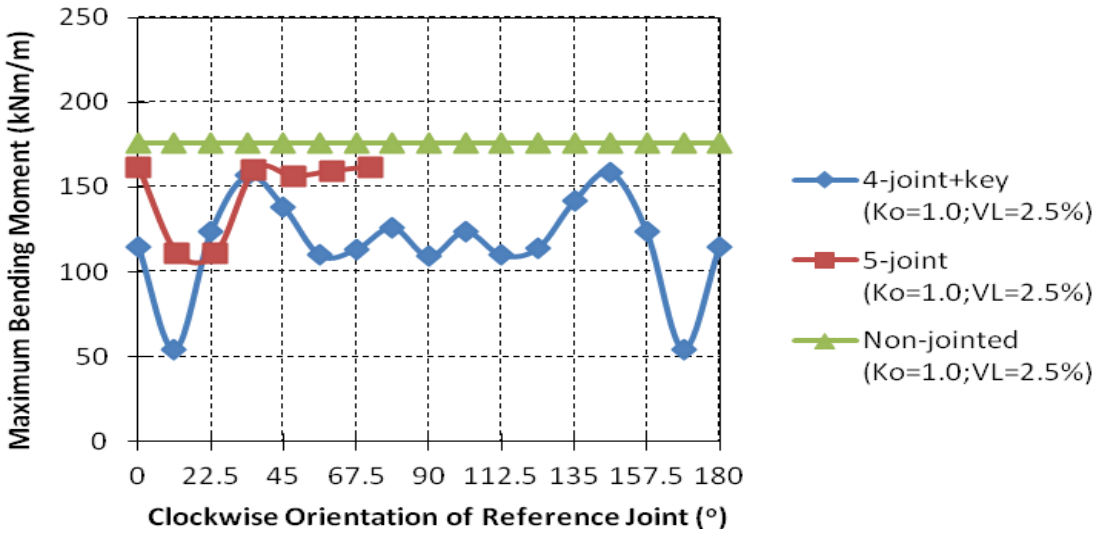
Maximum Bending Moment (kNm/m)
250
200
150
100
50
0
0 22.5 45 67.5 90 112.5 135 157.5 180
Clockwise Orientation of Reference Joint (°)
4-joint+key (Ko=1.0;VL=2.5%)
5-joint (Ko=1.0;VL=2.5%)
Non-jointed (Ko=1.0;VL=2.5%)

(b)

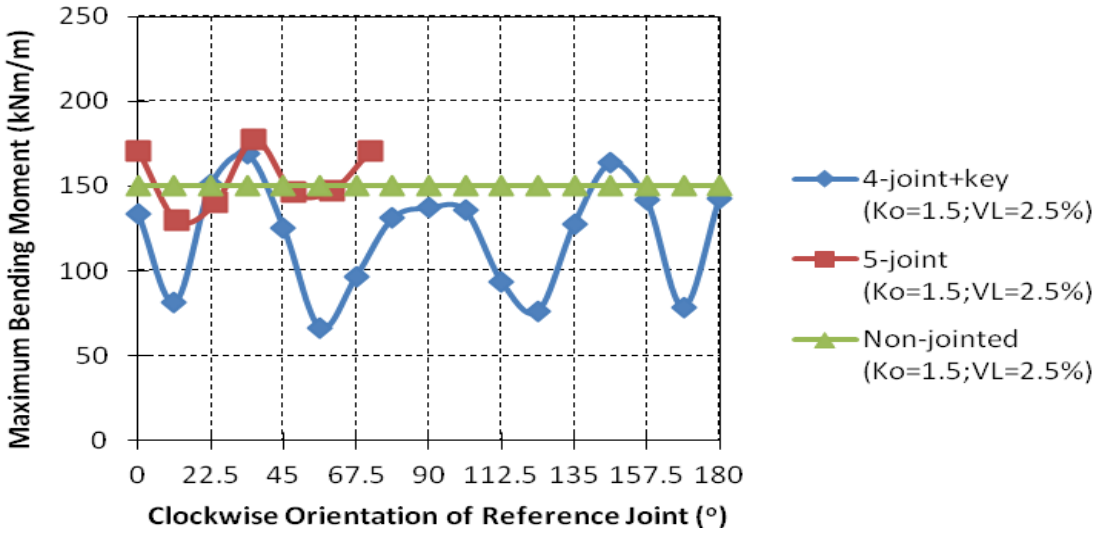

(c)

Figure 11.11 Variation of maximum bending moment with clockwise orientation of reference joint for (a) K_o=0.5; (b) K_o=1.0; and (c) K_o=1.5

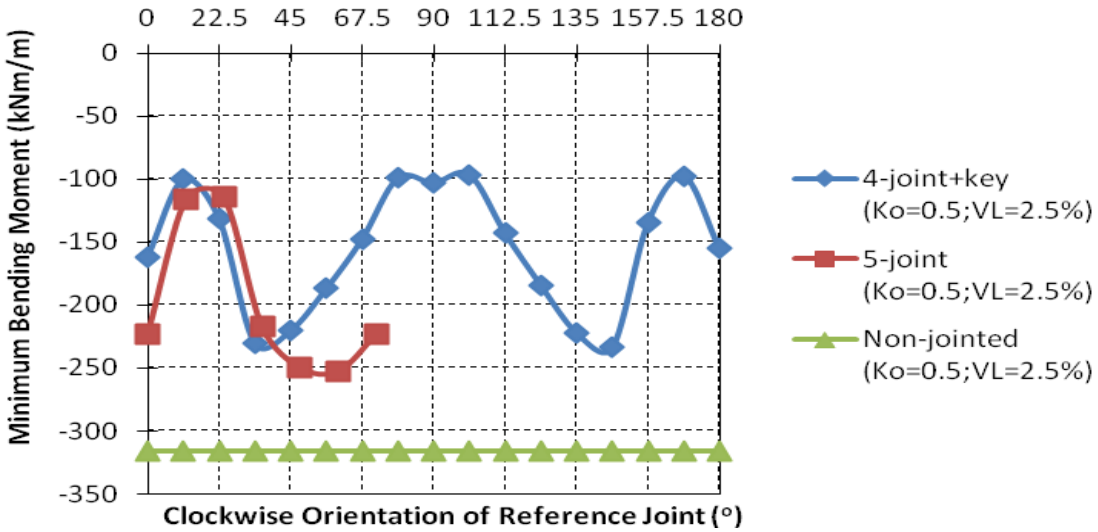

(a)

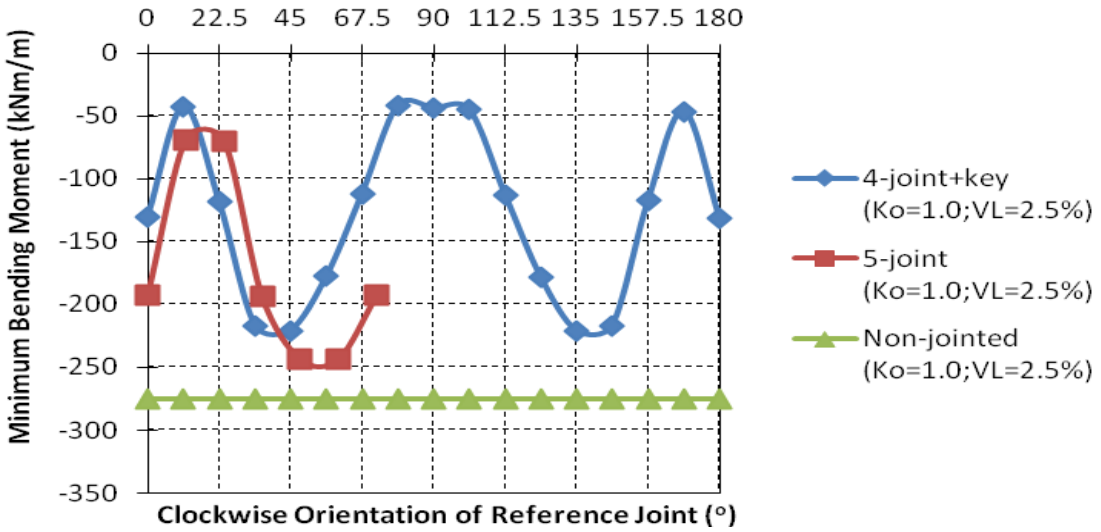

(b)

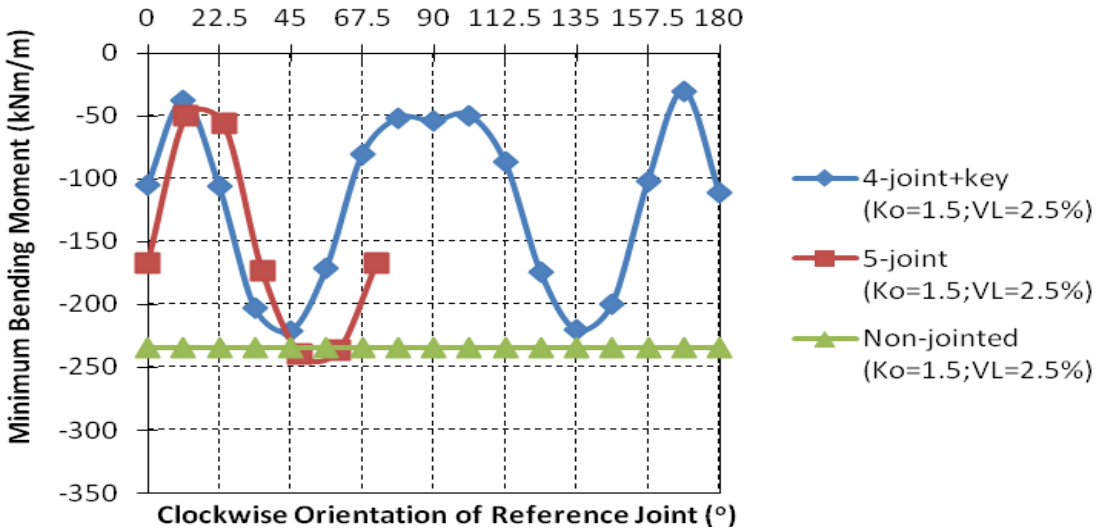

(c)

Figure 11.12 Variation of minimum bending moment with clockwise orientation of reference joint for (a) K_o=0.5; (b) K_o=1.0; and (c) K_o=1.5

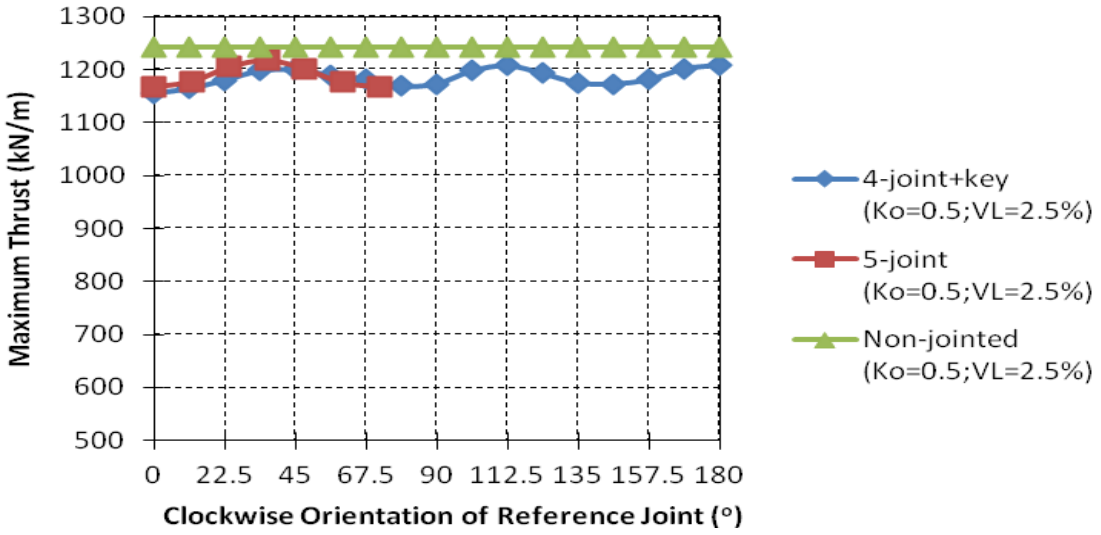
Maximum Thrust (kN/m)
1300
1200
1100
1000
900
800
700
600
500
0
22.5
45
67.5
90
112.5
135
157.5
180
Clockwise Orientation of Reference Joint (°)
4-joint+key (Ko=0.5;VL=2.5%)
5-joint (Ko=0.5;VL=2.5%)
Non-jointed (Ko=0.5;VL=2.5%)

(a)

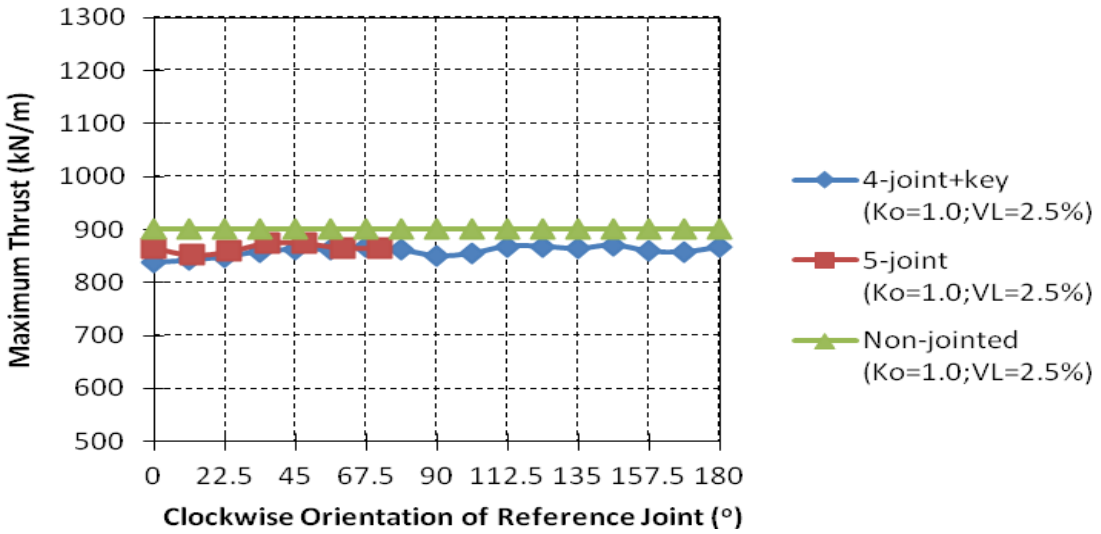
Maximum Thrust (kN/m)
1300
1200
1100
1000
900
800
700
600
500
0
22.5
45
67.5
90
112.5
135
157.5
180
Clockwise Orientation of Reference Joint (°)
4-joint+key (Ko=1.0;VL=2.5%)
5-joint (Ko=1.0;VL=2.5%)
Non-jointed (Ko=1.0;VL=2.5%)

(b)

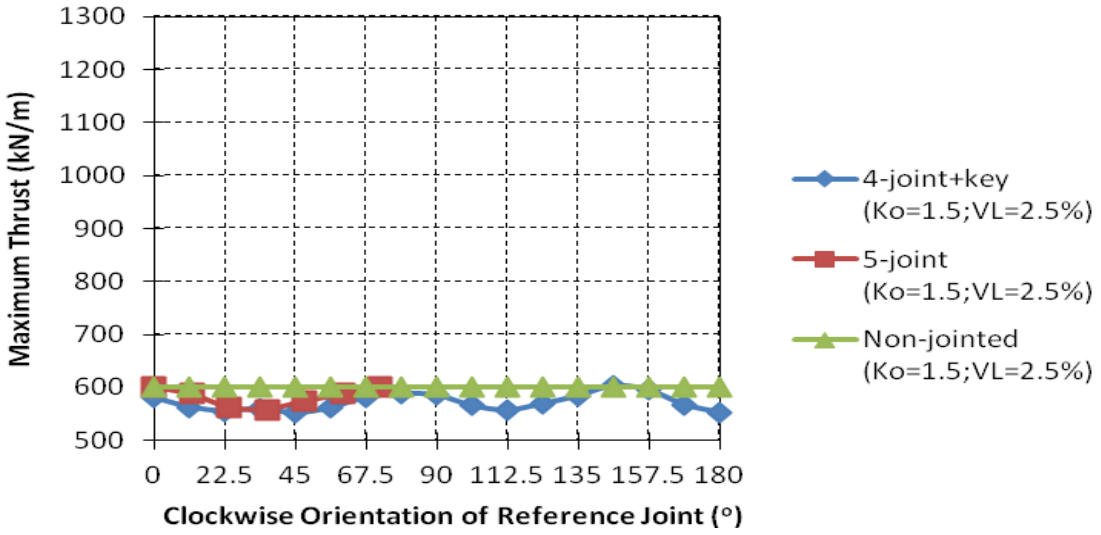

(c)

Figure 11.13 Variation of maximum thrust with clockwise orientation of reference joint for (a) K_o=0.5; (b) K_o=1.0; and (c) K_o=1.5

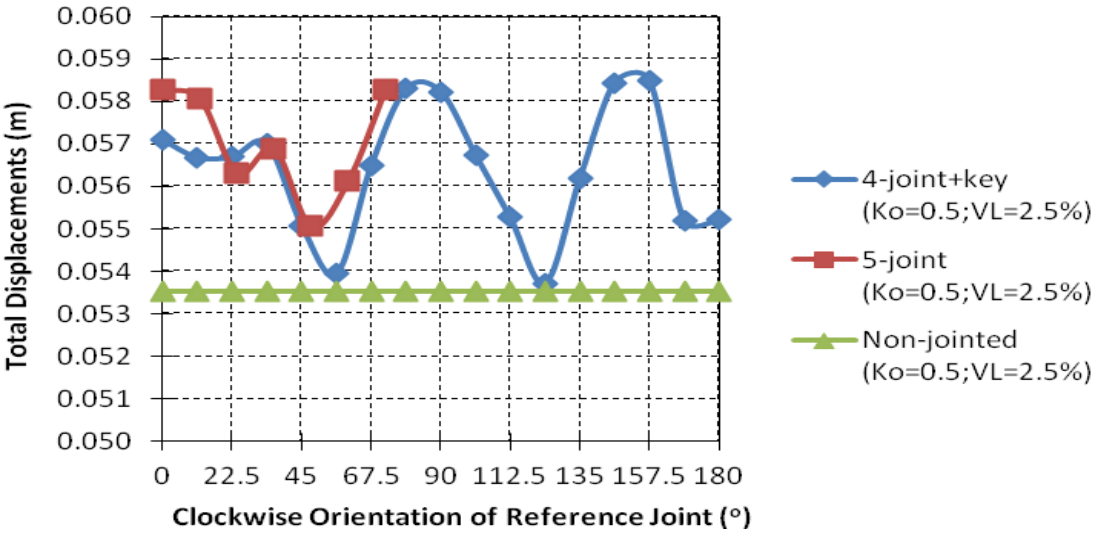

(a)

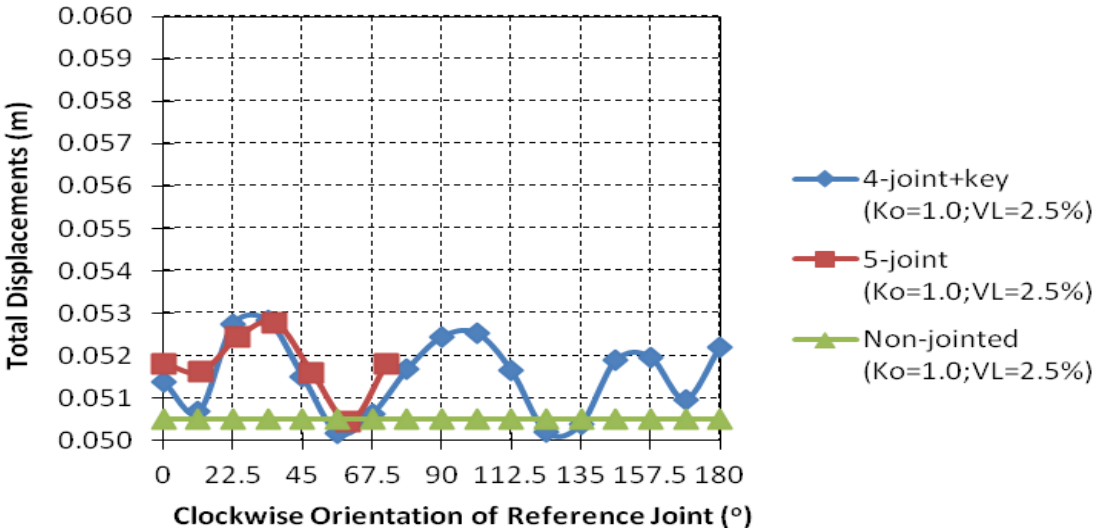

(b)

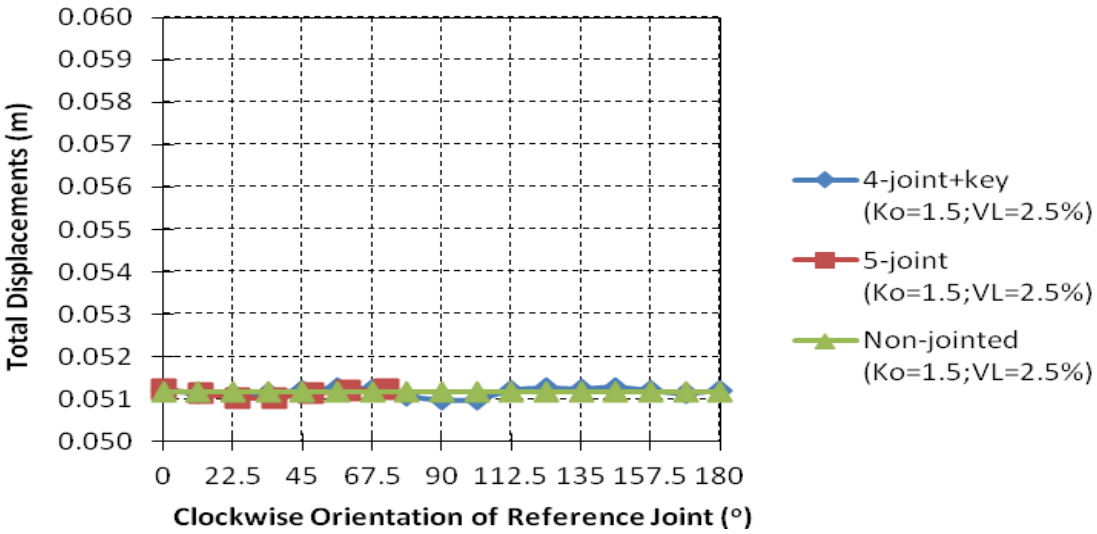

(c)

Figure 11.14 Variation of total displacements with clockwise orientation of reference joint for (a) K_o=0.5; (b) K_o=1.0; and (c) K_o=1.5

Counterclockwise Orientation of Reference Joint

Similar trends were observed between clockwise and counterclockwise orientation of reference joint for the maximum bending moment, minimum bending moment, maximum thrust and total displacements induced in the first bored tunnel for the 4-joint+key, the 5-joint and the non-jointed tunnel lining, as shown in Figures 11.15 to 11.18.

From Figure 11.18, it is noted that:

1. For K_o of 0.5, counterclockwise orientation of reference joint of 12^o and 24^o for the 5-joint induced much smaller total displacements as compared to the 4-joint+key. In this respect the location of the joint around the interaction face is moving away from the springline for both the 4-joint+key and the 5-joint. However, it must be pointed out that smaller total vertical stresses are experienced by the reference joint of the 5-joint as compared to the 4-joint+key.
2. For K_o of 1.0, similar trend as K_o of 0.5 was observed for counterclockwise orientation of reference joint of 12^o for the 5-joint.

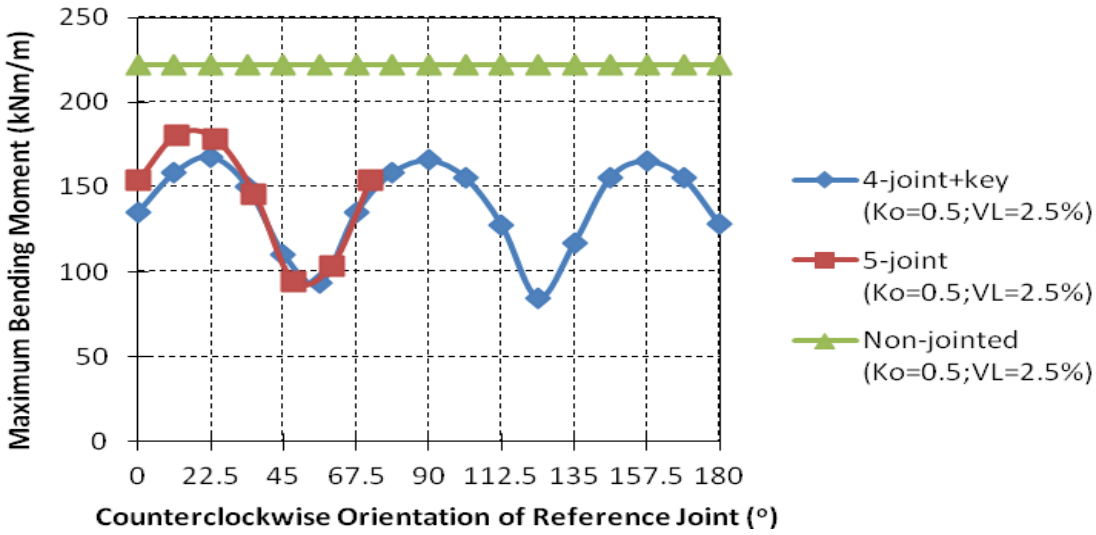

(a)

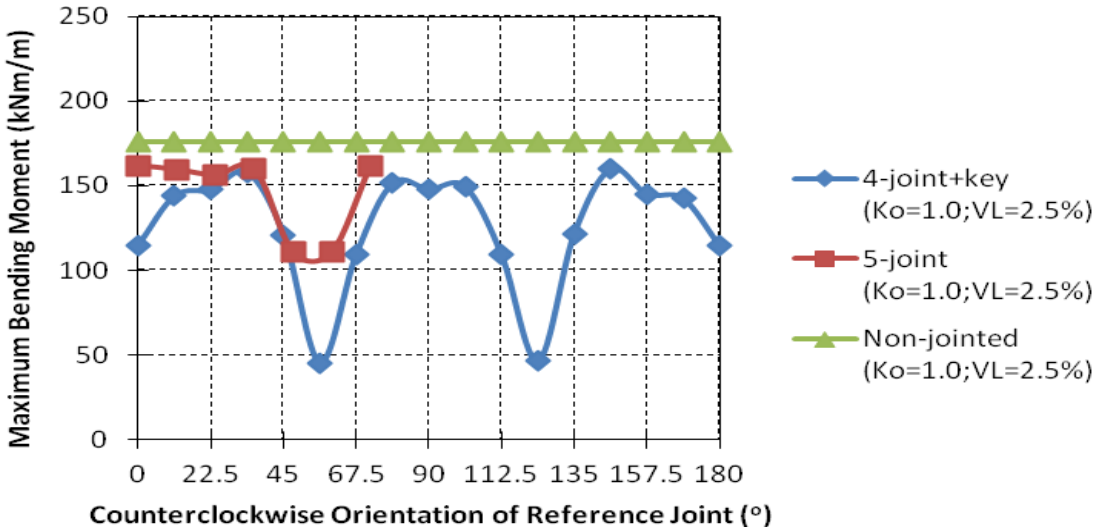

(b)

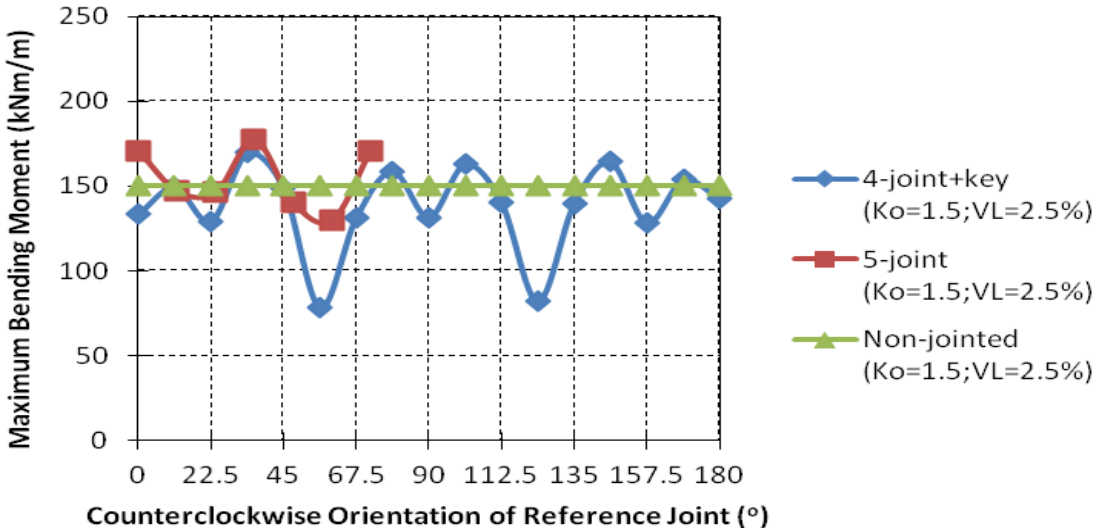

(c)

Figure 11.15 Variation of maximum bending moment with counterclockwise orientation of reference joint for (a) K_o=0.5; (b) K_o=1.0; and (c) K_o=1.5

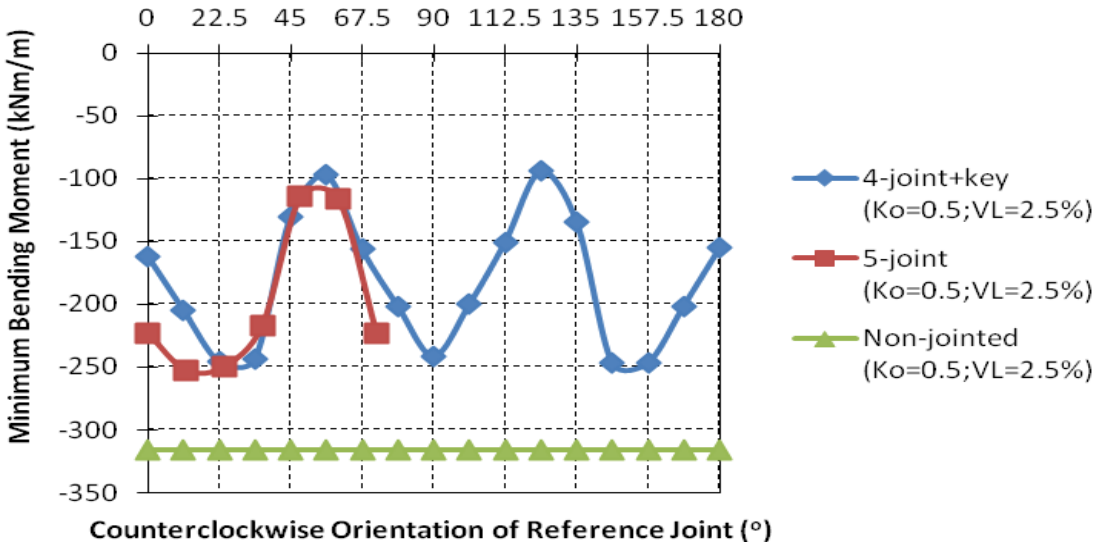
0 22.5 45 67.5 90 112.5 135 157.5 180
0
-50
-100
-150
-200
-250
-300
-350
Minimum Bending Moment (kNm/m)
Counterclockwise Orientation of Reference Joint (°)
4-joint+key (Ko=0.5;VL=2.5%)
5-joint (Ko=0.5;VL=2.5%)
Non-jointed (Ko=0.5;VL=2.5%)

(a)

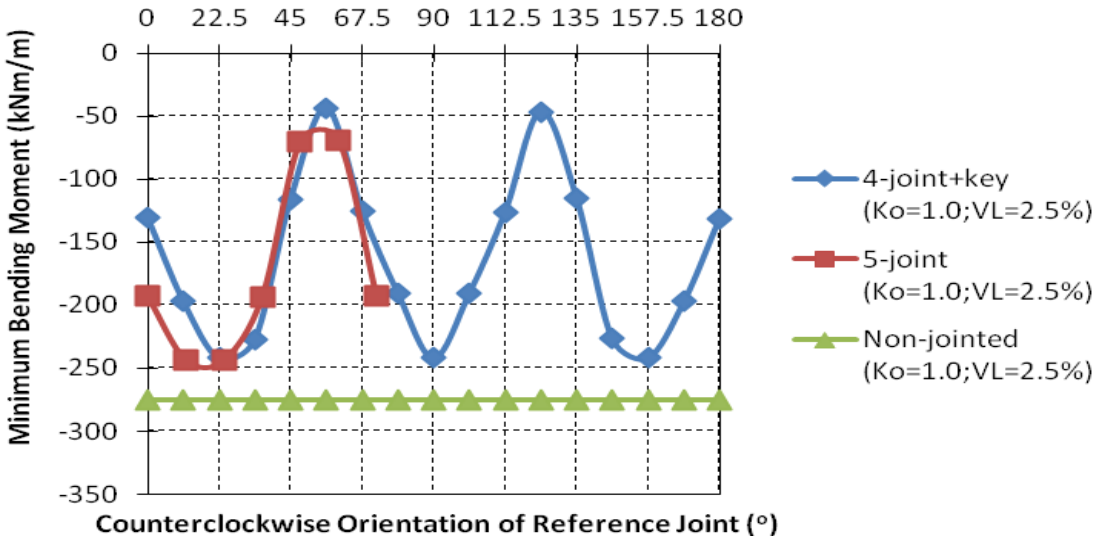
0 22.5 45 67.5 90 112.5 135 157.5 180
0
-50
-100
-150
-200
-250
-300
-350
Minimum Bending Moment (kNm/m)
Counterclockwise Orientation of Reference Joint (°)
4-joint+key (Ko=1.0;VL=2.5%)
5-joint (Ko=1.0;VL=2.5%)
Non-jointed (Ko=1.0;VL=2.5%)

(b)

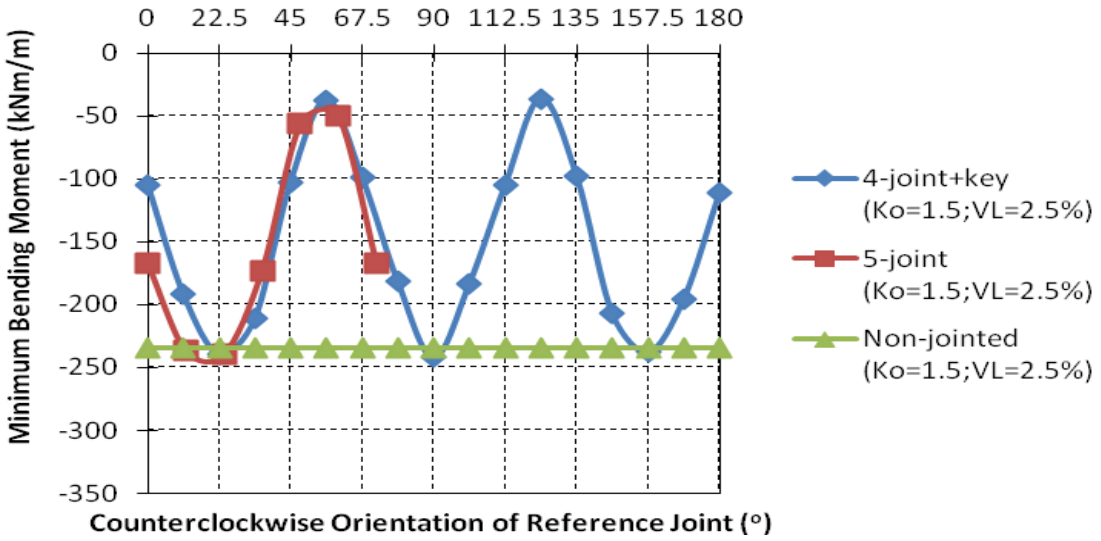

(c)

Figure 11.16 Variation of minimum bending moment with counterclockwise orientation of reference joint for (a) K_o=0.5; (b) K_o=1.0; and (c) K_o=1.5

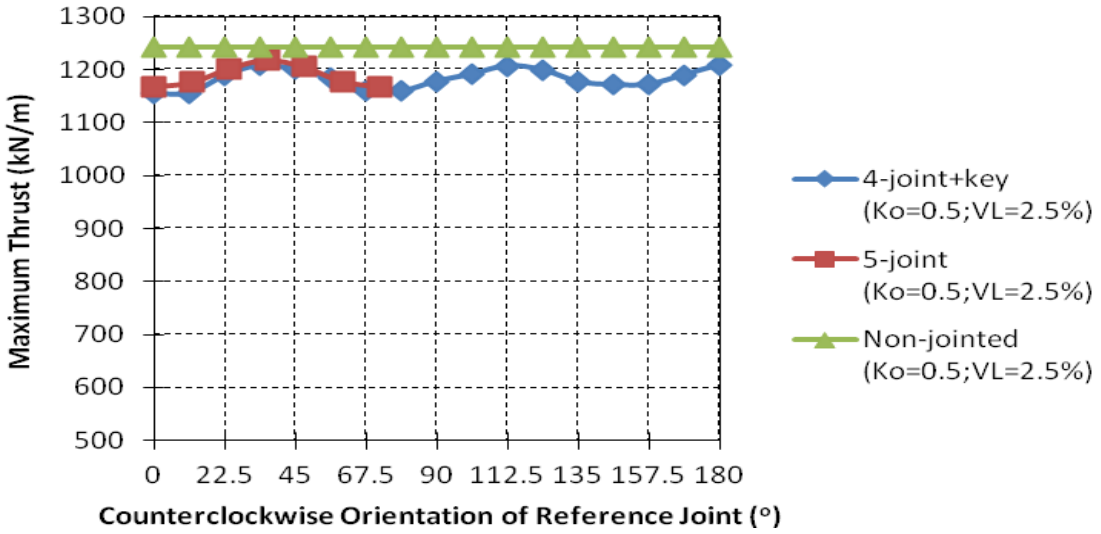

(a)

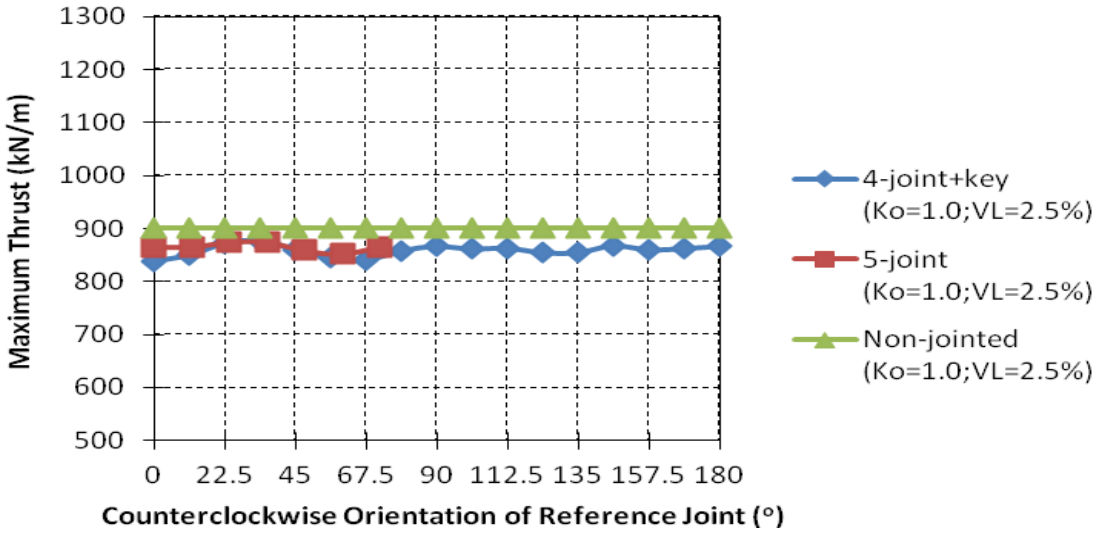

(b)

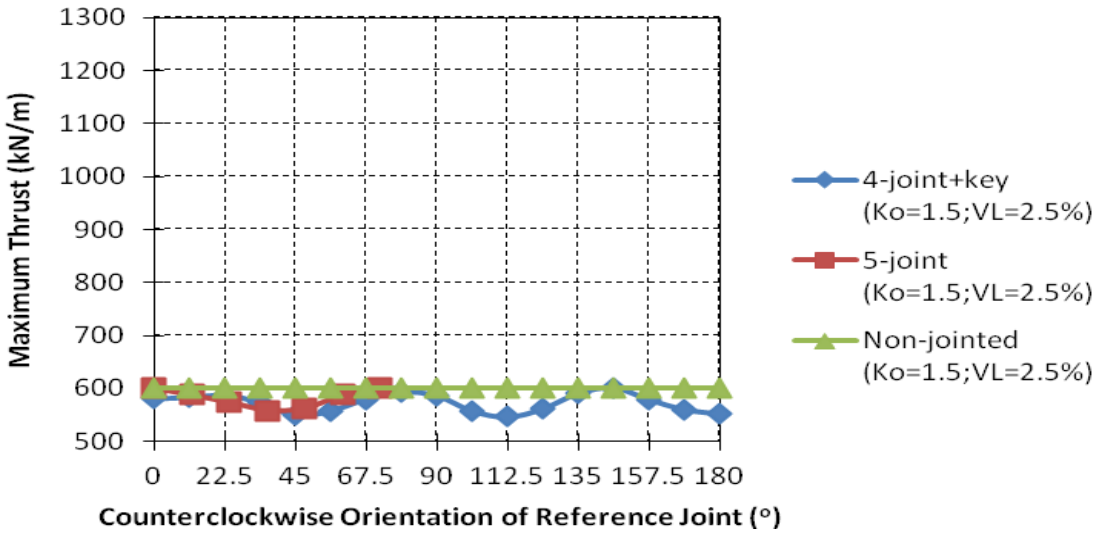

(c)

Figure 11.17 Variation of maximum thrust with counterclockwise orientation of reference joint for (a) K_o=0.5; (b) K_o=1.0; and (c) K_o=1.5

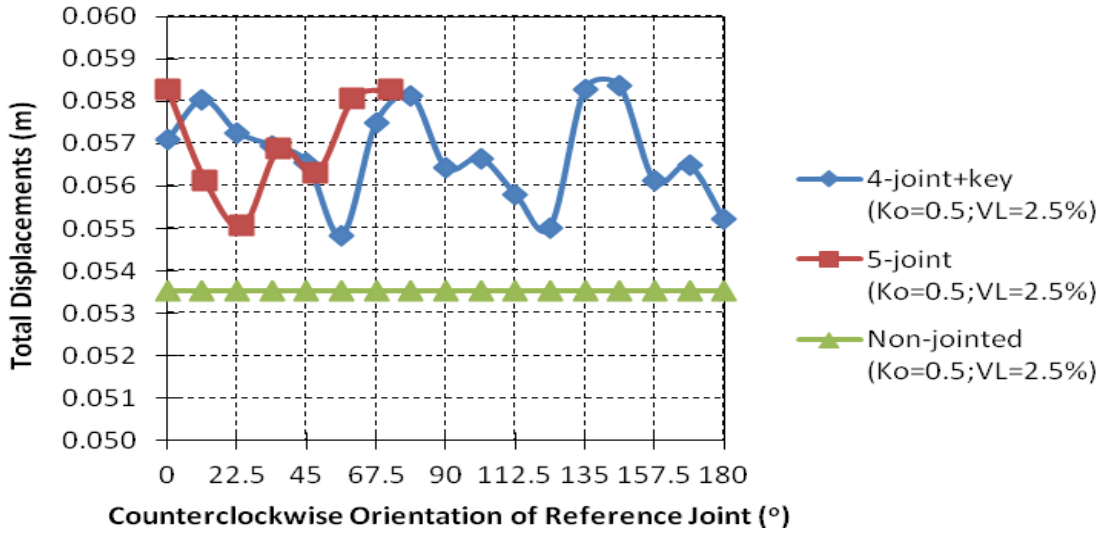
0.060
0.059
0.058
0.057
0.056
0.055
0.054
0.053
0.052
0.051
0.050
Total Displacements (m)
0
22.5
45
67.5
90
112.5
135
157.5
180
Counterclockwise Orientation of Reference Joint (°)
4-joint+key (Ko=0.5;VL=2.5%)
5-joint (Ko=0.5;VL=2.5%)
Non-jointed (Ko=0.5;VL=2.5%)

(a)

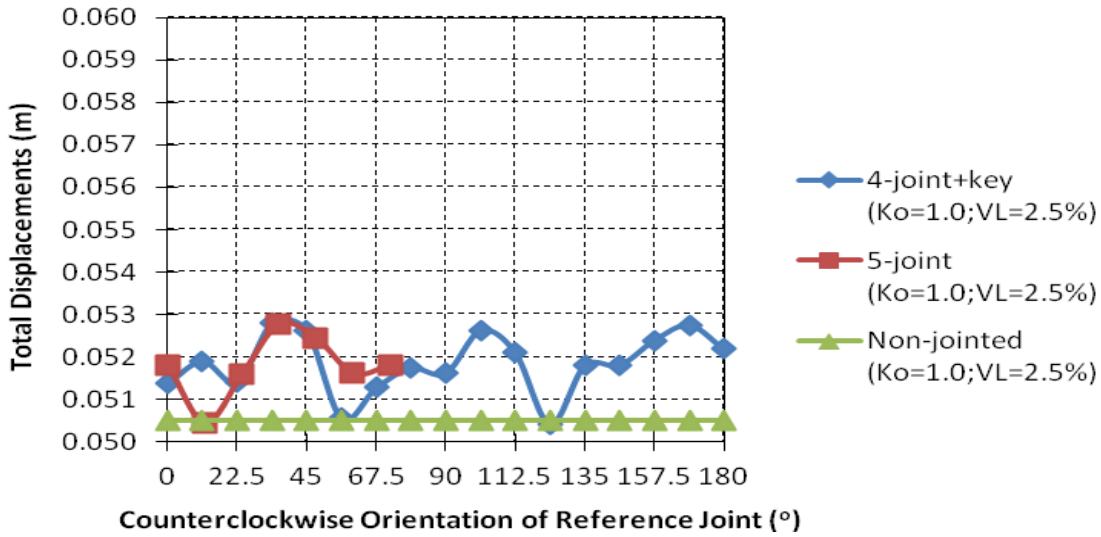
0.060
0.059
0.058
0.057
0.056
0.055
0.054
0.053
0.052
0.051
0.050
Total Displacements (m)
0
22.5
45
67.5
90
112.5
135
157.5
180
Counterclockwise Orientation of Reference Joint (°)
4-joint+key (Ko=1.0;VL=2.5%)
5-joint (Ko=1.0;VL=2.5%)
Non-jointed (Ko=1.0;VL=2.5%)

(b)

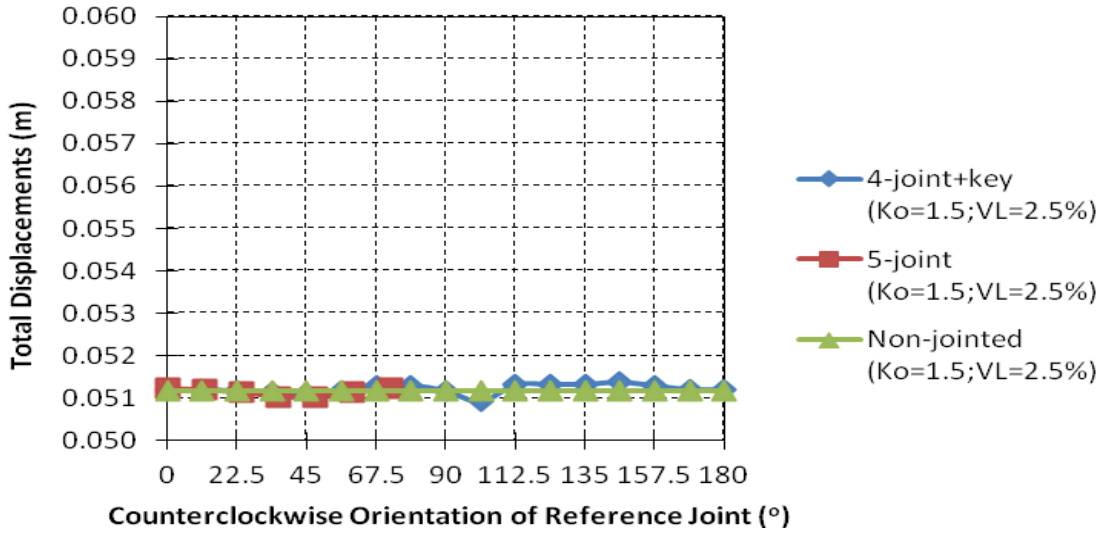

(c)

Figure 11.18 Variation of total displacements with counterclockwise orientation of reference joint for (a) K_o=0.5; (b) K_o=1.0; and (c) K_o=1.5

11.11 Summary

Based on the condition, i.e. flexibility ratio, defined in Section 11.8, both K_o and volume loss were observed to be the two important factors affecting the maximum bending moment, minimum bending moment, maximum thrust, minimum thrust and total displacements induced in jointed and non-jointed tunnel lining of single bored tunnel. In the case of interaction between closely spaced parallel bored tunnels, numerical simulation for a 4-joint+key can be simplified by using 5-joint, as it provides good approximation of the maximum bending moment, minimum bending moment, maximum thrust and total displacements. Further simplification using a non-jointed tunnel lining is possible with the following considerations:

1. For K_o of 0.5, appreciably larger maximum bending moment and minimum bending moment are induced in the non-jointed tunnel lining as compared to the 4-joint+key and the 5-joint, indicating conservative estimation of maximum and minimum bending moment using the non-jointed tunnel lining.
2. For K_o of 1.0, the non-jointed tunnel lining provides a good upper bound estimation of the maximum and minimum bending moment induced in the 4-joint+key and the 5-joint.

3. For K_o of 1.5, the maximum bending moment induced in the non-jointed tunnel lining could be slightly smaller than the 4-joint+key and the 5-joint. However, the non-jointed tunnel lining generally provides an approximately average estimate of the maximum bending moment induced in the jointed tunnel lining. In addition, the non-jointed tunnel lining also provides a reasonable upper bound approximation of the corresponding minimum bending moment of the 4-joint+key and the 5-joint.
4. For K_o of 0.5, 1.0 and 1.5, the non-jointed tunnel lining provides a good upper bound estimation of the maximum thrust induced in the 4-joint+key and the 5-joint.
5. For K_o of 1.5, the non-jointed tunnel lining provides a good estimation of the total displacements induced in the 4-joint+key and the 5-joint, despite smaller total displacements generated in the non-jointed tunnel lining for K_o of 0.5 and 1.0.

It is possible to incorporate the joint stiffness to represent the jointed tunnel lining that is adopted in actual construction. From this study, it is clear that the behaviour of the non-jointed tunnel lining is in broad agreement with the 4-joint+key and 5-joint. Hence, further increase in the joint stiffness could enhance the relationship between the 4-joint+key, the 5-joint and the non-jointed tunnel lining with a tendency for them to exhibit similar responses.

CHAPTER 12 CONCLUSIONS AND RECOMMENDATIONS

12.1 Introduction

This research study was set against the background of the construction of Circle Line (CCL) Mass Rapid Transit (MRT) Tunnels Contract 856 in Singapore. Apart from evaluating the field performance of bored tunnelling based on field measurements, the thesis presented back analyses using the two-dimensional (2D) finite element method program, PLAXIS with the aim to validate the use of empirical correlations and soil properties for subsequent numerical analyses. An effective method for estimating the trough width parameter i and location of maximum surface settlement Loc S_{max} for back analysis of single bored tunnel and closely spaced bored tunnels was proposed. Based on a series of parametric studies, empirical equations were derived using regression analysis for estimation of the trough width parameter i and location of maximum surface settlement Loc S_{max} for closely spaced bored tunnels. At tunnel level, the factors affecting the interaction between closely spaced bored tunnels were identified and design charts for estimating the magnitude of tunnel interaction were proposed and validated using published case records. An extensive study of the behaviour of jointed tunnel lining was performed to interprete the interrelationship between jointed tunnel lining and non-jointed tunnel lining. The following presents conclusions drawn from this study. Recommendations for future work are subsequently presented.

12.2 Field Performance of Bored Tunnelling through Jurong Formation and Mixed Ground of Jurong Formation and Kallang Formation

The comparative study of the EPBM parameters from Circle Line Contract 856 indicates the EPBM speed influences both the ground surface settlement and heave. The occurrence of ground surface heave may lead to smaller settlements above the EPBM face which results in smaller overall final settlement. In mixed grades ground conditions, the ground surface settlement for the first and second bored tunnel could be significantly different, despite similar EPBM parameters being

adopted during bored tunnelling. This suggests that the performance of the first EPBM tunnelling may not always be relevant to assess the performance for the second adjacent bored tunnelling. For tunnelling through mixed ground of Jurong Formation and Kallang Formation, sufficient grouting over EPBM shield and tail void is necessary to minimise the flowing or squeezing of Kallang Formation soils. In addition, the performance of EPBM could be in good qualitative agreement with the transient ground surface response.

12.3 Finite Element Analysis of Ground Surface Settlements Induced by Closely Spaced Bored Tunnels

A total of 13 case studies from Circle Line Contract 856 involving bored tunnelling through uniform grade of Jurong Formation, mixed grades of Jurong Formation and mixed ground of Jurong Formation and Kallang Formation were analysed using the 2D finite element method program, PLAXIS. For the Jurong Formation both the Hardening Soil (HS) model and Mohr-Coulomb (MC) model were used. Depending on the volume loss, the magnitude of maximum surface settlement computed using the HS model and MC model could be different. Both the HS and MC models provide good estimates of the transverse surface settlement and the location of the maximum surface settlement for closely spaced bored tunnels. The EPBM performance of the second bored tunnelling and pillar width which greatly influence the volume loss induced in the closely spaced bored tunnels are found to have a significant effect on the location of the maximum surface settlement. The close agreement between the field measurements and results from the numerical analysis is more meaningful than efforts to achieve a perfect match due to the pre-existing factors such as aboveground structures and heterogeneous soil profiles in the field that affect the field measurements.

12.4 Determination of Settlement Parameters for Single Bored Tunnel and Closely Spaced Bored Tunnels

The Excel spreadsheet built-in optimisation routine Solver provides a framework for the interpretation of the trough width parameter i and location of maximum surface settlement Loc S_{max} for good quality field measurements. These estimated trough width parameter i were generally similar to those recommended by various researchers, in particular Peck (1969). However, there were some discrepancies possibly because of errors during measurement and mixed ground condition. A greater trough width parameter i was observed for closely spaced bored tunnels as compared to single bored tunnel. In addition, the location of the maximum surface settlement Loc S_{max} for closely spaced bored tunnels is found to be offset from the tunnel axis of the first bored tunnel.

12.5 Empirical Equations for Predicting Settlement Parameters for Closely Spaced Bored Tunnels

Based on a comprehensive parametric study of ground surface settlement, empirical equations have been developed for estimating the trough width parameter i and location of maximum surface settlement Loc S_{max} for closely spaced bored tunnels. With volume loss of 0.5 per cent and 5 per cent being incorporated into these empirical equations, the trough width parameter i and location of maximum surface settlement Loc S_{max} in between these two volume loss values can be approximated. Based on these settlement parameters, the Gaussian probability curve of ground surface settlement can be generated for engineering analysis.

12.6 Effects of Tunnel Interaction on Stresses and Displacements Induced in the Pre-Existing Bored Tunnel

The interaction effects of closely spaced bored tunnels could be evaluated by observing the difference between various factors affecting the stiff lining and flexible lining. Both tunnel angular relative position and K_o provide a good

indication of the interaction mechanisms for stiff lining and flexible lining where the former are mainly governed by the lining deformation of the new adjacent bored tunnel whereas the latter is mainly controlled by the stress relief associated with the volume loss of the bored tunnels, which dominates the behaviour of the surrounding soil. This effect of volume loss diminishes gradually with increasing tunnel proximity. A comparison of the interaction mechanisms between stiff lining and flexible lining reveals no direct interpretation of the overall interaction effects can be achieved using a single approach.

12.7 Design Charts for Estimating Magnitude of Interaction Effects for Closely Spaced Tunnels

Due to the limitations that exist in direct interpretation of the overall interaction effects, a series of design charts have been developed to facilitate the determination of the incremental maximum bending moment and lining deformation of the pre-existing bored tunnel after interaction with the new adjacent bored tunnel. The proposed design charts take into account the effects of lining deformation, volume loss of pre-existing bored tunnel and volume loss of new adjacent bored tunnel. The proposed design charts were validated using seven published case records.

12.8 Analysis of Jointed Tunnel Lining

Values of K_o and volume loss have significant influence on the variation of the maximum bending moment, minimum bending moment and total displacements with orientation of reference joint for jointed tunnel lining of single bored tunnel. Numerical simulation of 5-joint is suitable for a relatively quick estimation of stresses and displacements for a lining with 4-joint+key. Numerical analysis of interaction between closely spaced parallel bored tunnels with 4-joint+key can be simplified to 5-joint in order to account for the effect of joints. At the limiting condition where the parameters of the joints are absent, further simplification of 4-joint+key to a non-jointed tunnel lining produces reasonable results that are sensitive to K_o.

12.9 Recommendations for Further Research

Based on the findings of this research study and the available literature, further research of the interaction between closely spaced bored tunnels for greenfield and non-greenfield sites in the following areas are recommended:

1. To investigate the effects of relative position of closely spaced bored tunnels on the ground surface response. Like the present research study, it is important to have good quality field measurements or data from well-documented sites reported in the literature to verify the approach of analysis.
2. To perform 3D numerical modelling on tunnel interaction. While confidence was gained in the predictability of the settlement parameters and magnitude of interaction effects for closely spaced bored tunnels through 2D numerical simulations, factors affecting the volume loss have not been examined. In this respect, 3D numerical modelling could assist in assessing the effects of TBM parameters on the magnitude of ground surface settlement.
3. To conduct research on long-term ground surface response induced by closely spaced bored tunnelling. The differences in composition and relative permeability of the various members of Kallang Formation to the tunnel lining affecting the long-term ground surface response could be assessed using 2D approach. However, one of the challenges of this kind of research is to obtain sufficient good quality long-term field measurements for numerical calibration.
4. To collate field measurements on building settlement above the alignments of closely spaced bored tunnelling through Jurong Formation and mixed ground of Jurong Formation and Kallang Formation. As a building will generally settle less than the ground. It would be beneficial to identify the relationship between non-greenfield ground surface settlement trough and greenfield ground surface settlement trough induced by closely spaced bored tunnelling. Accompanying the correlation, the present proposed empirical equations for settlement parameters can be utilised to estimate the non-greenfield ground surface settlement trough induced by closely spaced bored tunnelling for subsequent assessment of the severity of building response.

REFERENCES

Addenbrooke, T.I. and Potts, D.M. (2001). Twin Tunnel Interaction: Surface and Subsurface Effects. The International Journal of Geomechanics, Volume 1, Number 2, pp. 249-271.

Afifipour, M., Sharifzadeh M., Shahriar, K. and Jamshidi, H. (2011). Interaction of twin tunnels and shallow foundation at Zand underpass, Shiraz metro, Iran. Tunnelling and Underground Space Technology, Vol. 26, pp. 356-363.

Ahmed, M. and Iskander, M. (2011). Analysis of Tunneling-Induced Ground Movements Using Transparent Soil Models. Journal of Geotechnical and Geoenvironmental Engineering, Vol. 137, pp. 525-535.

Anagnostou, G. (1993). Modelling seepage flow during tunnel excavation. Proc. ISRM International Symposium – EUROCK'93, "Safety and Environmental Issues in Rock Engineering", 21-24 / 06 / 1993, Lisbon, Vol. 1, pp. 3-10. Rotterdam: A. A. Balkema.

Anagnostou, G. (1995). Influence of tunnel excavation on hydraulic head. Int. Journal of Num. and Analyt. Meth. in Geomechanics, 19, pp. 725-746.

Anagnostou, G. and Kovári, K. (1994). The Face Stability of Slurry-shield-driven-Tunnels. Tunnelling and Underground Space Technology, Vol. 9, No. 2, pp. 165-174.

Anagnostou, G. and Kovári, K. (1996). Face Stability Conditions with Earth-Pressure-Balanced Shields. Tunnelling and Underground Space Technology, Vol. 11, No. 2, pp. 165-173.

Atkinson, J.H. and Potts, D.M. (1977). Subsidence above Shallow Tunnels in Soft Ground. Proc. ASCE, Vol. 103, No. GT4, pp. 307-325.

Atkinson, J.H. and Potts, D.M. (1979). Subsidence above shallow tunnels in soft ground. Journal of Geotechnical Engineering, American Society of Civil Engineers, GT4, pp. 307-325.

Atkinson, J.H. and Sallfors, G. (1991). Experimental determination of soil properties. In: Proceedings of the 10th ECSMFE, vol. 3, Florence, pp. 915–956.

Attewell, P.B. (1977). Ground movements caused by tunnelling in soil. Proc. of the Large Ground Movements and Structures Conference, Cardiff, Edited by Geddes, Pentech Press, London, pp. 812-948.

Bilotta, E. (2008). Use of diaphragm walls to mitigate ground movements induced by Tunnelling. Géotechnique, Vol. 58, No. 2, pp. 143–155.

Breth, H. (1977). Tunnelling in Soft Ground. Proceedings of the 9th International Conference on Soil Mechanics and Foundation Engineering, Tokyo, Vol. 3, pp. 463-468.

Brinkgreve, R.B.J., Engin, E. and Swolfs, W.M. (2012). PLAXIS 2D 2012.

British Standard Code of practice for site investigations. (1999). BS 5930:1999

Broms, B.B. and Bennermark, H. (1967). Stability of clay at vertical openings. Journal of the Soil Mechanics and Foundations Division, Vol. 93(1), pp. 71-94.

Brown, E.T. and Hudson, J.A. (1984). Design and Performance of Underground Excavations. ISRM Symposium, Cambridge, pp. 221-229.

Burland, J.B. (2001). Assessment methods used in design. Building response to tunnelling: Case studies from construction of the Jubilee Line Extension, London, Editors: J.B. Burland, J.R. Standing, F.M. Jardine, Vol. 1, pp. 23-43.

Carter, J.P. and Booker, J.R. (1984). The behaviour of a lined circular tunnel in viscoelastic ground. In Proceedings of the Computational Techniques and Applications Conference, Amsterdam, North Holland, pp. 753-768.

Chakeri, H., Ozcelik, Y. and Unver, B. (2013). Effects of important factors on surface settlement prediction for metro tunnel excavated by EPB. Tunnelling and Underground Space Technology, Vol. 36, pp. 14-23.

Chapman, D.N., Ahn, S.K. and Hunt, D.V.L. (2007). Investigating ground movements caused by the construction of multiple tunnels in soft ground using laboratory model tests. Canadian Geotechnical Journal, Vol. 44, pp. 631–643.

Chen, R.P., Zhu, J., Liu, W. and Tang, X.W. (2011). Ground movement induced by parallel EPB tunnels in silty soils. Tunnelling and Underground Space Technology, Vol. 26, pp. 163-171.

Chen, S.L., Gui, M.W. and Yang, M.C. (2012). Applicability of the principle of superposition in estimating ground surface settlement of twin- and quadruple-tube tunnels. Tunnelling and Underground Space Technology, Vol. 28, pp. 135-149.

Chern, J.C. and Hsiao, F.Y. (2005). Interaction Behavior of the Hsuehshan Tunnels. World 2005 Long Tunnels, pp. 73-79.

Chi, S.Y., Chern, J.C. and Lin, C.C. (2001). Optimized back-analysis for tunneling-induced ground movement using equivalent ground loss model. Tunnelling and Underground Space Technology, Vol. 16, pp. 159-165.

Chou,W.I. and Bobet, A. (2002). Predictions of ground deformations in shallow tunnels in clay. Tunnelling and Underground Space Technology, Vol. 17, pp. 3-19.

Chu, B.L., Hsu, S.C., Chang, Y.L. and Lin, Y.S. (2007). Mechanical behavior of a twin-tunnel in multi-layered formations. Tunnelling and Underground Space Technology, Vol. 22, pp. 351–362.

Chu, J. Kay, R.E., Tay, T.H. and Wen, D. (2000). Engineering properties of fluvial sand at Race Course Road. Tunnels and Underground Structures, Zhao, Shirlaw & Krishnan (eds), pp. 591-596.

Clough, G.W. and Mana, A. (1976). Lessons learned in Finite Element Analyses of Temporary Excavations in Soft Clay. Proceedings of the 2nd International Conference on Numerical Methods in Geomechanics, Blacksburg, ASCE, pp. 496-510.

Clough, G.W. and Schmidt, B. (1977). Design and Performance of Excavations and Tunnels in Soft Clay. Int. Symp. on Soft Clay, Bangkok, 85 p.

Clough, G.W. and Schmidt, B. (1977). Three Dimensional Finite Element Analysis of Shallow Soil Tunneling. Int. Symp. on Soft Clay, Bangkok, pp. 10-22.

Clough, G.W. and Schmidt, B. (1981). Design and performance of excavations and tunnels in soft clay. Soft clay engineering, Ed. E.W. Brand and R.P. Brenner, Elsevier, Amsterdam, 1981, pp. 567-634.

Copsey, J.P. and Doran, S.R. (1987). Mass Rapid Transit Systems. Proc. of the Singapore Mass Rapid Transit Conference, pp. 225-235.

Cording, E.J. and Hansmire, W.H. (1975). Displacement around Soft Ground Tunnels. Proceedings of the 5th Pan American Conference on Soil Mechanics and Foundation Engineering, Buenos Aires, Vol. 4, pp. 571-630.

CPG Consultants Pte. Ltd. (2005). Contract 856 Construction & Completion of West Coast, Pasir Panjang, Alexandra & Telok Blangah Stations Including Harbourfront Fit Out Works & Tunnels. Geotechnical Interpretative Report, Vol. 1, 126 p.

Dang, H.K. and Meguid, M.A. (2008). Application of a multilaminate model to simulate the undrained response of structured clay to shield tunnelling. Canadian Geotechnical Journal, Vol. 45, pp. 14–28.

Deere, D.U., Peck, R.B., Monsees, J.E. and Schimdt, B. (1969). Design of Tunnel Liners and Support System. Final Report by the Department of Civil Engineering, University of Illinois at Urbana-Champaign for the Office of High Speed Ground Transportation, U.S. Dept. of Transp., Contr. No. 3-0152, 404 p.

Ding, W.Q., Yue, Z.Q., Tham, L. G., Zhu, H.H., Lee, C.F. and Hashimoto, T. (2004). Analysis of shield tunnel. International Journal for Numerical and Analytical Methods in Geomechanics, Vol. 28, pp. 57–91.

Divall, S. (2013). Ground movements associated with twin-tunnel construction in clay. Unpublished Doctoral thesis, City University London.

Duddeck, H. and Erdmann, J. (1982). Structural design models for tunnels. Tunnelling'82, Proceedings of the 3rd International Symposium, Institution of Mining and Metallurgy, London, pp. 83-91.

Duncan, J. M. and Buchignani, A. L. (1976). An engineering manual for settlement studies. Geotechnical Engineering Report, Department of Civil Engineering, University of California, Berkeley, 94 p.

EFNARC (2005). Specification and guidelines for the use of specialist products for mechanised tunnelling (TBM) in soft ground and hard rock.

Franzius, J.N., Potts, D.M., and Burland, J.B. (2005). The influence of soil anisotropy and K_o on ground surface movements resulting from tunnel excavation. Géotechnique, Vol. 55, No. 3, pp. 189–199.

Ghaboussi, J. and Ranken, R.E. (1977). Interaction between two parallel tunnels. International Journal for Numerical and Analytical Methods in Geomechanics, Vol. 1, pp.75-103.

Goh, K.H., Jeyatharan, K. and Wen, D. (2012). Understanding the stiffness of soils in Singapore from Pressuremeter Testing. Geotechnical Engineering Journal of the SEAGS & AGSSEA, Vol. 43, pp. 56-62.

González, C. and Sagaseta, C. (2001). Patterns of soil deformations around tunnels. Application to the extension of Madrid Metro. Computers and Geotechnics, Vol. 28, pp. 445-468.

Hansmire, W.H. (1975). Field Measurements of Ground Displacements About a Tunnel in Soil. Ph.D. Thesis, University of Illinois at Urbana-Champaign, 357 p.

Hansmire, W.H. and Cording, E.J. (1972). Performance of a Soft Ground Tunnel on the Washington, D. C. Metro. Proceeding of the 1st North American Rapid Excavation and Tunnelling Conference, Chicago, AIME, Vol. 1, pp. 371-389.

Herzog, M. (1985). Surface subsidence above shallow tunnels (in German). Bautechnik 62, pp. 375–377.

Heuer, R.E. (1974). Important ground parameters in soft ground tunneling. Subsurface exploration for underground excavation and heavy construction, New England College, Henniker, New Hampshire, American Society of Civil Engineers, New York, pp.41-55.

Heuer, R.E. and Virgens, D.L. (1987). Anticipated behavior of silty sands in tunneling. Rapid Excavation and Tunneling Conference, Louisiana, New Orleans, Society of Mining Engineers, Inc., Colorado, Littleton, v.1, pp. 221-237.

Hight, D. W. and Higgins, K. G. (1995). An approach to the prediction of ground movements in engineering practice background and application. Int. Symp. on pre-failure deformation charact. of geomaterials, pp. 909-945.

Horn, M. (1961). Alagutak homlokbiztositására ható vizszintes földnyomásvizsgálat néhány eredménye. Az országos mélyépitóipari konferencia elóadásai, Közlekedési Dokumentációs Vállalat, Budapest (in Hungarian). See also "Horizontaler Erddruck auf senkrechte Abschlussflächen von Tunneln", in Landeskonferenz der ungarischen Tiefbauindustrie, Budapest (German translation, STUVA, Düsseldorf).

http://www.itascacg.com

http://www.plaxis.nl

ITA/AITES Report 2006 (2007). Settlements induced by tunneling in Soft Ground. Tunnelling and Underground Space Technology, Vol. 22, pp. 119-149.

Janbu, N. (1963). Soil compressibility as determined by oedometer and triaxial tests. Proc. ECSMFE, Wiesbaden, 1, pp. 19-25.

Janssen, H.A. (1895). Versuche über Getreidedruck in Silozellen. Zeitschrift des Vereins deutscher lngenieure XXXIX (35), pp. 1045-1049 (in German).

Kasper, T. and Meschke, G. (2006). On the influence of face pressure, grouting pressure and TBM design in soft ground tunnelling. Tunnelling and Underground Space Technology, Vol. 21, pp. 160–171.

Kawaguchi, T., Mitachi, T., Shibuya, S. and Sato, S. (2003). Evaluation of deformation modulus of clay at small strains based on isotropic elasticity. Deformation Characteristics of Geomaterials, Ed. Di Benedetto, H., Doanh, T., Geoffroy, H. and Sauzéat, C., Swets & Zeitlinger B.V., Lisse, The Netherlands.

Kim, S.H. (1996). Model Testing and Analysis of Interactions between Tunnels in Clay. D.Phil. Thesis, University of Oxford.

Kim, S.H., Burd, H.J. and Milligan, G.W.E. (1996). Interaction between Closely Spaced Tunnels in Clay. Geotechnical Aspects of Underground Construction in Soft Ground, pp. 543-548.

Kim, S.H., Burd, H.J. and Milligan, G.W.E. (1998). Model testing of closely spaced tunnels in clay. Géotechnique, pp. 375-388.

Kimmance, J.P., Lawrence, S., Hassan, O. and Purchase, N.J. (1996). Observations of Deformations Created in Existing Tunnels by Adjacent and Cross Cutting Excavations. Geotechnical Aspects of Underground Construction in Soft Ground, pp.707-712.

Kirsch, G. (1898). VDI, Vol. 42, described in Timoshenko & Goodier.

Koungelis, D.K. and Augarde, C.E. (2004). Interaction between multiple tunnels in soft ground. Developments in Mechanics of Structures and Materials, pp. 1031-1036.

Land Transport Authority. (2010). Engineering Group Civil Design Criteria For Road And Rail Transit Systems, E/GD/09/106/A1, Controlled Document, 351 p.

Leach, G. (1985). Pipeline response to tunnelling. Unpublished paper presented to the North of England Gas Association, January 1985.

Lee, C.J., Wu, B.R., Chen, H.T. and Chiang, K.H. (2006). Tunnel stability and arching effects during tunneling in soft clayey soil. Tunnelling and Underground Space Technology, Vol. 21, pp. 119–132.

Lee, K.M. and Ge, X.W. (2001). The equivalence of a jointed shield-driven tunnel lining to a continuous ring structure. Canadian Geotechnical Journal, 38, pp. 461-483.

Lee, K.M., Hou, X.Y., Ge, X.W. and Tang, Y. (2001). An analytical solution for a jointed shield-driven tunnel lining. International Journal for Numerical and Analytical Methods in Geomechanics, 25, pp. 365–390.

Lee, S.C., LU, F.S. and Lee, K.W. (2005). Interaction Behaviors During The Excavation For Three-Parallel Tunnel. World 2005 Long Tunnels, pp. 91-103.

Leong, E.C., Rahardjo, H. and Tang, S.K. (2003). Characterisation and engineering properties of Singapore residual soils. Characterisation and Engineering Properties of Natural Soils, Ed. T.S. Tan, K.K. Phoon, D.W. Hight and S. Leroueil, Swets & Zeitlinger B.V., Lisse, The Netherlands, pp. 1279-1304.

Liakos, A.L., Nasri, V. and Jafari, M.R. (2003). Effect of soil consolidation on soil-lining interaction in tunnels. (Re)Claiming the Underground Space, pp. 1015-1017.

Lim, K.K., Chu, C.Y., Lim, T.F., Tan, M.W. and Wong, Y.K. (2008). Singapore Circle Line Stage 3 – The challenges of tunnelling in close proximity. Proceedings of International Conference on Deep Excavations (ICDE) 2008, 8 p.

Lin, D.G., Tseng, C.T., Phienwej, N. and Suwansawat, S. (2002). 3-D deformation analysis of earth pressure balance shield tunnelling in Bangkok subsoil. Journal of the Southeast Asian Geotechnical Society, Vol. 33(1), pp. 13-27.

Litwiniszyn, J. (1957). The theories and model research of movements of ground masses. In: Proceedings of European Congress Ground Movement, Leeds, UK, pp. 203–209.

Lo, K.W., Chang, L.K., Leung, C.F., Lee, S.L., Makino, H. and Mihara, T. (1987). Field measurements at a multiple tunnel interaction site, 2nd International Symposium on Field Measurements in Geomechanics, Ed. S. Sakurai, Balkema, Rotterdam.

Loganathan, N. and Flanagan, R.F. (2001). Predictions of Tunnelling-Induced Ground Movements: Assessment and Evaluation. Proceedings of Underground Singapore 2001, pp. 102-113.

Loganathan, N. and Poulos, H.G. (1998). Analytical prediction for tunneling-induced ground movements in clays. Journal of Geotechnical and Geoenvironmental Engineering, Vol. 124, No. 9, pp. 846–856.

Mair, R.J. (1978). Centrifugal Modelling of Tunnel Construction in Soft Clay. PhD Thesis, University of Cambridge.

Mair, R.J. (1993). Developments in geotechnical engineering research: application to tunnels and deep excavations. Unwin Memorial Lecture 1992, Proceedings of Institution of Civil Engineers: Civil Engineering, Vol. 93, pp. 27-41.

Mair, R.J., Gunn, M.J. and O'Reilly, M.P. (1981). Ground Movements around Shallow Tunnels in Soft Clay. Proceedings of the 10th International Conference on Soil Mechanics and Foundation Engineering, Stockholm, Vol. 1, pp. 323-328.

Mair, R.J. and Taylor, R.N. (1996). Design of twin-tube tunnel through soft rock. Proceedings of the International Symposium on Geotechnical Aspects of Underground Construction in Soft Ground. London, UK, pp. 15-17.

Mair, R. J., Taylor, R. N. and Bracegirdle, A. (1993). Subsurface settlement profiles above tunnels in clay. Géotechnique, 43, No. 2, pp. 315–320

Mair, R.J., Taylor, R.N. and Burland, J.B. (1996). Prediction of ground movements and assessment of risk of building damage due to bored tunnelling. In: Mair, Taylor (Eds.), Proc. Int. Symposium on Geotechnical Aspects of Underground Construction in Soft Ground, London, Balkema, pp. 623–628.

Mair, R. J. and Taylor, R. N. (1997). Bored Tunneling in the Urban Environment. Proceedings of the 14th International Conference on Soil Mechanics and Foundation Engineering, Hamburg, pp. 2353–2385.

Mathew, G.V. and Lehane, B.M. (2013). Numerical back-analyses of greenfield settlement during tunnel boring. Canadian Geotechnical Journal, Vol. 50, pp. 145–152.

McCabe, B.A., Orr, T.L.L., Reilly, C.C. and Curran, B.G. (2012). Settlement trough parameters for tunnels in Irish glacial tills. Tunnelling and Underground Space Technology, Vol. 27, pp. 1-12.

Melis, M., Medina, L. and Rodríguez, J.M. (2002). Prediction and analysis of subsidence induced by shield tunnelling in the Madrid Metro extension. Canadian Geotechnical Journal, Vol. 39, pp. 1273–1287.

Mirhabibi, A. and Soroush, A. (2012). Effects of surface buildings on twin tunnelling-induced ground settlements. Tunnelling and Underground Space Technology, Vol. 29, pp. 40-51.

Monsees, J.E. (1996). Soft Ground Tunneling. Tunnel Engineering Handbook, Ed. John O. Bickel, Thomas R. Kuesel and Elwyn H. King, Chapman & Hall, pp. 97-121.

Morgan, H. D. (1961). A contribution to the analysis of stress in a circular tunnel. Géotechnique, pp. 37-46.

Möller, S.C. (2006). Tunnel induced settlements and structural forces in linings. Dr.-Ing. Thesis, Universität Stuttgart.

Möller, S.C. and Vermeer, P.A. (2008). On numerical simulation of tunnel installation. Tunnelling and Underground Space Technology, Vol. 23(4), pp. 461–475.

Mroueh, H. and Shahrour, I. (2008). A simplified 3D model for tunnel construction using tunnel boring machines. Tunnelling and Underground Space Technology, Vol. 23, pp. 38–45.

Muir Wood, A.M. (1975). The circular tunnel in elastic ground. Géotechnique, Vol. 25, No. 1, pp. 115-127.

Ng, C.W.W. and Lee, G.T.K. (2005). Three-dimensional ground settlements and stress transfer mechanisms due to open-face tunnelling. Canadian Geotechnical Journal, Vol. 42, pp. 1015–1029.

Ng, C.W.W., Lee, K.M. and Tang, D.K.W. (2004). Three-dimensional numerical investigations of new Austrian tunnelling method (NATM) twin tunnel interactions. Canadian Geotechnical Journal, Vol. 41, pp. 523–539.

Nomoto, T., Imamura, S., Hagiwara, T., Kusakabe, O. and Fujii, N. (1999). Shield Tunnel Construction in Centrifuge. Journal of Geotechnical and Geoenvironmental Engineering, Vol. 125(4), pp. 289-300.

Nunes, M.A. and Meguid, M.A. (2009). A study on the effects of overlying soil strata on the stresses developing in a tunnel lining. Tunnelling and Underground Space Technology, Vol. 24, pp. 716-722.

O'Reilly, M.P. and New, B.M. (1982). Settlement above tunnels in the United Kingdom-their magnitude and prediction. Tunnelling 82, London, IMM, pp. 173-181.

Orihara, K., Chan, K.L., Chabayashi, K., Okamoto, S., Teo, P.T.P. and Tan, C.G. (2001). Excavation of New Dhoby Ghaut Station for MRT North East Line. Proceedings of Underground Singapore 2001, Session 5.

Orihara, K. and Khoo, K.S. (1998). Engineering properties of Old Alluvium in Singapore and its parameters for bored pile and excavation design. 13th Southeast Asian Geotechnical Conference, pp. 545-550.

Osman, A.S. (2010). Stability of unlined twin tunnels in undrained clay. Tunnelling and Underground Space Technology, Vol. 25, pp. 290-296.

Palmer, A.C. and Mair, R.J. (2011). Ground movements above tunnels: a method for calculating volume loss. Canadian Geotechnical Journal, Vol. 48, pp. 451–457.

Park, K.H. (2005). Analytical solution for tunnelling-induced ground movement in clays. Tunnelling and Underground Space Technology, Vol. 20, pp. 249–261.

Parker, H.W. (1996). Geotechnical Investigations. Tunnel Engineering Handbook, Ed. John O. Bickel, Thomas R. Kuesel and Elwyn H. King, Chapman & Hall, pp. 46-79.

Peck, R.B. (1969). Deep excavations and tunneling in soft ground. Proceedings of the 7th International Conference on Soil Mechanics and Foundation Engineering, Mexico City, State of the Art Volume, pp. 225-290.

Peck, R.B., Deere, D.U., Moness, J.E., Parker, H.W. and Schmidt, B. (1969). Some Design Considerations in the Selection of Underground Support System. Report for U.S. Dept. of Transportation, Office of High Speed Ground Transportation, Contract 3-0152.

Peck, R.B., Hendron, A.J. and Mohraz, B. (1972). State of the art of soft ground tunneling. Proc. 1st Rapid Excavation and Tunneling Conference, AIME, (1), pp. 259-286.

Phienwaja, N. (1987). Ground response and support performance in a sheared shale, Stillwater Tunnel, Utah. Ph.D. Thesis, University of Illinois at Urbana-Champaign.

Raju, G.V.R., Heath, G.R. and Lim, K. (2000). Lining design and ground response to the construction of the Clarke Quay tunnels. Proceeding of Underground Singapore 2000, pp. 213-218.

Sagaseta, C. (1987). Analysis of undrained soil deformation due to ground loss. Géotechnique, 37, pp. 301-320.

Sahoo, J.P. and Kumar, J. (2013). Stability of long unsupported twin circular tunnels in soils. Tunnelling and Underground Space Technology, Vol. 38, pp. 326-335.

Schmertmann, J. H. (1978). Guidelines for cone penetration test performance and design. Report FHWA-TS-78-209, U.S. Department of Transportation, Washington, 145 p.

Schmidt, B. (1969). A method of estimating surface settlement above tunnels constructed in soft ground. Canadian Geotechnical Journal, 20, pp. 11–22.

Schmidt, B. (1969). Settlements and Ground Movements Associated with Tunnelling in Soil. Ph.D. Thesis, University of Illinois at Urban-Champaign, 224 p.

Schmidt, B. (1974). Exploration for soft ground tunnels - a new approach. Subsurface exploration and heavy construction, New England College, Henniker, New Hampshire, American Society of Civil Engineers, New York.

Schmidt, B. (1977). Tunnels in Granular Soil: Washington and Baltimore Case Histories. Selected paper for Specialty Session 1, 9th ICSMFE, Tokyo.

Sebastian, P. and Nadarajah, P. (2000). Construction of North East Line Tunnels at Singapore River Crossing. Proceedings of the International Conference on Tunnels and Underground Structures, Singapore, pp. 191-198.

Sharma, J.S., Chu, J. and Zhao, J. (1999). Geological and Geotechnical Features of Singapore: an Overview. Tunnelling and Underground Space Technology, Vol. 14, pp. 419-431.

Shirlaw, J.N. (2002). Controlling the risk of excessive settlement during EPB tunnelling. Keynote lecture, Proc. Case studies in geotechnical engineering, NTU Singapore.

Shirlaw, J.N., Ong, J.C.W., Rosser, H.B., Osborne, N.H., Tan, C.G. and Heslop, P.J.E. (2001). Immediate Settlements Due to Tunnelling for the North East Line. Proceedings of Underground Singapore 2001, Session 3.

Sirivachiraporn, A. and Phienwej, N. (2012). Ground movements in EPB shield tunneling of Bangkok subway project and impacts on adjacent buildings. Tunnelling and Underground Space Technology, Vol. 30, pp. 10-24.

Soliman, E., Duddeck, H. and Ahrens, H. (1993). Two- and Three-Dimensional Analysis of Closely Spaced Double-Tube Tunnels. Tunnelling and Underground Space Technology, Vol. 8, pp. 13-18.

Standing, J.R. and Burland, J.B. (2006). Unexpected tunnelling volume losses in the Westminster area, London. Géotechnique, Vol. 56, No. 1, pp. 11–26.

Standing, J.R. and Selemetas, D. (2013). Greenfield ground response to EPBM tunnelling in London Clay. Géotechnique, Vol. 63, No. 12, pp. 989–1007.

Standing, J.R. and Selman, R. (2001). The Response to Tunnelling of Existing Tunnels at Waterloo and Westminster. Building Response to Tunnelling, Vol. 2, pp. 509-546.

Stroud, M.A. (1974). The standard penetration test in insensitive clays and soft rocks. Proc. European Symp. on Penetration Testing, Stockholm, 2.2, pp. 367-375.

Sture, S. (2004). Non-Linear Hyperbolic Model & Parameter Selection. Short Course on Computational Geotechnics + Dynamics, Boulder, Colorado, 24 p.

Suwansawat, S. and Einstein, H.H. (2006). Artificial neural networks for predicting the maximum surface settlement caused by EPB shield tunneling. Tunnelling and Underground Space Technology, Vol. 21, pp. 133–150.

Sweeney, P. (2006). A study of interaction effects due to bored tunnels in clay. M.Eng. Thesis, Massachusetts Institute of Technology.

Terzaghi, K. (1950). Geologic aspects of soft ground tunneling. Applied sedimentation, P.D. Trask, ed., John Wiley, New York.

Terzaghi, K. (1977). Earth tunneling with steel supports. Commercial Shearing and Stamping Co., Youngstown, Ohio.

Terzaghi, K. and Peck, R.B. (1948). Soil Mechanics in Engineering Practice, 1st Edition. John Wiley, New York.

Terzaghi, K. and Peck, R.B. (1967). Soil Mechanics in Engineering Practice, 2nd Edition. John Wiley, New York.

Timoshenko, S. and Goodier, J.N. (1951). Theory of Elasticity. 2nd Edition, McGraw-Hill Book Co., New York, pp. 78-80.

Toki, S., Shibuya, S. and Yamashita, S. (1994). Standardization of laboratory test methods to determine the cyclic deformation properties of geomaterials. Pre-failure Deformation of Geomaterials, 2, pp. 741-784, Balkema.

Verruijt, A. and Booker, J.R. (1996). Surface settlements due to deformation of a tunnel in an elastic half plane. Géotechnique, Vol. 46, No. 4, pp. 753-756.

von Soos, P. (1990). Properties of soil and rock (in German). In In: Grundbautaschenbuch Part 4, Ernst & Sohn, Berlin.

Vorster, T.E.B. (2005). The effect of tunnelling on buried pipes. Unpublished Ph.D. Thesis, University of Cambridge.

Ward, W.H. (1969). Discussion of: Peck, R.B., Deep Excavations and Tunnelling in Soft Ground. Proc. 7th ICSMFE, Vol. 3, pp. 320-325.

Ward, W.H., Samuels, S.G. and Butler, M.E. (1959). Further Studies of the Properties of London Clay. Géotechnique, Vol. 9, pp. 33-58.

Ward, W.H. and Thomas, H.S.H. (1965). The Development of Earth Loading and Deformation in Tunnel Linings in London Clay. Proc. 6th ICSMFE, Vol. 2, pp. 432-436.

Xu, Y.F., Sun, D.A., Sun, J., Fu, D.M. and Dong, P. (2003). Soil disturbance of Shanghai silty clay during EPB tunnelling. Tunnelling and Underground Space Technology, Vol. 18, pp. 537–545.

Yang, X.L. and Wang, J.M. (2011). Ground movement prediction for tunnels using simplified procedure. Tunnelling and Underground Space Technology, Vol. 26, pp. 462-471.

Zhang, Z., Huang, M. and Zhang, M. (2011). Theoretical prediction of ground movements induced by tunnelling in multi-layered soils. Tunnelling and Underground Space Technology, Vol. 26, pp. 345-355.

APPENDICES

Appendix A

Instrumentation Array D35

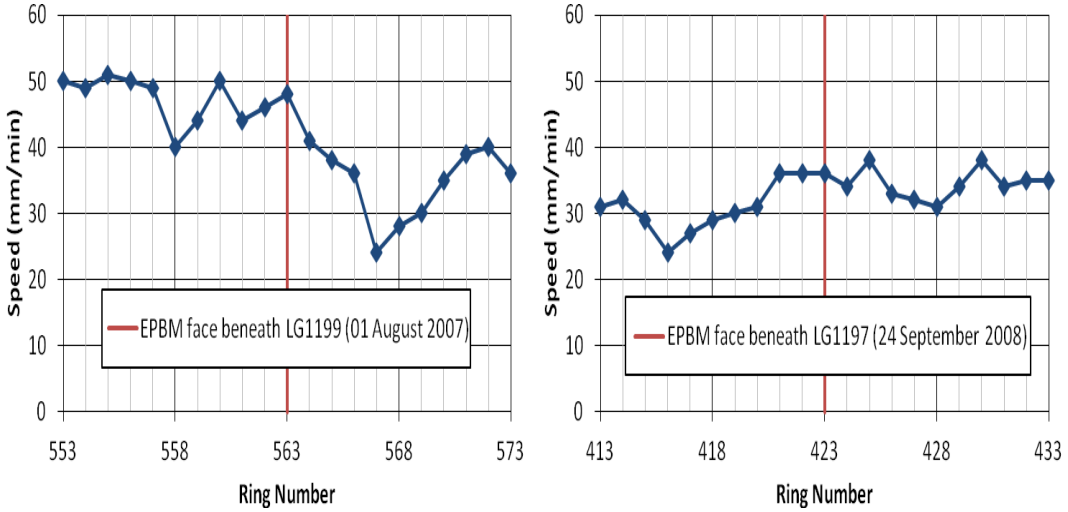

(a) (b)

Figure A.1 TBM speed for (a) first inner bound bored tunnelling; and (b) second outer bound bored tunnelling (Instrumentation Array D35)

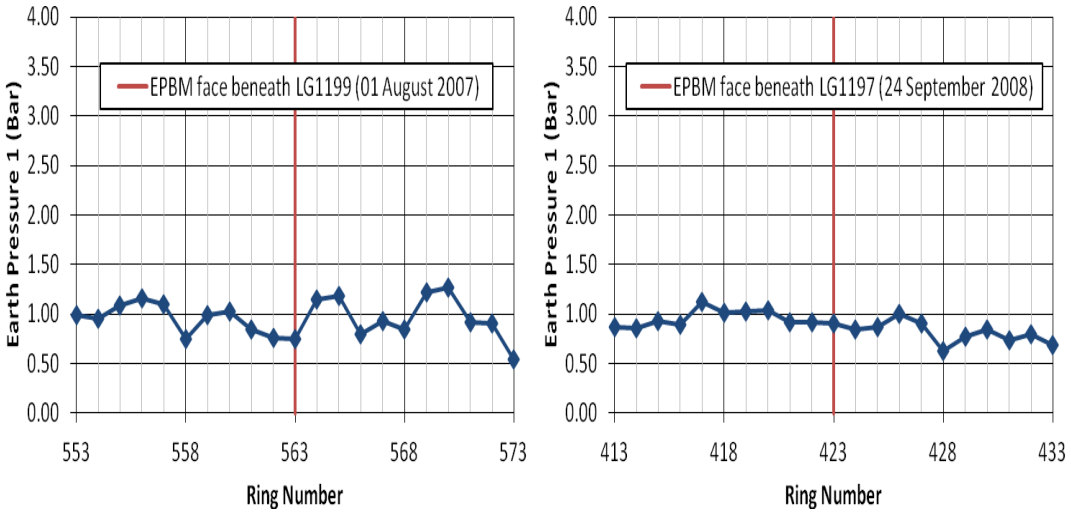

(a) (b)

Figure A.2 TBM earth pressure 1 for (a) first inner bound bored tunnelling; and (b) second outer bound bored tunnelling (Instrumentation Array D35)

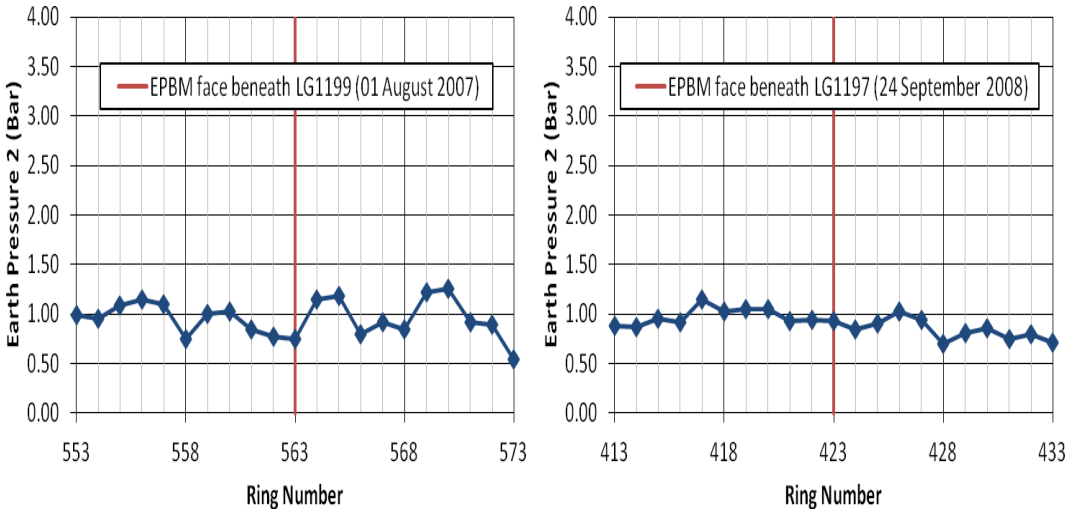

(a) (b)

Figure A.3 TBM earth pressure 2 for (a) first inner bound bored tunnelling; and (b) second outer bound bored tunnelling (Instrumentation Array D35)

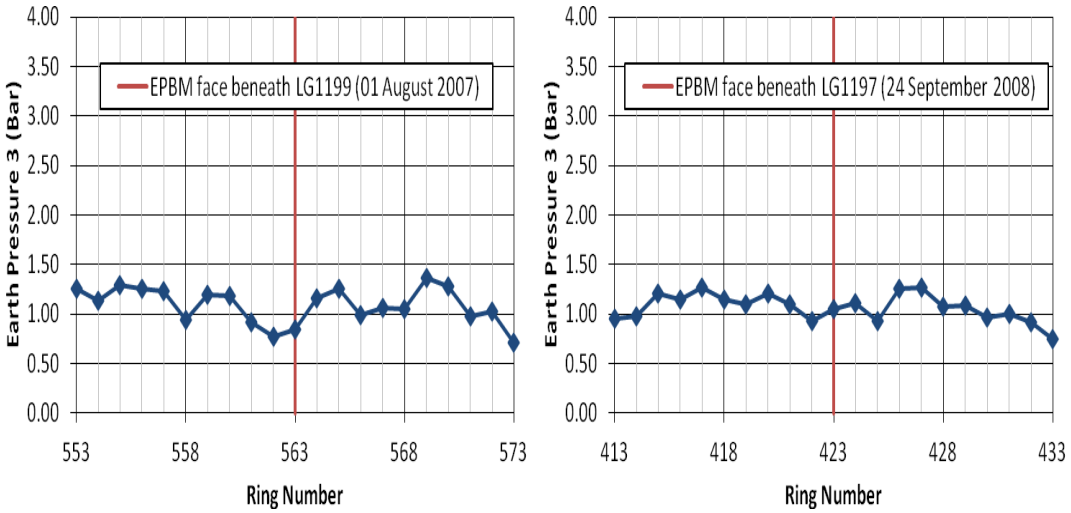

(a) (b)

Figure A.4 TBM earth pressure 3 for (a) first inner bound bored tunnelling; and (b) second outer bound bored tunnelling (Instrumentation Array D35)

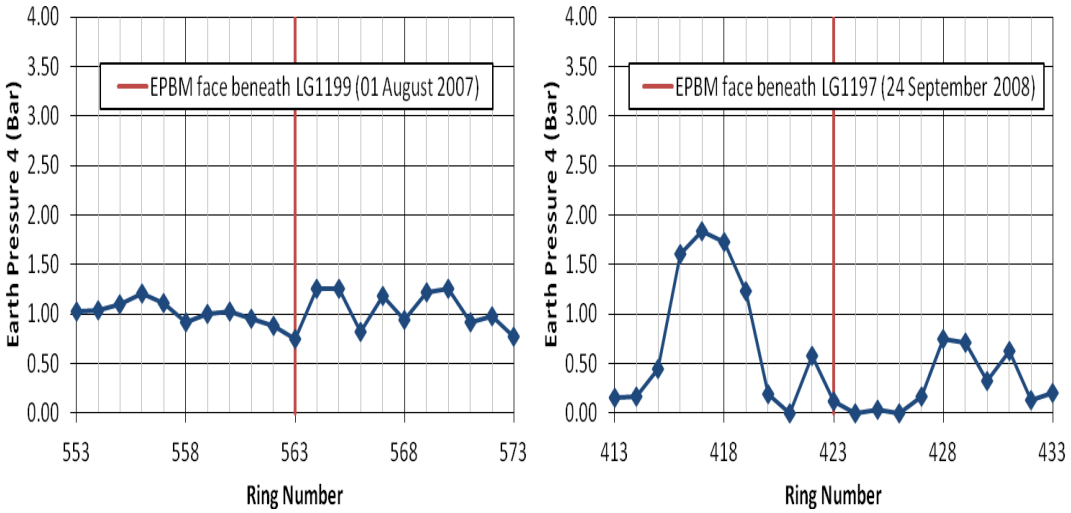

(a) (b)

Figure A.5 TBM earth pressure 4 for (a) first inner bound bored tunnelling; and (b) second outer bound bored tunnelling (Instrumentation Array D35)

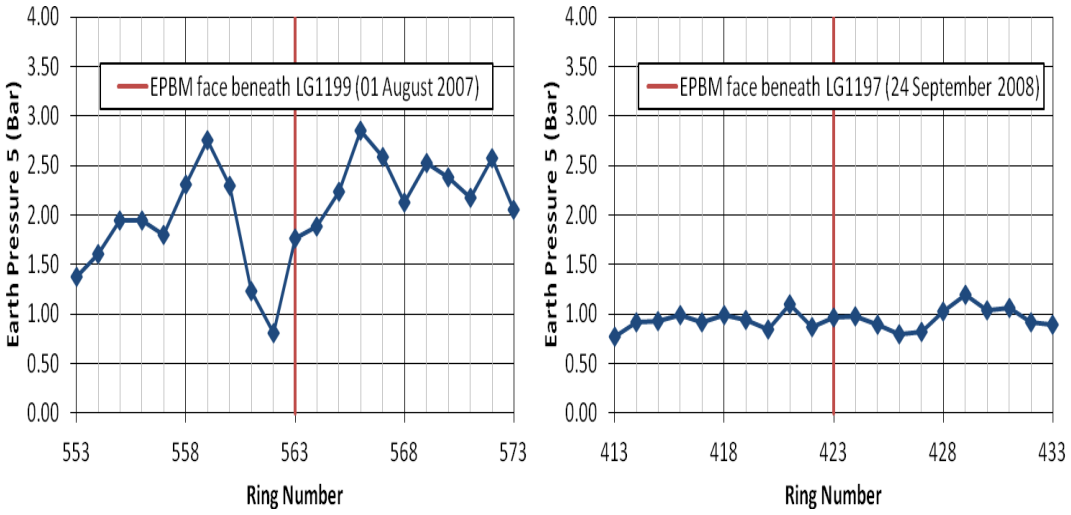

(a) (b)

Figure A.6 TBM earth pressure 5 for (a) first inner bound bored tunnelling; and (b) second outer bound bored tunnelling (Instrumentation Array D35)

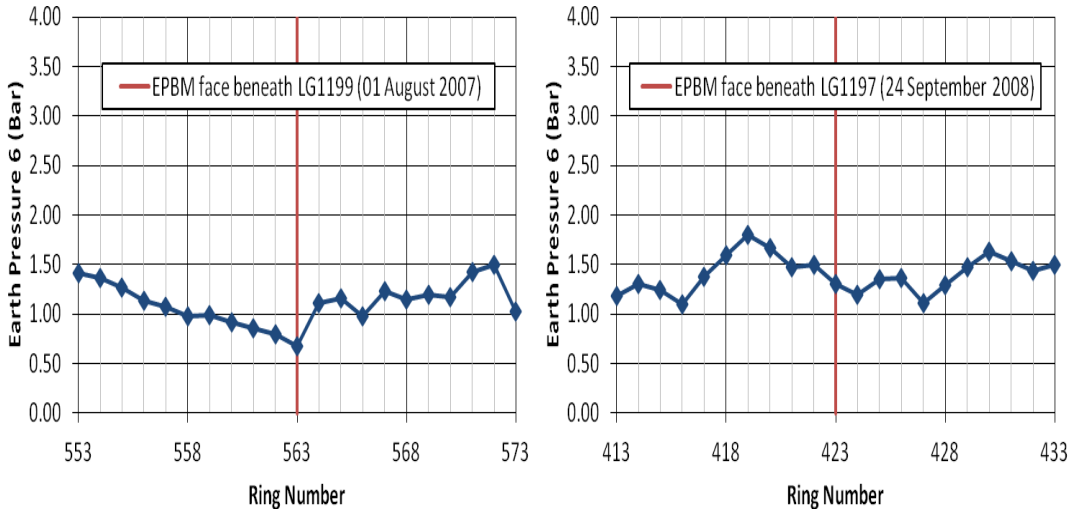

(a) (b)

Figure A.7 TBM earth pressure 6 for (a) first inner bound bored tunnelling; and (b) second outer bound bored tunnelling (Instrumentation Array D35)

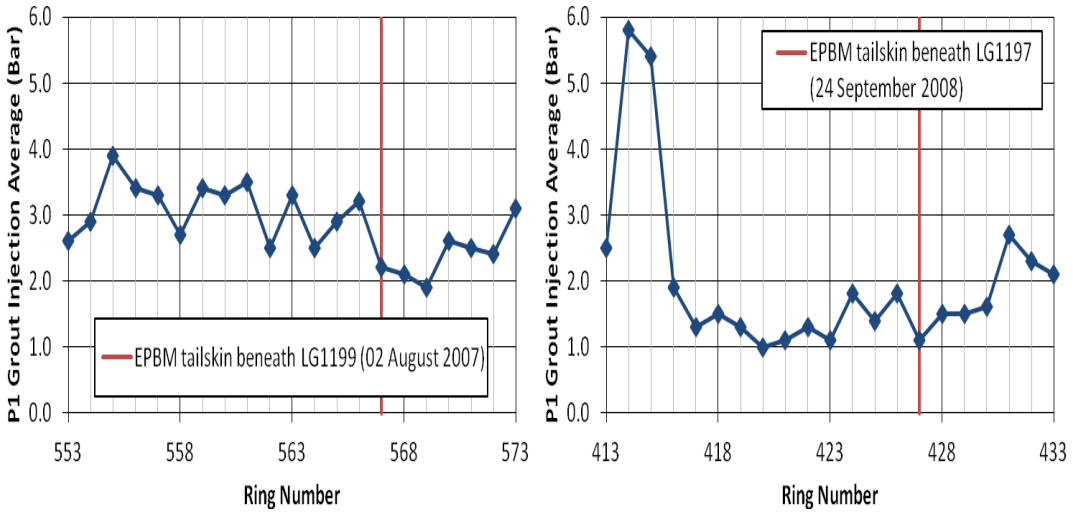

(a) (b)

Figure A.8 P1 grout injection average for (a) first inner bound bored tunnelling; and (b) second outer bound bored tunnelling (Instrumentation Array D35)

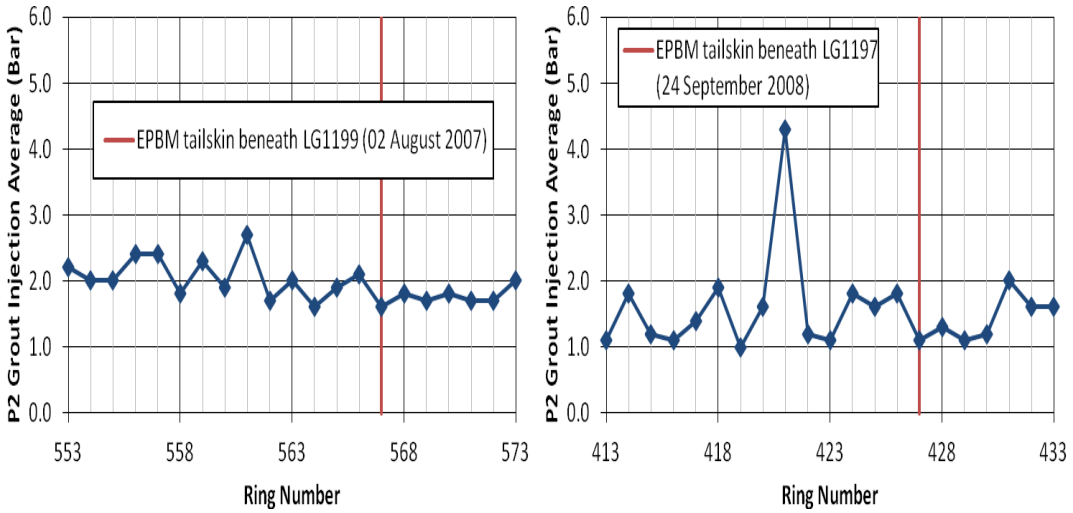

(a) (b)

Figure A.9 P2 grout injection average for (a) first inner bound bored tunnelling; and (b) second outer bound bored tunnelling (Instrumentation Array D35)

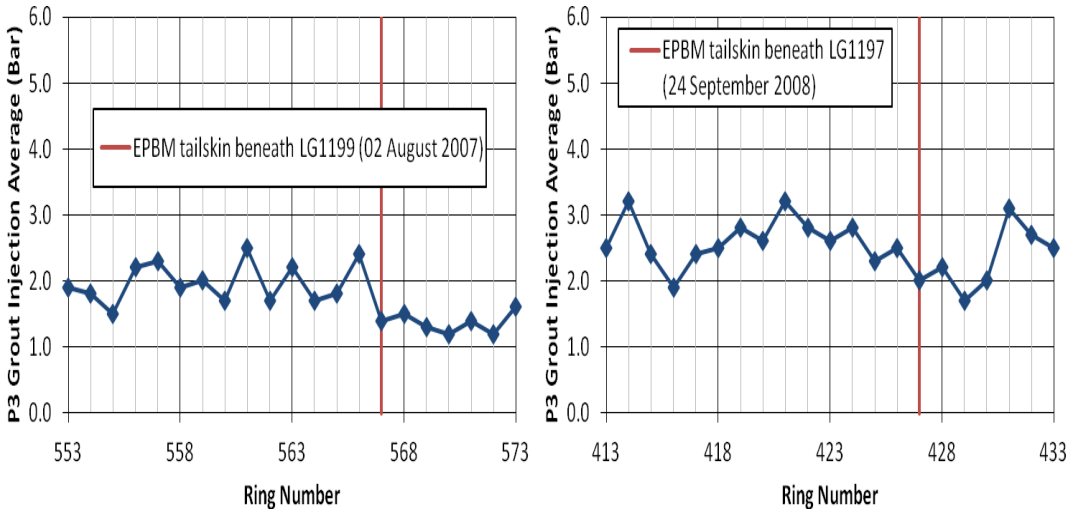

(a) (b)

Figure A.10 P3 grout injection average for (a) first inner bound bored tunnelling; and (b) second outer bound bored tunnelling (Instrumentation Array D35)

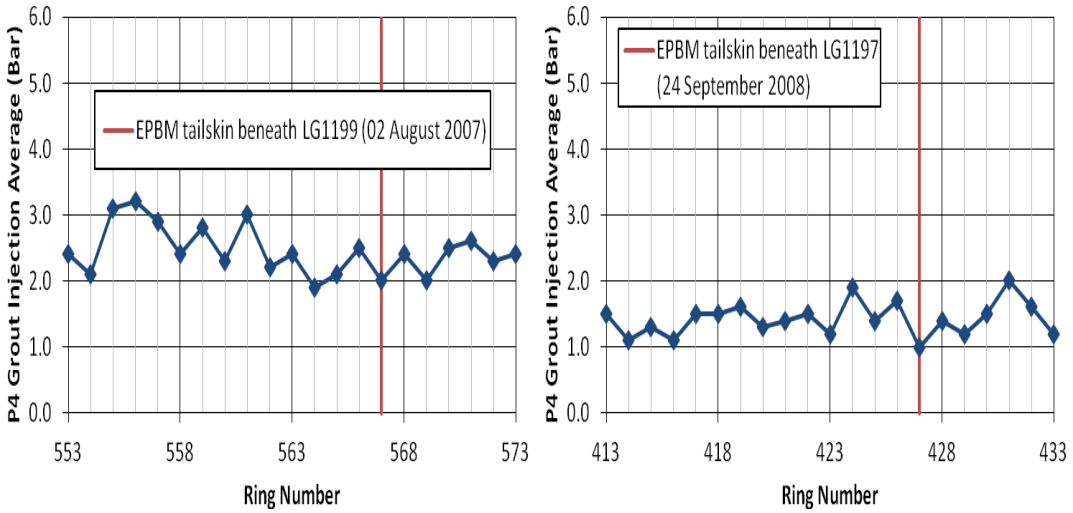

(a) (b)

Figure A.11 P4 grout injection average for (a) first inner bound bored tunnelling; and (b) second outer bound bored tunnelling (Instrumentation Array D35)

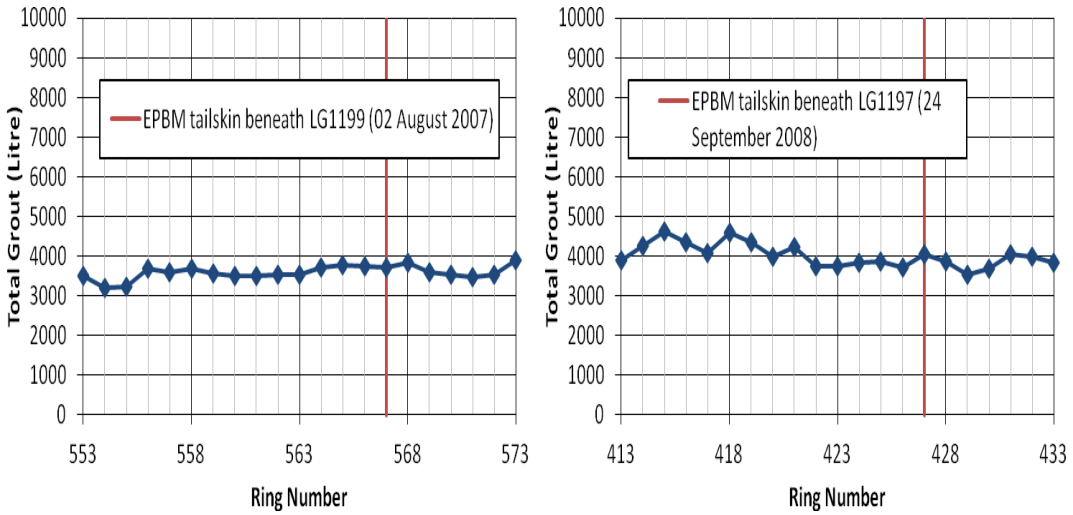

(a) (b)

Figure A.12 Total grout for (a) first inner bound bored tunnelling; and (b) second outer bound bored tunnelling (Instrumentation Array D35)

Instrumentation Array E9

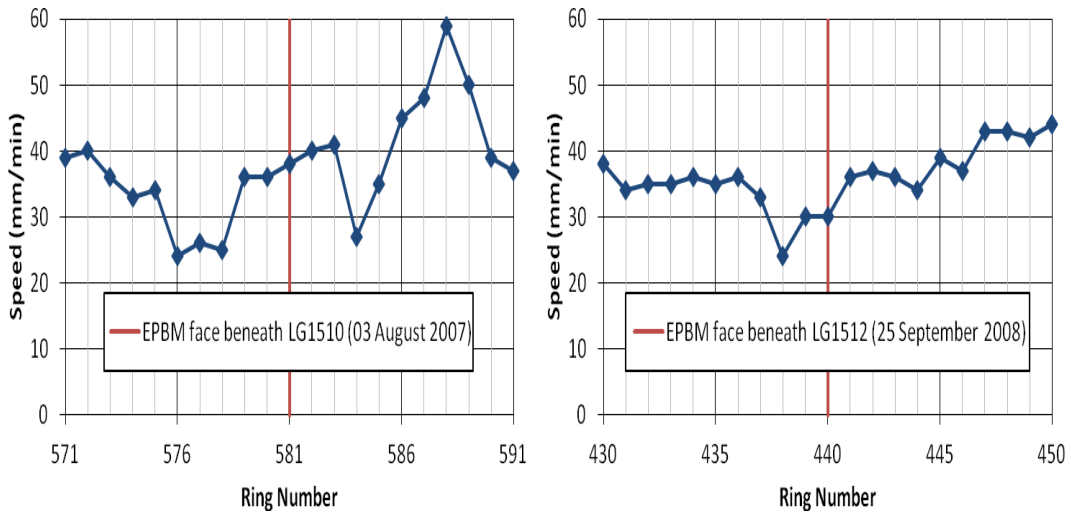

(a) (b)

Figure A.13 TBM speed for (a) first inner bound bored tunnelling; and (b) second outer bound bored tunnelling (Instrumentation Array E9)

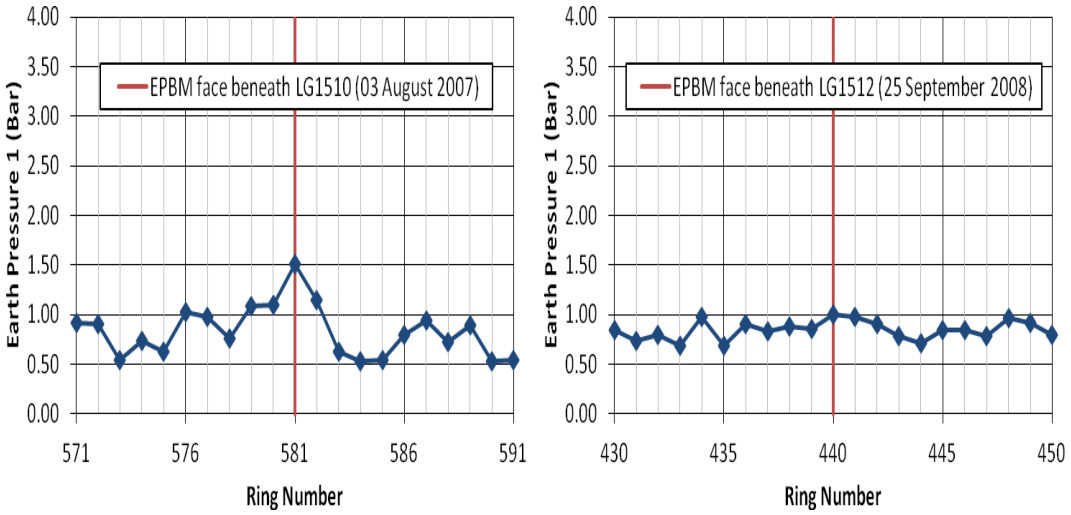

(a) (b)

Figure A.14 TBM earth pressure 1 for (a) first inner bound bored tunnelling; and (b) second outer bound bored tunnelling (Instrumentation Array E9)

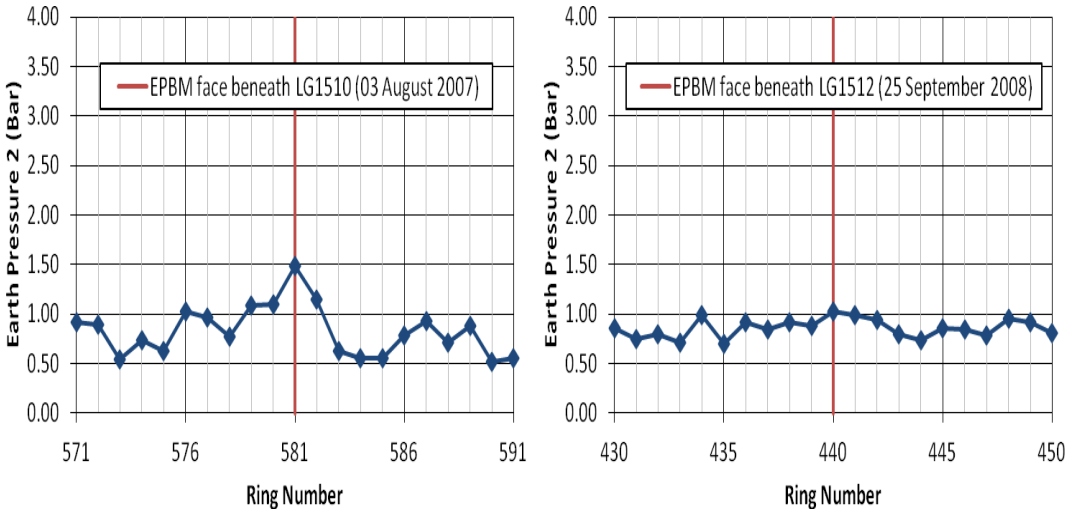

(a) (b)

Figure A.15 TBM earth pressure 2 for (a) first inner bound bored tunnelling; and (b) second outer bound bored tunnelling (Instrumentation Array E9)

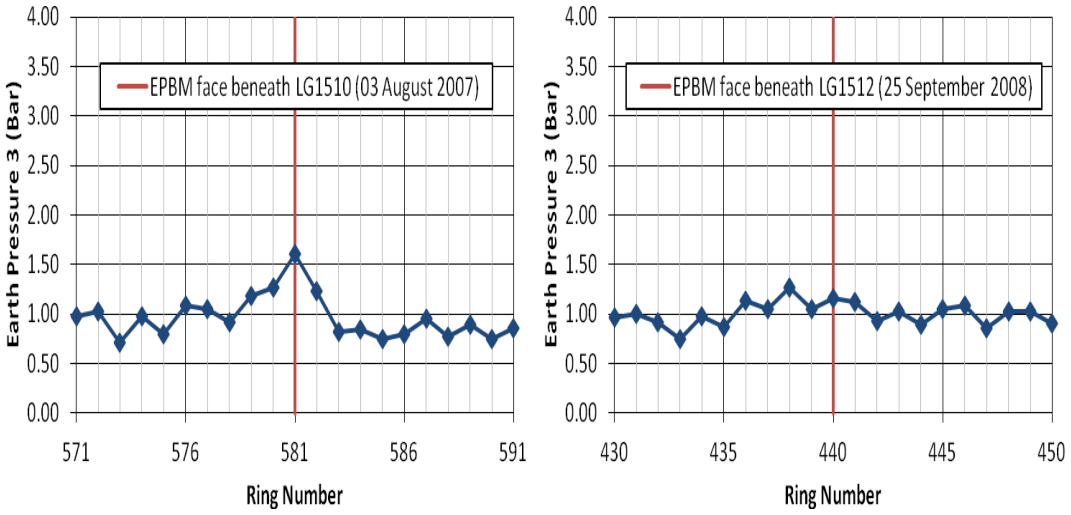

(a) (b)

Figure A.16 TBM earth pressure 3 for (a) first inner bound bored tunnelling; and (b) second outer bound bored tunnelling (Instrumentation Array E9)

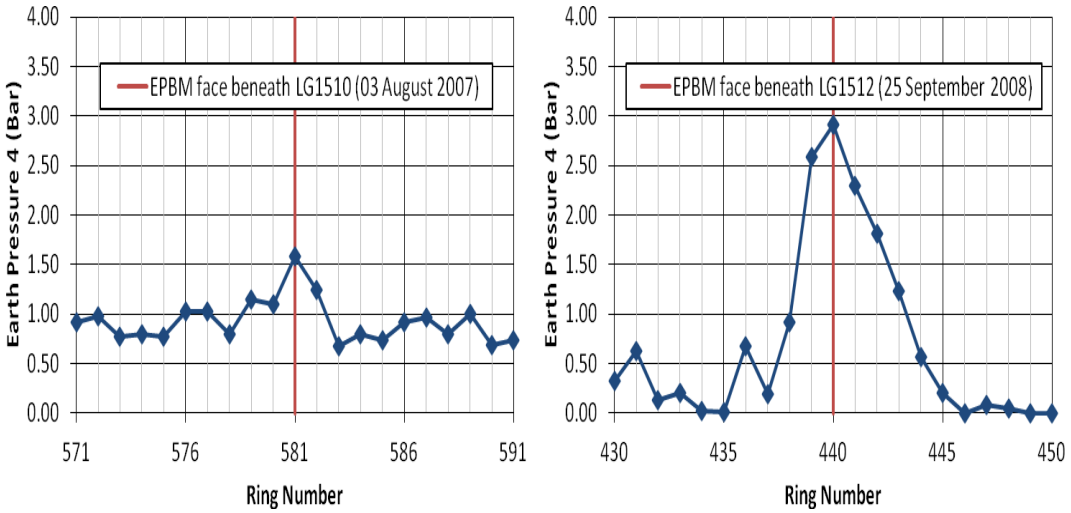

(a) (b)

Figure A.17 TBM earth pressure 4 for (a) first inner bound bored tunnelling; and (b) second outer bound bored tunnelling (Instrumentation Array E9)

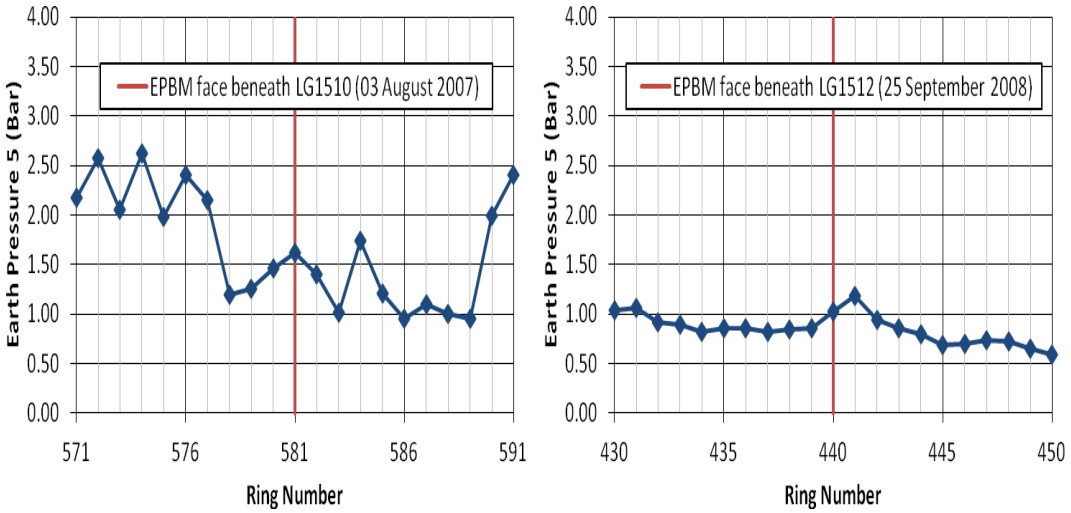

(a) (b)

Figure A.18 TBM earth pressure 5 for (a) first inner bound bored tunnelling; and (b) second outer bound bored tunnelling (Instrumentation Array E9)

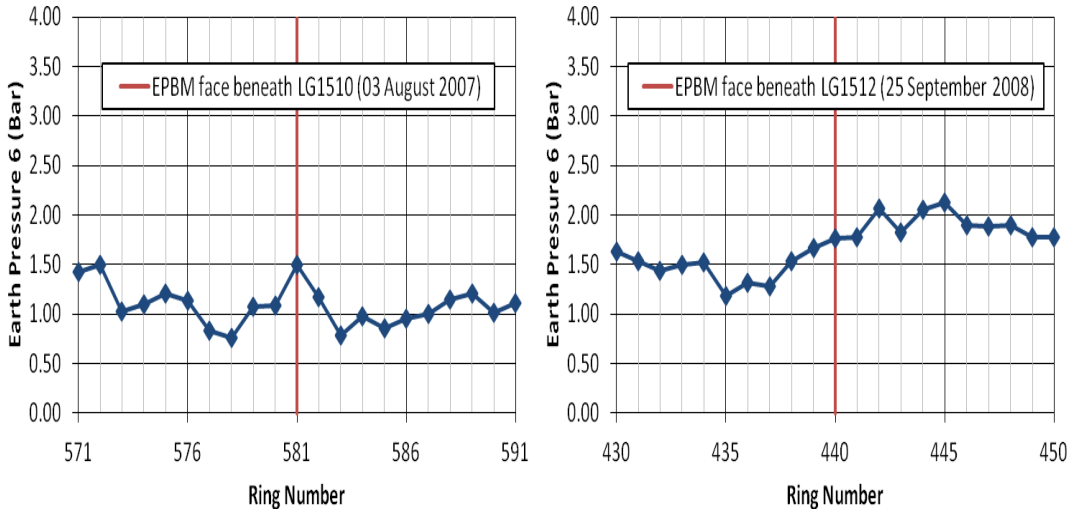

(a) (b)

Figure A.19 TBM earth pressure 6 for (a) first inner bound bored tunnelling; and (b) second outer bound bored tunnelling (Instrumentation Array E9)

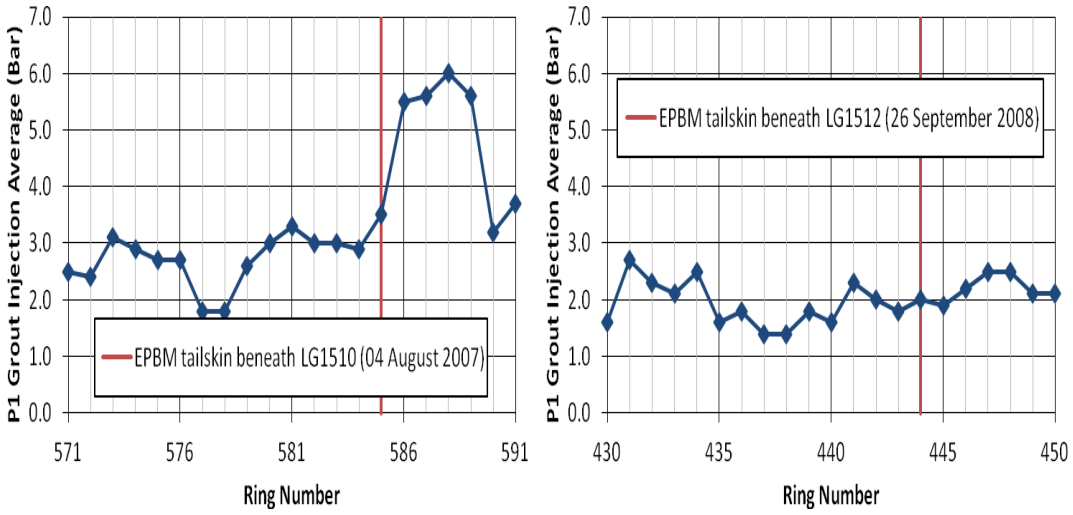

(a) (b)

Figure A.20 P1 grout injection average for (a) first inner bound bored tunnelling; and (b) second outer bound bored tunnelling (Instrumentation Array E9)

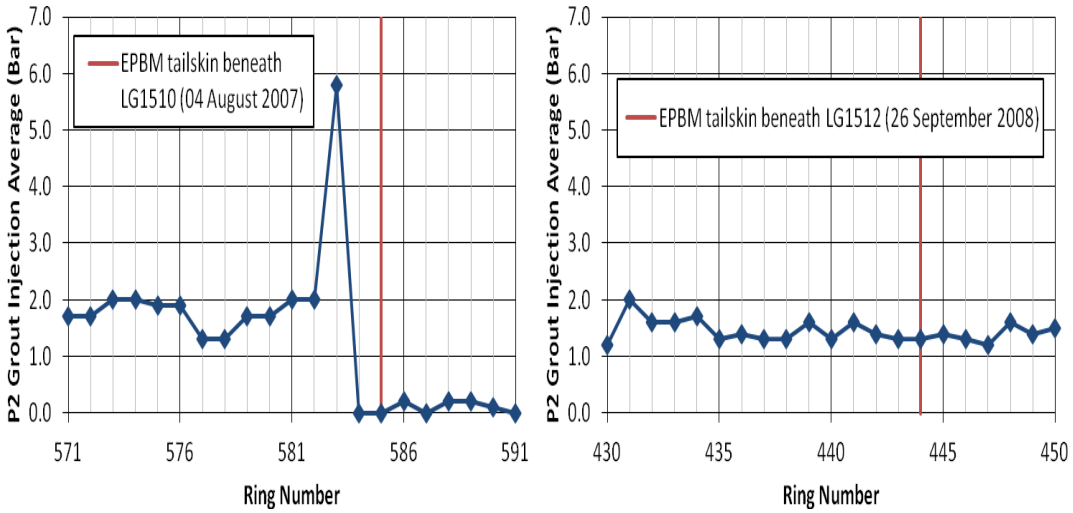

(a) (b)

Figure A.21 P2 grout injection average for (a) first inner bound bored tunnelling; and (b) second outer bound bored tunnelling (Instrumentation Array E9)

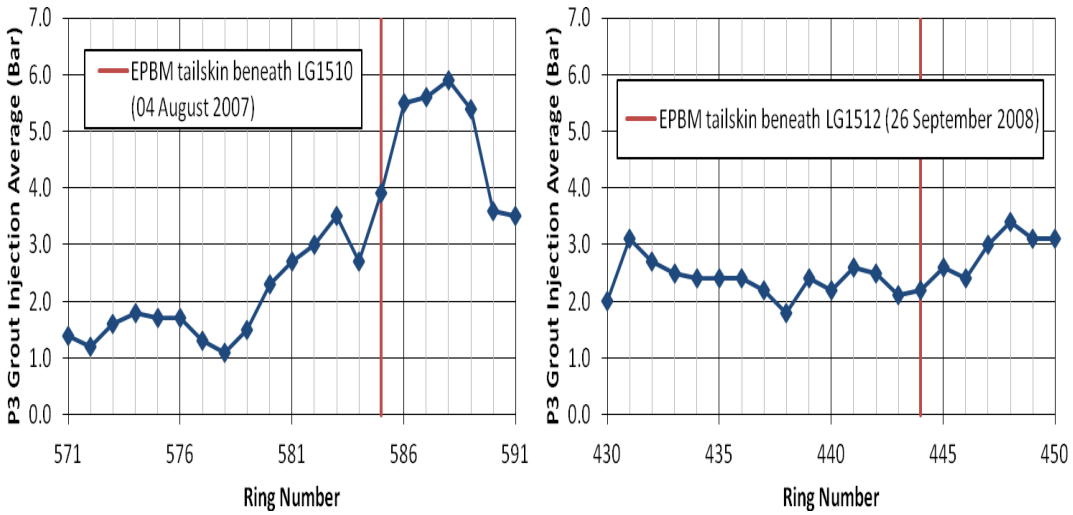

(a) (b)

Figure A.22 P3 grout injection average for (a) first inner bound bored tunnelling; and (b) second outer bound bored tunnelling (Instrumentation Array E9)

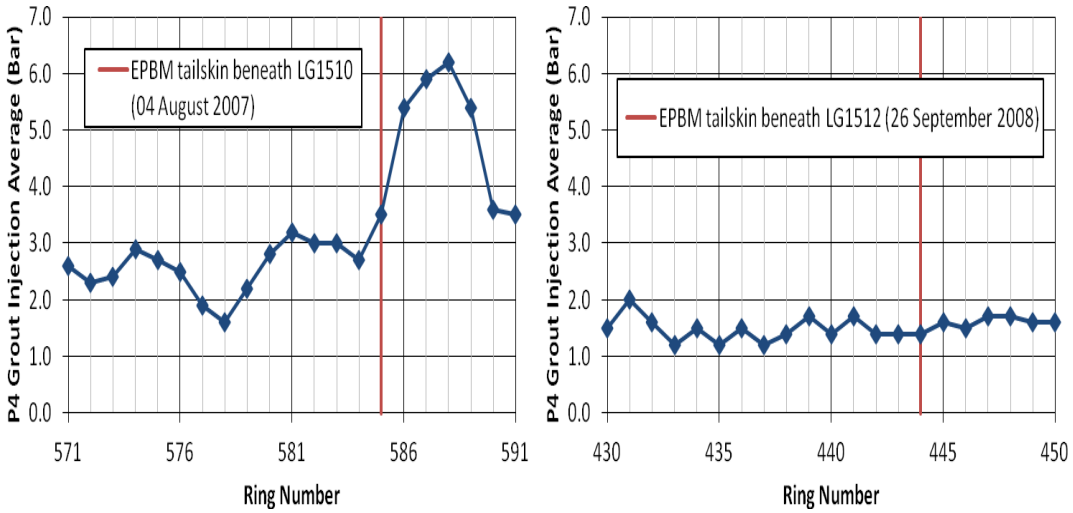

(a) (b)

Figure A.23 P4 grout injection average for (a) first inner bound bored tunnelling; and (b) second outer bound bored tunnelling (Instrumentation Array E9)

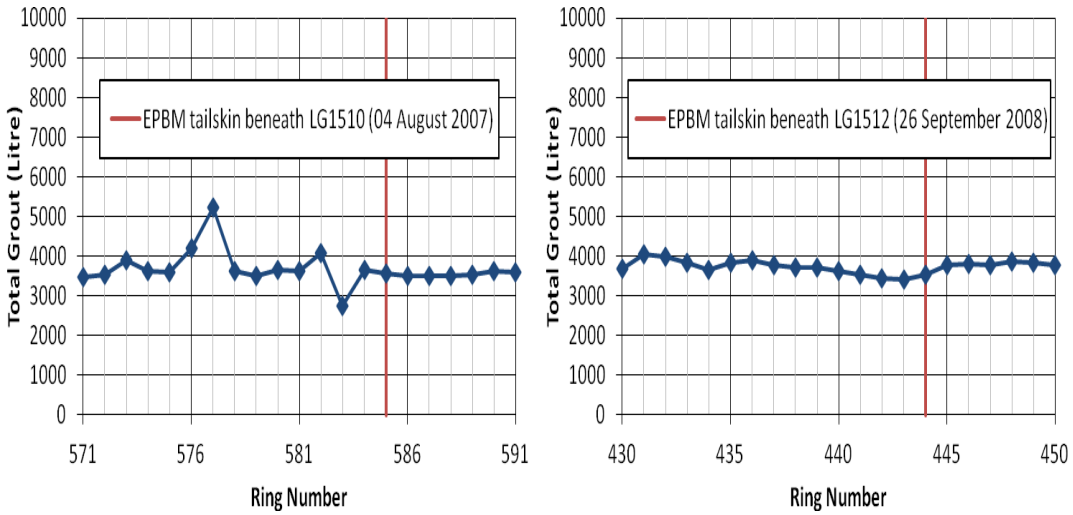

(a) (b)

Figure A.24 Total grout for (a) first inner bound bored tunnelling; and (b) second outer bound bored tunnelling (Instrumentation Array E9)

Instrumentation Array D34

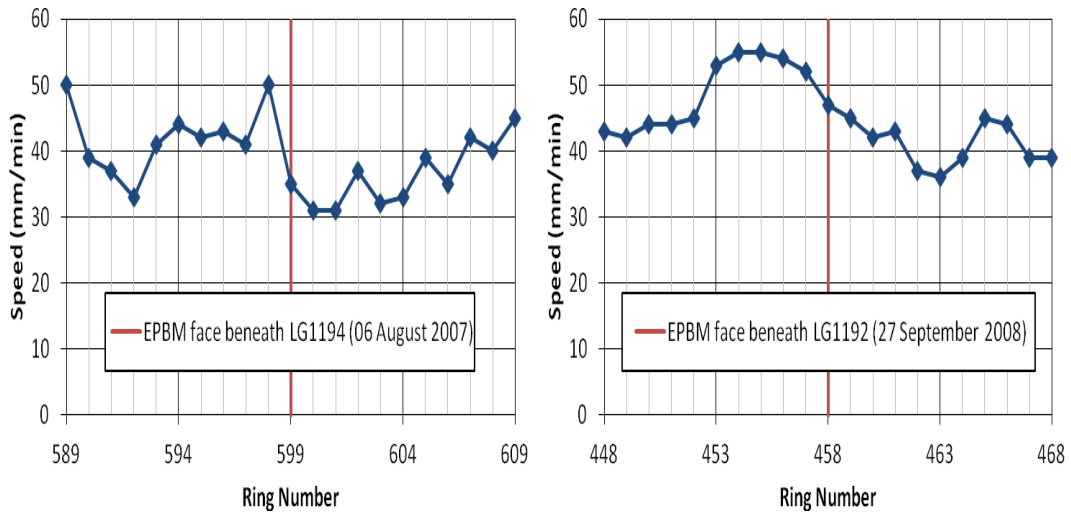

(a) (b)

Figure A.25 TBM speed for (a) first inner bound bored tunnelling; and (b) second outer bound bored tunnelling (Instrumentation Array D34)

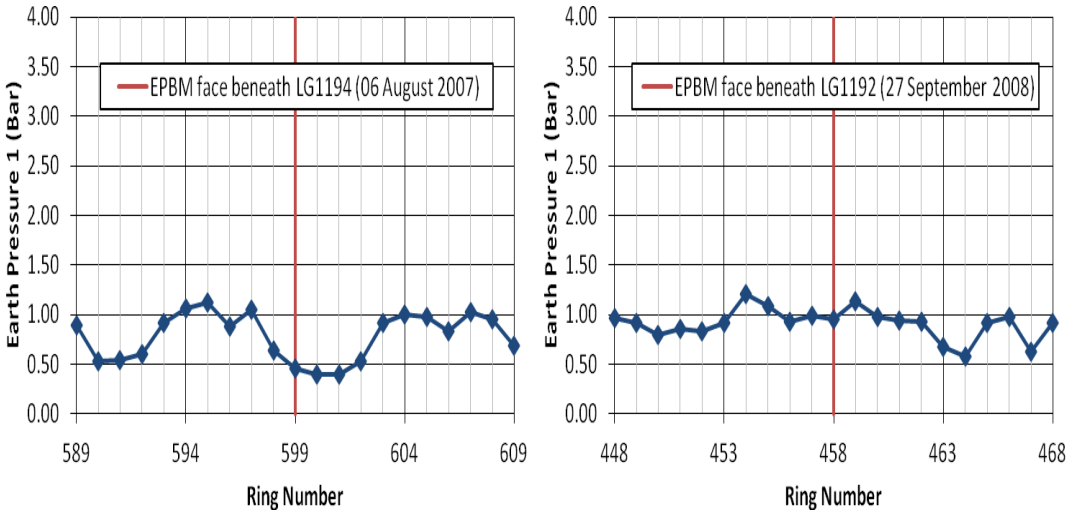

(a) (b)

Figure A.26 TBM earth pressure 1 for (a) first inner bound bored tunnelling; and (b) second outer bound bored tunnelling (Instrumentation Array D34)

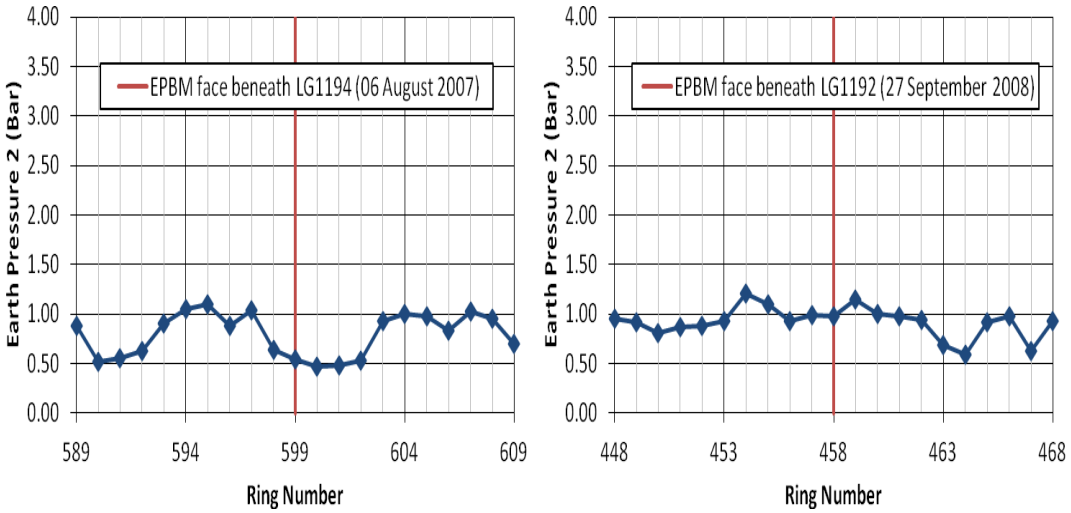

(a) (b)

Figure A.27 TBM earth pressure 2 for (a) first inner bound bored tunnelling; and (b) second outer bound bored tunnelling (Instrumentation Array D34)

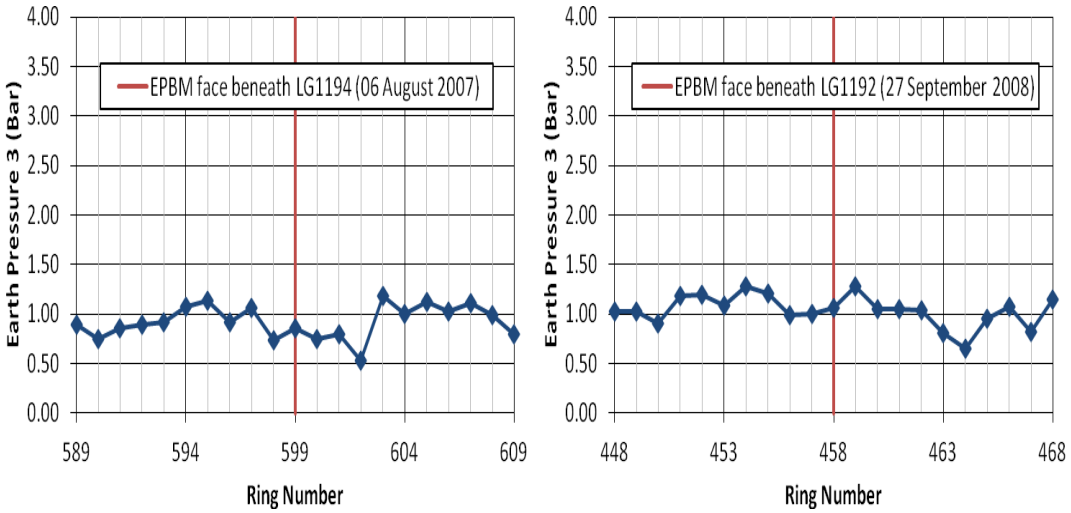

(a) (b)

Figure A.28 TBM earth pressure 3 for (a) first inner bound bored tunnelling; and (b) second outer bound bored tunnelling (Instrumentation Array D34)

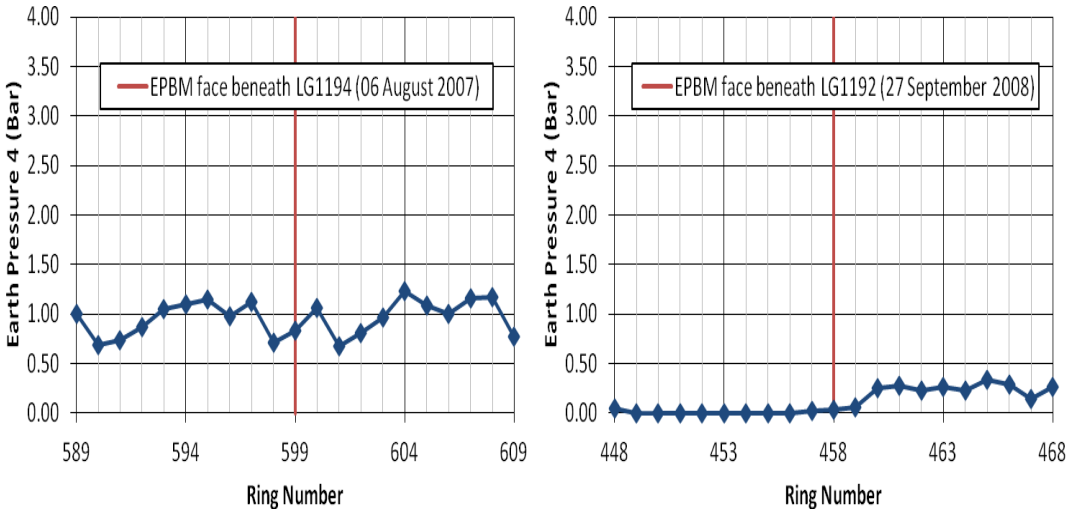

(a) (b)

Figure A.29 TBM earth pressure 4 for (a) first inner bound bored tunnelling; and (b) second outer bound bored tunnelling (Instrumentation Array D34)

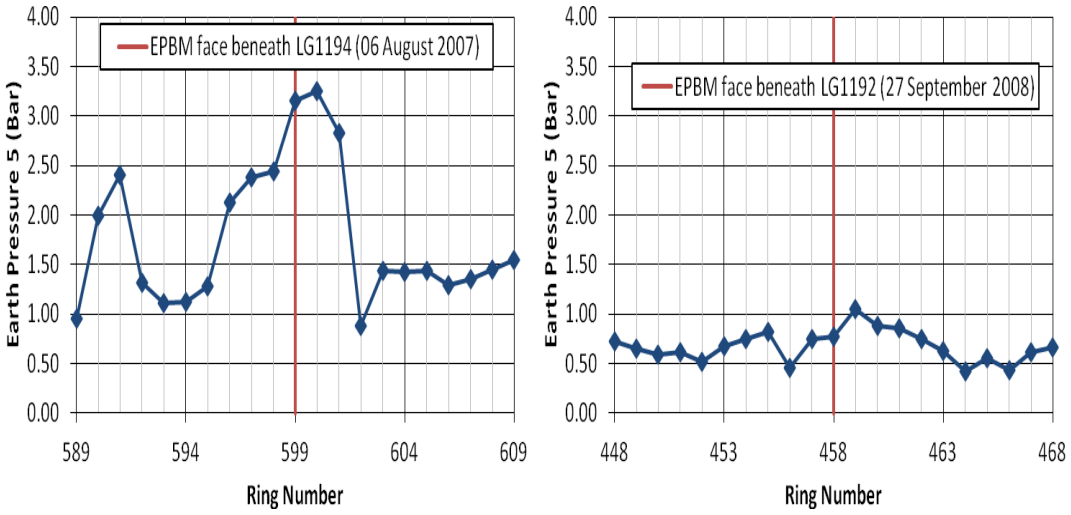

(a) (b)

Figure A.30 TBM earth pressure 5 for (a) first inner bound bored tunnelling; and (b) second outer bound bored tunnelling (Instrumentation Array D34)

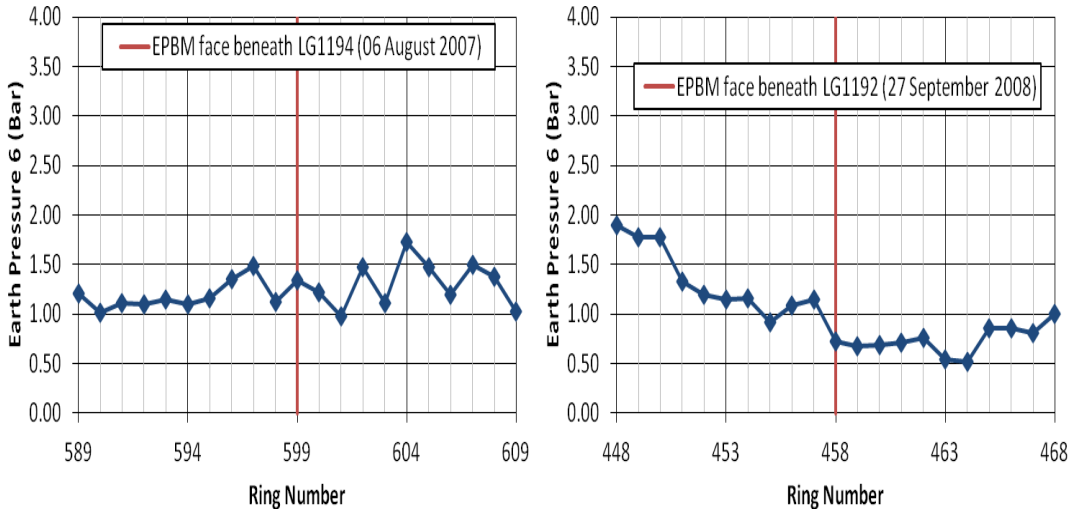

(a) (b)

Figure A.31 TBM earth pressure 6 for (a) first inner bound bored tunnelling; and (b) second outer bound bored tunnelling (Instrumentation Array D34)

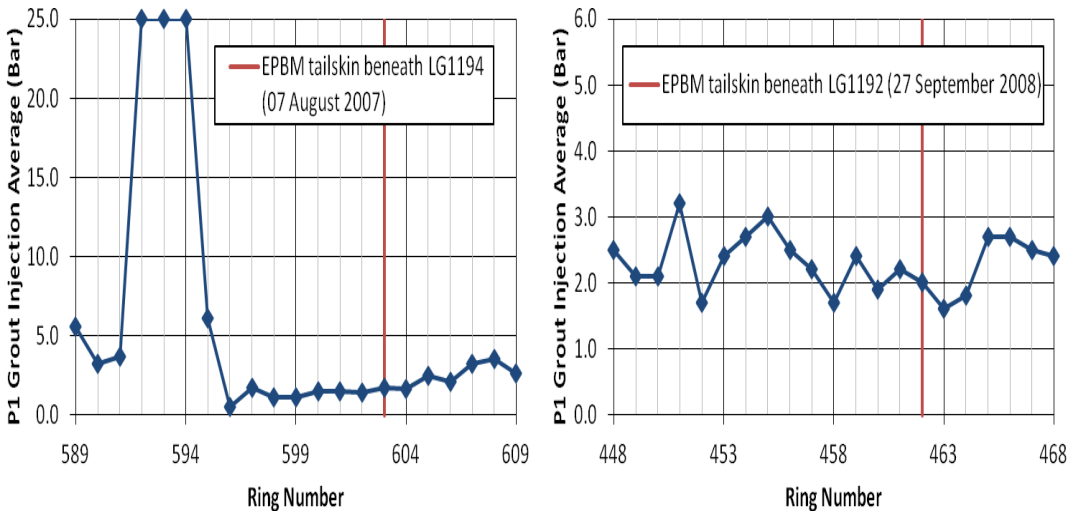

(a) (b)

Figure A.32 P1 grout injection average for (a) first inner bound bored tunnelling; and (b) second outer bound bored tunnelling (Instrumentation Array D34)

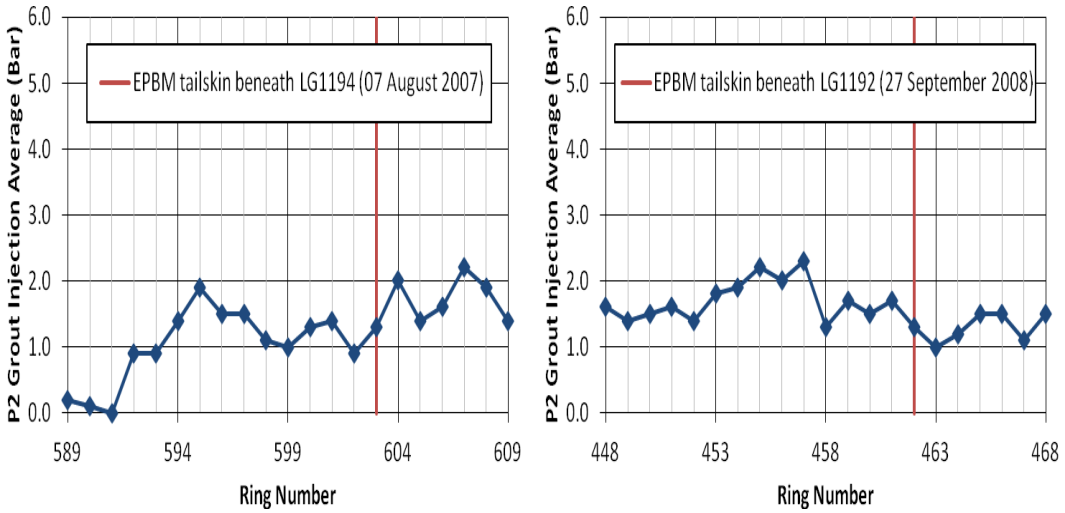

(a) (b)

Figure A.33 P2 grout injection average for (a) first inner bound bored tunnelling; and (b) second outer bound bored tunnelling (Instrumentation Array D34)

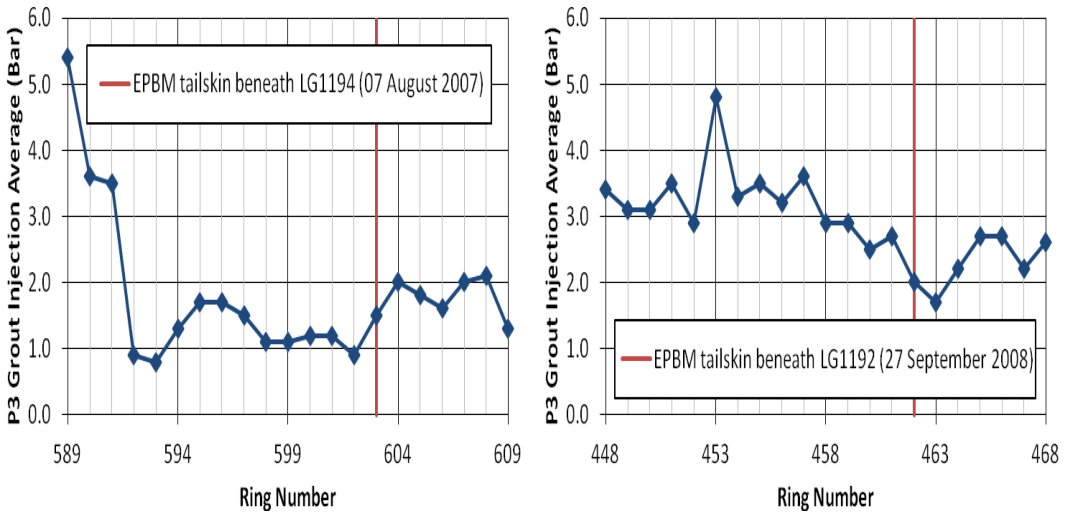

(a) (b)

Figure A.34 P3 grout injection average for (a) first inner bound bored tunnelling; and (b) second outer bound bored tunnelling (Instrumentation Array D34)

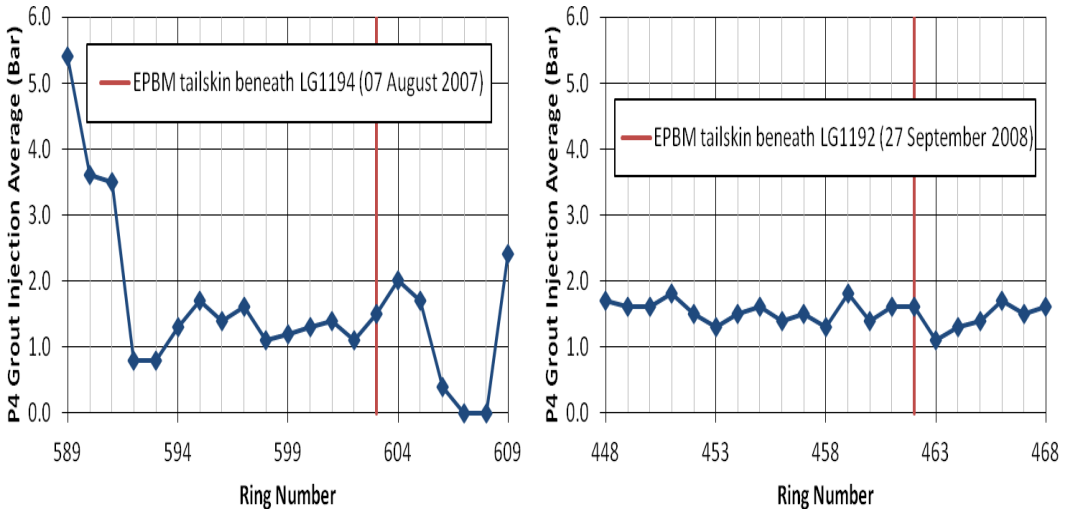

(a) (b)

Figure A.35 P4 grout injection average for (a) first inner bound bored tunnelling; and (b) second outer bound bored tunnelling (Instrumentation Array D34)

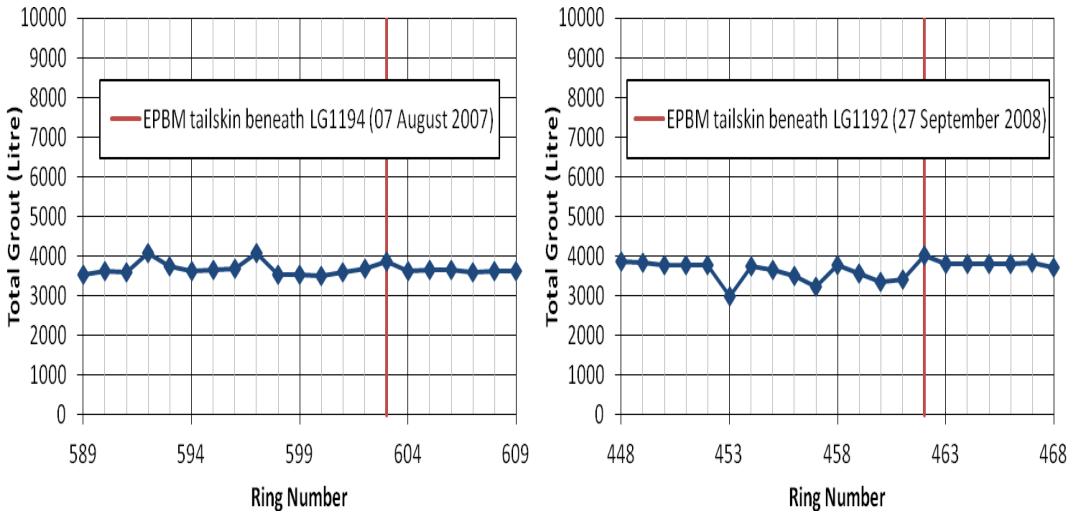

(a) (b)

Figure A.36 Total grout for (a) first inner bound bored tunnelling; and (b) second outer bound bored tunnelling (Instrumentation Array D34)

Instrumentation Array D7

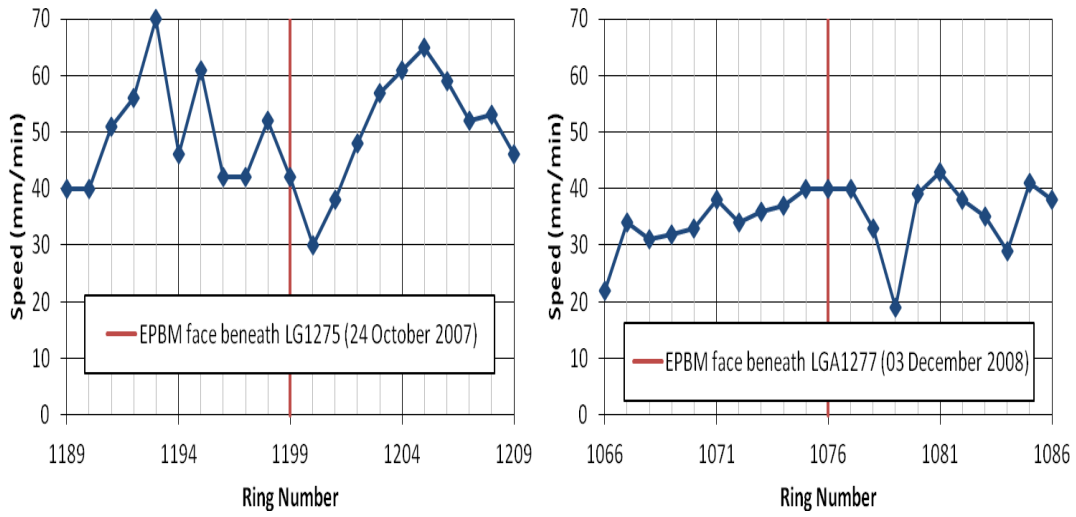

(a) (b)

Figure A.37 TBM speed for (a) first inner bound bored tunnelling; and (b) second outer bound bored tunnelling (Instrumentation Array D7)

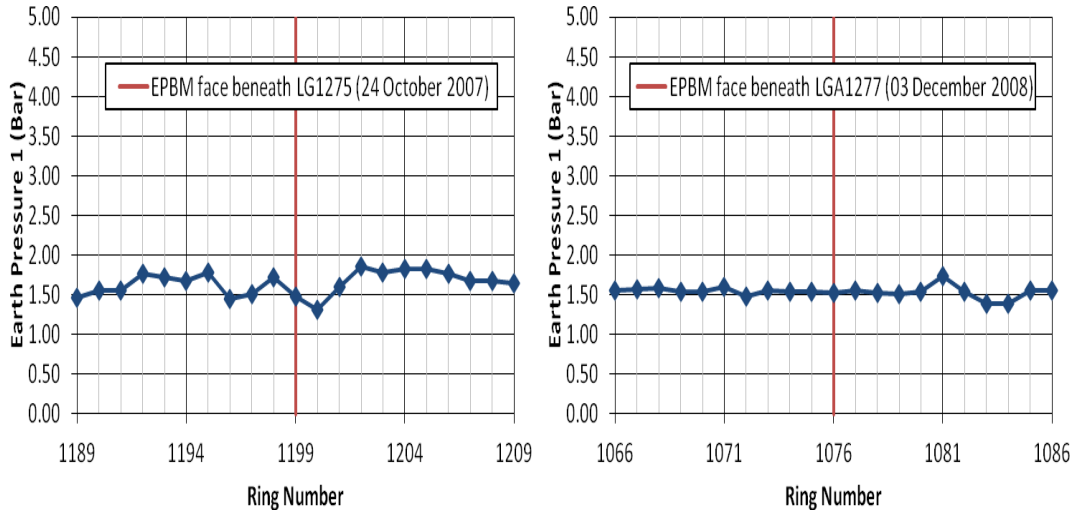

(a) (b)

Figure A.38 TBM earth pressure 1 for (a) first inner bound bored tunnelling; and (b) second outer bound bored tunnelling (Instrumentation Array D7)

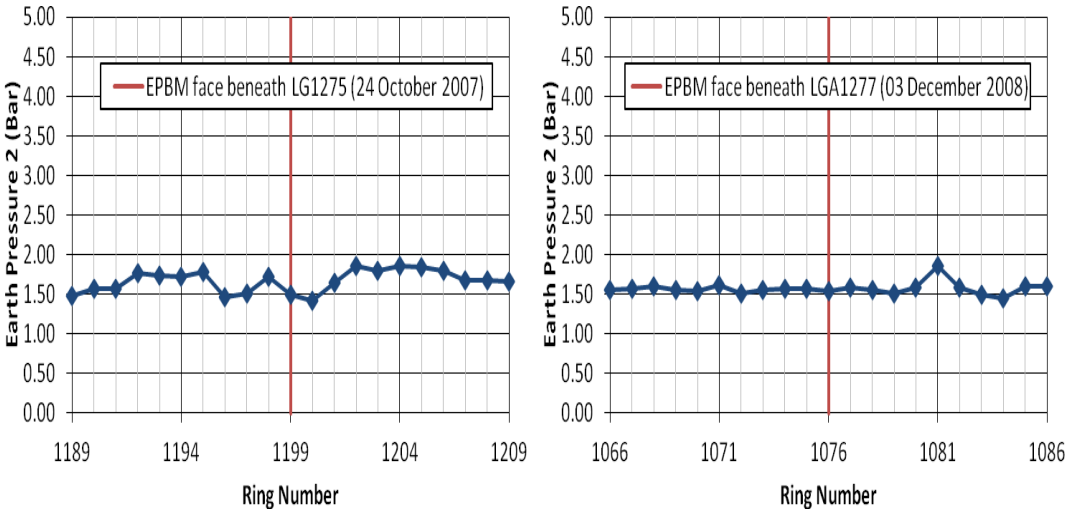

(a) (b)

Figure A.39 TBM earth pressure 2 for (a) first inner bound bored tunnelling; and (b) second outer bound bored tunnelling (Instrumentation Array D7)

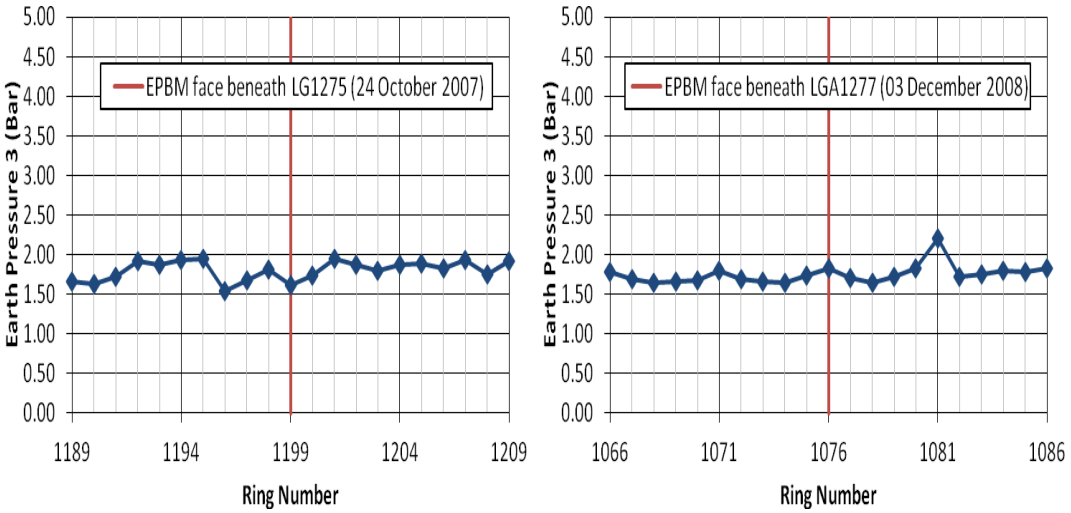

(a) (b)

Figure A.40 TBM earth pressure 3 for (a) first inner bound bored tunnelling; and (b) second outer bound bored tunnelling (Instrumentation Array D7)

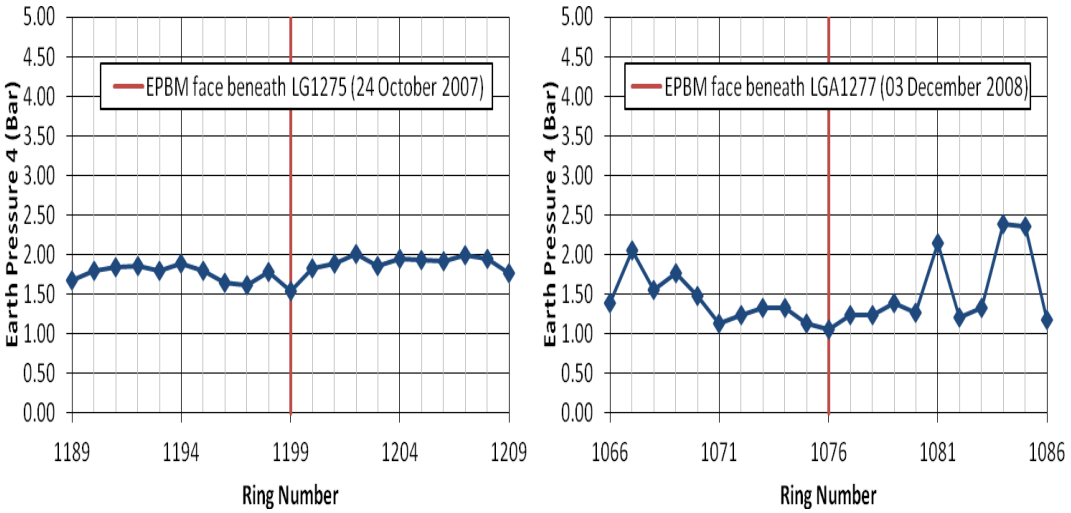

(a) (b)

Figure A.41 TBM earth pressure 4 for (a) first inner bound bored tunnelling; and (b) second outer bound bored tunnelling (Instrumentation Array D7)

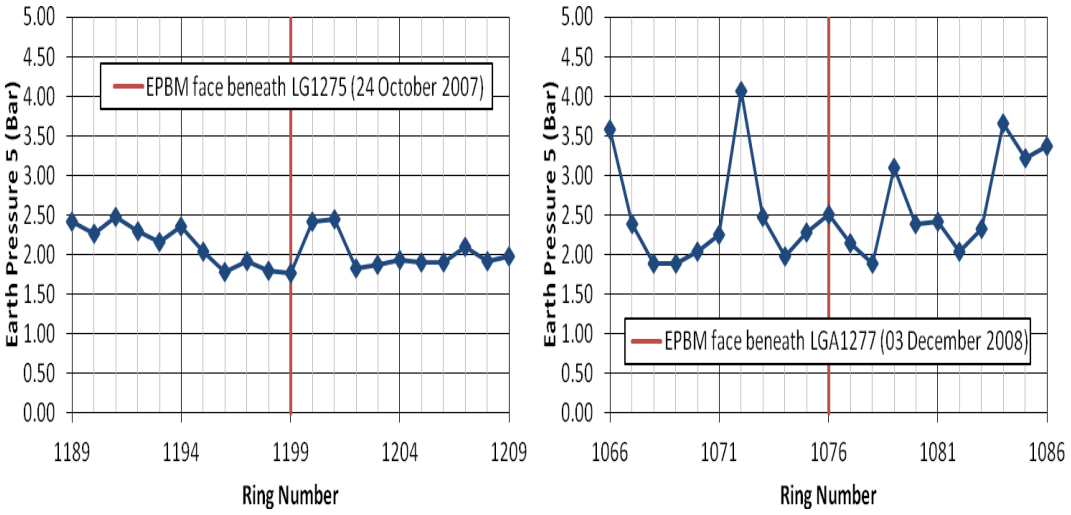

(a) (b)

Figure A.42 TBM earth pressure 5 for (a) first inner bound bored tunnelling; and (b) second outer bound bored tunnelling (Instrumentation Array D7)

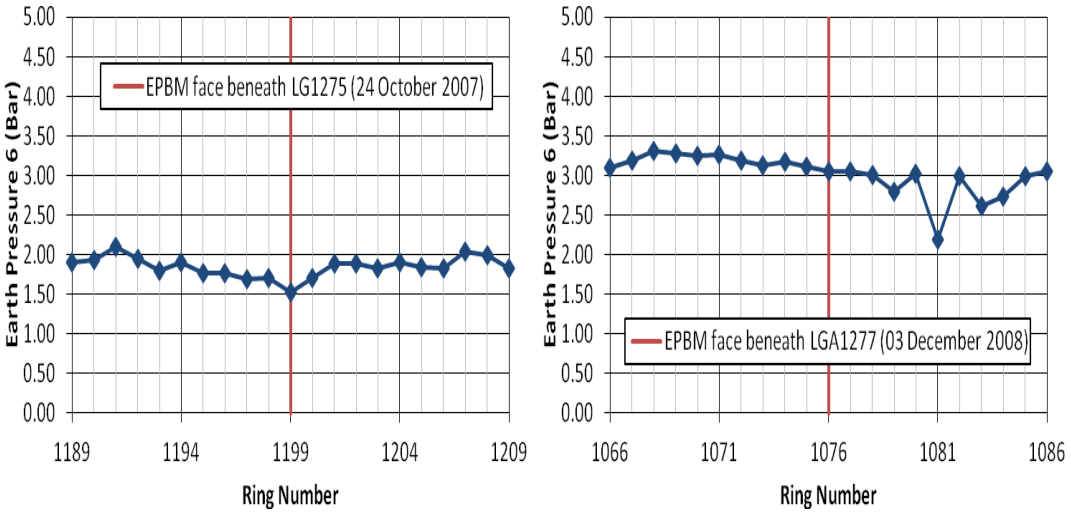

(a) (b)

Figure A.43 TBM earth pressure 6 for (a) first inner bound bored tunnelling; and (b) second outer bound bored tunnelling (Instrumentation Array D7)

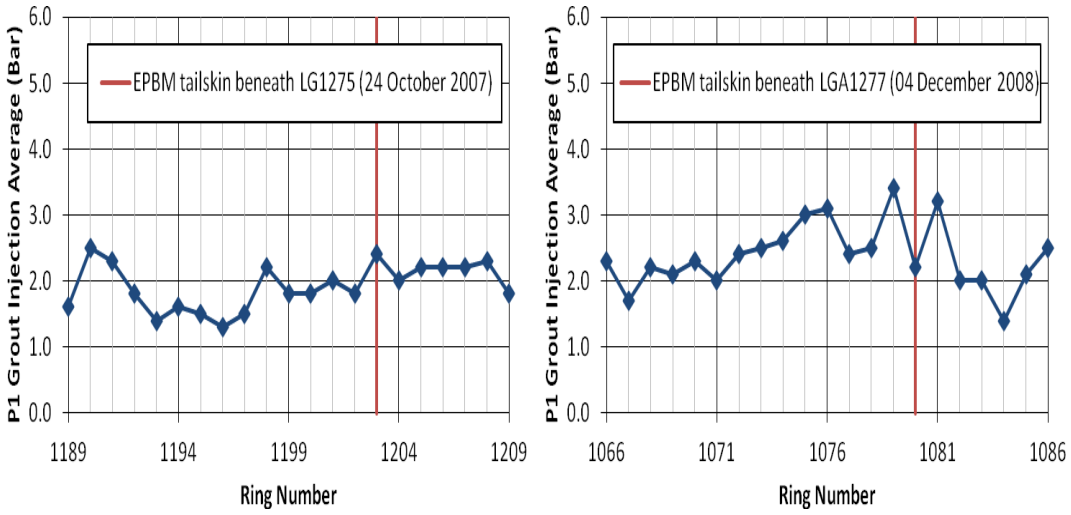

(a) (b)

Figure A.44 P1 grout injection average for (a) first inner bound bored tunnelling; and (b) second outer bound bored tunnelling (Instrumentation Array D7)

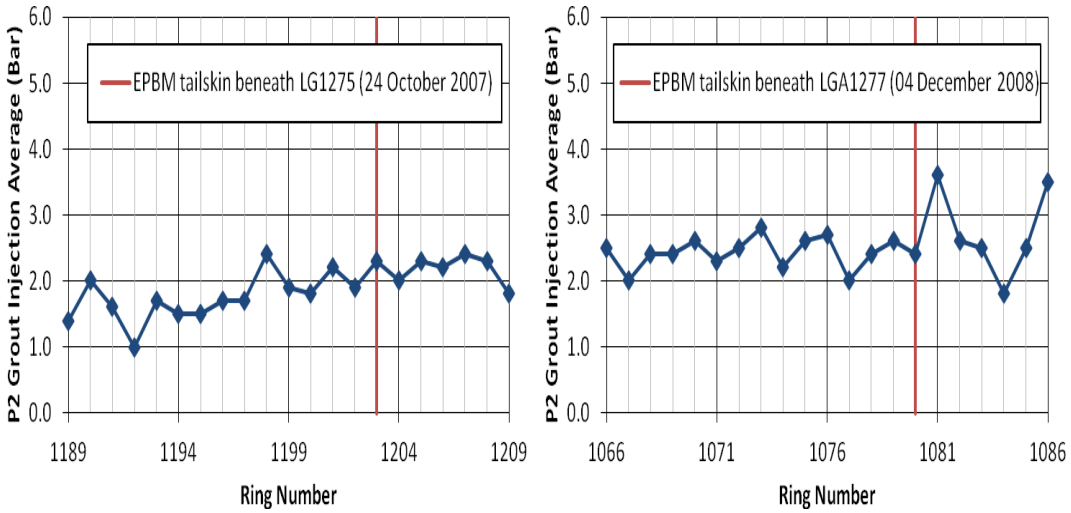

(a) (b)

Figure A.45 P2 grout injection average for (a) first inner bound bored tunnelling; and (b) second outer bound bored tunnelling (Instrumentation Array D7)

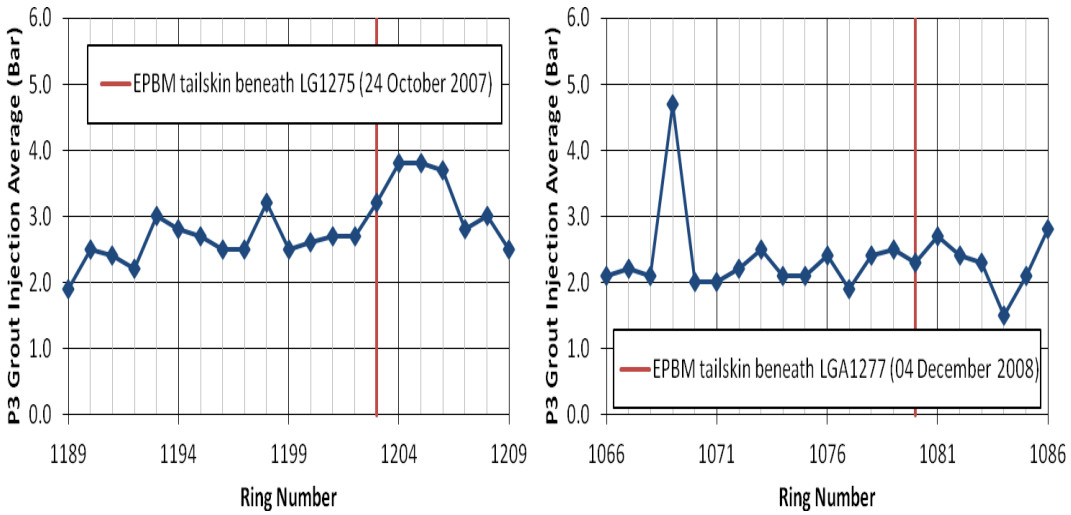

(a) (b)

Figure A.46 P3 grout injection average for (a) first inner bound bored tunnelling; and (b) second outer bound bored tunnelling (Instrumentation Array D7)

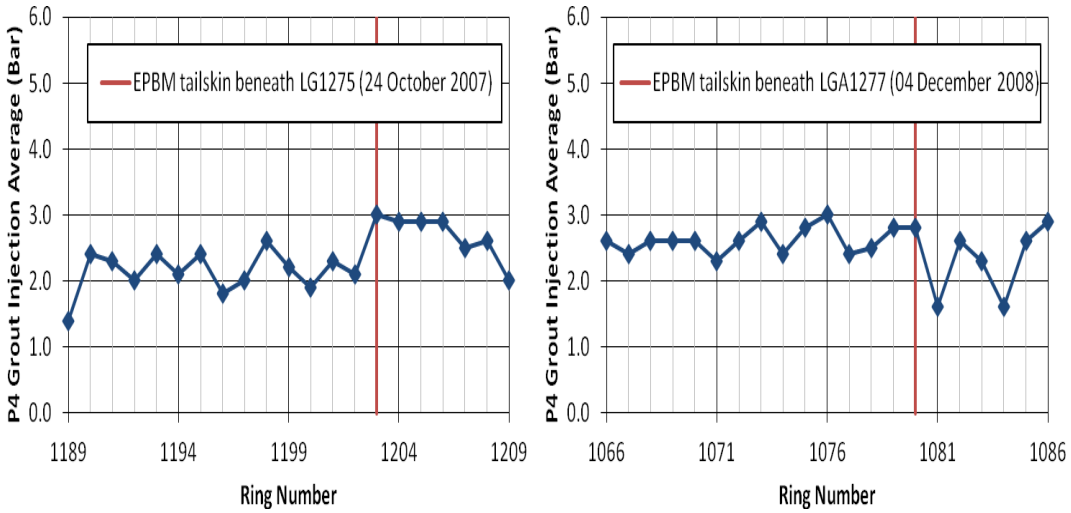

(a) (b)

Figure A.47 P4 grout injection average for (a) first inner bound bored tunnelling; and (b) second outer bound bored tunnelling (Instrumentation Array D7)

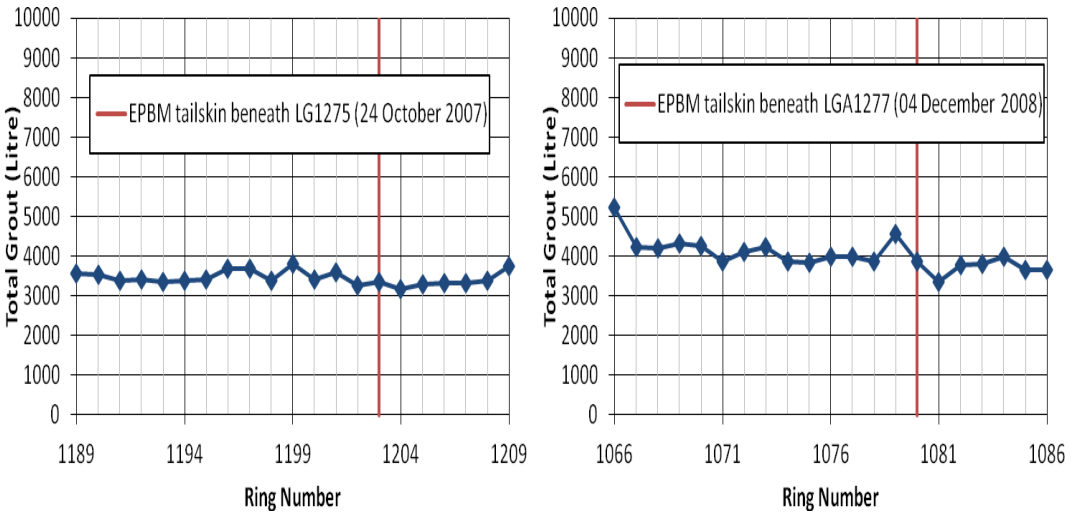

(a) (b)

Figure A.48 Total grout for (a) first inner bound bored tunnelling; and (b) second outer bound bored tunnelling (Instrumentation Array D7)

Instrumentation Array D38

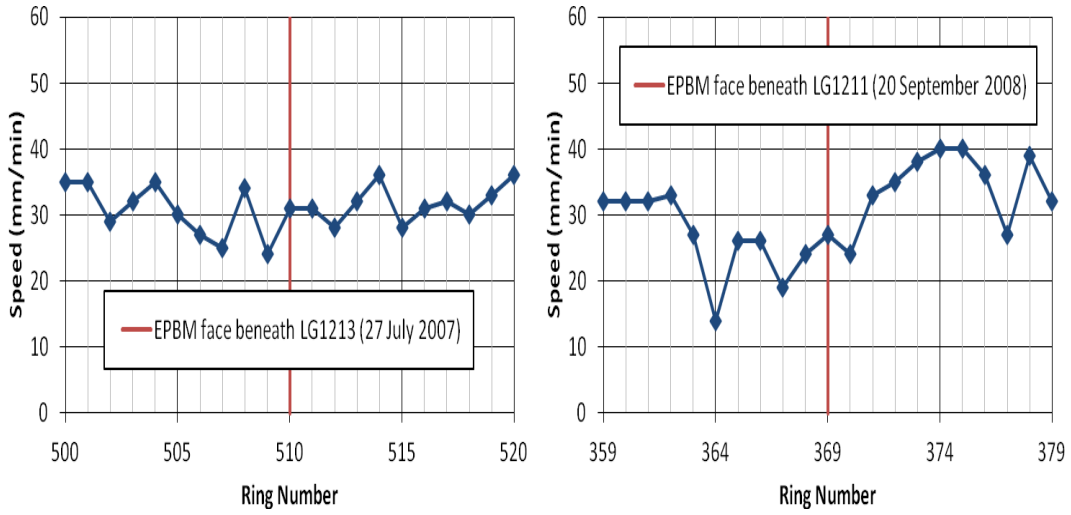

(a) (b)

Figure A.49 TBM speed for (a) first inner bound bored tunnelling; and (b) second outer bound bored tunnelling (Instrumentation Array D38)

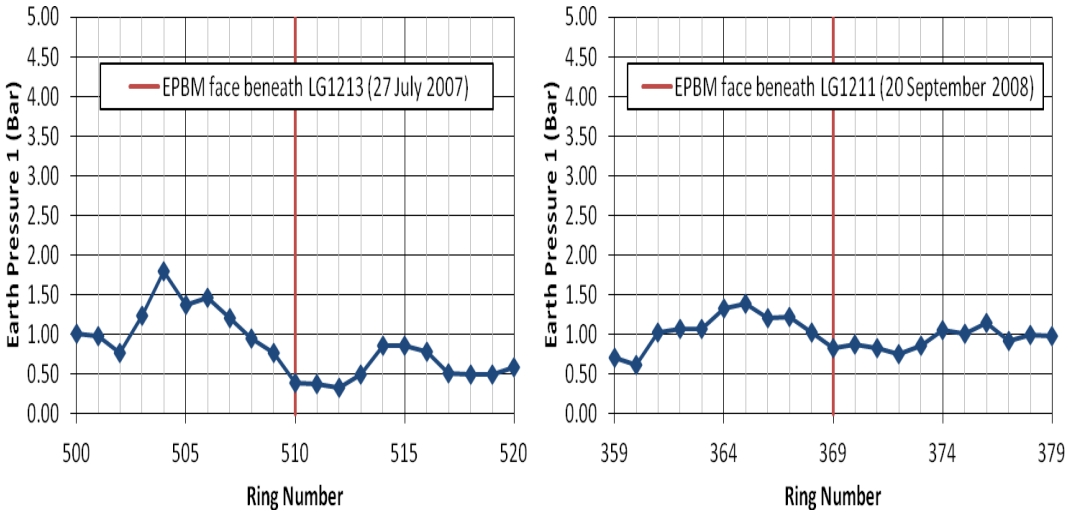

(a) (b)

Figure A.50 TBM earth pressure 1 for (a) first inner bound bored tunnelling; and (b) second outer bound bored tunnelling (Instrumentation Array D38)

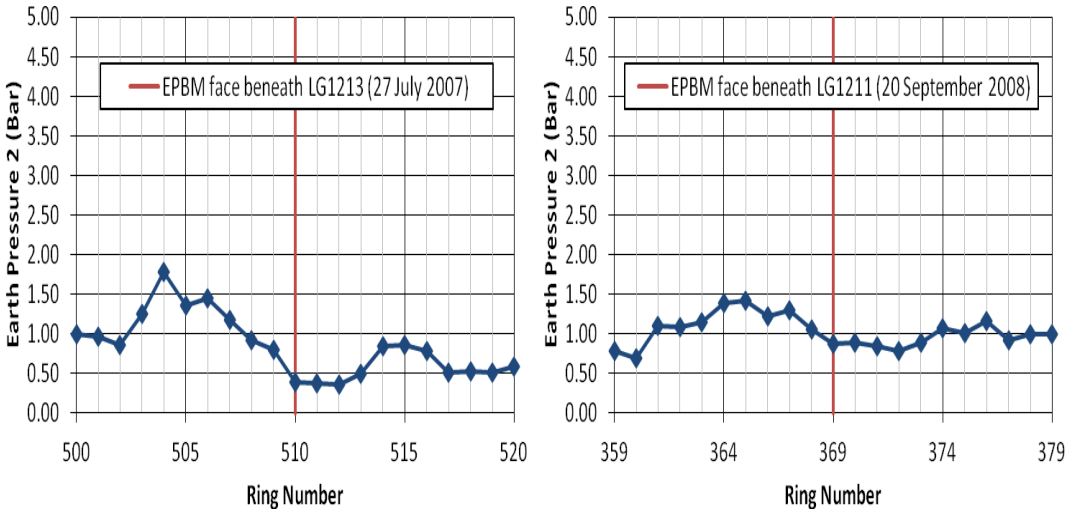

(a) (b)

Figure A.51 TBM earth pressure 2 for (a) first inner bound bored tunnelling; and (b) second outer bound bored tunnelling (Instrumentation Array D38)

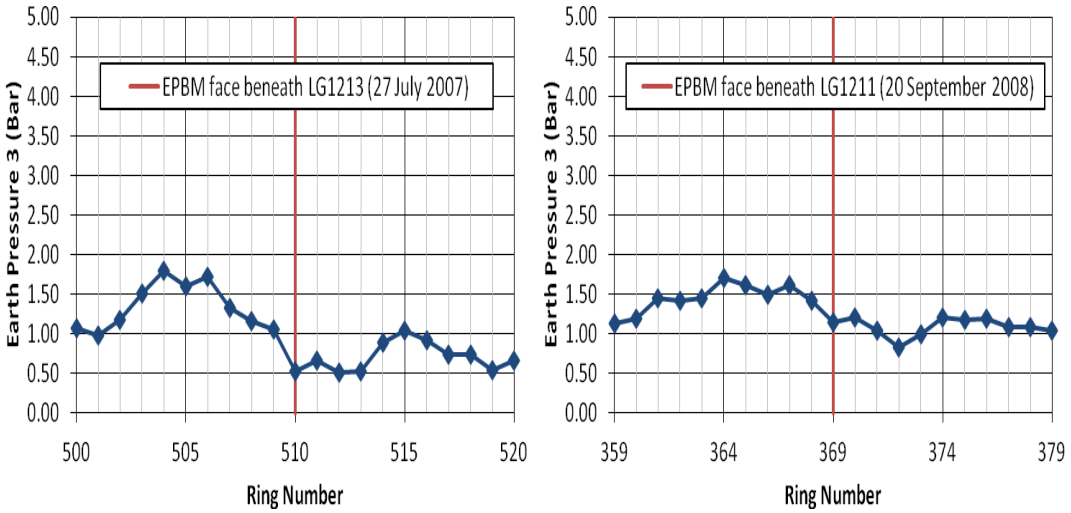

(a) (b)

Figure A.52 TBM earth pressure 3 for (a) first inner bound bored tunnelling; and (b) second outer bound bored tunnelling (Instrumentation Array D38)

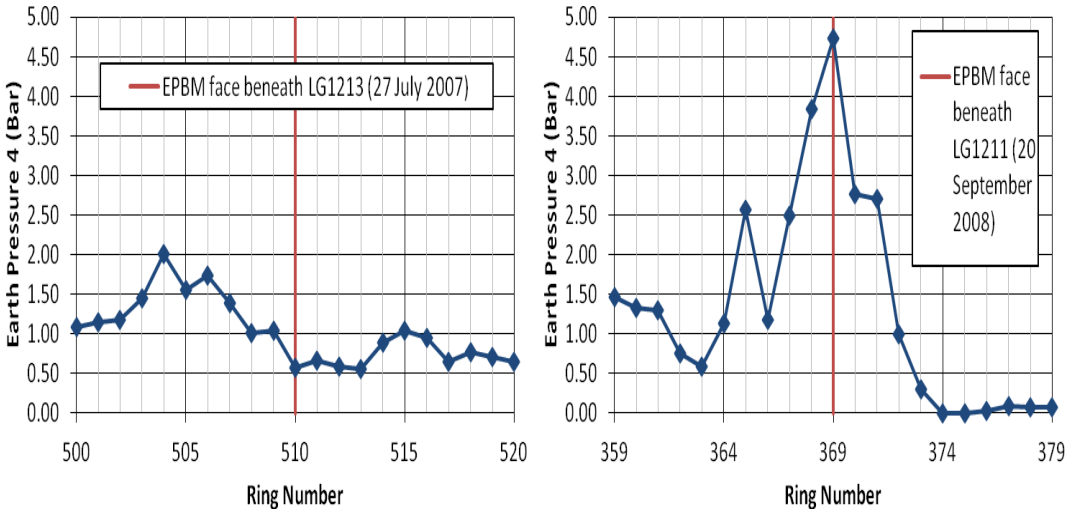

(a) (b)

Figure A.53 TBM earth pressure 4 for (a) first inner bound bored tunnelling; and (b) second outer bound bored tunnelling (Instrumentation Array D38)

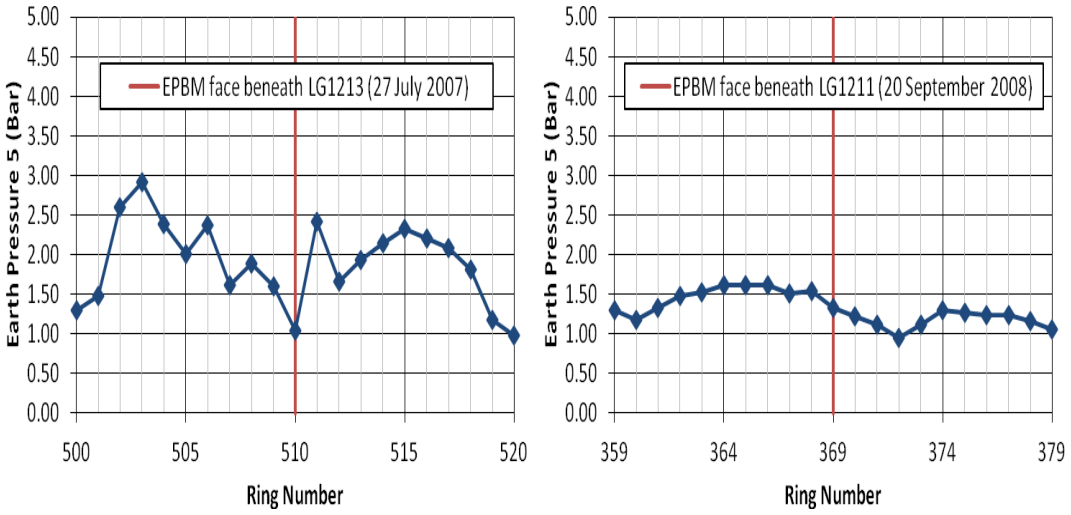

(a) (b)

Figure A.54 TBM earth pressure 5 for (a) first inner bound bored tunnelling; and (b) second outer bound bored tunnelling (Instrumentation Array D38)

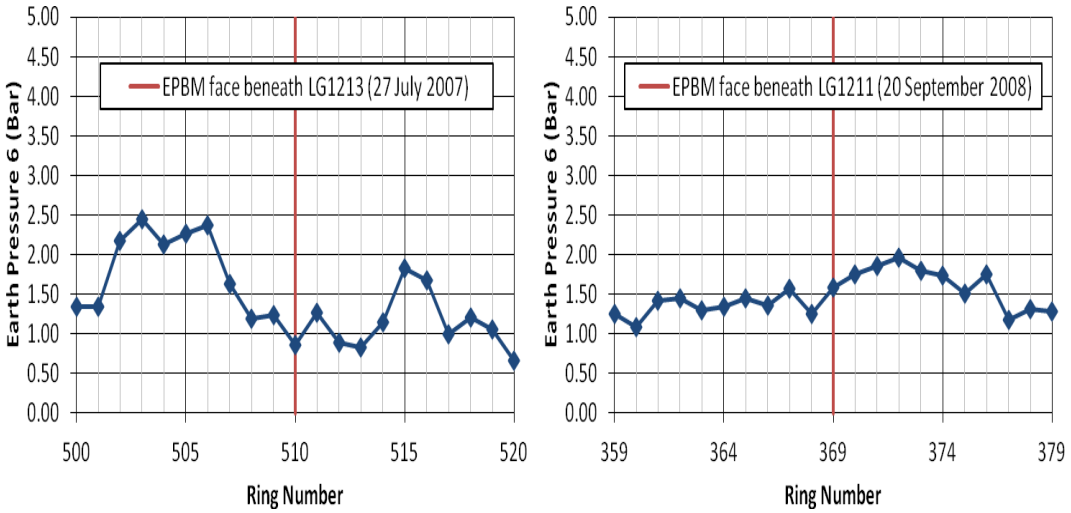

(a) (b)

Figure A.55 TBM earth pressure 6 for (a) first inner bound bored tunnelling; and (b) second outer bound bored tunnelling (Instrumentation Array D38)

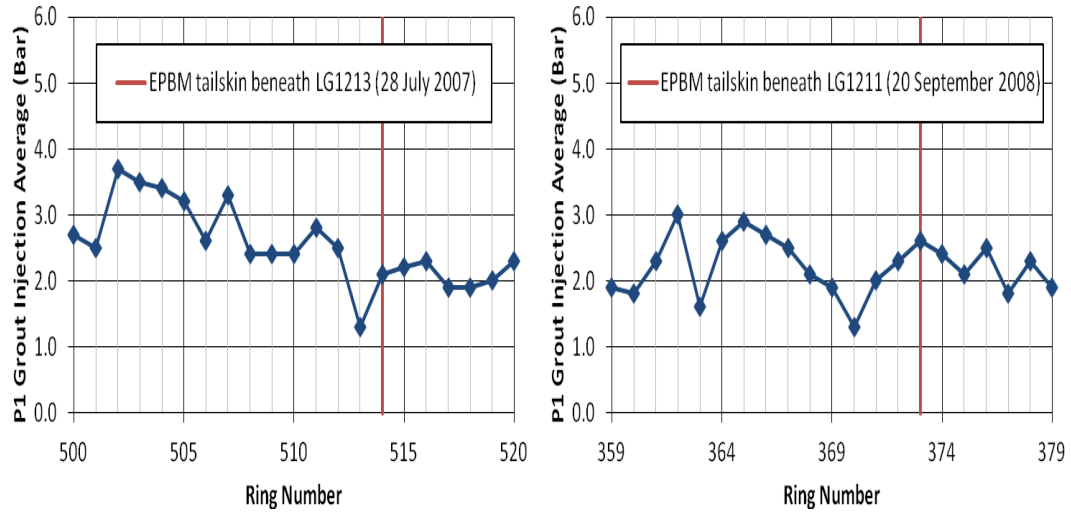

(a) (b)

Figure A.56 P1 grout injection average for (a) first inner bound bored tunnelling; and (b) second outer bound bored tunnelling (Instrumentation Array D38)

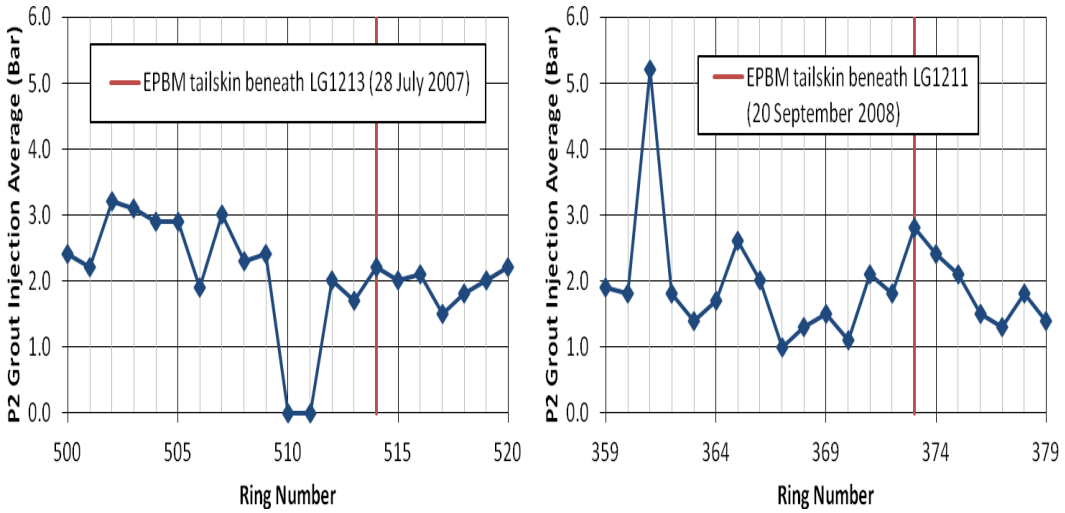

(a) (b)

Figure A.57 P2 grout injection average for (a) first inner bound bored tunnelling; and (b) second outer bound bored tunnelling (Instrumentation Array D38)

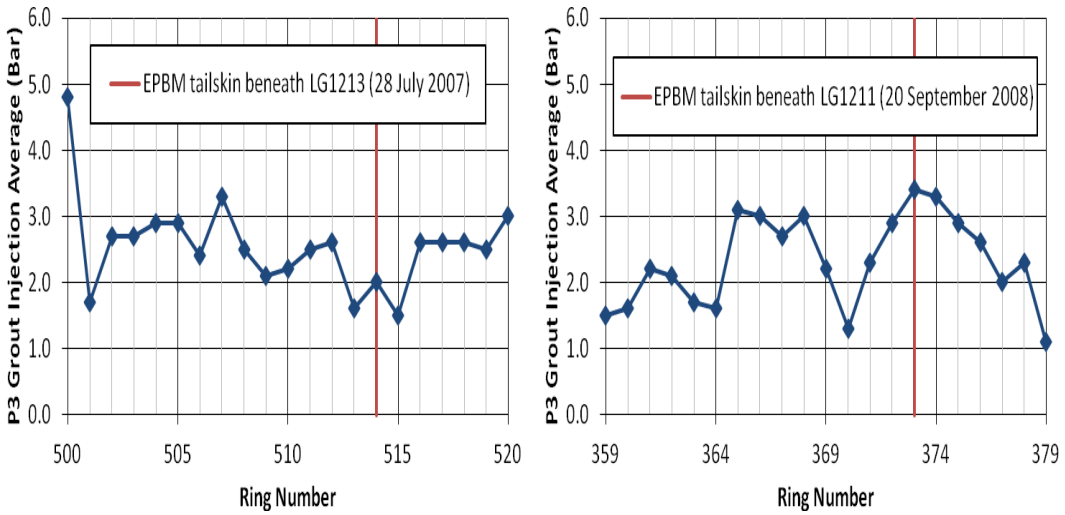

(a) (b)

Figure A.58 P3 grout injection average for (a) first inner bound bored tunnelling; and (b) second outer bound bored tunnelling (Instrumentation Array D38)

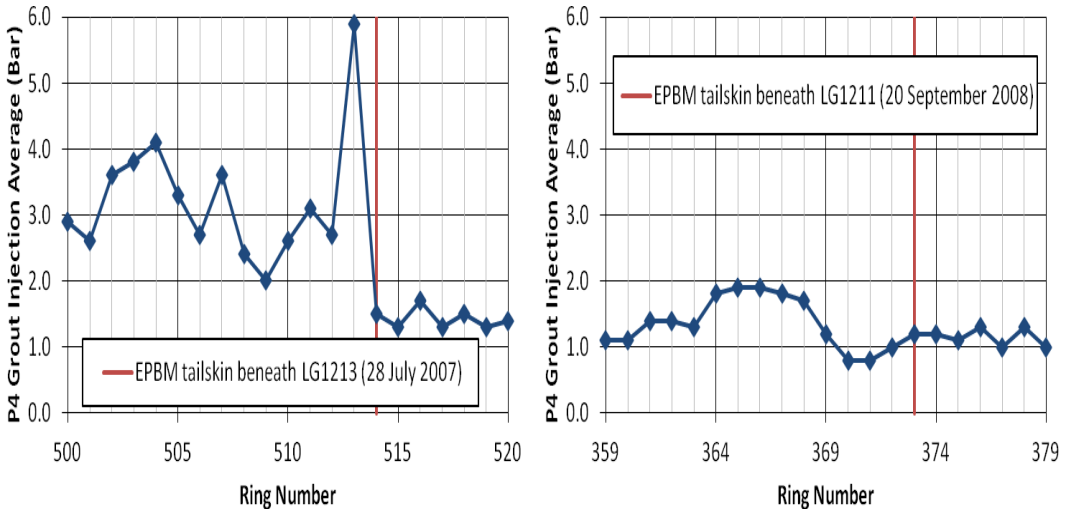

(a) (b)

Figure A.59 P4 grout injection average for (a) first inner bound bored tunnelling; and (b) second outer bound bored tunnelling (Instrumentation Array D38)

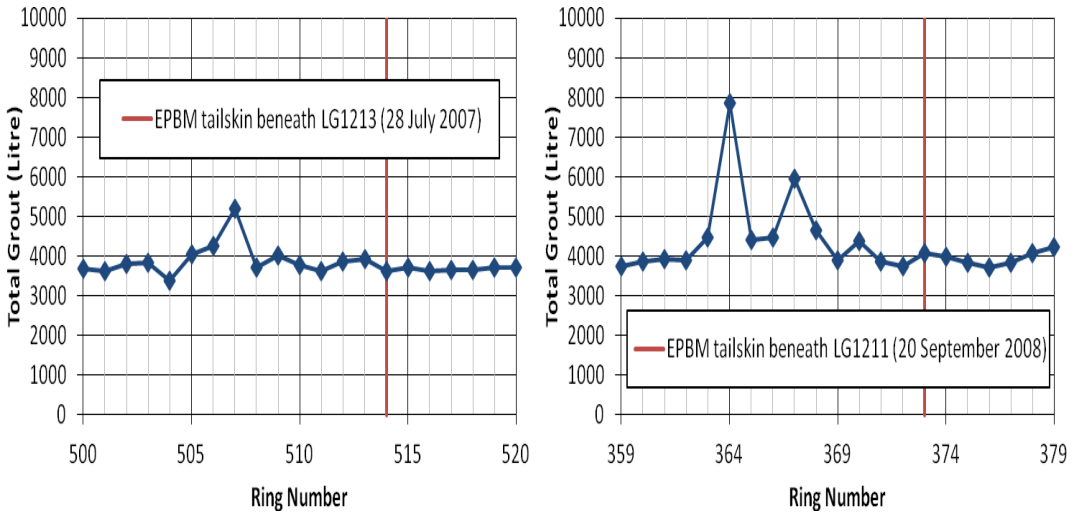

(a) (b)

Figure A.60 Total grout for (a) first inner bound bored tunnelling; and (b) second outer bound bored tunnelling (Instrumentation Array D38)

Instrumentation Array D37

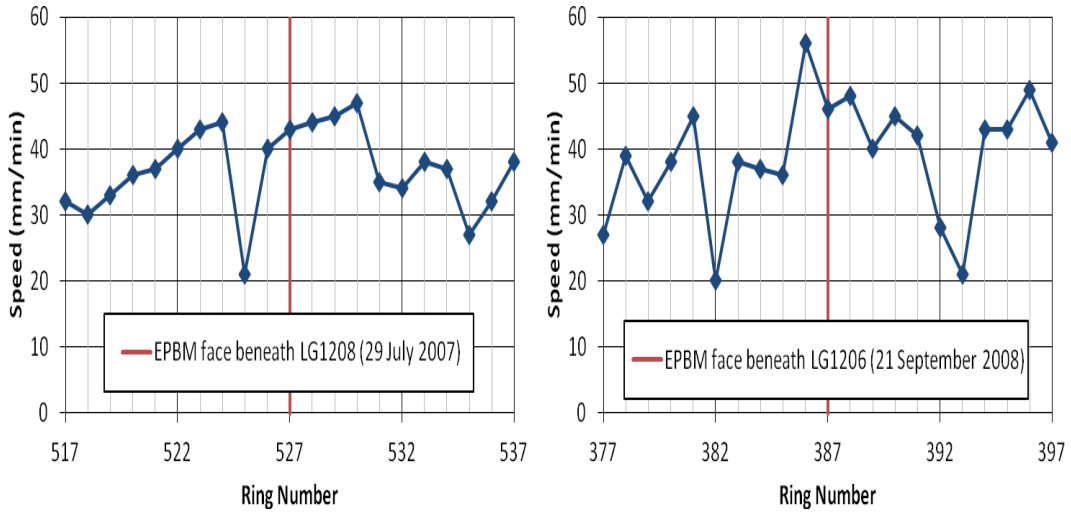

(a) (b)

Figure A.61 TBM speed for (a) first inner bound bored tunnelling; and (b) second outer bound bored tunnelling (Instrumentation Array D37)

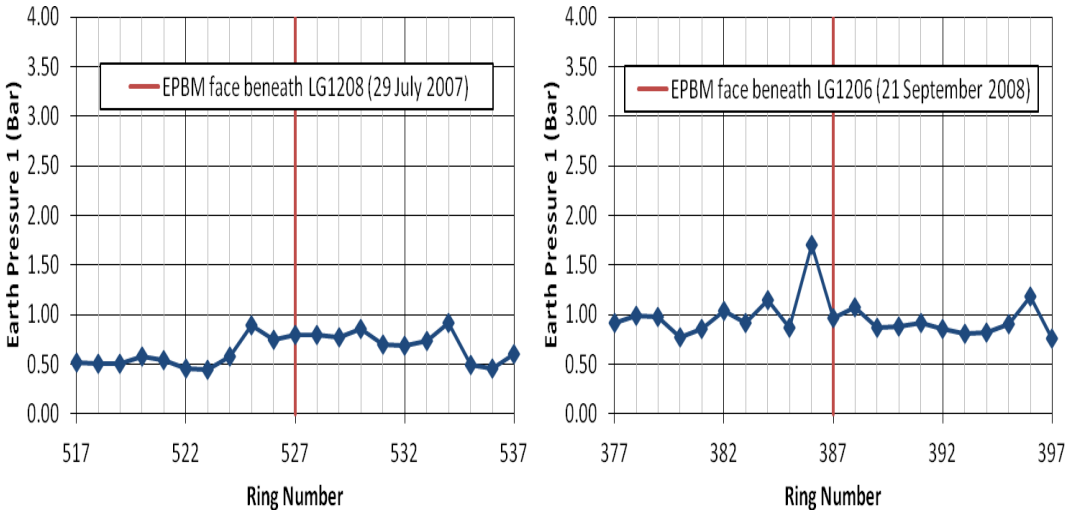

(a) (b)

Figure A.62 TBM earth pressure 1 for (a) first inner bound bored tunnelling; and (b) second outer bound bored tunnelling (Instrumentation Array D37)

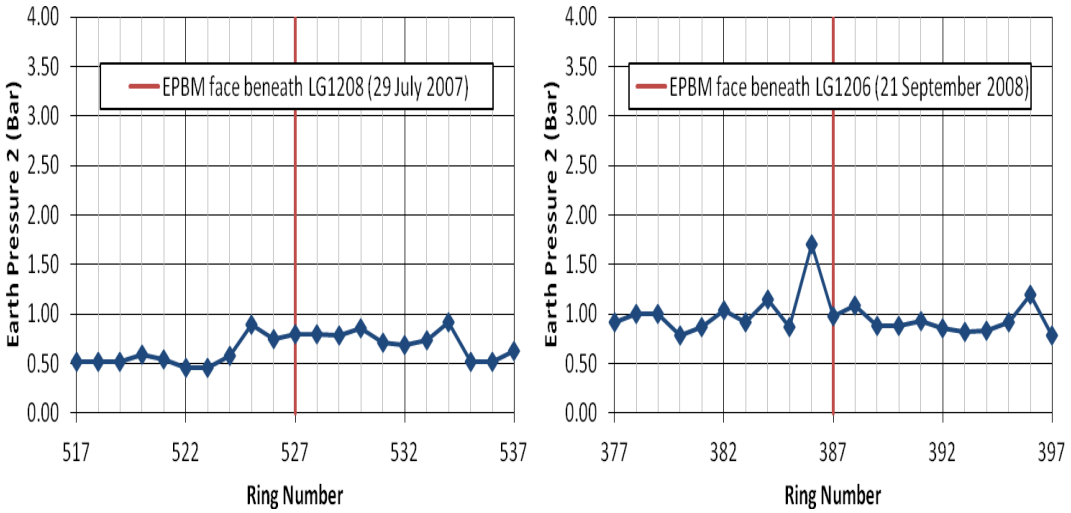

(a) (b)

Figure A.63 TBM earth pressure 2 for (a) first inner bound bored tunnelling; and (b) second outer bound bored tunnelling (Instrumentation Array D37)

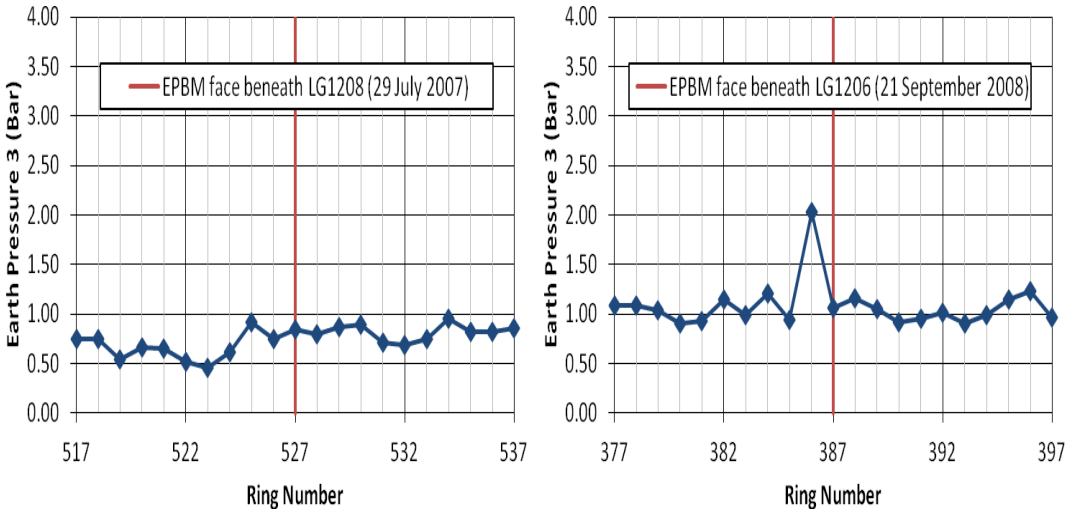

(a) (b)

Figure A.64 TBM earth pressure 3 for (a) first inner bound bored tunnelling; and (b) second outer bound bored tunnelling (Instrumentation Array D37)

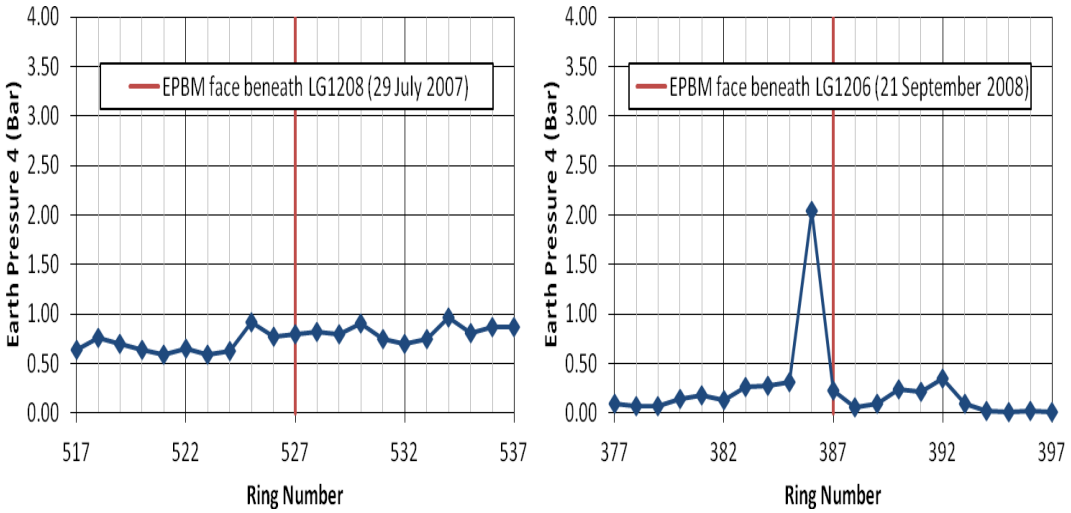

(a) (b)

Figure A.65 TBM earth pressure 4 for (a) first inner bound bored tunnelling; and (b) second outer bound bored tunnelling (Instrumentation Array D37)

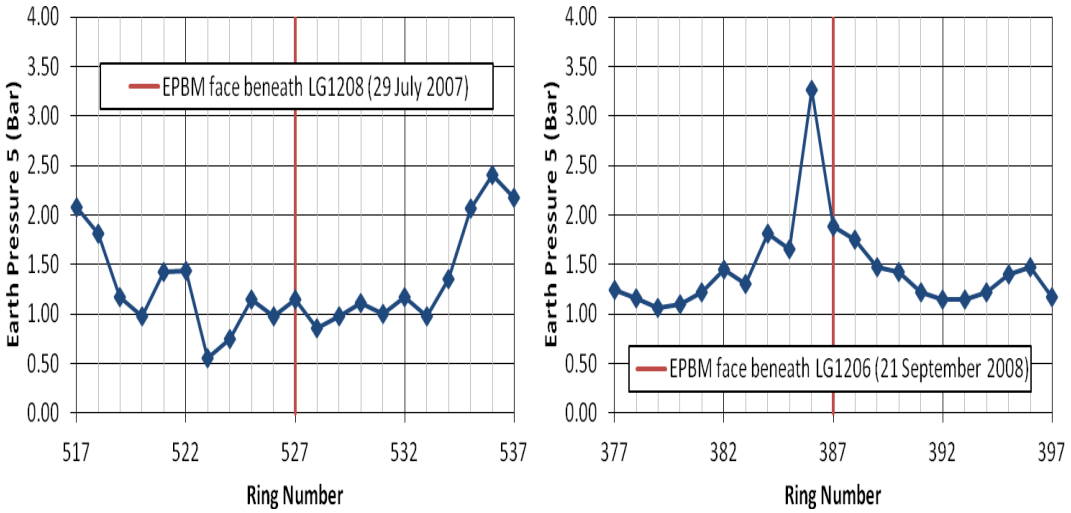

(a) (b)

Figure A.66 TBM earth pressure 5 for (a) first inner bound bored tunnelling; and (b) second outer bound bored tunnelling (Instrumentation Array D37)

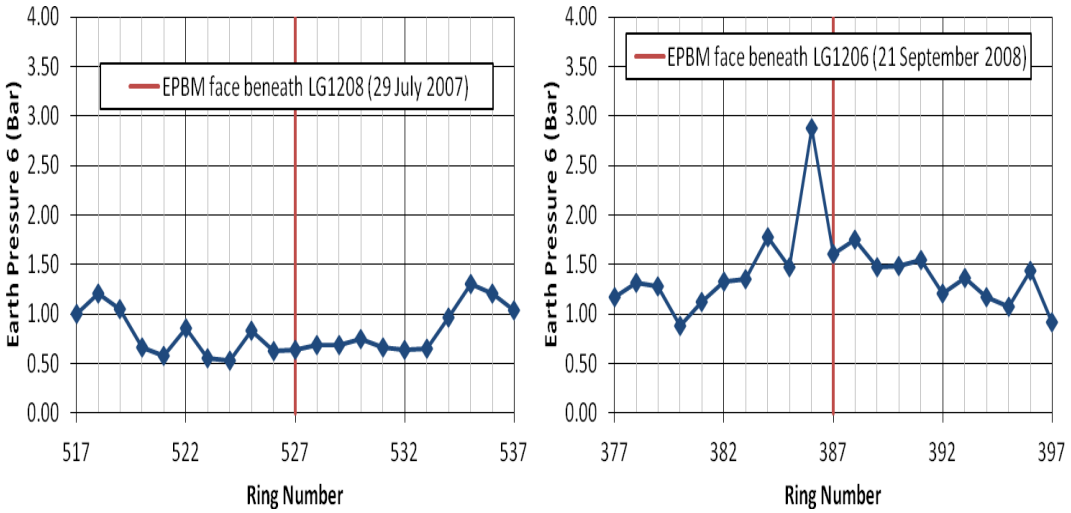

(a) (b)

Figure A.67 TBM earth pressure 6 for (a) first inner bound bored tunnelling; and (b) second outer bound bored tunnelling (Instrumentation Array D37)

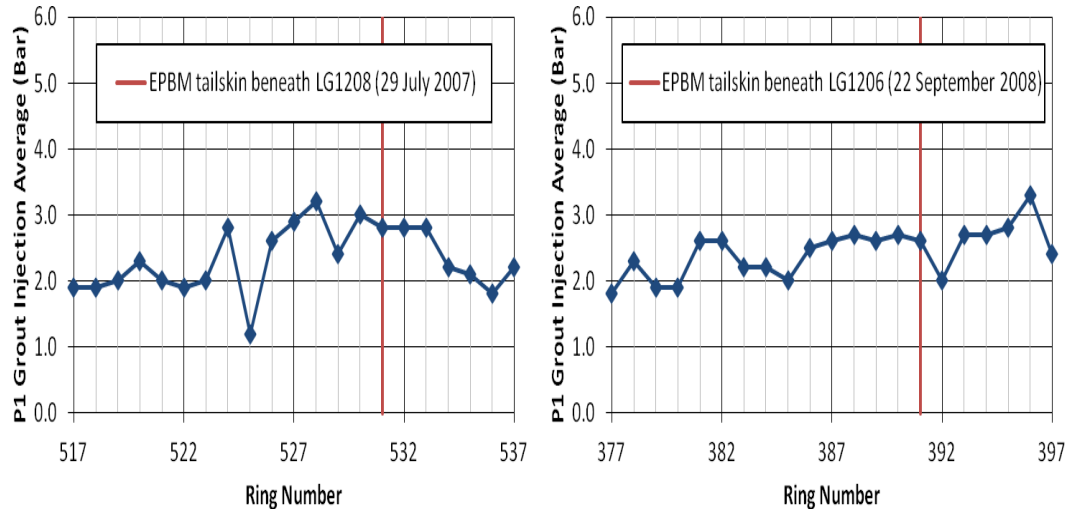

(a) (b)

Figure A.68 P1 grout injection average for (a) first inner bound bored tunnelling; and (b) second outer bound bored tunnelling (Instrumentation Array D37)

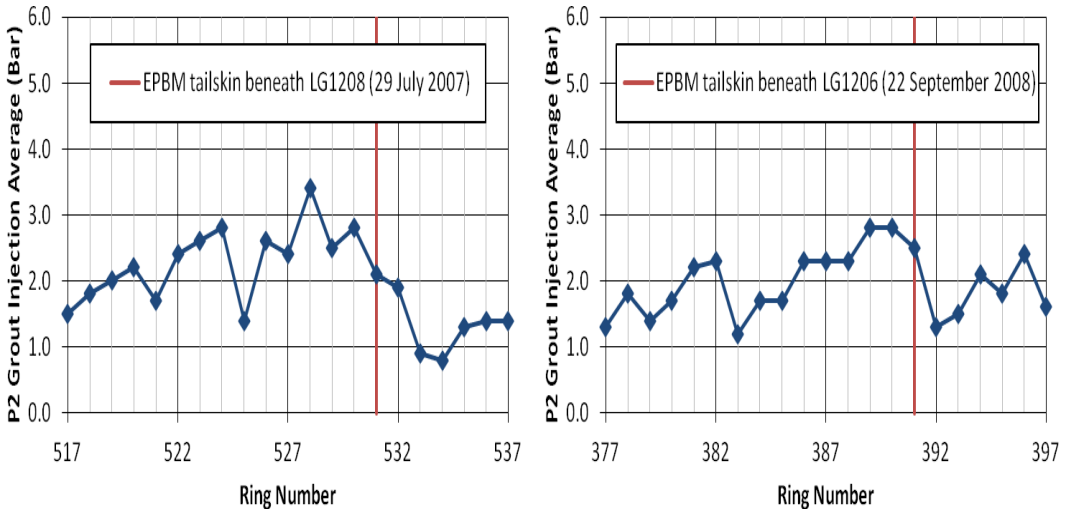

(a) (b)

Figure A.69 P2 grout injection average for (a) first inner bound bored tunnelling; and (b) second outer bound bored tunnelling (Instrumentation Array D37)

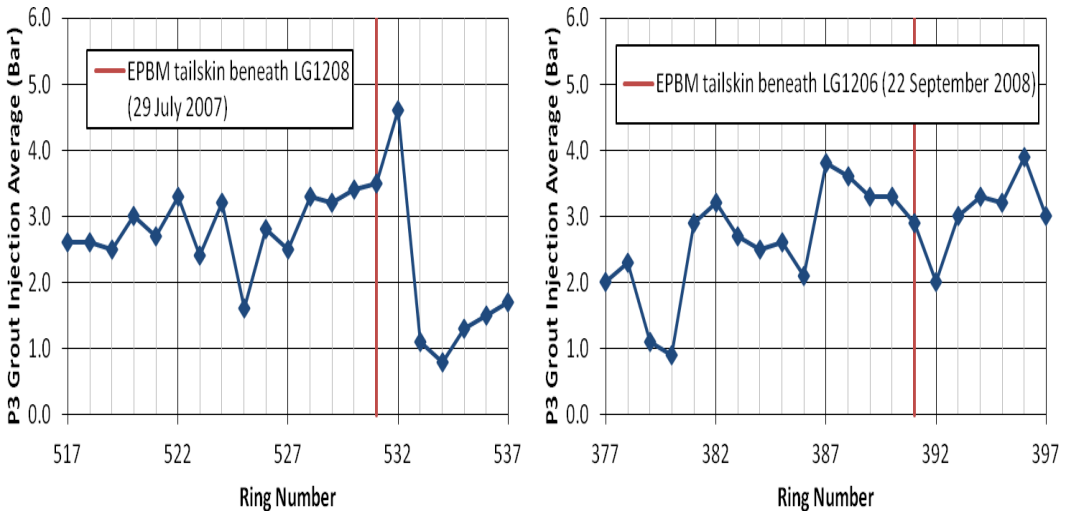

(a) (b)

Figure A.70 P3 grout injection average for (a) first inner bound bored tunnelling; and (b) second outer bound bored tunnelling (Instrumentation Array D37)

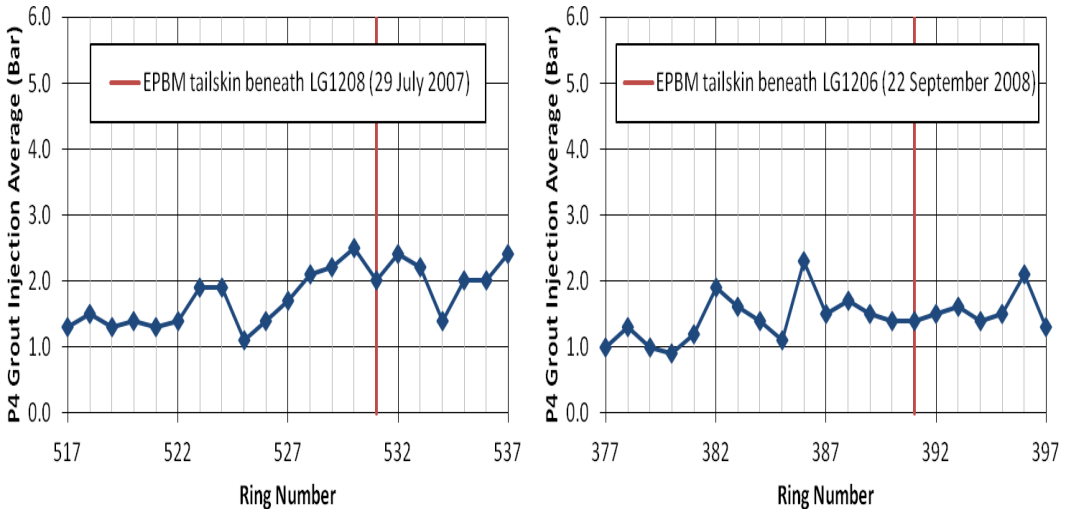

(a) (b)

Figure A.71 P4 grout injection average for (a) first inner bound bored tunnelling; and (b) second outer bound bored tunnelling (Instrumentation Array D37)

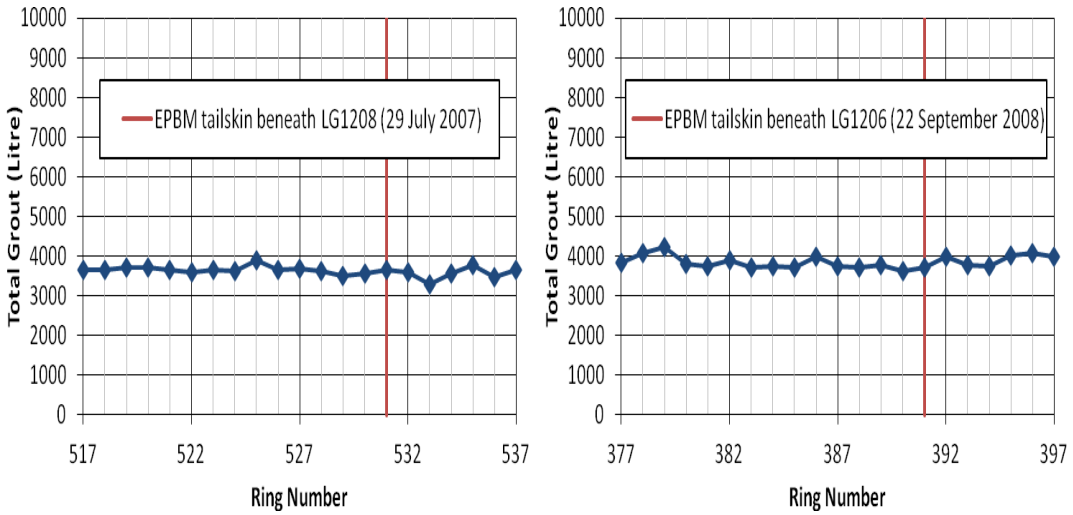

(a) (b)

Figure A.72 Total grout for (a) first inner bound bored tunnelling; and (b) second outer bound bored tunnelling (Instrumentation Array D37)

Instrumentation Array D33

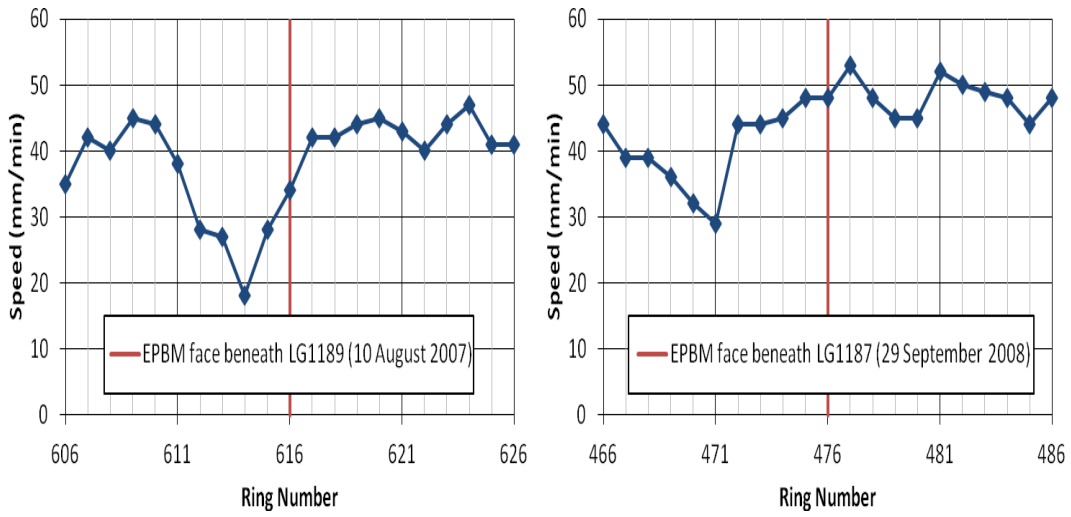

(a) (b)

Figure A.73 TBM speed for (a) first inner bound bored tunnelling; and (b) second outer bound bored tunnelling (Instrumentation Array D33)

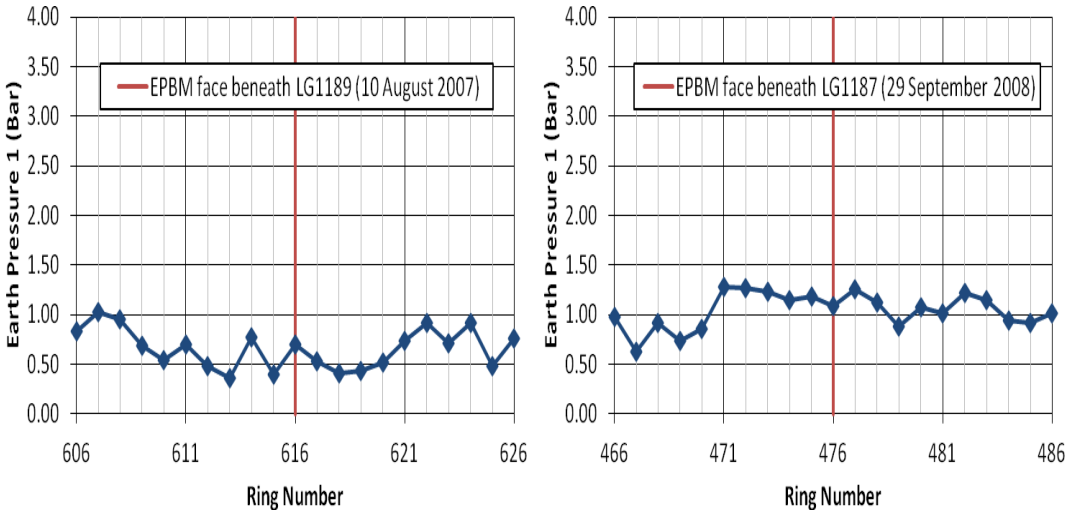

(a) (b)

Figure A.74 TBM earth pressure 1 for (a) first inner bound bored tunnelling; and (b) second outer bound bored tunnelling (Instrumentation Array D33)

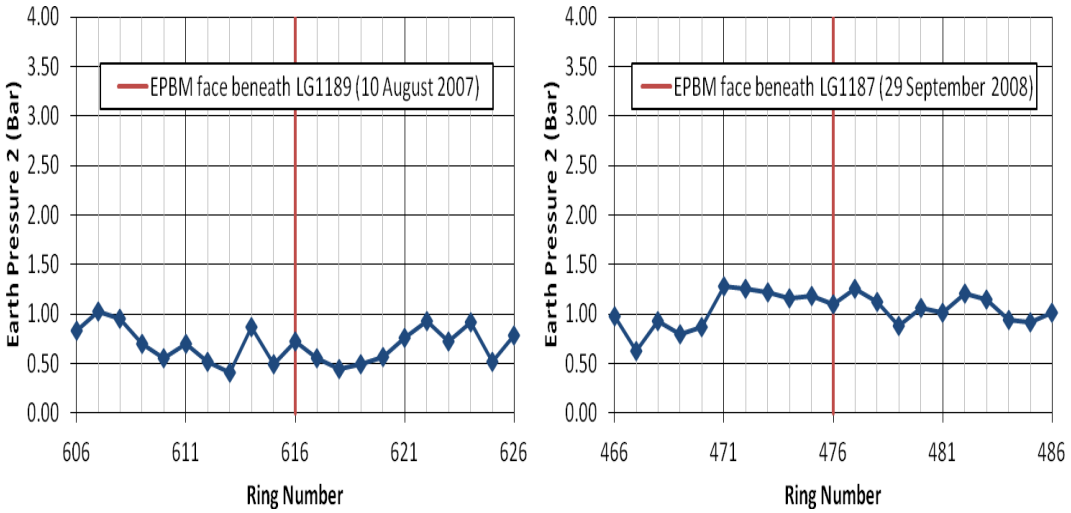

(a) (b)

Figure A.75 TBM earth pressure 2 for (a) first inner bound bored tunnelling; and (b) second outer bound bored tunnelling (Instrumentation Array D33)

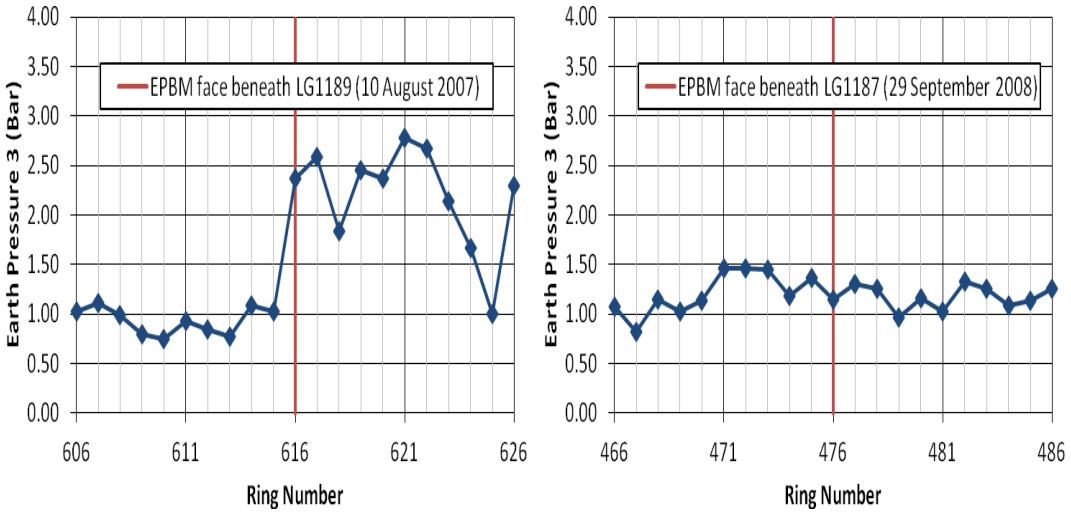

(a) (b)

Figure A.76 TBM earth pressure 3 for (a) first inner bound bored tunnelling; and (b) second outer bound bored tunnelling (Instrumentation Array D33)

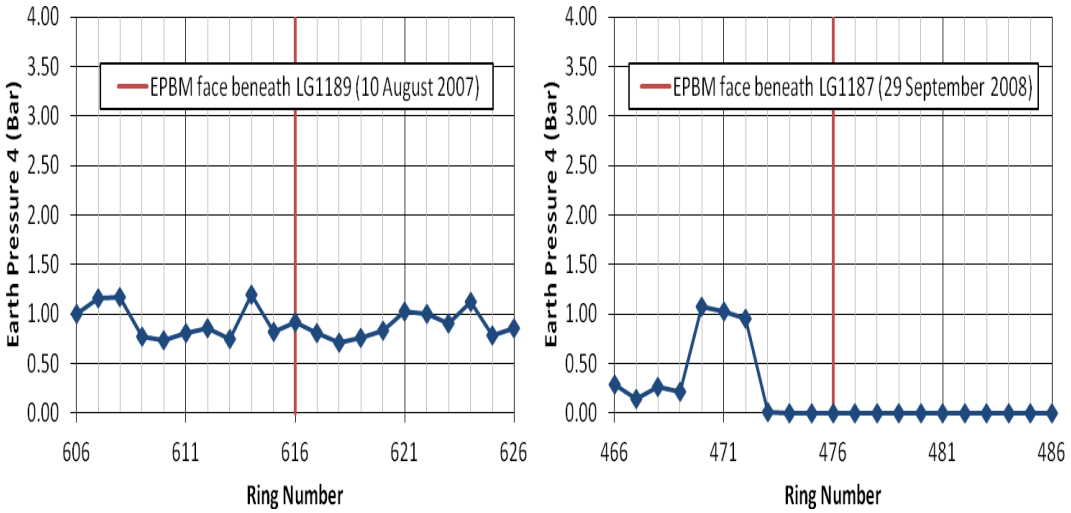

(a) (b)

Figure A.77 TBM earth pressure 4 for (a) first inner bound bored tunnelling; and (b) second outer bound bored tunnelling (Instrumentation Array D33)

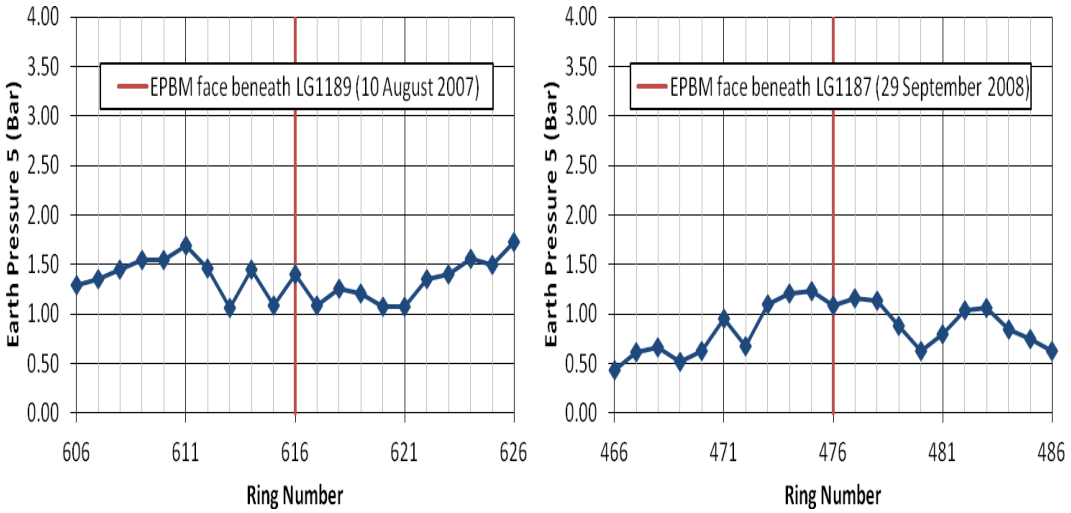

(a) (b)

Figure A.78 TBM earth pressure 5 for (a) first inner bound bored tunnelling; and (b) second outer bound bored tunnelling (Instrumentation Array D33)

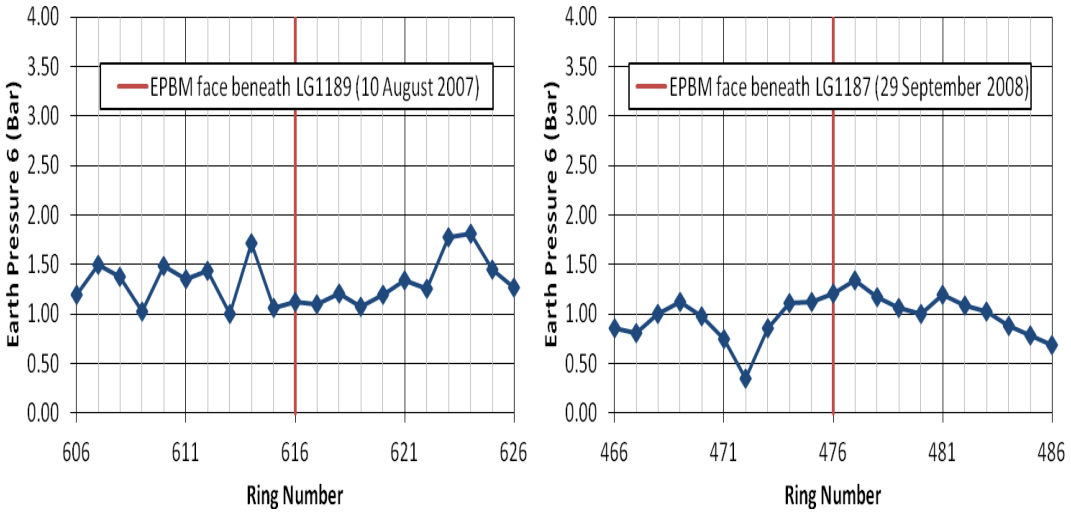

(a) (b)

Figure A.79 TBM earth pressure 6 for (a) first inner bound bored tunnelling; and (b) second outer bound bored tunnelling (Instrumentation Array D33)

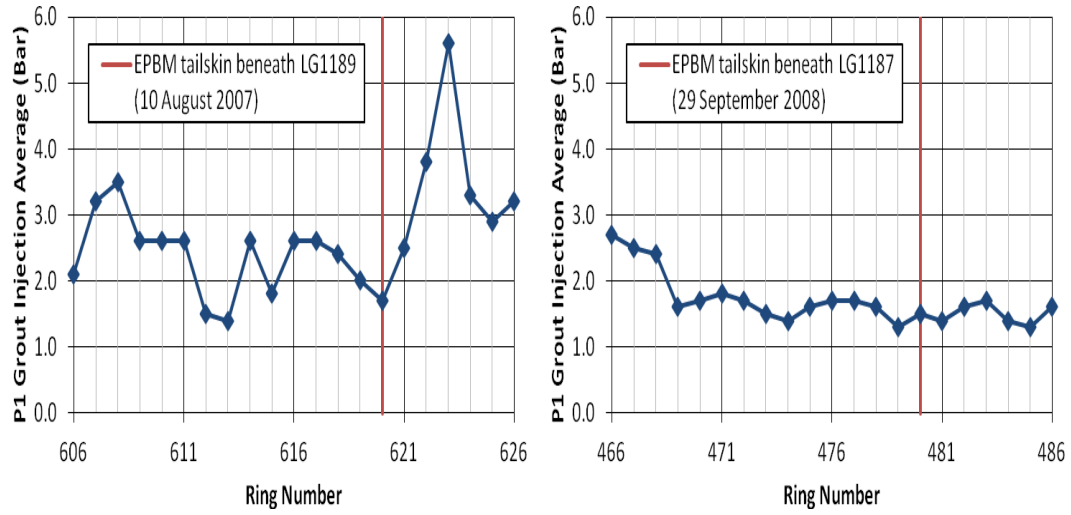

(a) (b)

Figure A.80 P1 grout injection average for (a) first inner bound bored tunnelling; and (b) second outer bound bored tunnelling (Instrumentation Array D33)

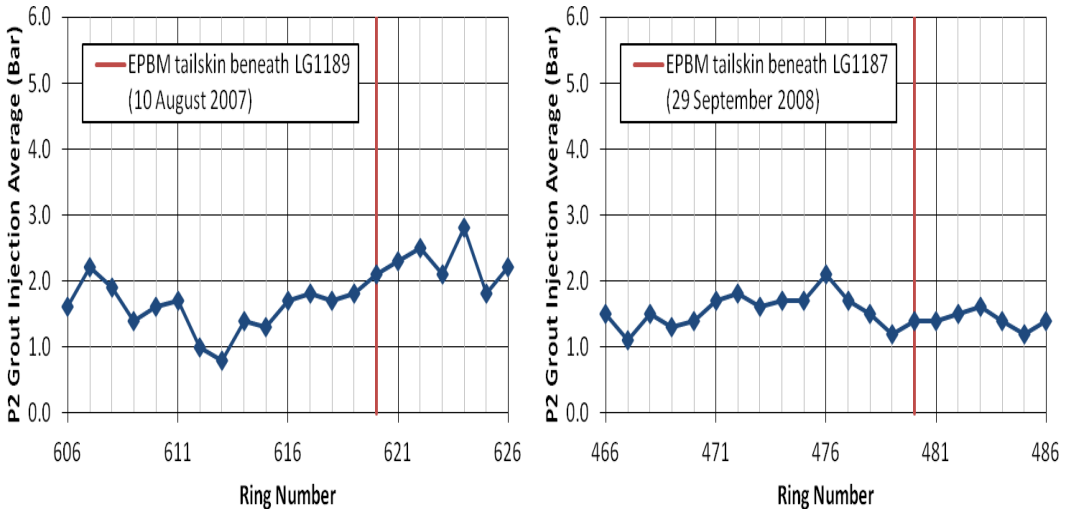

(a) (b)

Figure A.81 P2 grout injection average for (a) first inner bound bored tunnelling; and (b) second outer bound bored tunnelling (Instrumentation Array D33)

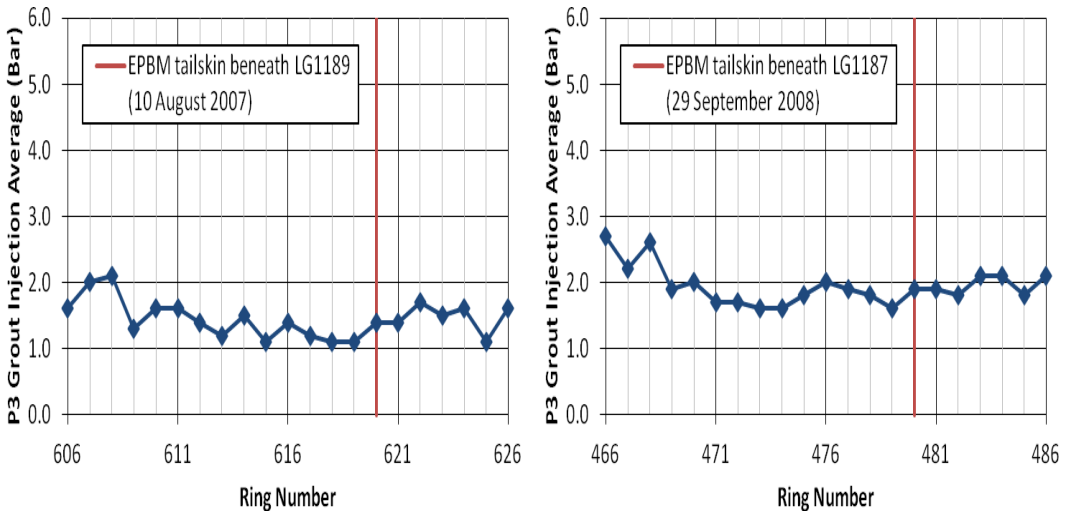

(a) (b)

Figure A.82 P3 grout injection average for (a) first inner bound bored tunnelling; and (b) second outer bound bored tunnelling (Instrumentation Array D33)

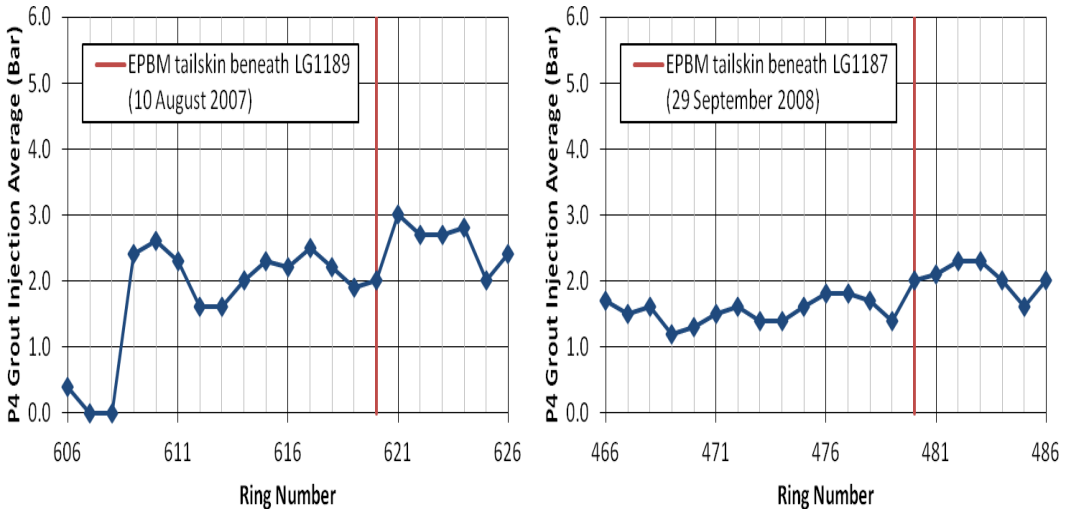

(a) (b)

Figure A.83 P4 grout injection average for (a) first inner bound bored tunnelling; and (b) second outer bound bored tunnelling (Instrumentation Array D33)

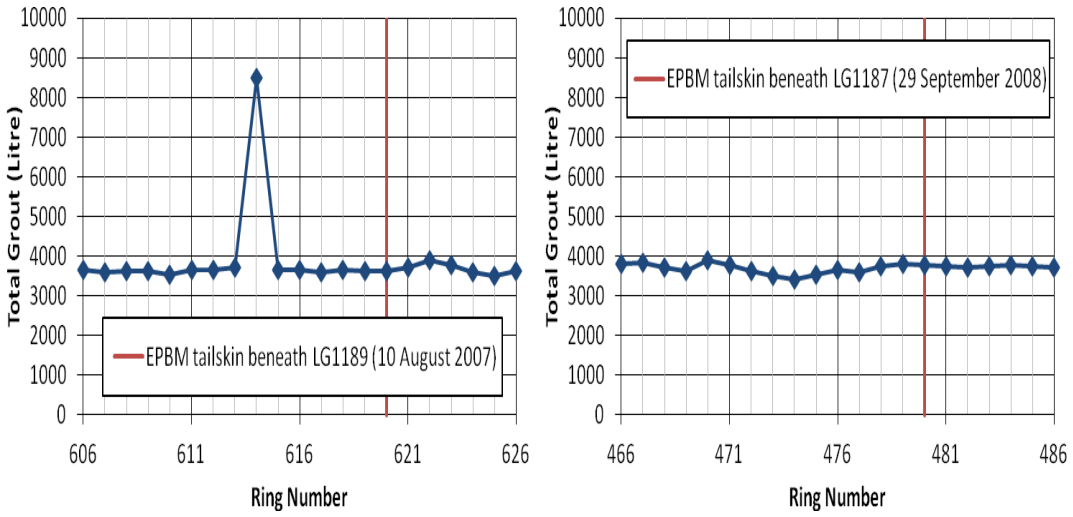

(a) (b)

Figure A.84 Total grout for (a) first inner bound bored tunnelling; and (b) second outer bound bored tunnelling (Instrumentation Array D33)

Instrumentation Array D32

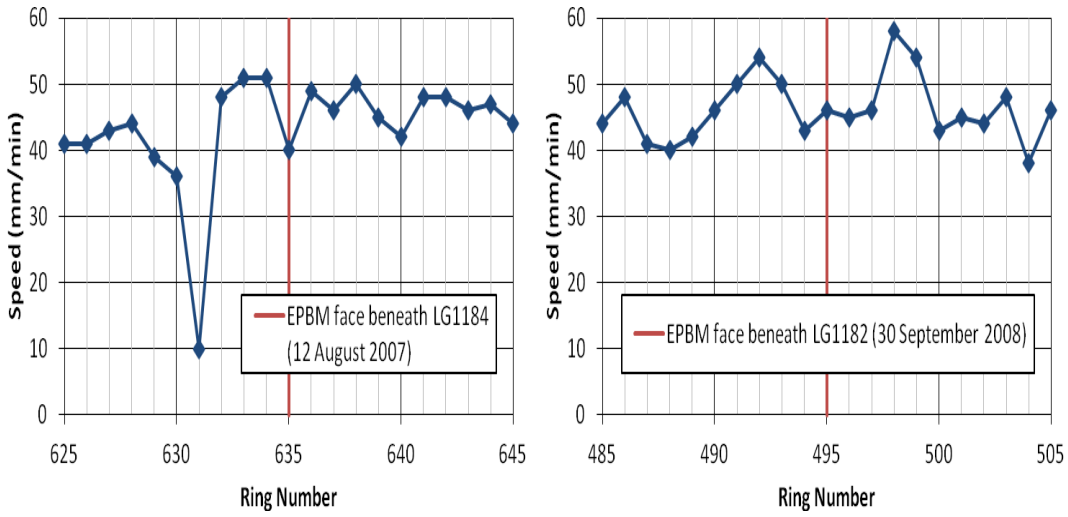

(a) (b)

Figure A.85 TBM speed for (a) first inner bound bored tunnelling; and (b) second outer bound bored tunnelling (Instrumentation Array D32)

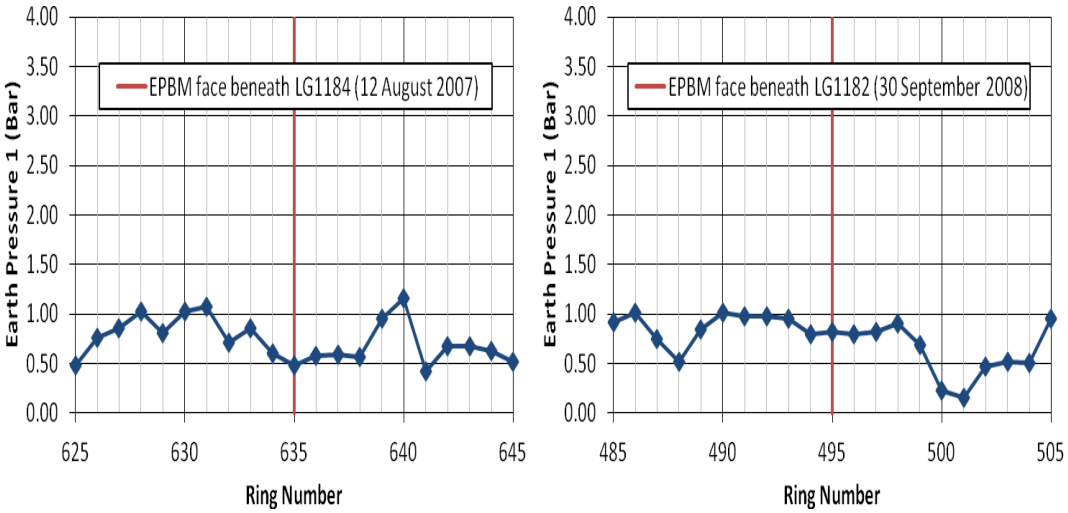

(a) (b)

Figure A.86 TBM earth pressure 1 for (a) first inner bound bored tunnelling; and (b) second outer bound bored tunnelling (Instrumentation Array D32)

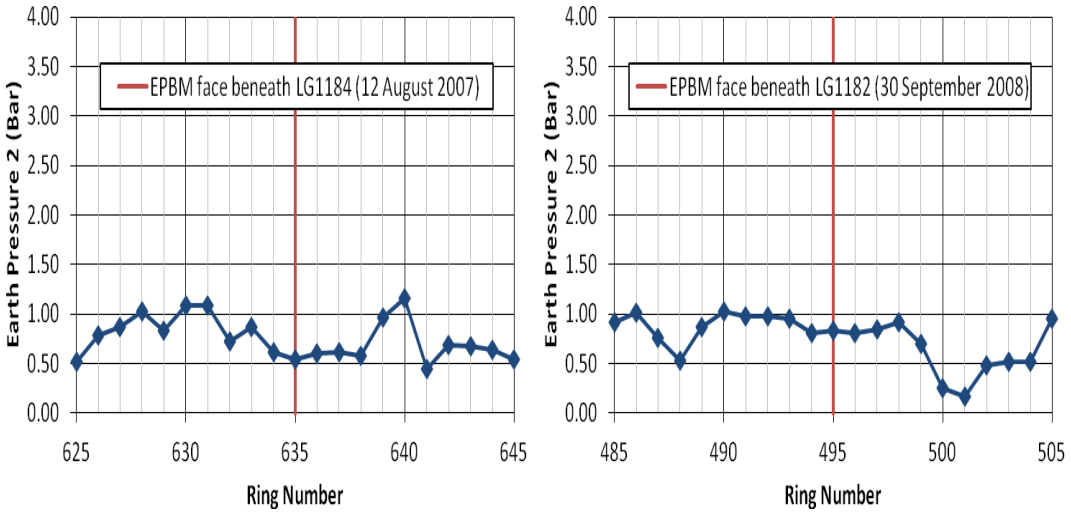

(a) (b)

Figure A.87 TBM earth pressure 2 for (a) first inner bound bored tunnelling; and (b) second outer bound bored tunnelling (Instrumentation Array D32)

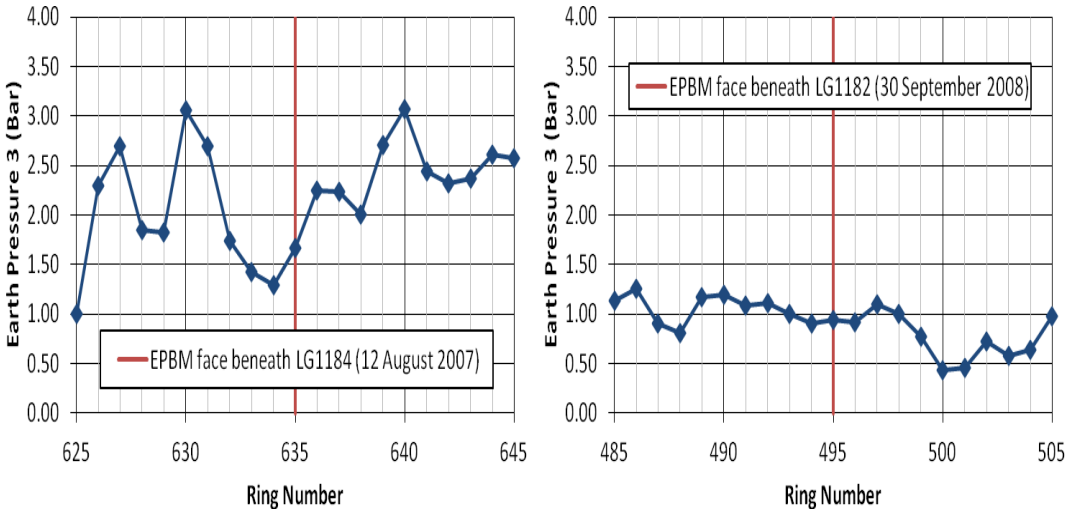

(a) (b)

Figure A.88 TBM earth pressure 3 for (a) first inner bound bored tunnelling; and (b) second outer bound bored tunnelling (Instrumentation Array D32)

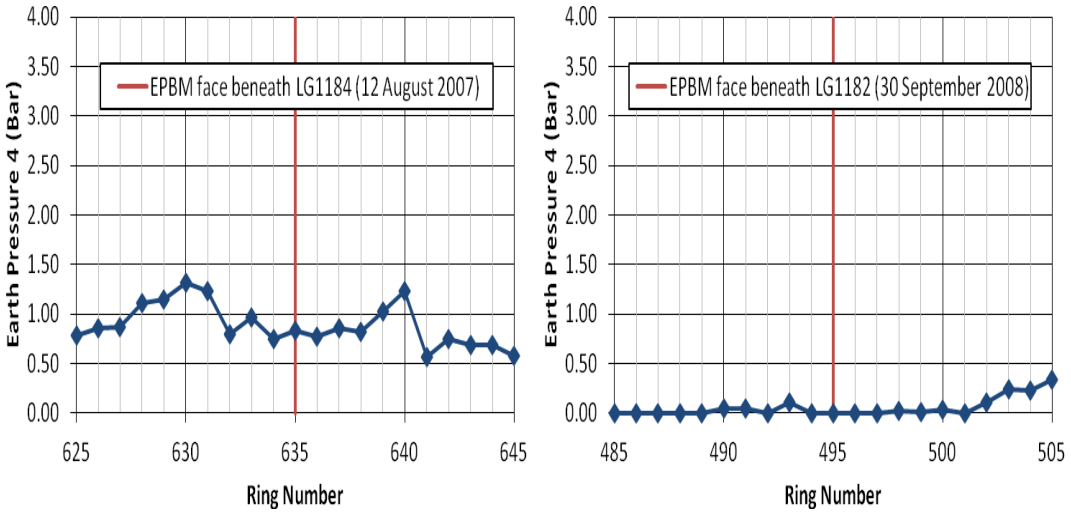

(a) (b)

Figure A.89 TBM earth pressure 4 for (a) first inner bound bored tunnelling; and (b) second outer bound bored tunnelling (Instrumentation Array D32)

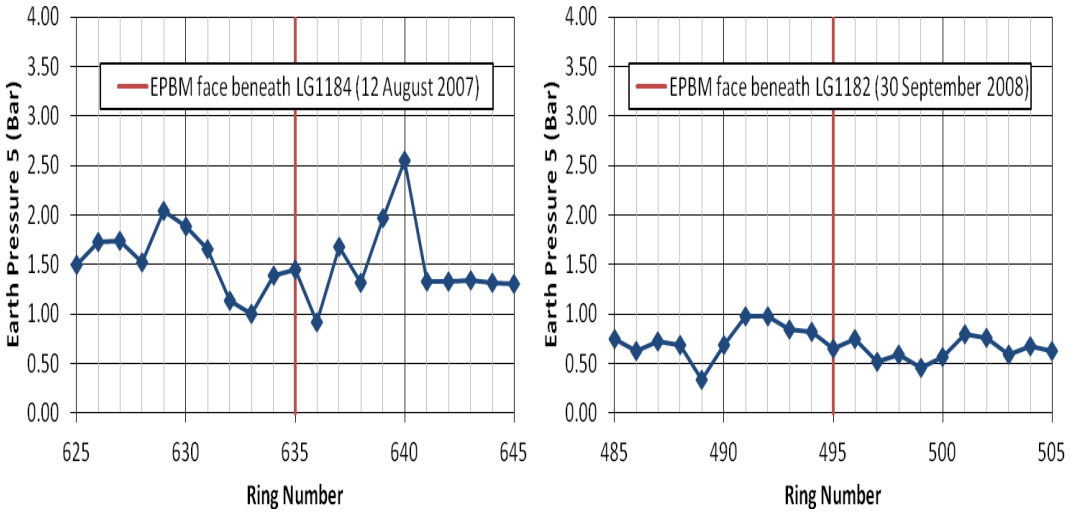

(a) (b)

Figure A.90 TBM earth pressure 5 for (a) first inner bound bored tunnelling; and (b) second outer bound bored tunnelling (Instrumentation Array D32)

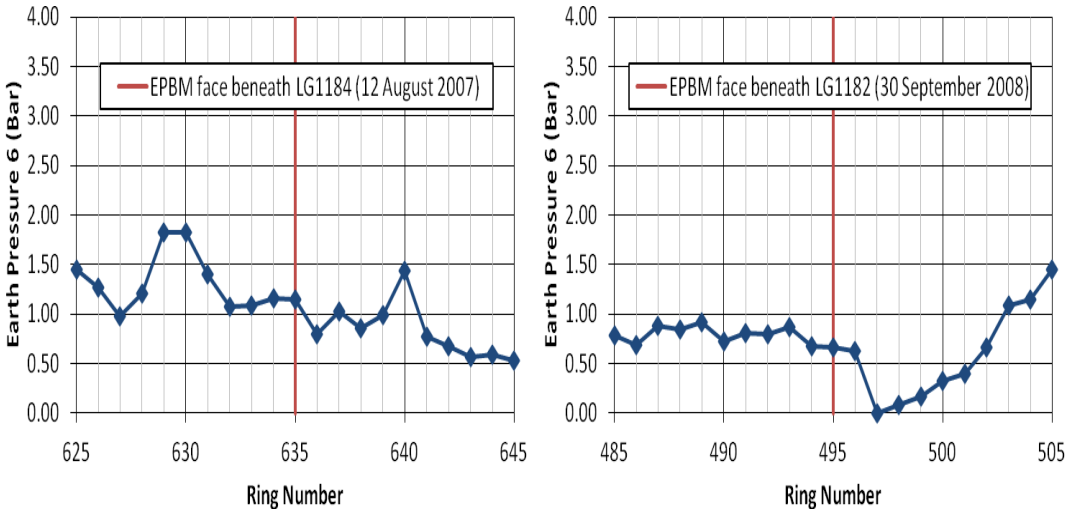

(a) (b)

Figure A.91 TBM earth pressure 6 for (a) first inner bound bored tunnelling; and (b) second outer bound bored tunnelling (Instrumentation Array D32)

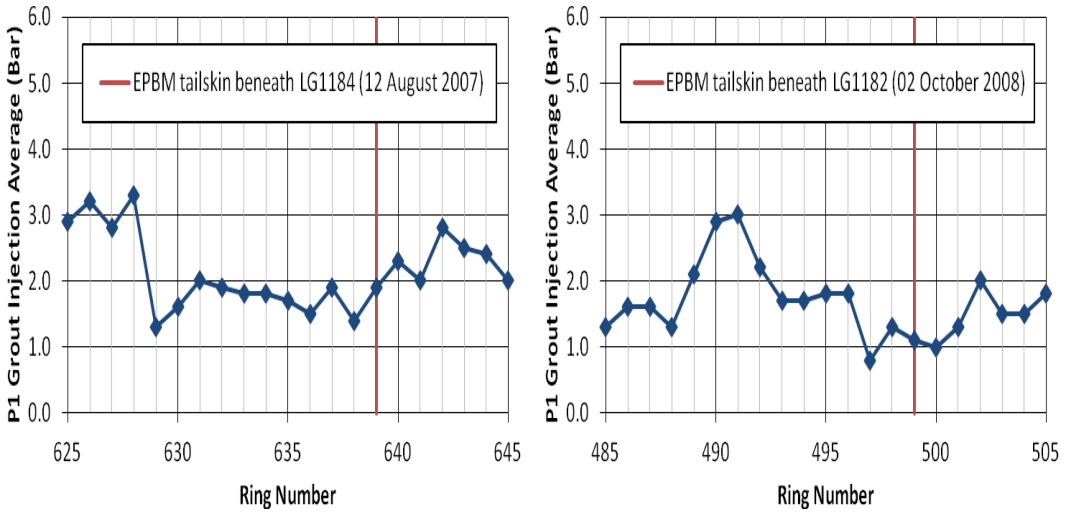

(a) (b)

Figure A.92 P1 grout injection average for (a) first inner bound bored tunnelling; and (b) second outer bound bored tunnelling (Instrumentation Array D32)

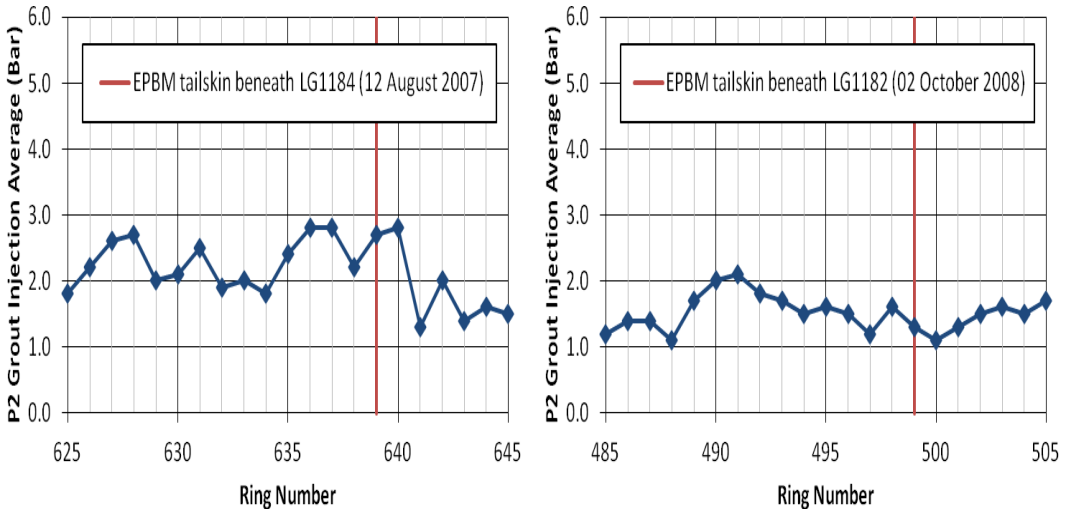

(a) (b)

Figure A.93 P2 grout injection average for (a) first inner bound bored tunnelling; and (b) second outer bound bored tunnelling (Instrumentation Array D32)

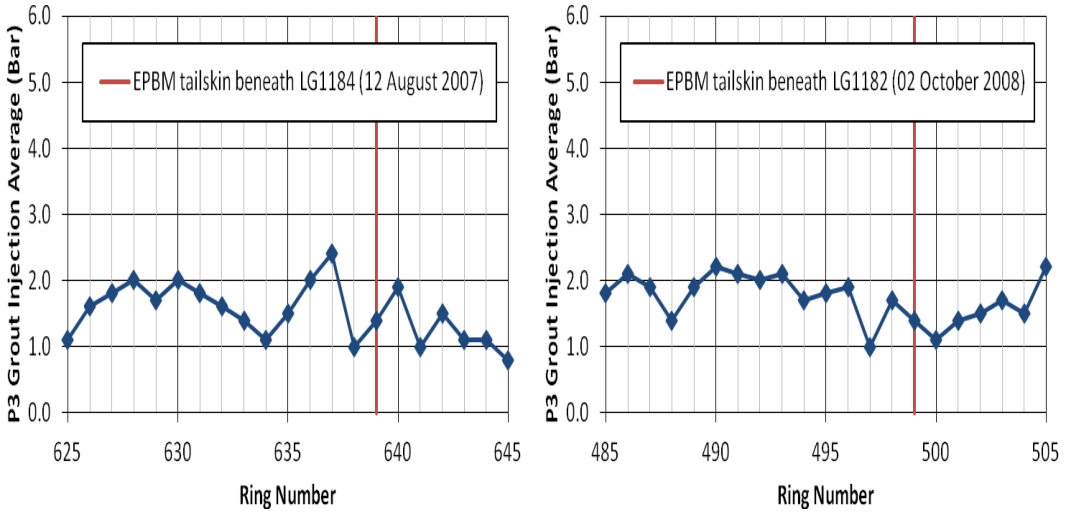

(a) (b)

Figure A.94 P3 grout injection average for (a) first inner bound bored tunnelling; and (b) second outer bound bored tunnelling (Instrumentation Array D32)

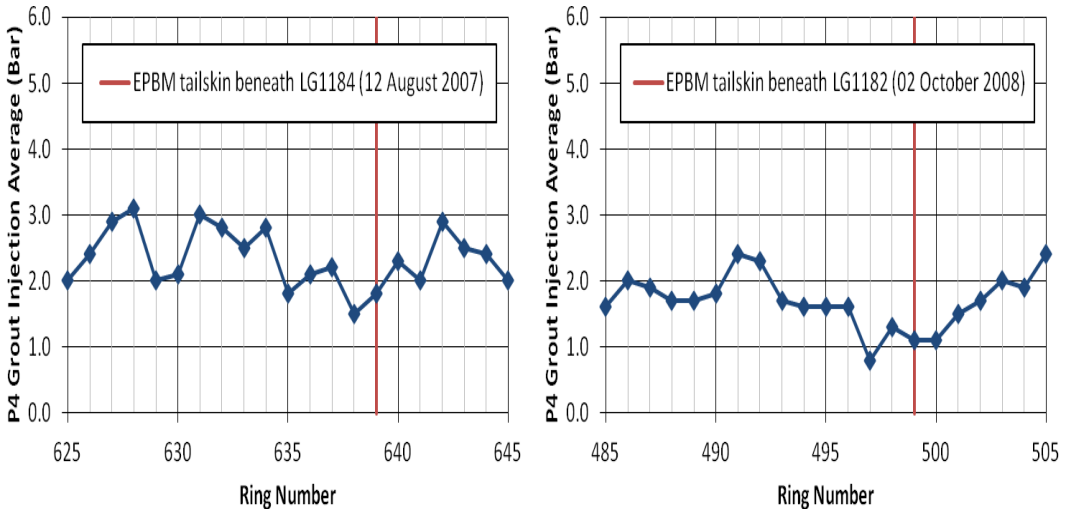

(a) (b)

Figure A.95 P4 grout injection average for (a) first inner bound bored tunnelling; and (b) second outer bound bored tunnelling (Instrumentation Array D32)

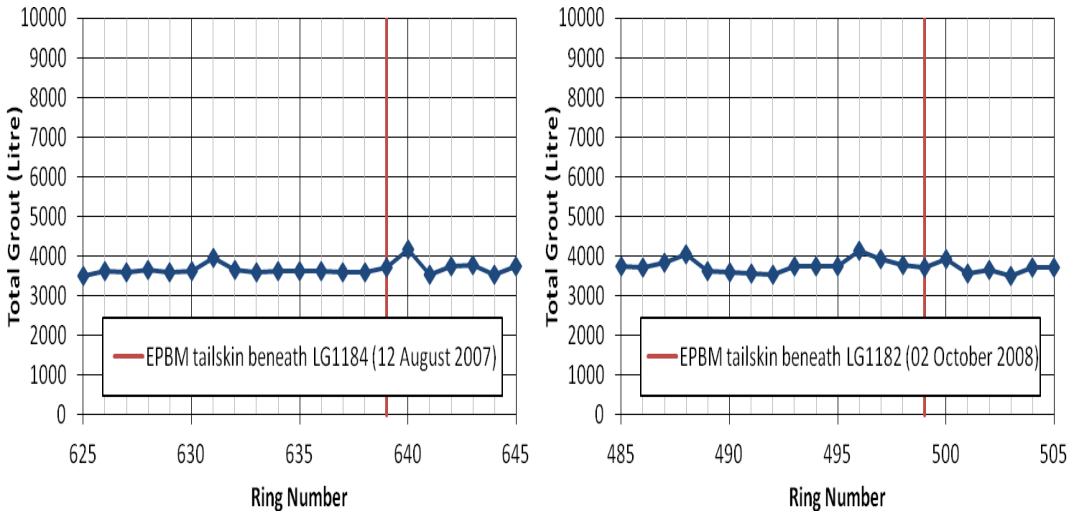

(a) (b)

Figure A.96 Total grout for (a) first inner bound bored tunnelling; and (b) second outer bound bored tunnelling (Instrumentation Array D32)

Instrumentation Array E14

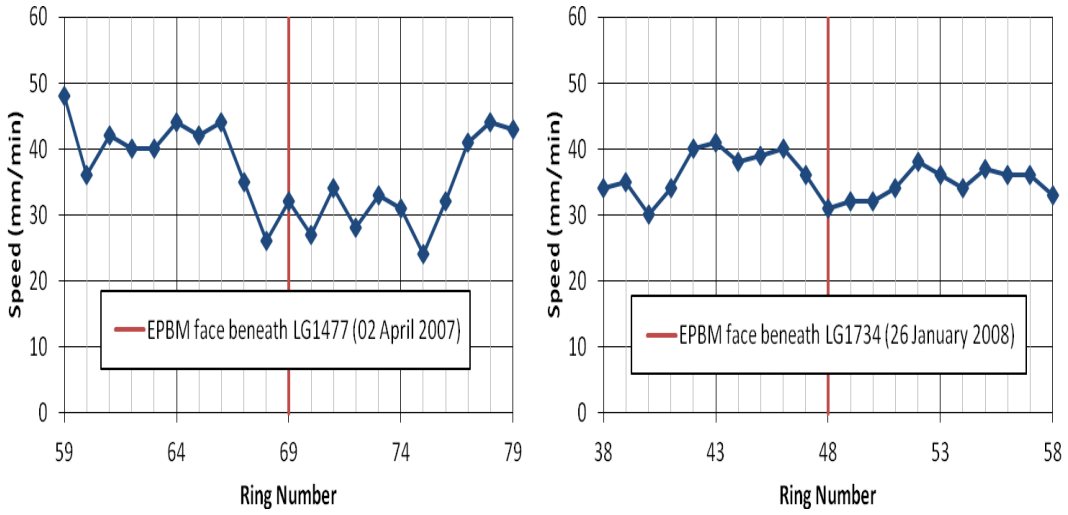

(a) (b)

Figure A.97 TBM speed for (a) first inner bound bored tunnelling; and (b) second outer bound bored tunnelling (Instrumentation Array E14)

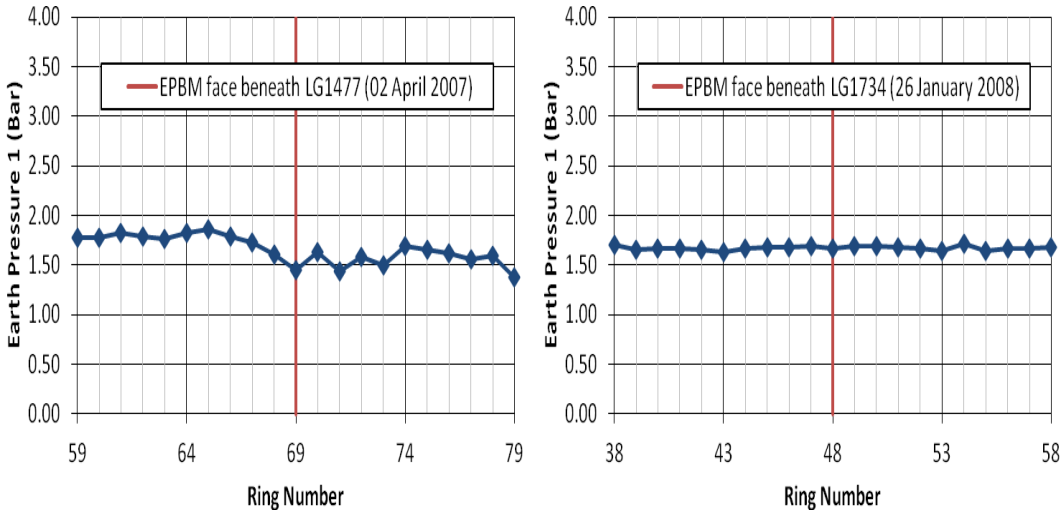

(a) (b)

Figure A.98 TBM earth pressure 1 for (a) first inner bound bored tunnelling; and (b) second outer bound bored tunnelling (Instrumentation Array E14)

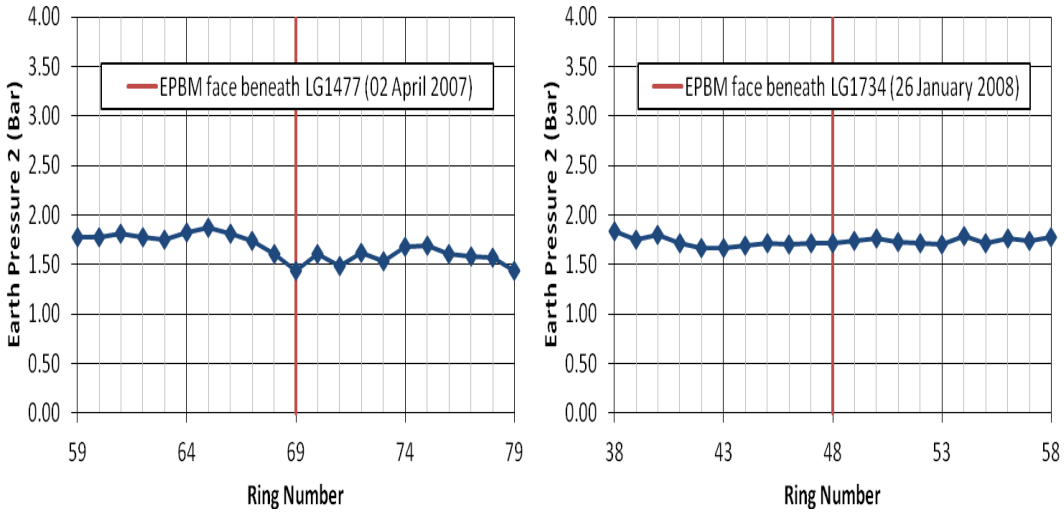

(a) (b)

Figure A.99 TBM earth pressure 2 for (a) first inner bound bored tunnelling; and (b) second outer bound bored tunnelling (Instrumentation Array E14)

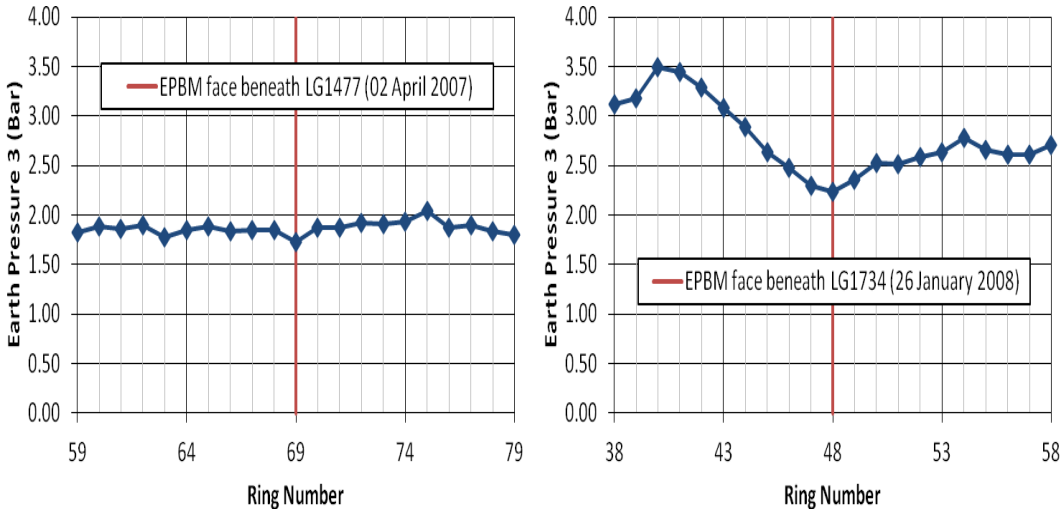

(a) (b)

Figure A.100 TBM earth pressure 3 for (a) first inner bound bored tunnelling; and (b) second outer bound bored tunnelling (Instrumentation Array E14)

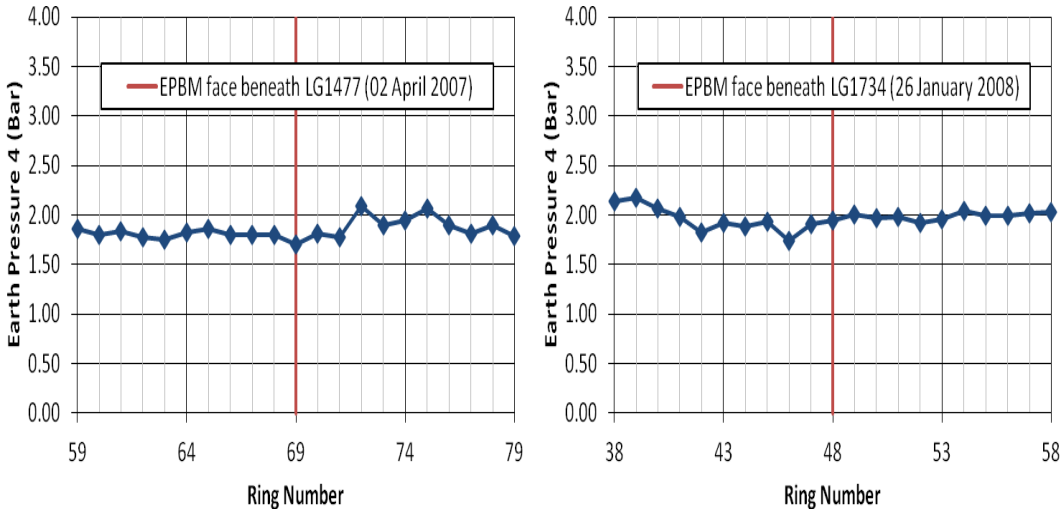

(a) (b)

Figure A.101 TBM earth pressure 4 for (a) first inner bound bored tunnelling; and (b) second outer bound bored tunnelling (Instrumentation Array E14)

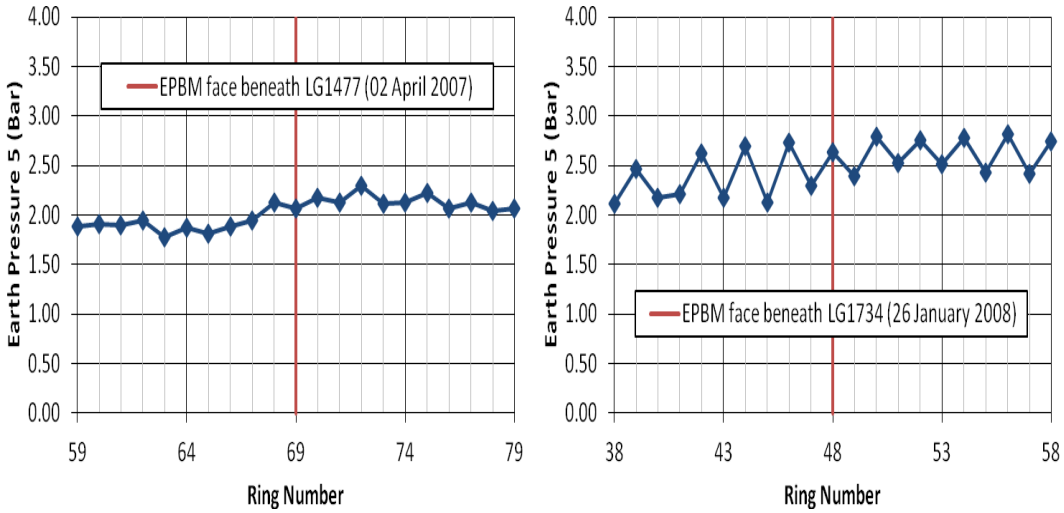

(a) (b)

Figure A.102 TBM earth pressure 5 for (a) first inner bound bored tunnelling; and (b) second outer bound bored tunnelling (Instrumentation Array E14)

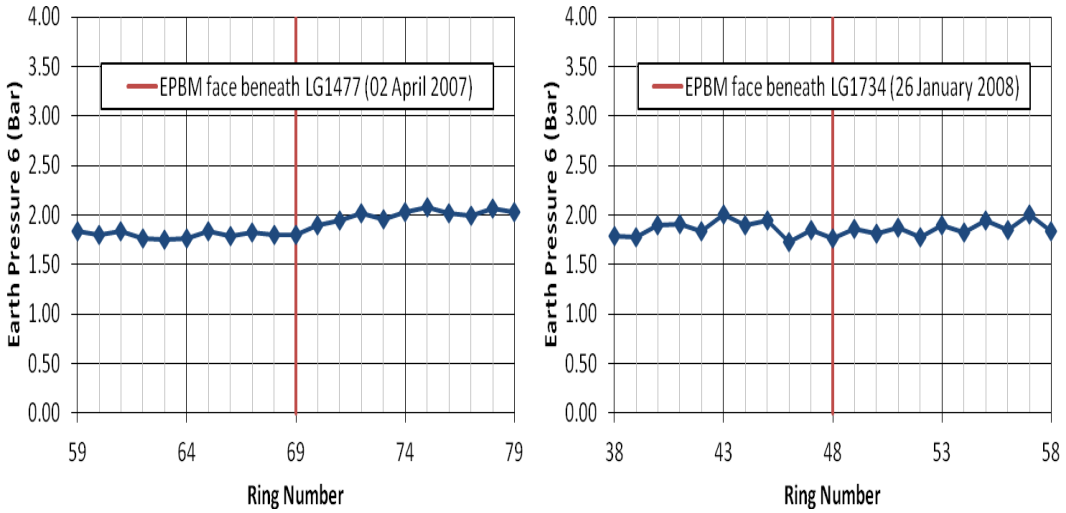

(a) (b)

Figure A.103 TBM earth pressure 6 for (a) first inner bound bored tunnelling; and (b) second outer bound bored tunnelling (Instrumentation Array E14)

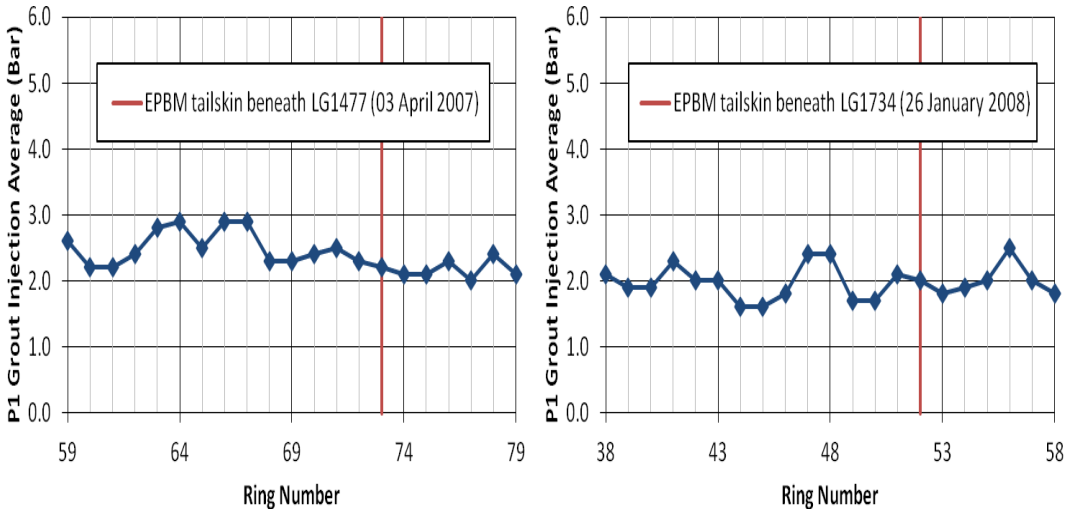

(a) (b)

Figure A.104 P1 grout injection average for (a) first inner bound bored tunnelling; and (b) second outer bound bored tunnelling (Instrumentation Array E14)

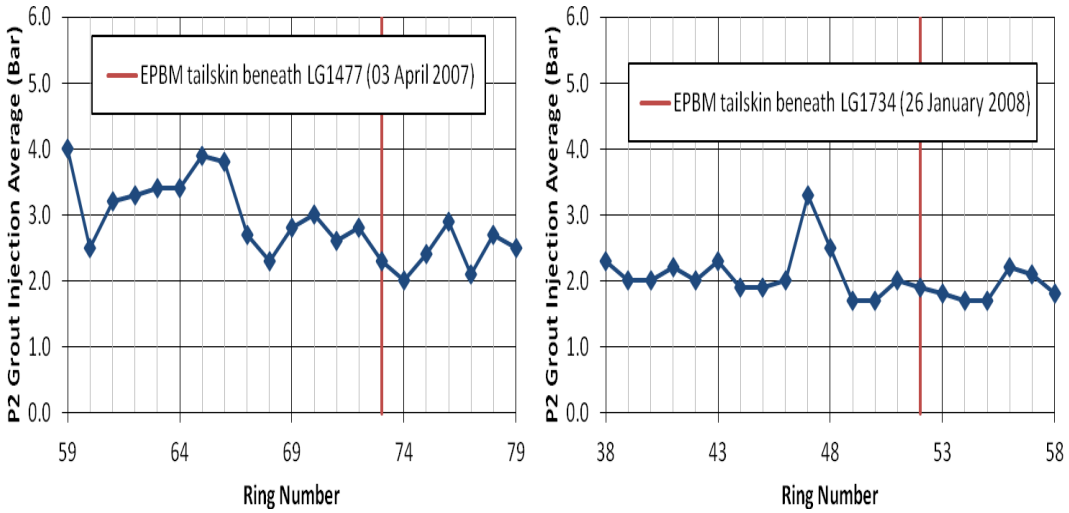

(a) (b)

Figure A.105 P2 grout injection average for (a) first inner bound bored tunnelling; and (b) second outer bound bored tunnelling (Instrumentation Array E14)

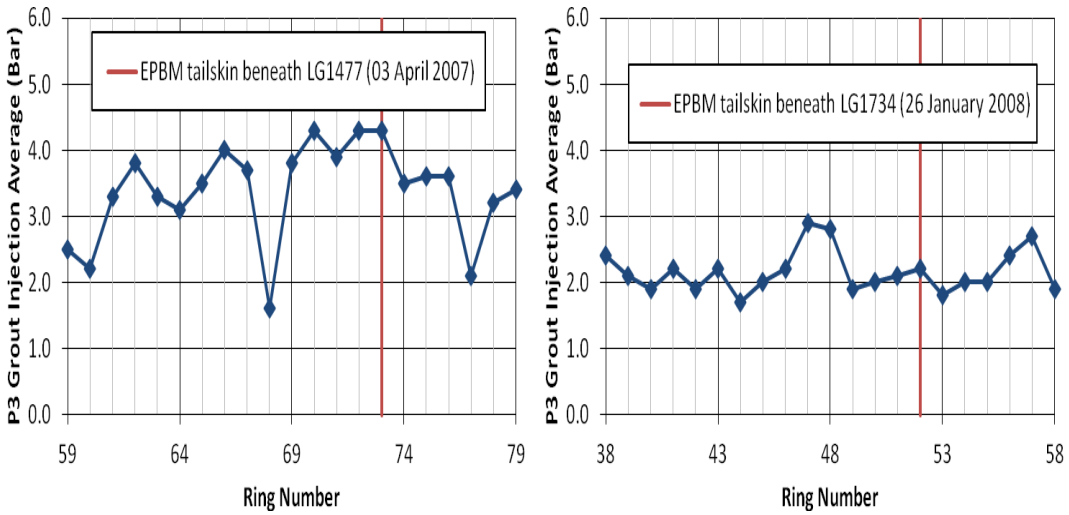

(a) (b)

Figure A.106 P3 grout injection average for (a) first inner bound bored tunnelling; and (b) second outer bound bored tunnelling (Instrumentation Array E14)

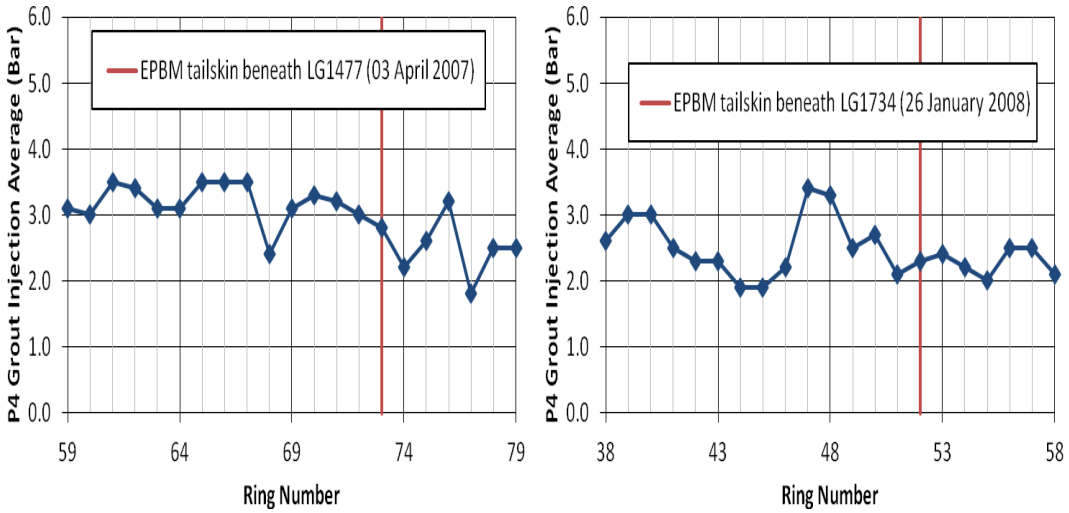

(a) (b)

Figure A.107 P4 grout injection average for (a) first inner bound bored tunnelling; and (b) second outer bound bored tunnelling (Instrumentation Array E14)

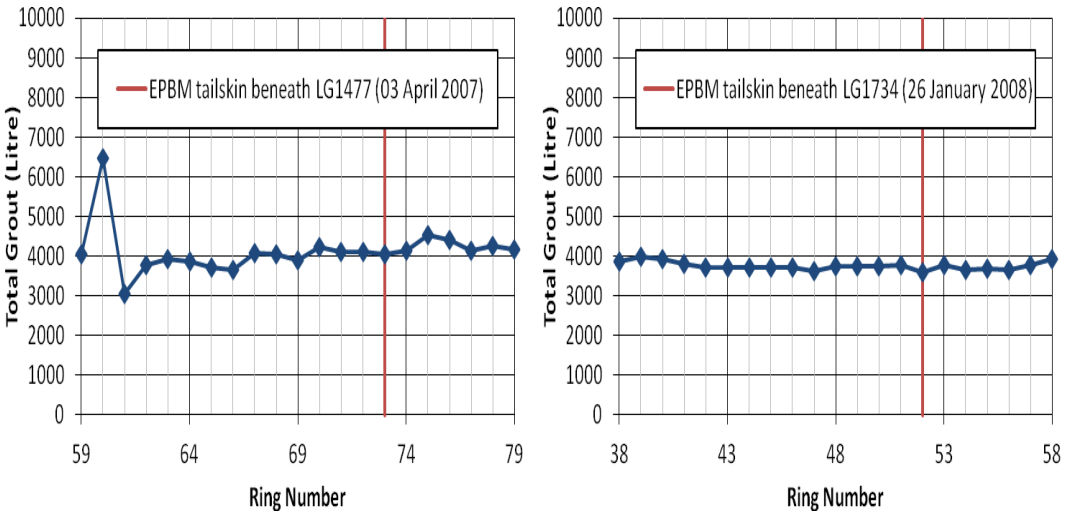

(a) (b)

Figure A.108 Total grout for (a) first inner bound bored tunnelling; and (b) second outer bound bored tunnelling (Instrumentation Array E14)

Instrumentation Array D49

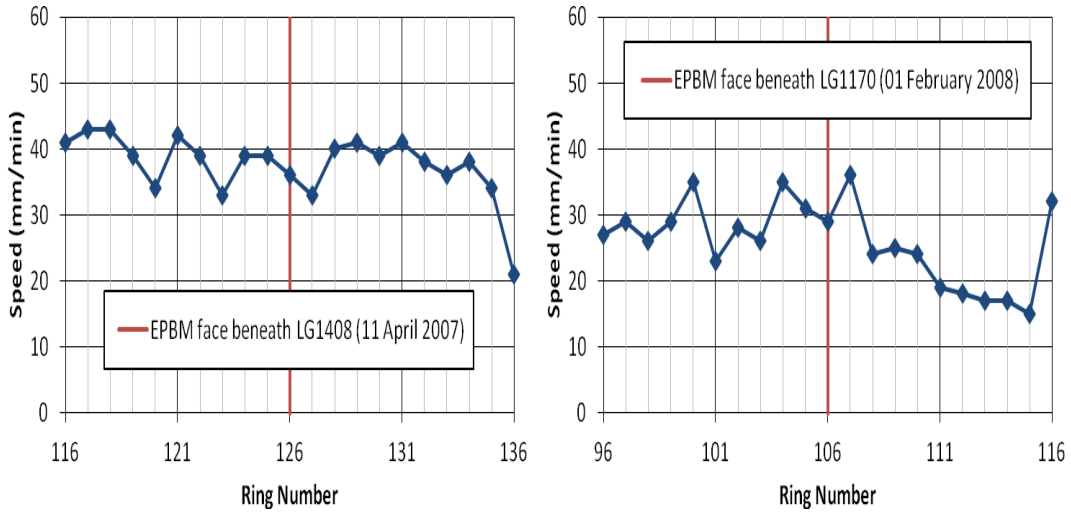

(a) (b)

Figure A.109 TBM speed for (a) first inner bound bored tunnelling; and (b) second outer bound bored tunnelling (Instrumentation Array D49)

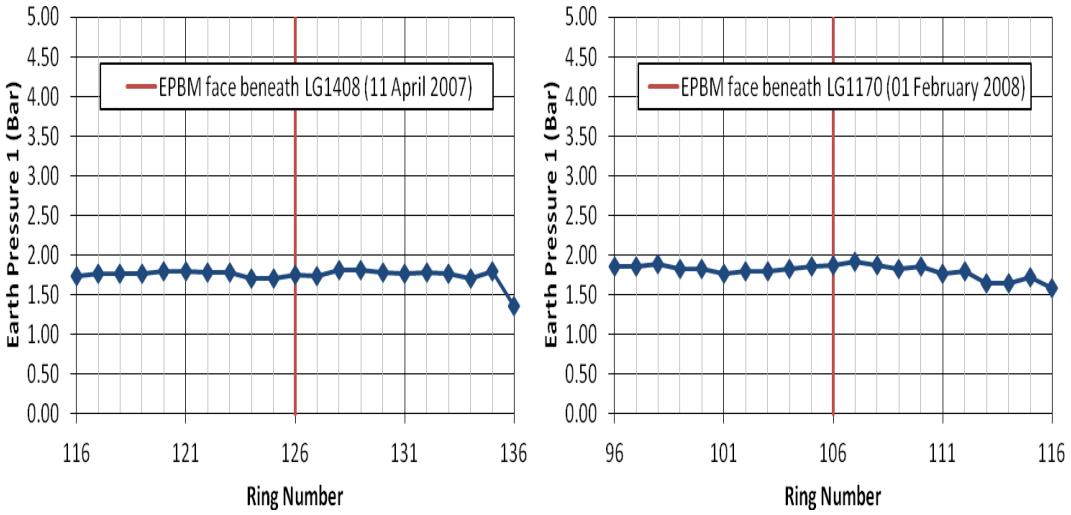

(a) (b)

Figure A.110 TBM earth pressure 1 for (a) first inner bound bored tunnelling; and (b) second outer bound bored tunnelling (Instrumentation Array D49)

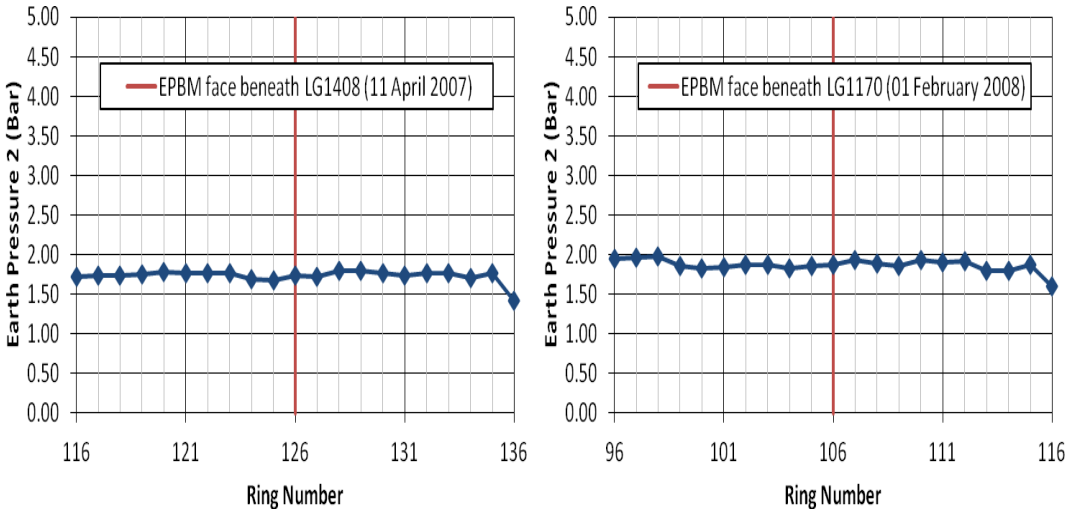

(a) (b)

Figure A.111 TBM earth pressure 2 for (a) first inner bound bored tunnelling; and (b) second outer bound bored tunnelling (Instrumentation Array D49)

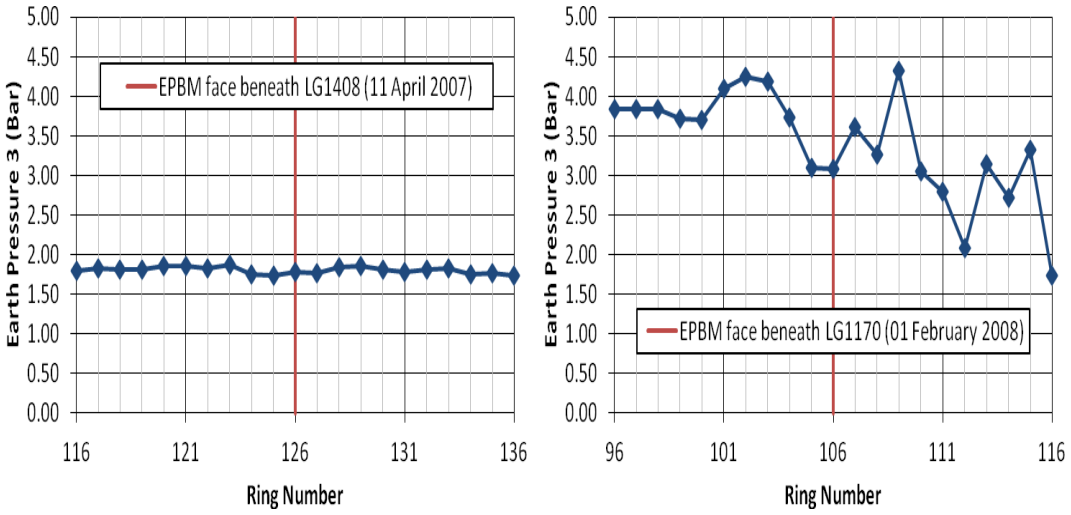

(a) (b)

Figure A.112 TBM earth pressure 3 for (a) first inner bound bored tunnelling; and (b) second outer bound bored tunnelling (Instrumentation Array D49)

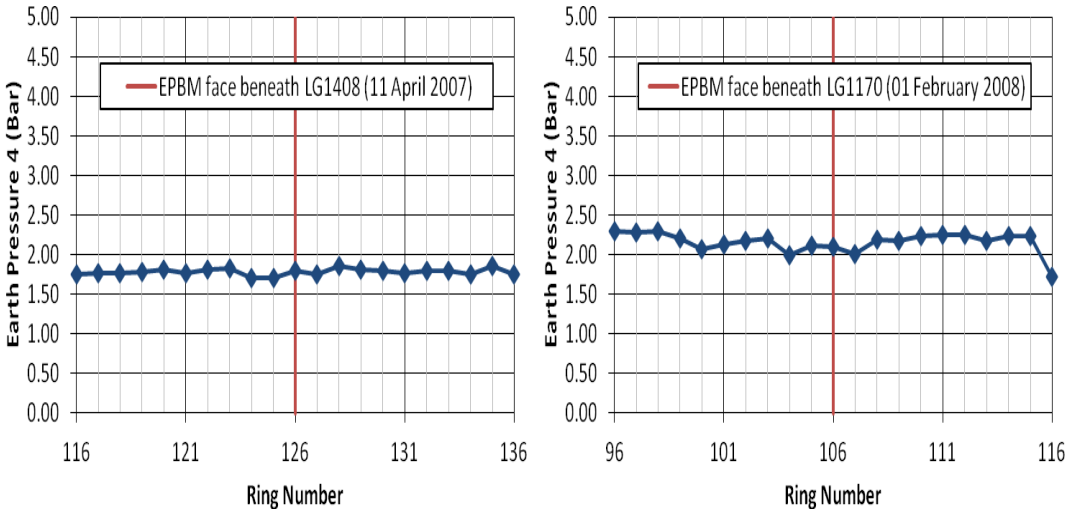

(a) (b)

Figure A.113 TBM earth pressure 4 for (a) first inner bound bored tunnelling; and (b) second outer bound bored tunnelling (Instrumentation Array D49)

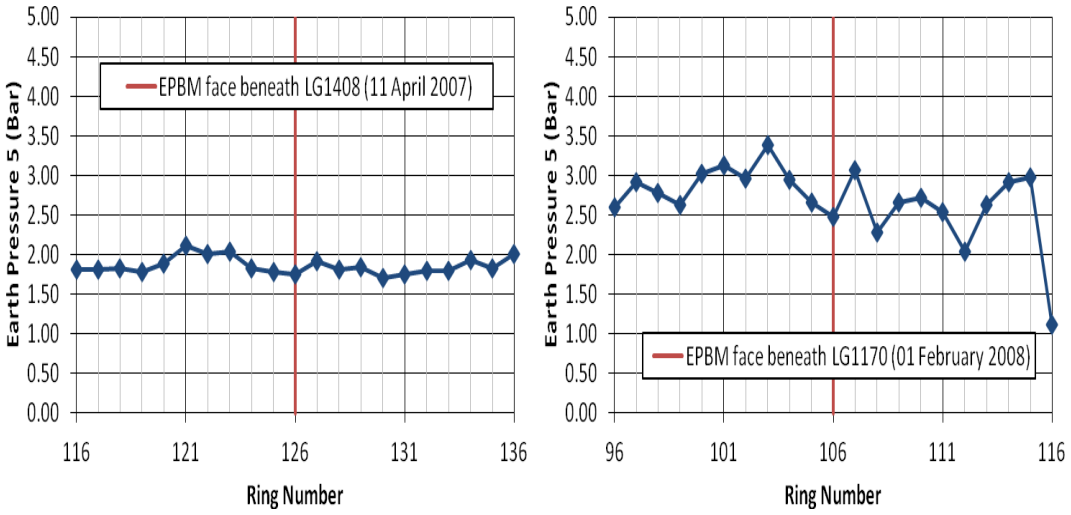

(a) (b)

Figure A.114 TBM earth pressure 5 for (a) first inner bound bored tunnelling; and (b) second outer bound bored tunnelling (Instrumentation Array D49)

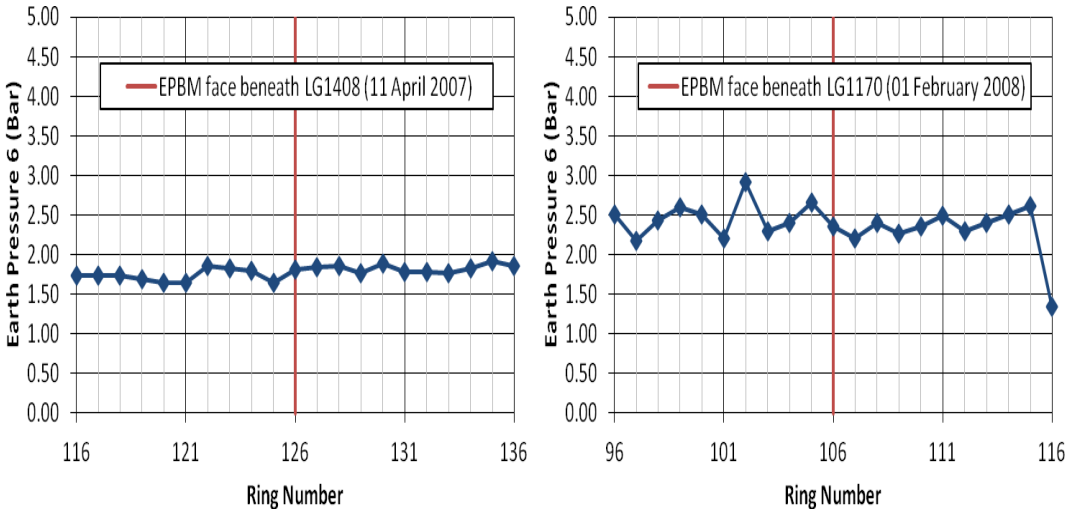

(a) (b)

Figure A.115 TBM earth pressure 6 for (a) first inner bound bored tunnelling; and (b) second outer bound bored tunnelling (Instrumentation Array D49)

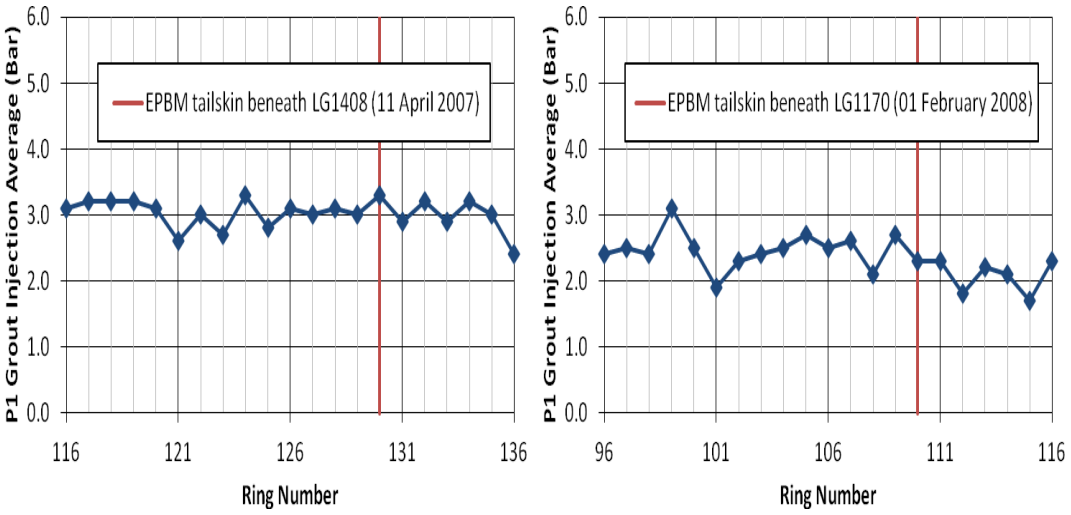

(a) (b)

Figure A.116 P1 grout injection average for (a) first inner bound bored tunnelling; and (b) second outer bound bored tunnelling (Instrumentation Array D49)

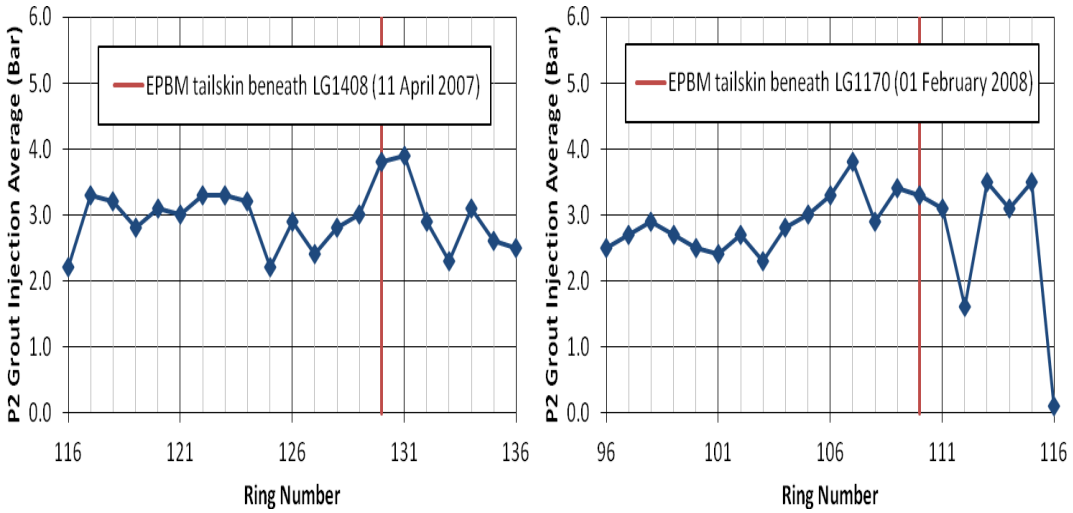

(a) (b)

Figure A.117 P2 grout injection average for (a) first inner bound bored tunnelling; and (b) second outer bound bored tunnelling (Instrumentation Array D49)

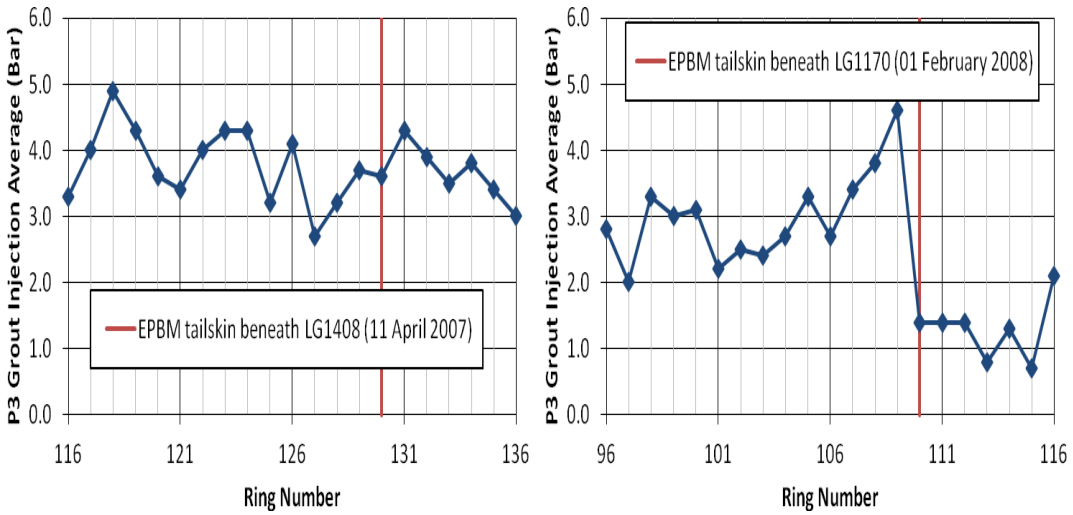

(a) (b)

Figure A.118 P3 grout injection average for (a) first inner bound bored tunnelling; and (b) second outer bound bored tunnelling (Instrumentation Array D49)

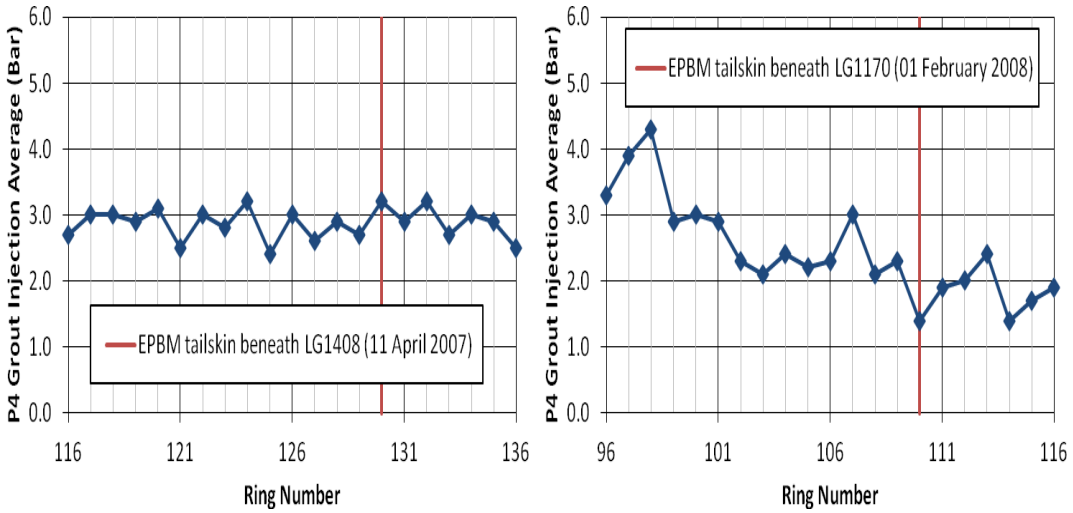

(a) (b)

Figure A.119 P4 grout injection average for (a) first inner bound bored tunnelling; and (b) second outer bound bored tunnelling (Instrumentation Array D49)

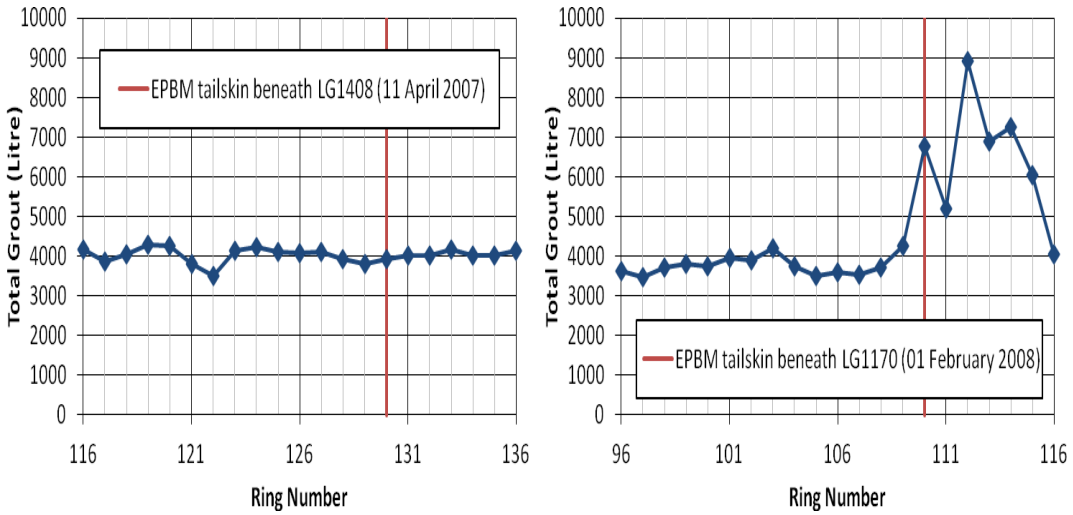

(a) (b)

Figure A.120 Total grout for (a) first inner bound bored tunnelling; and (b) second outer bound bored tunnelling (Instrumentation Array D49)

Instrumentation Array D47

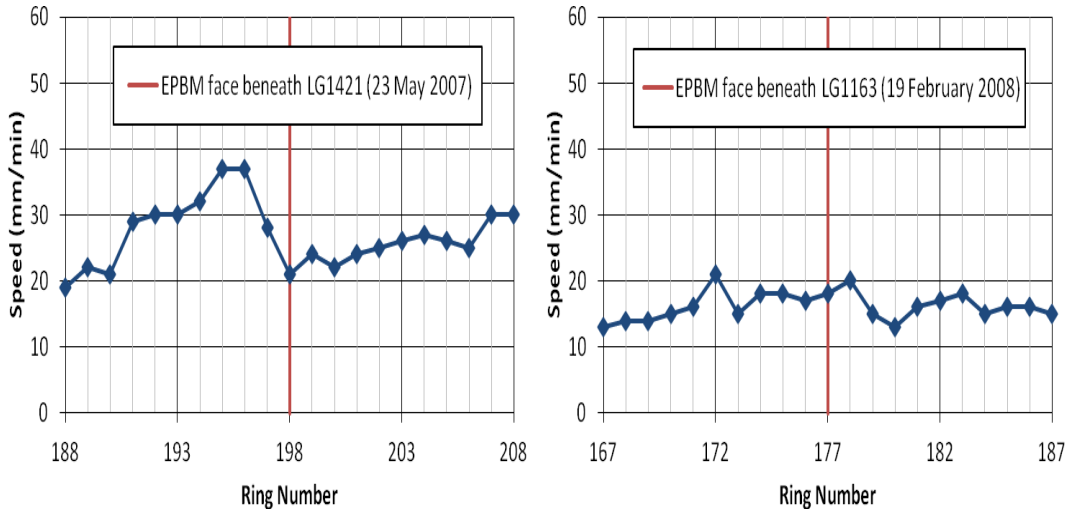

(a) (b)

Figure A.121 TBM speed for (a) first inner bound bored tunnelling; and (b) second outer bound bored tunnelling (Instrumentation Array D47)

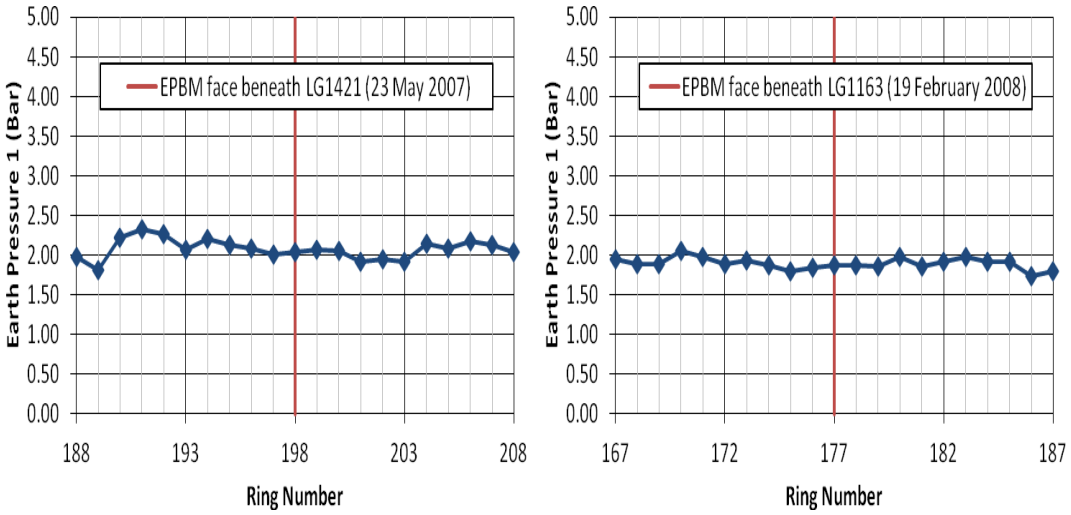

(a) (b)

Figure A.122 TBM earth pressure 1 for (a) first inner bound bored tunnelling; and (b) second outer bound bored tunnelling (Instrumentation Array D47)

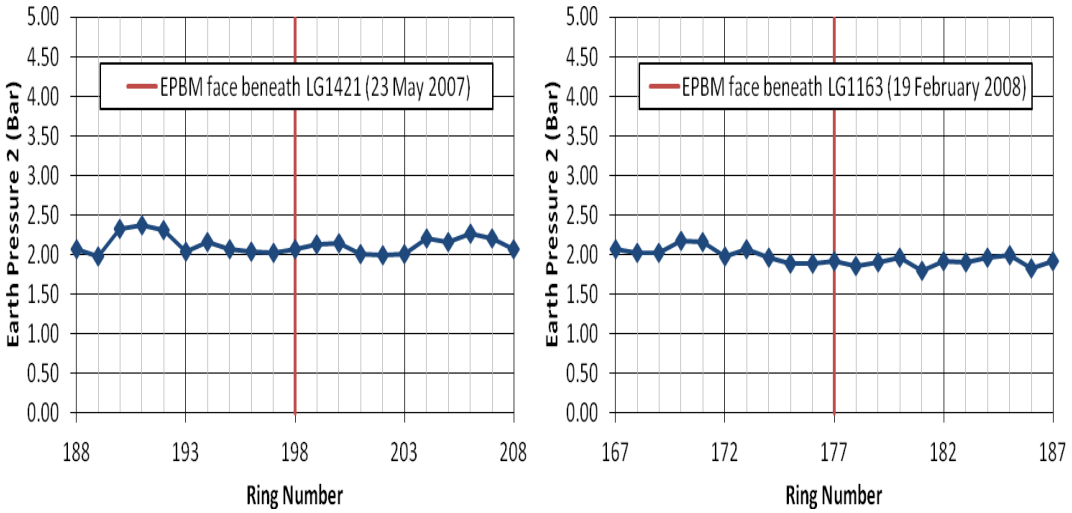

(a) (b)

Figure A.123 TBM earth pressure 2 for (a) first inner bound bored tunnelling; and (b) second outer bound bored tunnelling (Instrumentation Array D47)

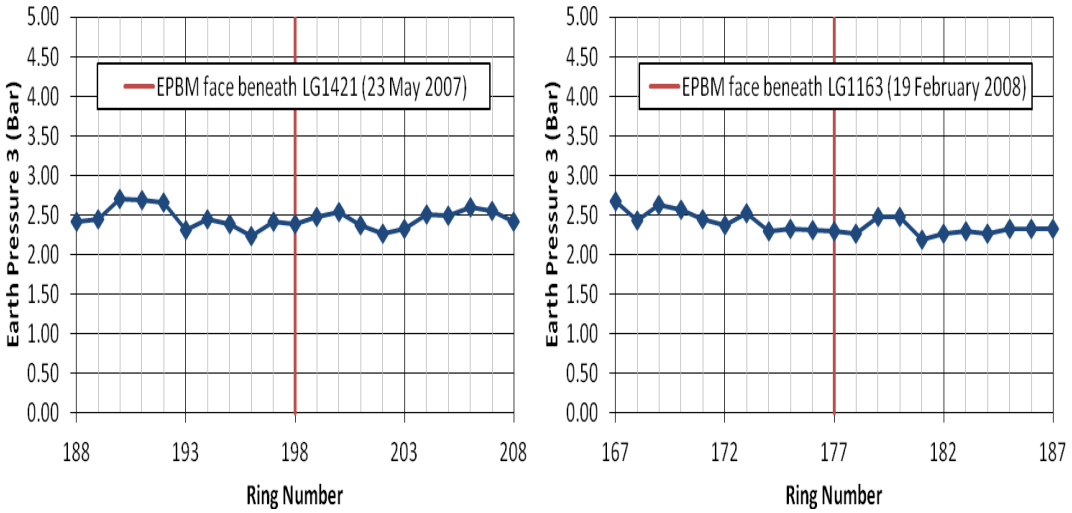

(a) (b)

Figure A.124 TBM earth pressure 3 for (a) first inner bound bored tunnelling; and (b) second outer bound bored tunnelling (Instrumentation Array D47)

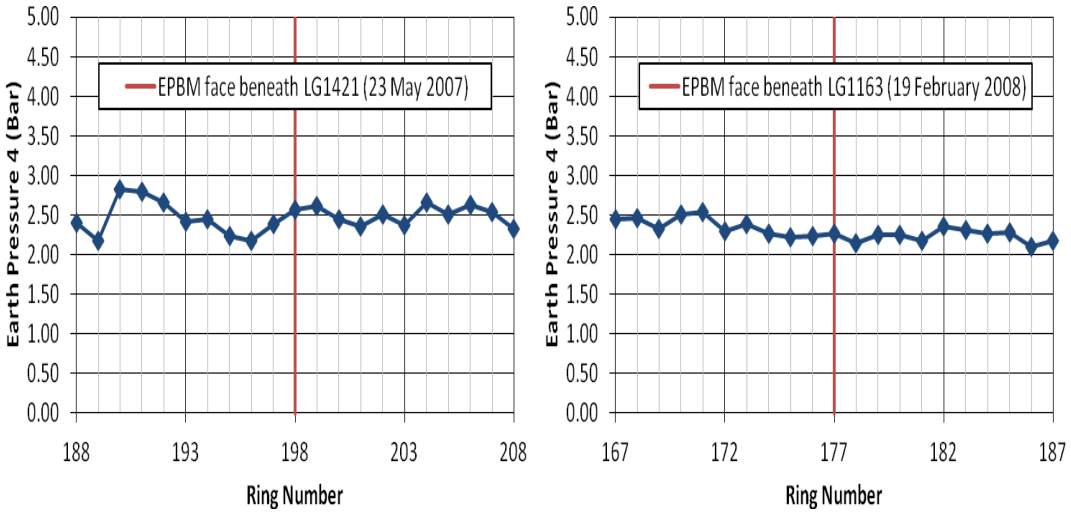

(a) (b)

Figure A.125 TBM earth pressure 4 for (a) first inner bound bored tunnelling; and (b) second outer bound bored tunnelling (Instrumentation Array D47)

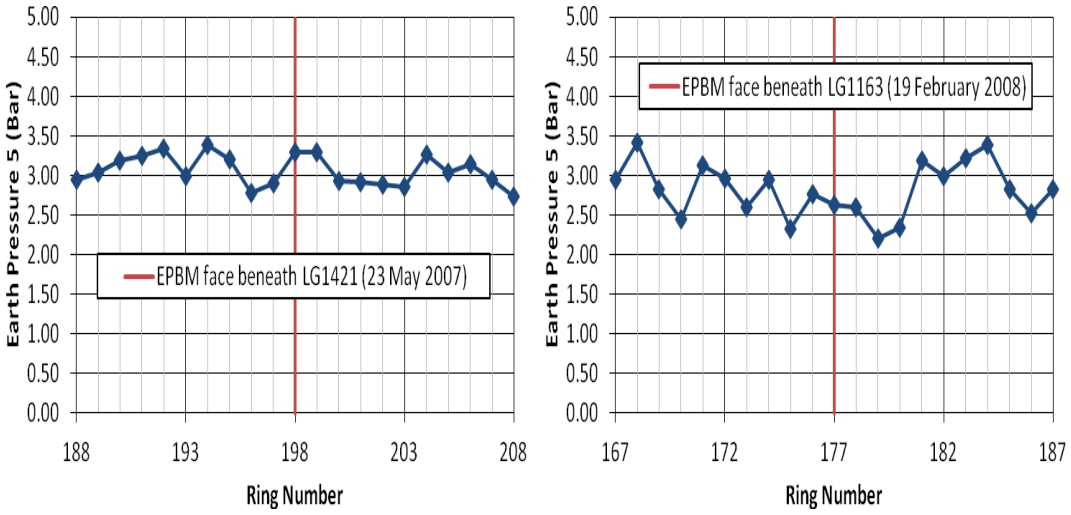

(a) (b)

Figure A.126 TBM earth pressure 5 for (a) first inner bound bored tunnelling; and (b) second outer bound bored tunnelling (Instrumentation Array D47)

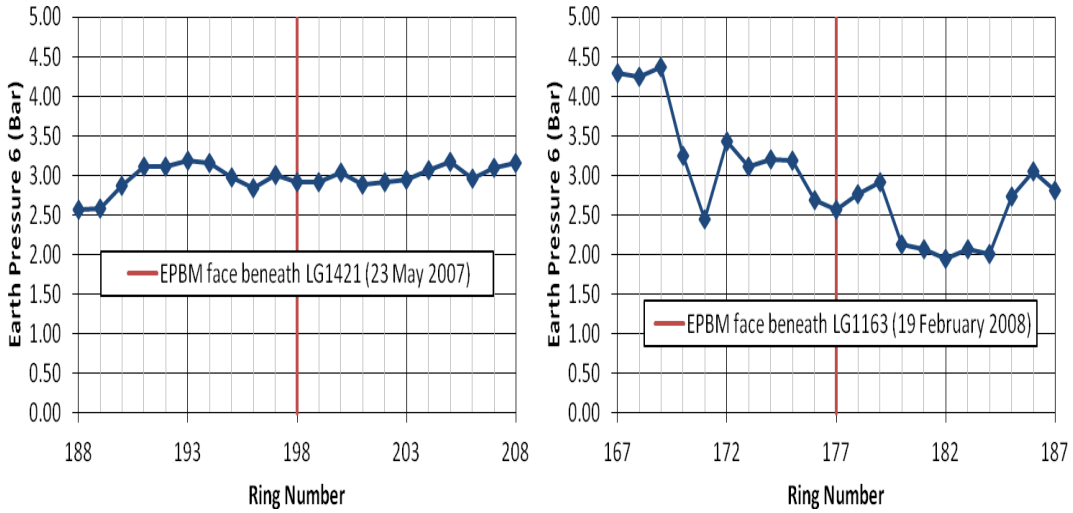

(a) (b)

Figure A.127 TBM earth pressure 6 for (a) first inner bound bored tunnelling; and (b) second outer bound bored tunnelling (Instrumentation Array D47)

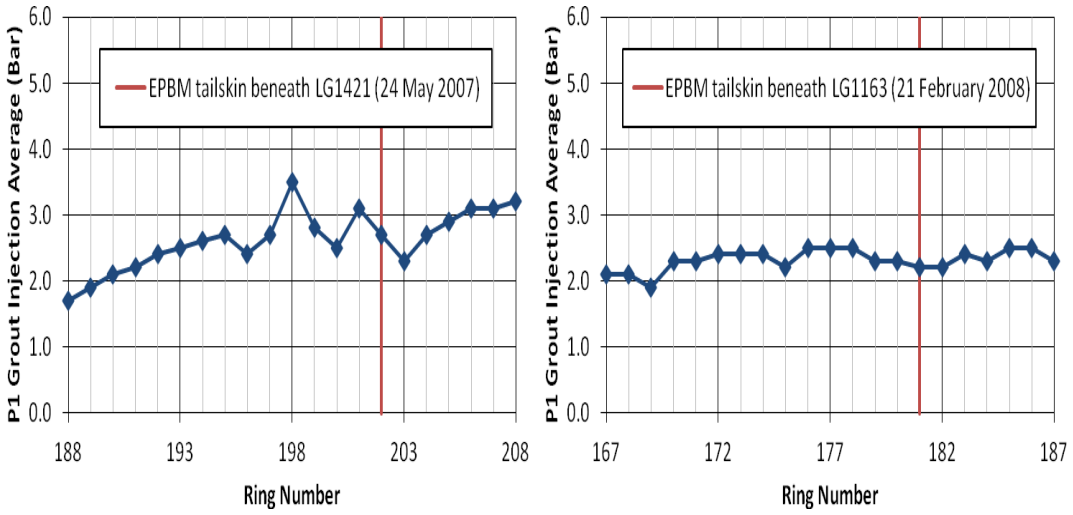

(a) (b)

Figure A.128 P1 grout injection average for (a) first inner bound bored tunnelling; and (b) second outer bound bored tunnelling (Instrumentation Array D47)

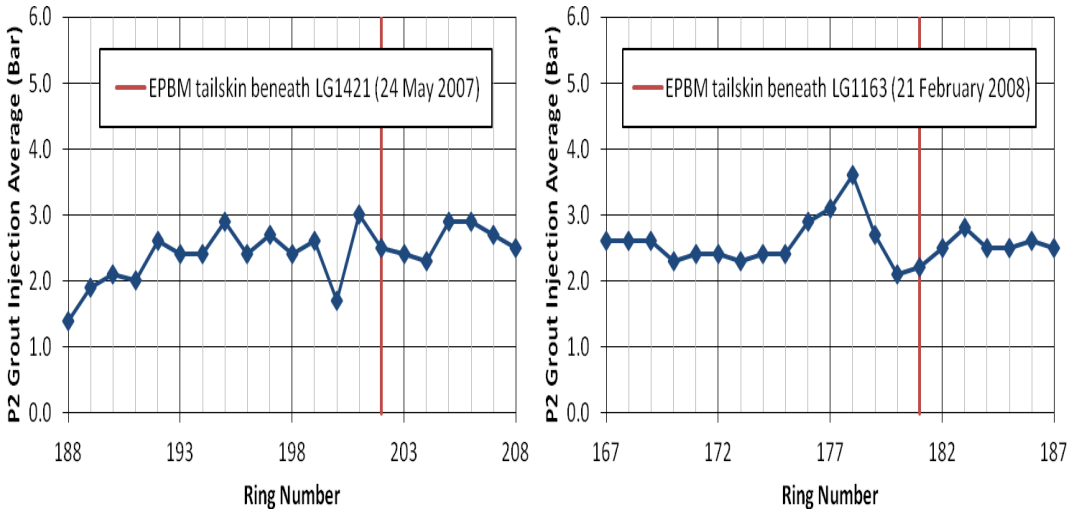

(a) (b)

Figure A.129 P2 grout injection average for (a) first inner bound bored tunnelling; and (b) second outer bound bored tunnelling (Instrumentation Array D47)

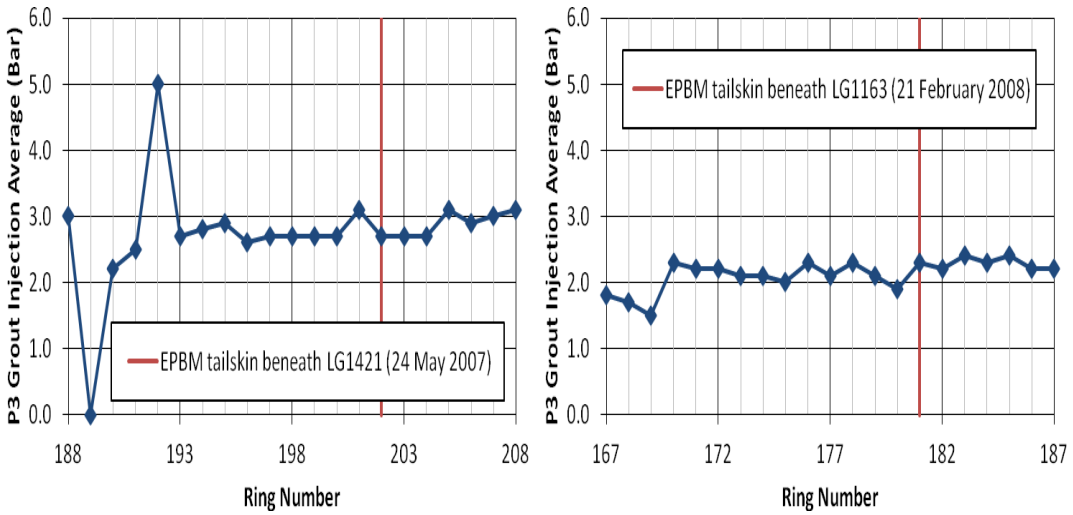

(a) (b)

Figure A.130 P3 grout injection average for (a) first inner bound bored tunnelling; and (b) second outer bound bored tunnelling (Instrumentation Array D47)

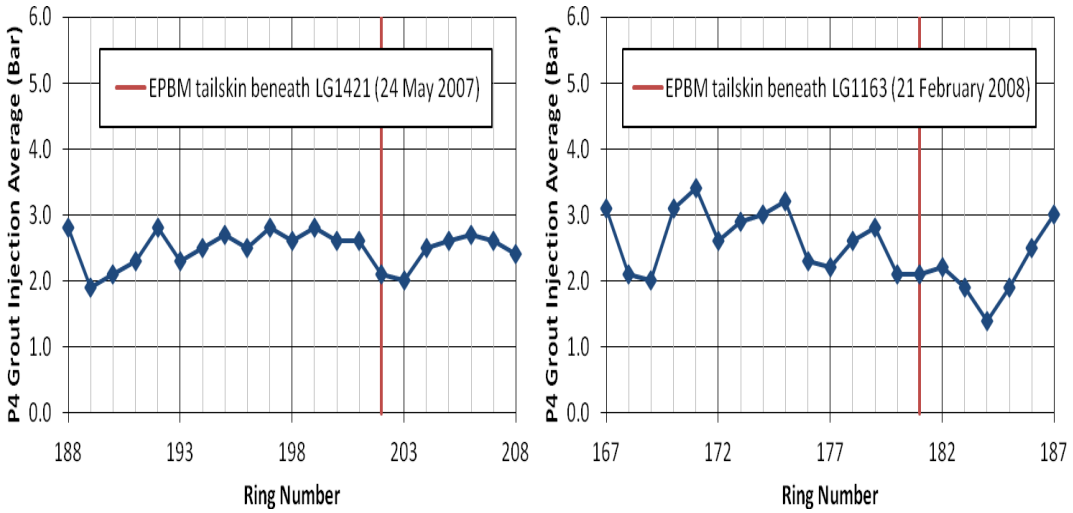

(a) (b)

Figure A.131 P4 grout injection average for (a) first inner bound bored tunnelling; and (b) second outer bound bored tunnelling (Instrumentation Array D47)

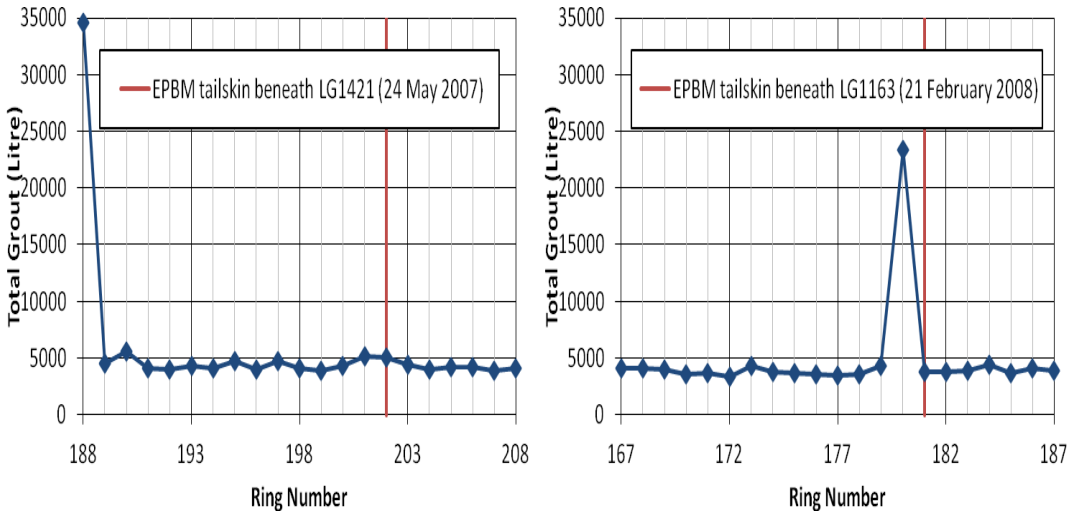

(a) (b)

Figure A.132 Total grout for (a) first inner bound bored tunnelling; and (b) second outer bound bored tunnelling (Instrumentation Array D47)

Instrumentation Array E10

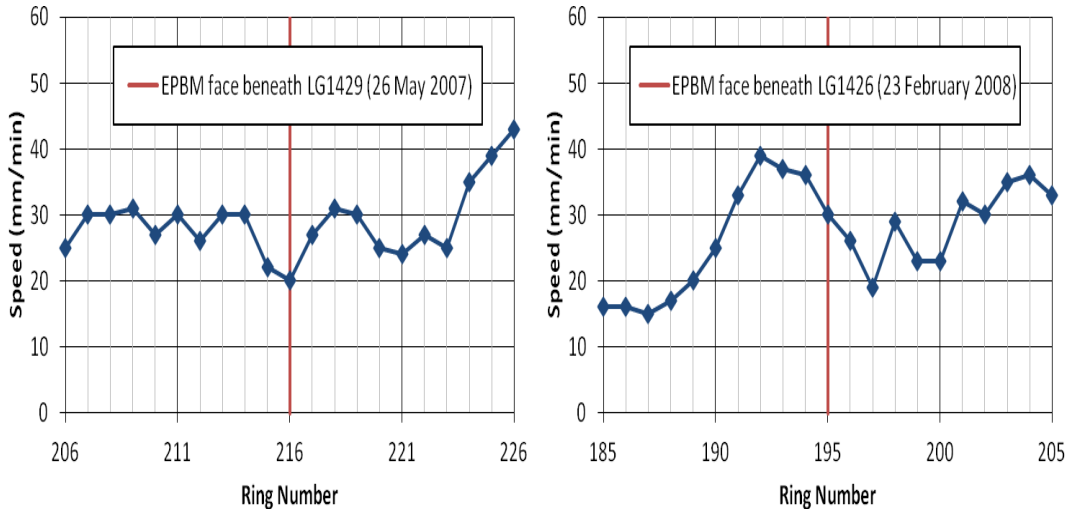

(a) (b)

Figure A.133 TBM speed for (a) first inner bound bored tunnelling; and (b) second outer bound bored tunnelling (Instrumentation Array E10)

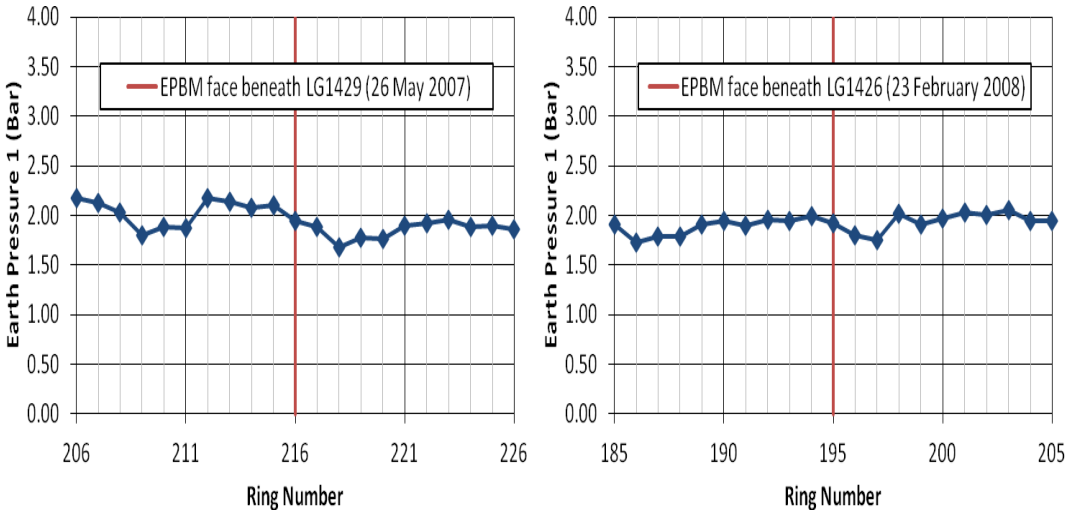

(a) (b)

Figure A.134 TBM earth pressure 1 for (a) first inner bound bored tunnelling; and (b) second outer bound bored tunnelling (Instrumentation Array E10)

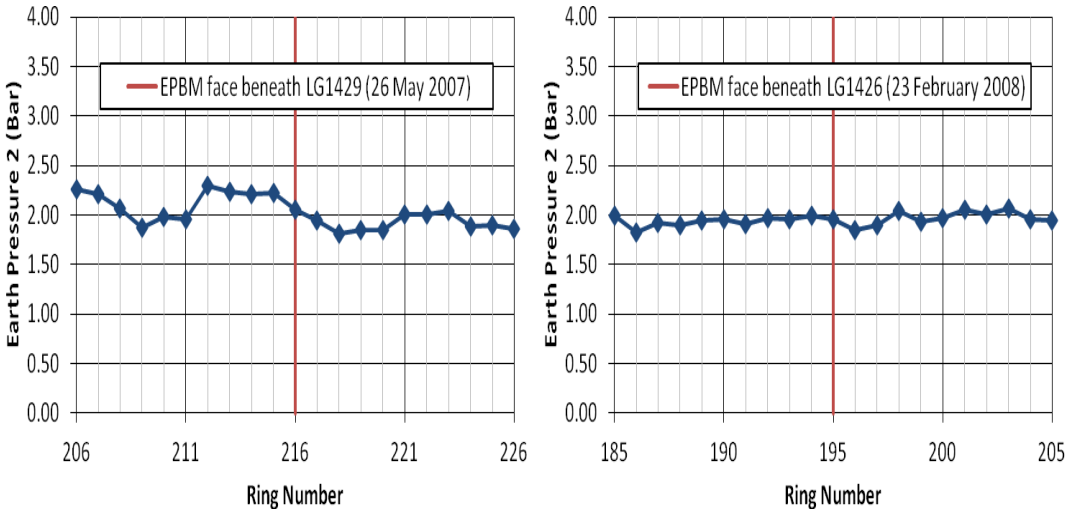

(a) (b)

Figure A.135 TBM earth pressure 2 for (a) first inner bound bored tunnelling; and (b) second outer bound bored tunnelling (Instrumentation Array E10)

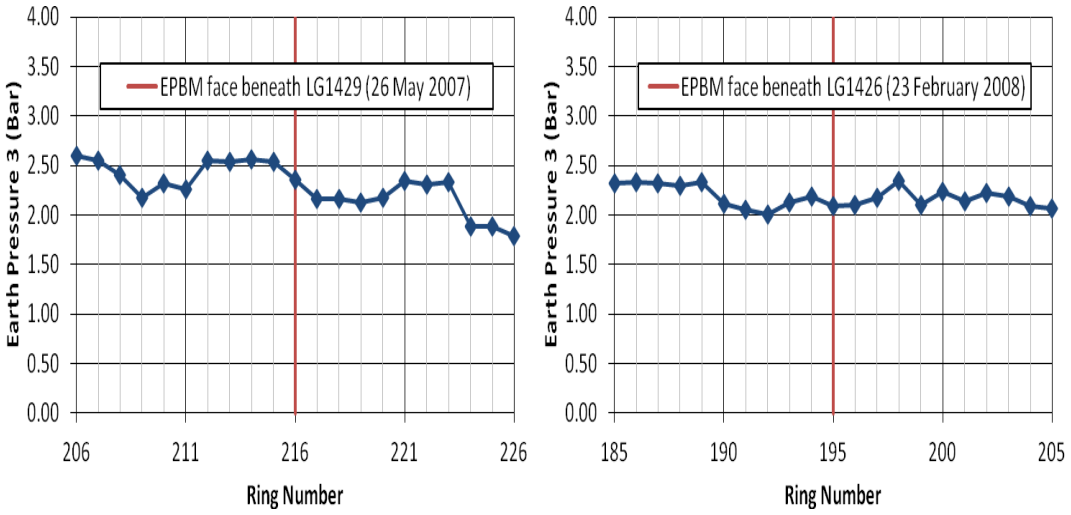

(a) (b)

Figure A.136 TBM earth pressure 3 for (a) first inner bound bored tunnelling; and (b) second outer bound bored tunnelling (Instrumentation Array E10)

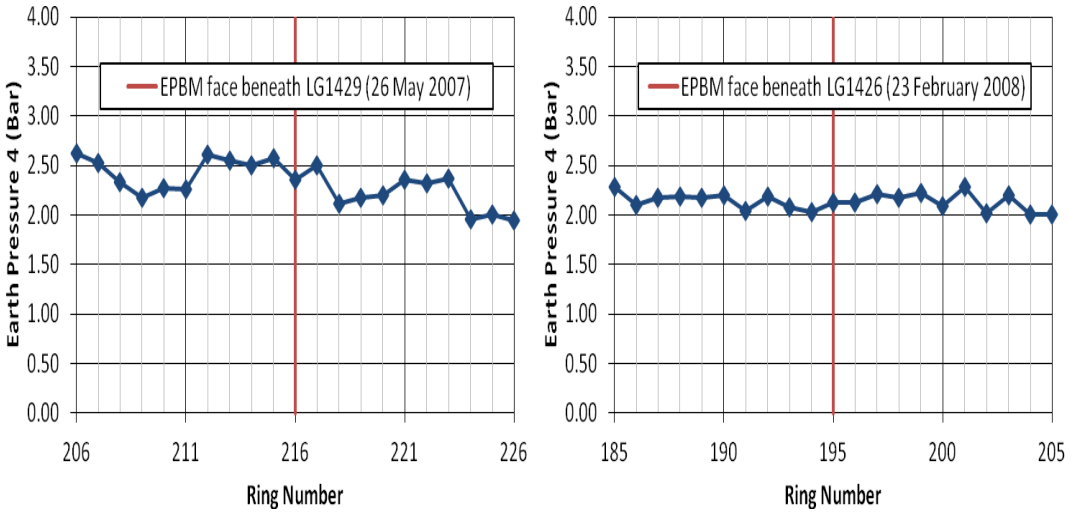

(a) (b)

Figure A.137 TBM earth pressure 4 for (a) first inner bound bored tunnelling; and (b) second outer bound bored tunnelling (Instrumentation Array E10)

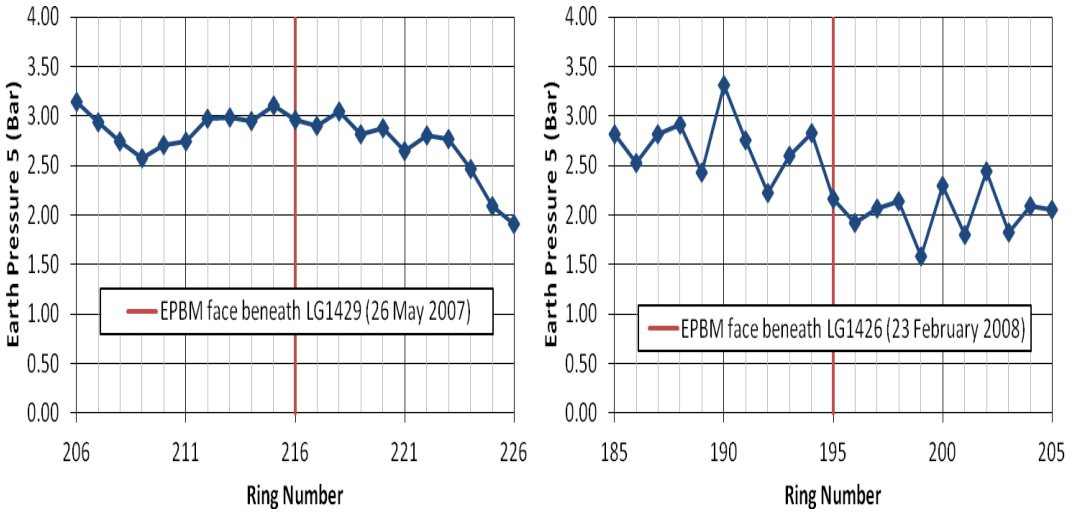

(a) (b)

Figure A.138 TBM earth pressure 5 for (a) first inner bound bored tunnelling; and (b) second outer bound bored tunnelling (Instrumentation Array E10)

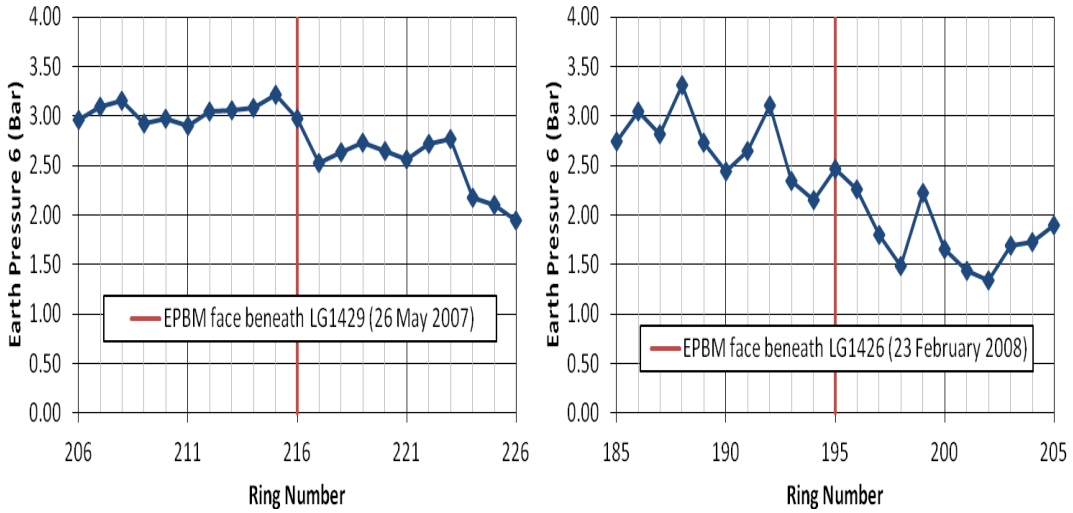

(a) (b)

Figure A.139 TBM earth pressure 6 for (a) first inner bound bored tunnelling; and (b) second outer bound bored tunnelling (Instrumentation Array E10)

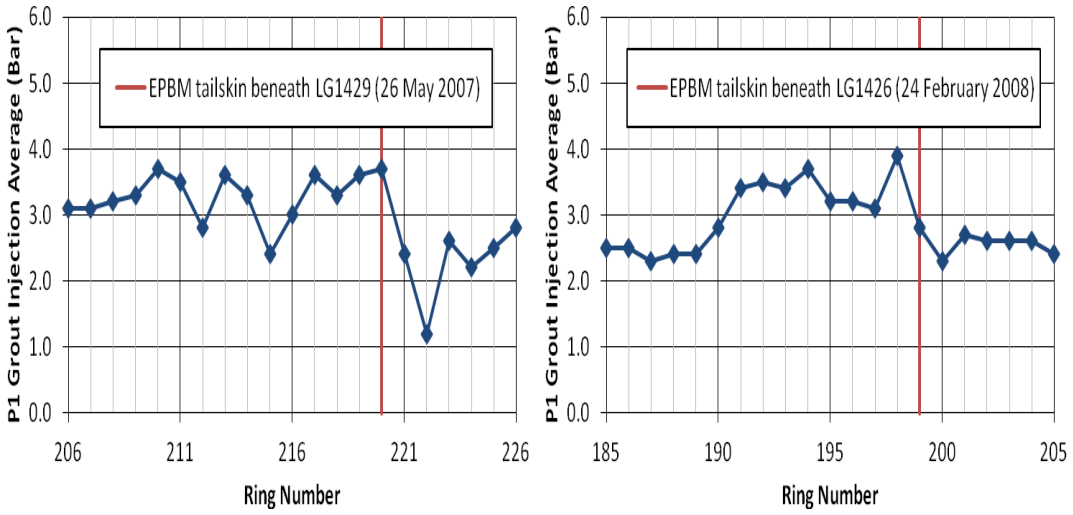

(a) (b)

Figure A.140 P1 grout injection average for (a) first inner bound bored tunnelling; and (b) second outer bound bored tunnelling (Instrumentation Array E10)

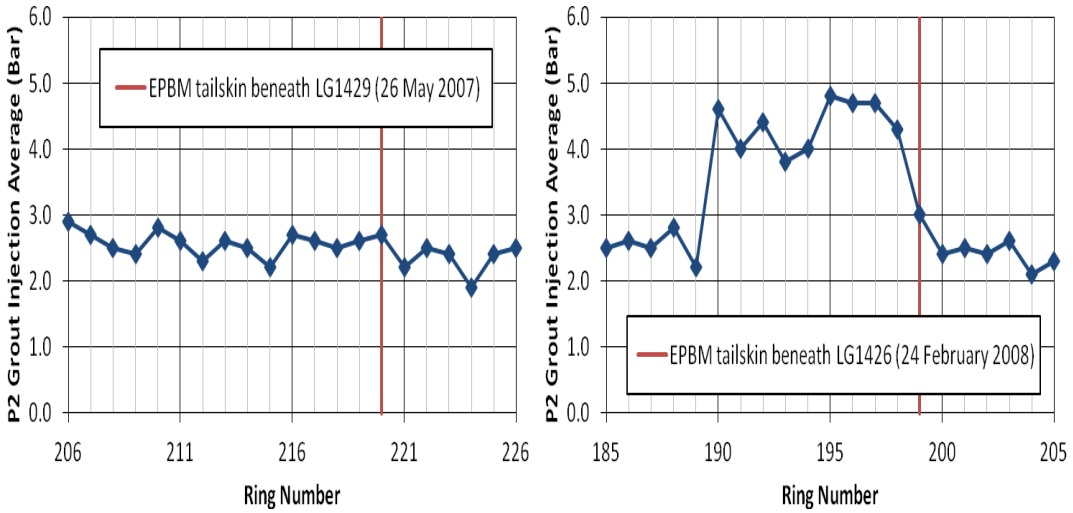

(a) (b)

Figure A.141 P2 grout injection average for (a) first inner bound bored tunnelling; and (b) second outer bound bored tunnelling (Instrumentation Array E10)

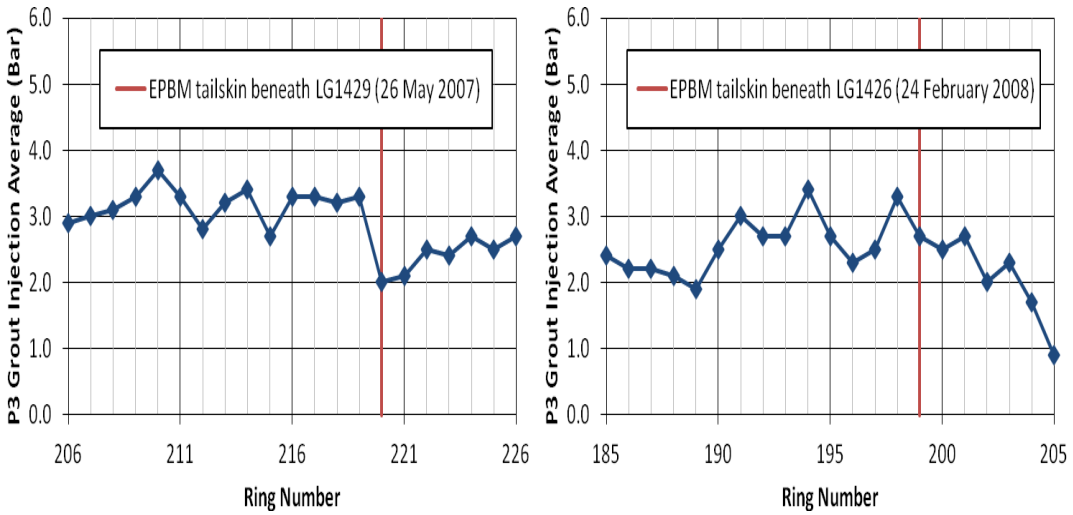

(a) (b)

Figure A.142 P3 grout injection average for (a) first inner bound bored tunnelling; and (b) second outer bound bored tunnelling (Instrumentation Array E10)

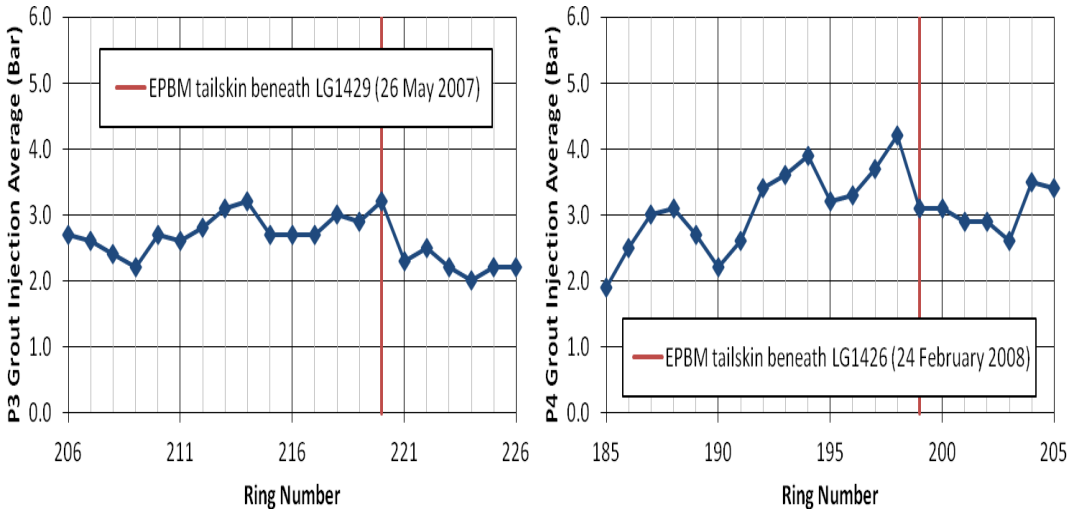

(a) (b)

Figure A.143 P4 grout injection average for (a) first inner bound bored tunnelling; and (b) second outer bound bored tunnelling (Instrumentation Array E10)

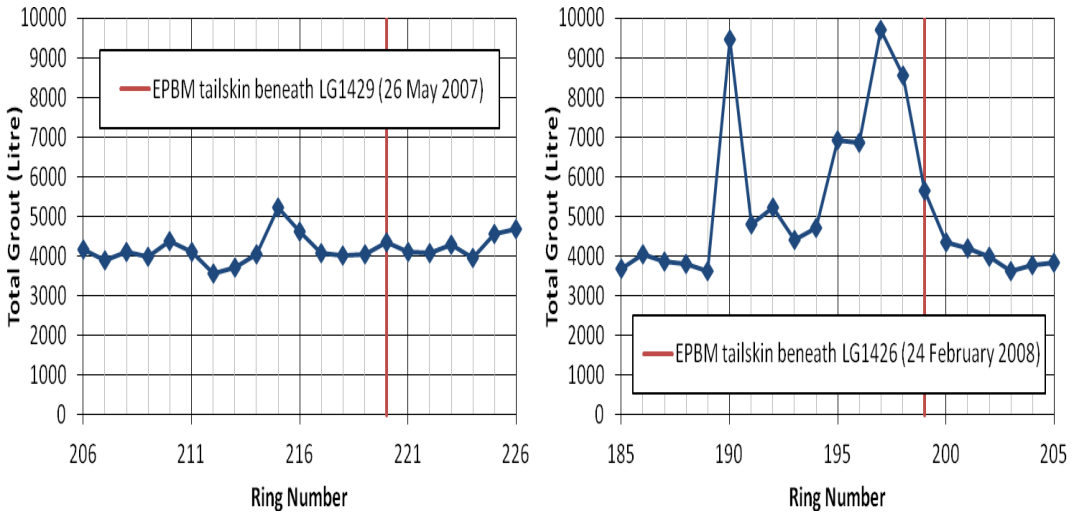

(a) (b)

Figure A.144 Total grout for (a) first inner bound bored tunnelling; and (b) second outer bound bored tunnelling (Instrumentation Array E10)

Instrumentation Array D46

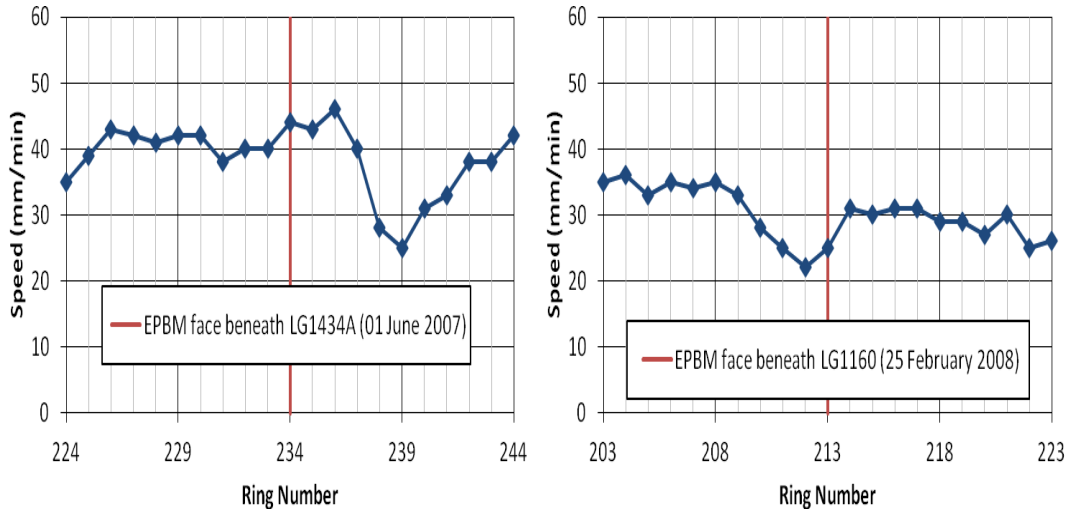

(a) (b)

Figure A.145 TBM speed for (a) first inner bound bored tunnelling; and (b) second outer bound bored tunnelling (Instrumentation Array D46)

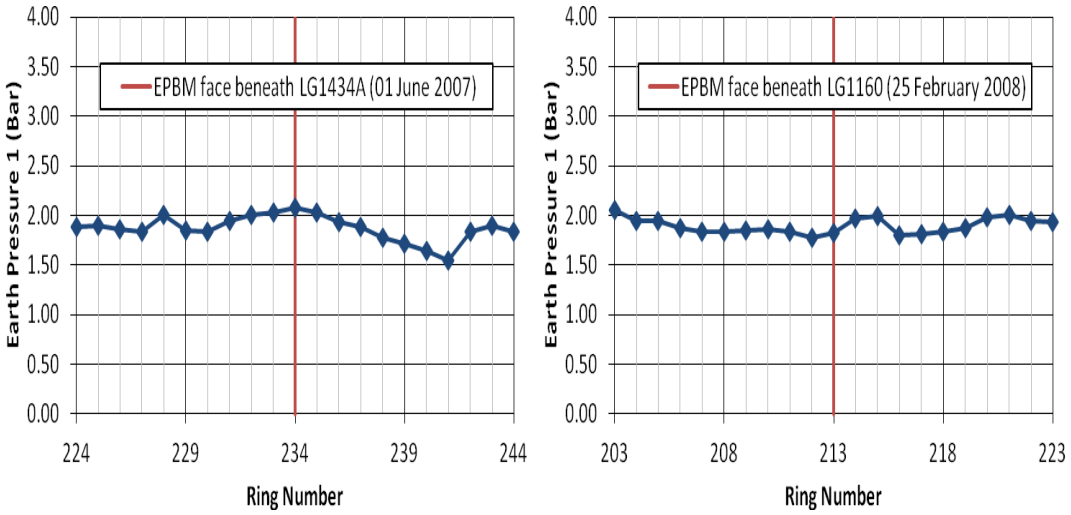

(a) (b)

Figure A.146 TBM earth pressure 1 for (a) first inner bound bored tunnelling; and (b) second outer bound bored tunnelling (Instrumentation Array D46)

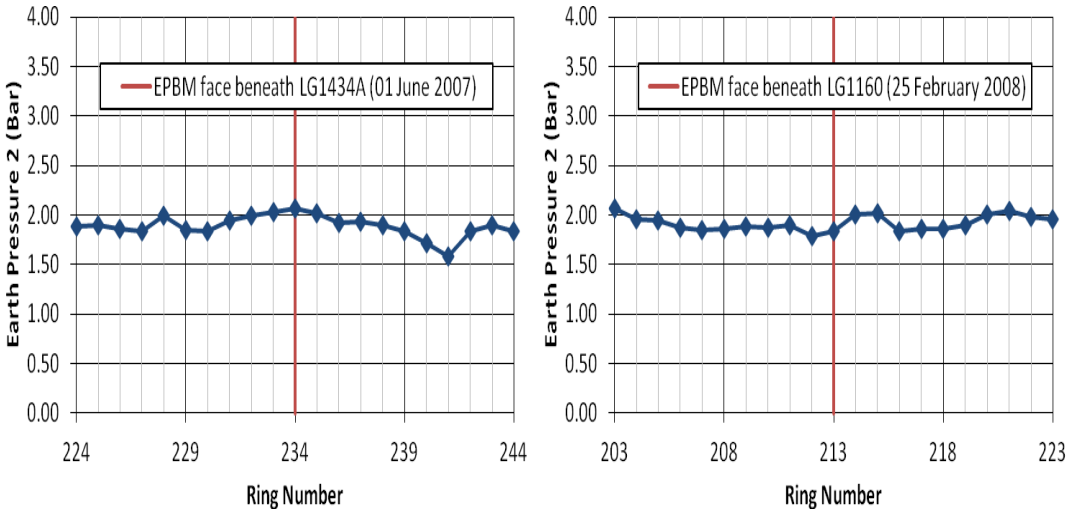

(a) (b)

Figure A.147 TBM earth pressure 2 for (a) first inner bound bored tunnelling; and (b) second outer bound bored tunnelling (Instrumentation Array D46)

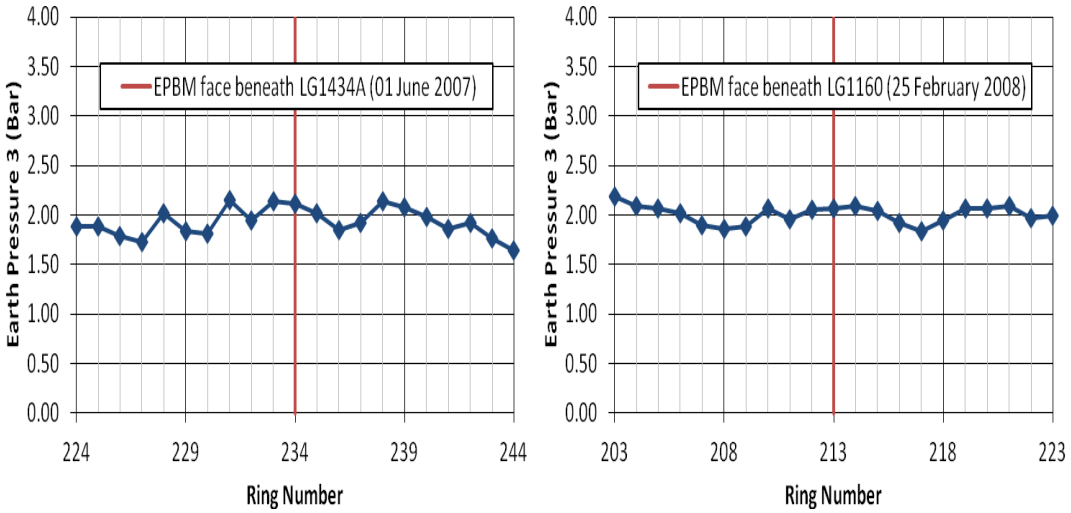

(a) (b)

Figure A.148 TBM earth pressure 3 for (a) first inner bound bored tunnelling; and (b) second outer bound bored tunnelling (Instrumentation Array D46)

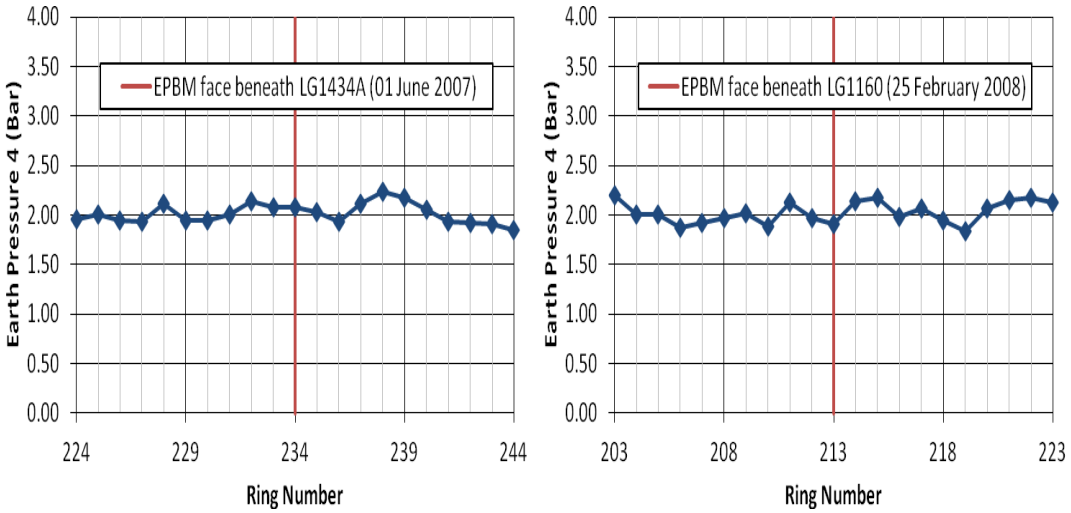

(a) (b)

Figure A.149 TBM earth pressure 4 for (a) first inner bound bored tunnelling; and (b) second outer bound bored tunnelling (Instrumentation Array D46)

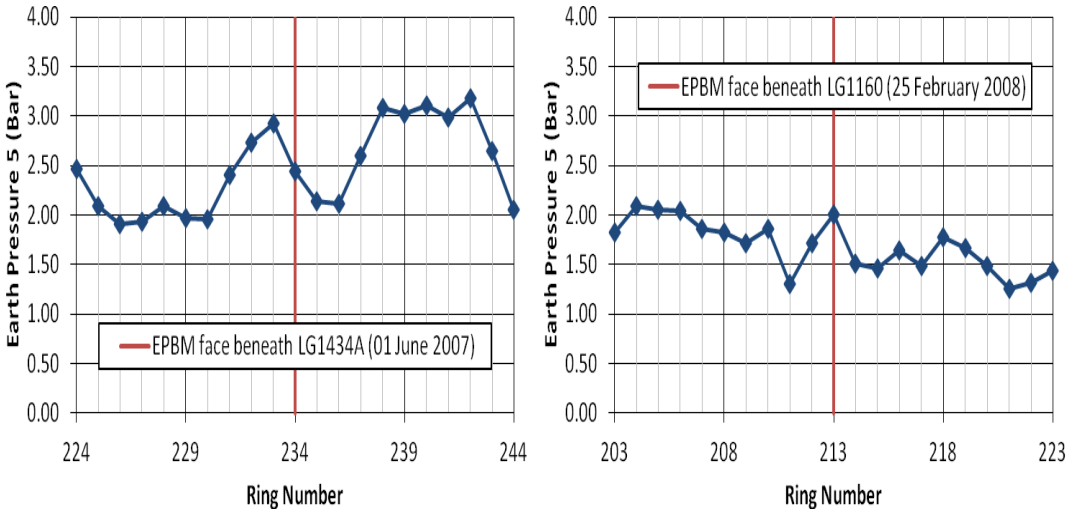

(a) (b)

Figure A.150 TBM earth pressure 5 for (a) first inner bound bored tunnelling; and (b) second outer bound bored tunnelling (Instrumentation Array D46)

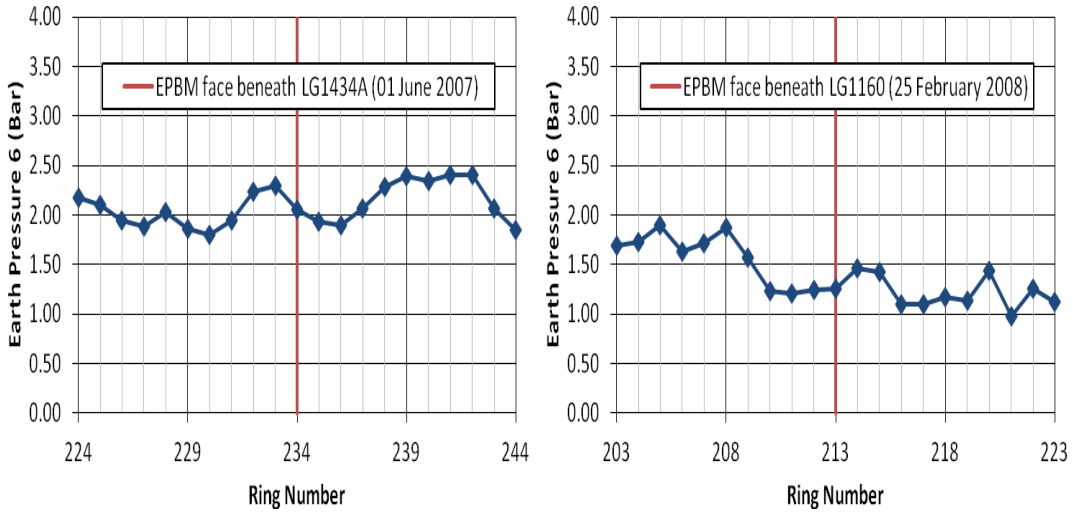

(a) (b)

Figure A.151 TBM earth pressure 6 for (a) first inner bound bored tunnelling; and (b) second outer bound bored tunnelling (Instrumentation Array D46)

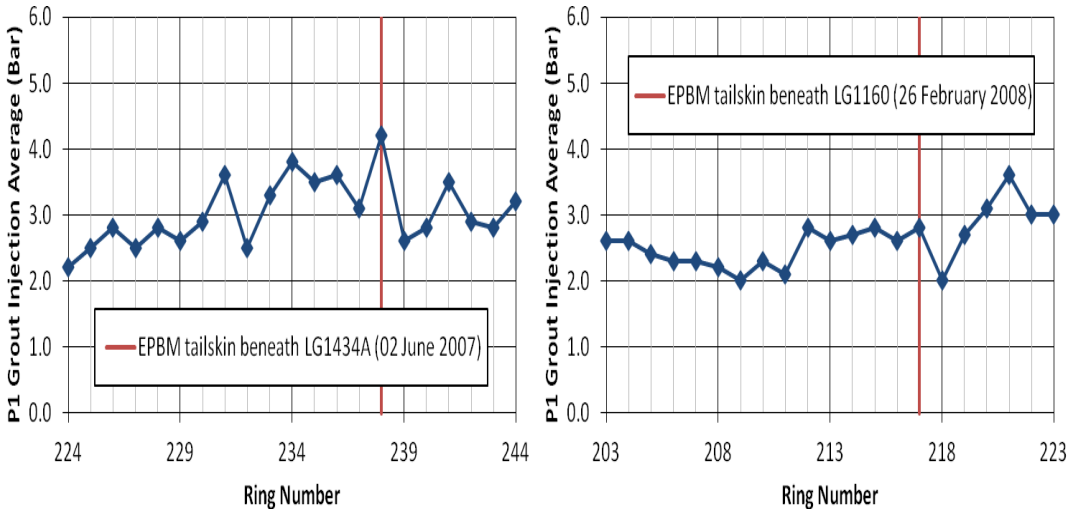

(a) (b)

Figure A.152 P1 grout injection average for (a) first inner bound bored tunnelling; and (b) second outer bound bored tunnelling (Instrumentation Array D46)

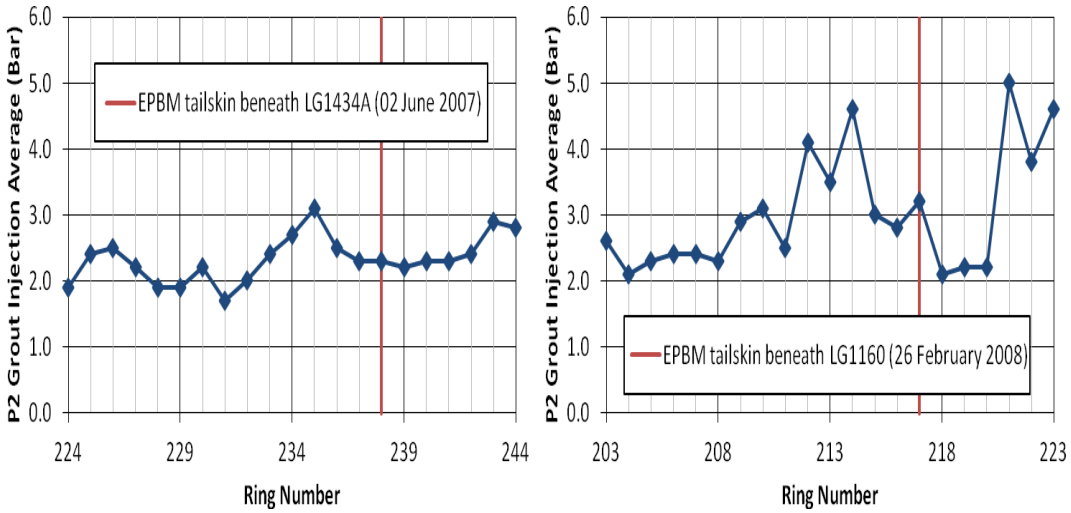

(a) (b)

Figure A.153 P2 grout injection average for (a) first inner bound bored tunnelling; and (b) second outer bound bored tunnelling (Instrumentation Array D46)

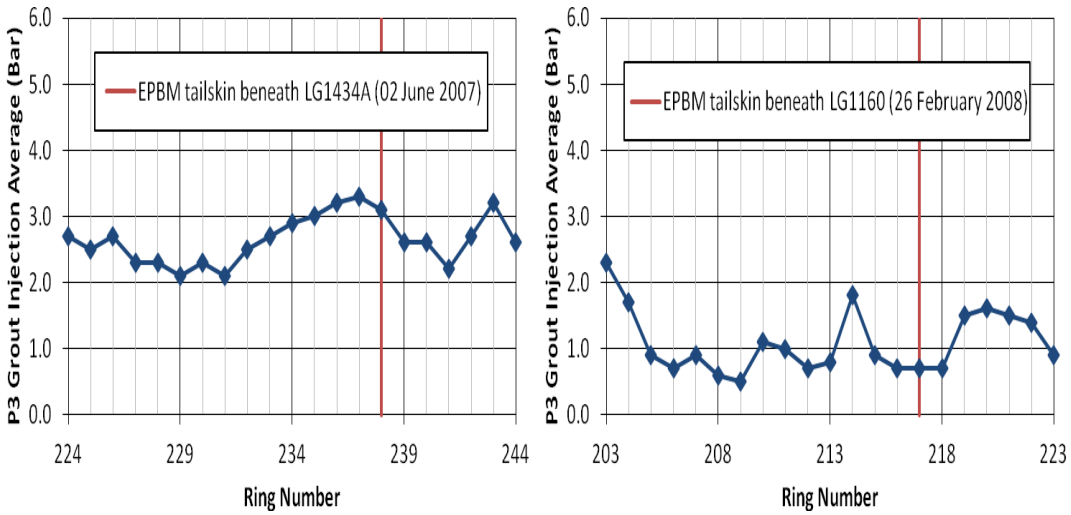

(a) (b)

Figure A.154 P3 grout injection average for (a) first inner bound bored tunnelling; and (b) second outer bound bored tunnelling (Instrumentation Array D46)

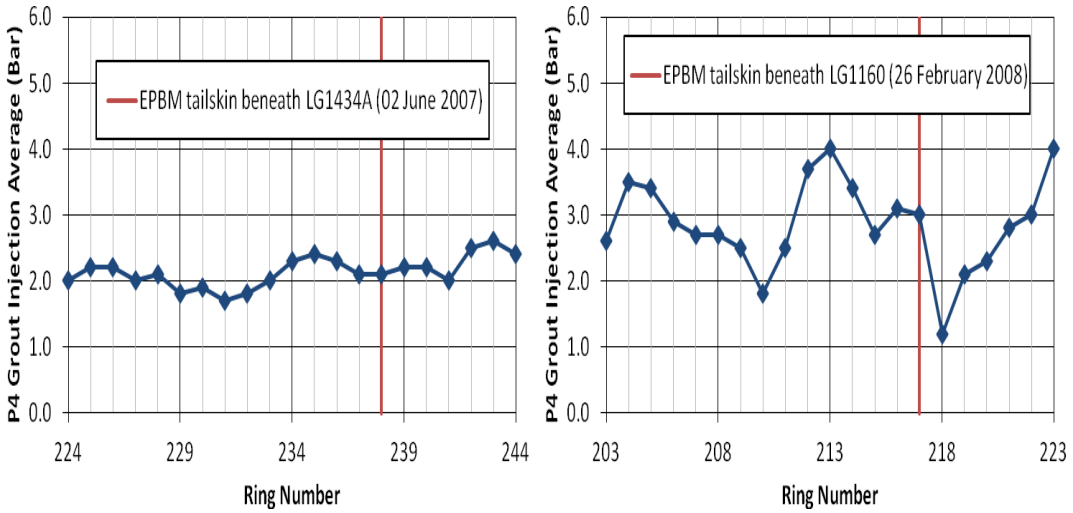

(a) (b)

Figure A.155 P4 grout injection average for (a) first inner bound bored tunnelling; and (b) second outer bound bored tunnelling (Instrumentation Array D46)

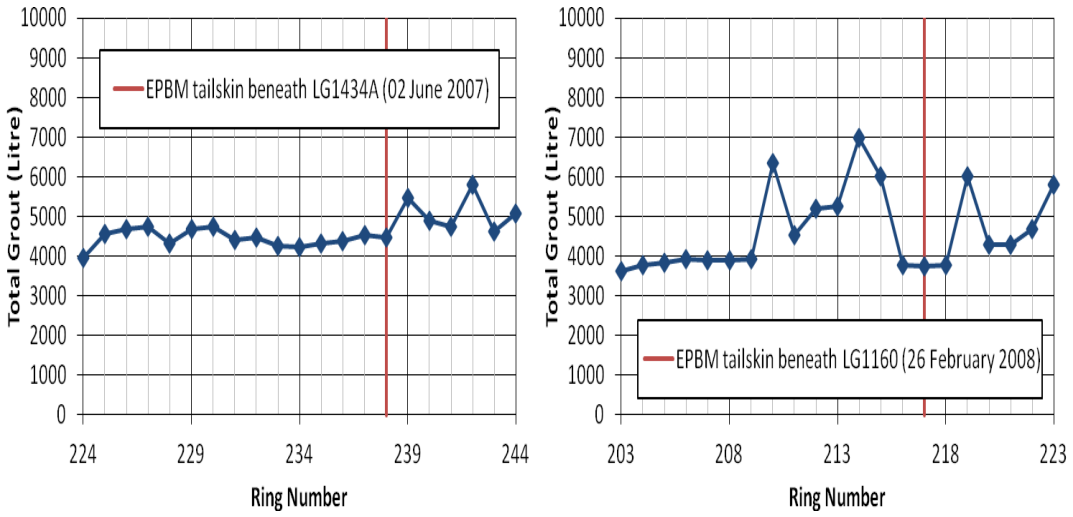

(a) (b)

Figure A.156 Total grout for (a) first inner bound bored tunnelling; and (b) second outer bound bored tunnelling (Instrumentation Array D46)

Appendix B

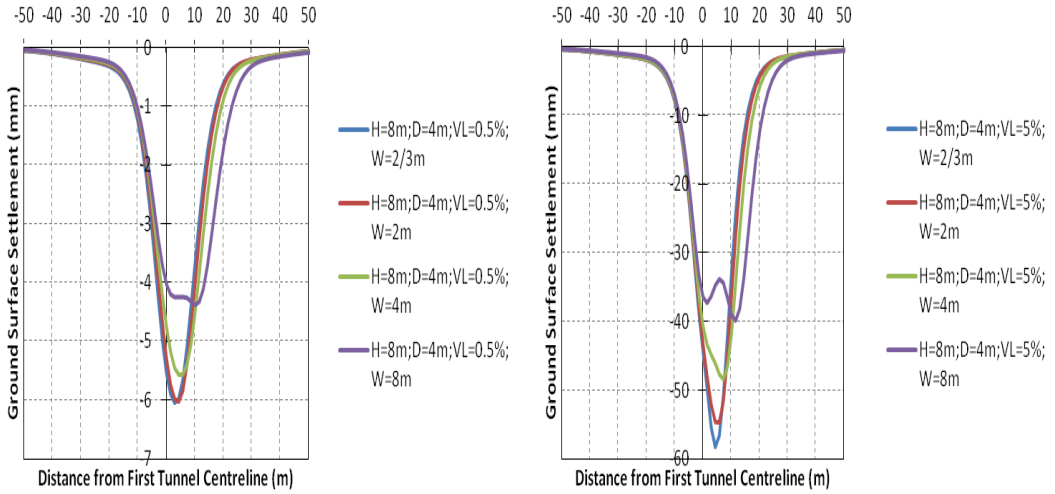

(a) (b)

Figure B.1 Variation of ground surface settlement for closely spaced bored tunnels (D=4 m; H=8 m) with pillar width, for volume loss of (a) 0.5%; and (b) 5% (Jurong Formation)

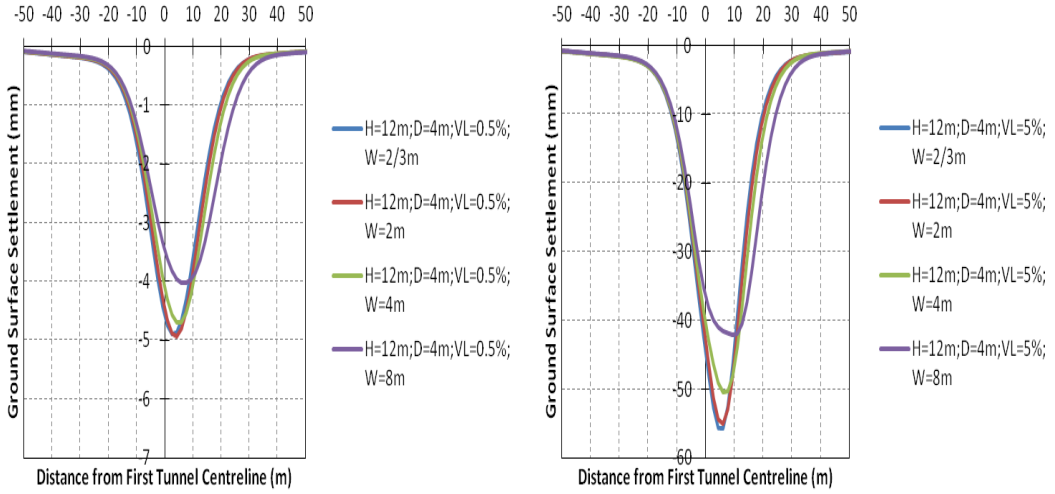

(a) (b)

Figure B.2 Variation of ground surface settlement for closely spaced bored tunnels (D=4 m; H=12 m) with pillar width, for volume loss of (a) 0.5%; and (b) 5% (Jurong Formation)

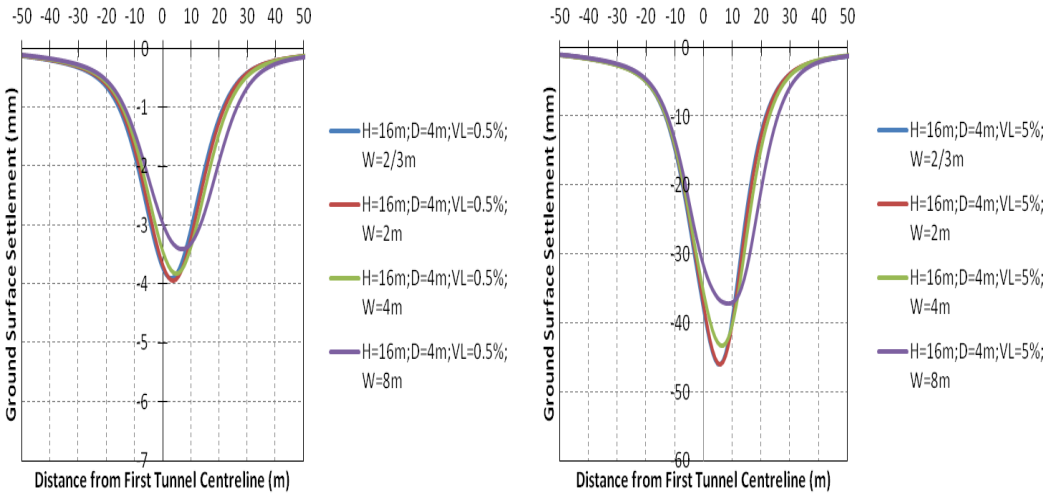

(a) (b)

Figure B.3 Variation of ground surface settlement for closely spaced bored tunnels (D=4 m; H=16 m) with pillar width, for volume loss of (a) 0.5%; and (b) 5% (Jurong Formation)

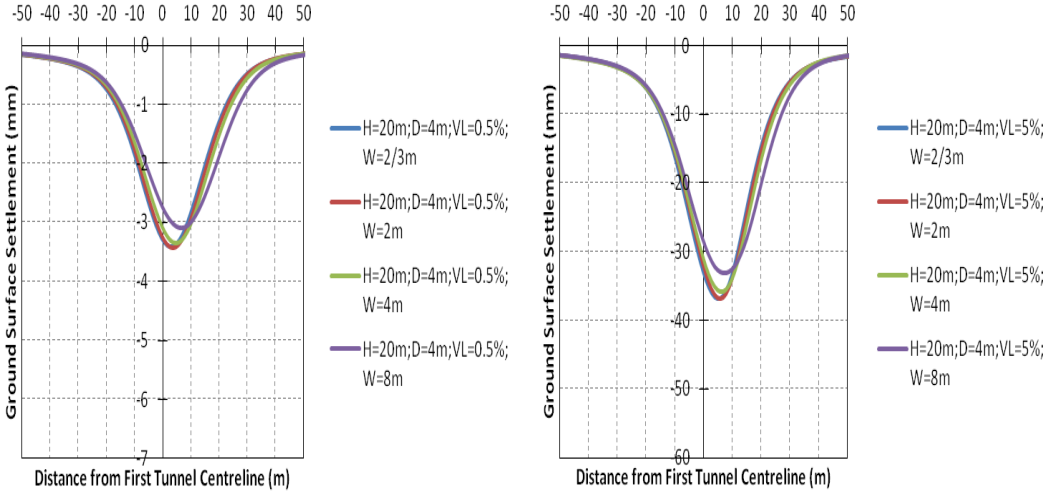

(a) (b)

Figure B.4 Variation of ground surface settlement for closely spaced bored tunnels (D=4 m; H=20 m) with pillar width, for volume loss of (a) 0.5%; and (b) 5% (Jurong Formation)

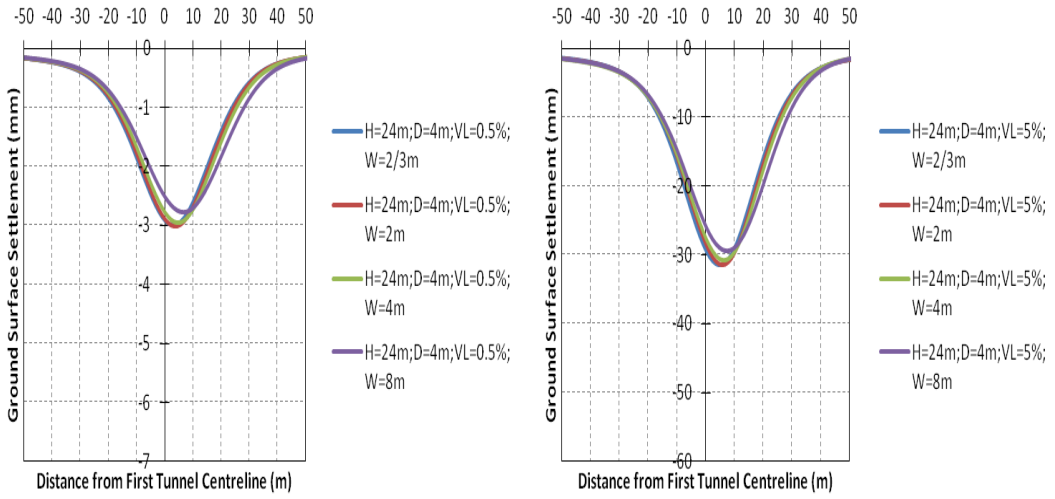

(a) (b)

Figure B.5 Variation of ground surface settlement for closely spaced bored tunnels (D=4 m; H=24 m) with pillar width, for volume loss of (a) 0.5%; and (b) 5% (Jurong Formation)

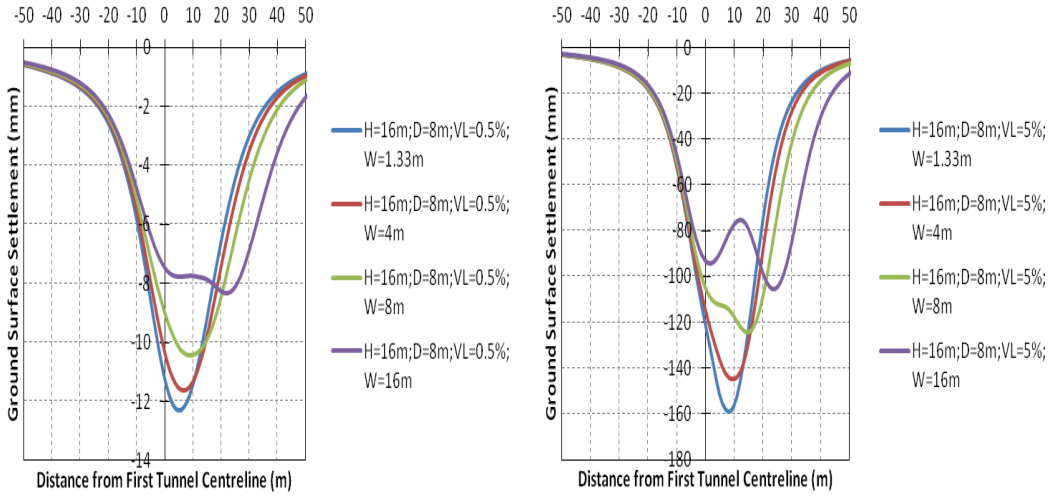

(a) (b)

Figure B.6 Variation of ground surface settlement for closely spaced bored tunnels (D=8 m; H=16 m) with pillar width, for volume loss of (a) 0.5%; and (b) 5% (Jurong Formation)

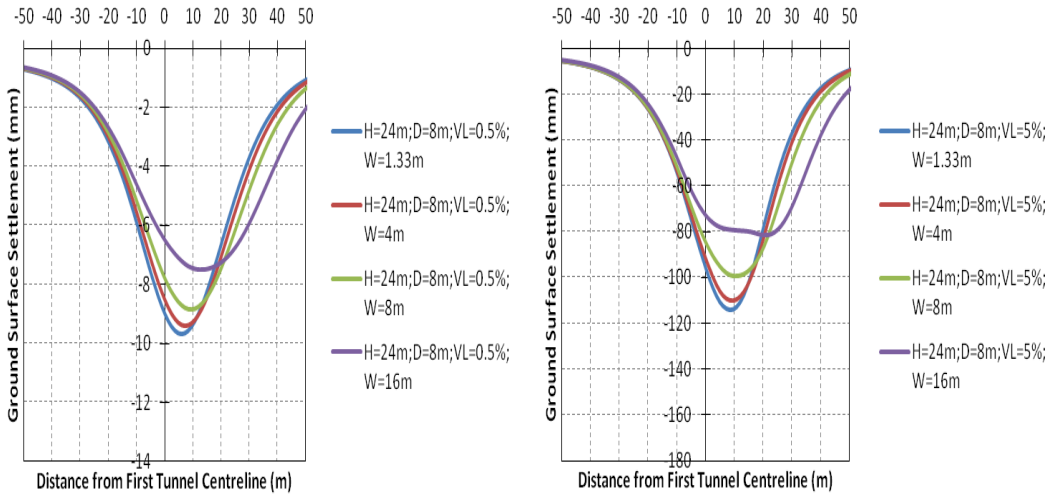

(a) (b)

Figure B.7 Variation of ground surface settlement for closely spaced bored tunnels (D=8 m; H=24 m) with pillar width, for volume loss of (a) 0.5%; and (b) 5% (Jurong Formation)

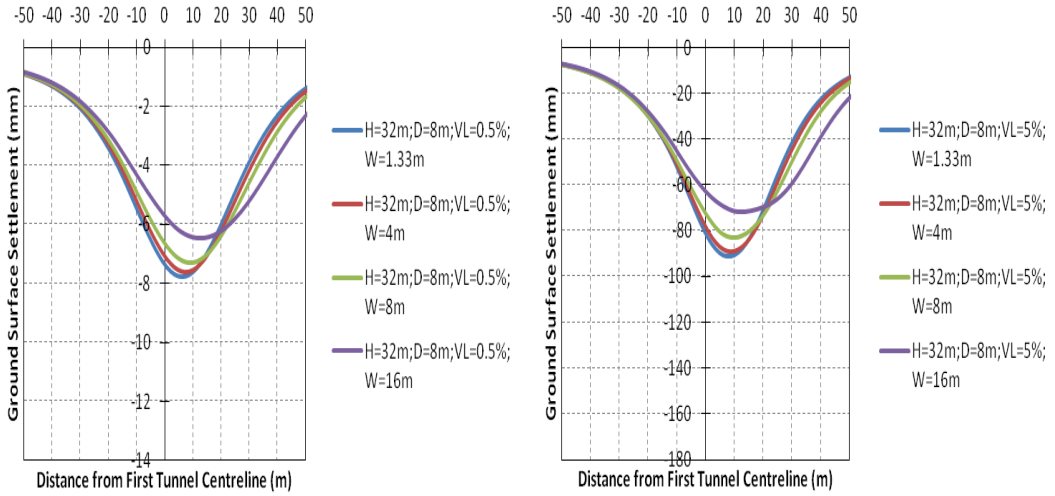

(a) (b)

Figure B.8 Variation of ground surface settlement for closely spaced bored tunnels (D=8 m; H=32 m) with pillar width, for volume loss of (a) 0.5%; and (b) 5% (Jurong Formation)

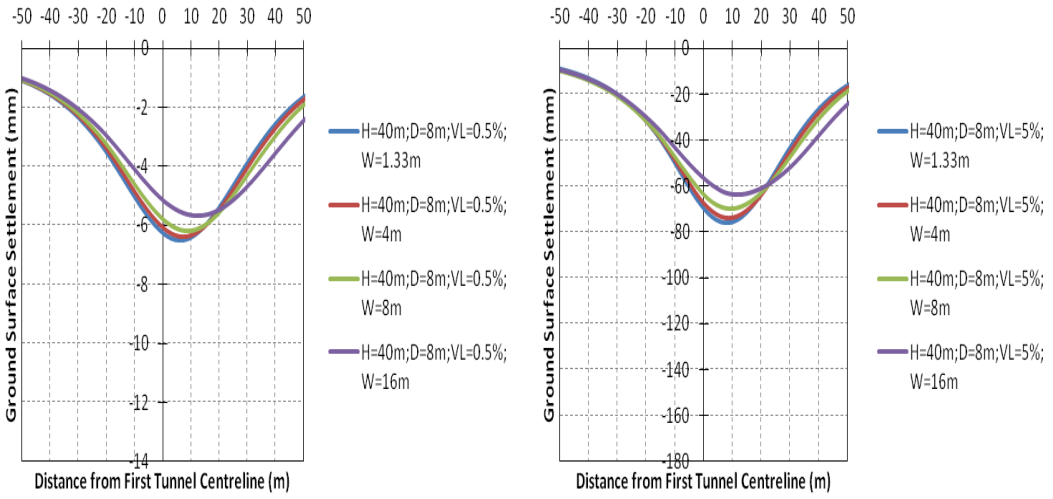

(a) (b)

Figure B.9 Variation of ground surface settlement for closely spaced bored tunnels (D=8 m; H=40 m) with pillar width, for volume loss of (a) 0.5%; and (b) 5% (Jurong Formation)

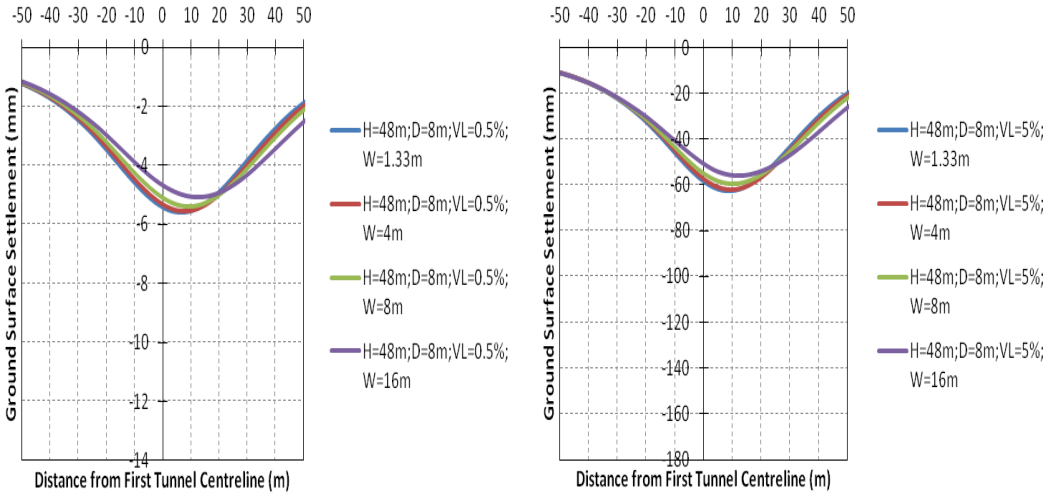

(a) (b)

Figure B.10 Variation of ground surface settlement for closely spaced bored tunnels (D=8 m; H=48 m) with pillar width, for volume loss of (a) 0.5%; and (b) 5% (Jurong Formation)

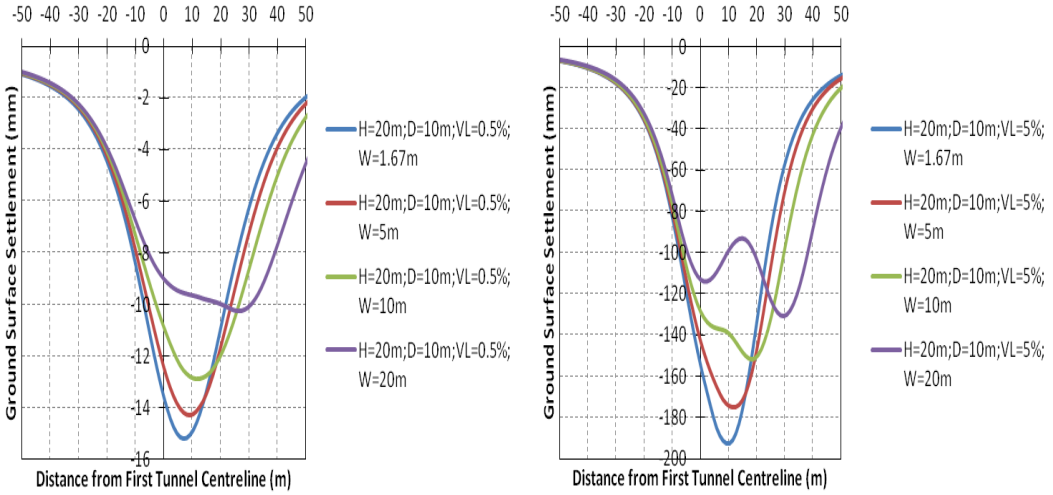

(a) (b)

Figure B.11 Variation of ground surface settlement for closely spaced bored tunnels (D=10 m; H=20 m) with pillar width, for volume loss of (a) 0.5%; and (b) 5% (Jurong Formation)

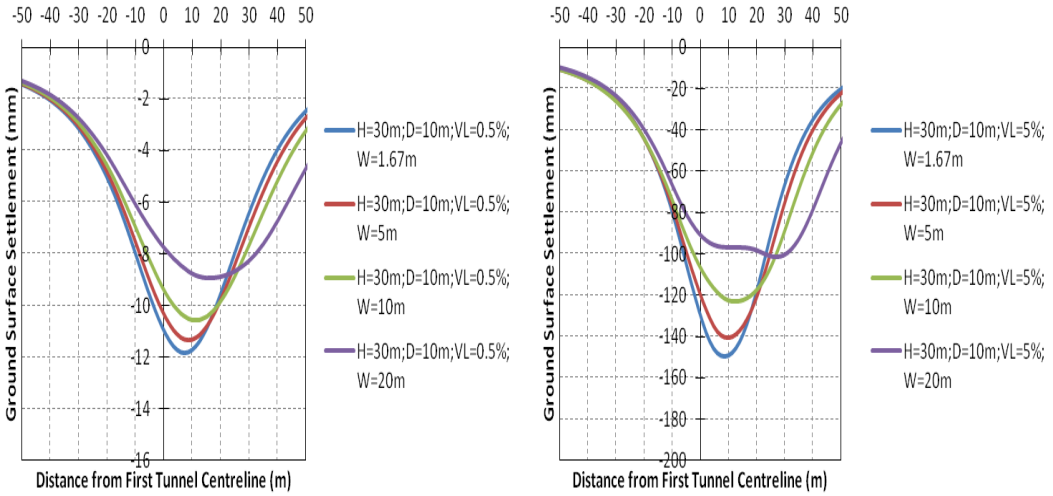

(a) (b)

Figure B.12 Variation of ground surface settlement for closely spaced bored tunnels (D=10 m; H=30 m) with pillar width, for volume loss of (a) 0.5%; and (b) 5% (Jurong Formation)

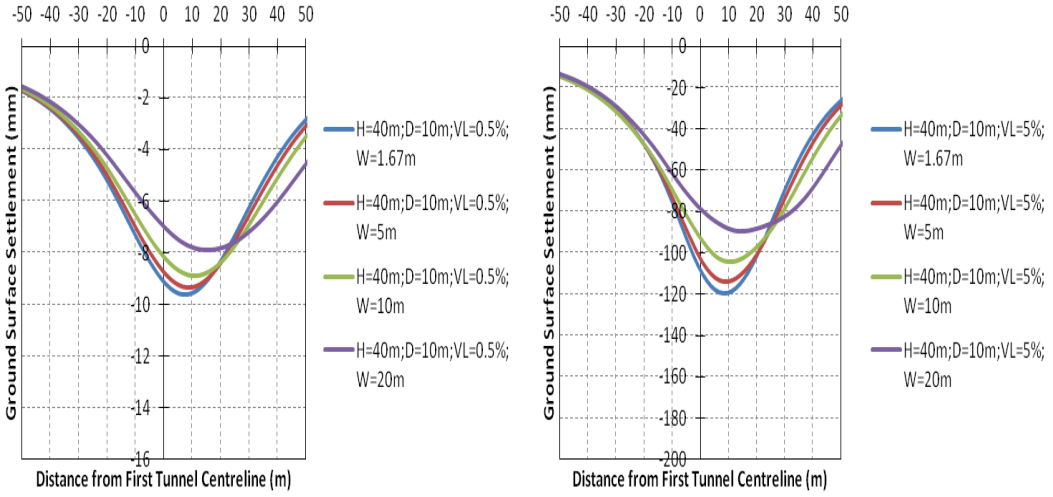

(a) (b)

Figure B.13 Variation of ground surface settlement for closely spaced bored tunnels (D=10 m; H=40 m) with pillar width, for volume loss of (a) 0.5%; and (b) 5% (Jurong Formation)

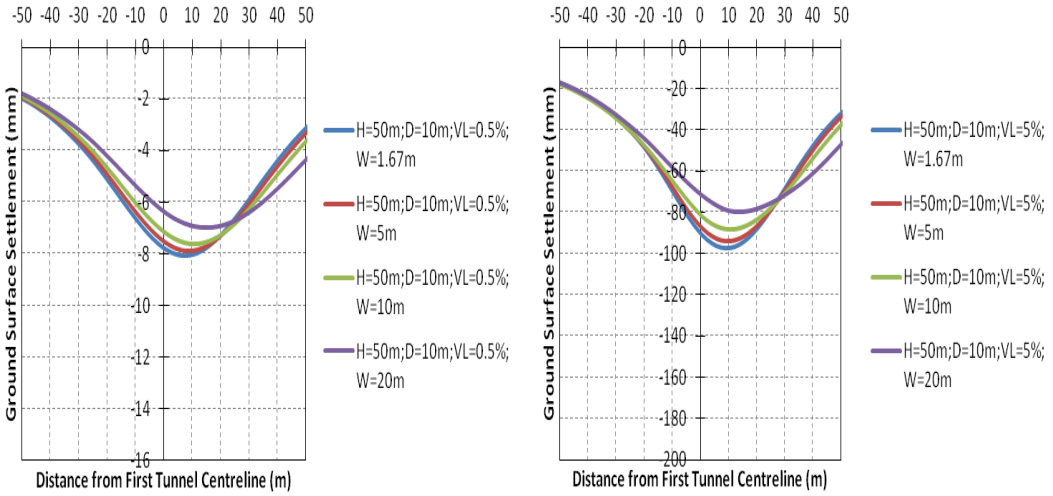

(a) (b)

Figure B.14 Variation of ground surface settlement for closely spaced bored tunnels (D=10 m; H=50 m) with pillar width, for volume loss of (a) 0.5%; and (b) 5% (Jurong Formation)

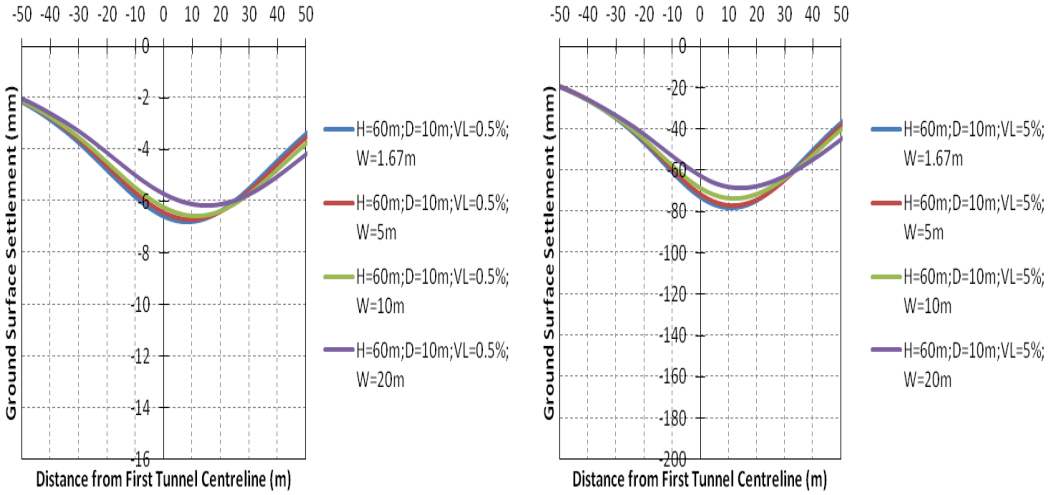

(a) (b)

Figure B.15 Variation of ground surface settlement for closely spaced bored tunnels (D=10 m; H=60 m) with pillar width, for volume loss of (a) 0.5%; and (b) 5% (Jurong Formation)

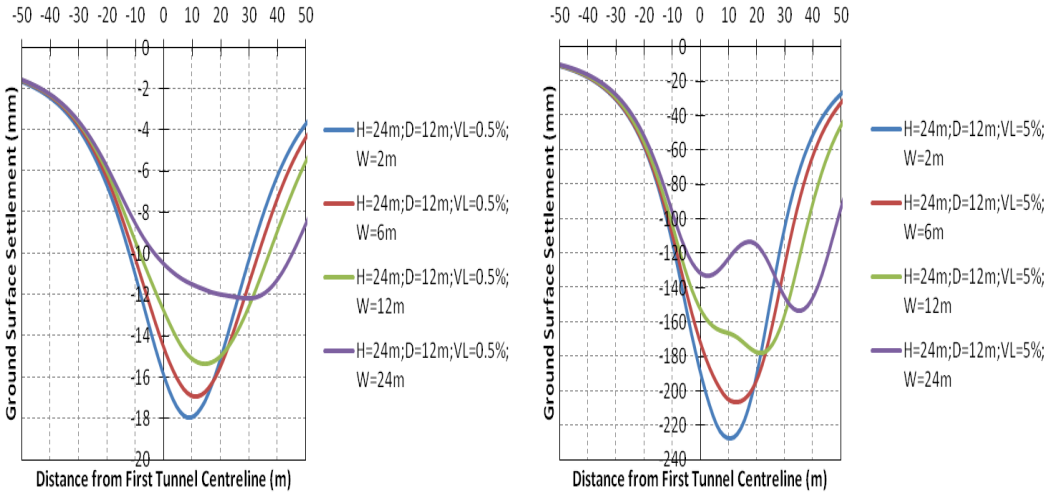

(a) (b)

Figure B.16 Variation of ground surface settlement for closely spaced bored tunnels (D=12 m; H=24 m) with pillar width, for volume loss of (a) 0.5%; and (b) 5% (Jurong Formation)

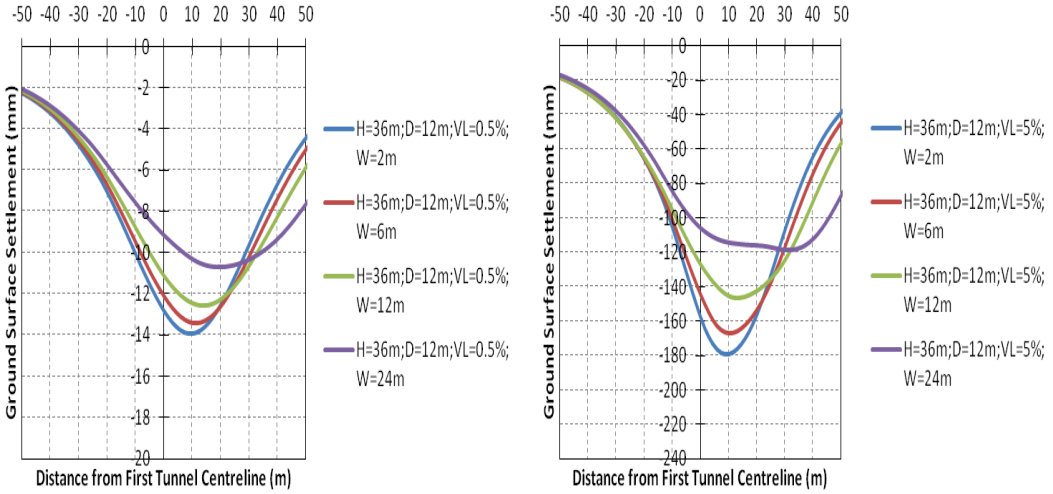

(a) (b)

Figure B.17 Variation of ground surface settlement for closely spaced bored tunnels (D=12 m; H=36 m) with pillar width, for volume loss of (a) 0.5%; and (b) 5% (Jurong Formation)

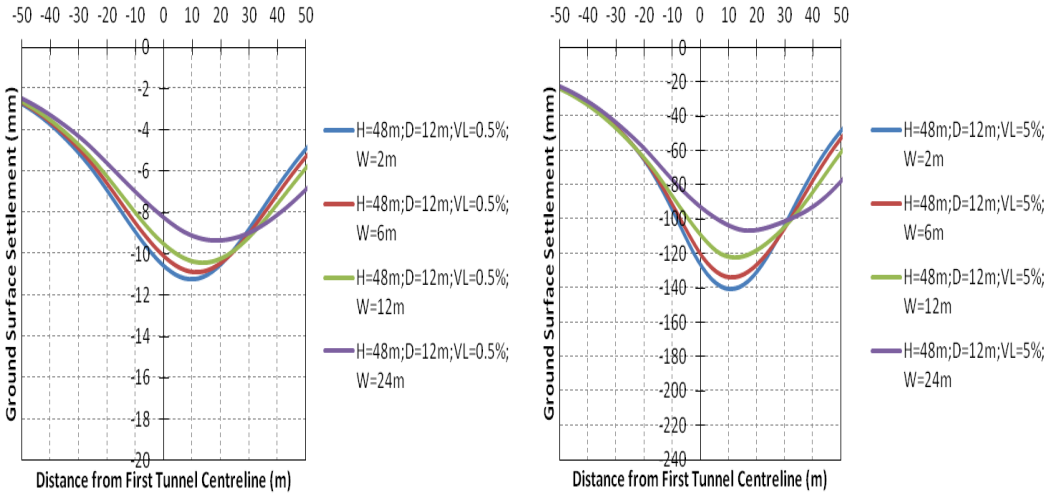

(a) (b)

Figure B.18 Variation of ground surface settlement for closely spaced bored tunnels (D=12 m; H=48 m) with pillar width, for volume loss of (a) 0.5%; and (b) 5% (Jurong Formation)

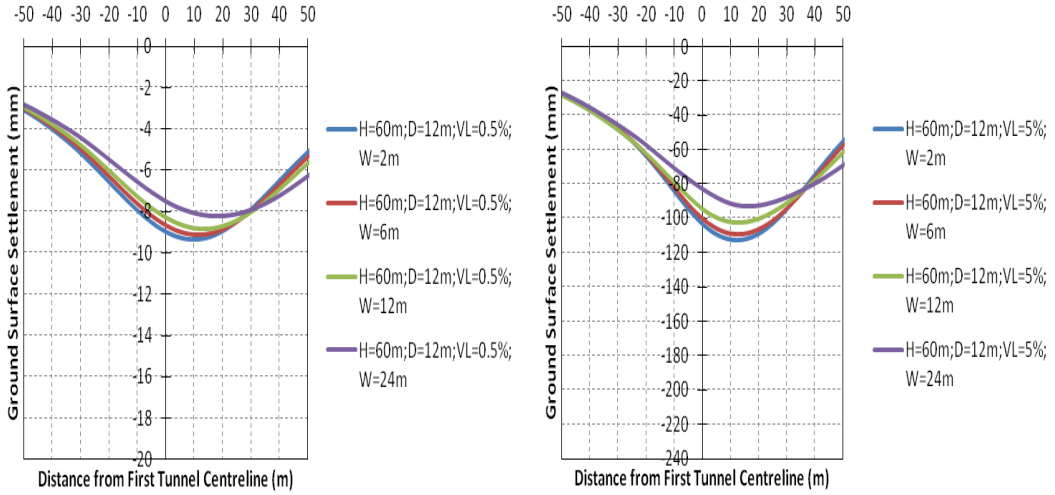

(a) (b)

Figure B.19 Variation of ground surface settlement for closely spaced bored tunnels (D=12 m; H=60 m) with pillar width, for volume loss of (a) 0.5%; and (b) 5% (Jurong Formation)

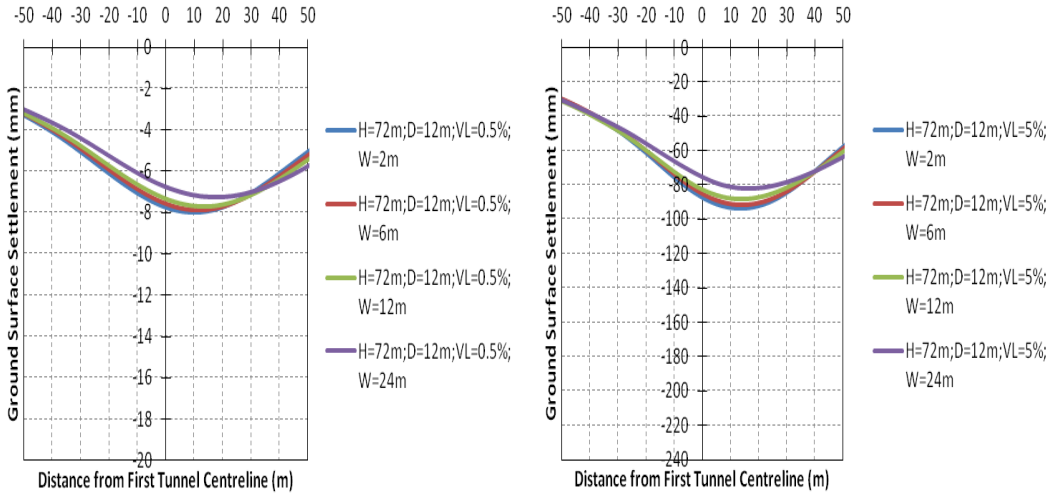

(a) (b)

Figure B.20 Variation of ground surface settlement for closely spaced bored tunnels (D=12 m; H=72 m) with pillar width, for volume loss of (a) 0.5%; and (b) 5% (Jurong Formation)

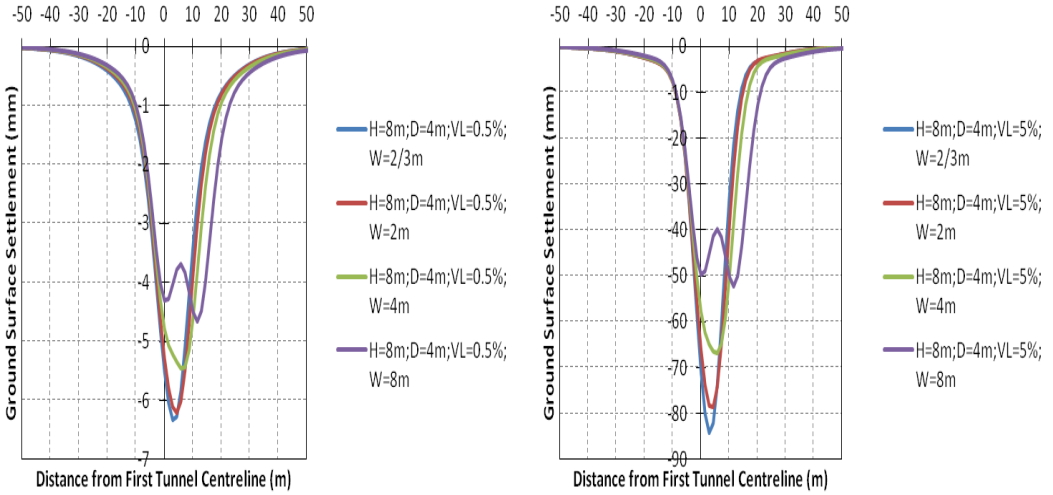

(a) (b)

Figure B.21 Variation of ground surface settlement for closely spaced bored tunnels (D=4 m; H=8 m) with pillar width, for volume loss of (a) 0.5%; and (b) 5% (mixed ground of Jurong Formation and Marine Clay)

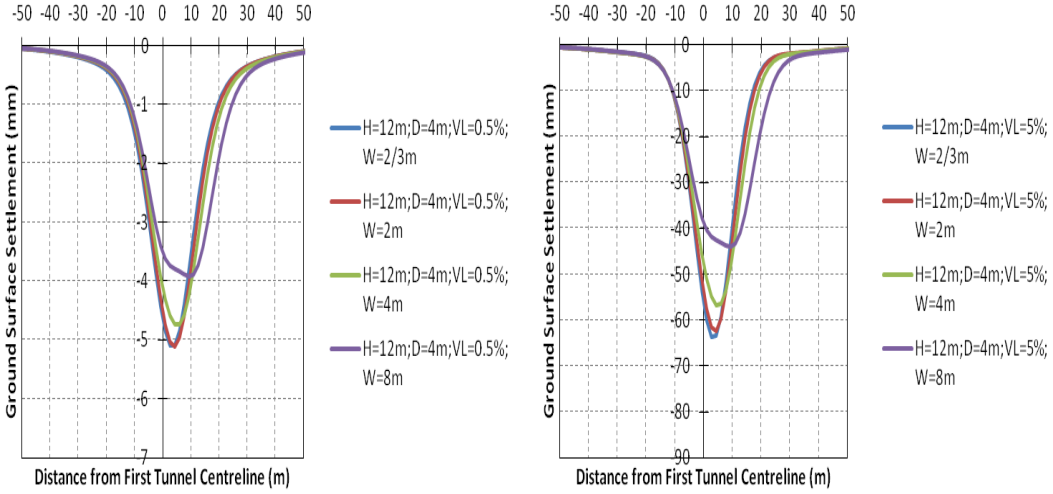

(a) (b)

Figure B.22 Variation of ground surface settlement for closely spaced bored tunnels (D=4 m; H=12 m) with pillar width, for volume loss of (a) 0.5%; and (b) 5% (mixed ground of Jurong Formation and Marine Clay)

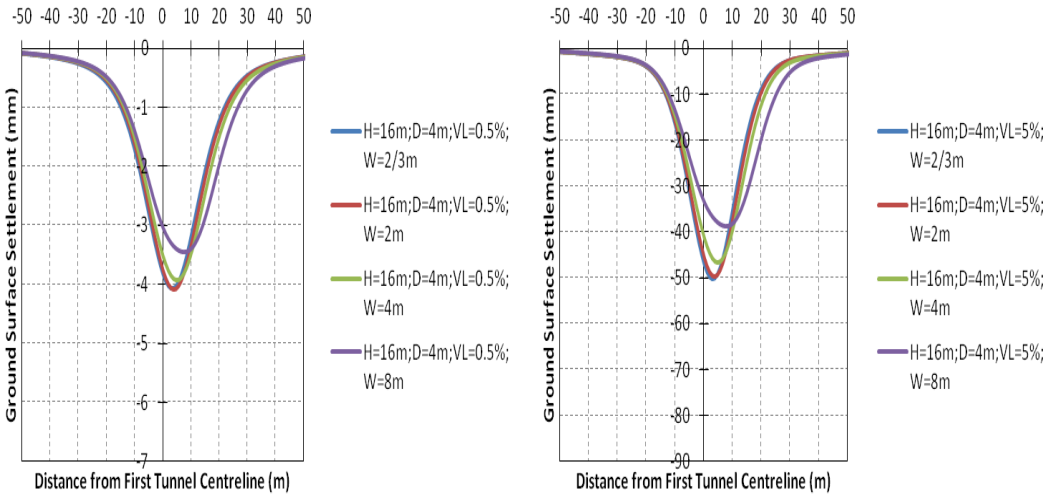

(a) (b)

Figure B.23 Variation of ground surface settlement for closely spaced bored tunnels (D=4 m; H=16 m) with pillar width, for volume loss of (a) 0.5%; and (b) 5% (mixed ground of Jurong Formation and Marine Clay)

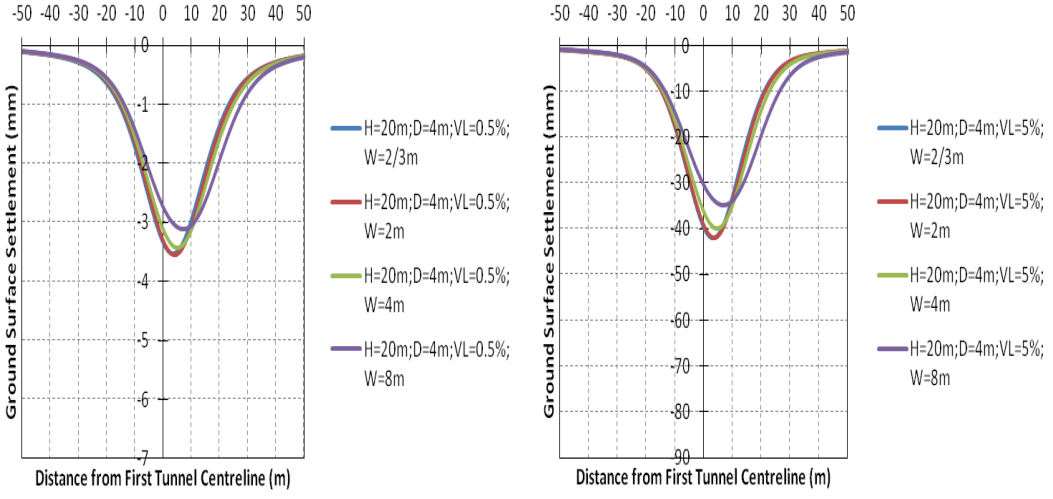

(a) (b)

Figure B.24 Variation of ground surface settlement for closely spaced bored tunnels (D=4 m; H=20 m) with pillar width, for volume loss of (a) 0.5%; and (b) 5% (mixed ground of Jurong Formation and Marine Clay)

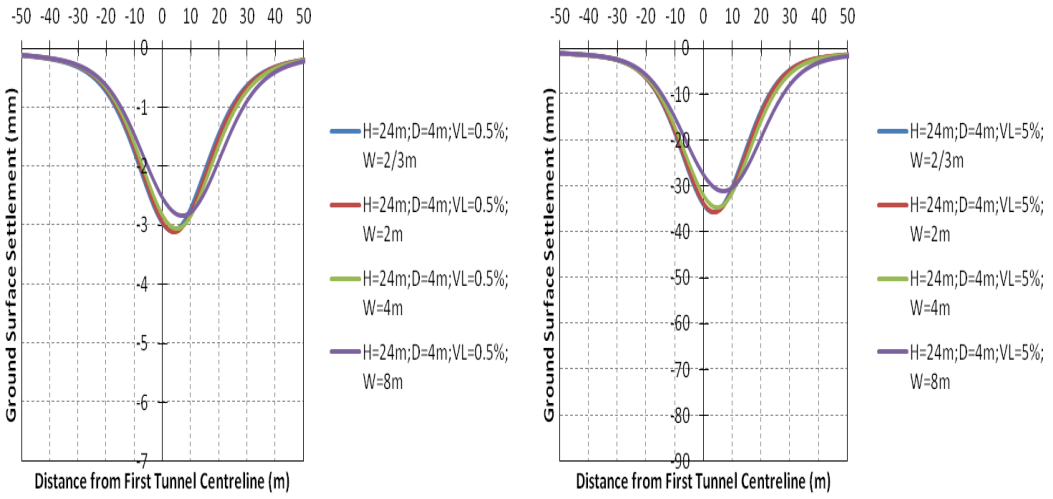

(a) (b)

Figure B.25 Variation of ground surface settlement for closely spaced bored tunnels (D=4 m; H=24 m) with pillar width, for volume loss of (a) 0.5%; and (b) 5% (mixed ground of Jurong Formation and Marine Clay)

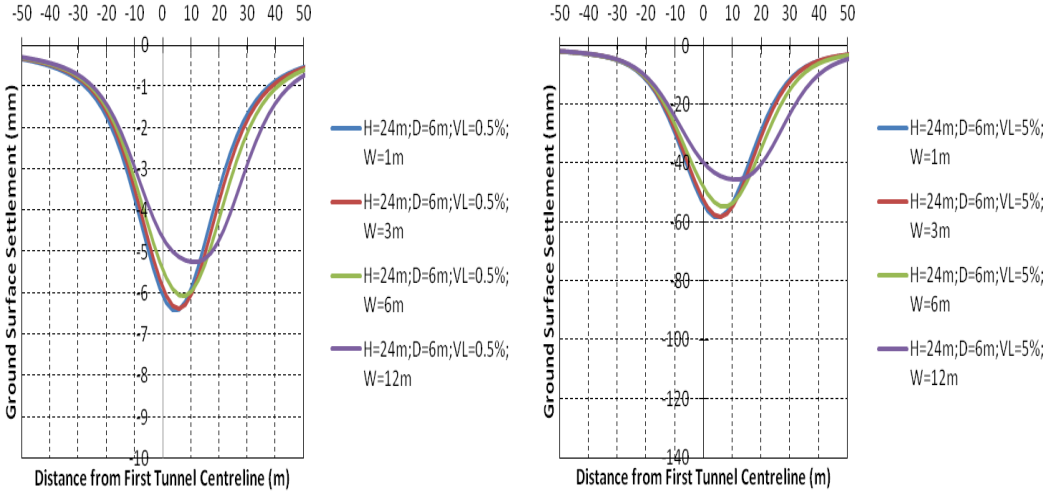

(a) (b)

Figure B.26 Variation of ground surface settlement for closely spaced bored tunnels (D=6 m; H=24 m) with pillar width, for volume loss of (a) 0.5%; and (b) 5% (mixed ground of Jurong Formation and Marine Clay)

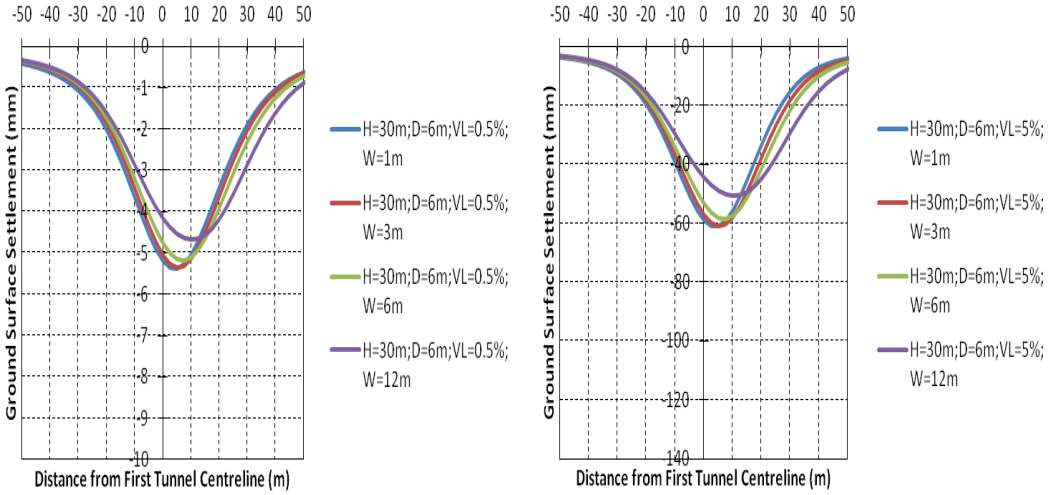

(a) (b)

Figure B.27 Variation of ground surface settlement for closely spaced bored tunnels (D=6 m; H=30 m) with pillar width, for volume loss of (a) 0.5%; and (b) 5% (mixed ground of Jurong Formation and Marine Clay)

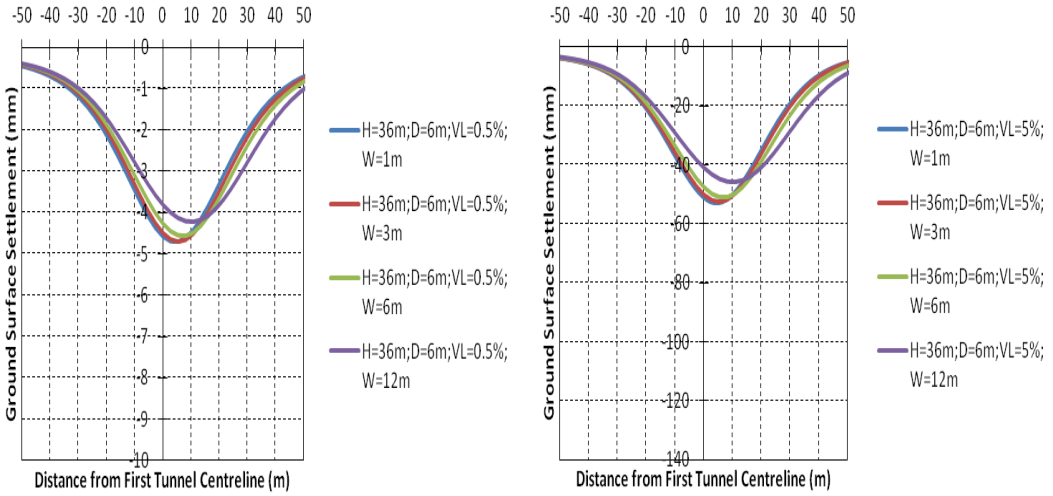

(a) (b)

Figure B.28 Variation of ground surface settlement for closely spaced bored tunnels (D=6 m; H=36 m) with pillar width, for volume loss of (a) 0.5%; and (b) 5% (mixed ground of Jurong Formation and Marine Clay)

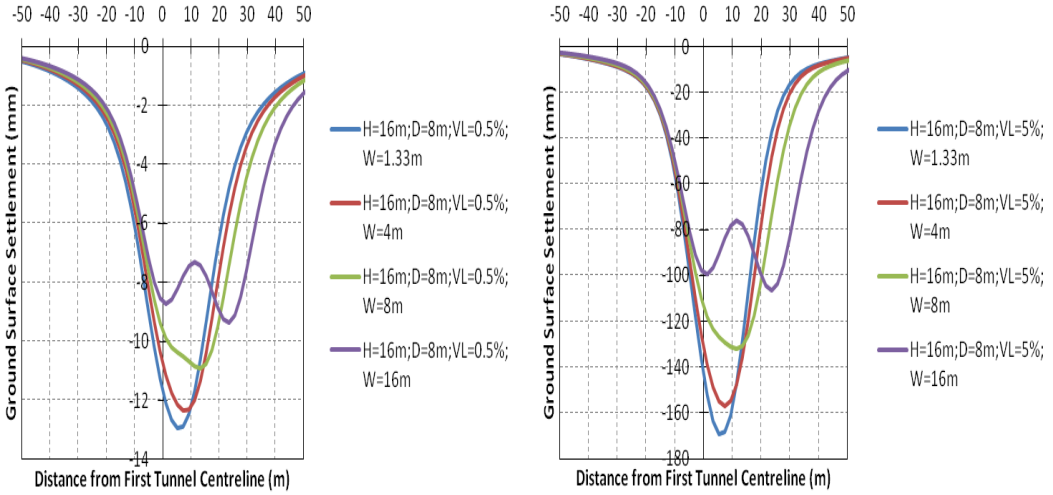

(a) (b)

Figure B.29 Variation of ground surface settlement for closely spaced bored tunnels (D=8 m; H=16 m) with pillar width, for volume loss of (a) 0.5%; and (b) 5% (mixed ground of Jurong Formation and Marine Clay)

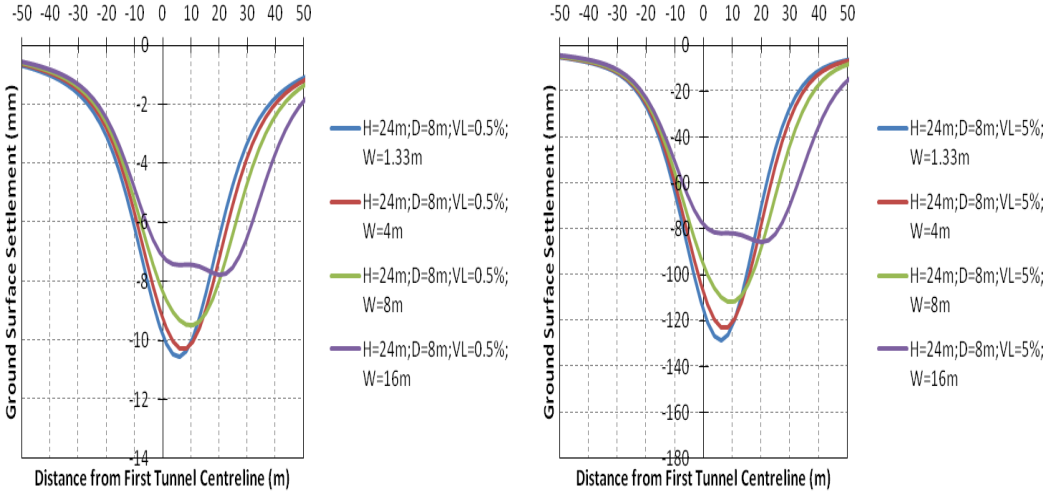

(a) (b)

Figure B.30 Variation of ground surface settlement for closely spaced bored tunnels (D=8 m; H=24 m) with pillar width, for volume loss of (a) 0.5%; and (b) 5% (mixed ground of Jurong Formation and Marine Clay)

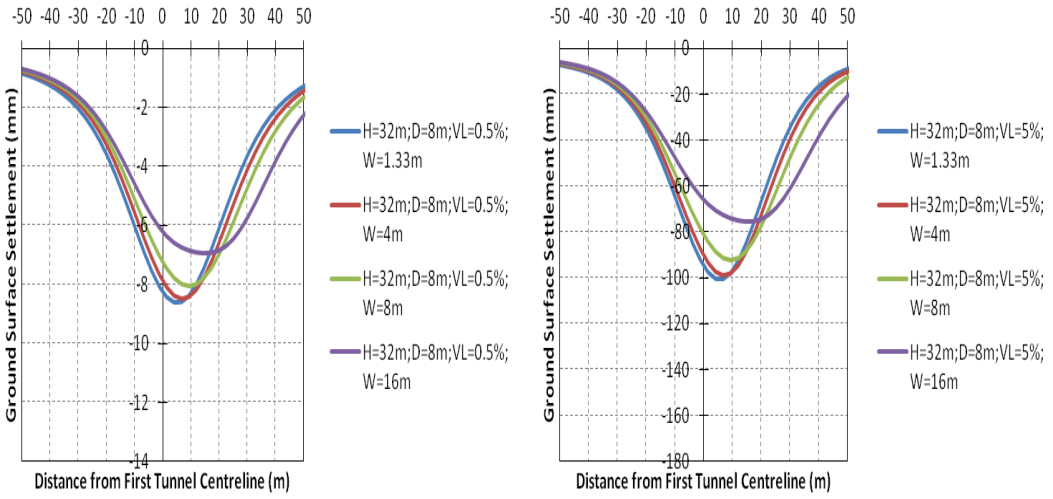

(a) (b)

Figure B.31 Variation of ground surface settlement for closely spaced bored tunnels (D=8 m; H=32 m) with pillar width, for volume loss of (a) 0.5%; and (b) 5% (mixed ground of Jurong Formation and Marine Clay)

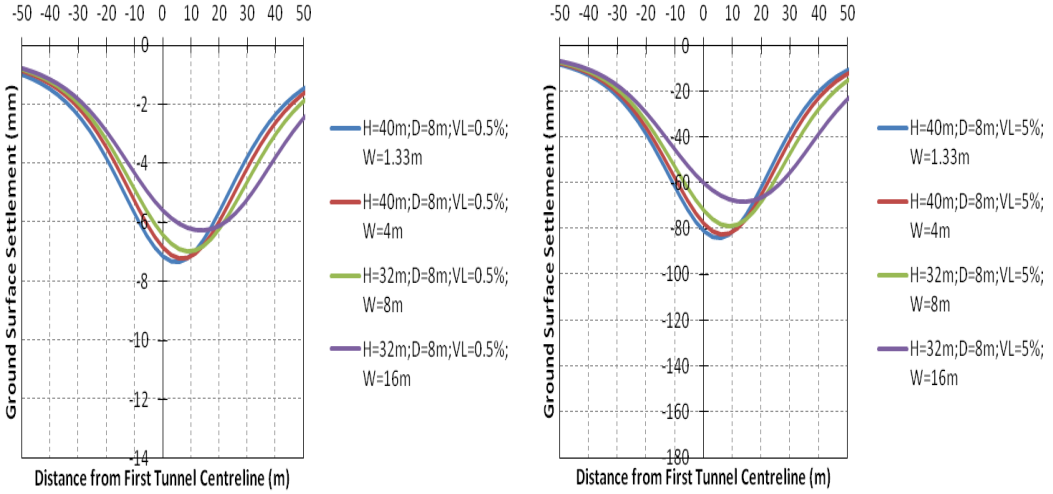

(a) (b)

Figure B.32 Variation of ground surface settlement for closely spaced bored tunnels (D=8 m; H=40 m) with pillar width, for volume loss of (a) 0.5%; and (b) 5% (mixed ground of Jurong Formation and Marine Clay)

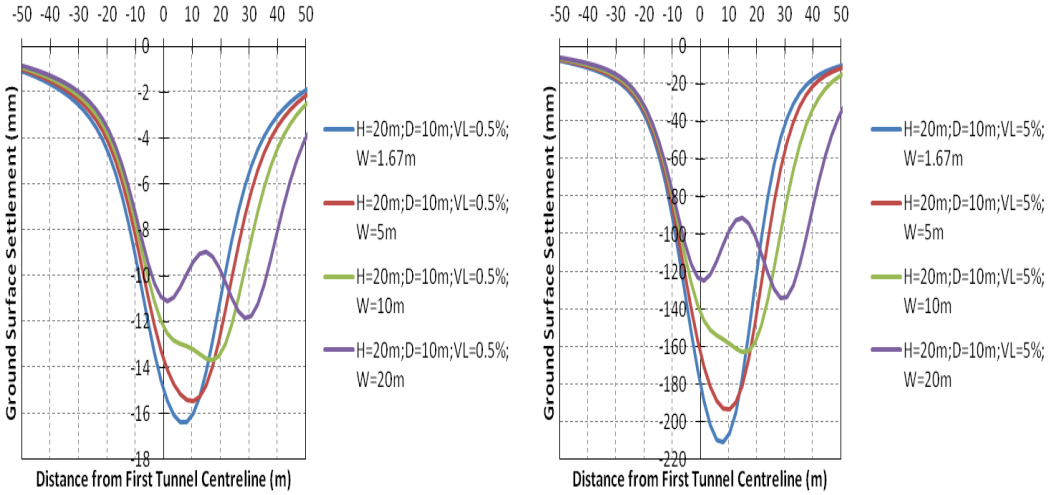

(a) (b)

Figure B.33 Variation of ground surface settlement for closely spaced bored tunnels (D=10 m; H=20 m) with pillar width, for volume loss of (a) 0.5%; and (b) 5% (mixed ground of Jurong Formation and Marine Clay)

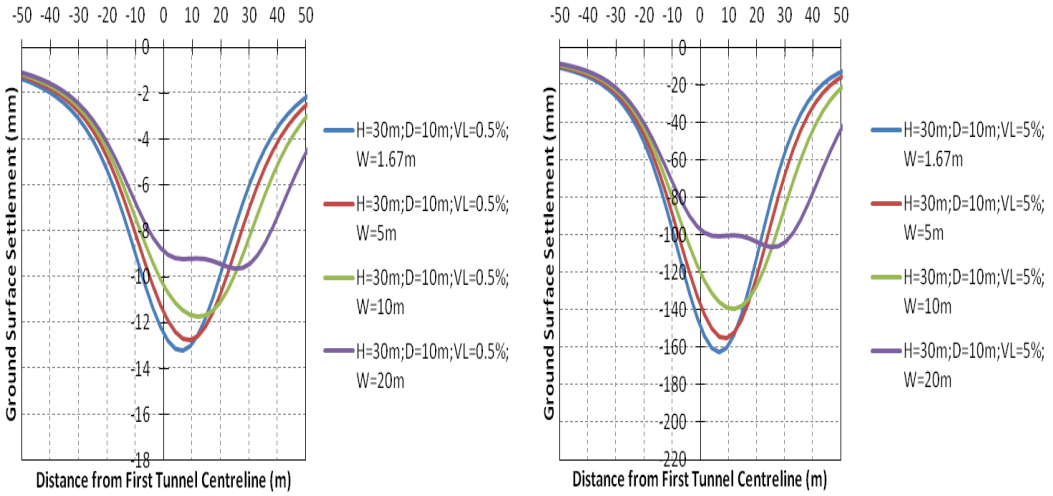

(a) (b)

Figure B.34 Variation of ground surface settlement for closely spaced bored tunnels (D=10 m; H=30 m) with pillar width, for volume loss of (a) 0.5%; and (b) 5% (mixed ground of Jurong Formation and Marine Clay)

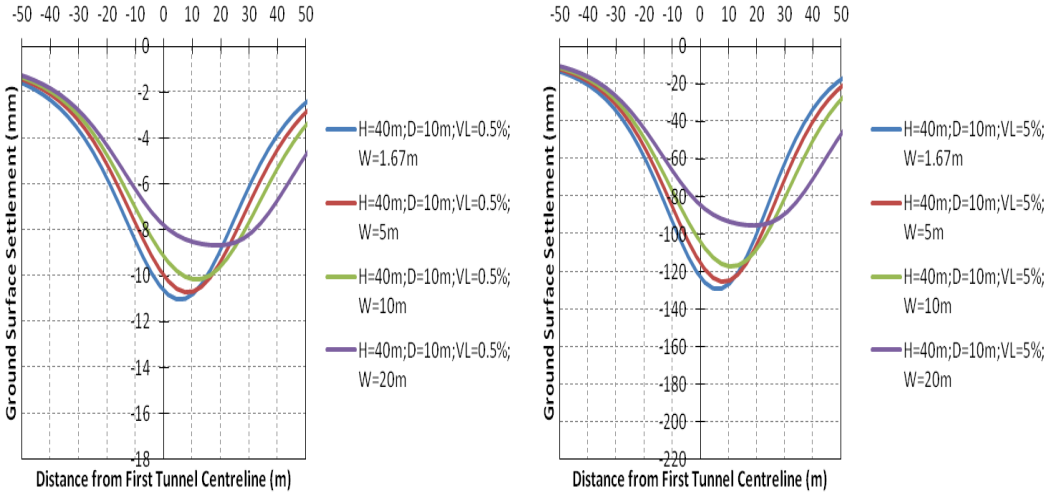

(a) (b)

Figure B.35 Variation of ground surface settlement for closely spaced bored tunnels (D=10 m; H=40 m) with pillar width, for volume loss of (a) 0.5%; and (b) 5% (mixed ground of Jurong Formation and Marine Clay)

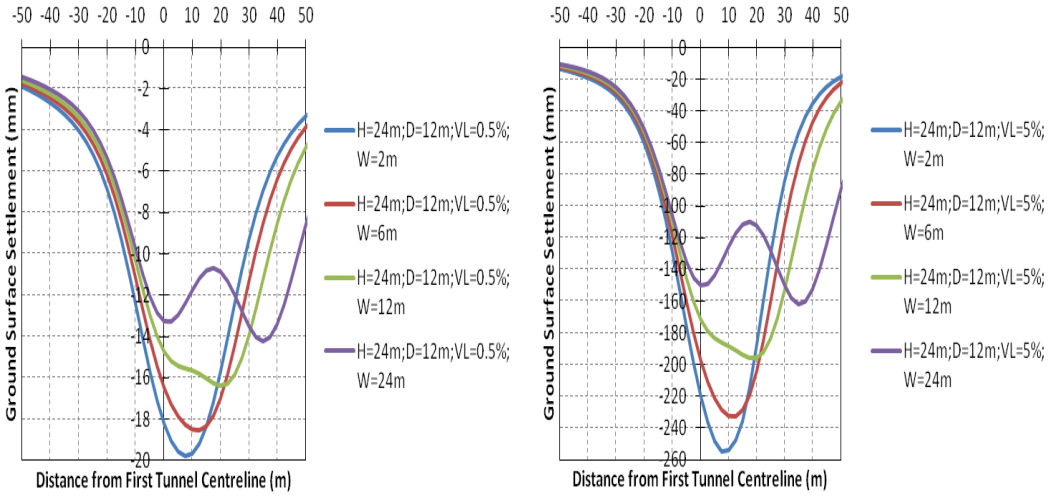

(a) (b)

Figure B.36 Variation of ground surface settlement for closely spaced bored tunnels (D=12 m; H=24 m) with pillar width, for volume loss of (a) 0.5%; and (b) 5% (mixed ground of Jurong Formation and Marine Clay)

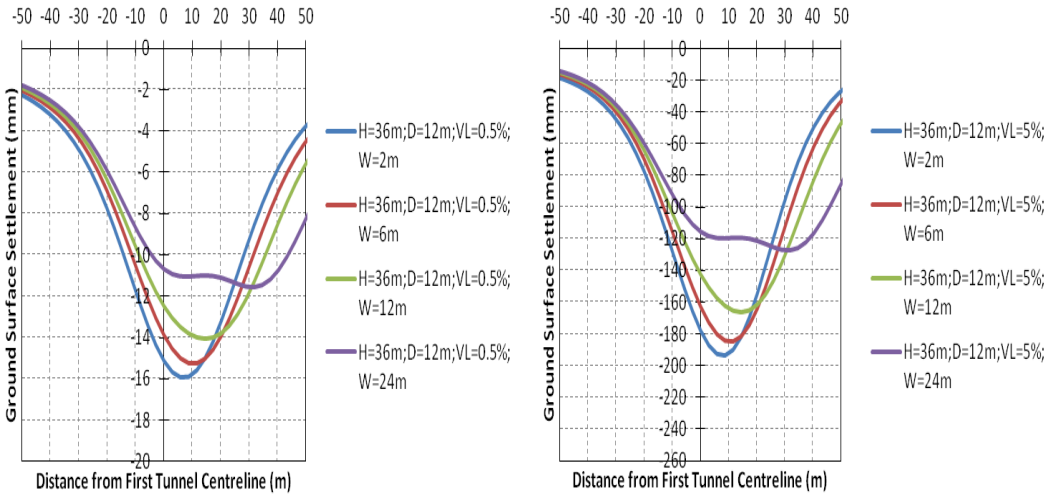

(a) (b)

Figure B.37 Variation of ground surface settlement for closely spaced bored tunnels (D=12 m; H=36 m) with pillar width, for volume loss of (a) 0.5%; and (b) 5% (mixed ground of Jurong Formation and Marine Clay)

D=4m			D=4m		
W/D	i (H=8m;VL=0.5%)	Loc S_{max}	W/D	i (H=8m;VL=5%)	Loc S_{max}
0.167	7.436	3.016	0.167	6.466	3.743
0.500	7.478	3.625	0.500	6.746	4.096
1.000	8.072	4.574	1.000	7.578	4.820
2.000	10.087	6.442	2.000	9.544	6.543
W/D	i (H=12m;VL=0.5%)	Loc S_{max}	W/D	i (H=12m;VL=5%)	Loc S_{max}
0.167	9.254	3.085	0.167	8.379	4.232
0.500	9.221	3.727	0.500	8.513	4.674
1.000	9.648	4.665	1.000	9.187	5.308
2.000	11.175	6.467	2.000	10.704	6.738
W/D	i (H=16m;VL=0.5%)	Loc S_{max}	W/D	i (H=16m;VL=5%)	Loc S_{max}
0.167	11.597	2.818	0.167	9.982	4.397
0.500	11.480	3.486	0.500	9.996	4.744
1.000	11.822	4.507	1.000	10.581	5.260
2.000	13.247	6.441	2.000	12.103	6.826
W/D	i (H=20m;VL=0.5%)	Loc S_{max}	W/D	i (H=20m;VL=5%)	Loc S_{max}
0.167	13.154	2.805	0.167	12.312	4.338
0.500	13.080	3.415	0.500	12.323	4.832
1.000	13.393	4.392	1.000	12.709	5.310
2.000	14.592	6.273	2.000	13.716	6.630
W/D	i (H=24m;VL=0.5%)	Loc S_{max}	W/D	i (H=24m;VL=5%)	Loc S_{max}
0.167	14.978	2.883	0.167	14.415	4.421
0.500	14.895	3.500	0.500	14.447	5.131
1.000	15.137	4.414	1.000	14.778	5.546
2.000	16.169	6.214	2.000	15.523	6.709

Figure B.38 Variation of trough width parameter i and location of maximum surface settlement Loc S_{max} with dimensionless pillar width at various depth (D=4 m) for volume loss of 0.5% and 5% (Jurong Formation)

D=6m			D=6m		
W/D	i (H=12m;VL=0.5%)	Loc S_{max}	W/D	i (H=12m;VL=5%)	Loc S_{max}
0.167	11.142	4.617	0.167	9.663	5.724
0.500	11.402	5.572	0.500	10.123	6.250
1.000	12.346	6.974	1.000	11.428	7.335
2.000	15.304	9.750	2.000	14.428	9.908
W/D	i (H=18m;VL=0.5%)	Loc S_{max}	W/D	i (H=18m;VL=5%)	Loc S_{max}
0.167	14.114	4.399	0.167	11.820	5.955
0.500	14.344	5.365	0.500	12.155	6.414
1.000	15.242	6.772	1.000	13.416	7.394
2.000	17.943	9.730	2.000	16.228	10.129
W/D	i (H=24m;VL=0.5%)	Loc S_{max}	W/D	i (H=24m;VL=5%)	Loc S_{max}
0.167	16.782	4.520	0.167	15.292	6.305
0.500	16.955	5.429	0.500	15.483	6.830
1.000	17.665	6.748	1.000	16.396	7.555
2.000	19.818	9.492	2.000	18.491	9.789
W/D	i (H=30m;VL=0.5%)	Loc S_{max}	W/D	i (H=30m;VL=5%)	Loc S_{max}
0.167	20.395	4.470	0.167	18.444	6.415
0.500	20.572	5.341	0.500	18.582	6.900
1.000	21.197	6.554	1.000	19.390	7.500
2.000	23.174	9.244	2.000	21.270	9.642
W/D	i (H=36m;VL=0.5%)	Loc S_{max}	W/D	i (H=36m;VL=5%)	Loc S_{max}
0.167	23.259	4.556	0.167	22.009	6.589
0.500	23.383	5.392	0.500	22.101	7.266
1.000	23.905	6.565	1.000	22.669	7.728
2.000	25.540	9.069	2.000	24.126	9.500

Figure B.39 Variation of trough width parameter i and location of maximum surface settlement Loc S_{max} with dimensionless pillar width at various depth (D=6 m) for volume loss of 0.5% and 5% (Jurong Formation)

D=8m			D=8m		
W/D	i (H=16m;VL=0.5%)	Loc S_{max}	W/D	i (H=16m;VL=5%)	Loc S_{max}
0.167	14.676	5.587	0.167	11.694	6.720
0.500	15.541	6.932	0.500	12.697	7.595
1.000	17.253	9.022	1.000	14.837	9.414
2.000	21.689	13.243	2.000	19.410	13.495
W/D	i (H=24m;VL=0.5%)	Loc S_{max}	W/D	i (H=24m;VL=5%)	Loc S_{max}
0.167	18.613	6.016	0.167	15.994	7.475
0.500	19.166	7.309	0.500	16.640	8.211
1.000	20.445	9.141	1.000	18.267	9.590
2.000	23.935	12.935	2.000	21.934	13.296
W/D	i (H=32m;VL=0.5%)	Loc S_{max}	W/D	i (H=32m;VL=5%)	Loc S_{max}
0.167	23.137	6.042	0.167	19.939	7.653
0.500	23.647	7.248	0.500	20.521	8.392
1.000	24.780	8.863	1.000	22.111	9.530
2.000	27.863	12.610	2.000	25.306	12.993
W/D	i (H=40m;VL=0.5%)	Loc S_{max}	W/D	i (H=40m;VL=5%)	Loc S_{max}
0.167	27.694	5.919	0.167	24.060	7.888
0.500	28.186	6.936	0.500	24.713	8.507
1.000	29.184	8.455	1.000	26.194	9.302
2.000	31.829	12.124	2.000	28.833	12.375
W/D	i (H=48m;VL=0.5%)	Loc S_{max}	W/D	i (H=48m;VL=5%)	Loc S_{max}
0.167	31.976	6.233	0.167	29.288	8.535
0.500	32.328	7.315	0.500	29.641	9.302
1.000	33.175	8.720	1.000	30.763	9.954
2.000	35.481	11.843	2.000	33.116	12.221

Figure B.40 Variation of trough width parameter i and location of maximum surface settlement Loc S_{max} with dimensionless pillar width at various depth (D=8 m) for volume loss of 0.5% and 5% (Jurong Formation)

	Z	AA	AB	AD	AE	AF
2	**D=10m**			**D=10m**		
3	W/D	i (H=20m;VL=0.5%)	Loc S_{max}	W/D	i (H=20m;VL=5%)	Loc S_{max}
4	0.167	18.655	7.400	0.167	14.930	8.194
5	0.500	19.820	9.131	0.500	16.279	9.546
6	1.000	21.972	11.654	1.000	18.985	11.951
7	2.000	27.387	16.660	2.000	24.687	17.179
9	W/D	i (H=30m;VL=0.5%)	Loc S_{max}	W/D	i (H=30m;VL=5%)	Loc S_{max}
10	0.167	23.900	7.335	0.167	18.984	8.362
11	0.500	24.930	8.836	0.500	20.359	9.524
12	1.000	26.722	11.134	1.000	23.053	11.508
13	2.000	31.317	16.283	2.000	27.717	16.716
15	W/D	i (H=40m;VL=0.5%)	Loc S_{max}	W/D	i (H=40m;VL=5%)	Loc S_{max}
16	0.167	29.302	7.230	0.167	23.895	8.722
17	0.500	30.187	8.602	0.500	25.230	9.582
18	1.000	31.711	10.699	1.000	27.714	11.161
19	2.000	35.592	15.713	2.000	31.775	16.034
21	W/D	i (H=50m;VL=0.5%)	Loc S_{max}	W/D	i (H=50m;VL=5%)	Loc S_{max}
22	0.167	34.720	7.154	0.167	29.473	9.349
23	0.500	35.463	8.512	0.500	30.610	9.993
24	1.000	36.764	10.448	1.000	32.810	11.165
25	2.000	40.143	15.010	2.000	36.467	15.211
27	W/D	i (H=60m;VL=0.5%)	Loc S_{max}	W/D	i (H=60m;VL=5%)	Loc S_{max}
28	0.167	41.234	7.908	0.167	36.872	10.699
29	0.500	41.778	9.182	0.500	37.440	11.486
30	1.000	42.932	10.738	1.000	39.226	12.114
31	2.000	45.874	14.534	2.000	42.443	14.976

Figure B.41 Variation of trough width parameter i and location of maximum surface settlement Loc S_{max} with dimensionless pillar width at various depth (D=10 m) for volume loss of 0.5% and 5% (Jurong Formation)

	AG	AH	AI	AJ	AK	AL	AM	AN	AO
1									
2		**D=12m**				**D=12m**			
3		W/D	i (H=24m;VL=0.5%)	Loc S_{max}		W/D	i (H=24m;VL=5%)	Loc S_{max}	
4		0.167	22.767	9.123		0.167	18.095	9.452	
5		0.500	24.173	11.280		0.500	19.867	11.231	
6		1.000	26.636	14.211		1.000	23.116	14.249	
7		2.000	32.956	20.091		2.000	29.892	20.710	
8									
9		W/D	i (H=36m;VL=0.5%)	Loc S_{max}		W/D	i (H=36m;VL=5%)	Loc S_{max}	
10		0.167	29.059	9.145		0.167	23.052	9.819	
11		0.500	30.288	11.083		0.500	24.969	11.287	
12		1.000	32.355	13.690		1.000	28.258	13.791	
13		2.000	37.744	19.652		2.000	33.917	20.185	
14									
15		W/D	i (H=48m;VL=0.5%)	Loc S_{max}		W/D	i (H=48m;VL=5%)	Loc S_{max}	
16		0.167	36.055	9.296		0.167	29.437	10.904	
17		0.500	37.100	11.035		0.500	31.051	11.883	
18		1.000	38.868	13.281		1.000	34.233	13.602	
19		2.000	43.406	18.905		2.000	39.181	19.299	
20									
21		W/D	i (H=60m;VL=0.5%)	Loc S_{max}		W/D	i (H=60m;VL=5%)	Loc S_{max}	
22		0.167	43.397	9.450		0.167	36.878	12.132	
23		0.500	44.371	11.042		0.500	38.076	12.829	
24		1.000	45.899	12.952		1.000	40.867	13.777	
25		2.000	49.879	17.997		2.000	45.378	18.338	
26									
27		W/D	i (H=72m;VL=0.5%)	Loc S_{max}		W/D	i (H=72m;VL=5%)	Loc S_{max}	
28		0.167	51.240	9.613		0.167	45.039	13.161	
29		0.500	52.146	11.050		0.500	45.818	13.772	
30		1.000	53.544	12.696		1.000	48.149	14.178	
31		2.000	57.186	17.175		2.000	52.253	17.627	
32									

Figure B.42 Variation of trough width parameter i and location of maximum surface settlement Loc S_{max} with dimensionless pillar width at various depth (D=12 m) for volume loss of 0.5% and 5% (Jurong Formation)

D=4m			D=4m		
W/D	i (H=8m;VL=0.5%)	Loc S_{max}	W/D	i (H=8m;VL=5%)	Loc S_{max}
0.167	7.189	3.039	0.167	5.429	2.873
0.500	7.310	3.642	0.500	5.808	3.299
1.000	8.182	4.585	1.000	6.733	4.171
2.000	10.382	6.528	2.000	9.418	6.256
W/D	i (H=12m;VL=0.5%)	Loc S_{max}	W/D	i (H=12m;VL=5%)	Loc S_{max}
0.167	8.877	3.217	0.167	7.151	3.047
0.500	8.872	3.800	0.500	7.367	3.460
1.000	9.498	4.712	1.000	8.055	4.308
2.000	11.292	6.557	2.000	10.182	6.290
W/D	i (H=16m;VL=0.5%)	Loc S_{max}	W/D	i (H=16m;VL=5%)	Loc S_{max}
0.167	11.205	3.314	0.167	9.032	2.836
0.500	11.156	3.937	0.500	9.179	3.344
1.000	11.620	4.892	1.000	9.780	4.369
2.000	13.064	6.757	2.000	11.663	6.542
W/D	i (H=20m;VL=0.5%)	Loc S_{max}	W/D	i (H=20m;VL=5%)	Loc S_{max}
0.167	12.786	3.422	0.167	10.716	2.966
0.500	12.719	4.023	0.500	10.824	3.294
1.000	13.153	4.931	1.000	11.363	4.237
2.000	14.422	6.758	2.000	12.992	6.386
W/D	i (H=24m;VL=0.5%)	Loc S_{max}	W/D	i (H=24m;VL=5%)	Loc S_{max}
0.167	14.457	3.528	0.167	12.563	3.101
0.500	14.366	4.133	0.500	12.629	3.449
1.000	14.724	5.020	1.000	13.095	4.348
2.000	15.824	6.796	2.000	14.508	6.423

Figure B.43 Variation of trough width parameter i and location of maximum surface settlement Loc S_{max} with dimensionless pillar width at various depth (D=4 m) for volume loss of 0.5% and 5% (mixed ground of Jurong Formation and Marine Clay)

D=6m			D=6m		
W/D	i (H=12m;VL=0.5%)	Loc S_{max}	W/D	i (H=12m;VL=5%)	Loc S_{max}
0.167	10.644	4.500	0.167	8.286	4.390
0.500	10.924	5.450	0.500	8.860	5.010
1.000	12.218	6.886	1.000	10.233	6.338
2.000	15.513	9.754	2.000	14.200	9.434
W/D	i (H=18m;VL=0.5%)	Loc S_{max}	W/D	i (H=18m;VL=5%)	Loc S_{max}
0.167	13.539	4.380	0.167	11.040	4.332
0.500	13.699	5.483	0.500	11.204	4.985
1.000	14.692	7.007	1.000	12.553	6.604
2.000	17.466	9.883	2.000	15.854	9.735
W/D	i (H=24m;VL=0.5%)	Loc S_{max}	W/D	i (H=24m;VL=5%)	Loc S_{max}
0.167	15.893	4.511	0.167	13.908	4.584
0.500	15.989	5.592	0.500	14.014	5.285
1.000	16.815	7.054	1.000	14.972	6.593
2.000	19.175	9.870	2.000	17.824	9.622
W/D	i (H=30m;VL=0.5%)	Loc S_{max}	W/D	i (H=30m;VL=5%)	Loc S_{max}
0.167	18.975	4.353	0.167	16.315	3.486
0.500	19.056	5.622	0.500	16.686	5.013
1.000	19.728	7.188	1.000	17.511	6.530
2.000	21.721	10.007	2.000	20.115	9.786
W/D	i (H=36m;VL=0.5%)	Loc S_{max}	W/D	i (H=36m;VL=5%)	Loc S_{max}
0.167	21.562	4.458	0.167	19.175	4.119
0.500	21.623	5.715	0.500	19.309	4.868
1.000	22.218	7.247	1.000	20.080	6.427
2.000	23.962	10.011	2.000	22.299	9.624

Figure B.44 Variation of trough width parameter i and location of maximum surface settlement Loc S_{max} with dimensionless pillar width at various depth (D=6 m) for volume loss of 0.5% and 5% (mixed ground of Jurong Formation and Marine Clay)

	D=8m			D=8m		
	W/D	i (H=16m;VL=0.5%)	Loc S_{max}	W/D	i (H=16m;VL=5%)	Loc S_{max}
	0.167	14.161	5.390	0.167	10.768	5.399
	0.500	14.762	7.035	0.500	11.648	6.432
	1.000	16.596	9.149	1.000	13.700	8.431
	2.000	20.999	13.025	2.000	19.256	12.815
	W/D	i (H=24m;VL=0.5%)	Loc S_{max}	W/D	i (H=24m;VL=5%)	Loc S_{max}
	0.167	17.269	5.382	0.167	14.209	5.319
	0.500	17.680	7.009	0.500	14.798	6.486
	1.000	19.095	9.110	1.000	16.338	8.392
	2.000	22.956	12.998	2.000	20.998	12.665
	W/D	i (H=32m;VL=0.5%)	Loc S_{max}	W/D	i (H=32m;VL=5%)	Loc S_{max}
	0.167	21.116	5.048	0.167	18.090	4.884
	0.500	21.462	7.001	0.500	18.506	6.430
	1.000	22.600	9.228	1.000	19.859	8.584
	2.000	25.839	13.111	2.000	23.909	12.899
	W/D	i (H=40m;VL=0.5%)	Loc S_{max}	W/D	i (H=40m;VL=5%)	Loc S_{max}
	0.167	24.717	4.767	0.167	21.643	4.502
	0.500	25.057	7.011	0.500	22.024	6.108
	1.000	26.034	9.318	1.000	23.144	8.332
	2.000	28.808	13.194	2.000	26.661	12.802
	W/D	i (H=48m;VL=0.5%)	Loc S_{max}	W/D	i (H=48m;VL=5%)	Loc S_{max}
	0.167	-	-	0.167	-	-
	0.500	-	-	0.500	-	-
	1.000	-	-	1.000	-	-
	2.000	-	-	2.000	-	-

Figure B.45 Variation of trough width parameter i and location of maximum surface settlement Loc S_{max} with dimensionless pillar width at various depth (D=8 m) for volume loss of 0.5% and 5% (mixed ground of Jurong Formation and Marine Clay)

	Z	AA	AB	AD	AE	AF
D=10m				D=10m		
W/D		i (H=20m;VL=0.5%)	Loc S_{max}	W/D	i (H=20m;VL=5%)	Loc S_{max}
0.167		17.393	6.382	0.167	13.457	6.503
0.500		18.335	8.554	0.500	14.664	8.096
1.000		20.589	11.298	1.000	17.356	10.664
2.000		26.207	16.207	2.000	24.354	16.136
W/D		i (H=30m;VL=0.5%)	Loc S_{max}	W/D	i (H=30m;VL=5%)	Loc S_{max}
0.167		21.618	5.988	0.167	17.560	5.898
0.500		22.384	8.540	0.500	18.438	7.778
1.000		24.231	11.353	1.000	20.437	10.406
2.000		29.050	16.241	2.000	26.531	15.936
W/D		i (H=40m;VL=0.5%)	Loc S_{max}	W/D	i (H=40m;VL=5%)	Loc S_{max}
0.167		25.783	5.573	0.167	22.042	5.326
0.500		26.456	8.434	0.500	22.721	7.541
1.000		27.981	11.355	1.000	24.346	10.290
2.000		32.107	16.250	2.000	29.497	15.860
W/D		i (H=50m;VL=0.5%)	Loc S_{max}	W/D	i (H=50m;VL=5%)	Loc S_{max}
0.167		-	-	0.167	-	-
0.500		-	-	0.500	-	-
1.000		-	-	1.000	-	-
2.000		-	-	2.000	-	-
W/D		i (H=60m;VL=0.5%)	Loc S_{max}	W/D	i (H=60m;VL=5%)	Loc S_{max}
0.167		-	-	0.167	-	-
0.500		-	-	0.500	-	-
1.000		-	-	1.000	-	-
2.000		-	-	2.000	-	-

Figure B.46 Variation of trough width parameter i and location of maximum surface settlement Loc S_{max} with dimensionless pillar width at various depth (D=10 m) for volume loss of 0.5% and 5% (mixed ground of Jurong Formation and Marine Clay)

D=12m				D=12m		
W/D	i (H=24m;VL=0.5%)	Loc S_{max}		W/D	i (H=24m;VL=5%)	Loc S_{max}
0.167	20.751	7.474		0.167	16.061	7.553
0.500	22.006	10.242		0.500	17.545	9.631
1.000	24.773	13.573		1.000	20.749	12.744
2.000	31.488	19.461		2.000	29.152	19.334
W/D	i (H=36m;VL=0.5%)	Loc S_{max}		W/D	i (H=36m;VL=5%)	Loc S_{max}
0.167	25.798	6.905		0.167	21.207	6.838
0.500	26.885	10.163		0.500	22.279	9.406
1.000	29.081	13.587		1.000	24.768	12.685
2.000	34.913	19.493		2.000	32.104	19.209
W/D	i (H=48m;VL=0.5%)	Loc S_{max}		W/D	i (H=48m;VL=5%)	Loc S_{max}
0.167	-	-		0.167	-	-
0.500	-	-		0.500	-	-
1.000	-	-		1.000	-	-
2.000	-	-		2.000	-	-
W/D	i (H=60m;VL=0.5%)	Loc S_{max}		W/D	i (H=60m;VL=5%)	Loc S_{max}
0.167	-	-		0.167	-	-
0.500	-	-		0.500	-	-
1.000	-	-		1.000	-	-
2.000	-	-		2.000	-	-
W/D	i (H=72m;VL=0.5%)	Loc S_{max}		W/D	i (H=72m;VL=5%)	Loc S_{max}
0.167	-	-		0.167	-	-
0.500	-	-		0.500	-	-
1.000	-	-		1.000	-	-
2.000	-	-		2.000	-	-

Figure B.47 Variation of trough width parameter i and location of maximum surface settlement Loc S_{max} with dimensionless pillar width at various depth (D=12 m) for volume loss of 0.5% and 5% (mixed ground of Jurong Formation and Marine Clay)

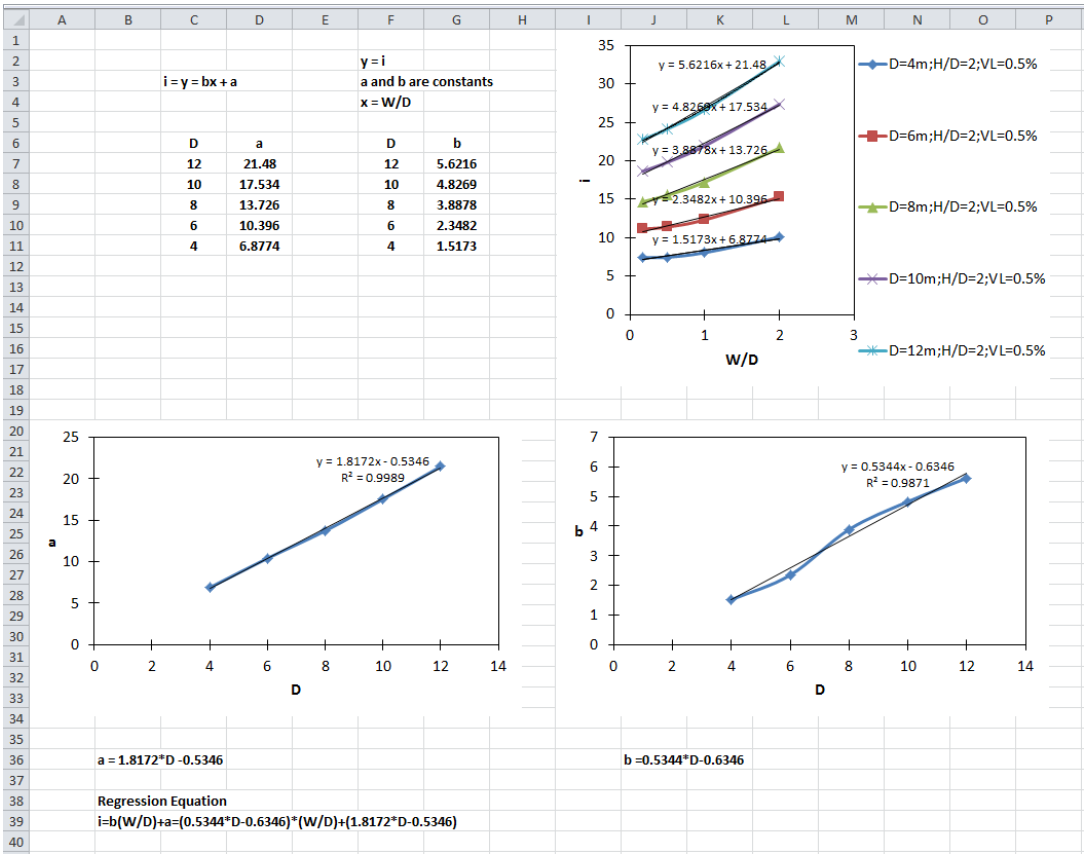

(a)

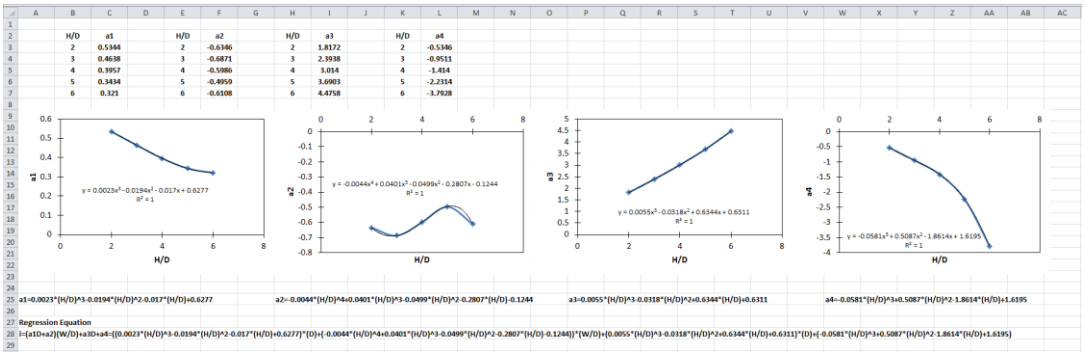

(b)

Figure B.48 Regression equations (a) i=b(W/D)+a; and (b) i=(a1D+a2)(W/D)+a3D+a4

Appendix C

F	W/D=1/6 H/D=1 Incre Max Moment Coefficient	W/D=1/6 H/D=1.25 Incre Max Moment Coefficient	W/D=1/6 H/D=2 Incre Max Moment Coefficient	W/D=1/6 H/D=6 Incre Max Moment Coefficient
0.5	0.021885	0.022106	0.019797	0.016382
1	0.022817	0.022568	0.020664	0.018618
3.1	0.017734	0.017067	0.015895	0.015182
15.6	0.006182	0.005852	0.005518	0.005383
70	0.001052	0.000939	0.000840	0.000801
200	-0.000050	-0.000105	-0.000143	-0.000149
400	-0.000240	-0.000268	-0.000279	-0.000272

F	W/D=0.5 H/D=1 Incre Max Moment Coefficient	W/D=0.5 H/D=1.25 Incre Max Moment Coefficient	W/D=0.5 H/D=2 Incre Max Moment Coefficient	W/D=0.5 H/D=6 Incre Max Moment Coefficient
0.5	0.010904	0.013320	0.013533	0.010894
1	0.013015	0.014638	0.014378	0.012602
3.1	0.011758	0.012119	0.011447	0.010676
15.6	0.004782	0.004626	0.004268	0.004094
70	0.001127	0.001012	0.000880	0.000838
200	0.000263	0.000192	0.000127	0.000115
400	0.000067	0.000020	-0.000017	-0.000019

F	W/D=1.0 H/D=1 Incre Max Moment Coefficient	W/D=1.0 H/D=1.25 Incre Max Moment Coefficient	W/D=1.0 H/D=2 Incre Max Moment Coefficient	W/D=1.0 H/D=6 Incre Max Moment Coefficient
0.5	0.001583	0.004986	0.007873	0.006462
1	0.003872	0.006669	0.008555	0.007385
3.1	0.004939	0.006369	0.006819	0.006105
15.6	0.002292	0.002567	0.002447	0.002229
70	0.000612	0.000616	0.000510	0.000449
200	0.000195	0.000165	0.000095	0.000072
400	0.000087	0.000060	0.000013	0.000001

Figure C.1 Incremental maximum moment coefficient for primary effect (K_o=0.5)

F	W/D=1/6 H/D=1 Incre Max Moment Coefficient	W/D=1/6 H/D=1.25 Incre Max Moment Coefficient	W/D=1/6 H/D=2 Incre Max Moment Coefficient	W/D=1/6 H/D=6 Incre Max Moment Coefficient
0.5	-0.009655	-0.008079	-0.010025	-0.015528
1	-0.015779	-0.014049	-0.015034	-0.018723
3.1	-0.017056	-0.015633	-0.015507	-0.016635
15.6	-0.008358	-0.007975	-0.007822	-0.007863
70	-0.003374	-0.003354	-0.003354	-0.003359
200	-0.001844	-0.001853	-0.001856	-0.001856
400	-0.001207	-0.001208	-0.001198	-0.001190

F	W/D=0.5 H/D=1 Incre Max Moment Coefficient	W/D=0.5 H/D=1.25 Incre Max Moment Coefficient	W/D=0.5 H/D=2 Incre Max Moment Coefficient	W/D=0.5 H/D=6 Incre Max Moment Coefficient
0.5	-0.012006	-0.008380	-0.006259	-0.009792
1	-0.015755	-0.012135	-0.009739	-0.012194
3.1	-0.015250	-0.012377	-0.010392	-0.011285
15.6	-0.006966	-0.005974	-0.005355	-0.005467
70	-0.002506	-0.002329	-0.002227	-0.002242
200	-0.001216	-0.001188	-0.001168	-0.001167
400	-0.000736	-0.000734	-0.000725	-0.000720

F	W/D=1.0 H/D=1 Incre Max Moment Coefficient	W/D=1.0 H/D=1.25 Incre Max Moment Coefficient	W/D=1.0 H/D=2 Incre Max Moment Coefficient	W/D=1.0 H/D=6 Incre Max Moment Coefficient
0.5	-0.012241	-0.009075	-0.004435	-0.005311
1	-0.013771	-0.010805	-0.006350	-0.006736
3.1	-0.011868	-0.009536	-0.006267	-0.006207
15.6	-0.004883	-0.003988	-0.002921	-0.002874
70	-0.001517	-0.001338	-0.001138	-0.001134
200	-0.000647	-0.000620	-0.000584	-0.000584
400	-0.000365	-0.000367	-0.000361	-0.000359

Figure C.2 Incremental maximum moment coefficient for primary effect (K_o=1.5)

F	W/D=1/6 H/D=1 Vertical Diameter Change Coefficient	W/D=1/6 H/D=1.25 Vertical Diameter Change Coefficient	W/D=1/6 H/D=2 Vertical Diameter Change Coefficient	W/D=1/6 H/D=6 Vertical Diameter Change Coefficient
0.5	0.032053	0.033907	0.030205	0.022368
1	0.062318	0.063857	0.056478	0.045755
3.1	0.127572	0.124521	0.105602	0.089362
15.6	0.169566	0.152815	0.113247	0.090753
70	0.108282	0.064822	0.001332	-0.020113
200	-0.038740	-0.114520	-0.193515	-0.198543
400	-0.198708	-0.294147	-0.370498	-0.350140

F	W/D=0.5 H/D=1 Vertical Diameter Change Coefficient	W/D=0.5 H/D=1.25 Vertical Diameter Change Coefficient	W/D=0.5 H/D=2 Vertical Diameter Change Coefficient	W/D=0.5 H/D=6 Vertical Diameter Change Coefficient
0.5	0.015634	0.021285	0.023142	0.017256
1	0.035805	0.044080	0.044984	0.036313
3.1	0.086159	0.096086	0.089965	0.075325
15.6	0.128461	0.132723	0.109917	0.087311
70	0.110070	0.096116	0.047178	0.019551
200	0.057525	0.016349	-0.062341	-0.087680
400	0.005028	-0.058285	-0.156373	-0.173719

F	W/D=1.0 H/D=1 Vertical Diameter Change Coefficient	W/D=1.0 H/D=1.25 Vertical Diameter Change Coefficient	W/D=1.0 H/D=2 Vertical Diameter Change Coefficient	W/D=1.0 H/D=6 Vertical Diameter Change Coefficient
0.5	0.001367	0.007726	0.014623	0.011727
1	0.010120	0.020601	0.030071	0.024879
3.1	0.037868	0.054586	0.064447	0.053197
15.6	0.066792	0.085048	0.086957	0.066694
70	0.065177	0.076293	0.058369	0.028650
200	0.051837	0.049722	0.004010	-0.033276
400	0.040558	0.026235	-0.041567	-0.081781

Figure C.3 Vertical diameter change coefficient for primary effect (K_o=0.5)

F	W/D=1/6 H/D=1 Vertical Diameter Change Coefficient	W/D=1/6 H/D=1.25 Vertical Diameter Change Coefficient	W/D=1/6 H/D=2 Vertical Diameter Change Coefficient	W/D=1/6 H/D=6 Vertical Diameter Change Coefficient
0.5	-0.013342	-0.008062	-0.008278	-0.019654
1	-0.042448	-0.030880	-0.027550	-0.043659
3.1	-0.123931	-0.093086	-0.075368	-0.096092
15.6	-0.226219	-0.170722	-0.136436	-0.159852
70	-0.326320	-0.279354	-0.254902	-0.277959
200	-0.490529	-0.467561	-0.451547	-0.457584
400	-0.669433	-0.658113	-0.631006	-0.609089

F	W/D=0.5 H/D=1 Vertical Diameter Change Coefficient	W/D=0.5 H/D=1.25 Vertical Diameter Change Coefficient	W/D=0.5 H/D=2 Vertical Diameter Change Coefficient	W/D=0.5 H/D=6 Vertical Diameter Change Coefficient
0.5	-0.021821	-0.014531	-0.007585	-0.014301
1	-0.053389	-0.039204	-0.024303	-0.033173
3.1	-0.138800	-0.105287	-0.068221	-0.077264
15.6	-0.239529	-0.183390	-0.123301	-0.130677
70	-0.302736	-0.252901	-0.203583	-0.212556
200	-0.378484	-0.350818	-0.323794	-0.327041
400	-0.452214	-0.442267	-0.426979	-0.417684

F	W/D=1.0 H/D=1 Vertical Diameter Change Coefficient	W/D=1.0 H/D=1.25 Vertical Diameter Change Coefficient	W/D=1.0 H/D=2 Vertical Diameter Change Coefficient	W/D=1.0 H/D=6 Vertical Diameter Change Coefficient
0.5	-0.023090	-0.018008	-0.007998	-0.008820
1	-0.049477	-0.040472	-0.021860	-0.021278
3.1	-0.117852	-0.097980	-0.058177	-0.051820
15.6	-0.194876	-0.162333	-0.102665	-0.090339
70	-0.231994	-0.201950	-0.152468	-0.143972
200	-0.263175	-0.245020	-0.219648	-0.214744
400	-0.289186	-0.282493	-0.275590	-0.269139

Figure C.4 Vertical diameter change coefficient for primary effect (K_o=1.5)

F	W/D=1/6 H/D=1 Horizontal Diameter Change Coefficient	W/D=1/6 H/D=1.25 Horizontal Diameter Change Coefficient	W/D=1/6 H/D=2 Horizontal Diameter Change Coefficient	W/D=1/6 H/D=6 Horizontal Diameter Change Coefficient
0.5	-0.034028	-0.035755	-0.032074	-0.024358
1	-0.066880	-0.068331	-0.061327	-0.051013
3.1	-0.141133	-0.138829	-0.122395	-0.107726
15.6	-0.200412	-0.190694	-0.163375	-0.146633
70	-0.146666	-0.129213	-0.098783	-0.089172
200	-0.042091	-0.017277	0.013842	0.013554
400	0.029524	0.058824	0.090732	0.084526

F	W/D=0.5 H/D=1 Horizontal Diameter Change Coefficient	W/D=0.5 H/D=1.25 Horizontal Diameter Change Coefficient	W/D=0.5 H/D=2 Horizontal Diameter Change Coefficient	W/D=0.5 H/D=6 Horizontal Diameter Change Coefficient
0.5	-0.016596	-0.022182	-0.024016	-0.018242
1	-0.038242	-0.046399	-0.047425	-0.039077
3.1	-0.094513	-0.104351	-0.099421	-0.086056
15.6	-0.150199	-0.156422	-0.141125	-0.123939
70	-0.131853	-0.130378	-0.107408	-0.093773
200	-0.081770	-0.072203	-0.042152	-0.033341
400	-0.048478	-0.034135	0.001187	0.008147

F	W/D=1.0 H/D=1 Horizontal Diameter Change Coefficient	W/D=1.0 H/D=1.25 Horizontal Diameter Change Coefficient	W/D=1.0 H/D=2 Horizontal Diameter Change Coefficient	W/D=1.0 H/D=6 Horizontal Diameter Change Coefficient
0.5	-0.001570	-0.008020	-0.014919	-0.012112
1	-0.010837	-0.021458	-0.030957	-0.026001
3.1	-0.040937	-0.057939	-0.068102	-0.057802
15.6	-0.075192	-0.094526	-0.099424	-0.083706
70	-0.069691	-0.085680	-0.082444	-0.066674
200	-0.046248	-0.058389	-0.046771	-0.031604
400	-0.029684	-0.040297	-0.023336	-0.007423

Figure C.5 Horizontal diameter change coefficient for primary effect (K_o=0.5)

F	W/D=1/6 H/D=1 Horizontal Diameter Change Coefficient	W/D=1/6 H/D=1.25 Horizontal Diameter Change Coefficient	W/D=1/6 H/D=2 Horizontal Diameter Change Coefficient	W/D=1/6 H/D=6 Horizontal Diameter Change Coefficient
0.5	0.014948	0.009949	0.010457	0.021753
1	0.047494	0.036520	0.033638	0.049278
3.1	0.144433	0.115486	0.098247	0.116349
15.6	0.303305	0.253164	0.216903	0.229583
70	0.517138	0.472409	0.435766	0.436639
200	0.766345	0.736429	0.705147	0.692624
400	0.943647	0.923023	0.895108	0.874072

F	W/D=0.5 H/D=1 Horizontal Diameter Change Coefficient	W/D=0.5 H/D=1.25 Horizontal Diameter Change Coefficient	W/D=0.5 H/D=2 Horizontal Diameter Change Coefficient	W/D=0.5 H/D=6 Horizontal Diameter Change Coefficient
0.5	0.022754	0.015449	0.008695	0.015362
1	0.056246	0.041999	0.027482	0.036148
3.1	0.150768	0.117154	0.081138	0.089032
15.6	0.287220	0.231764	0.173484	0.174981
70	0.423403	0.374013	0.321647	0.315542
200	0.567612	0.534583	0.498586	0.486423
400	0.670724	0.648171	0.623993	0.609386

F	W/D=1.0 H/D=1 Horizontal Diameter Change Coefficient	W/D=1.0 H/D=1.25 Horizontal Diameter Change Coefficient	W/D=1.0 H/D=2 Horizontal Diameter Change Coefficient	W/D=1.0 H/D=6 Horizontal Diameter Change Coefficient
0.5	0.023782	0.018505	0.008470	0.009266
1	0.051308	0.041874	0.023192	0.022544
3.1	0.124827	0.103717	0.063701	0.057020
15.6	0.221225	0.186090	0.125955	0.111272
70	0.297556	0.265027	0.213561	0.196775
200	0.374338	0.349812	0.317377	0.302307
400	0.432446	0.411818	0.392225	0.379982

Figure C.6 Horizontal diameter change coefficient for primary effect (K_o=1.5)

F	W/D=1/6 H/D=1 Incre Max Moment Coefficient	W/D=1/6 H/D=1.25 Incre Max Moment Coefficient	W/D=1/6 H/D=2 Incre Max Moment Coefficient	W/D=1/6 H/D=6 Incre Max Moment Coefficient
0.5	0.000034	0.000036	0.000038	0.000039
1	0.000091	0.000095	0.000100	0.000102
3.1	0.000322	0.000335	0.000345	0.000346
15.6	0.001098	0.001150	0.001175	0.001177
70	0.002301	0.002418	0.002505	0.002528
200	0.003217	0.003410	0.003559	0.003666
400	0.003764	0.004014	0.004234	0.004430

F	W/D=0.5 H/D=1 Incre Max Moment Coefficient	W/D=0.5 H/D=1.25 Incre Max Moment Coefficient	W/D=0.5 H/D=2 Incre Max Moment Coefficient	W/D=0.5 H/D=6 Incre Max Moment Coefficient
0.5	0.000011	0.000012	0.000013	0.000014
1	0.000030	0.000032	0.000034	0.000035
3.1	0.000094	0.000103	0.000110	0.000111
15.6	0.000242	0.000271	0.000295	0.000296
70	0.000365	0.000416	0.000460	0.000468
200	0.000412	0.000475	0.000531	0.000551
400	0.000429	0.000498	0.000571	0.000595

F	W/D=1.0 H/D=1 Incre Max Moment Coefficient	W/D=1.0 H/D=1.25 Incre Max Moment Coefficient	W/D=1.0 H/D=2 Incre Max Moment Coefficient	W/D=1.0 H/D=6 Incre Max Moment Coefficient
0.5	0.000003	0.000004	0.000004	0.000004
1	0.000007	0.000009	0.000010	0.000010
3.1	0.000021	0.000025	0.000029	0.000030
15.6	0.000045	0.000054	0.000065	0.000067
70	0.000058	0.000071	0.000086	0.000092
200	0.000063	0.000076	0.000093	0.000101
400	0.000065	0.000079	0.000096	0.000106

Figure C.7 Incremental maximum moment coefficient for volume loss effect of pre-existing tunnel

F	W/D=1/6 H/D=1 Incre Max Moment Coefficient	W/D=1/6 H/D=1.25 Incre Max Moment Coefficient	W/D=1/6 H/D=2 Incre Max Moment Coefficient	W/D=1/6 H/D=6 Incre Max Moment Coefficient
0.5	-0.000456	-0.000485	-0.000502	-0.000492
1	-0.000740	-0.000784	-0.000804	-0.000785
3.1	-0.001398	-0.001468	-0.001485	-0.001452
15.6	-0.002749	-0.002855	-0.002868	-0.002829
70	-0.004338	-0.004455	-0.004514	-0.004500
200	-0.005432	-0.005576	-0.005687	-0.005685
400	-0.006016	-0.006232	-0.006309	-0.006411

F	W/D=0.5 H/D=1 Incre Max Moment Coefficient	W/D=0.5 H/D=1.25 Incre Max Moment Coefficient	W/D=0.5 H/D=2 Incre Max Moment Coefficient	W/D=0.5 H/D=6 Incre Max Moment Coefficient
0.5	-0.000205	-0.000235	-0.000263	-0.000259
1	-0.000335	-0.000384	-0.000422	-0.000413
3.1	-0.000595	-0.000691	-0.000757	-0.000739
15.6	-0.001021	-0.001184	-0.001277	-0.001252
70	-0.001327	-0.001513	-0.001617	-0.001596
200	-0.001451	-0.001649	-0.001746	-0.001734
400	-0.001499	-0.001700	-0.001796	-0.001788

F	W/D=1.0 H/D=1 Incre Max Moment Coefficient	W/D=1.0 H/D=1.25 Incre Max Moment Coefficient	W/D=1.0 H/D=2 Incre Max Moment Coefficient	W/D=1.0 H/D=6 Incre Max Moment Coefficient
0.5	-0.000078	-0.000098	-0.000130	-0.000134
1	-0.000120	-0.000154	-0.000208	-0.000212
3.1	-0.000197	-0.000267	-0.000358	-0.000364
15.6	-0.000284	-0.000416	-0.000555	-0.000559
70	-0.000332	-0.000498	-0.000657	-0.000660
200	-0.000346	-0.000527	-0.000686	-0.000685
400	-0.000347	-0.000536	-0.000697	-0.000693

Figure C.8 Incremental maximum moment coefficient for volume loss effect of new adjacent tunnel

F	W/D=1/6 H/D=1 Vertical Diameter Change Coefficient	W/D=1/6 H/D=1.25 Vertical Diameter Change Coefficient	W/D=1/6 H/D=2 Vertical Diameter Change Coefficient	W/D=1/6 H/D=6 Vertical Diameter Change Coefficient
0.5	0.000035	0.000035	0.000035	0.000038
1	0.000084	0.000084	0.000082	0.000086
3.1	0.000224	0.000214	0.000199	0.000204
15.6	0.000391	0.000353	0.000312	0.000321
70	0.000392	0.000333	0.000290	0.000312
200	0.000298	0.000231	0.000202	0.000249
400	0.000201	0.000132	0.000121	0.000191

F	W/D=0.5 H/D=1 Vertical Diameter Change Coefficient	W/D=0.5 H/D=1.25 Vertical Diameter Change Coefficient	W/D=0.5 H/D=2 Vertical Diameter Change Coefficient	W/D=0.5 H/D=6 Vertical Diameter Change Coefficient
0.5	0.000014	0.000015	0.000015	0.000016
1	0.000034	0.000037	0.000036	0.000037
3.1	0.000089	0.000094	0.000089	0.000089
15.6	0.000152	0.000155	0.000140	0.000137
70	0.000159	0.000155	0.000131	0.000134
200	0.000142	0.000128	0.000100	0.000112
400	0.000125	0.000104	0.000075	0.000093

F	W/D=1.0 H/D=1 Vertical Diameter Change Coefficient	W/D=1.0 H/D=1.25 Vertical Diameter Change Coefficient	W/D=1.0 H/D=2 Vertical Diameter Change Coefficient	W/D=1.0 H/D=6 Vertical Diameter Change Coefficient
0.5	0.000004	0.000005	0.000006	0.000006
1	0.000010	0.000012	0.000013	0.000013
3.1	0.000024	0.000029	0.000032	0.000031
15.6	0.000039	0.000048	0.000051	0.000047
70	0.000042	0.000050	0.000050	0.000047
200	0.000041	0.000047	0.000042	0.000041
400	0.000040	0.000044	0.000035	0.000035

Figure C.9 Vertical diameter change coefficient for volume loss effect of pre-existing tunnel

F	W/D=1/6 H/D=1 Vertical Diameter Change Coefficient	W/D=1/6 H/D=1.25 Vertical Diameter Change Coefficient	W/D=1/6 H/D=2 Vertical Diameter Change Coefficient	W/D=1/6 H/D=6 Vertical Diameter Change Coefficient
0.5	-0.000514	-0.000564	-0.000604	-0.000592
1	-0.000780	-0.000854	-0.000906	-0.000878
3.1	-0.001214	-0.001322	-0.001374	-0.001311
15.6	-0.001566	-0.001693	-0.001715	-0.001609
70	-0.001705	-0.001809	-0.001798	-0.001659
200	-0.001817	-0.001893	-0.001832	-0.001646
400	-0.001893	-0.001960	-0.001832	-0.001632

F	W/D=0.5 H/D=1 Vertical Diameter Change Coefficient	W/D=0.5 H/D=1.25 Vertical Diameter Change Coefficient	W/D=0.5 H/D=2 Vertical Diameter Change Coefficient	W/D=0.5 H/D=6 Vertical Diameter Change Coefficient
0.5	-0.000261	-0.000307	-0.000361	-0.000359
1	-0.000396	-0.000467	-0.000548	-0.000539
3.1	-0.000607	-0.000722	-0.000840	-0.000816
15.6	-0.000754	-0.000910	-0.001054	-0.001007
70	-0.000808	-0.000970	-0.001105	-0.001037
200	-0.000860	-0.001026	-0.001135	-0.001044
400	-0.000901	-0.001066	-0.001155	-0.001045

F	W/D=1.0 H/D=1 Vertical Diameter Change Coefficient	W/D=1.0 H/D=1.25 Vertical Diameter Change Coefficient	W/D=1.0 H/D=2 Vertical Diameter Change Coefficient	W/D=1.0 H/D=6 Vertical Diameter Change Coefficient
0.5	-0.000116	-0.000141	-0.000194	-0.000206
1	-0.000175	-0.000213	-0.000295	-0.000311
3.1	-0.000262	-0.000324	-0.000453	-0.000473
15.6	-0.000317	-0.000400	-0.000568	-0.000587
70	-0.000329	-0.000423	-0.000602	-0.000611
200	-0.000333	-0.000442	-0.000621	-0.000610
400	-0.000335	-0.000455	-0.000635	-0.000610

Figure C.10 Vertical diameter change coefficient for volume loss effect of new adjacent tunnel

F	W/D=1/6 H/D=1 Horizontal Diameter Change Coefficient	W/D=1/6 H/D=1.25 Horizontal Diameter Change Coefficient	W/D=1/6 H/D=2 Horizontal Diameter Change Coefficient	W/D=1/6 H/D=6 Horizontal Diameter Change Coefficient
0.5	-0.000038	-0.000039	-0.000039	-0.000042
1	-0.000095	-0.000095	-0.000094	-0.000098
3.1	-0.000271	-0.000267	-0.000257	-0.000260
15.6	-0.000617	-0.000608	-0.000584	-0.000587
70	-0.000955	-0.000962	-0.000955	-0.000965
200	-0.001211	-0.001249	-0.001264	-0.001297
400	-0.001398	-0.001461	-0.001496	-0.001549

F	W/D=0.5 H/D=1 Horizontal Diameter Change Coefficient	W/D=0.5 H/D=1.25 Horizontal Diameter Change Coefficient	W/D=0.5 H/D=2 Horizontal Diameter Change Coefficient	W/D=0.5 H/D=6 Horizontal Diameter Change Coefficient
0.5	-0.000015	-0.000016	-0.000017	-0.000017
1	-0.000036	-0.000039	-0.000040	-0.000040
3.1	-0.000099	-0.000106	-0.000104	-0.000104
15.6	-0.000192	-0.000207	-0.000204	-0.000200
70	-0.000247	-0.000271	-0.000275	-0.000275
200	-0.000277	-0.000311	-0.000324	-0.000331
400	-0.000299	-0.000341	-0.000367	-0.000374

F	W/D=1.0 H/D=1 Horizontal Diameter Change Coefficient	W/D=1.0 H/D=1.25 Horizontal Diameter Change Coefficient	W/D=1.0 H/D=2 Horizontal Diameter Change Coefficient	W/D=1.0 H/D=6 Horizontal Diameter Change Coefficient
0.5	-0.000004	-0.000005	-0.000006	-0.000006
1	-0.000010	-0.000012	-0.000014	-0.000014
3.1	-0.000025	-0.000031	-0.000035	-0.000034
15.6	-0.000044	-0.000055	-0.000062	-0.000060
70	-0.000053	-0.000067	-0.000078	-0.000077
200	-0.000057	-0.000073	-0.000088	-0.000091
400	-0.000061	-0.000079	-0.000098	-0.000101

Figure C.11 Horizontal diameter change coefficient for volume loss effect of pre-existing tunnel

F	W/D=1/6 H/D=1 Horizontal Diameter Change Coefficient	W/D=1/6 H/D=1.25 Horizontal Diameter Change Coefficient	W/D=1/6 H/D=2 Horizontal Diameter Change Coefficient	W/D=1/6 H/D=6 Horizontal Diameter Change Coefficient
0.5	0.000548	0.000597	0.000636	0.000624
1	0.000840	0.000913	0.000963	0.000936
3.1	0.001354	0.001463	0.001517	0.001459
15.6	0.001943	0.002088	0.002133	0.002051
70	0.002303	0.002455	0.002535	0.002476
200	0.002451	0.002627	0.002753	0.002717
400	0.002499	0.002718	0.002848	0.002872

F	W/D=0.5 H/D=1 Horizontal Diameter Change Coefficient	W/D=0.5 H/D=1.25 Horizontal Diameter Change Coefficient	W/D=0.5 H/D=2 Horizontal Diameter Change Coefficient	W/D=0.5 H/D=6 Horizontal Diameter Change Coefficient
0.5	0.000273	0.000319	0.000372	0.000369
1	0.000417	0.000489	0.000568	0.000560
3.1	0.000654	0.000774	0.000891	0.000870
15.6	0.000866	0.001037	0.001189	0.001157
70	0.000934	0.001116	0.001286	0.001270
200	0.000928	0.001117	0.001296	0.001312
400	0.000911	0.001100	0.001292	0.001330

F	W/D=1.0 H/D=1 Horizontal Diameter Change Coefficient	W/D=1.0 H/D=1.25 Horizontal Diameter Change Coefficient	W/D=1.0 H/D=2 Horizontal Diameter Change Coefficient	W/D=1.0 H/D=6 Horizontal Diameter Change Coefficient
0.5	0.000119	0.000144	0.000198	0.000209
1	0.000180	0.000219	0.000302	0.000317
3.1	0.000272	0.000339	0.000469	0.000490
15.6	0.000336	0.000433	0.000606	0.000631
70	0.000352	0.000454	0.000639	0.000676
200	0.000350	0.000448	0.000630	0.000680
400	0.000345	0.000438	0.000619	0.000680

Figure C.12 Horizontal diameter change coefficient for volume loss effect of new adjacent tunnel

CURRICULUM VITAE

Personal Details:

Name: Chua Heng Choon
Nationality: Malaysian (Singapore Permanent Resident) Phone: +65 96231382
Date of Birth: 14 February 1978 Email: chuahengchoon@gmail.com

Education:

- **2016: Doctor of Philosophy**
  - Nanyang Technological University, Singapore
  - PhD Thesis: Field Measurements and Numerical Analysis of Interaction between Closely Spaced Bored Tunnels

- **2007: Master of Science (Civil Engineering)**
  - Nanyang Technological University, Singapore
  - Dissertation: Distinct Element Modelling of Cavern Construction

- **2003: Bachelor of Engineering (Civil)**
  - Nanyang Technological University, Singapore
  - Final Year Project: Effect of New Bored Tunnels on the Stresses Induced in the Lining of Existing Adjacent Tunnels

Engineering Experience:

- **2003-2012: Project Officer, School of Civil and Environmental Engineering, Nanyang Technological University, Singapore**

  - **2007-2012: Jurong Rock Caverns Project**
    - ✓ Numerical modelling using UDEC, 3DEC and Phase2
    - ✓ Knowledgeable about rock cavern and rock engineering

  - **2006-2007: Complementary Site Investigation at Banyan Basin, Jurong Island, for the Jurong Rock Caverns Project**
    - ✓ Collation of site investigation data
    - ✓ Knowledgeable about in-situ and laboratory rock testings

  - **2003-2006: Deep Tunnel Sewerage System Project**
    - ✓ Numerical modelling using PLAXIS
    - ✓ Knowledgeable about bored tunnelling

- **2002: Industrial Attachment with Ching Soon Construction Pte. Ltd.**
    - ✓ Design and construction of pile foundations

Achievements:

- 2006: The Hulme Prize (First Prize) for the best technical paper related to tunnelling and underground construction
- 2002: Industrial Attachment Book Prize

Publications:

Chua, H.C., Goh, A.T.C. and Zhao, Z.Y. (2009). Distinct Element Analysis of Staged Constructed Underground Cavern in the Vicinity of a Fault. Analysis of Discontinuous Deformation: Proceedings of the 9th International Conference on Analysis of Discontinuous Deformation: New Developments and Applications, pp. 429-435.

Chua, H.C. and Leong, E.C. (2007). Numerical Analysis of Interaction between Underground Caverns. Numerical Models in Geomechanics: Proceedings of the 10th International Symposium on Numerical Models in Geomechanics (NUMOG X), pp. 393-398.

Chua, H.C. and Leong, E.C. (2006). Effect of Excavation Sequence and Fault Orientation on Stresses and Deformation around a Cavern. Proceedings of the ISRM International Symposium 2006 and the 4th Asian Rock Mechanics Symposium: Rock Mechanics in Underground Construction, p. 361.

Hefny, A.M. and Chua, H.C. (2006). An Investigation into the Behaviour of Jointed Tunnel Lining. Tunnelling and Underground Space Technology, Vol. 21(3-4), p. 428.

Hefny, A.M., Chua, H.C. and Zhao, J. (2004). Parametric Studies on the Interaction between Existing and New Bored Tunnels. Tunnelling and Underground Space Technology, Vol. 19(4-5), p. 471.

MEMORABILIA

A revelatory insigh+

I guess I really lucked out when I accidentally (honest!) hit…. your face while making a stand from the step of the staircase after the annual group photo-taking for faculty and graduating students of School of Civil and Environmental Engineering (CEE) on 27 January 2016. Surprisingly, you accepted hit…. with good grace! Since both of us were surrounded mostly by the final year undergraduate students, it seems that… by degrees our friendship grew into love. Yes, get hitched! Haha…

Intermittently, we spent seconds chatting about the prospect of Singapore Permanent Resident being recruited as police officer during the recess for Lecture on Shallow and Deep Foundations on 29 January 2016, where I initially ruled out such possibility before saying "很难讲". Surprisingly, you repeated the same "很难讲". What a refreshing and energising repetition and I looked at you queerly. It seems that… you agreed both of us are a perfect match for each other. In every sense of the word "很难讲" carries the meaning of "夫唱妇随", i.e. "唱" serves as an alternative for "难讲" and your repetition is definitely as good as "妇随". Yahoo, "夫唱妇随"! Haha…

But…but… the whole thing became a regular "disaster" after you walked passing me at the bus stop after the lecture! This action allows of only one explanation "It isn't love, it's just a passing in…fat…ua…tion." I know you jerked me around but this wasn't even remotely funny! Anyway, I, Chua Heng Choon, hope you, (see ACKNOWLEDGEMENTS), enjoy reading my "Unproven Theories" submitted to you on 01 February 2016 in fulfilment of the requirement for the degree of Fiancé.

《礼记·大学》

When not otherwise engaged, I cast my eyes to the sky…

AS IF: THE LONG ARM OF 内圣外王 (MARRIAGE LINES)

(Photo by Chua Heng Choon on 16 January 2013 at 7:03:16 PM)

AS IF: COMPENDIUM

(Photo by Chua Heng Choon on 06 January 2013 at 7:00:26 PM)

AS IF: PhO…spho…res…cent 修身

(Photo by Chua Heng Choon on 10 February 2012 at 7:10:26 PM)

AS IF: -ish…ome 齐家

(Photo by Chua Heng Choon on 15 January 2013 at 5:34:36 PM)

AS IF: PEEKING~PEKING~BEIJING 治国 (wonderFULI expressI'VE eyes)

(Photo by Chua Heng Choon on 13 January 2013 at 4:59:10 PM)

AS IF: Dip…lo…ma…–cy 平天下 (the horse slowed to a trot)

(Photo by Chua Heng Choon on 03 January 2013 at 5:56:24 PM)

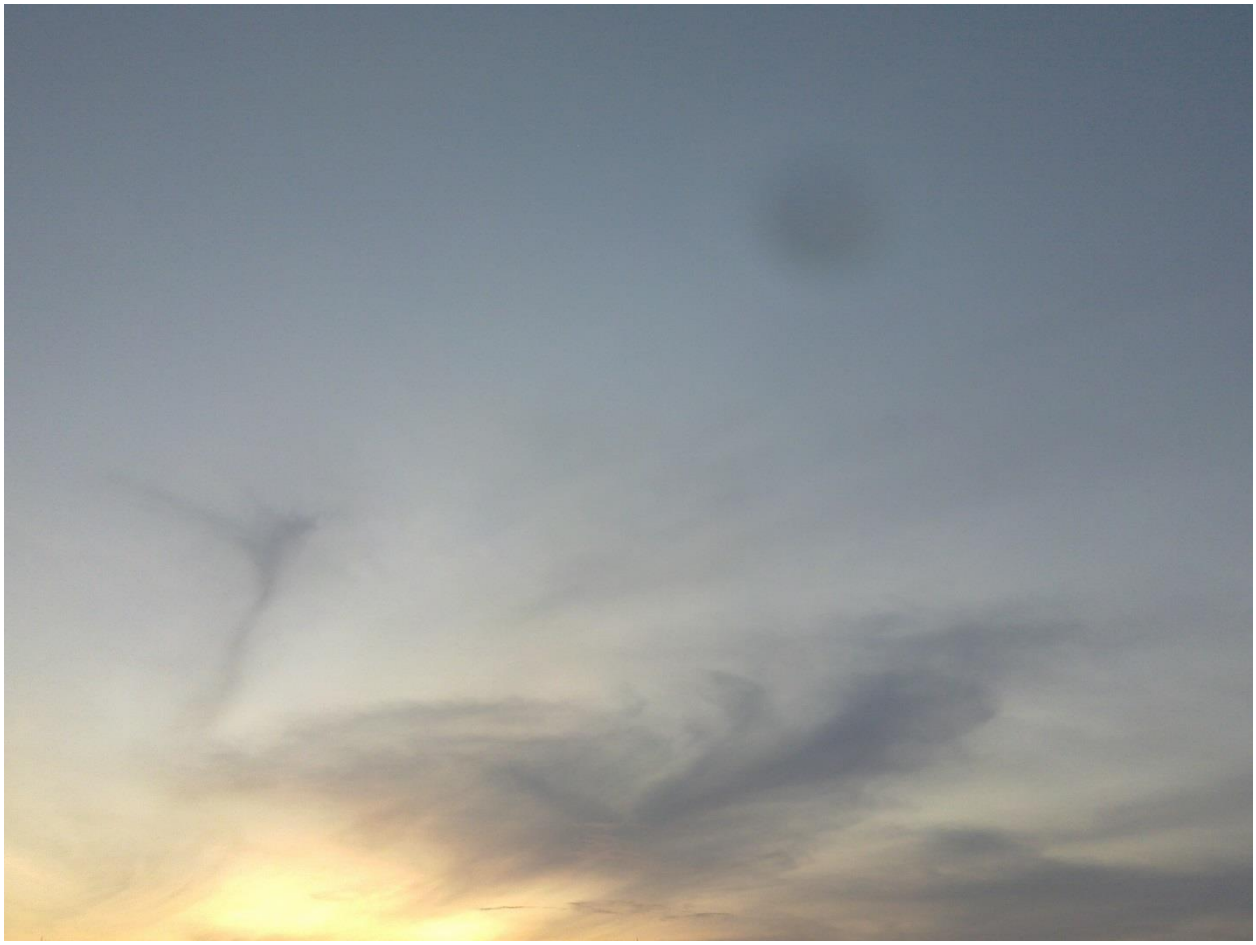

AS IF: plover? dialectic (plight your troth)

(Photo by Chua Heng Choon on 16 January 2012 at 7:16:12 PM)